BIOPHYSICS 241:\MEMBRANE BIOLOGY



Roland Faller
University of California, Davis



University of California, Davis

UCD Biophysics 241: Membrane Biology

Roland Faller

This text is disseminated via the Open Education Resource (OER) LibreTexts Project (https://LibreTexts.org) and like the thousands of other texts available within this powerful platform, it is freely available for reading, printing, and "consuming."

The LibreTexts mission is to bring together students, faculty, and scholars in a collaborative effort to provide an accessible, and comprehensive platform that empowers our community to develop, curate, adapt, and adopt openly licensed resources and technologies; through these efforts we can reduce the financial burden born from traditional educational resource costs, ensuring education is more accessible for students and communities worldwide.

Most, but not all, pages in the library have licenses that may allow individuals to make changes, save, and print this book. Carefully consult the applicable license(s) before pursuing such effects. Instructors can adopt existing LibreTexts texts or Remix them to quickly build course-specific resources to meet the needs of their students. Unlike traditional textbooks, LibreTexts' web based origins allow powerful integration of advanced features and new technologies to support learning.



LibreTexts is the adaptable, user-friendly non-profit open education resource platform that educators trust for creating, customizing, and sharing accessible, interactive textbooks, adaptive homework, and ancillary materials. We collaborate with individuals and organizations to champion open education initiatives, support institutional publishing programs, drive curriculum development projects, and more.

The LibreTexts libraries are Powered by NICE CXone Expert and was supported by the Department of Education Open Textbook Pilot Project, the California Education Learning Lab, the UC Davis Office of the Provost, the UC Davis Library, the California State University Affordable Learning Solutions Program, and Merlot. This material is based upon work supported by the National Science Foundation under Grant No. 1246120, 1525057, and 1413739.

Any opinions, findings, and conclusions or recommendations expressed in this material are those of the author(s) and do not necessarily reflect the views of the National Science Foundation nor the US Department of Education.

Have questions or comments? For information about adoptions or adaptions contact info@LibreTexts.org or visit our main website at https://LibreTexts.org.

This text was compiled on 06/12/2026

TABLE OF CONTENTS

Licensing

1: Lipids

- 1.1: Charged Lipids
- 1.2: Lipid Headgroup Types
- 1.3: Lipid Tails and Saturation
- 1.4: Glycolipids
- 1.5: Sphingolipids
- 1.6: Sterols and Sterol Induced Phases
- 1.7: Lipids in Non-Aqueous Environments

2: Membranes - Aggregated Lipids

- 2.1: Membrane Fluctuations
- 2.2: Membrane Asymmetry
- 2.3: Membrane Curvature
- 2.4: Membrane Compressibility
- 2.5: Surface Tension and Line Tension
- 2.6: Vesicles
- 2.7: Diffusion in Membranes

3: Membrane Phases and Morphologies

- 3.1: Membrane Phase Transitions
- 3.2: The Main Phase Transition
- 3.3: The Fluid Phase
- 3.4: The Gel Phase
- 3.5: The Ripple Phase
- 3.6: Rafts
- 3.7: Lipid Phase Coexistence

4: Membrane-Protein Interactions

- 4.1: Membrane Permeability
- 4.2: Insertion of Membrane Proteins into Lipid Membranes
- 4.3: Protein-lipid Interactions
- 4.4: Physical Lipid Protein Interactions
- 4.5: Nanoparticle Spontaneous Penetration and Assembly in and Through Membranes
- 4.6: Non-Membrane Lipid Assemblies (Micelles)

5: Experimental Characterization - Spectroscopy and Microscopy

- 5.1: Model Membranes vs. Biological Membranes
- 5.2: Supported and Tethered Membranes
- 5.3: Styrene Maleic Acid Lipid Particles (SMALP) Technology
- 5.4: Lipid Probes
- 5.5: Fluorescence on Membranes
- 5.6: Near-field Scanning Optical Microscopy (NSOM)
- 5.7: Single Molecule Tracking
- 5.8: FTIR on Membranes

- 5.9: Raman Spectroscopy on Membranes
- 5.10: Nuclear Magnetic Resonance (NMR) Theory and Solution NMR
- 5.11: Solid-state NMR
- 5.12: Electron Paramagnetic Resonance (EPR) of Membranes
- 5.13: Membrane X-ray Scattering

6: Experimental Characterization - Mass Spectrometry and Atomic Force Microscopy

- 6.1: Atomic force microscopy (AFM) on Membranes
- 6.2: Mass Spectrometer Ionization Techniques for Membrane Proteins
- 6.3: Electrospray Ionization (ESI) Mass Spectrometry
- 6.4: Mass Analyzer Orbitrap
- 6.5: Mass Analyzer - Time of Flight

7: Computational Characterization of Membranes

- 7.1: Mathematical Continuum Descriptions of Membranes
- 7.2: Monte Carlo for Biomembranes
- 7.3: Molecular Dynamics for Biomembranes
- 7.4: Designing Molecular Membranes Models with VMD
- 7.5: Coarse Grain Simulations of Membranes

Index

Glossary

Detailed Licensing

Licensing

*A detailed breakdown of this resource's licensing can be found in **Back Matter/Detailed Licensing**.*

CHAPTER OVERVIEW

1: Lipids

Lipid is a loosely defined term for substances of biological origin that are soluble in nonpolar solvents. It comprises a group of naturally occurring molecules that include fats, waxes, sterols, fat-soluble vitamins (such as vitamins A, D, E, and K), monoglycerides, diglycerides, triglycerides, phospholipids, and others. The main biological functions of lipids include storing energy, signaling, and acting as structural components of cell membranes. Lipids have applications in the cosmetic and food industries as well as in nanotechnology. Lipids may be broadly defined as *hydrophobic* or *amphiphilic* small molecules; the amphiphilic nature of some lipids allows them to form structures such as vesicles, multilamellar/unilamellar liposomes, or membranes in an aqueous environment.

1.1: Charged Lipids
1.2: Lipid Headgroup Types
1.3: Lipid Tails and Saturation
1.4: Glycolipids
1.5: Sphingolipids
1.6: Sterols and Sterol Induced Phases
1.7: Lipids in Non-Aqueous Environments

1: Lipids is shared under a CC BY 4.0 license and was authored, remixed, and/or curated by LibreTexts.

1.1: Charged Lipids

Lipids comprise a diverse group of compounds that include fats, waxes, sterols, phospholipids and many others. The functions associated with lipids are just as diverse, and include membrane structure, signaling, and energy storage. While most lipids are composed of non-polar hydrocarbon structures, other lipids can contain positively and/or negatively charged elements, the nature of which imparts particular physical properties that give charged lipids structural and functional versatility. This page will describe the structure and function of some of the charged lipids commonly encountered in biology.

Types of charged lipids

Fatty acids

The simplest of the charged lipids, fatty acids are a large group of amphipathic molecules consisting of short, medium or long-chain hydrocarbon "tails" (C4 to C36) and a polar carboxylic acid "head". The aliphatic chains can be fully saturated or unsaturated to some extent, and provide the hydrophobic character of the fatty acid. Regardless of the length of the aliphatic tail group the hydrophilic carboxylic acid group will have a pKa around 4.0, which means that under physiological conditions, the majority of fatty acids will have a negative charge of -1. The tails can also contain carbon ring structures, hydroxyl groups, and additional methyl group branches (Figure 1.1.1).

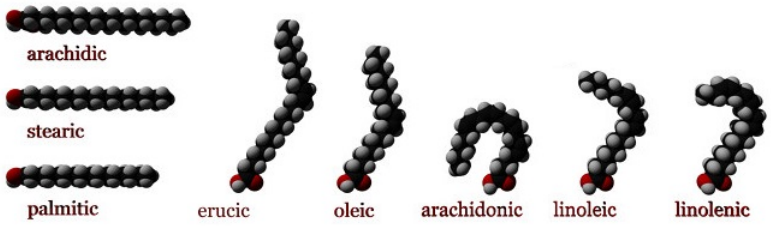


Figure 1.1.1: An example of fatty acids with differing chain length, saturation, and linearity. (CC BY-SA 3.0; Lojban via Wikipedia).

The physical properties of fatty acids are largely dependent on the length and degree of unsaturation of the hydrocarbon tail group. The major factor influencing properties such as melting point and water solubility is the ordering of water molecules around the hydrophobic tails. Fatty acids will cluster together as result of the hydrophobic effect. The clustering of the aliphatic tail groups forms a crystalline lattice, minimizing the exposed hydrophobic surface area and the formation of a hydration shells around individual fatty acid tails. With increasing degrees of unsaturation in the tails (increased number of double bonds), the effect is reversed. Unsaturation introduces kinks into the tails so that they no longer pack as uniformly and tightly, which allows water molecules to become ordered around the individual tails. As such, the crystalline lattice is weakened, increasing the solubility of the fatty acid and decreasing its melting point.

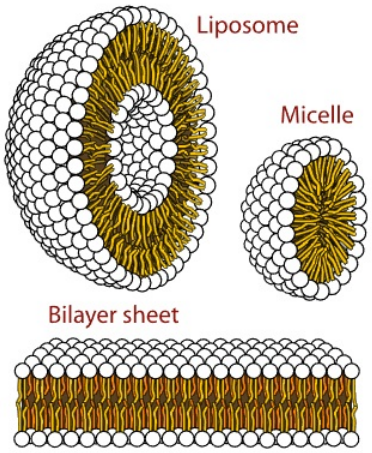


Figure 1.1.2: Image depicting the various structures formed by charged lipids. Image source: Wikipedia

Fatty acids have a variety of important roles. The hydrocarbon tails are a major source of energy when each successive two-carbon unit is converted into acetyl-CoA during beta-oxidation, the process of which generates NADH and $FADH_2$ which are subsequently used in the formation of ATP in oxidative phosphorylation. Fatty acids and their derivatives also function as soaps and detergents.

At high enough concentrations, fatty acids will aggregate to form spherical structures called micelles, which are energetically favorable structures that increase the entropy of water by minimizing water clathrate formation around the hydrophobic regions. They accomplish this by clustering the hydrophobic tails into the center of the sphere, while the hydrophilic heads form a shell that is water soluble. The spherical structure is favored by fatty acids because the cross-sectional area of the head group is larger than that of the tail, forming a conical shape. When soaps (the salts of fatty acids) are mixed with water, the micelles that are formed sequester oils and hydrophobic "dirt" into the micelle center, while the hydrophilic outer shell helps to wash the dirt-carrying micelles away. Lastly, fatty acids form the foundation of di- and triacylglycerols, a family of molecules with two or three fatty acid chains bound by glycerol. When the third hydroxyl group of the glycerol is bound to a charged molecule such as phosphate instead of a hydrocarbon chain, the diacylglycerol is known as a phospholipid.

Phospholipids

As with any molecule, the formation of a charge requires the inclusion of an ionizable element, most often covalently bound to the parent compound. In the case of diacylglycerols, non-ionizable hydrocarbons require the covalent addition of an ionic group to the glycerol to impart a charge. By far the most common of these is the negatively charged phosphate group (PO_4^{3-}) which, when covalently bound to the glycerol moiety of a two-chain fatty acid, forms the main group of charged fatty acids known as phospholipids. Phospholipids are amphipathic molecules composed of three sections: a diglycerol, a hydrophilic "head" consisting of the charged phosphate moiety, and a small organic molecule covalently bound to the phosphate (Figure 1.1.3).

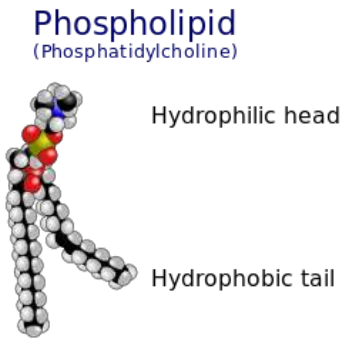


Figure 1.1.3: Structure of a phospholipid, containing the fatty acid tails, glycerol, phosphate moiety, and an additional head-group structure. Image source: Wikipedia

Phospholipids comprise the major components of lipid bilayers in cellular membranes. Similar to fatty acids, phospholipids will favor the clustering of the hydrophobic tails to exclude water as much as possible. Unlike fatty acids, however, the presence of two tails favors the formation of a more planar membrane because the cross-sectional area of the head and tail groups is similar, forming a cylindrical shape which is most efficiently packed as a bilayer. In the bilayer, the hydrophobic tails interact with one another, whereas the hydrophilic head groups interact with the aqueous environment on either side of the bilayer. While the bilayer is most practical as a two dimensional planar structure, it can fold in on itself to form a closed, vesicle called a **liposome**. Unlike the micelle, the liposome has a bilayer wall enclosing a hollow, aqueous cavity, and is used organisms as a transport mechanism for any number of substances.

The structural complexity of the membrane bilayer goes beyond a single type of phospholipid molecule. There exist a variety of phospholipids with varying head groups and hydrocarbon tails. Additionally, membrane lipids are not symmetrically distributed throughout the membrane bilayer, whereby certain phospholipids are more likely to be found in the inner monolayer with the others more likely to be found in the outer leaflet. On the other hand, the physical properties of the different head groups dictate the interactions of each phospholipid with the aqueous environment, and resulting in the movement of the lipids across the bilayer in both the vertical and horizontal directions, continuously changing its shape and phospholipid organization. To give a better idea of the different phospholipid head groups, the following sections will describe the structural features some of the more common ones.

Types of Phospholipids

Phosphatidic acid

As the sole member of the head group, the phosphate imparts a -2 charge to the lipid molecule and is referred to as phosphatidic acid (PA). The phosphate moiety exhibits several different levels of protonation, depending on the pH. Below a pH of 4.0, it carries

a charge of zero, whereas above pH 12, it is fully deprotonated and with a -2 charge. Thus, it goes to reason that at physiological pH, the phosphate group is only partially protonated, carrying a -1 charge, and imparting a net charge of -1 to the PA molecule.

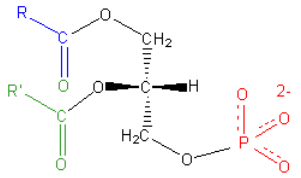


Figure 1.1.4: Chemical structure of phoshatidic acid. Fatty acid groups (blue and green), glycerol moiety (black), phosphate head group (red). Image source: Wikipedia

PA's greatest role is in the biosynthesis of triacylglycerols and other phospholipids, as its structure serves as the backbone these compounds. Although PA is the simplest of all the phospholipids, it occurs only in small amounts in biological membranes. Because of the unique ionization properties of its head-group, which can deprotonate to a -2 charge in the process of forming an intermolecular hydrogen bond, it serves a crucial role in the binding of basic protein and small molecule compounds (**2**). This property not only makes PA an important phospholipid for protein-membrane docking, but also has implications in membrane dynamics and cellular signaling.

Phosphatidylcholine

Phosphatidylcholine (PC) adds an additional positively-charged group, choline, to the phosphate head group of phosphatidic acid. Choline is an N,N,N-trimethylethanolammonium cation and an essential nutrient required for membrane structural integrity, signaling, and neurotransmission. Once choline binds to phosphatidic acid, the phosphate group loses one of its negative charges, making PC an overall neutral molecule: a positive charge on the choline and a negative charge on the phosphate. The nature of the hydrocarbon tails determines the type of phosphatidylcholine molecule, where one tail is usually an unsaturated hydrocarbon such as oleic acid and the other a fully saturated one.

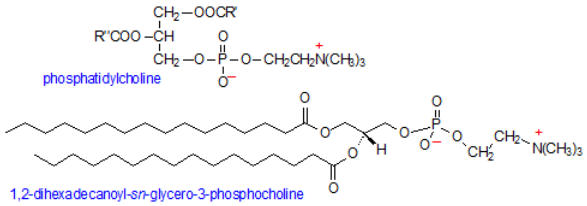


Figure 1.1.5: Chemical structure of phosphatidylcholine. Image source: Wikipedia

PC is one of the more abundant phospholipids in cellular membranes, where it can comprise up to 50% of the total membrane phospholipid composition and is found primarily in the outer leaflet of membranes. PC's other major role is as an integral component of plasma lipoproteins, where it accounts for 60-80 mol% of total phospholipids. (**3**)

Sphingomyelin

Similar to phosphatidylcholine, zwitterionic sphingomyelin contains the phosphocholine head group. Unlike PC and other phospholipids containing glycerol, however, the sphingomyelin backbone is an unsaturated 18-carbon amino-alcohol group called sphingosine. An additional hydrocarbon chain, typically of a different length, is attached to the other sphingosine hydroxyl group.

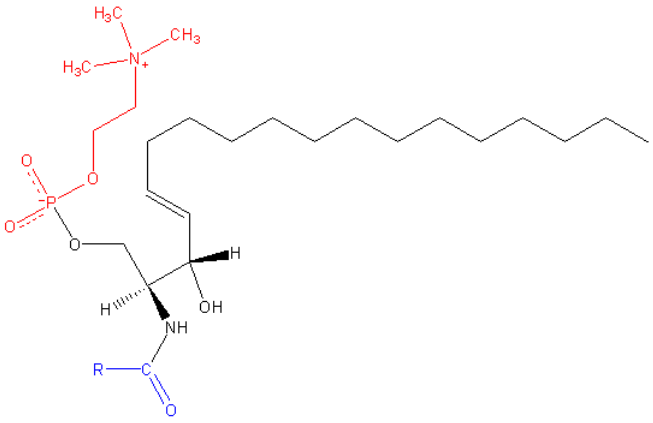


Figure 1.1.6: Chemical structure of sphingolmyelin. Sphingosine (black), fatty acid (blue), phosphocholine head group (red). Image source: Wikipedia

Next to PC, sphingomyelin (SM) is the most abundant charged lipid, and the most abundant sphingolipid, found in the outer leaflet of cellular membranes. SMs are important molecules in membrane fluidity, as they are heavily involved in the formation of lipid rafts and ordered domains on the membrane surface, binding to membrane-spanning proteins, and are involved in cellular signaling and membrane homeostasis. (**4**) SMs come in a variety of long-chain bases depending tissue distribution, with the most common one being sphingosine (pictured above). Others include palmitic acid, a common *N*-linked acyl chain of SM in mammalian peripheral cells, and stearic acid, which is more common to neuronal tissues.

Phosphatidylethanolamine

Phosphatidylethanolamine (PE) is the second most abundant phospholipid and is comprised of the typical phosphatidic acid with an additional head group component, namely ethanolamine. Ethanolamine is both a primary amine and alcohol, and attaches to the PA head group via the hydroxyl. Because the amino group has a pKa of about 9.5, it is protonated under physiological pH, making PE a zwitterionic and neutral molecule.

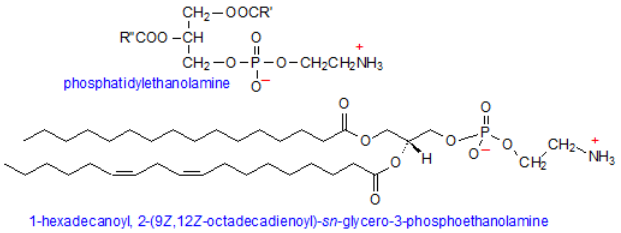
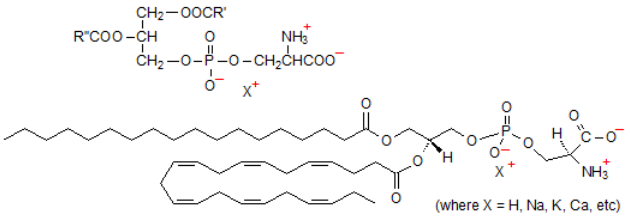


Figure 1.1.7: Chemical structure of phosphatidylethanolamine. Upper image is a basic skeletal structure with R-groups representing hydrocarbon tails. The lower image is an example of two different tail types. Image source: Lipid Library

While PE is just as (if not more) abundant in lipid membranes as PC and SMs, it prefers to occupy the inner leaflet of the membrane, facing the cytoplasm. Because of its smaller head group, the molecule takes on a conical shape which can exert lateral pressure on the membrane, thus modulating its curvature and stabilizing membrane proteins. (**5**) Additionally, the positive charge on the head group is able to bind to a variety of signaling proteins and balance local negative charge on the membrane.

Phosphatidylserine

Phosphatidylserine (PS) is composed of phosphatidic acid (PA), with the negatively charged phosphate group attached to the amino acid serine at the hydroxyl end. Because of the carboxyl and amino groups on serine, in addition to the negatively charged phosphate group, it is possible for PS to have net charge of -1. This is because the carboxyl and amino groups of serine have pKas of 2.21 and 9.15, respectively, so that the carboxyl group will be have a -1 charge at physiological pH; the reverse will be true for the amino group.



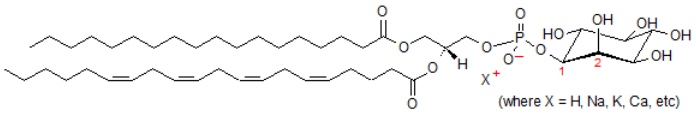
1-octadecanoyl, 2-(4*Z*,7*Z*,10*Z*,13*Z*,16*Z*,19*Z*-docosahexaenoyl)-*sn*-glycero-3-phosphoserine

Figure 1.1.8: Chemical structure of phosphatidylserine. Upper image is a basic skeletal structure with R-groups representing hydrocarbon tails. The lower image is an example of two different tail types. Image source: Lipid Library

Phosphatidylserine comprises only about 10% of total cell membrane phospholipids and is found almost exclusively in the inner monolayer, most prominently in myelin of brain tissue. One of the most prominent functions of PS is in blood coagulation, whereby its transport to the outer membrane layer in activated platelets is thought to either enhance the rate of prothrombin formation, or to allosterically alter the proteolytic and cofactor capabilities of prothrombin factors X_a and V_a in thrombin activation. (**6**) In a completely different role, exposure of PS to the extracellular side of a membrane is often a cellular marker for apoptosis, or programmed cell death. (**7**)

Phosphatidylinositol

Phosphatidylinositol (PI) is a unique phospholipid in that the head group is a cyclohexane carbohydrate called inositol, which is attached to the phosphate moiety at the 1’ carbon. Unique to inositol is the ability to become phosphorylated at the 3’, 4’, and 5’ carbons by a host of PI-kinases, which can add up to three phosphate groups at those positions, per molecule. This phenomenon can impart up to a -4 charge on the PI molecule. Although comprising only about 5% of total lipid content in membranes, phosphoinositols (PIs) are concentrated on the inside leaflet of the lipid bilayer where they play crucial roles in cellular signaling, protein binding, and membrane dynamics. (**8**)



1-octadecanoyl, 2-(5*Z*,8*Z*,11*Z*,14*Z*-eicosatetraenoyl)-*sn*-glycero-3-phospho-(1’-*myo*-inositol)

Figure 1.1.9: Chemical structure of phosphotidylinositol, showing the inositol sugar moiety attached at the 1' carbon to phosphatidic acid. Image source: Lipid Library

References

1. David L. Nelson & Michael M. Cox, "Principles of Biochemistry, fourth edition." W. H. Freeman and Company, New York. 2005
2. Edgar Eduard Kooijman & Koert N. J. Burger (2009). "Biophysics and function of phosphatidic acid: A molecular perspective". *Biochimica et Biophysica Acta* **1791** (9): 881-888.
3. Cole, L.K., Vance, J.E., Vace, D.E. (2012). "Phosphatidylcholine biosynthesis and lipoprotein metabolism". *Biochimica et Biophysica Acta (BBA) - Molecular and Cell Biology of Lipids* **1821** (5): 754-761.
4. Petter J. Slotte (2013). "Molecular properties of various structurally defined sphingomyelins – correlation of structure with function". *Progress in Lipid Research* **52** (2): 206-219.
5. Suetsugu, S., Kurisu, S., Takenawa, T. (2014). "Dynamic Shaping of Cellular Membranes by Phospholipids and Membrane-Deforming Proteins". *Physiological Reviews* **94** (4): 1219-1248.
6. Barry R. Lentz (2003). "Exposure of platelet membrane phosphatidylserine regulates blood coagulation". *Progress in Lipid Research* **42** (5): 423-428.
7. Peter A. Leventis & Sergio Grinstein (2010). "The Distribution and Function of Phosphatidylserine in Cellular Membranes". *Annual Reviews of Biophysics* **39**: 407-27
8. Gilbert Di Paolo & Pietro De Camilli (2006). "Phosphoinositides in cell regulation and membrane dynamics". *Nature* **443**: 651-657.

1.1: Charged Lipids is shared under a CC BY 4.0 license and was authored, remixed, and/or curated by LibreTexts.

1.2: Lipid Headgroup Types

Lipid headgroups comprise part of the hydrophilic backbone of membrane phospholipids. There are a number of headgroups, each of which correlates with a particular type of backbone. Membrane lipids are split into three categories: phospholipids and glycolipids (Figure 1.2.1). Sterols are the third type of membrane lipid (not pictured) that will be discussed.

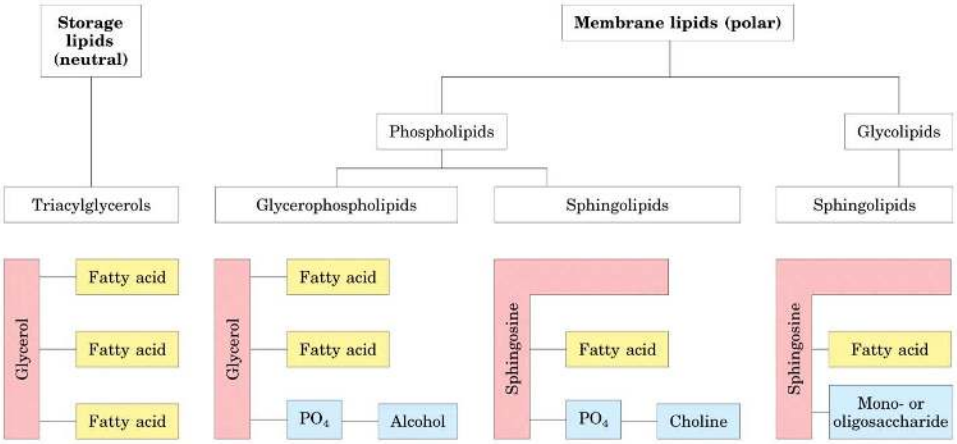


Figure 1.2.1: Membrane lipids are polar and can be separated into phospholipids and glycolipids, for which the basic structures are shown. Note the difference in the third binding site. Phospholipids have a phosphate bound to an alcohol (glycerol-) or choline (sphingo-), while glycolipids have a sugar group. Source: Lafer, Eileen. "Membrane Lipids I and II: Glycerophospholipids and Sphingolipids." Lecture. San Antonio, Texas. December 6, 2011

Lipid headgroups are substituents that attach to the glycerol, sphingosine, or cholesterol backbones of polar membrane lipids. Phospho- and glycolipids have headgroups linked to the backbone through a phosphodiester bond (Figure 1.2.2).

Understanding head group behavior is necessary for the study of membrane biology. The high structural diversity allows for a large range of functions, including effects on membrane curvature [1] cell signaling, substrate transport [2], and more. Consequently, their crucial role in membrane biology also ties them in with a broad range of diseases, from cardiovascular defects to cancer.

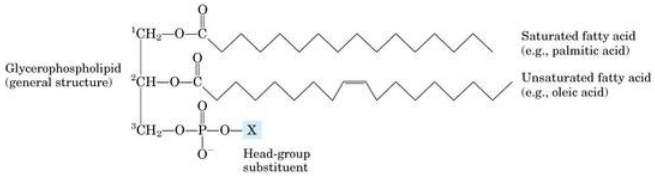


Figure 1.2.2: headgroups are the substituent bound to the phosphate group of a hydrophilic lipid backbone. Source: Lafer, Eileen. "Membrane Lipids I and II: Glycerophospholipids and Sphingolipids." Lecture. San Antonio, Texas. December 6, 2011

II. PHOSPHOLIPIDS

A. GLYCEROPHOSPHOLIPIDS

Glycerophospholipids are classified by the alcohol that is bound to the phosphate group on the glycerol backbone. The backbone always consists of a glycerol esterified to fatty acids in positions *Csn*-1 and *Csn*-2, with the head group substituent bound to the phosphate in position *Csn*-3 [2]. Interestingly, archaebacteria have the headgroup at the *Csn*-1 position [3]. The headgroup classes are differentiated by the *Csn*-1 and *Csn*-2 substituents. If the *Csn*-1 and *Csn*-3 substituents are unique, the *Csn*-2 carbon becomes a chiral center [4].

Phosphatidic acid has the simplest substituent: hydrogen. This parent compound, phosphomonoester, is then built upon by naming the derivatives for the head-group alcohol (X, Figure 1.2.2) with "phosphatidyl-" as a prefix. For example, phosphatidyl-choline, phosphatidyl-ethanolamine, and phosphatidyl-serine are other common membrane lipids [4].

Some of the common glycerophospholipid head groups are shown in Table 1:

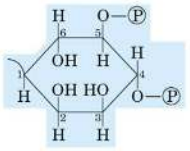
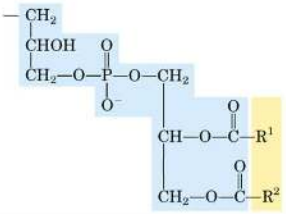
Name of glycerophospholipid	Name of X	Formula of X	Net charge (at pH 7)
Phosphatidic acid	—	— H	−1
Phosphatidylethanolamine	Ethanolamine	— CH_2—CH_2—$\overset{+}{N}H_3$	0
Phosphatidylcholine	Choline	— CH_2—CH_2—$\overset{+}{N}(CH_3)_3$	0
Phosphatidylserine	Serine	— CH_2—$CH(COO^-)$—$\overset{+}{N}H_3$	−1
Phosphatidylglycerol	Glycerol	— CH_2—$CH(OH)$—CH_2—OH	−1
Phosphatidylinositol 4,5-bisphosphate	*myo*-Inositol 4,5-bisphosphate		−4
Cardiolipin	Phosphatidyl-glycerol		−2

Table 1: common head groups found in glycerophospholipids and their basic characteristics. Source: Lafer, Eileen. “Membrane Lipids I and II: Glycerophospholipids and Sphingolipids.” Lecture. San Antonio, Texas. December 6, 2011

Phosphatidylinositol (PI) is interesting in that it can be phosphorylated to make PI phosphate (PIP), PI bisphosphate (PIP_2), and PI trisphosphate (PIP_3). These compounds are found on the cytoplasmic leaflet of membranes and therefore heavily influence the membrane-cytosol interface. This makes them particularly relevant to membrane trafficking, regulating cell growth, proliferation, and apoptosis [2].

B. SPHINGOLIPIDS

Sphingolipids have a base made of a long (carbon) chain called sphingosine, which is bound with fatty acids using amide linkages to make ceramides (Figure 1.2.3). The sphingoid base backbone is synthesized from a long-chain fatty acyl-CoA and serine. Ceramide is the most basic sphingolipid, with only a hydrogen in the *Csp*-3 position and an amide-linked fatty acid [4] (Table 2). More complex (phosphor)sphingolipids have headgroups attached via phosphodiester linkages [4]. The Sphingosine backbone, fatty acid, and headgroup of a sphingolipid are also highlighted in Table 2.

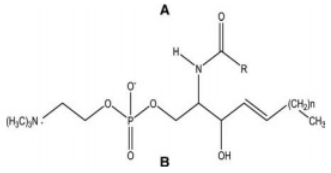


Figure 1.2.3: Structure of sphingolipids in which R represents a fatty acid. Source: Montealegre, C., et al., Analysis of glycerophospho- and sphingolipids by CE. Electrophoresis, 2014. 35(6): p. 779-92.

Some common sphingolipids headgroups are depicted in Table 2:

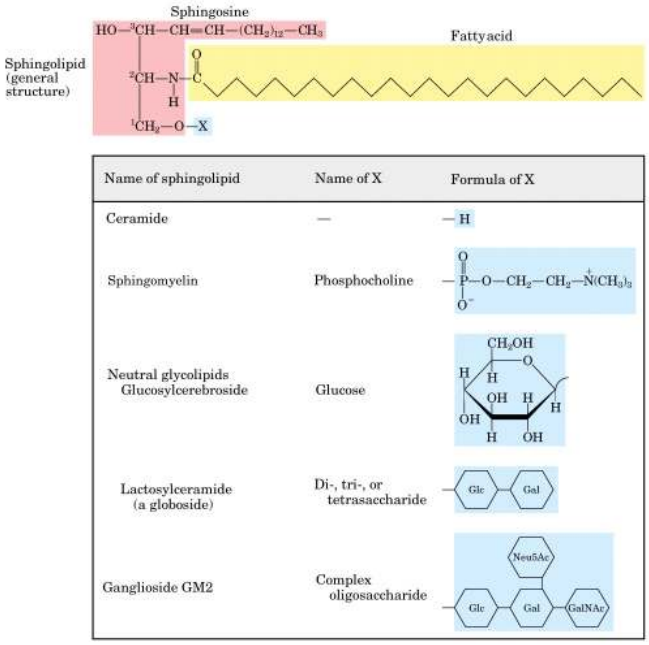


Table 2: Sphingolipid structure and common head groups. Source: Lafer, Eileen. “Membrane Lipids I and II: Glycerophospholipids and Sphingolipids.” Lecture. San Antonio, Texas. December 6, 2011

Sphingomyelin is a common sphingolipid that is prominent in the myelin sheaths of neurons. The head groups have a large effect on overall lipid structure, which is why phosphatidyl choline (gylerophospholipid) and sphingomyelin (sphingolipid) look so similar (Figure \(\PageIndex{4}\)).

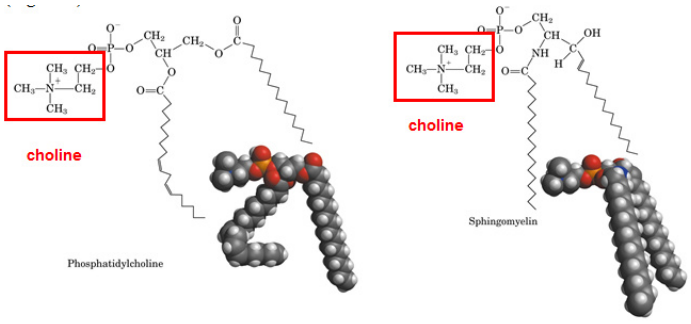


Figure 1.2.4: Both phosphatidylcholine and sphingomyelin have a choline head group attached to a phosphate group. Despite the different backbone molecule, the two molecules are remarkably similar in shape. Source: Lafer, Eileen. “Membrane Lipids I and II: Glycerophospholipids and Sphingolipids.” Lecture. San Antonio, Texas. December 6, 2011

III. GLYCOLIPIDS

Glycolipids contain a sub-group of sphingolipids that have a similar backbone structure to phosphosphingolipids (Figure 1.2.3), but have a mono- or oligosaccharide bound to the *Csn*-3 position instead of a phosphate-choline group (Table 2). Glycosphingolipids

are especially relevant to neuronal membranes, where D-glucose is added to the hydroxyl group of ceramide to create GlcCer. If the headgroup has any (one to four) silica acid(s) attached to it, the new molecule is referred to as a ganglioside [2].

Interestingly, the carbohydrate head group portions of sphingolipids are what define the human blood groups. The oligosaccharide head groups are composed of D-glucose (Glc), D-galactose (Gal), N-acetyl-D-galactosamine (GalNAc), and fucose (Fuc). The addition of an extra GalNAc creates the A antigen/blood type, and the addition of a Gal creates the B antigen/blood type (Figure 1.2.5).

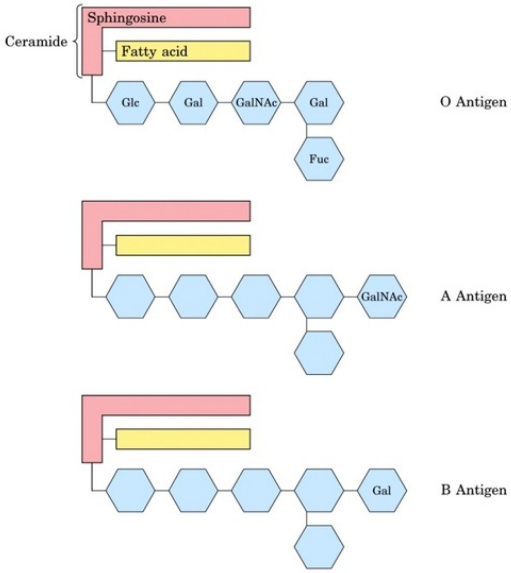


Figure 1.2.5: Blood group types in humans are determined by the glycolipid headgroup; source: Lafer, Eileen. “Membrane Lipids I and II: Glycerophospholipids and Sphingolipids.” Lecture. San Antonio, Texas. December 6, 2011

STEROLS

Sterols in mammals stem primarily from cholesterol (Figure 1.2.6) and its derivatives. Sterols are subdivided primarily based on biological function; steroids, a set of important hormones and signaling molecules [5] can also be subdivided by the number of carbons in the core skeleton. Estrogens fall into the C_{18} family, while androgens make up the C_{19} family [4]. A broad representation of sterols can be seen below (Figure 1.2.6).

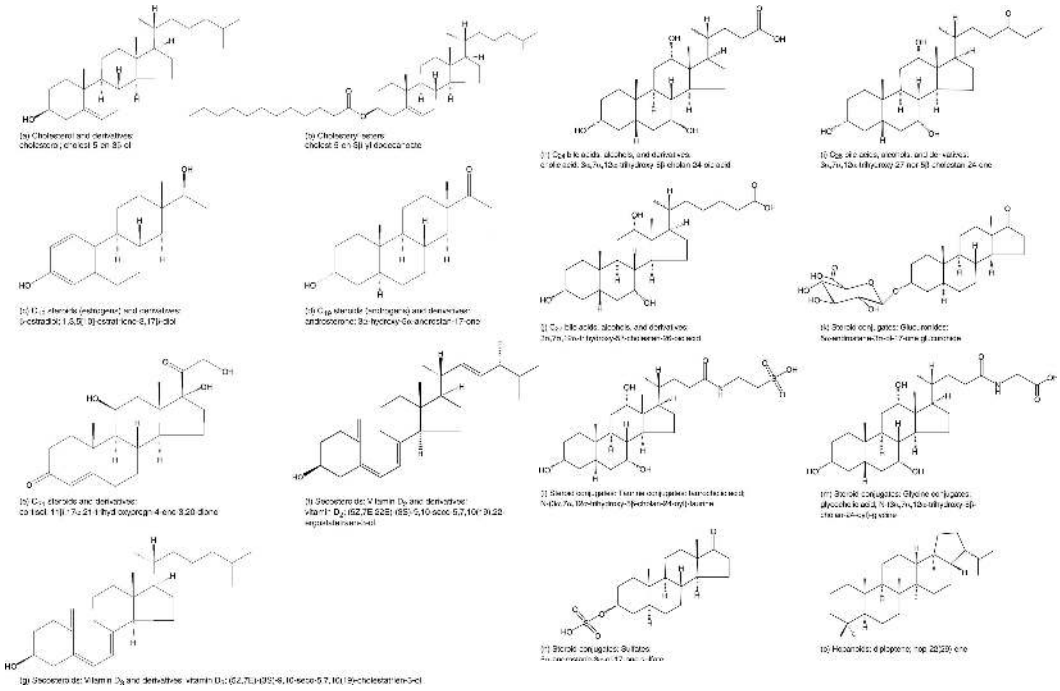


Figure 1.2.6: Representative structures for sterol lipids; source: Fahy E et al. J. Lipid Res. 2005;46:839-862, ©2005 by American Society for Biochemistry and Molecular Biology

CHARGED HEADGROUPS

Many lipids (both glycerophospholipids and sphingolipids) have charged headgroups. This charge is incredibly important in determining headgroup behavior, as it affects repulsion with other molecules and other membrane characteristics. For example, phospholipid headgroups interact with other membrane proteins like the P-glycoprotein multidrug transporter, which is linked to cancer resistance [6]. Similarly, charge density and headgroup structure influence membrane rigidity [7], create variation in protein-lipid interactions and liposome membrane mobility [8], and determine the ability of lipid-DNA complexes to transfect DNA *in vitro* [9].

There are many negatively charged headgroups, whereas positive charges are much less common. Phosphatidic acid is a dynamic headgroup that is uncharged below pH 4, but has a -1 charge at physiological (human) pH and a -2 charge above pH 14. Similarly, phosphatidylserine has a -1 charge and phosphatidylcholine is zwitterionic (Figure 1.2.7).

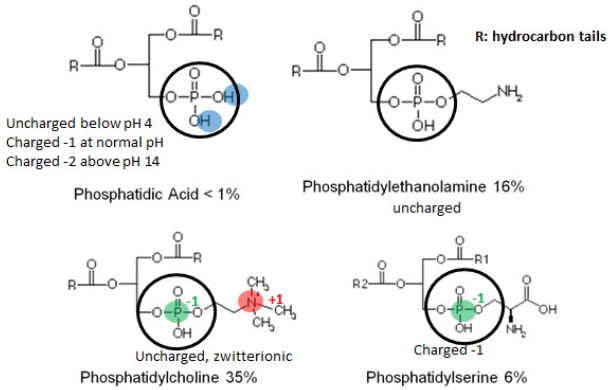


Figure 1.2.7: Headgroups found in cell membranes with various charges. Percentages represent relative abundance in human red blood cell membranes. Source: Faller, Roland. “Introduction to Membrane and Lipid Fundamentals.” Lecture. Davis, CA. April 3, 2014

The presence and concentration of charge has direct effects on headgroup orientation. If the electric surface charge of a membrane is positive, the N+ component of the P—N dipole (see phosphatidylcholine, Figure 1.2.7) moves toward the water phase, which

causes a large (>30˚) change in orientation of the phosphate segment. A negative surface charge has the opposite effect, moving the N+ end of the dipole toward the interior area of the membrane [10]. The orientation of lipids, and therefore the movement of headgroups, is important for lipid-protein binding and membrane topology. Finally, headgroup charge is notably related to membrane curvature. Studies have shown that the negatively charged headgroups phosphatidic acid and phosphatidylserine favor negative membrane curvature when excess ion are present (due to charge repulsion) and nearly flat surfaces in pure water. However, it is important to consider salt and pH conditions, as these may have an effect on the data [1, 11, 12].

CONCLUSION

In summary, there are three major membrane lipid groups: sterols, glycolipids, and phospholipids. These groups are determined based on the molecular backbone of the lipid. A variety of headgroups can then attach and alter structure and function. Many of these membrane lipids are directly associated with cellular processes, and therefore present health risks if perturbed. One case study showed that higher levels of plasma sphingolipids increases risk or occurence of lung cancer [13]. Headgroups also largely affect biological functions due to their ability to be charged, and often to change charge at different various pH values.

References

1. Sodt, A.J. and R.W. Pastor, *Molecular modeling of lipid membrane curvature induction by a Peptide: more than simply shape.* Biophys J, 2014. **106**(9): p. 1958-69.
2. Montealegre, C., et al., *Analysis of glycerophospho- and sphingolipids by CE.* Electrophoresis, 2014. **35**(6): p. 779-92.
3. Pereto, J., P. Lopez-Garcia, and D. Moreira, *Ancestral lipid biosynthesis and early membrane evolution.* Trends Biochem Sci, 2004. **29**(9): p. 469-77.
4. Fahy, E., et al., *A comprehensive classification system for lipids.* J Lipid Res, 2005. **46**(5): p. 839-61.
5. Tsai, M.J. and B.W. O'Malley, *Molecular mechanisms of action of steroid/thyroid receptor superfamily members.* Annu Rev Biochem, 1994. **63**: p. 451-86.
6. Sharom, F.J., *Complex Interplay between the P-Glycoprotein Multidrug Efflux Pump and the Membrane: Its Role in Modulating Protein Function.* Front Oncol, 2014. **4**: p. 41.
7. Bruning, B., et al., *Influence of charge density on bilayer bending rigidity in lipid vesicles: a combined dynamic light scattering and neutron spin-echo study.* Eur Phys J E Soft Matter, 2013. **36**(7): p. 77.
8. Shimanouchi, T., et al., *Relationship between the mobility of phosphocholine headgroup and the protein-liposome interaction: A dielectric spectroscopic study.* Colloids Surf B Biointerfaces, 2014. **116**: p. 343-50.
9. Zhang, X.X., et al., *Lipid-mediated DNA and siRNA Transfection Efficiency Depends on Peptide Headgroup.* Soft Matter, 2013. **9**(17).
10. Scherer, P.G. and J. Seelig, *Electric charge effects on phospholipid headgroups. Phosphatidylcholine in mixtures with cationic and anionic amphiphiles.* Biochemistry, 1989. **28**(19): p. 7720-8.
11. Fuller, N., C.R. Benatti, and R.P. Rand, *Curvature and bending constants for phosphatidylserine-containing membranes.* Biophys J, 2003. **85**(3): p. 1667-74.
12. Kooijman, E.E., et al., *Spontaneous curvature of phosphatidic acid and lysophosphatidic acid.* Biochemistry, 2005. **44**(6): p. 2097-102.
13. Alberg, A.J. et al., *Plasma sphingolipids and lung cancer: a population-based, nested case-control study.* *Cancer Epidemiol Biomarkers Prev.* 2013. 22(8): p. 1374-82.

1.2: Lipid Headgroup Types is shared under a CC BY 4.0 license and was authored, remixed, and/or curated by LibreTexts.

1.3: Lipid Tails and Saturation

Lipids are molecules that are composed of a hydrophilic head group and a hydrophobic tail. Lipid bilayers form to remove the hydrophobic tails from the aqueous phase. The lipid tails face the interior of a biological membrane (Figure 1.3.1). Phospholipids, glycerolipids, and sphingolipids contain one or more (usually two) fatty acid chains as hydrophobic tails. A portion of the sphingoid base also makes up part of the hydrophobic tail of a sphingolipid. The hydrophobic tail dominates the size of the structure of sterols, excluding the hydroxl group. The shape and size of the lipid tail contribute significantly to the physical properties of the membrane.

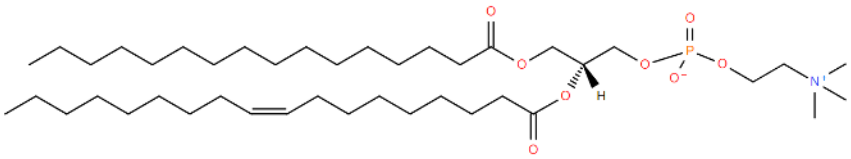


Figure 1.3.1: Structure of the Palmitoyloleoylphosphatidylcholine Esterfied Fatty Acid (1-hexadecanoyl-2-(9Z-octadecenoyl)-sn-glycero-3-phosphocholine). Image used from LipidsMaps.org

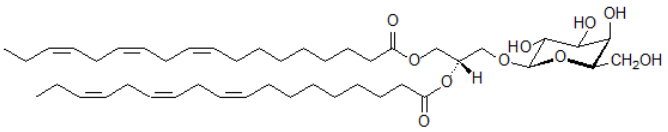
Fatty acids

The majority of membrane lipid tails are made up of esterified fatty acids. This means that the carboxylic acid group forms a bond with the glycerol backbone resulting in an ester group. The hydrophobic tails consists of fatty acids. Fatty acids vary in both chain length and degree of saturation. The chain length is the number of carbons in the fatty acid. The fatty acids can be completely saturated, meaning the carbons are all connected by single bonds, or unsaturated, meaning the chain contains one or more double bonds. A given fatty acid can be named in three ways based off of their chain length and degree of saturation. First, many have common, or trivial names. For example, a 16 carbon fully saturated fatty acid is palmitic acid. An 18 carbon fatty acid with one cis double bond at the 9th position is oleic acid. Another naming system is the shorthand structural. This consists of 2 numbers separated by a colon. The first number is the number of carbons in the chain while the second is the number of double bonds. Additional numbers are added after a delta (Δ) symbol to indicate the positions of the double bonds. Since most biologically occurring unsaturated fatty acid have cis double bonds, there is nothing added after the number to signify cis. However, if the double bond is trans, the number will be followed by a “t”. Palmitic acid and oleic acid are thus 16:0 and $18{:}1^{\Delta 9}$ respectively (Sitwell 2013). Lastly, there is the system of nomenclature supported by IUPAC and IUBMB. In this system, the fatty acid takes its carboxylic acid name. A 16 carbon saturated fatty acid is hexadecanoic acid. An 18 carbon mono-unsaturated at the 9th position fatty acid is 9Z-octadecenoic acid. The “9Z” at the beginning specifies the location of the double bond and that it is cis. When naming a phospholipid or glycerolipid containing fatty acid tails, the name of the tails precede the name of the headgroup. Since the fatty acids are esterified, the suffix is changed from -oic to -oyl. The systematic name for a common phospholipid is 1-hexadecanoyl-2-(9Z-octadecenoyl)-*sn*-glycero-3-phosphocholine (Fahy et al 2011). This has hexadecanoic acid at position 1 and 9Z-octadecenoic acid at position 2 of the glycerol backbone (Figure 1.3.2A). Fatty acids can also be given an omega designation which is determined by the position of the double bond carbon nearest to the methyl end. An omega 3 fatty acid is one were the 3rd and 4th carbons from the methyl are connected by a double bond (Uttaro 2008).

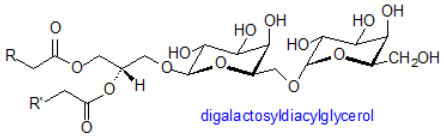
Glycerophospholipids

The most common type of membrane lipids are glycerophospholipids or glycerolipids. Phosphoglycerides are prominent in higher animals (such as vertebrates) while glycosylglycerides are important in plants. There are three chief classes of membrane lipid which are widely distributed- glycerolipids, sphingolipids, and steroids. Glycerolipids, related to their abundance, are the most important group. They can be divided into two main groups – phosphoglycerides (containing phosphorus) and glycosylglycerides (without phosphorus but containing a sugar constituent) Phosphoglycerides are the major lipid components of most biological membranes. Phosphoglycerides consist of a diverse and vast array of structures. They are the primary lipid components in most membranes, excluding photosynthetic membranes of plants, algae, and cyanobacteria as well as archaebacterial membranes. Typically, phosphoglycerides contain fatty acids esterified at positions 1 and 2 of glycerol making them diacylphosphoglycerides. The names of these lipids come from the component which is attached to the phosphate esterified at position 3 of glycerol. Therefore, the compounds are essentially derivatives of diacylglycerols in which the hydroxyl on the carbon 3 atom is esterified with phosphoric acid. Moreover, the simplest phosphoglyceride contains only phosphoric acid attached to diacylglycerol which is called phosphatidic acid. (Gurr, 2005)

Glucosylglycerides are predominant components of photosynthetic membranes and play major role in some micro-organisms. Their structure is comparable to that of glycerophospholipids with the sugars attached glycosidically to position 3 of glycerol and fatty acids esterified at the other two positions. Roughly 40% of the dry weight of photosynthetic membranes of higher plants consists of two galactose-containing lipids – monogalactosyldiacylglcerol and digalactosyldiacylglycerol. There is a β-link in the first position of the galactose ring to glycerol while in digalactosyldiacylglycerol there is an α, 1,6-bond between sugars. Many combinations of residues in diglycosyldiacylglycerols can be found in bacteria-most abundantly are two glucose, two galactose, or two mannose residues linked α,1-2 or β,1-6.



1,2-di-(9*Z*,12*Z*,15*Z*)-octadecatrienoyl-3-*O*-β-*D*-galactosyl-*sn*-glycerol



digalactosyldiacylglycerol

Aside from galactose-containing lipids, a third glycosylglyceride, plant sulpholipid, is found in chloroplasts. It is more formally referred to as sulphoquinovosyliacylglycerol and it contains a sulphonate constituent on carbon 6 of a deoxyglucose residue. This is a naturally occurring negatively charged molecule with a very stable sulphonic acid group. This sulpholipid is highly characteristic of the photosynthetic membranes of chloroplasts and cyanobacteria. All of the chloroplast glycolipids usually consists of great amounts of α-linolenic acid. Moreover, monogalactosyldiacylglycerol may have up to 97%of its total acyl groups as this one component in some plants. (Gurr,2005)

Sterols

Since the hydrophobic tail of a sterol is essentially a steroid, it is named accordingly. The suffix -ol is added to designate that it is a sterol (Figure 1.3.2B).

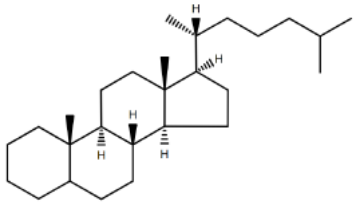
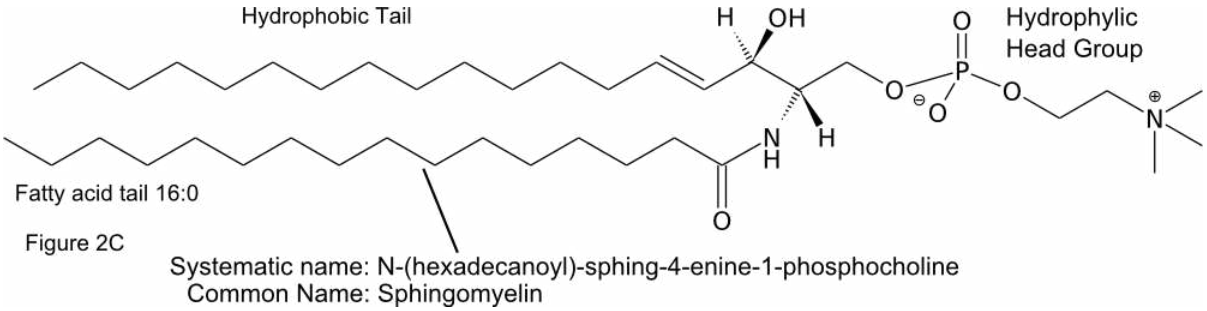


Figure 1.3.2B: Cholesterol

Many sterols are significant units of many organisms especially their external cellular membranes. However, sterols are not necessary or crucial components by all organisms even organisms with significant sterol content. Sterols are widespread in eurkaryotes, but are rare in prokaryotes. Yeast and fungi have side chain alkylated compounds while plants and algae contain sitosterol and stigmasterol as their most com common sterols. The primary function for membrane sterol is the modulation of fluidity which is resolved by the interaction of sterol with the glycerolipid components.

Sphingolipids

The hydrophobic tails of sphingolipids are made up of a fatty acid and a long carbon chain on the sphingoid base. The name of the lipid is thus a combination of the name of the sphingoid base and the fatty acid (Figure 1.3.2C) (Fahy et al 2011).



Figured out from the use of glucosidase enzymes or by permethylation analysis. (Gurr,2002)

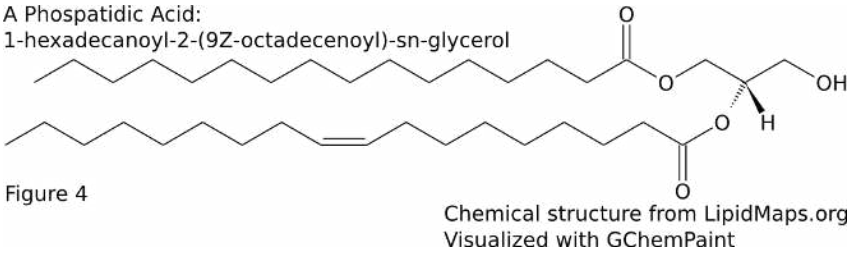
Fatty Acid Biosynthesis

Fatty acid synthesis pathways are placed in two classes, type I and II. The steps in the type II pathway are catalyzed by separate enzymes. In type I, multienzymes contain multiple domains that catalyze several steps in the synthesis pathway. Type II is found in eubacteria and organelles of prokaryotic origin (mitochondria and plastids) while Type I is found in eukaryotes (Schweizer and Hofmann 2004). Although the enzyme organization is different, the basic steps of fatty acid synthesis are conserved across bacteria and eukaryotes and involve the sequential addition of acetyl groups from acetyl-coA to a growing fatty acid chain. To produce saturated fatty acids addition of acetyl groups proceeds to form a chain of usually 16 or 18 carbons (Figure 1.3.3).

$$\begin{aligned} &8\text{Acetyl-coA} + 7\text{ATP} + 14\text{NADPH} \\ &\rightarrow \text{Palmitic Acid} + 7\text{ADP} + 7\text{P}_\text{i} + 14\text{NADP} + 6\text{H}_2\text{O} + 8\text{coA} \end{aligned} \tag{1.3.1}$$

Synthesis of an unsaturated fatty acid in bacteria occurs in a similar manner to saturated fatty acid synthesis up to the 10 carbon intermediate. At this point a double bond is formed between the 3rd and 4th carbons on the chain (numbering from the side of addition). After the cis double bond is added, the addition of acetyl units continues to 16 or 18 carbons, meaning the double bond will be at positions 9 and 11 respectively (Chan and Vogel 2010). In eukaryotes, double bonds are added after fatty acid synthesis. The enzymes that produce mono-unsaturated fatty acids preferentially introduce a double bond between carbons 9 and 10. This means that $16{:}1^{\Delta 9}$ and $18{:}1^{\Delta 9}$ are common on lipid tails. Another set of enzymes adds double bonds near the methyl end of already unsaturated fatty acids. These preferentially produce bonds between the 3rd and 4th carbons and between the 6th and 7th carbons from the methyl end (omega 3 and 6). Mammals do not have the enzymes needed to add double bonds near the methyl end. Additional double bonds are added near the carboxyl end of fatty acids that already contain double bonds added by the other two enzyme classes (Uttaro 2008). Thus, the degree of unsaturation and placement of the double bonds is determined by these enzymes.

Two fatty acid chains are attached to positions 1 and 2 of glycerol-3-phosphate to form phospatidic acid (Figure 1.3.4). This is later converted to several other lipids by addition of diverse head groups . Some bacteria are able to introduce double bonds to the fatty acid chain after the lipid is formed (Zhang and Rock 2008).



Effects on membranes

Membrane fluidity and phase: The fluidity of a biological membrane is related to the melting temperature of the lipid tails within it. The melting temperature is affected by both the chain length and saturation of the tail. Longer chains lead to higher melting temperature because they are able to form stronger van der Waals forces between molecules. Higher degrees of unsaturation lead to lower melting temperature. This is because the double bonds add kinks to the fatty acid chains which prevent tight packing of lipid molecules. In general, the degree of saturation impacts the fluidity of the membrane to a greater extent than chain length (Sitwell 2013). Membranes of single lipid composition exist in two phases. At high temperatures they are in a highly fluid liquid-crystalline phase. At low temperatures they are at a rigid gel phase. In membranes that contain cholesterol, the gel phase is replaced by a liquid-ordered phase that maintains some fluidity (Komura and Andelman 2014). Lipids with saturated tails are prone to the liquid-

ordered phase, while lipids with unsaturated tails are prone to the liquid-crystalline, or liquid-disordered phase. In the liquid-ordered phase, the carbon-carbon bonds maintain trans-rotomers, meaning the tails straighten out as much as possible. The width of the hydrophobic portion of lipids with long saturated tails will be greater than those with shorter or unsaturated tails because double bonds can prevent the tails from straightening out completely and packing closely. The difference in the hydrophobic width can lead to hydrophobic mismatch and phase separation (Komura and Andelman 2014).

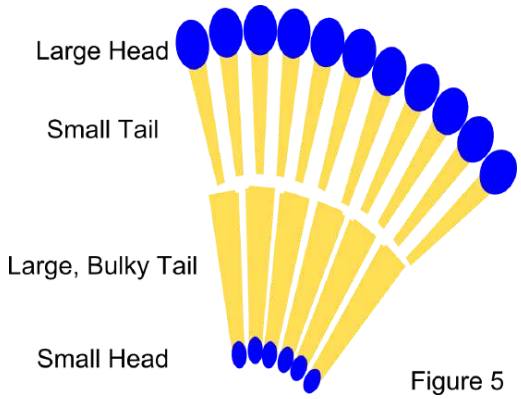


Figure 1.3.5. While there is evidence for this in synthetic membranes, biological membranes largely use proteins to produce membrane curvature (Shibata et al 2009).

Interactions with membrane proteins: The hydrophobic lipid tails are responsible for solublizing the trans-membrane portions of a membrane protein within the membrane which illustrates one of the their many roles. A ring of lipids, referred to as a lipid annulus, surrounds the protein and the relatively flexible tails cover the surface of protein (Lee 2011). Properties of the membrane conferred by the lipid tail, such as the thickness of the hydrophobic phase, compressibility, and intrinsic curvature can significantly impact protein folding and function within the membrane (Andersen et al 2007).

Citations

1. Stillwell, William. *An Introduction to Biological Membranes: From Bilayers to Rafts. Chapter 4 - Membrane Lipids: Fatty Acids.* Amsterdam: Elsevier/Academic, 2013. pg 43-56
2. Fahy E, Cotter D, Sud M, Subramaniam S. Lipid classification, structures and tools. Biochim Biophys Acta. 2011;1811(11):637-47.
3. Uttaro AD. Biosynthesis of polyunsaturated fatty acids in lower eukaryotes. IUBMB Life. 2006;58(10):563-71.
4. Schweizer E, Hofmann J. Microbial type I fatty acid synthases (FAS): major players in a network of cellular FAS systems. Microbiol Mol Biol Rev. 2004;68(3):501-17
5. Chan DI, Vogel HJ. Current understanding of fatty acid biosynthesis and the acyl carrier protein. Biochem J. 2010;430(1):1-19.
6. Zhang YM, Rock CO. Membrane lipid homeostasis in bacteria. Nat Rev Microbiol. 2008;6(3):222-33.
7. Komura S, Andelman D. Physical aspects of heterogeneities in multi-component lipid membranes. Adv Colloid Interface Sci. 2014;208C:34-46.
8. Shibata Y, Hu J, Kozlov MM, Rapoport TA. Mechanisms shaping the membranes of cellular organelles. Annu Rev Cell Dev Biol. 2009;25:329-54.
9. Andersen OS, Koeppe RE. Bilayer thickness and membrane protein function: an energetic perspective. Annu Rev Biophys Biomol Struct. 2007;36:107-30.
10. Sud M, Fahy E, Cotter D, Brown A, Dennis EA, Glass CK, Merrill AH Jr, Murphy RC, Raetz CR, Russell DW, Subramaniam S. LMSD: LIPID MAPS structure database *Nucleic Acids Research* 35: p. D527-32.
11. GChemPaint Chemical Structures Editor. http://savannah.nongnu.org/projects/gchempaint/
12. Gurr, M. I., J. L. Harwood, and K. N. Frayn. *Lipid Biochemistry*. Oxford, UK: Blackwell Science, 2005

Contributors and Attributions

- Philip Day (UC Davis) and William Scott (UC Davis)

1.3: Lipid Tails and Saturation is shared under a CC BY 4.0 license and was authored, remixed, and/or curated by LibreTexts.

1.4: Glycolipids

Glycolipids are components of cellular membranes comprised of a hydrophobic lipid tail and one or more hydrophilic sugar groups linked by a glycosidic bond. Generally, glycolipids are found on the outer leaflet of cellular membranes where it plays not only a structural role to maintain membrane stability but also facilitates cell-cell communication acting as receptors, anchors for proteins and regulators of signal transduction [1]. Glycolipids are found widely distributed throughout all cells and primarily localized, but not exclusively, to the plasma membrane.

Structure and Synthesis

The basic structure of a glycolipid consists of a mono- or oligosaccharide group attached to a sphingolipid or a glycerol group (can be acetylated or alkylated) with one or two fatty acids. These make up the classes of glycosphingolipids and glycoglycerolipids, respectively. Glycolipids interact and bind to the lipid-bilayer through the hydrophobic nature of the lipid tail which anchors it to the surface of the plasma membrane.

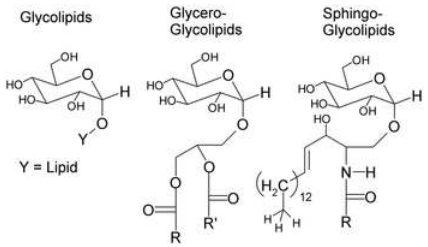


Figure 1.4.1. Structure of glycolipids

Synthesis of glycolipids proceed by a series of enzymes that sequentially add sugars to the lipid. Glycosphingolipids are derived from lactosylceramide (LacCer; β-D-galactosyl(1→4)-β-D-glucosyl-ceramide) where the first step is the acylation and desaturation of D-erythro-sphinganine. Ceramide is glucosylated then β-galactosylated extracellularly to form lactosylceramide. Further elongation can occur via glycosyltransferases and sulfotransferases. For example, the biosynthesis of a major glycoglycerolipid in plants involves the transfer of a galactosyl from UDP-Gal onto diacylglycerol to produce β-galactosyldiacylglycerol via galactosyltransferases. An additional transfer of a galactosyl from UDP-Gal forms α-D-galactosyl-(1,6)-*O*-β-D-galactosyldiacylglycerol [2].

Metabolism

Degradation of glycosphingolipids are mediated by internalization by endocytosis. They are transported to the lysosomes where enzymes degrade the glycosphingolipids through hydrolytically and irreversible cleavage of bonds. Sphingolipidoses, which are present in the membrane, also mediate the degradation of these class of glycolipids [4].

Dysfunction of glycolipid metabolism is linked to several different diseases from the disruption of glycolipid degradation leading to the accumulation of glycolipids. Figure 1.4.2 illustrates diseases associated with different disruptions in the metabolism of glycolipids. For example, Tay-Sachs disease is an autosomal recessive disease that is a member of the G_{M2} gangliosidotic disease. The disease portrays symptoms of severe psycho-motor developmental disordered which is caused by the inabiligy to properly degrade membrane associated gangliosides. This occurs because the enzyme required to break down gangliosides, β-hexosamindase A, is dysfunctional due to mutations in the HEXA gene. The accumulation of these gangliosides in the neurons results in neural cell death.

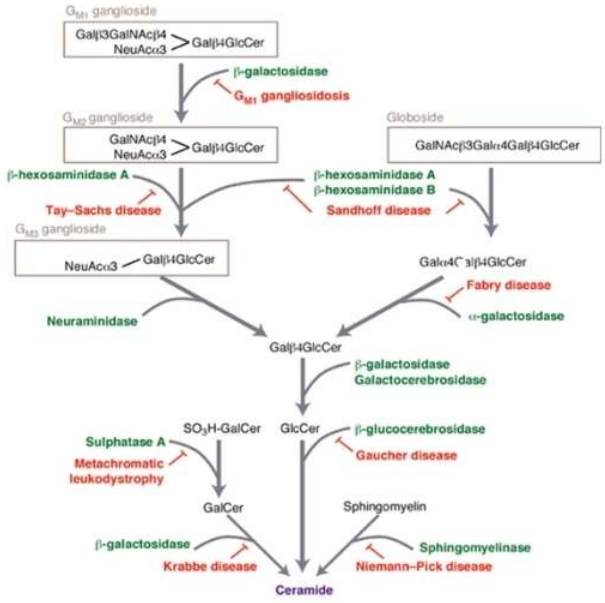


Figure 1.4.2. Diseases associated with dysfunction of glycolipid metabolism

Distribution

The majority of glycolipids are located in membrane structures in the cell. Two-thirds of total glycolipids are distributed in intracellular membranes such as the golgi-apparatus, endosomes, lysosomes, nuclear membrane, and mitochondria [4]. Glycolipids are synthesized in the golgi-apparatus where the majority are transported to membranes to maintain the bilayer. Few glycolipids can be found in the cystol; approximately 5% of the total glycolipids in the brain are found in the soluble fraction.

Glycosphingolipids in the plasma membrane can cluster with cholesterol to for rafts which contains less phospholipids relative to other portions of the membrane; approximately 70% of total glycolipids are found in these rafts which form hydrophobic interactions [5]. In addition, sphingolipids and glycosphingolipids form weak interactions between the carbohydrate head groups and the hydrophobic saturated side chain lipids with cholesterol filling any voids [6]. The strong interactions between glycolipids and cholesterol is the driving force which segregates them from the fluid phospholipids in the membrane [7].

Function

Carbohydrates on glycolipids are the most exposed structures on the extracellular surface of cells and are flexible with numerous binding sites which make them optimal for cell signaling. Since the lipid moiety is usually buried within the membrane, carbohydrate-carbohydrate interactions are the predominant interactions that may occur between glycolipids. They can interact side by side within the same membrane or trans interactions between two membranes. Trans interactions between glycolipids was reported to be the basis for glycosphingolipid-dependent cell to cell adhesion which involves calcium ions [8]. Further studies reported that cell surface carbohydrates play major roles in cell-substrate recognition in oncogenesis, myelin sheath regulation, and cell adhesion in metastasis [9-11]. Glycolipids play an important role in several biological functions such as recognition and cell signaling events; below are a few biological functions glycolipids play a role in.

Signal Transduction

Glycosphingolipids and sphingomyelin are clustured into microdomains where they can associate with serveral different proteins such as cSrc, G-proteins, and focal adhesion kinase to mediate cellular events [12]. In the plasma membrane, glycosphingolipids form rafts with cholesterol where these regions have relatively less phospholipids. Shown in Figure 1.4.3, glycosphingolipids form rafts with cholestorol to anchor GPI proteins to the extracellular leaflet and src family kinases to the cystolic leaflet. Thus, glycosphingolipids have been These microdomains can cause cellular responses by associating with GPI-anchored proteins which may induce activation of specific kinases to transduce the phosphorylation of different substrates [13]. The glycosphingolipid microdomains have also been associated with mediating immunoreceptors and growth factor receptors [14].



Figure 1.4.3. Interaction Glycolipids and membrane bound proteins.

Cell Proliferation

Glycolipids have been observed to play a role in the regulation of cell growth via interactions with growth factor receptors. Intracellular ceramide stimulated DNA synthesis in endothelial smooth muscle cells and also induced mitogenesis by platelet-derived growth factor [15]. Lactosylceramide activates NADPH oxidase to modulate interacellular adhesion molecule -1 expression on human umbilical vein endotheial cells and to induce proliferation of human aortic smooth muscle cells. With the reduction of ceramide, there was increased ceramidase activity, sphingomyelin synthase which is associated with the proliferation of smooth muscle cells. In addition, gangliosides are known to be involved in inducing apoptosis. Apoptotic signal triggered by CD95 in lymphoid and myeloid tumor cells increase ceramide levels which results in the increase in ganglioside GD3 synthesis; GD3 is known to be a potent mediatior of cell death. Abundant amounts of glycosphingolipids are found in the plasma membrane of cancer cells where antibodies targeting these gangliosides result in apoptosis [16]. Treatment with anti-ganglioside GD2 monoclonal antibodies induces apoptosis in GD2 expressing human lung cancer cells.

Calcium Signaling

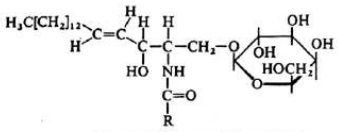
Gangliosides are associated with calcium ions which is thought to have a role in neuronal function. Ganglioslide micelles bind to calcium ions with high affinity and may play a significant role in synaptic transmission. It has been reported that sphingosine and ceramide mediate the release of calcium from intracellular stores. Gangliosides may also play a role in calcium homeostasis and signaling. These glycolipids induce changes in cellular calcium through the modulation ofcalcium influx channels, calcium exchange proteins, and calcium dependent enzymes which were altered through the association of gangliosides. [17]. In addition, increased levels of intracellular glucosylceramide resulted in increased calcium stores in neurons [18]. Glycolipid galactocerebroside have been observed in the opening of calcium channels in oligodendrocyte cells.

Types of Glycolipids

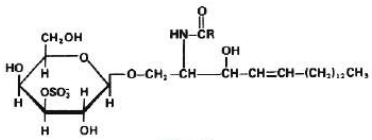
Glycosphingolipids

Glycosphingolipids are a class of glycolipids which contain ceramide as the lipid complex. Ceramides are amides of fatty acids with long chain di- or trihydroxy bases. The acyl group of ceramides is a long chain saturated or monounsaturated fatty acids. These lipids are primarily found in nerve tissue nerve tissue and mediate cell signaling. The glycophingolipids can be subdivided into the following groups:

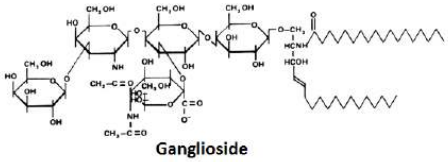
1. **Neutral glycosphingolipids**: Cerebrosides also known as monoglycosylceramides are glycolipids primarily found in the brain and peripheral nervous tissue. The most common cerebroside contains a molecule of galactose found in myelin. Their function is to provide a protective coating to each nerve acting as an insulator with high concentrations in the myelin sheath.
2. **Acidic glycosphingolipids**: These lipids are negatively charged at physiological pH which is provided by N-acetylneuraminic acid (NANA) or by sulfate groups in sulfatides. Gangliosides contain a sialic acid (NANA) making them negatively charged. These are found in the ganglion cells of the CNS and are predominantly at nerve endings. Sulfatides are sulfated galactocerebrosides which are found in the brain and kidneys. They are primarily found in the medulated nerve fibers and have been linked to immune responses to nervous system signaling.
3. **Basic glycosphingolipids**
4. **Amphoteric glycosphingolipids**



Neutral Glycosphingolipid
(monoglycosylceramide)



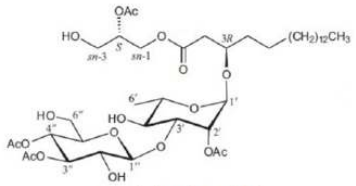
Sulfatide



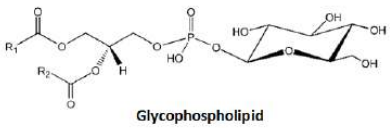
Ganglioside

Glycoglycerolipids

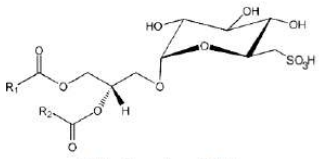
1. **Neutral glycoglycerolipids**: These usually contain one or two sugars linked to glycerol or diacylglycerol. These lipids have important roles in higher plants, algae, and bacteria in which they are localized to photosynthetic membranes. Photosynthetic membranes are comprised of about 85% of neutral glycoglycerolipids [6]. neutral glycoglycerol lipids can be separated into non-acylated or acylated glycoside moieties.
2. **Glycophospholipids**: These compounds are glycoglycerolipids containing at least one phosphate group attached to either the sugar or glycerol. The simpliest of these compounds are found in red blood cells called glucosylated phosphatidic acid.
3. **Sulfoglycoglycerolipids**: These compounds contain a sulfur atom and are proposed to be localized to acidic membranes (surface membrane strongly acidic). Sulfolipids are shown to be present in the thylakoid membranes of plants within the photosynthetic membranes.



Neutral glycoglycerolipid
(2-Acetoxy-1-(3-glycosyloxyoctadecanoyl)glycerol)



Glycophospholipid



Sulfoglycoglycerolipids

References

1. "Glycolipids". Nature. Nature Publishing Group. Retrieved May 2016.
2. Yu et al., R.K. Yu, Y. Suzuki, M. Yanagisawa. Membrane glycolipids in stem cells. FEBS Lett., 584 (2010), p. 1694
3. C. Neil Hunter, Fevzi Daldal, Marion C. Thurnauner, J. Thomas Beaty. Advances in Photosynthesis and Respiration, Vol. 28. The Purple Phototrophic Bacteria. Springer. 2009.

4. Gillard BK, Thurmon, LT, Marcus DM (1993) Variable subcellular localization of glycosphingolipids. Glycobiology 3: 57-67.
5. Edidin M (2003)
5. Simons K, Toomre D (2000) Lipid rafts and signal tranduction. Nat Rev Mol Cell Biol 1: 31-41.
6. Brown DA, London E (2000) Structure and functions of sphingolipid- and cholesterol-rich membrane rafts. J Biol Chem 275: 17221-17224.
7. Shaul PW, Anderson RG (1998) Role of plasmalemnal caveolae in signal transduction. Am J Physiol 275: 843-851.
8. Marrow MR, Singh D, Lu D, Grant CW (1995) Glycosphingolipid fatty acid arrangement in phospholipid bilayer: Cholesterol effects. Biophys J 68: 179- 186
9. Kojima N, Hakomori S (1991) Cell adhesion, spreading, and motility of GM3- expressing cells based on glycolipid-glycolipid interaction. J Biol Chem 266: 17552-17558.
10. Boggs JM, Menikh A, Rangaraj G (2000) Trans interaction between galactosyl ceramide and cerebroside sulphate across opposed bilayers. Biophys J 78: 874-885.
11. Schnaar RL (2004) Glycolipid-mediated cell-cell recognition in inflammation and nerve regeneration. Arch Biochem Biophys 426: 163-172.
12. Malhotra R (2012) Membrane Glycolipids: Functional Heterogeneity: A Review. Biochem Anal Biochem 1:108. doi:10.4172/2161- 1009.1000108
13. Hakamori SI (2000) Cell adhesion, recognition and signal transduction through glycosphingolipid microdomain. Glycoconj J 17: 143-151.
14. Jordan S, Rodgers W (2003) T-cell glycolipid-enriched membrane domains are constitutively assembled as membrane phases that translocate to immune synapses. J Immunol 171: 78-87.
15. Auge N, Andrieu N, Negre-Salvayre A, Thiers JC, Levade T, et al. (1996) The sphingomyelin-ceramide signaling pathway is involved in oxidized low density lipoprotein-induced cell proliferation. J Biol Chem 271: 19251–19255.
16. De Maria R, Lenti L, Malisan F, d'Agostino F, Tomassini B, et al. (1997) Requirement for GD3 ganglioside in CD95- and ceramide induced apoptosis. Science 277: 1652-1655.
17. Nagatsuka Y et al., FEBS Lett 2001, 497, 141
18. Benson AA et al., Proc Natl Acad Sci USA 1959, 45, 1582

1.4: Glycolipids is shared under a CC BY 4.0 license and was authored, remixed, and/or curated by LibreTexts.

1.5: Sphingolipids

Sphingolipids are a type of lipids made up of fatty acid chains that were first mentioned in 1884 in J.L.W. Thudichum's *A Treatise on the chemical composition of the brain.* They were named after the Greek mythological creature, the sphinx, due to the unknown riddle of their function.[1] Sphingolipids are found in essentially all plants, animals, fungi and in some prokaryotes and viruses. Specifically, they are found in membranes and as a major component of lipoproteins.[2]

Structure

Sphingolipids are amphipathic molecules; they have hydrophobic and hydrophilic properties. In the hydrophobic region there is a sphingoid long chain base (aliphatic chains with attached hydroxyl groups) with a fatty acid chain attached by amide bond at carbon 2. In the hydrophilic region, there are phosphate groups, sugar residues, and/or hydroxyl groups.[3] This amphipathic nature allows for the diffusion of sphingolipids between membranes and for the flipping of sphingolipids between membrane leaflets. However, sphingolipids are still more likely to accumulate in acidic environments because of the possible ionization of a free amino group.[4] There are several classes of sphingolipids: the sphingoid base and simple derivatives, ceramides, and complex sphingolipids (Figure 1.5.1).

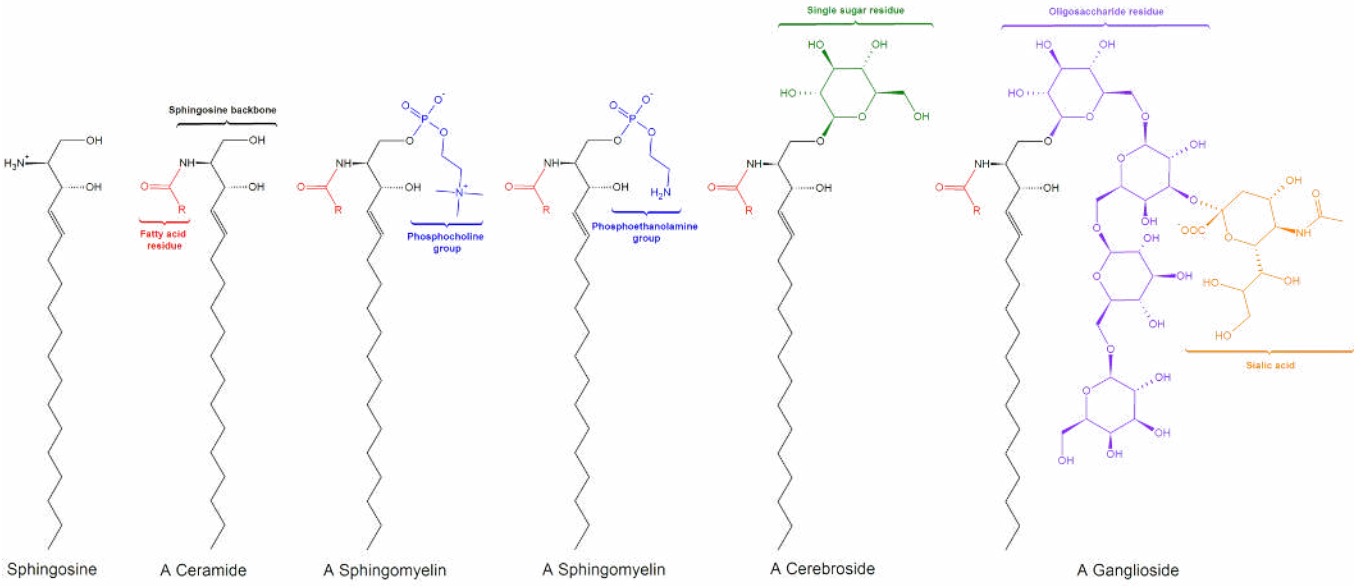


Figure 1.5.1: Sphingolipids general structure. (CC BY-3.0; LHcheM).

Sphingoid base & simple derivatives

Sphingolipids are composed of many backbone "sphingoid bases" which are synthesized from serine and a long-chain fatty acyl-CoA.[2,5] If a backbone has not yet been analyzed, it is referred to as a *sphinosine*, after the original name for the fundamental component of these lipids. Sphingoid bases can vary in alkyl chain length/branching, the number and position of double bonds, the number and locations of hydroxyl groups, etc. A simple sphinosine base can be seen in Figure 1.5.1.

These simple derivatives exist mainly as the backbone of more complex sphingolipids, but they do exist on their own. They are mainly used in intra-and extra-cellular signaling.[2] The exact structure of the sphingolipid determines the function. For example, in the dermis, there are additional hydroxyl groups at positions 4 and/or 6 that interact with neighboring molecules to strengthen the permeability of the skin barrier.[5]

Ceramides

Ceramides, which are synthesized in the endoplasmic reticulum, are the simplest sphingolipid after the backbone.[3] They are fatty acid derivatives of sphingoid bases, linked by amide bonds. They are usually fully saturated or mono-unsaturated and consist of 14-26 carbons, but are sometimes longer. There is sometimes a hydroxyl group on the ω or ω-carbon atom.[2,5] The structure can be seen in Figure 1.5.2. Ceramides have high phase transition temperatures of greater than 37°C. This is due to their predominately saturated nature, which allows for the tight packing of lipids. This also favors the segregation of ceramides (and more complex sphingolipids) into regions called membrane "rafts."[2,6]

Ceramides are key to cell signaling processes.[3] They generally serve as second messengers by regulating cell growth, senescence, and apoptosis. The exact function depends on the type of sphingolipid base and fatty acid.[2] For example, ceramides containing palmitic acid for a fatty acid chain are generated in response to apoptosis. Much of the specifics of ceramide function is still under investigation. Ceramides also serve as a precursor to more complex sphingolipids.[3]

Ceramides can only exist in membranes but they have a rapid flip rate between leaflets. This means they cannot leave the organelle they are created in, but will have access to binding proteins and enzymes on both sides of the bilayer. As such, ceramides can usually only be modified by enzymes that exist in the membrane compartment that the ceramide was produced in.[4]

Complex Sphingolipids

The synthesis of complex sphingolipids occurs in the Golgi apparatus.[3] The bulky headgroups of these sphingolipids make flipping between membrane leaflets very unlikely without the aid of flippases. This means that without flippases, sphingolipids are restricted to the lumenal Golgi leaflet/outer leaflet of the plasma membrane.[4] The two main type of complex sphingolipids are phospho- and glycol-sphingolipids.

Phosphosphingolipids

Phosphosphingolipids are linked by phosphodiester bonds.[5] In mammals, the major phosphosphingolipids are gomyelins (ceramide phosphocholines). In insects, it is ceramide phosphoethanolamines. The major phosphosphingolipids in fungi are phytoceramidesphosphoinositols and inositol phosphates. Aquatic organisms typically have sphingolipids where the phosphate has been replaced with a phosphono- or arsenate group.[2] Example phosphosphingolipids can be seen in Figure 1.5.3.

Glycosphingolipids

Glycosphingolipids have one or more carbohydrate groups in a glycosidic linkage (usually; ceramide phophonositols are an exception). The structure can be seen in Figure 1.5.4. There are four classifications of glycosphingolipids:

1. Neutral glycosphingolipids: 1 or more uncharged sugars (i.e. glucose, galactose, N-acetylglucosamine, N-acetylgalacoseamine, fucose)[2]
2. Acid glycosphingolipids: ionized functional groups (i.e. phosphate or sulfate) attached to neutral or charged sugars[2]
3. Basic glycosphingolipids[5]
4. Amphoteric glycosphingolipids[5]

Naming of Sphingolipids

Sphingolipids are named using IUPAC nomenclature for lipids (http://www.chem.qmul.ac.uk/iupac/lipid/). The most common sphingoid base is sphingosine. The official names of sphingosine are (2S,3R,4E)-2-aminooctadec-4-ene-1,3-diol or D-*erythro*-sphingosine & E-sphing-4-enine. The abbreviation is d18:1. The first number represents the number of carbon atoms. The second number is the number of double bonds. In this case, the letter ‘d’ refers to the 2 (di-) hydroxyl groups.[2,5]

Biological Functions

There are many biological functions associated with sphingolipids, including cellular regulation, signaling and metabolism.

Biophysical Properties

Sphingolipids tend to form clustered structured called microdomains, rafts, or caveolae (when containing caveolin). Saturated alkyl sidechains allow for strong van der Waals interactions. Ceramide hydroxyls, amide bonds, and polar headgroups allow for hydrogen bonding and dipole interactions. Sphingolipids are enriched in growth factor receptors, transporteres and proteins with glycosylphosphatidylinositiol-lipid anchors. Sphingolipids help stabilize the membrane bilayer which helps structures such as the lamellar bodies that maintain the permeability of skin. Their water solubility allows for rapid movement between membranes. Sphingolipids can exist in cationic and neutral forms.[2]

There are three major phases that a lipid membrane can take (Figure 1.5.5).

- In the gel phase, the lipid bilayers are in the solid state. The packing of the lipid molecules is very tight and ordered, leading to little movement of lipids across the membrane surface.
- In the liquid disordered phase, are highly fluid states in which the individual lipids can move unhindered across the surface of the membrane. The packing of the lipids is highly irregular and the lipids themselves are often kinked due to unsaturated fatty acids.

- The liquid ordered phase in a cross between the gel phase and the liquid disordered phase. There is still the relatively easy movement of lipid molecules across the membrane, but the membrane itself is more tightly packed, leading to a more solid structure. This phase comes about through the presence of sterol molecules within the membrane.

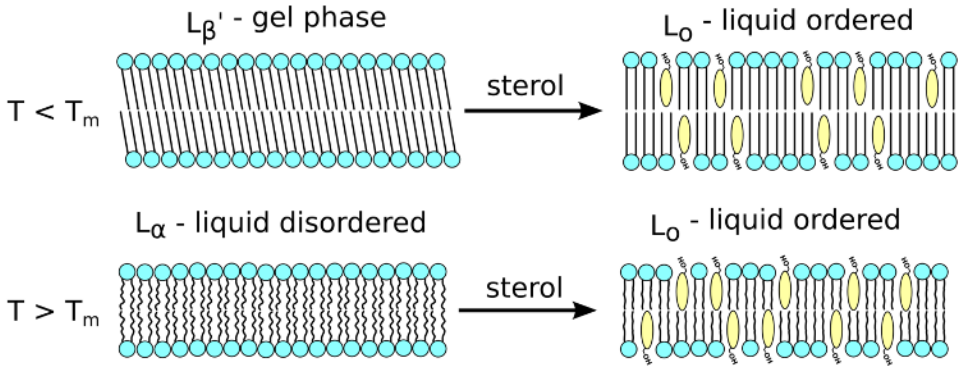


Figure 1.5.5: The gel, liquid disordered and liquid ordered phases of membranes (Faller 2016)

Membrane rafts are caused by a phase separation in the membrane. They occur when the liquid ordered phase and the disordered phase coexist. Tight packing of lipids is key to raft formation. In the liquid ordered phase, like the ordered gel phase, lipids are elongated and tightly packed, but they still have a higher degree of lateral mobility.[6] Figure 1.5.7 shows a membrane with a lipid raft.

Membrane rafts are abundant in membranes that are cholesterol and sphingolipid rich (i.e. the plasma membrane). They are important in sorting in the trans-Golgi network, sorting in the endocytic pathway, as a docking site for pathogens and toxins, and as integrin receptors.[6]

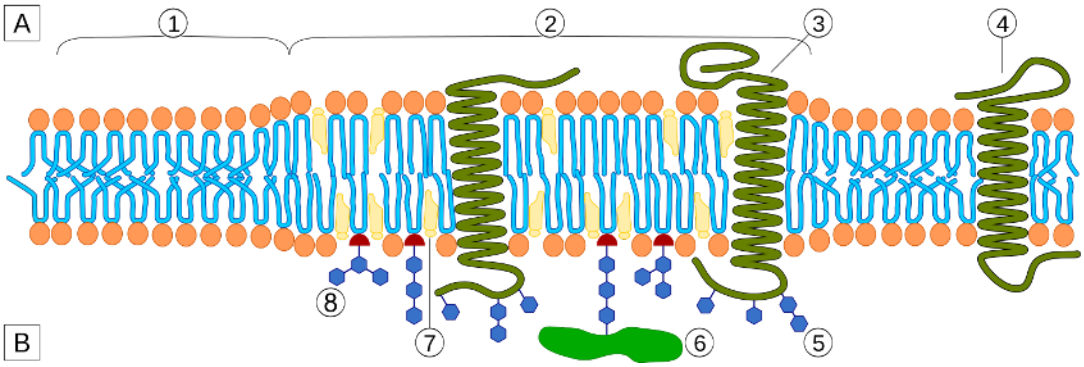


Figure 1.5.7: A membrane containing a lipid raft. Section 1 is a standard lipid bilayer and section 2 is the lipid raft

Cellular Regulation

Cellular sphingolipids are located in many places throughout the cell. They are found in the outer leaflet of the plasma membrane, in the lumen of intracellular vesicles/organelles (i.e. endosomes, Golgi membranes), and in undefined locations in the mitochondria, nuclei, and intracellular compartments. This abundance makes them ideal candidates for cell regulation.[2]

Cellular sphingolipids interact with complementary ligands (i.e. extracellular matrix proteins/receptors), with other carbohydrates (i.e. glycosynapse) and with proteins on the same cell surface. Through these interactions, they can control the location of a protein (i.e. in membrane rafts) and modify the conformation of the protein and its activity. They can also be recognized by viruses, bacteria and bacterial toxins as a means of attachment and entry.[2]

Ceramides have multiple roles in membrane biogenesis and regulation. They can influence ER to Golgi trafficking. They can help with the formation of autophagosomes. It is also likely that they influence the ER interactions with the nuclear membrane, outer membrane of mitochondria, and the plasma membrane.[2]

Cellular Signaling

Sphingolipids affect cell signaling by influencing the properties of receptors directly. The exact pathway for signal transduction varies depending on the exact function of the sphingolipids but there is a general pathway.[2]

1. Receptors are activated by cytokines (i.e. IL1, tumor necrosis factor-ω), growth factors (i.e. platelet derived growth factor), or other agonists.
2. Hydrolysis of membrane sphingolipid to ceramide is induced.
3. Sphingolipids either serve as a lipid second messenger, or can be converted to downstream metabolites (i.e. sphingosine, sphingosine 1-phosphate, ceramide 1-phosphate).
4. Downstream targets (i.e. proteins kinases, phosphoprotein phosphatases) that control cell behavior are either activated or inhibited.

Sometimes, multiple sphingolipids within the same cell have opposing signaling function. For example, ceraminde and sphingosine 1-phosphate signal for conflicting functions of cell growth. One signals for the inhibition of growth, while the other signals for the stimulation of growth. (Or in other words, the induction vs. inhibition of apoptosis.) The cellular pathway taken is determined by a ceraminde/sphingosine 1-phosophate “rheostat” in deciding between growth arrest/apoptosis and proliferation/survial.[2]

Because sphingolipids are complex molecules, they can take diverse input signals and produce multiple coordinated outputs. Signaling from sphingolipids also alters membrane structure and behavior of other membrane receptors and/or proteins.[2]

Metabolism

Sphingolipid base acylation is done through ceramide synthases which are highly specific for acyl chain lengths.[2] Regulation occurs through control of enzyme expression, post-translational modifications, and allosteric mechanisms. These can be cell specific – they can control sphingolipid synthesis during specific phases of the cell cycle, in response to specific signals.[3] Figure 1.5.8 shows several metabolic pathways of sphingolipids.

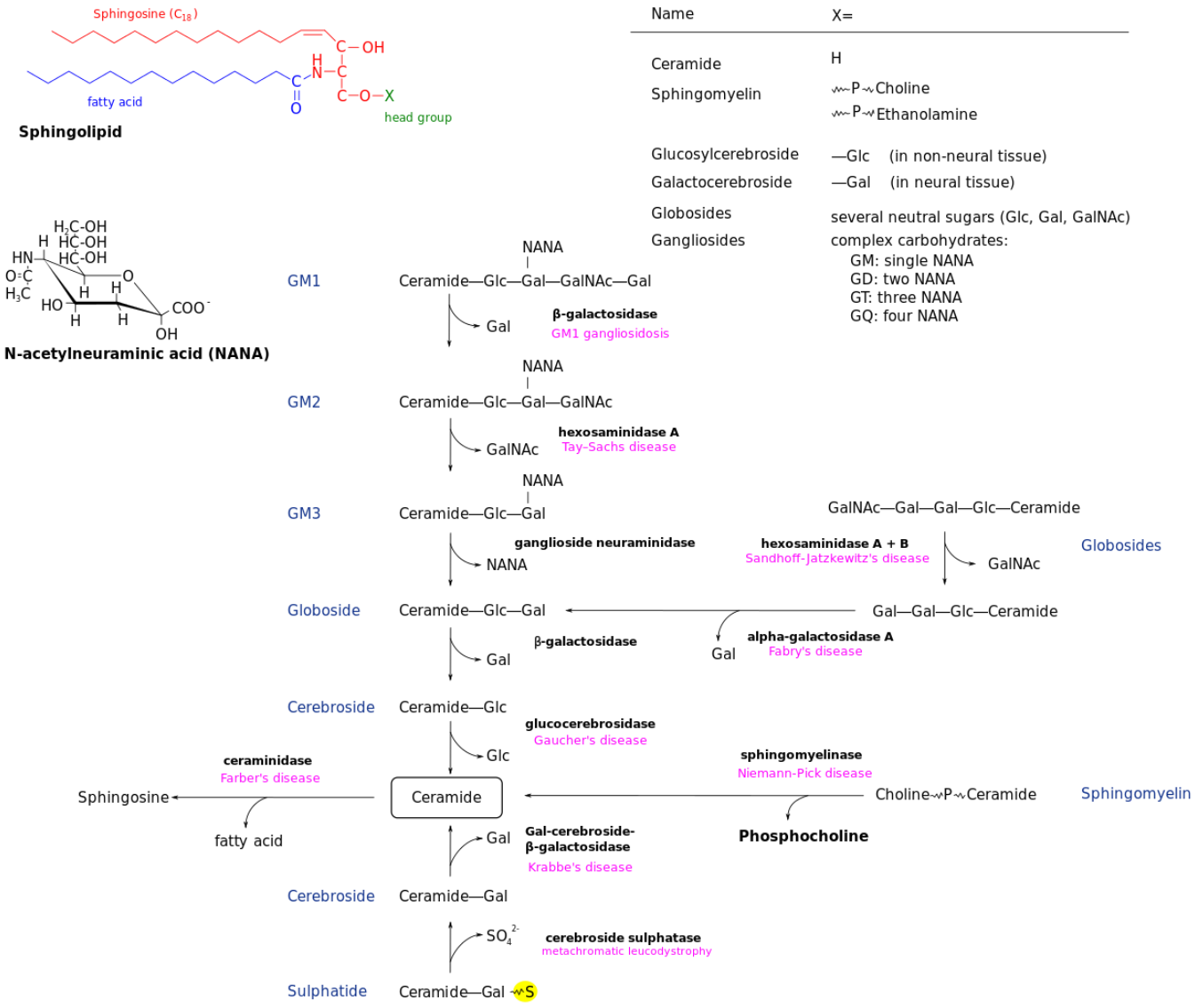


Figure 1.5.8 – Sphingolipid metabolic pathways

During sphingolipid metabolism, sphingomyelin turnover produces signaling metabolites and alters the structure of membrane domains, depending on its presence. In addition, changing the glycosphingolipid composition affects the properties of the cell surface and its interaction with the extracellular matrix and neighboring cells. Because of this, sphingolipid metabolism and signaling are basically the same.[2]

Sources

1. Thudichum, J. L. W. 1884. “A Treatise on the Chemical Constitution of Brain”. Bailliere, Tindall, and Cox, London.
2. Hirabayashi, Y., Igarashi, Y., Merrill, A.H. (2006). Sphingolipid Biology Springer, Japan.
3. Futerman, A. H., Hannun, Y. A. (2004). "The complex life of simple sphingolipids." EMBO Rep **5**(8): 777-782.
4. Gault, C., et al. (2010). "An overview of sphingolipid metabolism: from synthesis to breakdown." Adv Exp Med Biol **688**: 1-23.
5. Fahy, E., et al. (2005). "A comprehensive classification system for lipids." J Lipid Res **46**(5): 839-861.
6. Brown, D. A. and E. London (2000). "Structure and Function of Sphingolipid- and Cholesterol-rich Membrane Rafts." J Biol. Chem. **275**(23): 17221-17224.

1.5: Sphingolipids is shared under a CC BY 4.0 license and was authored, remixed, and/or curated by LibreTexts.

1.6: Sterols and Sterol Induced Phases

Sterols are a class of hydrophobic ringed lipid molecules found in biological membranes throughout eukarya. Sterols can comprise greater than 50% of the membrane lipid content in cells, and are known to alter membrane fluidity and structure [1]. Though the mechanisms of these effects are still under debate, sterols have been shown to induce altered lipid phases in bilayer systems, generally increasing the order of acyl chains while maintaining lipid translational fluidity. Their actions are thought to be essential to the formation of lipid rafts with various effects on cell biology and serve as precursors to steroid hormones in animals.

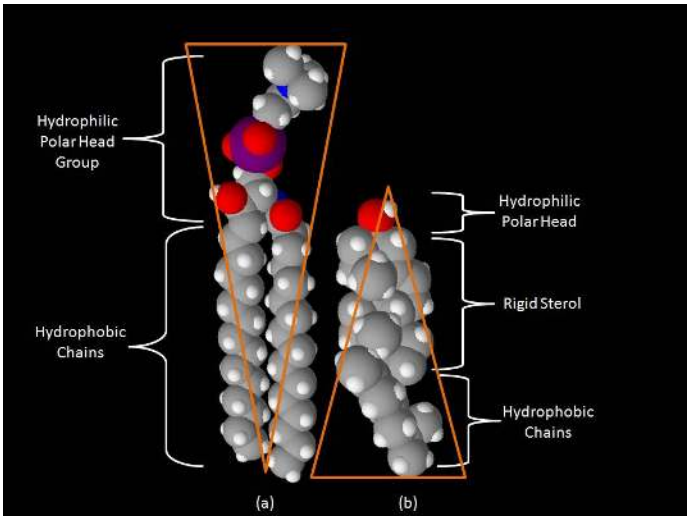


Figure 1.6.1: Space-filling diagram of (a) sphingomyelin and (b) cholesterol depicting relative size and depth in membrane. (Public Domain; Wlstutts via Wikipedia)

Sterol Structure

All naturally occurring sterols are comprised of a hydrocarbon tetrameric fused ring structure and acquire a small degree of polarity from a 3-hydroxyl in the β configuration (fig 2); α-hydroxyl sterols are not found in natural membranes. The most common sterols also have a short aliphatic tail on the opposite end on C17. In lipid bilayers the hydroxyl acts as the polar head group and orients towards the phospholipid head groups of the bilayer, while the rings and short hydrophobic tail extend into the hydrophobic core of the membrane, aligning with the acyl chains of the phospholipids. The topography of sterols is such that the α side of the relatively rigid ring structure is flat while the β side has protruding methyl groups; this structure constrains their interactions with lipids allowing significant contact on the flat surface.

Common Sterols

Many different sterols are found in biological membranes and are specific to certain phyla. Subtle differences in their structure can change their effect on membrane structure and dynamics as discussed below. Cholesterol is the most common sterol in animal membranes accounting for approximately 20-30% of sterols found therein [2]. It is characterized by a single double bond in ring B (C5-C6) and the lack of a branching carbon at position 24. Ergosterol is found in the membranes of fungi and protists and differs from cholesterol by containing two more carbon-carbon double bonds (one in ring B, another between carbons 22 and 23 in the tail region) and a methyl group at position 24.

Sterols from plants are known as phytosterols. Common phytosterols include campesterol, stigmasterol and sitosterol, though hundreds of different compounds have been isolated from plants. Hopanoids are pentacyclic compounds that share a similar structure with sterols and are often found in prokaryotic membranes, where they are thought to have an effect on membrane stability and structure similar to sterols [3].

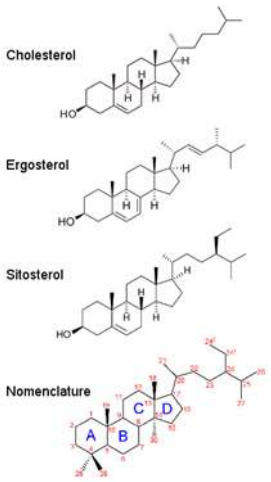


Figure 1.6.2: Backbone structures of common sterols and nomenclature of the conserved backbone carbons. Source: Ian Kimball.

Liquid-ordered Phase (l_o)

Sterols have pronounced effects on the phase behavior of lipid membranes. When added to lipids in the gel phase ($L_{\beta'}$) sterols tend to liquefy the membrane structure by disrupting the highly ordered tilted structure of the hydrocarbon chains. At low temperatures this induces the liquid crystal phase ($L_{c'}$) where the lipid tails are fully extended, but not tilted [4]. Conversely, cholesterol tends to solidify lipids in the liquid disordered phase (L_α). In both cases, higher cholesterol concentration leads to the formation of an intermediate phase, known as the liquid ordered (l_o) phase. In the l_o phase, the phospholipid tails have higher order similar to the gel phase, but maintain lateral fluidity similar to the L_α phase [2,5] (fig. 3). The area per molecule is also reduced (see condensation effect below)

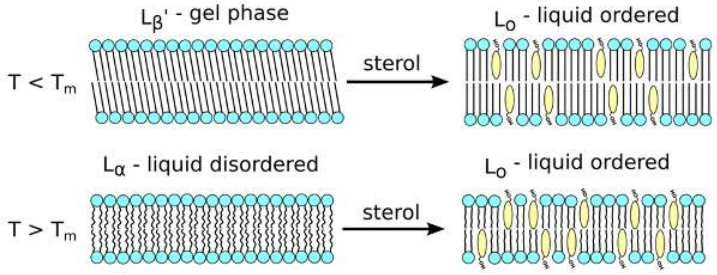


Figure 1.6.3: Sterol-induced liquid-ordered phase. Source: [6]

Lipid phase diagrams (fig 4) show the phase coexistence of l_o and either L_α or the ripple phase P_β (sometimes called pre-transition phase), depending on temperature in lower cholesterol content. As the relative concentration of sterol in the membrane increases, the l_o phase dominates as all phospholipids come in near contact with sterols [7]. The ordering of saturated acyl chains in the presence of cholesterol has been studied by many different methods including ^{2}H-NMR, EPR, and MD simulations [2], which show that sterols induce order in neighboring fatty acid tails. Headgroup type, tail length and saturation, and whether the lipids are glycerol or sphingosine-based all influence the effects of sterols [2]. Notably, sterols have the most pronounced effect on the phase behavior of long saturated phospholipids like dipalmitoylphosphatidylcholine (DPPC); however, the presence of one saturated tail is sufficient for the effect [7]. Likewise, sterols with an α conformation or methyl groups in the trans conformation are incapable of affecting the phase behavior of lipids [1].

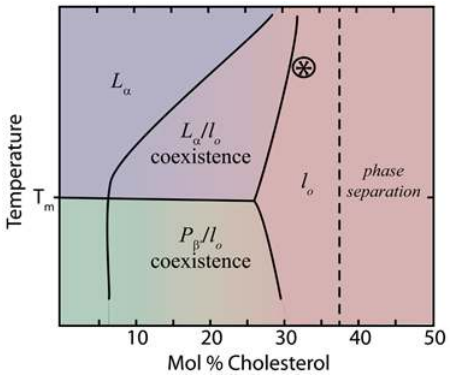


Figure 1.6.4: Lipid phase diagram as function of temperature and cholesterol content. [7] (CC BY 4.0; Armstrong et al. via PLOS)

Cholesterol and the main phase transition

The effect of cholesterol on lipid phases has been extensively studied with a method known as differential scanning calorimetry (DSC). With DSC the rate of heat flow can be measured as the temperature of a sample is increased or decreased at a constant rate. When the sample transitions between phases, the excess heat flow is recorded as a spike around the temperature at which that phase transition occurs. When heated or cooled past their phase transitions, pure lipids will display a sharp peak. The addition of sterols leads to a dampening and broadening of the enthalpy spikes associated with pre-transition and the main phase transition, effectively eliminating the phase transitions at higher cholesterol concentrations as the membrane enters the l_o phase [1]. This effect is dependent on the type and amount of sterol as well as the type of phospholipid [9]. For example, a precursor to cholesterol known as lathosterol differs in structure only by the placement of one double bond. This small difference means the lathosterol decreases the temperature of the main phase transition while cholesterol increases it, though cholesterol is eliminates the transition at high molar percent while lathosterol does not [9]

The Condensation Effect

When cholesterol is added to a membrane, the 2-dimensional area per molecule decreases while the membrane thickness increases; this is known as the condensation effect. The mechanism for this effect is unclear [4], but the rigid structure of cholesterol means that the reduction in surface area must be due to changes in the order of the lipid tails (fig 5). In DMPC membranes, increasing cholesterol from 0 to 50 mol% can lead to 25% reduction in area per DMPC molecules [2]. This condensation augments membrane strength and decreases permeability, and is strongest when paired with phosphatidylcholine-based lipids [10].

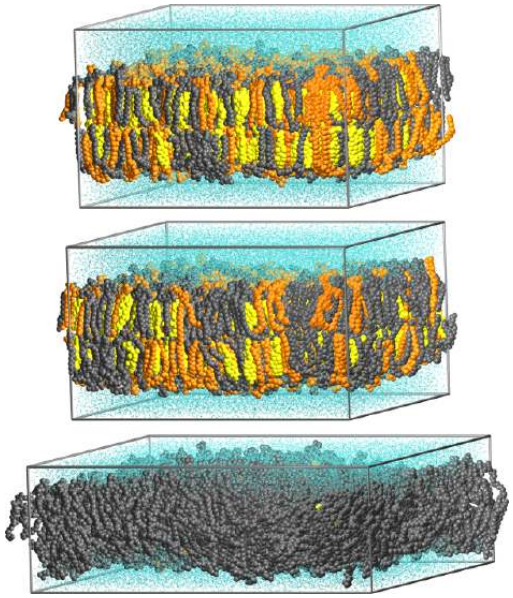


Figure 1.6.5: Simulation of sterol-induced phases. Palmitoyloleoylphosphatidylcholine (POPC) appears in grey, palmitoylsphingomelin in orange, and cholesterol in yellow. Note the increased order in the l_o phase and the change in dimensions of the membrane when cholesterol and PSM are present. Cholesterol also tends to interact with PSM more than POPC. Source: [11]

Sterols in Rafts

In biological membranes sterols are essential components of lipid rafts. Cholesterol makes a hydrogen bond with the sphingosine head group and preferentially associates with the fatty acid tails of sphingomyelin over other lipid tails. Cholesterol and sphingomyelin together solidify the membrane and decrease the lateral diffusion of lipids leading to long-lasting l_o domains amid $L_\alpha$lipids [11]. The lipid characteristics of rafts are thought to be important in determining membrane protein function.

Steroid Hormones

In animals, cholesterol serves as a precursor for all steroid hormones such as estradiol, aldosterone and cortisol, which act via intracellular receptors to regulate gene transcription in target tissues. These hormones are vital to nearly all physiological function including growth and reproduction, the stress response, water balance and metamorphosis (in invertebrates).

References

1. R.A. Demel, B. De Kruyff, Biochimica et Biophysica Acta (BBA) - Reviews on Biomembranes 457 (1976) 109.
2. T. Róg, M. Pasenkiewicz-Gierula, I. Vattulainen, M. Karttunen, Biochimica et Biophysica Acta (BBA) - Biomembranes 1788 (2009) 97.
3. M. Rohmer, P. Bouvier-Nave, G. Ourisson, Journal of General Microbiology 130 (1984) 1137.
4. F. de Meyer, B. Smit, Proceedings of the National Academy of Sciences 106 (2009) 3654.
5. K.J. Tierney, D.E. Block, M.L. Longo, Biophys J 89 (2005) 2481.
6. R. Faller. BPH 241 Lecture slides, UC Davis (2014)
7. C.L. Armstrong, D. Marquardt, H. Dies, N. Kučerka, Z. Yamani, T.A. Harroun, J. Katsaras, A.-C. Shi, M.C. Rheinstädter, PLoS ONE 8 (2013) e66162.
8. M.G.K. Benesch, R.N. McElhaney, Biochimica et Biophysica Acta (BBA) - Biomembranes 1838 (2014) 1941.
9. M.G. Benesch, D.A. Mannock, R.N. Lewis, R.N. McElhaney, Biochemistry 50 (2011) 9982.
10. P.J. Quinn and C. Wolfe, Biochimica et Biophysica Acta 1788 (2009) 33
11. P.S. Niemelä, S. Ollila, M.T. Hyvönen, M. Karttunen, I. Vattulainen, PLoS Comput Biol 3 (2007) e34.

Contributors and Attributions

- Ian Kimball

1.6: Sterols and Sterol Induced Phases is shared under a CC BY 4.0 license and was authored, remixed, and/or curated by LibreTexts.

1.7: Lipids in Non-Aqueous Environments

It is widely known that in the presence of aqueous solutions, lipids will spontaneously form ordered structures such as micelles and bilayers. This process is driven by the structure of the lipid, consisting of an ionic polar group at the head of the lipid and a long hydrocarbon chain which is nonpolar. The head group of the lipid is hydrophilic, while the long nonpolar portion is hydrophobic or lipophilic. In the presence of water, a polar molecule, the structures organize themselves in order to minimize the exposure of the hydrophobic ends to the water molecules in the solution. This interaction is driven by the formation of hydrogen bonds and the arrangement of water around the polar head groups of the lipids (the formation hydration shells).

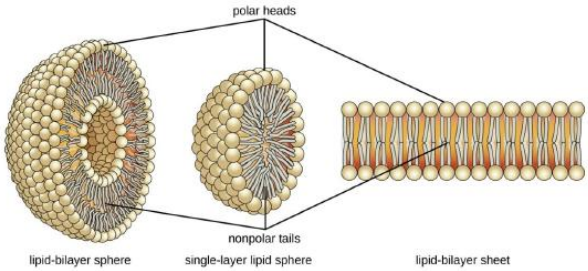


Figure 1.7.1: Structures formed by lipids in aqueous environments[1]

In the absence of water, the observed interactions between the lipids are free of the effects of the hydrogen bonding. These non-aqueous environments allow for the study of lipid behaviors in the absence of water.[2] There are three main classifications of non-aqueous solvents used for the replacement of water in lipid bilayer systems: organic solvents, “dry” solvents, and purely ionic mediums. [2]

Organic Solvents

Organic solvents are a non-aqueous class of liquid solvents which have a common structure containing at least one carbon and one hydrogen atom. They are generally lipophilic, allowing for their use in dissolving lipids. Organic solvents have been used to study the effect of water on lipid structures, specifically the structure and behavior of the lipids in the absence of water.

Glycerol is an organic solvent that has been used to substitute for water in the study of biological membranes; glycerol has been shown to substitute for water in biological systems. Multilamellar liposomes can be formed from phospholipids in pure glycerol. [3] Under pure glycerol conditions, the liposomes exhibit the same fluid space (fluid spacing between bilayers) that is measured in water. In solutions of glycerol and water, however, fluid spacing between the lipid bilayers is a function of the glycerol mole fraction in water due to glycerol changing the dielectric permittivity of fluid space. The dielectric constant of glycerol is around 42.5 compared to the dielectric constant of water of ~80. The effect of changing dielectric permittivity is to change the long-range Van der Waals forces between the lipid bilayers. [3]

Interdigitated hydrocarbon chain packing

Alcohols, including ethanol, have been shown to have a biphasic effect on the gel to liquid-crystalline phase transition temperatures of saturated phosphatidylcholine bilayers. It is observed that at low concentrations of alcohol in solution, the lipids exhibit a decrease in Tm with increasing concentration. At higher alcohol concentrations there is a reversal in the slope of the changing Tm with respect to increasing concentration of alcohol; at high concentrations there in an increase of Tm with increasing alcohol concentration. [4,5]

The concentration at which the reversal takes place is also dependent on the length of the hydrocarbon tails of the lipids; it is more energetically favorable for long chain lipids to interdigitate than short chained lipids due to Van der Waals interactions. The decrease in Tm in the low concentration ranges is explained by freezing point depression as a result of the preferential interaction of the alcohol with the liquid-crystalline phase of the lipid. The reversal in the trend at higher concentrations of alcohol is due to an induced gel phase in which the phospholipids from opposing monolayers interdigitate/interlock.

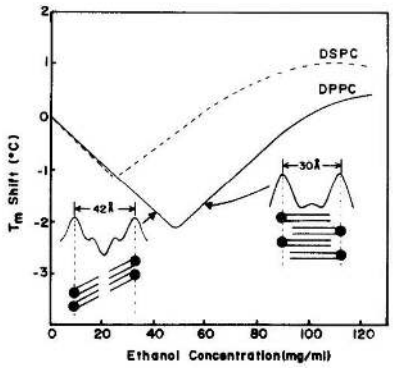


Figure 1.7.2: Effect of ethanol concentration on main transition temperature shift in DSPC and DPPC bilayers. Inset diagrams of normally spaced and interdigitated bilayers [4]

"Dry" Solvents

It is possible to maintain the integrity of lipid membranes in the absence of water using certain molecules. These molecules, usually a sugar such as trehalose, serve to act as substitutes for water in the structure of the lipid bilayers. [6]

“Wet” Interactions

The roles dry solvents play in interacting with phospholipids can best understood in the context of the interactions water has with the lipids. There are several things to consider regarding the interactions of water with these lipids, namely the affects of hydration such as shell formation, swelling, and headgroup separation between bilayers. For example, when water hydrates phospholipids, the lipids swell as water becomes bound to the headgroup of the lipids. Phosphatidylcholines can bind 10-12 mol of water per mol of lipid. [7] The water which binds to the lipids forms the hydration shell of the lipid. Increase in hydration of phospholipid bilayers can result in increased area per lipid molecule, increased disorder among hydro carbon chains, and increased lamellar repeat distances. The lamellar repeat distance is the separation of head groups between stacked lipid bilayers.

Decreased hydration levels (generally below 20%) result in increased van der Waal’s interactions, which increase the likelihood of the lipid undergoing a liquid crystalline to gel phase transition. [7]

Dehydration

Dehydration of lipid bilayers can result in fusion. Dehydration causes a reduction in the force of hydration which opposes the fusion of lipid bilayers. Fusion of lipid bilayers during dehydration has been shown using freeze-fracturing techniques. In the cases where fusion has been observed, the fusion is between adjacent bilayers. [7] The implications of this fusion are evident in cellular membranes that undergo dehydration. Fusion of cellular membranes can result in leakages during the transitions from liquid-crystalline to gel phase (drying) and gel to liquid-crystalline (rehydration).

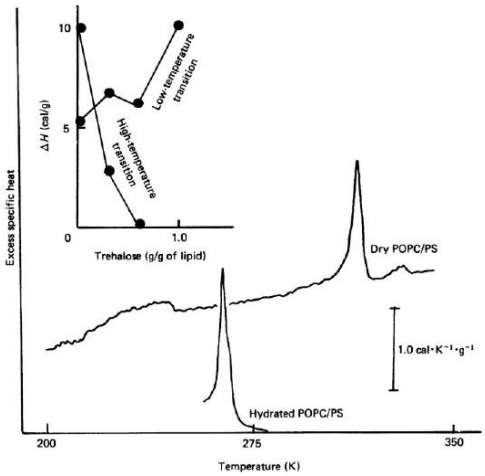


Figure 1.7.3: Melting endotherms for dry and hydrated multilamellar vesicles of POPC. Inset: Changes in enthalpy of high and low temperature endotherms for dry POPC and trehalose [7]

Sugar Protectants

Membranes may be stabilized in the absence of water in presence of dry sugars such as trehalose. The sugars are theorized to stabilize lipid bilayers by inhibiting the fusion of the lipids in the absence of water. In the case of trehalose, the addition of small amounts of the dry solvent (~1g trehalose/g phospholipid) preserves phospholipids in the “dry” state while maintaining the phospholipid's liquid crystalline phase. High resolution proton NMR can be used to demonstrate that phospholipids dried without a dry/stabilizing sugar present result in gelling of the hydrocarbon chains, while in the presence of trehalose the hydrocarbon chains remain in a fluid phase. [7]

There is likely a direct interaction between the phosphate head groups of the lipid and the hydroxyl groups of the trehalose due to hydrogen bonding. Other sugars such as sucrose, which are not as readily able to form hydrogen bonds, can also be used with varying degrees of success (Figure 1.7.4).

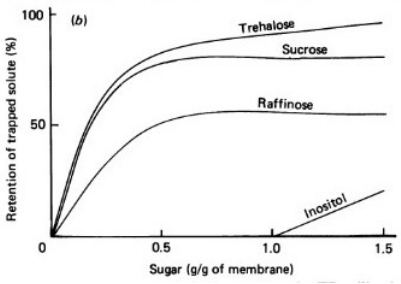


Figure 1.7.4: Plot of retention of trapped solute after removal of water (drying) in presence of various sugars [7]

Purely Ionic Solvents

Purely ionic salts, also known as fused salts are unique solvents in that they are able to provide purely ionic medium in the absence of water. Thus, these solvents can be used to study the role of ionic bonding between the phosphate head groups of phospholipids and the corresponding interactions resulting from hydrogen bonding in water. [8] Similar to the organic solvents and dry solvents, the fused salt is used to replace water in studies concerning phospholipid bilayers.

Ethylammonium nitrate

Ethylammonium nitrate (EAN) is one of the earliest identified room temperature ionic liquids with a melting point of 12 degrees C. The ionic fluid has been used to study the interactions of distearoylphospatidylcholine (DSPC) and L-dipalmitoylphospatidylcholine (DPPC). [9] The presence of EAN had little effect in the phase transition of DSPC, however in subsequent studies with DPPC in the presence of EAN it has been observed that a subgel to liquid crystalline transition is observed. The subgel transition is unique to the purely ionic solvents. In the interaction of the ionic fluid with the lipids, the acyl chains are disordered, forcing a transformation from the subgel bilayer to a Hexagonal array of cylinders (HII) without passing through L-beta, L-beta', or L-alpha intermediate forms. [9]

Additionally, the acyl chain packing structure (also known as subcells) for DPPC in EAN were found to be larger than the DPPC subcells in water. [8] The implications of these observations in EAN may be that the gel-phase observed in water is characteristic of the water's interaction with the lipid, but not the ionic fluid's; the gel phase may only be a metastable phase. [9] In the case of the presence of the ionic fluid, the larger DPPC subcells may allow for the thermodynamically stable Hexagonal array to be the high-temperature liquid crystalline phase.

The evidence of these phase transitions is shown below in the following differential scanning calorimetry thermogram. In (a) the DPPC in EAN undergoes a transition from L-c to an H-alpha or some non lamellar phase.(b) Initial cooling results in a transition from the non lamellar phase to a gel phase. It is unlikely that during cooling the process would result in the formation of an L-c phase. (c) The reheating results in two phase transitions possibly from the L-c to the L-alpha phase and then from the L-alpha to the Hexagonal array phase.

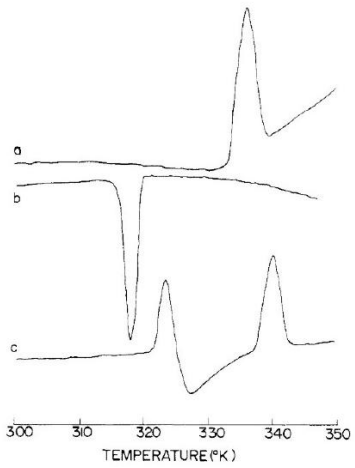


Figure 1.7.5: DSC curves of multilamellar dispersion of DPPC in EAN (a) first heating, (b) cooling (c) reheating [9]

Liquid Crystal Formation

Liquid crystal formation of DSPC in the presence of totally ionic fluid EAN can be viewed by polarizing microscopy. In a 1:1 mixture of DSPC to EAN was micrographed in the range of 57 to 100 degrees C. In this range the micrographs show a texture of oily streaks. Below a measured temperature of 56.7 degrees, the oily streaks take on the appearance of rigid, angular bundles. [9]

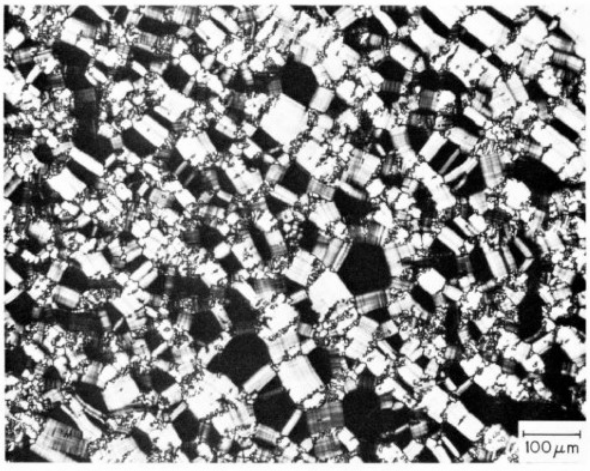


Figure 1.7.6: Micrograph of DSPC - EAN (1:1 mixture), T=57.6 C. Note "oily streak" appearance [9]

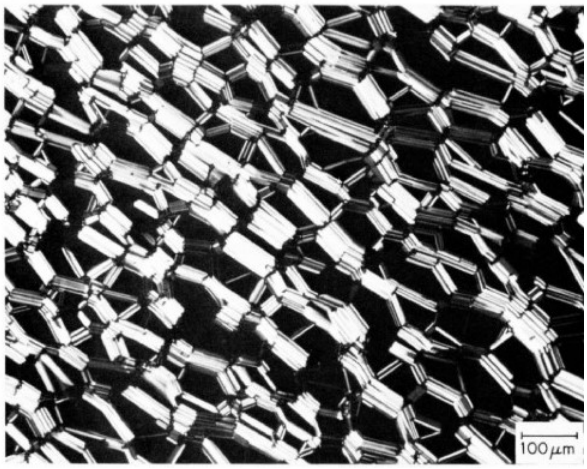


Figure 1.7.7: Micrograph of DSPC - EAN (1:1 mixture), T=56.1 C. Note rigid bundle appearance [9]

The evidence of these two phase transitions are analogous to well-known order-disorder or gel-liquid crystalline transitions that are observed in lecithin-water mixtures. [9]

Summary

The three main classifications of non-aqueous environments with applications to the study of lipids are organic solvents, dry solvents, and purely ionic salts. Each of these environments give insight into the behavior of lipids in the absence of water, providing invaluable information regarding the importance of water on the structure of lipids. Organic solvents are generally used to dissolve lipids. In the case of some solvents, like alcohols, the solvent can replace water in the fluid space between lipids, influencing the interactions and spacing between the lipid bilayers. Dry solvents can come in the form of dry sugars and other molecules. These sugars serve to protect lipid membranes by preventing fusion via hydrogen bond interactions with the hydrophilic headgroups of the phospholipid. Fused salts are used to determine the influence of purely ionic interactions in the the absence of hydrogen bonding. Each of these environments are used to create simple models systems for studying the phase changes, the bilayer structure, thermal behaviors, and interaction forces between bilayers. Practical applications of the study of these environments are numerous, including the preservation of the lipid membranes of cells during drying/rehydrating. [7]

References

1. Lipids | Microbiology. https://courses.lumenlearning.com/mi...hapter/lipids/. Accessed May 15, 2019.

2. Lis, L J;Tamura-Lis W. Structures and Mechanisms of Lipid Phase Transitions in Nonaqueous Media : Dipalmitoylphosphatidylcholine in Fused Salt. 1987;(6):4625-4627. doi:10.1021/j100301a039

3. McDaniel R V., McIntosh TJ, Simon SA. Nonelectrolyte substitution for water in phosphatidylcholine bilayers. *BBA - Biomembr*. 1983;731(1):97-108. doi:10.1016/0005-2736(83)90402-9

4. Simon SA, McIntosh TJ. Interdigitated hydrocarbon chain packing causes the biphasic transition behavior in lipid/alcohol suspensions. *BBA - Biomembr*. 1984;773(1):169-172. doi:10.1016/0005-2736(84)90562-5

5. McIntosh TJ, McDaniel R V., Simon SA. Induction of an interdigitated gel phase in fully hydrated phosphatidylcholine bilayers. *BBA - Biomembr*. 1983;731(1):109-114. doi:10.1016/0005-2736(83)90403-0

6. Crowe, Lois M.;Womersley, Christopher;Crowe, John H.; Reid, David; Appell, Lori; Rudolph A. Prevention of fusion and leakage in freeze-dried liposomes by carbohydrates. *Biochemistry*. 1986;861:131-140.

7. Crowe JH, Crowe LM, Carpenter JF, Wistrom CA. REVIEW ARTICLE Stabilization of dry phospholipid bilayers and proteins by sugars. *Biochem J*. 1987;242:1-10. https://www.ncbi.nlm.nih.gov/pmc/art...00261-0011.pdf.

8. Leary TJC, Levin IW. Effects of solvent on biomembrane structure: Raman spectroscopic investigation of dipalmitoylphosphatidylcholine dispersed in N-ethylammonium nitrate. *J Phys Chem*. 1984;88(18):4074-4078. doi:10.1021/j150662a044

9. Evans DF, Kaler EW, Benton WJ. Liquid crystals in a fused salt: .beta.,.gamma.-distearoylphosphatidylcholine in N-ethylammonium nitrate. *J Phys Chem*. 1983;87(4):533-535. doi:10.1021/j100227a003

1.7: Lipids in Non-Aqueous Environments is shared under a CC BY 4.0 license and was authored, remixed, and/or curated by LibreTexts.

CHAPTER OVERVIEW

2: Membranes - Aggregated Lipids

Biological membranes consist of a phospholipid bilayer with embedded, integral and peripheral proteins used in communication and transportation of chemicals and ions. The bulk of lipid in a cell membrane provides a fluid matrix for proteins to rotate and laterally diffuse for physiological functioning. Proteins are adapted to high membrane fluidity environment of lipid bilayer with the presence of an annular lipid shell, consisting of lipid molecules bound tightly to surface of integral membrane proteins.

2.1: Membrane Fluctuations
2.2: Membrane Asymmetry
2.3: Membrane Curvature
2.4: Membrane Compressibility
2.5: Surface Tension and Line Tension
2.6: Vesicles
2.7: Diffusion in Membranes

2: Membranes - Aggregated Lipids is shared under a CC BY 4.0 license and was authored, remixed, and/or curated by LibreTexts.

2.1: Membrane Fluctuations

In 1972, Singer and Nicolson [1], proposed a fluid mosaic model for the cell membrane, which viewed the entire membrane as a dynamic system constantly in flux. Since then, the dynamics of cell membranes were studied extensively and have shown that the membrane is in even more flux than the fluid mosaic model had claimed. The membrane is inhomogeneous, with some parts changing their position and composition more rapidly than others. Proteins get inserted and reinternalized, rafts form and dissolve, cytoskeleton is remodeled, and the membrane itself changes its thickness and curvature. Together, all of these perturbations are called membrane fluctuations.

Membrane Composition

In order to understand the fluctuations that happen within a membrane, a brief overview of the membrane components is required. The membrane consists of a phospholipid bilayer. This bilayer can be thought of as a sea, in which proteins are floating. Proteins can be inserted in either both or a single layer of the membrane. Also in the membrane, there are sterol molecules, which add rigidity. On the inside, the membrane is supported by a cytoskeletal network, which consists mainly of actin (Figure 2.1.1).

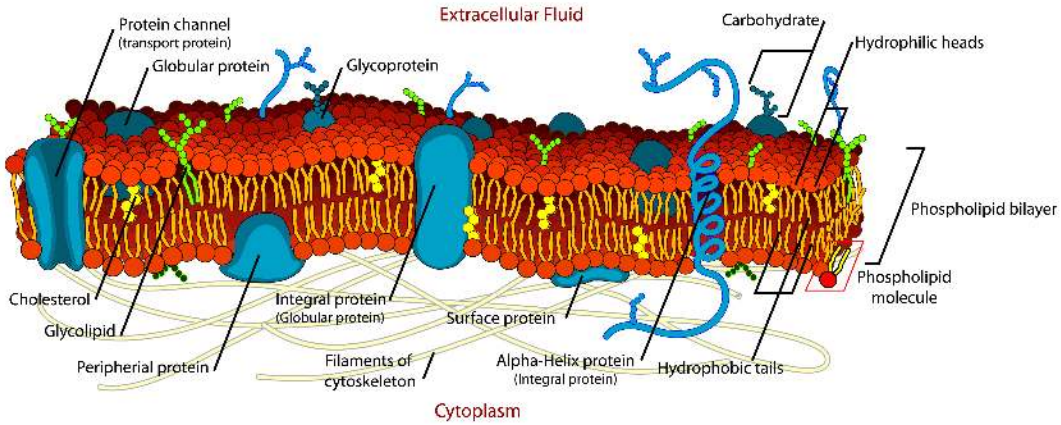


Figure 2.1.1: General organization of cell membrane. (Copyright; author via source)

Lipid Rafts

The membrane is not homogeneous; it is full of rafts, or areas of lipids that are in liquid ordered state, which is more ordered than the surrounding area. These rafts are important for a number of reasons; they are thicker than the lesser ordered membrane, and there are transmembrane proteins that only fit in these thicker rafts [2]. These rafts may act as a means to concentrate proteins to an area of the membrane.

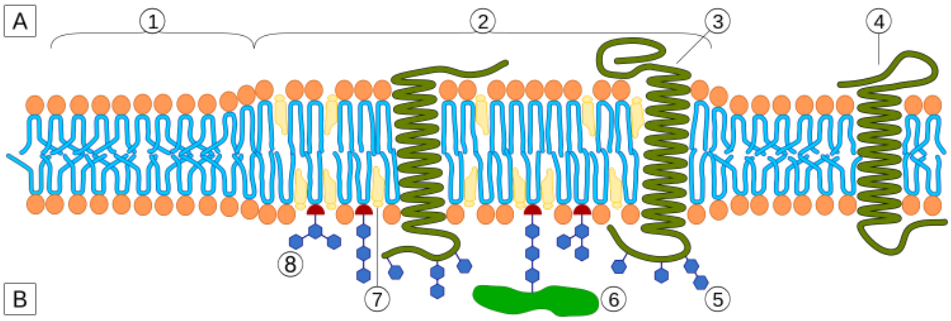


Figure 2.1.2: A representation of a lipid raft. Region 1 is normal bilayer, 2 is raft. 3 and 4 are transmembrane proteins, positioned in and out of the raft, respectively. 5 denotes protein glycosylation, 7 is cholesterol, and 8 is a glycosylated lipid.

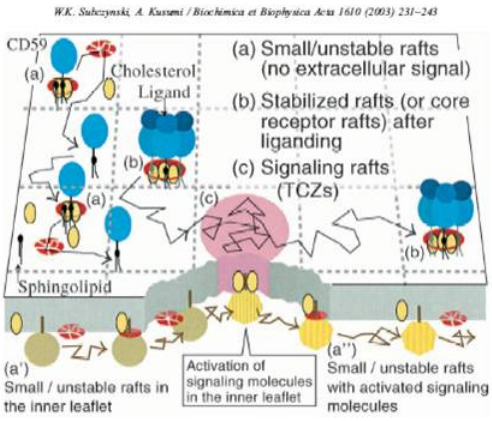


Figure 2.1.3: Diffusion of raft proteins vs non-raft proteins. The patterns are similar, indicating that the rafts are dynamic.

Studies of diffusion rates of raft versus non-raft proteins suggest that the rafts diffuse at a rate similar to that of non-raft transmembrane proteins (Fig 3). This indicates that the rafts are very small, and of similar size to transmembrane proteins.

Proteins

Transmembrane Proteins

There are a multitude of proteins embedded in the membrane. These proteins are continuously recycled, with new proteins being delivered by vesicles. Typically, a transmembrane protein would be synthesized in the rough endoplasmic reticulum (rER) and then transported in a clathrin-coated vesicle to the cell membrane. The vesicle fuses with the membrane, and the proteins become a part of it. Vesicle fusion is a major process of membrane remodeling.

Membrane Remodeling Proteins

There is a number of proteins that can remodel the membrane. One of them is known as BAR (Figure 4) This protein has an inherent curvature, which allows it to sense membrane curvature and induce further curvature by binding. When multiple subunits bind to the membrane, they can cause tubulation.

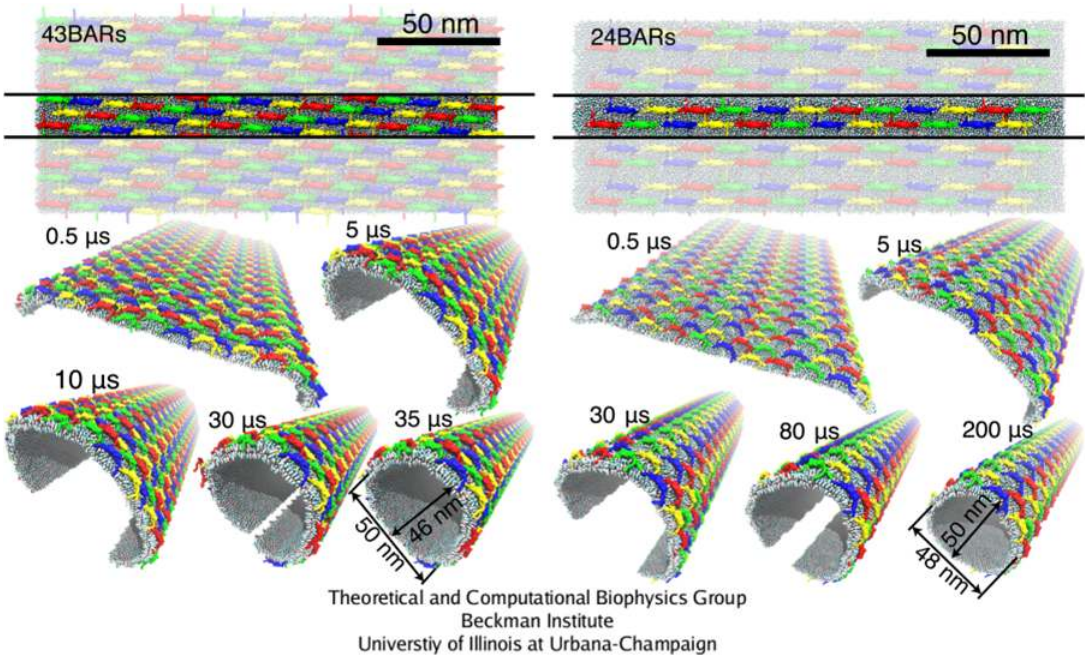


Figure 2.1.4: BAR protein action on membrane. Y. Yin, A. Arkhipov, K. Schulten. Structure, 17,882-892(2009)

Actin Network

The cell membrane is anchored to the cytoskeleton, which mainly consists of actin [3], (Fig.5, 6). Actin in itself is a dynamic polymer that is both depolymerizing and polymerizing, depending on the concentration of monomers. This activity is tightly controlled and is extremely important for mobility, phagocytosis, and most processes that require large scale membrane remodeling. By growing actin in a certain point in the cell, membrane can be made to grow protrusions, which can be used to engulf foreign particles or move.

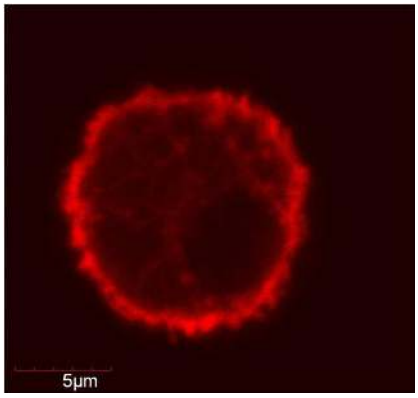


Figure 2.1.5: Confocal image of a BV2 cell. The cell is transfected with an actin-specific RFP-conjugated probe. Note the higher concentration around next to the cell membrane.

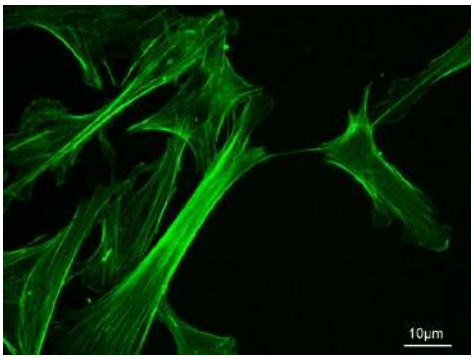


Figure 2.1.6: Fluorescent image of F-actin in rat fibroblasts

Layer to Layer Fluctuations

It is extremely energetically unfavorable for a lipid from one leaflet of the membrane to flip over to the other. However, this is a process necessary for membrane remodeling and it does occur. A group of enzymes, know as flippases, assists this flipping of lipids [4]. A number of flippases have been identified [5], but the mechanism remains unclear.

Protrusions and Bending

Lipids can move laterally within the membrane, or they can protrude from it. If they form a protrusion, it can be detected with neutron scattering (Figure 7) Bending of the membrane has been suggested to be important in clathrin aggregation using computational methods [6].

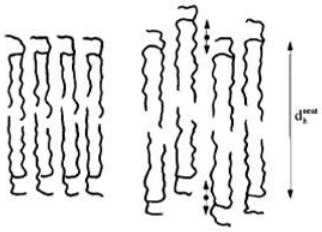


Figure 7. Schematic comparison of bilayer hydrophobic thickness as measured from NMR and neutron diffraction. In the absence of protrusion, NMR (by taking twice the chain length plus one glycerol–ester thickness, see text) and neutron diffraction lead to the same estimate for bilayer thickness. In the presence of protrusion the bilayer thickness as obtained from neutron diffraction is greater than that estimated from NMR.

.

References

1. Singer SJ, Nicolson GL (Feb 1972). "The fluid mosaic model of the structure of cell membranes". *Science* **175** (4023): 720– 31
2. Jérémie Rossy, Yuanqing Ma, Katharina Gaus, "The organisation of the cell membrane: do proteins rule lipids?", Current Opinion in Chemical Biology, Volume 20, June 2014, Pages 54-59, ISSN 1367-5931
3. Mithilesh Mishra, Junqi Huang, Mohan K. Balasubramanian, "The yeast actin cytoskeleton" FEMS Microbiology Reviews Mar 2014, 38 (2) 213-227;
4. Bretscher, MS. (1972). "Asymmetrical lipid bilayer structure for biological membranes." *Nature New Biology* 236:11-12
5. Islam, S. T. and Lam, J. S. (2013), "Wzx flippase-mediated membrane translocation of sugar polymer precursors in bacteria. Environmental Microbiology", 15: 1001–1015
6. Cordella, Nicholas et al. “Membrane Fluctuations Destabilize Clathrin Protein Lattice Order.” *Biophysical Journal* 106.7 (2014): 1476–1488

2.1: Membrane Fluctuations is shared under a CC BY 4.0 license and was authored, remixed, and/or curated by LibreTexts.

2.2: Membrane Asymmetry

The purpose of biological membranes is to create compartments suitable for specific biological functions. Biological membranes include a lipid bilayer which functions as a selective permeable barrier to generate internal environments, as well as proteins which participate in molecular transport, catalysis, signaling, cell-cell recognition and forming junctions, and adherence to extracellular spaces. Biomembranes also carry out critical functions in signal transduction and vesicle (de)formation [1].

An asymmetrical membrane lacks uniformity in molecular composition and distribution, and structurally has a variable degree of leaflet curvature. The degree of asymmetry covers a wide range as asymmetry is any deviation of the 50:50 proportion when comparing two surfaces [2]. Asymmetry can occur on both sides of a biological membrane when the inner and outer leaflet have different molecular architecture. One leaflet shows asymmetry (transverse asymmetry) when the molecular components are not homogeneously distributed. Phase separation is one of the simplest examples of transverse membrane asymmetry (Figure 2.2.1). Lipid rafts are a specific example of membrane asymmetry. They are lateral regions of the bilayer with specific lipid composition that are involved in lipid trafficking and contain proteins participating in various biological functions. The wide variety of lipids, sterols, and membrane-associated proteins evolved correspond to the diverse forms of membrane asymmetry. The loss of physiological membrane asymmetry in cells is deleterious and often results in cell death [18].

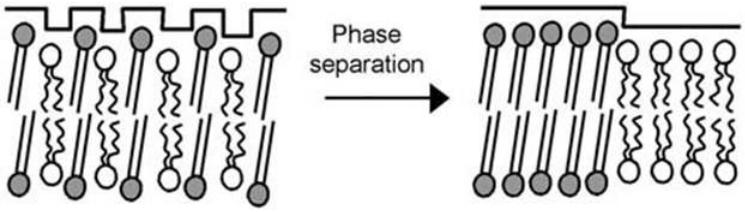


Figure 2.2.1. The different phase transitions of different lipids form the basis of lipid rafts.

This wiki briefly explains the characteristics of the molecular components of membrane bilayers. The contribution of lipids, sterols, and proteins to membrane asymmetry are reflected in specific examples. The last section acknowledges some of the techniques used to assess the presence and degree of membrane asymmetry.

Lipids

Phospholipids

From a historical perspective, lipid asymmetry was first established in the erythrocyte plasma membrane, which has been extensively used as a model for biological membranes [3]. The phospholipid composition in the outer leaflet of the erythrocyte membrane is rich in sphingomyelin and phophatidylcholine (PC). Conversely, the inner leaflet is enriched in phosphatidylethanolamine (PE), phosphatidylinositol (PI), and phosphatidylserine (PS), all of which form more fluid bilayers than the phospholipids of the outer leaflet [8] (Figure 2.2.2). Furthermore, PS and PI of the inner leaflet carry a negative charge that interacts with positively-charged residues near the cytoplasmic end of the transmembrane domain of simgle-pass membrane proteins. In some cases, the same phospholipid species can have different acyl chains compared to the opposite leaflet [4, 18]. Remarkably, translocation of phospholipis to maintain the asymmetry in the lipid bilayer is an active process carried out by flippases and floppases via ATP hydrolysis [18].

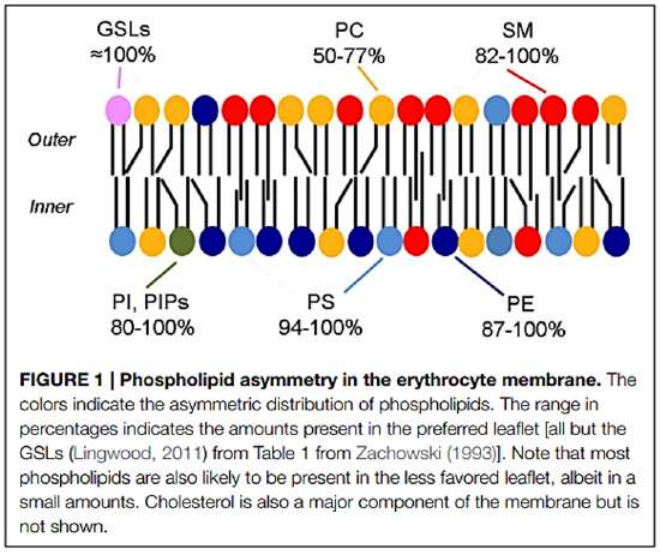


FIGURE 1 | Phospholipid asymmetry in the erythrocyte membrane. The colors indicate the asymmetric distribution of phospholipids. The range in percentages indicates the amounts present in the preferred leaflet [all but the GSLs (Lingwood, 2011) from Table 1 from Zachowski (1993)]. Note that most phospholipids are also likely to be present in the less favored leaflet, albeit in a small amounts. Cholesterol is also a major component of the membrane but is not shown.

Figure 2.2.2. Phospholipid distribution in the leaflets of the membrane in human erythrocytes (From: Fujimoto & Parmryd, Front. Cell Dev. Biol., 4:155, 2017).

Nowadays, it is known that the membrane lipids are responsible for the overall cell shape. The charge and size of the head group as well as the number, length and saturation of the acyl chains are all important factors determining membrane symmetry. For example, large, charged head groups are more likely to form curved structures. On the other hand, uncharged lipids with longer acyl chains and smaller head groups would be less likely to form curved structures (Figure 2.2.3). Thus, local enrichment of specific lipids can induce different curvatures and domains [5]. Lipid molecules tend to group thermodynamically with those that have similar tail length and saturation thus leading to phase separation and domains within the membrane.

Phophatidylserine (PS) on the outer leaflet illustrates the biological importance of maintaining membrane asymmetry. This phospholipid is commonly found in the inner leaflet, but flippases are known to catalyze PS translocation from the inner to the outer leaflet [6]. PS on the extracellular face is known to trigger signaling pathways through activation of ADAM proteins, which cleave transmembrane proteins involved in cell growth and homeostasis. Extracellular PS functions as a tag on apoptotic cells to be phagocyted and participate in platelet activation. A defect in PS translocation to the outer leaflet can result in diseases such as Scott syndrome, where an enzyme, the scramblase, fails to traslocate PS to the outer leaflet as a part of plateler activation [7]. Conversely, Neo1, a P4-ATPase, is a floppase that was recently found to maintain membrane asymmetry translocating PS and phosphatidylethanolamine (PE) to the inner leaflet in yeast [8]. Moreover, translocation of PS to the outer leaflet occurs in erythrocyte adhesion, myotube formation as well as apoptosis, recognition of cells to be phagocyted by macrophages, and malignization of tumor cells [18].

The origin of the lipid asymmetry lays in the organelles of the cell secretory pathway [9]. The endoplasmic reticulum and the Golgi apparatus synthesize and insert the phospholipids specifically in one of the leaflets. Phosphoglycerides, such as phosphatidylcholine, are translocated to the opposite leaflets by flippases and floppases via ATP hydrolysis .

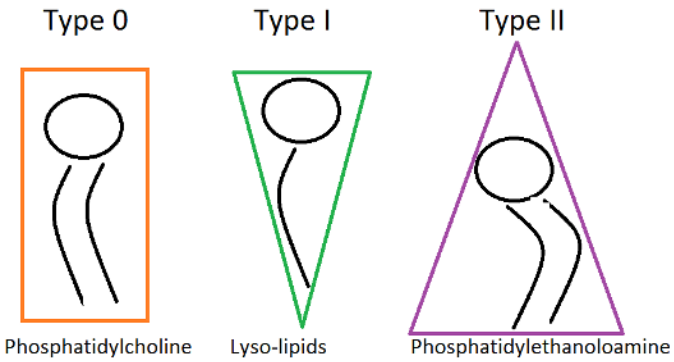


Figure 2.2.3. Intrinsic lipid properties cause zero, positive, or negative curvature, respectively. Lipid types have different phase transitions and preferences of interactions. An example of each type is listed below the representation.

As stated earlier, phospholipids are not the sole reason for membrane asymmetry. Other lipids, carbohydrates and proteins also have a key role in changing the phase and shape of the membrane.

Sterols: Cholesterol

Sterols are four-ring isoprenoid-based hydrocarbons that modulate the fluidity of the lipid bilayers in eukaryotic cells [9]. Among sterols, cholesterol is found in the plasma membrane of animal cells and it is one of the most recently evolved sterols (Figure 2.2.4). Cholesterol is amphypathic given that is mainly hydrophobic, but also has a hydrophilic hydroxil group.

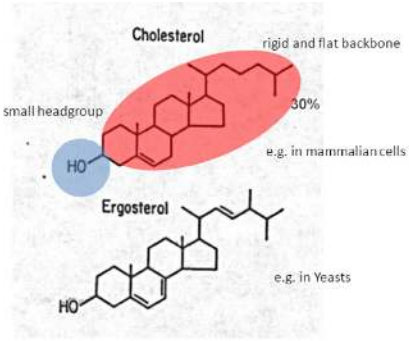


Figure 2.2.4. Examples of sterols in lipid bilayers of eukaryotic cells (supl. ref.)

Cholesterol can be thought of as the moderator of order within the lipid bilayer causing membrane asymmetry. Through its simultaneously bulky head and long tail, cholesterol is able to disorder the gel phase and order the liquid phase of lipids [10]. The presence of cholesterol prevents the phospholipids from being too close to one another, maintaining the membrane fluidity. Likewise, cholesterol provides structural support to the bilayer. The presence of cholesterol buffers the Tm (Transition Temperature) (Figure 2.2.5) [9]. In lipid rafts, which are in gel phase, the polar head group in cholesterol binds to the amide group in sphingomyelin. This bond prevents the formation of H -bonds between water and cholesterol, which would increase disorder. Cholesterol is also able to order the liquid phase in long-chained lipid-saturated phospholipids in membrane domains. Moreover, cholesterol has recently reported to be a factor that inhibits translocation of PS to the outer leaflet in human erythrocytes, presumably by inhibition of PLSCR1 scramblase. Preventing PS translocation to the extracellular face is important to maintain membrane asymmetry regarding phospholipid composition [11].

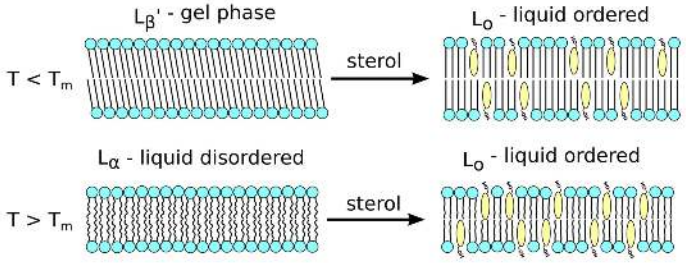


Figure 2.2.5. Sterols are able to modulate the order of lipid bilayers. Both the gel phase and the liquid disordered phase are mediated toward the liquid ordered phase.

The functional role of the membrane proteins and carbohydrates constitute another factor that influences membrane asymmetry. Proteins and carbohydrates tie into the earlier concepts discussed because they interact preferentially with different lipid head groups and tails.

Carbohydrates: Lectins

Carbohydrates are bound to the outer surface of the plasma membrane [3]. This asymmetrical distribution of carbohydrates is related to their functions on the cell surface, such as intercellular adhesion and recognition, and cellular anchorage to the extracellular matrix. Lectins form a group of sugar-binding proteins that participate in cell-cell recognition. Lectins bind to carbohydrates attached to membrane-bound proteins. Glucose, mannose, galactose, N-acetyl galactosamine, sialic acid and fucose are among the most recurrent lectin ligands.

Lipid Rafts

Biological membranes have also lateral asymmetry, evidentially shown by lipid rafts -regions of the outer leaflet involved in specific functions such as lipid trafficking and signaling. The idea of lipid “rafts”, or distinct domains within the membrane, has been proposed as a way to spatially and temporally regulate membrane function [12]. Theoretically, the formation of rafts is thermodynamically favorable. In order to maximize the exclusion of water and increase entropy, acyl chains of similar lengths interact with one another. Similarly, transmembrane (TM) proteins, depending on the length of their TM domain, also preferentially interact with acyl chains of a similar length. The matching of hydrophobic chains and TM domains decreases enthalpy which is even more favorable. The thermodynamic separation of lipids results in phase separations throughout the membrane. The diameter of a lipid raft is 50nm in diameter on average (range: 10-100nm) [4,9].

Lipid rafts are enriched in glycosphingolipids and cholesterol, mainly having saturated acyl chains. As a consequence, lipid rafts are in a liquid-ordered state (Lo), and are thicker than the rest of the bilayer. The uniqueness of the lipid rafts' molecular composition is consistent with their variety of functions [4]. As a matter of fact, polarized cells are known to have specialized domains, like epithelial cells which have apical and basolateral regions. Another example comes from viruses, which only recognize and attach to specific non-random regions in the membrane of the host cells [4]. In addition, only particular membrane domains can participate in cell-cell fusion. Lastly, lipid rafts can be considered as signaling platforms as their proteins are commonly involved in reception and transduction of extracellular signals [9].

Proteins and Membrane Domains

Proteins are asymmetrically distributed across biological membranes according to the different functions carried out in the cytoplasmic and extracellular faces of the membrane [3]. Transmembrane proteins have a specific topology, which is set at the time of their synthesis. As a consequence, the cytoplasmic and extracellular domains can have different structure and function. Most of the extracellular domains of the transmembrane proteins are glycosylated (glycoproteins), and carbohydrates chains are linked to serine, threonine, and asparagine, whereas lipoproteins have lipids attached [9]. Peripheral membrane proteins are anchored to the plasma membrane by electrostatic interactions with either lipids, membrane proteins, or both. In animal cells, a subset of peripheral membrane proteins are linked to the membrane by Glucosyl-phosphatidyl-inositol (GPI) acyl chain on the outer leaflet, and have an important role in signal transduction. In the inner leaflet, membrane proteins are mainly anchored to lipids such as myristic acid, palmitic acid, and prenylated hydrophobic acid chains [3,4].

BAR proteins

Although many proteins are asymmetrically distributed to participate in signaling pathways and catalitic processes, some others have a structural role in maintaining cell shape. Perhaps the best example of protein’s influence on membrane curvature are the Bin-amphiphysin-Rvs (BAR) domain proteins [13]. BAR domains are seen in many important biological context including vesicle and exosome budding. It is no surprise that proteins containing a BAR domain are among the most conserved in biology. BAR domains are banana-shaped dimers that both sense and induce membrane curvature (Figure 2.2.6). They interact with the negatively charged lipids electrostatically with positively charged residues on one side of their surface, leading to the amphipathic nature of these helical domains.

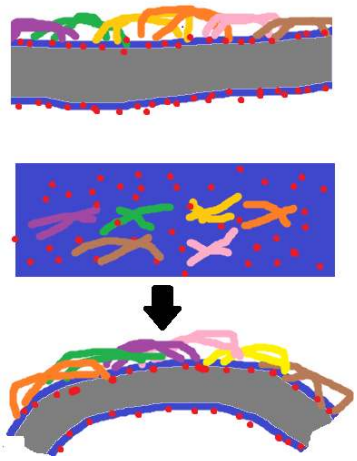


Figure 2.2.6. The effect of the BAR activity is additive. A simulation visualizes 6 BAR domains cooperate over time to bend a lipid bilayer.

The computational study in the Figure above was important because it suggested the additive model was correct. This simulation provided some of the first evidence that BAR domains bind linearly along a membrane and that their effects are cooperative [13].

Amphipathic helices

Membrane spanning proteins have an extremely important role in the spatial arrangement of membranes. Local curvature of membranes can be heavily influenced by helical protein insertion [14]. This is true for both anchored and membrane-spanning proteins. The former are typically amphipathic helices, which means they have both a polar and a non-polar face. Non-polar faces typically embed in the membrane and interact with the hydrophobic acyl chains while the polar surface remains near the phospholipid head groups. This kind of asymmetric insertion induces positive curvature in the membrane (Figure 2.2.7).

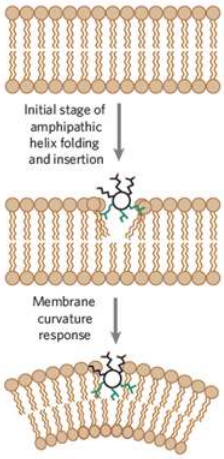


Figure 2.2.7. Example of amphipathic helix anchoring. The hydrophobic face buries into the acyl tails; the polar face remains solvent exposed. H.T. McMahon, J. L. Gallop Nature 438, 590-596 (2005).

One way to study the effects of proteins on membrane curvature is to utilize light microscopy to visualize liposomes or giant lamellar vesicles (GUVs) with and without the presence of protein. With these methods it has been determined that membrane-spanning helices can also manipulate membranes. One common mechanism is by protein oligomerization within the membrane. An example of this membrane manipulation is seen within a specific subdomain of the mitochondrial inner membrane called the cristae junction (CJ). CJs connect the inner boundary membrane to the cristae membranes where oxidative phosphorylation takes place. CJs are highly curved membranes that are responsible for the large surface area of the inner membrane. In fact, Mic10, a subunit of the mitochondrial contact site and cristae organizing system, coordinates the curvature of CJs by oligomerization through its transmembrane helices [15].

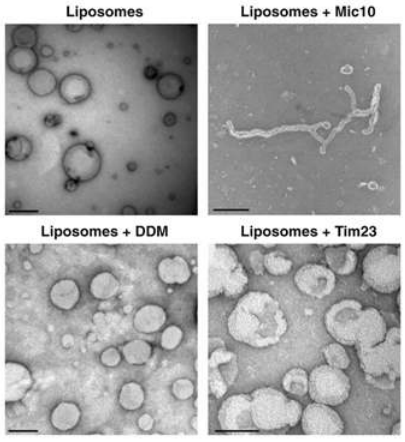


Figure 2.2.8. Mic10 is able to curve lipid bilayers via two glycine-rich motifs. Mic10 is able to cause liposomes to form tubule structures vs the control detergent (DDM) and protein (Tim23). Barbot et al, Cell Metabolism (2015). Copyright © 2015 Elsevier Inc. All rights reserved. This is an unofficial translation of an article that appeared in an Elsevier publication. Elsevier has not endorsed this translation.

Through a glycine-rich oligomerization domain in the transmembrane helices, Mic10 is able to self-assemble and curve membranes (Figure 2.2.8). Deletion of Mic10 has severe consequences in respiration due to loss of membrane surface area.

Manipulating membrane asymmetry

The membranes in live cells are shown to be inherently asymmetric. Membrane models used for in vitro studies have been difficult to produce asymmetrical bilayers as in living cells [16]. Supported lipid bilayer (SLB) methodology was one of the first approaches aiming to manipulate membrane asymmetry. SLB consist on a lipid bilayer extended on a physical support (surface), which can be a solid, a polymer "cushion" or a self-assembled monolayer [17]. Additionally, SLB can be tethered to the surface, freely-suspended, or a solid-supported lipid bilayer can be the support for vesicular layers (Figure 2.2.9). The vesicles are initially placed on the surface, and they rupture after support-induced deformation. Ultimately the bilayers from the broken vesicles coalesce and form the SLB (Figure 2.2.10). Studies with SLB allow to analyze molecular composition, molecular distribution and the curvature of membranes, which are the factors responsible for membrane asymmetry.

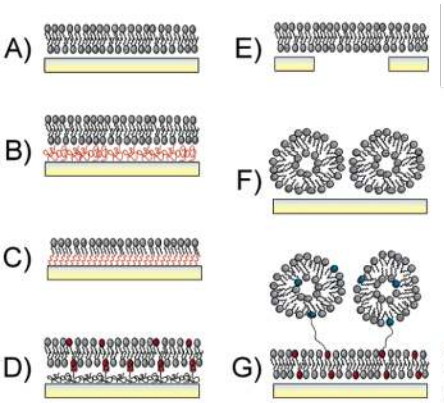


Figure 1. Surface-confined membrane models: (A) solid-supported lipid bilayer; (B) polymer-cushioned lipid bilayer; (C) hybrid bilayer, consisting of a self-assembled monolayer (e.g., thiols on Au or silanes on glass or silica) and a lipid monolayer; (D) tethered lipid bilayer; (E) freely suspended lipid bilayer; (F–G) supported vesicular layers.

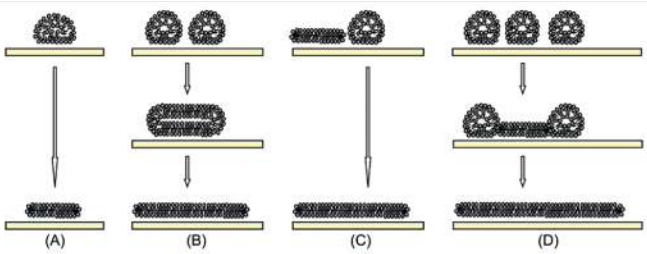


Figure 3. Mechanisms of vesicle rupture: (A) an isolated adsorbed vesicle ruptures spontaneously, driven by its support-induced deformation; (B) neighboring adsorbed vesicles fuse and eventually rupture; (C) the active edge of a supported bilayer patch induces the rupture of a neighboring vesicle; (D) the cooperative action of several neighboring vesicles leads to the rupture of a first vesicle (at the critical vesicular coverage). The active edge thereby exposed triggers the rupture of adjacent vesicles.

Figure 2.2.9. Supported lipid bilayers: Basic types, and Figure 2.2.10. SLB formation (From: Richter et al, Langmuir, Vol. 22 No. 8, 2006).

Issues such as bilayer-support unwanted interactions, and the fact that in some cases the supported bilayer becomes completely immobile, account for the difficulties to control membrane asymmetry [16]. Plus, a substantial part of research with SLBs have used vesicles with symmetrical compositions in both leaflets [18]. There are new ongoing approaches in recent years aiming to specifically manipulate membrane asymmetry. These methodologies include droplet-interface bilayers, inverted emulsion techniques, as well as methyl-beta-cyclodextrin catalyzed exchange. The latter approach basically consists of transporting phospholipids from the outer leaflet of a donor liposomes into the outer leaflet of an acceptor liposome [19]. This method is capable to produce asymmetric liposomes in a wide range of diameters, and is considered an easy method of transferring anionic phospholipids such as PS to an outer leaflet of a lipid bilayer, thus resembling membrane asymmetry of biological membranes. In recent years, it has been possible to conduct quantitative studies in lipid flip/flop rates, giving new possibilities for analysis of molecular composition and distribution of biological membranes [18].

References

1. Brown, D. A., & London, E. (1998). Functions of lipid rafts in biological membranes. *Annual review of cell and developmental biology*, *14*(1), 111-136.
2. Fujimoto, T., & Parmryd, I. (2016). Interleaflet Coupling, Pinning, and Leaflet Asymmetry—Major Players in Plasma Membrane Nanodomain Formation. *Frontiers in cell and developmental biology*, *4*.
3. Stillwell, W. (2013). *An introduction to biological membranes: from bilayers to rafts*. 1e. Academic Press. Elsevier. 367 p.
4. Luckey, M. (2014). *Membrane structural biology: with biochemical and biophysical foundations*. 2e. Cambridge University Press. 411p.
5. Harder, T., Scheiffele, P., Verkade, P., & Simons, K. (1998). Lipid domain structure of the plasma membrane revealed by patching of membrane components. *The Journal of cell biology*, *141*(4), 929-942.
6. Sommer, A., Bhakdi, S., & Reiss, K. (2016). How membrane asymmetry regulates ADAM17 sheddase function. *Cell Cycle*, *15*(22), 2995.

7. Zwaal, R. F., Comfurius, P., & Bevers, E. M. (2004). Scott syndrome, a bleeding disorder caused by defective scrambling of membrane phospholipids. *Biochimica et Biophysica Acta (BBA)-Molecular and Cell Biology of Lipids*, *1636*(2), 119-128.
8. Takar, M., Wu, Y., & Graham, T. R. (2016). The essential Neo1 protein from budding yeast plays a role in establishing aminophospholipid asymmetry of the plasma membrane. *Journal of Biological Chemistry*, *291*(30), 15727-15739.
9. Lodish, H., Berk, A., Kaiser, C., Krieger, M., Bretscher, A., Ploegh, H., Amon, A., Scott, M. (2013). *Molecular cell biology* . 7e. New York: Scientific American Books. 1154p.
10. Bacia, K., Schwille, P., & Kurzchalia, T. (2005). Sterol structure determines the separation of phases and the curvature of the liquid-ordered phase in model membranes. *Proceedings of the National Academy of Sciences of the United States of America*, *102*(9), 3272-3277.
11. Arashiki, N., Saito, M., Koshino, I., Kamata, K., Hale, J., Mohandas, N., ... & Takakuwa, Y. (2016). An unrecognized function of cholesterol: regulating the mechanism controlling membrane phospholipid asymmetry. *Biochemistry*, *55*(25), 3504-3513.
12. Risselada, H. J., & Marrink, S. J. (2008). The molecular face of lipid rafts in model membranes. *Proceedings of the National Academy of Sciences*, *105*(45), 17367-17372.
13. Arkhipov, A., Yin, Y., & Schulten, K. (2008). Four-scale description of membrane sculpting by BAR domains. *Biophysical journal*, *95*(6), 2806-2821.
14. Zimmerberg, J., & Kozlov, M. M. (2006). How proteins produce cellular membrane curvature. *Nature reviews Molecular cell biology*, *7*(1), 9-19.
15. Barbot, M., Jans, D. C., Schulz, C., Denkert, N., Kroppen, B., Hoppert, M., ... & Meinecke, M. (2015). Mic10 oligomerizes to bend mitochondrial inner membranes at cristae junctions. *Cell metabolism*, *21*(5), 756-763.
16. Purdie, J. A., & Sanderson, J. M. (2016). Tuning Membrane Asymmetry. *Biophysical Journal*, *110*(3), 85a.
17. Richter, R. P., Bérat, R., & Brisson, A. R. (2006). Formation of solid-supported lipid bilayers: an integrated view. *Langmuir*, *22*(8), 3497-3505.
18. Marquardt, D., Geier, B., & Pabst, G. (2015). Asymmetric lipid membranes: towards more realistic model systems. *Membranes*, *5*(2), 180-196.
19. Markones, M., Zorzin, C., Kalie, L., Fiedler, S., & Heerklotz, H. (2017). Tuning Membrane Asymmetry: Controlled Uptake of Negatively Charged Lipids into the Outer Leaflet of Liposomes. *Biophysical Journal*, *112*(3), 43a.

Supplementary references:

Faller, R., Lecture: Membrane and lipids fundamentals. In: Membrane Biology, UC Davis. April 11th 2017.

2.2: Membrane Asymmetry is shared under a CC BY 4.0 license and was authored, remixed, and/or curated by LibreTexts.

2.3: Membrane Curvature

There is a large variety of complex shapes of cells and cell organelles found in nature, and understanding functions of the morphology and how it is produced has been an intriguing question and a challenge. For example, cells without internal membranes, such as prokaryotic cells and erythrocytes can take different shapes suited for their purposes. Spirochetes, a type of bacteria, has corkscrew shape which may be an advantage for penetration and packing into host cells while the biconcave disk-like shape of erythrocytes provides the optimal surface-to-volume ratio for the oxygen exchange between haemoglobin and the outside medium [4].

There are significant local differences in membrane curvature even within one single cell with internal membranes giving intercellular organelles a variety of shapes. Plasma membranes, organelle membranes of Golgi, endosome and endoplasmic reticulum (ER), as seen in Figure 2.3.1, all have varied curvature and their membrane curvature regularly goes through dynamic remodeling for their specific functions [1]. The shapes defined by the curvatures of their intercellular membranes of Golgi and ER, for example, maximize the surface area while keeping the internal volume low, which allows efficient and fast protein trafficking in and out of these organelles [4].

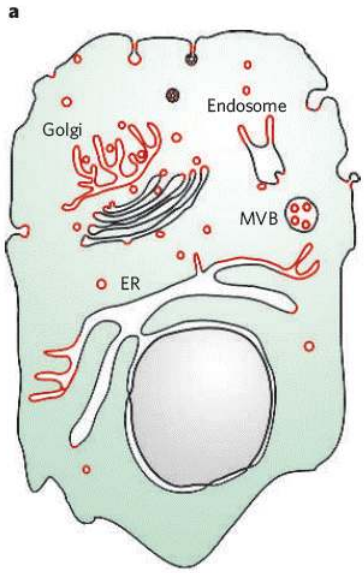


Figure 2.3.1 Local differences in membrane curvature in a cell [1].

Conformation (Curvature and shape) of cellular or intercellular membranes consisting of semi-permeable phospholipid bilayers are actively modulated by the interaction between phospholipids, cholesterols and proteins. It is essential for living organisms to regulate membrane curvatures because this allows cells and organelles take specific shapes that are suitable for their functions, and processes, such as endocytosis and exocytosis depend, which are vital in living organisms, on membrane remodeling to sustain life and malfunction of the regulating system can lead to serious diseases [2, 3].

Definition of curvature

A biological membrane is commonly described as a two-dimensional surfaces, which spans a three-dimensional space. There are two curvatures that characterize the shape of a membrane at each point in space, and mathematically, they are called the principal curvatures and are expressed as c_1 and c_2 [4]. These curvatures are equal to the inverse values of the radii of curvature and Figure 2.3.2 shows how the radii are determined. Two different combinations of the curvatures are used to describe the shape of a membrane. One is as **total curvature**,

$$J = c_1 + c_2 \tag{2.3.1}$$

and the other is **Gaussian curvature**

$$K = c_1 \times c_2. \tag{2.3.2}$$

The basic membrane shapes and the corresponding total curvatures and Gaussian curvatures are indicated in Figure 2.3.3 [4]. Total curvature is a measure in terms of its "curvedness," torsion and direction and takes into account the 2- and 3-dimensional space while the Gaussian curvature is a measure of the "curvedness" a surface displays and is an intrinsic property of a membrane, which means that this measure does not change as long as the surface is not stretched nor compressed [4].

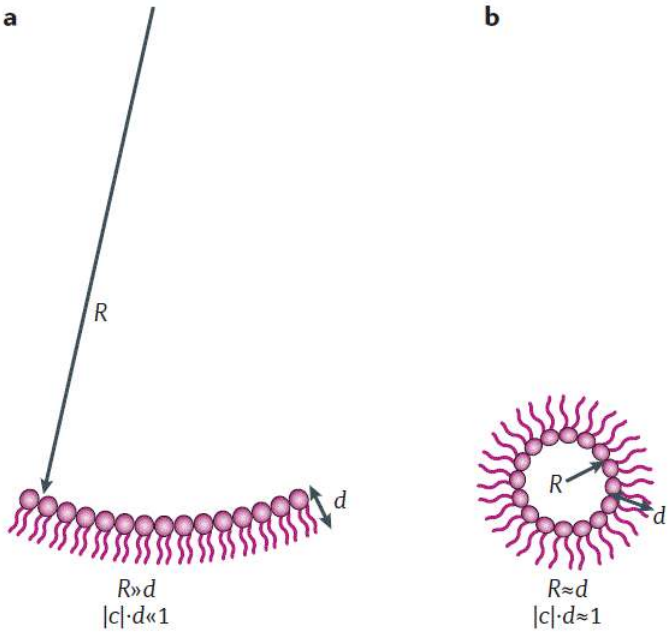


Figure 2.3.2 Determining membrane curvature [4].

As can be seen from Figure 2.3.3, curvatures can be positive or negative. For cellular membranes, positive or negative curvature is determined by curve directionality toward or away relative to the compartment or volume contained by the membrane [1]. Positive curvature builds a sphere while negative curvature is in the opposite direction, like at the neck of a vesicle budding.

The Helfrich theories allows calculation of bending energy required to produce these curvatures using two principal curvature values, c_1 and c_2, spontaneous curvature of a membrane, c_0, and the membrane bending modulus κ_b (Equation 2.3.3) [5]. Spontaneous curvature is intrinsic to lipid types and depending on their chemical compositions and structures, different lipids prefer different curvatures as further mentioned in Section 2. Typical value for bending modulus of a phospholipid membrane is about 10^{-19} J and it can be measured using a technique called micropipette aspiration.

$$E_{bend} = \frac{1}{2}\kappa_b(c_1 + c_2 - c_0)^2 \tag{2.3.3}$$

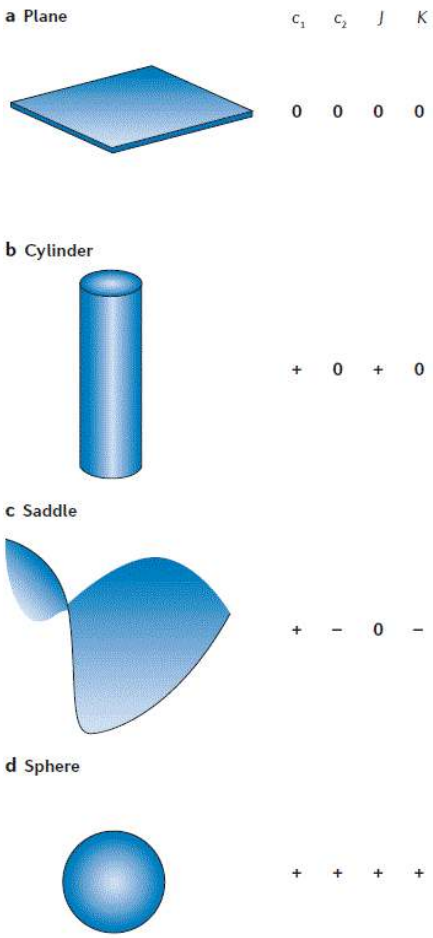


Figure 2.3.3 Basic membrane shapes [4].

Lipid Composition

Although many curvature-generating proteins have larger effects in membrane dynamics, lipid composition influences curvatures because the chemical properties of different lipid acyl chains or head groups favor different membrane curvatures [1]. Based on their preferred curvatures, also referred to as spontaneous curvatures, lipids can be classified into three types: type 0, type I, and type II (Figure 2.3.4). Type 0 lipids such as phosphatidylcholines (DOPC) prefer no curvature and often form flat bilayers. Type I lipids are found in modified forms of DOPC where one fatty acid residue is removed, for example lyso-PC [5]. Their larger head groups relative to their long fatty acid chains lead to cone-shaped structure, inducing positive curvature, and therefore, formation of micelles [5]. Due to their smaller headgroups compared to their wider fatty acid chains, type II lipids such as phosphatidylethanolamine (PE) prefer negative curvature, and often form what is called H_{II}-phase.

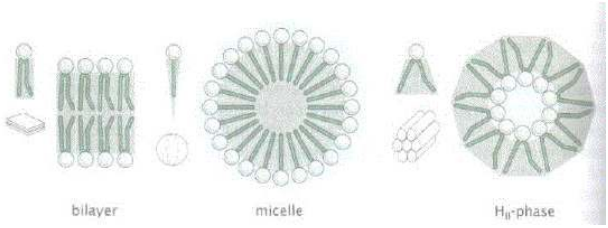


Figure 2.3.4 The shapes of lipid molecules can induce spontaneous curvature on membranes [5].

In membranes with multiple lipid components, lipids can respond to curvature by concentrating in domains of curvature that they prefer [1, 6]. Baumgart et al. used freely suspended giant unilamellar vesicles (GUVs), consisting of ternary mixture of the lipids sphingomyelin, dioleoylphophatidylcholine (DOPC) and cholesterol, to directly observe this correlation between domain composition and local membrane curvature. (Figure5) In there experiments, they observed the lipid membrane of this composition

phase separated into a short-range order phase (L_o), which favored lower curvature suggesting their higher membrane rigidity, and a disordered liquid phase (L_d), which favored higher curvature suggesting their lower membrane rigidity.

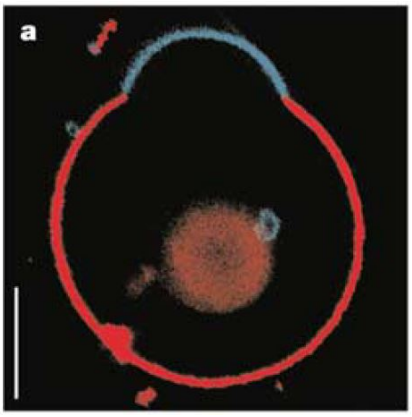


Figure 2.3.5 Structure of multicomponent vesicles [6].

Membrane Proteins

Proteins can generate membrane curvatures either by transporting lipids across the membrane or templating the membrane. Flippase is one protein known to transfer lipids from one leaflet to the other creating membrane asymmetry which leads to membrane curvatures. There are four types of proteins which act as mechanisms for templating membrane curvatures: transmembrane proteins, cytoskeletal proteins and microtubule motor activity, peripheral membrane proteins as scaffolds and amphipathic helices that are inserted into the bilayer [1].

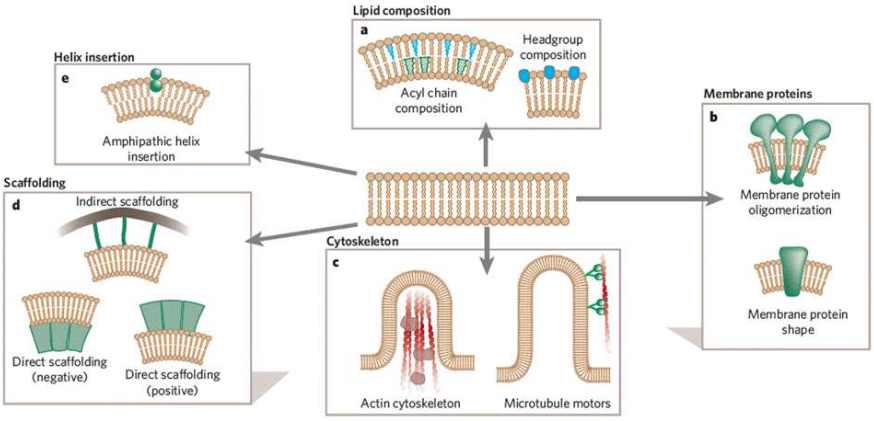


Figure 2.3.6 Mechanisms of membrane deformation [1].

Transmembrane proteins such as ion channels, transporters and receptors that have a conical or inverted conical shape prefer curvatures that mold around their shapes, causing their associated membranes to bend. Extramembrane domains can play a role in generating membrane curvatures when there are not symmetric on both sides of the membranes [7, 8]. The membrane may bend away from the side with the largest extramembrane domain to avoid protein crowding on one side [8]. Transmembrane proteins can also oligomerize and form clusters and scaffold membranes leading to an even greater effect on local curvature [1, 7].

Generation of high membrane curvature structures often involve macroscopic scaffolding by cytoskeletal proteins and microtubule motor activity [7]. The cytoskeleton has a large role in maintaining membrane tension which affects membrane shape by connecting to the bilayer at regular intervals and providing an underlying scaffold [1, 7]. Active membrane pulling or pushing by molecular motors such as kinesins, dynein and myosin also induces membrane reorganization and supports some of the membrane curvatures that shape organelles [7, 9].

Peripheral membrane proteins can interact with membranes in a scaffold-like manner [1]. Dynamin family proteins, including classical dynamin and dynamin-related proteins, play active roles in membrane dynamics to catalyze membrane remodeling, such as in organelle division and vesicle invagination [1, 10]. Commonly, dynamin proteins interact with inositol lipids and self-assemble into oligomers that form helical structures to induce tubular membranes. Interestingly, cryo-EM data has shown that the

yeast dynamin-related protein Dnm1 assembles into distinct helical structures, and *in vitro* liposome assays showed that Dnm1 constricts synthetic membranes [10]. These data further supported the role of this dynamin-related protein in membrane dynamics, in particular, for mitochondrial membrane division [10]. Oligomerized hydrophilic protein domains can generate curvatures through nanoscopic scaffolding. For example, coat proteins such as clathrin, COPI and COPII can influence membrane bending by polymerizing into curved structures. However, these proteins do not have direct associations with membrane and rely on adaptor proteins to link them to membranes [1, 7]. Another example of peripheral membrane scaffolding membranes is through BAR (Bin-Amphiphysin-Rvs) domains which are protein dimerization domains found in many proteins. They are banana-shaped which allow them to preferentially bind to concave membrane surfaces that are negatively-charged and function as a curvature-sensing protein.

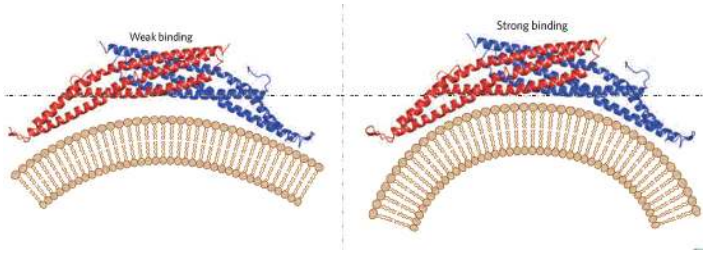


Figure 2.3.7 BAR domain with low-curvature membrane and high-curvature membrane [1].

Proteins with amphipathic helices insert into bilayers to induce positive curvature [1]. Amphipathic helices are alpha helices with a charged, polar side and a hydrophobic side, allowing them to act like wedges to insert into one leaflet of the membrane. Commonly, these helices are not structured until inserted into a membrane where lipid headgroups are displaced and acyl chains are reoriented. For example, epsin is a protein involved in clathrin-coated pit formation in endocytosis that helps to drive membrane curvature by the insertion of its amphipathic helix (Figure 2.3.8) [1].

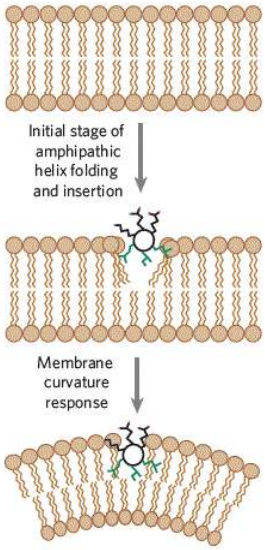


Figure 2.3.8 Amphipathic helices and membrane curvature [1].

Functions of Dynamic Membrane Remodeling

The generation and maintenance of curvature is essential in eukaryotic life as they have trafficking and cellular functions. The formation of high-curvature transport intermediates is necessary for compartmentalization and the characteristic shapes of organelles are maintained by their membrane curvatures as shown in Figure 2.3.1 [7]. These organelles shapes are dynamic constantly going through changes in response to the needs of the cell.

For example, membrane scission, a processes involved in exocytosis and in generation of transport carriers, requires the localized and timely connection in trans of two bilayer membranes to separate an organelle from its membrane of origin. Members of the dynamin superfamily mainly drives membrane scission by oligomerizing at the neck of nascent vesicles and triggering fusion between the two lipid bilayers. This can cause the scission of th eneck and detachment of the vesicle. High local concentrations of hydrophobic insertions at the neck of constricted vesicle carriers supports the fission sf nascent membrane-trafficking vesicles by creating sufficient stress on the bilayer to favor scission in vesicles such as COPII vesicles [7].

References

1. McMahon, H. T.; Gallop, J. L. Membrane curvature and mechanisms of dynamic cell membrane remodeling. *Nature*, **2005**, *438*, 590- 596.
2. Sodt, A.; R. Paster. Molecular modeling of lipid membrane curvature induction by a peptide: More than simply shape. *Biophysical Journal*. **2014**, *106*, 1958-1969.
3. Baumgart, T.; Capraro, B. R.; Zhu, C.; Das, S. L. Thermodynamics and mechanics of membrane curvature generation and sensing by proteins and lipids. *Annu. Rev. Phys. Chem.* **2011**, *62*, 483-506.
4. Zimmerberg, J.; Kozlov, M. M. How proteins produce cellular membrane curvature. *Nature*, **2005**, *7*, 9-19.
5. Phillips, R.; Kondev, J.; Theriot, J.; Garcia, H. G. *Physical Biology of the Cell*, **2013**, Garland Science, Taylor & Francis Group, LLC: Abingdon, UK.
6. Baumgart, T.; Hess, S. T.; Webb, W. W. Imaging coexisting fluid domains in biomembrane models coupling curvature and line tension. *Nature*, **2003**, *425*, 821-824.
7. McMahon, H. T.; Boucrot, E. Membrane curvature at a glance. *J. Cell Sci*. **2015**, *128*, 1065-1070.
8. Copic, A.; Latham, C. F.; Horlbeck, M. A; D'Accangelo, J. G.; Miller, E. A. ER cargo properties specify a requirement for COPII coat rigidity mediated by Sec 13p. *Science*, **2012**, *335*, 1359-1362.
9. Leduc, C.; Campas, O.; Joanny, J. F.; Prost, J.; Basserearu, P. Mechanism of membrane nanotube formation by molecular motors. *Biochim. Biophys. Acta*, **2010**, *1798*, 1418-1426.
10. Mears, J. A.; Lackner, L. L.; Fang, S.; Ingerman, E.; Nunnari, J.; Hinshaw, J. E. Conformational changes in Dnm1 support a contractile mechanism for mitochondrial fission. *Nat. Struct. Mol. Biol.* **2011**, *18*, 20-26.

2.3: Membrane Curvature is shared under a CC BY 4.0 license and was authored, remixed, and/or curated by LibreTexts.

2.4: Membrane Compressibility

Compressibility is a measure of the relative volume change of a substance in response to stress. **Lipid membrane** compressibility has been extensively studied and multiple models developed. Researchers have employed a combination of classic biochemical methods and computational analyses for the purpose of characterizing the elastic nature of mono- and bilayers. Membrane compressibility can also be understood in the context of **biological systems**. It is theorized that cell membranes evolved billions of years ago to provide a barrier between the cell and its surrounding environment. This barrier is elastic by nature, giving it the ability to compress and spread to protect the structural integrity of the cell even in times of mechanical deformation.

For example, under conditions of osmotic stress or during inclusion of proteins, phospholipid bilayers respond by expanding and shrinking. These processes have evolved to effectively preserve vital intercellular, intracellular, and intramembranous biological processes. **Red blood cells (RBC)** were the first cell used as a model system by which to study biological membrane compressibility. Much of the early insights into membrane deformations were gleamed by these studies conducted in the 1970s and 1980s. RBCs continue to be a great model in which to investigate membrane compressibility, due in part to the fact that they contain a variety of biologically important lipid types including Phosphatidic acid (PA), Phosphatidylethanolamine (PE), Phosphatidylcholine (PC), Phosphatidylserine (PS), Phosphatidylinositol (PI), Lysophosphatidylcholine (LPC), and Sphingomycin (SPH).

Membrane Elasticity

Elasticity refers to the ability of a system to reverse a deformation when the deformation is independent of elongation and contraction. In other words, a membrane essentially acts like a rubber band and so to understand membrane compressibility, we study membrane elasticity. The elasticity of a membrane directly determines the possible area per lipid molecule ration that a membrane can have.

Hooke's Law states that the force needed to extend or compress a spring by some distance, X, is proportional to that distance. To some extent, all materials exhibit Hookean behavior when under a small strain or stress. – including biological systems. This is again a simplified way in which to study a biological lipid membrane, but it does prove useful for some applications.

Young's modulus is used to predict how much a material sample will extend under a specific tension or shorten under a specific compression. Therefore, Young's modulus is also known as the tensile modulus or elastic modulus and is the main modulus studied for biological applications (more below). The Young's modulus of small inhomogeneous samples - such as cells and tissues - an be studied using atomic force microscopy (AFM). For example, AFM has been used to determine the Young's modulus of cells, which range from approximately 500 Pa – 100 kPa depending on the cell type. Actin filaments and microtubules have a Young's modulus magnitudes higher – measured at approximately 1 GPa (109 Pa), indicating that actin filaments are exponentially more "stiff" than cell membranes.

Elasticity refers to the ability of a system to reverse a deformation when the deformation is independent of elongation and contraction. Hooke's Law states that the force needed to extend or compress a spring by some distance, X, is proportional to that distance. To some extent, all systems can be thought of in terms of Hooke's Law – including biological systems. This is of course a simplified way in which to study a biological lipid membrane, but it does prove useful for some applications.

Stretching and Shearing of Biological Membranes

Classical elasticity theory is used to investigate energy changes that result from stretching or shearing. When studying fluid phospholipid bilayers, one does not need to account for shear since the lipids are in a "fluid" liquid crystalline state at physiological conditions (with the exception of myelin sheaths that surround neuronal axons). Thus the shear modulus is by definition zero. Instead, we use viscosity as a similar measure.

Stretching, however, is important to understand in relation to biological membranes as it does cost energy and therefore directly affects the structure and potential function of the membrane itself. In the most simplistic form, we can model the energy change (E_{stretch}) for a membrane at zero external stress with an area A_0 that is stretched to a size $A > A_0$ using the following equation:

$$E_{\text{stretch}} = \frac{1}{2} K_{\text{stretch}} \frac{(A - A_0)^2}{A_0}, \tag{2.4.1}$$

where the modulus $K_{stretch}$ is a proportionality constant between a quadratic deviation of the area from its unstressed state and the respective energy.

The lateral stress (Σ) represents the tension in the membrane when it is under such a strain:

$$\Sigma := \frac{\partial E_{stretch}}{\partial A} = K_{stretch}\frac{A - A_0}{A_0} =: K_{stretch}u \tag{2.4.2}$$

where the **dimensionless strain** is defined as

$$u = \frac{A}{A_0} - 1. \tag{2.4.3}$$

Recall Hooke's law mentioned above: stress is proportional to strain. For this application, the constant of proportionality is the stretching modulus $K_{stretch}$. Unlike the elastic area **compressibility modulus** (K_a) (also just called "compressibility modulus"), $K_{stretch}$ can be measured experimentally with relative ease using micropipette experiments to determine area change. Typical $K_{stretch}$ values are around 250 mN/m.

Researchers have used this equation to mathematically determine the rupture strain of biological membranes – and have determined it is only a few percent. This means that, compared to more elastic materials, biological membranes have a low stretch ability – or in other words, they can only stretch a small amount before they will "break" and the cell will burst.

However, some specialized membranes – such as membranes involved in endocytosis and exocytosis - can undergo more extreme deformation. This is to be expected, as these membranes must move large molecular "packages" in and out of cell membrane compartments without resulting in membrane collapse and subsequent cell death.

Mechanical Elastic Moduli of Homogeneous Lipid Layers

As opposed to heterogeneous phospholipid layers, homogeneous bilayers are often characterized using only three mechanical elastic moduli:

1. The area expansion (compression) modulus (K_a)
2. The bending modulus (K_b)
3. Edge energy (Λ) – not described here. See Evans *et al.* 2003 for further reading

Elastic area compressibility modulus

Homogeneous lipid mono- and bilayers can be modeled as two-dimensional structures, and therefore the membrane compression modulus K_a is defined within one plane. The bulk compressibility of a lipid bilayer is reported to be approximately 5.6 x 10^{-7} kPa^{-1}. For comparison, the value for water is 4.5 x 10^{-7} kPa^{-1}.

Studies show that monolayer compressibility is largely dependent on membrane thickness. Bilayer compressibility, on the other hand, is less dependent on thickness. This idea seems counterintuitive and therefore has been studied in depth. The reason for this: bilayers resist expansion mostly to decrease the exposure of their hydrophobic tails to water – which due to the hydrophobic effect is more thermodynamically favorable. Because of this, bilayer compressibility is less dependent on thickness and more dependent on the surrounding solution.

Studies have attempted to quantify the elastic area compressibility (K_a) modulus of one leaflet of a homogeneous lipid bilayer, and the most simple approximation is that it is equal to 2γ, where gamma is the surface tension of the water-lipid interface. With typical gamma values for one leaflet ranging from 20-50mN/m (or J/m2) per leaflet, K_a is approximated to be 80-200mN/m for a lipid bilayer.

Bending modulus

The bending modulus (K_b) is defined as the amount of energy that is required to deform a membrane from its "normal" curvature to a different curvature. We know that a lipid bilayer is composed of two monolayer leaflets, so you can imagine that for one leaflet to be bent, the other must be stretched. Because of this relationship, researchers have observed that as membrane thickness increases, the more each leaflet must deform to accommodate the curvature. The area compression modulus, bending modulus and bilayer thickness (t) have been related using the following equation (Boal *et al.* 2002):

$$K_b = K_a\, t \tag{2.4.4}$$

This relationship, although profoundly simplified, can be extremely useful. If one experimentally determines K_b and t, then K_a can be estimated with ease – acting as a starting point for more accurate measurements. Again, you must keep in mind that this is an

approximation and one that is generally limited to small deformations. However, since most biological membranes can only support a few percent strain before rupturing, this equation has served as a good general model.

To determine the energy of bending for a biological membrane, one can essentially consider a membrane as a two-dimensional surface that bends into a third dimension. Weak bending is a type of deformation that costs significantly less energy than stretching. The bending modulus of a general single elastic sheet (shown here as '*K*') is defined according to:

$$\kappa = \frac{1}{12} K_{stretch} h^2 \tag{2.4.5}$$

where h is membrane thickness; with the bending energy per area written as:

$$e_{bend} = \frac{1}{2} \kappa \frac{1}{R^2} \tag{2.4.6}$$

where R is the radius. Since lipid bilayers are composed of two sheets, one change must be made to the equation for K shown above. The modified relation between stretching and bending modulus is often found in the literature as follows (for two uncoupled sheets):

$$\kappa = \frac{1}{48} K_{stretch} h^2 \tag{2.4.7}$$

This equation allows for the bending modulus to be calculated by directly measuring $K_{stretch}$.

Last, the **Helfrich model** of membrane bending elasticity is used to describe the energy associated with membrane curvature. This model is far more advanced than earlier, more simplistic ones – modeling a lipid monolayer as a three-dimensional elastic layer. Because of this, Helfrich theory has been extensively used in studying the biology of cells, and has proven an excellent tool for quantifying biologically relevant membrane phenomena. For further reading and quantification of this theory, see further readinga.

Studying Unilamellar Vesicles: Adiabatic Volume Compressibility

Adiabatic compressibility is often used to study unilamellar lipid vesicles. The adiabatic (or isentropic) compressibility is the compressibility of a system in which no heat is exchanged with the environment. Adiabatic compressibility is typically used to understand the compressibility in a homogenous system, and becomes simply a function of isothermal compressibility, heat capacity coefficient and volume expansion coefficient – all of which can be determined by the heat capacity of a lipid system.

Because of this, one must ask to what extent the water surrounding a membrane contributes to heat buffering during transient membrane compression. There is some controversy over whether or not heat is exchanged between a lipid membrane and the surrounding water. However, this approach has been successful and therefore many researchers have concluded that heat exchange between membranes and the aqueous environment must be negligible in the megahertz regime.

Studying Lateral Compressibility of Phospholipid Bilayers

Many models have attempted to accurately describe cell membranes and cell membrane deformation. The most widely accepted is the fluid mosaic model, proposed by Singer and Nicolson in 1972. This model looks at biological membranes as two-dimensional fluid-like bilayers in which the lipids can move freely about. However, this is only a starting point.

A more accurate, yet also simplified, model is to look at a cell membrane as a lipid bilayer plus a membrane skeleton composed of two main categories of proteins: those that are partially embedded in the bilayer (**peripheral membrane proteins**) and those that are fully embedded in the bilayer (**integral membrane proteins**). This model incorporates more heterogeneity when performing calculations – which is essential to studying highly heterogeneous phospholipid bilayers.

One of the earlier attempts to characterize phospholipid bilayer deformation was by a study in 1982 (Lis *et al.* 1982). The researchers claim that the deformation of a phospholipid bilayer is highly non-linear, and therefore cannot be described in terms of a simple modulus.

In performing these experiments, researchers have found distinct differences between lipid monolayers, homogeneous lipid bilayers, and phospholipid bilayers. For example, upon compression, monolayers do not undergo a phase transition whereas some bilayers do. For example, the lateral compression of certain lipids (e.g. dilauryl PC and dimyristoyl PC) forces their acyl chains through a "melted" to "frozen" transition at temperatures higher than their T_M.

Current state of this research: many have argued that the lateral compressibility of phospholipid bilayers must be studied experimentally instead of modeled. This is largely because of the heterogeneous nature of phospholipid bilayers found in living systems. These studies continue today, and probably will for a while to come – as phospholipid systems are not only complex, but can also be unpredictable and even technically difficult to study in their natural (not reconstituted) environment.

Therefore, additional studies must be conducted to better understand lateral compressibility on critical cellular processes such as:

- membrane assembly
- mobility and segregation of membrane components
- enzyme-mediated membrane permeability
- incorporation of proteins or drugs into the membrane

Factors Affecting Compressibility in Biological Systems

Temperature

Most phospholipid bilayers exist in a liquid-crystalline state near physiological temperature, but will undergo a phase transition from a liquid-crystalline state to the gel phase as it approaches its melting temperature (T_m). This transition takes place when temperatures are lowered. Studies have shown that during the phase transition, lateral area of the membrane decreases by approximately 25%.

Pressure

Interestingly, compressing a biological membrane under otherwise physiological conditions can induce phase transition. Thus, an increase in pressure mimics the effects of a decrease in temperature. This relationship is modeled using the Clausius-Clapeyron equation:

$$\frac{dT_m}{dp} = \frac{T_m \Delta V}{\Delta H} \tag{2.4.8}$$

Thus the pressure raises the T_M without affecting ΔV or ΔH. However, due to their heterogeneous nature biological membranes do not often undergo phase transitions. Instead the effects of pressure are confined to ordering the bilayer. Because of this increase, when pressure is applied to a phospholipid bilayer, it can result in the membrane releasing some of their peripheral and/or integral membrane proteins.

Lipid Tail Length and Saturation

Studies have shown that the membrane compression modulus (K_a) varies with tail length and unsaturation.

Solution Type

Because membrane stretching and compression exposes hydrophilic phospholipid tales to the aqueous environment, K_a of lipid bilayers varies strongly with solution conditions.

Membrane Composition

Since biological membranes consist of lipids, proteins, cholesterols, and other molecules, they cannot be characterized in the same manner in which unilamellar vesicles or even homogeneous monolayers can be understood. The compressibility of bilayers is directly dependent on their composition – such as presence of cholesterol or presence of double bonds. For example, the area compressibility modulus (K_A) of a membrane increases as the percent cholesterol increases. Additionally, proteins can induce curvature in membranes by transporting lipids or by embedding themselves into the bilayer.

Molecular packing

As membranes cool, they lose fluidity. This results in the acyl groups fully extending and the head groups packing tightly and dehydrating. In respect to hydration, another study in 1985 determined the effects of hydration on egg and dioleoyl lecithin and found that at low hydrations, the head groups are much less tightly packed compared to those more hydrated (White *et al.* 1985). This is assumed to be due to osmotic pressure driving the head groups apart.

Tools are used to study membrane compressibility?

It is difficult to experimentally determine the compression modulus of a phospholipid bilayer. Therefore, one method often employed is to measure how vesicles swell in response to osmotic stress. However, this is an indirect and sometimes inaccurate

method due to polydispersity in vesicle size.

A more direct method of measuring K_a is the pipette aspiration method. This too can pose issues, as biological membranes are thin and fragile by nature and are difficult to study in this capacity without the cell dying. However, much important information has been gleamed using this method. Put in simple terms, this assay is essentially one where the researchers sucks part of a membrane up into a pipette, measures the length that is sucked into the pipette, then calculates the change in area to determine the elasticity of that particular membrane.

Atomic force microscopy (AFM) – also mentioned briefly above - has also been used to directly measure mechanical properties of bilayers, but this method is still under development. Because of these difficulties, the compression modulus is often calculated using the values of its determining characteristics.

Additional methods and techniques used to study lipid mechanics include (but are not limited to):

1. Single molecule tracking (fluorescent or radiolabeled probes): to asses the movement of lipids under certain conditions
2. ^{2}H-NMR: to determine bilayer dimensions
3. Langmuir Trough: to measure area per lipid
4. NEMD method: membrane area change
5. Phase contrast microscopy
6. Differential scanning calorimetry: to measure exotherms during a liquid crystalline to gel phase transition and endotherms during the reverse.
7. Fourier transform infrared spectroscopy (FTIR): lipid phase transitions
8. X-ray diffraction: to determine area per lipid as a function of water activity for different lipids (molecular packing)
9. Optical microscopy: to measure the volume of a bilayer during pressurization
10. Neutron diffraction: to determine molecular packing

Applications of Membrane Compressibility

Ion movement

When an ion penetrates a membrane, a very slight shape change takes place and thus has a corresponding energy cost – known as the **membrane deformation energy**

$$\Delta G_{\text{mem}} = \frac{1}{2}\int_{\Omega}\left[\frac{K_a}{L_0^2}(u^- - u^+)^2 + \frac{K_c}{2}\left(\left(\nabla^2 u^-\right)^2 + \left(\nabla^2 u^+\right)^2\right) + \frac{\alpha}{2}\left(\left(\nabla u^-\right)^2 + \left(\nabla u^+\right)^2\right)\right]\mathrm{d}x\mathrm{d}y \tag{2.4.9}$$

where u^+ is the shape of the upper leaflet and u^- the lower leaflet; L_0 the equilibrium thickness of the membrane; K_a the compression modulus; K_c the membrane bending modulus; and α the surface tension. Furthermore, this equation in combination with a domain of interest, X, ranging from position x-y, and with respect to variations in u+ and u^-, can be additionally used as a tool to determine the shapes of each leaflet.

Protein and small molecule movement

The values of K_a and K_b affect the ability of proteins and small molecules to insert into the phospholipid bilayer. The reverse is also true: bilayer mechanical properties have been demonstrated to affect the function of mechanically activated ion channels.

Ordering effects of pressure on cell structures

The ordering effects of pressure were discussed earlier. Examples of this include the rat liver mitochondria, human erythrocytes, and fish synaptic and brain myelin vesicles in which the ordering effect of pressure can be determined by measuring the increase in temperature required to offset the pressure. These values have been determined to be approximately 0.13 – 0.21 °C mPa^{-1}.

Effects of high pressure on cells

Cells are often exposed to hydrostatic pressure. This affects numerous cellular processes and reactions – albeit in a reversible manner. For example, the cytoplasm of eukaryotic cells can be reversibly “liquefied” under conditions of high pressure. Additionally, studies on amphibian epithelia have shown that changes in pressure can affect the passive permeability of sodium through the cell membrane.

References

1. Boal, D. *Mechanics of the Cell*. Cambridge, UK: Cambridge University Press. 2002
2. Campelo, F. et al. Helfrich model of membrane bending: From Gibbs theory of liquid interfaces to membranes as thick anisotropic elastic layers. 28: 25–33, 2014
3. Deserno, Markus. *Fluid Lipid Membranes – A Primer*. Max-Planck-Institut fu¨r Polymerforschung. Mainz, Germany. 2006
4. Determining the elastic modulus of biological samples using atomic force microscopy. Product Application Note.JPK Instruments. www.jpk.com.
5. Evans, E. *et al.* Dynamic tension spectroscopy and strength of biomembranes. *Biophysical Journal.* 85, pp.2342-2350, 2003
6. Hallett, FR. et al. Mechanical properties of vesicles: II A model for osmotic swelling and lysis. *Biophysical Journal.* 64. (1993) 435-442.
7. Heimburg, Thomas. *Thermal Biophysics of Membranes*. Wiley-VCh, Germany. 2007
8. Koenig, BW. et al. Membrane Lateral Compressibility Determined by NMR and X-Ray Diffraction: Effect of Acyl Chain Polyunsaturation. *Biophysical Journal*. 73: pp. 1954-1966, 1997
9. Latorraca, NR. et al. Continuum Approaches to Understanding Ion and Peptide Interactions with the Membrane. *J Memb Biol*. 22 Feb 2014.
10. Lis, LJ. et al. Measurement of the Lateral Compressibility of Several Phospholipid Bilayers. *Biophysical Journal.* Volume 37. March 1982. 667-672.
11. Nagle, JF. and Scott, HL. Lateral compressibility of lipid mono- and bilayers. Theory of membrane permeability. *Biochim Biophys Acta*. 513(2): 236-43, 1978
12. Rutkowski, CA. et al. The elasticity of synthetic phospholipid vesicles obtained by photon correlation spectroscopy. *Biochemistry.* 30: 5688-5696, 1991
13. Sperelaki, Nicholas. *Cell Physiology Source Book: Essentials of Membrane Biophysics.* Academic Press. London, UK. 2001
14. Waheed, Q. and Edholm, O. Undulation contributions to the area compressibility in lipid bilayer simulations. *Biophys J.* 97(10): 2754-2760, 2009
15. White, SH. and King, GI. Molecular packing and area compressibility of lipid bilayers. *Biophysics.* Vol. 82, pp.6532-6536, 1985

Contributors and Attributions

- Trisha Pfluger (University of California, Davis)

2.4: Membrane Compressibility is shared under a CC BY 4.0 license and was authored, remixed, and/or curated by LibreTexts.

2.5: Surface Tension and Line Tension

Cell membranes are composed of phospholipids (most abundant), proteins, and glycolipids (Figure 1)[1,2]. Generally, phospholipids in cell membranes will aggregate together in order to maximize hydrophobic interactions among their tails and hydrophilic interactions among their heads. Any in-plane stretching of cell membrane will disrupt the interaction between phospholipids. However, in-plane membrane tension (T_m), which is the force needed to stretch the membrane, will counteract any membrane deformation[3]. T_m, which seems to be constant across the whole cell membrane[4], depends on lipid composition and surface area of the cell membrane. Without changing the amount of lipid, increasing the surface area of cell membrane will increase membrane tension[5]. For example, cells will swell when they are in a hypotonic environment. Cell swelling will cause an increase in cell membrane surface area without changing the the amount of lipid in the membrane. In addition, cell membranes are connected to a cross-linked actin network named the cortex[6]. The cortex is demonstrated as a purple mesh under the membrane in Figure 1. Actin cytoskeleton supports cell membrane and helps cells maintain their shape[6]. Membrane surface tension, which consist of T_m and membrane-cytoskeleton adhesion, is the cohesive force that keep cell membranes intact. In order to deform cell membrane, you need to overcome both T_m and membrane-cytoskeleton adhesion[3,4]. Membrane surface tension helps cell maintain a small surface area.

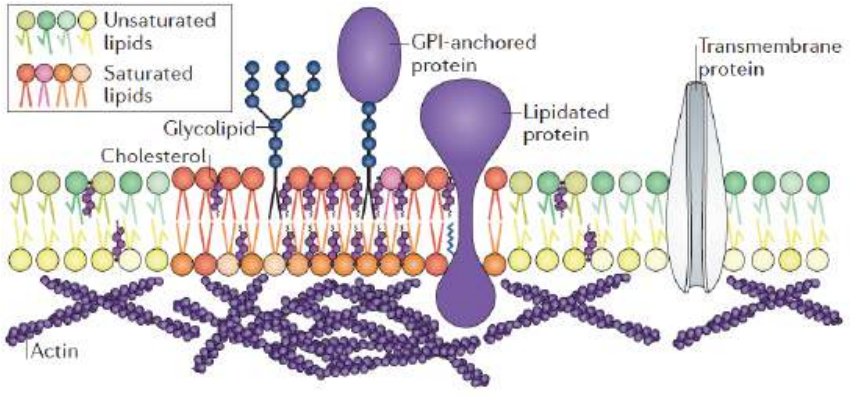


Figure 2.5.1: Cell membrane composition. Image adapted from reference 2.

As shown in Figure 1, cell membranes consist of various types of lipid (e. g. cholesterol, saturated/unsaturated phospholipids, and glycosylated lipids)[2]. Interactions between lipids in the membrane lead to formation of ordered membrane regions that recruit other lipids and proteins[2]. Consequently, there is a wide variety membrane domains with different molecular composition and properties[7]. In addition, lateral segregation of lipids leads to phase separations within cell membranes. Phase separation within cell membrane depends on temperature, pressure, and structural properties (e. g. hydrocarbon tails length or degrees of unsaturation, and the composition of the head group) of various lipid within the membrane[1]. For more info, refer to the wiki pages for Phase Coexistence and Membrane Phase Transitions. At the edge of membrane domains or at the lipid phase separations, phospholipid height mismatch and steric interactions have an energetic cost that depends on the length of the phase/domain boundary[8]. Line tension is the interfacial energy at the edge of membrane domain or at the lipid phase separation in cell membrane[9]. In order to minimize line tension, membrane domains tend to assume circular shapes (Figure 2)[9]. The free energy penalty associated with the line tension is compensated by the decrease in free energy due to membrane domain formations. Membrane tension plays important role in many biological processes, such as cell motility, endocytosis/exocytosis, and viral infection. Many techniques, such as atomic force microscopy (AFM) and micropipette aspiration, are used to study membrane tension.



Figure 2.5.2: Atomic force microscopy images of phase-separated lipid membranes with different lipid compositions. Image adapted form reference 9.

Biological Relevance

Membrane Tension and Cell Movement

Cell motility involves continuous cycles of protrusion, adhesion, and contraction of the cell membrane[10]. Actin-polymerization-mediated protrusion of cell membrane called lamellipodia influence the direction of migration. In the region of cell with low membrane tension, multiple lamellipodia that point in different directions coexist (Figure 3, left)[11]. As a result, cell migration in any particular direction is not favored. Cells can migrate toward a particular direction by increasing the membrane tension at a specific region of the membrane. Increasing the membrane tension will decrease the number of lamellipodia (Figure 3, right)[11]. Cells tend to migrate in the direction with fewer lamellipodia[11].

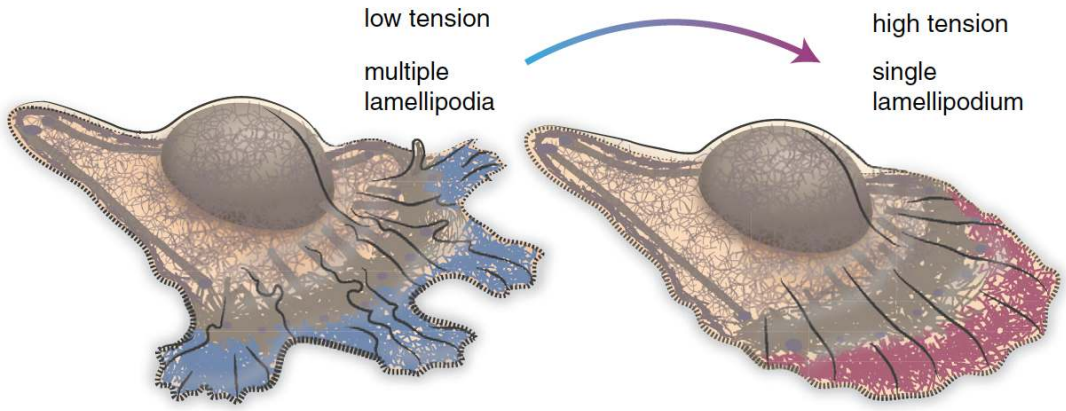


Figure 2.5.3: Membrane tension influences the formation of lamellipodia. Image adapted from reference 11.

Membrane Tension and Endocytosis/Exocytosis

Endocytosis involves formation of cell membrane invaginations, which eventually detach from cell membrane and form vesicles[12]. Increasing membrane tension or membrane-cytoskeleton adhesion will hinder both invagination and neck formation step (**Figure 4**)[12]. Both steps involves membrane deformation.

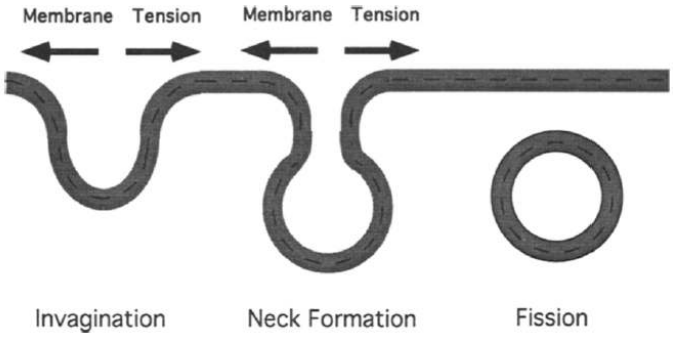


Figure 2.5.4: High membrane tension hinder endocytosis. Image adapted from reference 12.

Exocytosis involves vesicles docking to cell membrane and fuse with it[12]. Unlike endocytosis, increasing membrane tension will favor vesicle and membrane fusion (**Figure 5**)[12]. Unlike endocytosis, exocytosis requires minimal membrane deformation.

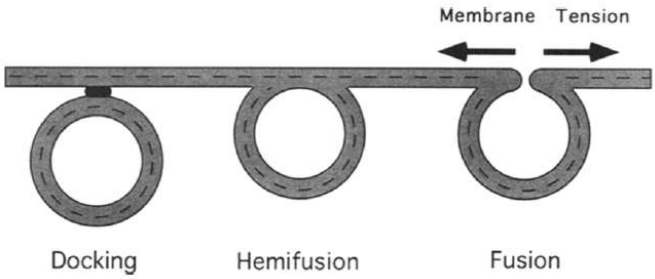


Figure 2.5.5: High membrane tension favors exocytosis. Image adapted from reference 12.

Membrane Tension and Viral Infections

Polyomaviruses (e. g. Simian virus 40 (SV40), Murine polyomavirus, and BK virus) are nonenveloped DNA viruses[13]. Capsid protein VP1[13], a main component of polyomavirus capsid, allows polyomaviruses to overcome membrane tension and infect cells. VP1 binds to glycosphingolipids on cell surface.[13] Different types of virus will bind to different types of glycosphingolipids[13]. For example, VP1 from SV40 binds to GM1 glycosphingolipid[13]. VP1 binding to GM1 reduces membrane tension by triggering actin cytoskeleton breakdown[13]. As a result, an invagination of cell membrane is formed, which eventually lead to the endocytosis of the virus[13]. SV40 endocytosis is shown in Figure 6.

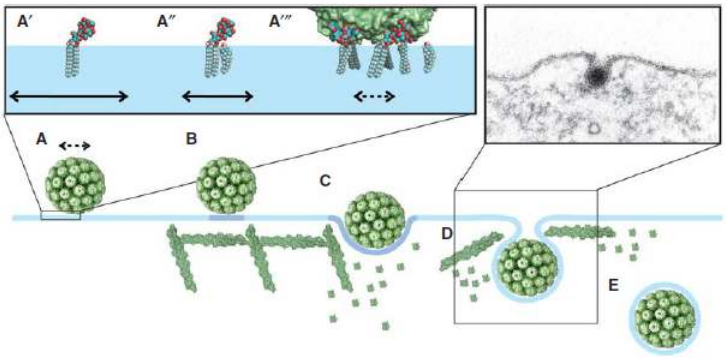


Figure 2.5.6: Simian virus 40 infect cell by triggering the breakdown of actin cytoskeleton. Image adapted from reference 13.

Methods Used to Study Membrane Tension and Line Tension

Methods Used to Measure Surface Tension:

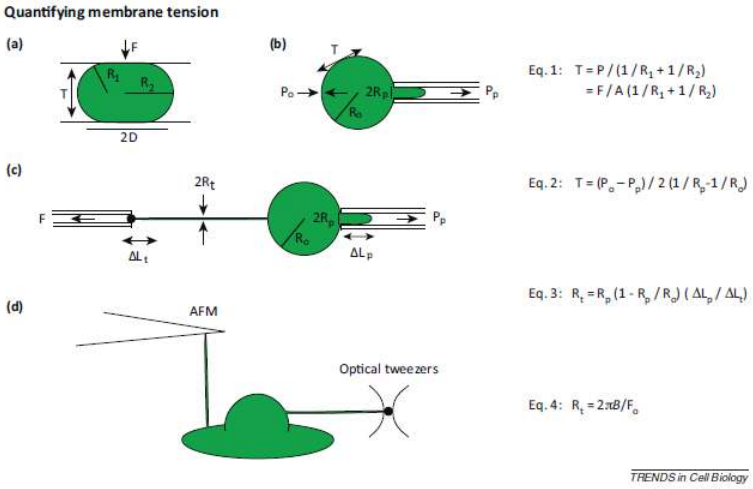


Figure 2.5.7: Common methods used to measure membrane tension. (a) Parallel plate confinement. (b) Micropipette aspiration. (c) Membrane tether extraction with micropipette. (d) Membrane tether extraction with AFM and optical tweezers. Image adapted from reference 3.

Common methods used to measure membrane tension is shown in Figure 7. One assay for measuring membrane tension is parallel plate confinement assay. In this assay, cells are compressed between two parallel plates. The radii of the principal curvatures of the membrane are measured[3]. Since the amount of force used to compress the cell is known, you can calculate the membrane tension with the equation shown in Figure 7 (Eq.1)[3]. Another method of measuring membrane tension is micropipette aspiration. For this method, a small section of the cell membrane is pulled using a micropipette, and the membrane tension is calculated from the cell radius, micropipette tip radius, extracellular pressure, and the suction pressure (Figure 7b, Equation 2)[3]. Micropipette aspiration can also be used to measure membrane tension from membrane tethers. Since membrane tethers lack continuous cytoskeleton, membrane-cytoskeleton adhesion will have very little (if any) contribution to the membrane tension measured[3]. Generally, cells are hold in place with a micropipette, and then tethers can be extracted from the cell membrane (Figure 7c, Equation 3)[3]. Other methods of tether extraction include atomic force microscopy (AFM) and optical tweezers (Figure 7d)[3]. The cantilever used in AFM can also be used to extract a membrane tether[3]. To extract membrane tether, optical tweezers can be used to pull on a uncoated polystyrene bead that was attached to the cell membrane[14].

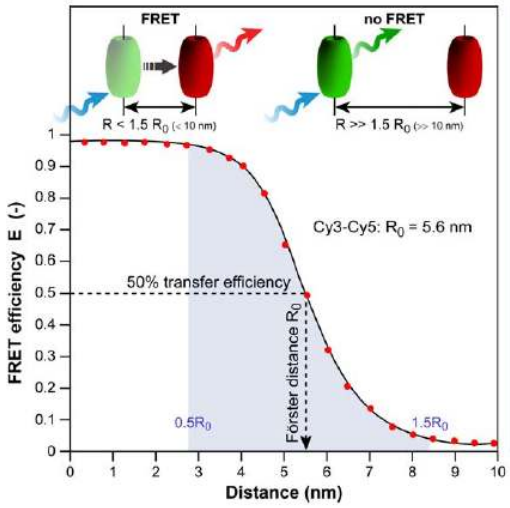


Figure 2.5.8: FRET between donor fluorophore (green) and acceptor fluorophore (red). FRET efficiency decreases as distance between the two fluorophores increases. Image adapted from reference 15.

Fluorescence resonance energy transfer (FRET) refers to the distance-dependent transfer of energy from one fluorophore to another fluorophore (**Figure 8**)[15]. For a more detail explanation of FRET refer to reference 15. Typical FRET experiment involves a pair of flourophores called a FRET pair (a donor fluorophore and an acceptor flourophore). Fluorescence emission spectra of the donor fluorophore must overlap with the fluorescence absorption spectra of the acceptor fluorophore. In practice, only the donor flourophore will be excited. Generally, the florescence intensity ratio of acceptor fluorophore to donor fluorophore is measured. The distance between the donor and acceptor fluorophores affects the FRET efficiency. FRET efficiency increases as the distance between the two fluorophores decreases. Grashoff et al. developed a FRET-base biosensor for membrane tension[16]. A brief description of the method used in reference 16 is presented here. The biosensor consists of a tension sensor module in-between two halves (Vh and Vt) of vinculin, a membrane-cytoskeletal protein (**Figure 9c**). The tension sensor module consists of two fluorophores, mTFP1 and venus(A206K), linked together by a spider silk protein flagelliform linker sequence, $(GPGGA)_8$ (**Figure 9a**). The linker acts as a spring that holds the FRET pair, mTFP1 and venus(A206K), together. Vh and Vt help localized the biosensor to the cell membrane. Once cells are transfected with this biosensor, you can measure the membrane tension by measuring FRET efficiency. As the membrane tension increases, the FRET efficiency decreases because the distance between the two fluorophores increases (**Figure 9b**). In order to convert FRET efficiency to force, you need to construct a calibration curve (FRET efficiency vs Force). Grashoff et al. attached a similar FRET-base biosensor to a polymer-coated glass surface and a microsphere. They can apply force to the sensor by pulling on the microsphere with an optical tweezer. They then construct the calibration curve by measuring the change in FRET efficiency in response to the amount of force applied to the sensor.

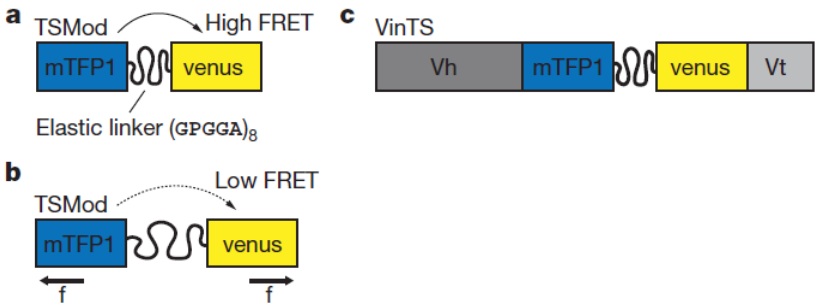


Figure 2.5.9: FRET-base biosensor for membrane tension. (a) Tension sensor module. (b) An increase in distance between the two fluorophores due to an increase in-plane membrane leads to a decrease in FRET. (c) FRET-base biosensor for membrane tension. Image adapted from reference 16.

Calculating Line Tension from Domain Nucleation Rate

Blanchette et al. developed a way to calculate line tension from nucleation rate of membrane domain[17]. A summary of the method used in reference 17 is presented here. First, supported lipid bilayers are heated to 55℃ and then cool down slowly until domain nucleation occurs. Domain nucleation events can be imaged with AFM. Next, lipid bilayers are heated slowly until membrane domains disappear. Averaging the nucleation and melting temperatures will give you the liquidus or miscibility temperature (T_{trans})

for liquid-solid and liquid-liquid phase coexistence, respectively[18]. Then, lipid bilayers are kept 5 ℃ above phase transition temperature. After the lipid bilayers are homogenized, they are rapidly cool down to various temperatures below T_{trans}. During the cooling process, domain nucleation events are imaged with AFM. The line tension (γ) is calculated by fitting the nucleation rate (J) vs $1/T\Delta T$ curve with equation 1 for symmetrical domain nucleation, which occurs on both side of the membrane, and equation 2 for asymmetrical domain nucleation, which only occurs on one side of the membrane.

$$J = A \exp\left(\frac{-\pi\gamma^2 a_g T_{trans}}{2k_B \Delta H} \times \frac{1}{T\Delta T}\right) \tag{1}$$

$$J = A \exp\left(\frac{-\pi\gamma^2 a_g T_{trans}}{k_B \Delta H} \times \frac{1}{T\Delta T}\right) \tag{2}$$

J (obtained with AFM) is number of nuclei that form per unit area per unit time. The molar area of the gel phase, a_g, and the enthalpy of the phase transition, ΔH, depend on the lipid composition of the lipid bilayer. T is the temperature, and ΔT is $T_{trans} - T$. A is a pre-exponential factor[18].

References

1. Kranenburg, M. & Smit, B. Phase Behavior of Model Lipid Bilayers. *J. Phys. Chem. B* **109**, 6553-6563 (2005).
2. Sezgin, E., Levental, I., Mayor, S. & Eggeling, C. The mystery of membrane organization: composition, regulation and roles of lipid rafts. *Nat. Rev. Mol. Cell. Biol.* (2017).
3. Diz-Muñoz, A., Fletcher, D.A. & Weiner, O.D. Use the force: membrane tension as an organizer of cell shape and motility. *Trends Cell Biol.* **23**, 47-53 (2013).
4. Sheetz, M.P. Cell control by membrane–cytoskeleton adhesion. *Nat. Rev. Mol. Cell. Biol.* **2**, 392-396 (2001).
5. Lieber, Arnon D., Yehudai-Resheff, S., Barnhart, Erin L., Theriot, Julie A. & Keren, K. Membrane Tension in Rapidly Moving Cells Is Determined by Cytoskeletal Forces. *Curr. Biol.* **23**, 1409-1417 (2013).
6. Salbreux, G., Charras, G. & Paluch, E. Actin cortex mechanics and cellular morphogenesis. *Trends Cell Biol.* **22**, 536-545.
7. Sonnino, S. & Prinetti, A. Membrane Domains and the “Lipid Raft” Concept. *Curr. Med. Chem.* **20**, 4-21 (2013).
8. García-Sáez, A.J. & Schwille, P. Stability of lipid domains. *FEBS Lett.* **584**, 1653-1658 (2010).
9. García-Sáez, A.J., Chiantia, S. & Schwille, P. Effect of Line Tension on the Lateral Organization of Lipid Membranes. *J. Biol. Chem.* **282**, 33537-33544 (2007).
10. Vicente-Manzanares, M., Webb, D.J. & Horwitz, A.R. Cell migration at a glance. *J. Cell. Sci.* **118**, 4917-4919 (2005).
11. Pierre, S. & Julie, P. Membrane tension and cytoskeleton organization in cell motility. *J. Phys. Condens. Matter* **27**, 273103 (2015).
12. Dai, J. & Sheetz, M.P. Regulation of Endocytosis, Exocytosis, and Shape by Membrane Tension. *Cold Spring Harb. Symp. Quant. Biol.* **60**, 567-571 (1995).
13. Ewers, H. & Helenius, A. Lipid-Mediated Endocytosis. *Cold Spring Harb. Symp. Quant. Biol.* **3**(2011).
14. Pontes, B., *et al.* Cell Cytoskeleton and Tether Extraction. *Biophys. J.* **101**, 43-52 (2011).
15. Ishikawa-Ankerhold, H.C., Ankerhold, R. & Drummen, G.P.C. Advanced Fluorescence Microscopy Techniques—FRAP, FLIP, FLAP, FRET and FLIM. *Molecules* **17**, 4047 (2012).
16. Grashoff, C., *et al.* Measuring mechanical tension across vinculin reveals regulation of focal adhesion dynamics. *Nature* **466**, 263-266 (2010).
17. Blanchette, C.D., Lin, W.-C., Orme, C.A., Ratto, T.V. & Longo, M.L. Using Nucleation Rates to Determine the Interfacial Line Tension of Symmetric and Asymmetric Lipid Bilayer Domains. *Langmuir* **23**, 5875-5877 (2007).
18. Blanchette, C.D., Lin, W.-C., Orme, C.A., Ratto, T.V. & Longo, M.L. Domain Nucleation Rates and Interfacial Line Tensions in Supported Bilayers of Ternary Mixtures Containing Galactosylceramide. *Biophys. J.* **94**, 2691-2697 (2008).

2.5: Surface Tension and Line Tension is shared under a CC BY 4.0 license and was authored, remixed, and/or curated by LibreTexts.

2.6: Vesicles

The most basic definition of a vesicle is a compartment composed of many phospholipids with some form of head group. In a biological context, vesicles are typically formed by cells to uptake, excrete, or otherwise transport materials between membranous compartments in the cell. A synthetic vesicle, called a liposome, can be created by mixing phospholipid molecules in an aqueous environment. This article outlines some fundamental properties of vesicles, then goes on to discuss them in a biological context.

Formation of a Vesicle

Firstly, curvature must be established in a bilayer. Eventually, the indentation must protrude farther and farther, until a neck can be formed. Scission of the neck occurs to free the newly formed vesicle from the membrane. [8]

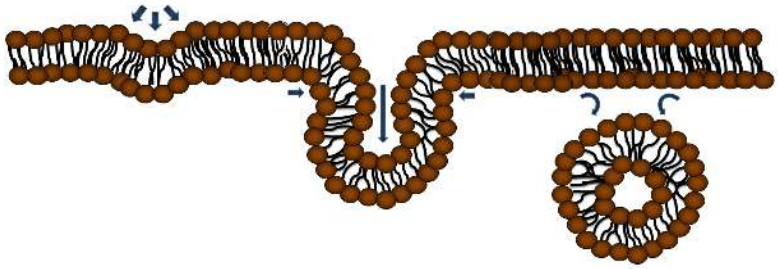


Figure 2.6.1: displays the initial membrane deformation by indentation (left), invagination and development of positive and negative curvatures (middle) and the development of complete curvature then scission to form complete vescicle.

The initial indentation into the bilayer necessitates a difference in the radius of curvature between the inner and outer leaflet. Compensation for this physical requirement can happen in several ways. One method involves leaflet asymmetry, where more phospholipids are shifted to the outside leaflet to compensate for the larger radius. If different types of phospholipids with varying geometries are used, these may also be incorporated in a fashion that compensates for the difference in radii equally well. The same balance can be struck using proteins incorporated into the membrane. [8,17]

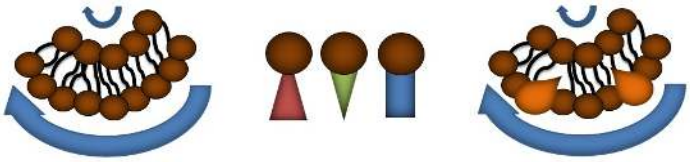


Figure 2.6.2: Differences in radii between the inner and outer leaflet (left), different geometry of lipids (middle), and proteins used in compensation for the different leaflet radii (right).

In an *in vitro* setting, phospholipids that are introduced to an aqueous environment can form several structures to optimize the arrangement of its hydrophobic and hydrophilic portions. Among these are micelles, liposomes, and multilamellar vesicles. Sonication of multilamellar vesicles can yield unilamellar vesicles and giant unilamellar vesicles (GUVs). Using a single type of phospholipid under these conditions yields a closed pure lipid bilayer membrane, which has been a useful model for understanding phase shifts among the lipids of the membrane, the mechanics of membrane formation and deformation, the dynamic behavior of elements that reside within the membrane, and the interactions between membranes and their environments. [2,4]

Biological Context

Vesicles mainly serve to hold some biological element apart from the surroundings. This may include biological molecules that must be transported from site to site or housing a particular chemical reaction until the products can be released into the cell.

Vesicles are most notably involved in taking nutrients in and excreting waste products out of the cell, called endocytosis and exocytosis, respectively. Vesicles serve as the chief mode of transport between the extracellular environment and various compartments in the cell such as the exosome, endosome, the trans golgi network (TGN), and the endoplasmic reticulum. Extracellular messaging works along this same system. As signals diffuse throughout the extracellular environment, they may interact with receptors that are then taken inside the cell in a vesicle or taken up inside a vesicle themselves. A number of secondary messengers may come into play to transduce the signal, or the signal may have an immediate intracellular target that elicits some change – expression of a particular gene or initiation of some post-translational modification, for example. Neuronal vesicles can carry signals between cells across the synaptic cleft or within the neuron itself.

In the cell, formation of any vesicle begins with a lipid bilayer. Perturbation and deformation at a section of this bilayer creates the proper combination of negative and positive curvature to develop the vesicle, a structure with wholly positive curvature.[8] The range of vesicles studied in a cell stretches anywhere between 30nm to 1.2µm. [6]

Vesicle Formation *in vivo*

The formation, or budding, of a vesicle in a cell involves deforming the membrane and creating specificity for a certain cargo. Early electron microscopy studies detected electron dense 'coats' in budding intermediates. The electron dense areas were later discovered to be coat proteins involved in creation of a vesicle.[10] These proteins coat a membrane section to create and stabilize curvature, then select the proper cargo. The vesicle then must be pinched off at the neck to create a membraneous structure separate from the larger membrane. These processes are typically mediated by groups of proteins. The best characterized mechanisms involve the clathrin protein, **co**at **p**rotein **I** (COPI), and **co**at **p**rotein **II** (COPII). [1, 9, 10]

Clathrin proteins are trimers, called triskellions, best represented as a central domain composed of three heavy chains (~190kDa) interacting with each other at their C-termini, bound with three light chains (~25kDa) extending outwards. Distal to the central domain are the N-termini, seven-bladed β-propeller structures with binding sites for a multitude of adaptor proteins to transfer a variety of cargo types in the potential vesicle. In solution, triskelia form flat hexagonal rings with relative ease. For the formation of a vesicle, triskelia must also form pentagonal rings, in addition to hexagonal rings, to generate enough curvature for the encapsulation of a vesicle. At least 12 pentagons must be present in the lattice to form a full vesicle. N-terminal repeat domains of a triskelion bind different adaptor proteins that can then in turn bind cargo as well as membrane directly. A single triskelion will bind others, forming the aforementioned shapes and eventually a cage that can encapsulate a vesicle. [9,10]

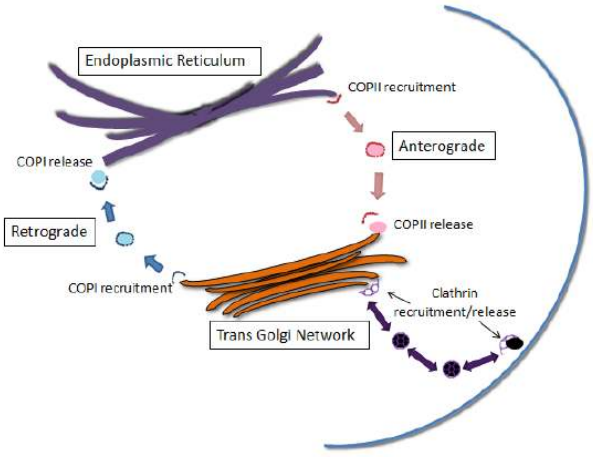


Figure 3 shows transport between the ER and the TGN. COPI is associated with retrograde transfer, and can be seen at the TGN membrane forming vesicles targeted to the ER. In anterograde transfer, COPII coatomers accumulate at the ER membrane to stabilize buds and similarly allow creation of vesicles targeted to the TGN. Clathrins also stabilize buds for the formation of vesicles, and can be seen here at the lower right corner.

COPI is a heptameric protein complex associated with shuttling substrates from the cis-golgi to the rough endoplasmic reticulum, called retrograde traffic. It is composed of seven subunits (α, β, β', δ, γ, ε and ζ), comprising the F subcomplex (a heteromer of β, δ, γ and ζ subunits) and B subcomplex (a heteromer of α and β' subunits). The α and β' subunits contain WD40 repeats, much like that of clathrin. COPII coat proteins are associated with the transportation of materials outward from the ER to the TGN and the cell membrane, or anterograde transfer. COPII proteins might be considered as subcomplexes of Sec13/31p and Sec23/Sec24p. Portions of the Sec13/31p have WD40 repeats, again like that of clathrin. [1,9]

Other Mechanisms of Vesicle Formation

Cytoskeletal branching, treadmilling and catastrophe affect membrane shape in the development of pseudopodia and lamellopodia, and can conceivably contribute to vesicle formation. Proteins with a BAR (Bin/amphiphysin/Rvs) domain specifically insert helices into membranes with curvature and play an important role in stabilizing curvature established by coat proteins. [8, 11, 17]

Multivesicular Bodies and Intralumenal vesicles

In the endocytic pathway, multivesicular bodies (MVB) are organelles that have vesicles inside their lumen, called intralumenal vesicles (ILT). They typically carry ubiquinated cargo to the lysosome, but can perform other functions as well. These vesicles require the **e**ndosomal **s**orting **c**omplex **r**equired for **t**ransport (ESCRT) proteins to form. ESCRTI, -II, and –III work alongside other associated proteins like vacuolar sorting protein 4 (Vsp4) to choose cargo, create a small bud, eventually perform scission on the bud, and target the vesicle to a final destination. A complex interplay between ESCRT proteins, associated targeting proteins that work with the ESCRT proteins, and post-translational modifications of the cargo governs these processes. [7] There is evidence that ESCRT proteins also participate in viral budding, cytokinesis, cell signaling, and development through its membrane interactions. [13,14,15,16]

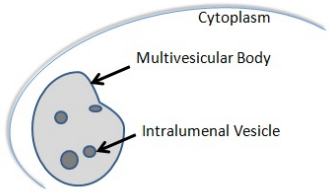


Figure 4 shows MVBs and ILVs within the cytoplasm.

References

1. Aridor, M., & Traub, L. M. (2002). Cargo selection in vesicular transport: the making and breaking of a coat. Traffic, 3(8), 537-546.
2. Basu, S. C., & Basu, M. (Eds.). (2002). Liposome methods and protocols (No. 199). Springer Science & Business Media.
3. Chenette, E. J. (2014). ESCRTing intraluminal vesicle formation. Nature cell biology, 16(5), 400-400.
4. Dua, J. S., Rana, A. C., & Bhandari, A. K. (2012). Liposome: methods of preparation and applications. Int J Pharm Stud Res, 3, 14-20.
5. Hanson, P. I., & Cashikar, A. (2012). Multivesicular body morphogenesis. Annual review of cell and developmental biology, 28, 337-362.
6. Jena, B. P. (2008). Intracellular Organelle Dynamics at nm Resolution. Methods in cell biology, 90, 19-37.
7. Jouvenet, N. (2012). Dynamics of ESCRT proteins. Cellular and Molecular Life Sciences, 69(24), 4121-4133.
8. McMahon, H. T., & Gallop, J. L. (2005). Membrane curvature and mechanisms of dynamic cell membrane remodelling. Nature, 438(7068), 590-596.
9. McMahon, H. T., & Mills, I. G. (2004). COP and clathrin-coated vesicle budding: different pathways, common approaches. Current opinion in cell biology, 16(4), 379-391.
10. Pearse BM (April 1976). "Clathrin: a unique protein associated with intracellular transfer of membrane by coated vesicles". Proceedings of the National Academy of Sciences of the United States of America 73 (4): 1255–9.
11. Peter, B. J., Kent, H. M., Mills, I. G., Vallis, Y., Butler, P. J. G., Evans, P. R., & McMahon, H. T. (2004). BAR domains as sensors of membrane curvature: the amphiphysin BAR structure. Science, 303(5657), 495-499.
12. Piper, R. C., & Katzmann, D. J. (2007). Biogenesis and function of multivesicular bodies. Annual review of cell and developmental biology, 23, 519.
13. Rusten, T. E., Vaccari, T., & Stenmark, H. (2012). Shaping development with ESCRTs. Nature Cell Biology, 14(1), 38-45.
14. Slagsvold, T., Pattni, K., Malerød, L., & Stenmark, H. (2006). Endosomal and non-endosomal functions of ESCRT proteins. Trends in cell biology, 16(6), 317-326.
15. Tu, C., Ahmad, G., Mohapatra, B., Bhattacharyya, S., Ortega-Cava, C., Chung, B. M., et. al & Band, H. (2011). ESCRT proteins: Double-edged regulators of cellular signaling. Bioarchitecture, 1(1), 45-48.
16. Wegner, C. S., Rodahl, L. M., & Stenmark, H. (2011). ESCRT proteins and cell signalling. Traffic, 12(10), 1291-1297.
17. Zimmerberg, J., & Kozlov, M. M. (2006). How proteins produce cellular membrane curvature. Nature Reviews Molecular Cell Biology, 7(1), 9-19.

2.6: Vesicles is shared under a CC BY 4.0 license and was authored, remixed, and/or curated by LibreTexts.

2.7: Diffusion in Membranes

Eukaryotic cells are surrounded by a flexible and dynamic barrier known as a membrane. These biological membranes are composed of lipids, which aggregate to form a bilayer with particular biochemical properties. The amphipathic nature of the lipid bilayer, whose tails are hydrophobic and associate with each other and whose head groups are hydrophilic and interact with the aqueous environment, are critical to its structure. The composition of the lipid bilayer is also important for the diffusion both across and within the membrane. This membrane diffusion is important for a variety of functions, some of which include regulating the fluidity of the membrane, the uptake of metabolites into the cell from the outside, and the removal of waste products from the inside of the cell.

Fluid Mosaic Model

Each membrane protein has a particular orientation within the membrane and cannot flip-flop form one bilayer to the other after it has assumed its mature conformation. However, lateral movement within the same lipid bilayer is still possible. Lateral diffusion is a key feature of the fluid mosaic model of membrane structure that was first described in 1972 by S. Jonathan Singer and Garth Nicolson (1).

This model was supported by experiments previously done by L.D. Frye and M. Edidin in 1970, which showed that cells taken from mouse and human lines could be fused together using the Sedani virus (Figure 2.7.1). The resulting fusion cell expressed both mouse and human antigens, which could be labeled indirectly by fluorescent antibodies and followed. Mixing of both parental antigens occurred forty minutes after fusion, suggesting that lateral diffusion within the membrane can occur (2). However, the time that it takes for lateral diffusion to occur depends on membrane fluidity, which ultimately depends on both temperature and lipid composition.

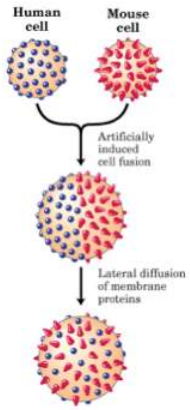


Figure 2.7.1: Experimental design originally performed by Frye and Edidin in 1970, in which they took cells from a human and a mouse and fused them using the Sedani virus. The species-specific antigens were then labeled with fluorescent antibodies and followed. The results of this experiment showed fusion and mixing of antigens, suggesting lateral diffusion within the membrane.

Types of Diffusion Across the Plasma Membrane

There are general thermodynamic principles that govern the transfer of molecules across the membrane. Figure 2.7.2 represents the equation that shows the amount of free energy that is required for a substrate to cross a membrane. In order for diffusion to occur, ΔG must be negative and as ΔG moves away from zero and becomes more positive, work becomes required. When the concentrations become equal on both sides of the membrane and $\Delta G = 0$ and the rates of transport in both directions will be the same and no net transport will occur.

$$\Delta G = RT \ln \left(\frac{C_2}{C_1} \right) \tag{2.7.1}$$

If C_2, the concentration of a substrate in the cytosol, is less than C_1, the concentration of a substrate outside of the cell, then ΔG is negative and the process is favorable. Gradually, as more substrate is transferred across the membrane, C_1 decreases as C_2 increases until $C_2 = C_1$and at this point delta G =0 and the system is at equilibrium.

Simple Diffusion

Simple diffusion occurs by the diffusion of molecules, such as O_2 and CO_2, across the hydrophobic core of the membrane (Figure 2.7.3). Therefore, no ATP is required for this type of diffusion across the membrane, it is simply a matter of molecules moving down a concentration gradient. As simple diffusion does not require ATP, large polar molecules or ions cannot diffuse across the membrane. This is due to the hydrophobic tail region of the membrane, which presents too large of an energy barrier to be overcome by the potential stored in the gradient.

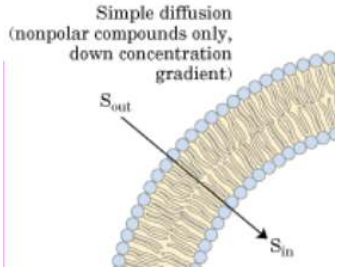


Figure 2.7.3: An image of simple diffusion in which nonpolar compounds diffuse across the membrane through the use of a concentration gradient. This process does not require any mediator proteins or pores.

The net rate of transport is proportional to the concentration difference ($C_2 - C_1$) across the membrane (Figure 2.7.4).

$$J = -\frac{KD_1(C_2 - C_1)}{l} \tag{2.7.2}$$

where

- J is the net rate of transport,
- K is the partition coefficient for the ratio of solubilities of the material in lipid and water,
- D_1 is the diffusion coefficient of the diffusing substance in the membrane, and
- l is the thickness of the membrane.

For ions and other hydrophilic substances, K is a very small number, given that diffusion of such molecules across the membrane is very slow.

Facilitated Transport

As opposed to simple diffusion, which does not require ATP, facilitated transport needs ATP in order to overcome the energy barrier of the hydrophobic tail region of the membrane. In addition, this type of diffusion is dependent on cargo binding the membrane-embedded channel or carrier protein.There are two types of facilitated transport, pore-facilitated transport and carrier-facilitated transport. In order to distinguish between pore-facilitated transport and carrier-facilitated diffusion, one can fluctuate the membrane fluidity by altering the temperature. This change in temperature will stop carrier-facilitated diffusion due to the fact that carrier-facilitated diffusion must move through the membrane in order to function and cannot do so when the membrane is in a non-fluid state.

Pore-Facilitated Transport

Pore-facilitated transport uses proteins embedded within the membrane that can open and close in order to facilitate diffusion. This type of diffusion allows for selected ions to pass through the pore, such as Cl-. An important example of pore-facilitated transport is the transport of glucose through the use of a gated pore mechanism, in which the pore is never open at both ends at once (Figure 2.7.5). Instead, the pore opens at the exterior to allow the entry of glucose, closes the exterior opening, opens the interior opening, releases glucose into the cytosol, and finally returns to its state of binding on the exterior (15).

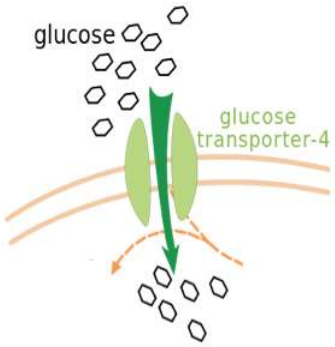


Figure 2.7.5: An image of glucose using the pore-facilitated transport system (light green) as a means for crossing the membrane, this is a simplified diagram that does not show the gated pore mechanism.

Carrier-Facilitated Transport

Antibiotic ionophores, such as valinomycin, a cation carrier, are an example of carrier-facilitated transport. Its folded conformation allows for the protein to have an outer hydrophobic surface, making it soluble in the lipid bilayer, with an internal conformation that mimics the hydration shell that the cation would have in an aqueous solution. This conformation allows valinomycin to diffuse from one surface of a membrane, pick up an ion, and then diffuse to the other surface to release it (Figure 2.7.6).

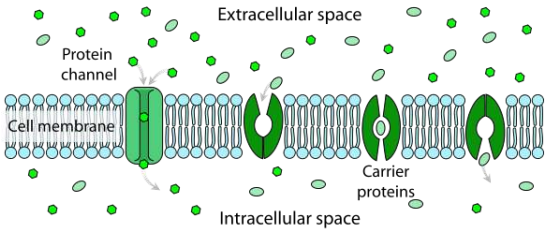


Figure 2.7.6: Facilitated diffusion involves the use of a protein to facilitate the movement of molecules across the membrane. In some cases, molecules pass through channels within the protein,In other cases, the protein changes shape, allowing molecules to pass through. (Public Domain).

Factors that Influence Membrane Diffusion

There are several factors that can influence the diffusion of molecules both within and across a membrane; physical barriers, electrostatic attraction or repulsion nodes, and partitioning phenomena (3), are just a few examples.

Physical Obstacles

Physical obstacles can become considerably crowded, which can obstruct the free passage of molecules. Several adaptor proteins (alpha-actinin, talin, vinculin, etc.) can attach the cortical cytoskeleton to the long cytosolic tails of transmembrane proteins within the plasma membrane and act as a fence, which restricts the movement of molecules across the membrane (4,5). Such obstruction by the cortical cytoskeleton has lead to the observation that molecules undergo a “hop diffusion” in which they “hop” intermittently between confinement zones (4,5) in order to diffuse (Figure7).

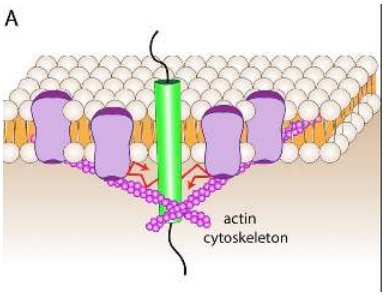


Figure 2.7.7: An image of the mesh actin cytoskeleton (light purple) attaching to transmembrane proteins (dark purple) and tightly associated lipids to form a barrier that limits the diffusion of molecules (3). The red arrows indicate limited diffusion.

Membrane-matrix junctions can also contribute to a physical obstruction that impedes membrane diffusion. This is due to the binding between integrin receptors located in the plasma membrane and the extracellular matrix (fibrous network of proteins that cells attach to) (Figure 2.7.8). If this interaction is increasingly accumulated at a high enough density, then diffusion is limited. A recent study showed that this type of physical barrier blocked the diffusion of membrane molecules whose dimensions exceeded the width of the integrin-matrix interaction (6).

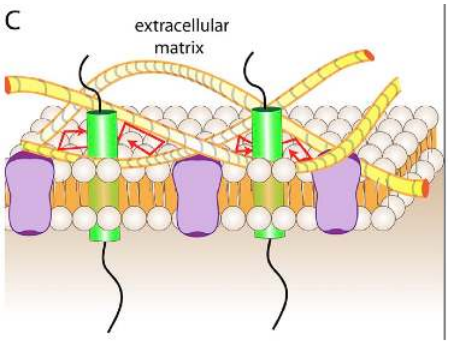


Figure 2.7.8: An image of the extracellular matrix (yellow) linking to membrane receptors (purple) to generate a mesh that limits diffusion (3). The red arrows indicate limited diffusion.

Electrostatic Impediments

Electrostatic interactions can also interfere with free diffusion, as charged proteins or lipids can be repelled by like charges or attracted by opposite ones (Figure 2.7.9). McLaughlin and Murray in 2005 showed that proteins have natively unfolded regions that have both basic and hydrophobic residues that allow them to exist within the bilayer and at the same time attract anionic lipids electrostatically (7). As a result, the membrane-associated cationic residues associate together, creating a negatively charged ring around the protein. Thus, the resulting ring of anionic lipids can alter the mobility of other charged molecules in the plane of the membrane (8).

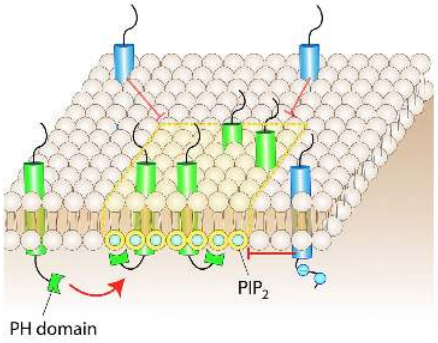


Figure 2.7.9: A protein bearing a PH domain is shown to be recruited to a patch that is rich in its ligand lipid. The negative charge on PIP_2 (green) accumulates and deflects proteins with a like negative charge (blue) (3).

Partition-Induced Barriers

In a membrane, certain types of lipids or proteins can partition into defined regions, resulting in an area of subdiffusive behavior (3). The association between lipids and proteins is often driven by the recognition of particular binding domains, for example, the association of protein PH domains with phosphoinositides (9). Another way for these lipid-protein complexes to form is through hydrophobic interactions. An example of this hydrophobic interaction-driven complex is the saturated lipid- and cholesterol- rich microdomains, known as lipid rafts (10). Lastly, membrane curvature can play a role in the obstruction of diffusion (Figure10). The bent region of the membrane has distinct properties, as the head groups of the lipids constituting the concave monolayer are unusually close, whereas the head groups on the convex monolayer are uncharacteristically far apart. The concave side of the bent bilayer can alter diffusion physically or electrostatically, while the convex side creates a more accessible membrane due to reduced packing of the head groups.

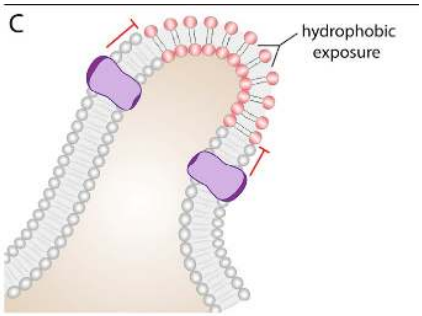


Figure 2.7.10: An area where the membrane undergoes sharp curvature can force the exposure of hydrophobic regions on the outer leaflet of the membrane in addition to forcing the lipid heads on the inner leaflet to compact. Curvature can alter the partition of lipids and proteins.

Techniques to Monitor Diffusion

- **Fluorescence recovery after photobleaching (FRAP)** was initially very useful in studying the lateral diffusion of membrane components (11). This technique uses fluorescently labeled probes to follow a molecule of interest. By using a high intensity laser, the fluorophores in a region of interest will become bleached and lose signal (Figure11). The probes that were not bleached will then diffuse throughout the sample and replace the bleached region. Since this method measures the average behavior of molecule, it ultimately has limited temporal resolution (seconds).
- **Fluorescence correlation spectroscopy (FCS)** is a correlation analysis that measures fluctuation in fluorescence intensity. This technique provides high spatial precision and can measure diffusion coefficients of molecules (12,13). Unlike FRAP, FCS can acquire the time resolution, but lacks the ability to capture defined transient events.
- **Imaging total internal reflection (ITIR)-FCS** is a technique that can circumvent both of the problems in other techniques, as it can probe diffusion in membranes with good temporal and spatial resolution (12). ITIR-FCS can be applied to diffusion, active transport, or even both.

References

1. Singer S.J. and Nicolson G.L. 1972. The Fluid Mosaic Model of the Structure of Cell Membranes. *Science*. 175:720-31.
2. Frye L.D. and Edidin M. 1970. The Rapid Intermixing of Cell Surface Antigens After Formation of Mouse-Human Heterokaryons. *Journal of Cell Science*. 7:319-35.
3. Mathews C.K. and Van Holde K.E. 1996. *Biochemistry.* Second Edition. Menlo Park, CA: The Benjamin/Cummings Publishing Company, Inc.
4. Fujiwara T.K., Ritchie H., Murakoshi K., Jacobson, Kusumi 2002. Phospholipids undergo hop diffusion in compartmentalized cell membrane. *Journal of Cell Biology*. 157:1071-82.
5. Suzuki K.G., Fujiwara T.K., Sanematsu F., Iino R., Edidin M., Kusumi A 2007. GPI-anchored receptor clusters transiently recruit Lyn and G-alpha for temporary cluster immobilization and Lyn activation: single molecule tracking study. *Journal of Cell Biology*. 177:717-30.
6. Paszek M.J., DuFort C.C., Rossier O., Bainer R., Mouw J.K., Godula K., Hudak J.N., Lakins A.C., Wijekoon L., Cassereau 2014. The cancer glycocalyx mechanically primes integrin-mediated growth and survival. *Nature*. 511:319-25.
7. McLaughlin S. and Murray D. 2005. Plasma membrane phosphoinositide organization by protein electrostatics. *Nature*. 438:605-611.
8. Van den Boggart G., Meyenberg K., Risselada H.J., Amin K.I., Willig B.E., Hubrich M., Dier S.W. Hell, H., Grubmuller U., Diederichsen, Jahn R., 2011. Membrane protein sequestering by ionic protein-lipid interactions. *Nature.* 479: 552-55.
9. Trimble W.S. and Grinstein S. 2015. Barriers to the free diffusion of proteins and lipids in the plasma membrane. *Journal of Cell Biology.* 208:259- 71
10. Lemmon M.A. 2008. Membrane recognition by phospholipid-binding domains. *Nature Review Molecular and Cell Biology.* 9: 99-111.
11. Lingwood D. and Simons K., 2010. Lipid rafts as a membrane-organizing principle. *Science*. 327: 46-50.
12. Chen Y., Lagerholm B.C., Yang B., Jacobson K., 2006. Methods to measure the lateral diffusion of membrane lipids and proteins. *Methods.* 39:147-53.
13. Sankaran J., Manna M., Guo L., Kraut R., Wohland T. 2009. Diffusion, transport, and cell membrane organization investigated by image fluorescence cross-correlation spectroscopy. *Biophysical Journal*. 97:2630-39.
14. Magde D., Elson E.L., Webb W.W. 1974. Fluorescence correlation spectroscopy. *Biopolymers*. 17:361-76.

15. Oka Y., Asaon T., Shibasaki Y., Lin J.L., Tsukuda K., Katagiri H., Akanuma Y., Takaku F. 1990. C-terminal truncated glucose transporter is locked into an inward-facing form without transport activity. *Nature*. 345:550-53.

2.7: Diffusion in Membranes is shared under a CC BY 4.0 license and was authored, remixed, and/or curated by LibreTexts.

CHAPTER OVERVIEW

3: Membrane Phases and Morphologies

One of the most important properties of a lipid bilayer is the relative mobility (fluidity) of the individual lipid molecules and how this mobility changes with temperature. This response is known as the phase behavior of the bilayer. The phase behavior of lipid bilayers is largely determined by the strength of the attractive Van der Waals interactions between adjacent lipid molecules. The extent of this interaction is in turn governed by how long the lipid tails are and how well they can pack together.

3.1: Membrane Phase Transitions
3.2: The Main Phase Transition
3.3: The Fluid Phase
3.4: The Gel Phase
3.5: The Ripple Phase
3.6: Rafts
3.7: Lipid Phase Coexistence

3: Membrane Phases and Morphologies is shared under a CC BY 4.0 license and was authored, remixed, and/or curated by LibreTexts.

3.1: Membrane Phase Transitions

Biological membranes are primarily composed of phospholipids—a diverse class of compounds composed of a hydrophilic head group covalently attached to a pair of hydrophobic fatty acids. This amphipathic structure leads phospholipid molecules to spontaneously form bilayers when placed in water, as the phospholipids are driven to orient their head groups towards water and shield their fatty acid tails from it via the hydrophobic effect.

While these bilayers tend to exist in a fluid phase under physiological conditions, their component phospholipids can undergo phase transitions under the correct environmental conditions. Similarly to the familiar transitions between the liquid, solid, and gas phases of simpler systems, these lipid phase transitions represent changes in the entropy of the system through reorganization of the system's components in response to changes in the free energy of the system. Lipids can exist in a number of phases, which are summarized below.

L_α: The Liquid Disordered Phase

The liquid disordered phase, as its name implies, is a highly fluid state in which individual lipids can move laterally across the surface of the membrane relatively unhindered. Liquid-disordered bilayers are often characterized by irregular packing of individual lipid molecules, as well as the presence of kinks in unsaturated fatty acids. These kinks effectively reduce the surface area accessible to other fatty acid chains, weakening Van der Waals interactions.

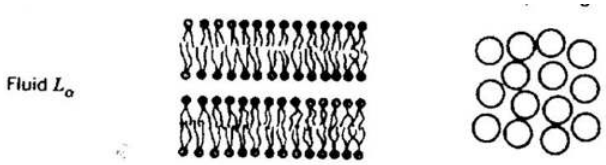


Figure 3.1.1: A depiction of the liquid-disordered phase, with a cross-sectional view to the left, and a top view at right illustrating packing irregularity. Note the irregular orientation of the fatty acid tails, indicating a high degree of fluidity. (Faller 2015)

L_β: The Gel Phase

At temperatures below Tm (melting temperature), lipid bilayers enter a solid-like phase known as the gel phase. Fatty acids with kinks often undergo trans isomerization, allowing the chains to be fully extended and strengthening Van der Waals interactions. Stronger Van der Waals interactions lead to tighter, more ordered lipid packing, impeding lateral movement across the surface of the membrane.

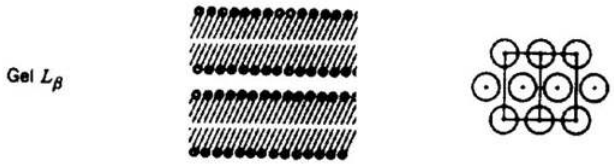


Figure 3.1.2: A depiction of the gel phase, with a cross-sectional view to the left, and a top view at right illustrating the highly ordered packing arrangement. Note the straight orientation of the fatty acid tails, indicating a low degree of fluidity. (Faller 2015)

L_o: The Liquid Ordered Phase

The liquid ordered phase represents something of a hybrid of the liquid disordered and gel phases. Sufficiently high membrane sterol concentration combined with the relative rigidity of sterol molecules leads to tighter packing of liquid phase membranes, while separating gel phase lipids. The result is a "liquid ordered phase" with solid-like qualities similar to the gel phase without sacrificing the high rate of lateral diffusion attainable in the liquid-disordered phase.

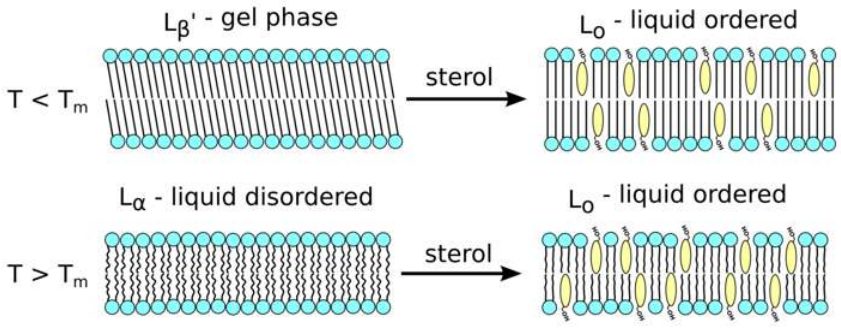


Figure 3.1.3: A a cross-sectional view of the liquid ordered phase as compared to the gel and liquid-disordered phases, with cholesterol molecules depicted in yellow. Note the straight orientation of the fatty acid tails, as well as the spacing between phospholipids provided by the cholesterol. (Faller 2015)

P_β: The Ripple Phase



Figure 3.1.4: A depiction of the ripple phase, with a cross-sectional view to the left, and a top view at right illustrating the highly ordered packing arrangement. Note the straight orientation of the fatty acid tails, indicating a low degree of fluidity, similar to the gel phase. (Faller 2015)

L_c: The Pseudocrystalline phase

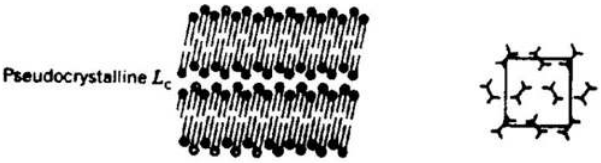


Figure 3.1.5: A depiction of the pseudocrystalline phase, with a cross-sectional view to the left. Note the straight orientation of the fatty acid tails, indicating a low degree of fluidity, similar to the gel phase. (Faller 2015)

Factors Affecting Lipid Phase Transitions

The primary factor driving most phase transitions is the temperature of the environment. Temperatures above a lipid's Tm will transition lipids to a liquid phase, while colder temperatures will cause a transition to a solid-like phase. However, Tm can vary between lipids due to differing structural properties. Furthermore, some phase transitions, such as the liquid-ordered phase transition, more strongly depend on environmental conditions other than temperature.

Chain Length

Longer fatty acid chains have higher surface areas than smaller ones, resulting in stronger Van der Waals interactions between long lipid chains. This leads to increasing Tm's with increasing chain length, as shown in Figure 3.1.1.

Table 2.1. Thermodynamic data for thermotropic phase transitions of a series of diacyl-saturated phosphatidylcholines determined by DSC[a].

Lipid	Tm_1 (°C)	Tm_2 (°C)	ΔH_1 (kcal/mol)	ΔH_2 (kcal/mol)	ΔS_2 (cal/°K mol)
DMPC (C_{14})	15.3	24.0	1.3	6.5	21.9
DPPC (C_{16})	35.5	41.5	1.6	8.7	27.7
DSPC (C_{18})	51.0	54.3	1.8	10.4	33.3
DAPC (C_{20})	62.1	64.1	1.7	12.3	37.6

[a]From ref. 112. Abbreviations: DMPC, dimyristoyl phosphatidylcholine; DPPC, dipalmitoyl phosphatidylcholine; DSPC, distearoyl phosphatidylcholine; DAPC, diarachidoyl phosphatidylcholine. The subscripts (1, 2) refer to the pretransition (1) and main transition (2).

Figure 3.1.6: Tabulation of Tm and enthalpy data for lipids of differing lengths. Notice how the Tm and ΔHfusion increase with chain length. (Faller 2015)

Furthermore, increasing the length of a hydrocarbon chain simultaneously increases the number of degrees of freedom, thereby increasing the lipid's heat capacity—thereby also increasing the enthalpy of fusion.

Unsaturation

Lipid unsaturation—the presence of one or more double bonds in the lipid's fatty acid tails—also affects Tm by altering the strength of Van der Waals interactions between lipid tails. Unlike chain length, however, increasing unsaturation reduces the Tm of the lipid by reducing the accessible surface area of the fatty acid tail by forming kinks that prevent nearby tails from packing together as tightly. This weakens inter-lipid Van der Waals interactions, and lowers the Tm of the lipid.

The positioning of double bonds in the fatty acid chain influences the degree to which Tm is lowered—with double bonds closer to the middle of the chain producing larger kinks, thereby decreasing Tm more than double bonds located closer to either end of the chain.

Sterols

Sterols, such as cholesterol, play a large role in modulating the fluidity of membranes. Sterols are—compared to neighboring phospholipids—small, rigid molecules that are largely hydrophobic, with the exception of a single hydroxyl group. The accumulation of sterols in a lipid bilayer causes tighter packing of fatty acid tails in liquid phase lipids and separates gel phase lipids. The result is a "liquid ordered phase" with solid-like qualities similar to the gel phase without sacrificing the high rate of lateral diffusion attainable in the liquid-disordered phase.

Membrane Protein Concentration

High local concentrations of membrane-associated proteins can decrease the Tm of sections of membrane through steric interactions between crowded proteins. Although elevated local protein concentrations can be critical for facilitating certain cellular processes, collisions between crowded proteins creates lateral pressure that renders lipid domain separation more thermodynamically favorable—possibly leading to phase transitions, as shown in Figure 3.1.7.

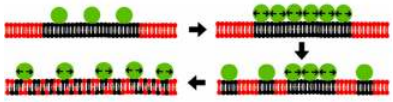


Figure 3.1.7: A diagram illustrating how steric interactions between crowded membrane proteins can result in the separation of ordered membrane domains. Membrane proteins are represented by green orbs and ordered domain lipids are colored black, with other membrane lipids indicated in red. (Scheve et al, 2013)

Outcomes of Lipid Phase Transitions

Phase Separation

Membranes often contain a mixture of lipids of different lengths and degrees of unsaturation, resulting in differing Tm's. If such a membrane system is cooled, the longer, more saturated lipids will undergo the transition to the gel phase before other shorter, less saturated lipids, as their Tm will be reached first. The resulting straightening of the fatty acid chains causes part of the gel phase lipids' chains to be exposed to water, resulting in a hydrophobic effect-driven aggregation of the long, newly gel-phase lipids. This results in the formation of patches of long, saturated, gel-phase lipids in the membrane.

Protein Aggregation

Phase separation between lipids surrounding integral membrane proteins can briefly expose the hydrophobic residues of the middle of the protein to water. If enough other exposed proteins are nearby, this can result in a hydrophobic effect-mediated protein aggregation event, as displayed in Figure 3.1.8.

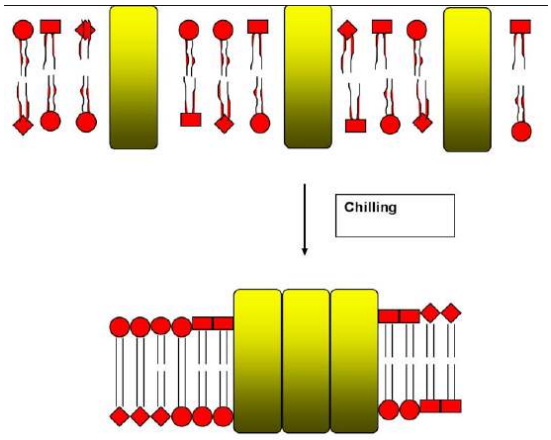


Figure 3.1.8: Illustration of phase separation-driven protein aggregation. Different lipid types (indicated by differently-shaped head groups) are sorted together through the process of phase separation, which can result in aggregation of membrane proteins through the hydrophobic effect.

Membrane Leakage

The differential rates of phase transition between lipids composing a membrane can lead to packing defects as gel-phase fatty acid chains straighten out, forming a short-lived gap between the now gel-phase chains and neighboring, still-liquid chains. Such gaps can allow cytoplasmic contents to leak out of the cell until they are plugged via lateral diffusion of neighboring lipids.

References

1. Benalcazar, Wladimir A. "Phase Transitions in Lipid Bilayers". Physics 563 Term Essay. University of Illinois, Urbana-Champaign. May, 2012.
2. Faller, R. BPH241 Lecture Notes. University of California, Davis. April, 2015.
3. Raghunathan, V. A., and John Katsaras. "L β ′ → L C ′ Phase Transition in Phosphatidylcholine Lipid Bilayers: A Disorder-order Transition in Two Dimensions." Physical Review E Phys. Rev. E: 4446-449. Web. 14 May 2015. .
4. Rangamani, Padmini, Shachi Katira, Berend Smit, and George Oster. "Lipid Tilt Regulates Ripple Phase Behavior in Lipid Bilayer." Biophysical Journal. Cell Press. Web. 14 May 2015.
5. Scheve, Christine S., Paul A. Gonzales, Noor Momin, and Jeanne C. Stachowiak. "Steric Pressure between Membrane-Bound Proteins Opposes Lipid Phase Separation." J. Am. Chem. Soc. Journal of the American Chemical Society (2013): 1185-188. Print.

3.1: Membrane Phase Transitions is shared under a CC BY 4.0 license and was authored, remixed, and/or curated by LibreTexts.

3.2: The Main Phase Transition

The membranes that provide structure and definition to cellular compartments are composed of dynamic and heterogeneous lipids whose varying chemical properties allow for their function. The transition between the two main phases of a lipid bilayer, the liquid crystalline phase (L_α) and the gel phase (L_β) determines how the membrane will behave in terms of fluidity at a particular temperature and the formation of biologically useful membrane microdomains.

Relevant Properties of Lipid Phases

Membranes composed of a lipid bilayer can exist in either the liquid or gel phase, depending on the strength of interaction between the molecules. The two phases are quite different in their physical properties and biological relevance.

A. L_α

The L_α, or "liquid" phase, is characterized by more thermal motion than the gel phase. Head groups in the liquid phase are loosely packed with rotational freedom, giving rise to a larger area per molecule at room temperature than observed in the gel phase[1]. The acyl chain tails are not rigid or efficiently packed due to the presence of "kinks" caused by gauche orientation of the alkane chain.
In the liquid phase, phospholipid molecules can move freely in the X and Y axis, but distance between the bilayers (the Z axis direction) is shorter in than in the gel phase, as would be expected due to the kinks in the hydrophobic tails[2]. The presence of gel phase domains within the bilayer can inhibit the lateral diffusion of liquid phase molecules[3].

B. L_β

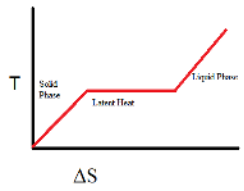
In the L_β phase, or "gel" phase, acyl chain tails are fully extended and a uniform trans orientation is present for the length of the alkyl chain. This gives the gel phase a longer Z axis, or length, because the acyl chains are more rigid and straight.
Tightly packed head groups result in a lower area per molecule at room temperature than in the liquid phase[1].

Ehrenfest's Definition of Phase Transition

The Austrian physicist Paul Ehrenfest provided a definition for phase transitions, where phase behavior is described in terms of free energy (ΔG) as a function of different thermodynamic variables. The "order" is the derivative of ΔG (as a function of some physical or chemical variable) and the point at which it is discontinuous is the point of phase change[4].

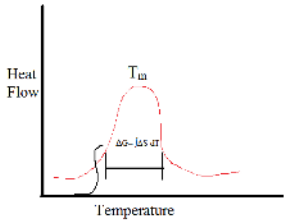
Physical state phase changes, such as the transition between a solid, liquid, gas (or liquid to gel state of a lipid bilayer) are first order phase transitions because they are discontinuous in density at their T_m, which is the first derivative of ΔG with respect to chemical potential.

In a second order phase transition, the first derivative of ΔG is continuous but the second derivative is discontinuous for the second derivative of ΔG. Magnetization is an example of a second order phase transition process.
The phase transition of gel to liquid is a first order process and involves a latent heat, in which the thermodynamic system (membrane) absorbs or emits a fixed amount of enthalpy ΔS. During phase transition, the temperature stays constant while heat is added to the system[4].



A simplified diagram of phase change

The heat flow required for a first order phase change can be modeled as $T\Delta S$. Plotting heat flow versus temperature shows intuitively the energy required for phase transition, with an integral of the curved area representing the free energy of the process:



Hysteresis is the phenomenon where there is a difference in T_m depending on which direction the phase transition is going (a difference between $T_{liquid \rightarrow gel}$and $T_{gel \rightarrow liquid}$).This phenomenon occurs only in first and not second order phase transitions[5].

Characteristics of Phase Transitions

The close packing of the gel phase is accomplished in part by the long and straight acyl chains. These chains are kept straight and rigid by the trans orientation of the alkane chain. During phase transitions, the acyl chain portion of the phospholipid hydrophobic tail undergoes a trans-gauche isomerization produces kinks, a shorter and skewed tail, and leads to less efficient packing[6].

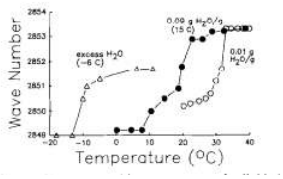
Biologically relevant membranes exist as complex mixtures of different lipids with varying melting temperatures. As a fraction of the membrane reaches its phase transition temperature (T_m) a mixed phase will exist with a heterogenous mixture of liquid and gel phases. Should a sufficient amount of mixed phase exist, a substantial amount of lipid molecules may become exposed to an aqueous environment as the liquid phase molecules will be shorter in the Z axis than the gel phase, making the membrane thinner and exposing a portion of the hydrophobic tails of adjacent phospholipid molecules. This phenomenon is known as “Hydrophobic mismatch” and is the driving force for phase separation. Thus, the disparity of phase transition temperatures in complex lipid mixtures of a lipid bilayer can be thought of as a driving force for phase separation and microdomain formation[7].

Forces Driving Phase Transition

Lipids undergo temperature specific phase transitions from liquid crystalline to gel phase. The specific temperature at which this transition occurs is referred to as T_m and varies depending on the specific molecule. Lipid molecules with longer acyl chains tend to have higher T_m than shorter tailed phospholipids because the longer tail provides more opportunity for Van der Waals interactions to occur between two adjacent molecules, lowering over all energy and requiring more thermal energy to reach the point of phase transition and making the phospholipid more likely to exist in the gel phase[5].

Double bonding within the acyl chain also affects T_m[8]. Unsaturated lipids have a lower T_m whereas saturated lipids have a higher T_m. In addition to the degree of unsaturation or number of double bonds, the position of the double bond in the acyl chain also affects phase behavior[7].

In addition to the acyl tail, the lipid headgroup also influences phase behavior. The size of the headgroup is thought to have a strong influence on T_m. Glycocylated head groups have been shown to exhibit less hydrogen bonding than normal phosphatidylcholine resulting in a more fluid and flexible membrane[9]. Somewhat related, the surrounding pH and the hydration of the membrane can also affect T_m, with lower pH and higher hydration state resulting in a higher T_m for the same lipid composition by affecting the hydrogen bonding between the lipid components[10].

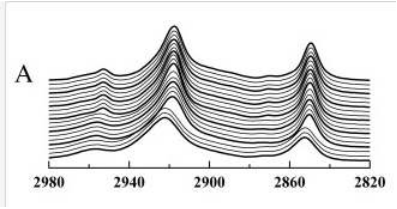


Change in melting temperature for lipids in pollen grains containing different water contents[11]

Techniques for Detecting and Measuring Phase Transitions

Differential scanning calorimetry (DSC) is a technique that can be used to measure phase transitions in lipid samples and even in simple cells like intact bacteria[12]. DSC works by measuring the amount of heat energy required to raise the temperature of the sample. By slowly ramping the temperature of the sample and accurately measuring temperature change, DSC can determine phase transition phases. By conducting a DSC scan in both directions, hysteresis can be identified.

Fourier transform infrared spectroscopy (FTIR) is a powerful technique that can provide a wealth of information about lipid structure, membrane organization and phase behavior[13]. FTIR detects the absorbance of IR type light emission, which at certain wavelengths is absorbed by different carbon-carbon bonds. From FTIR absorbance spectra, information about lipid conformation can be extrapolated. For example, the phase transition from gel to liquid phase represent change from a more ordered to a more disordered state; the disordered state provides for more rotational and vibrational freedom of the lipid molecules, which is accompanied by a broadening of the IR absorbance of the higher energy molecule[14]. It has been used to find T_m of intact cells, including human platelets[15].



FTIR spectra showing the C-H stretch at 6° of DMPS in an aqeous buffer[14]

Biological Consequences

Packing defects of the lipid bilayer can lead to leakage during phase transition the formation of microdomains that occurs as consequence of phase separation can alter the curvature and fluidity of the membrane, which can impart new biological characteristics to the plasma membrane, tonoplast or a vesicle. In addition, protein movement through the membrane can be impaired, or a protein could be restricted to a lipid environment in which it does not optimally function.[16]

Myelin is a notable exception to the general rule that lipids are fluid during physiological temperatures. In persons with multiple sclerosis, the T_m of myelin is lowered by 20°C[17], altering the physical properties of neuronal myelin sheath and possibly causing increased susceptibility to degradation[18].

References

1. Nagle, J.F., *Theory of lipid monolayer and bilayer phase transitions: Effect of headgroup interactions.* The Journal of Membrane Biology, 1976. **27**(1): p. 233-250.
2. John, K., et al., *Transbilayer Movement of Phospholipids at the Main Phase Transition of Lipid Membranes: Implications for Rapid Flip-Flop in Biological Membranes.* Biophysical Journal, 2002. **83**(6): p. 3315-3323.
3. Ratto, T.V. and M.L. Longo, *Obstructed diffusion in phase-separated supported lipid bilayers: a combined atomic force microscopy and fluorescence recovery after photobleaching approach.* Biophys J, 2002. **83**(6): p. 3380-92.
4. Jaeger, G., *The Ehrenfest Classification of Phase Transitions: Introduction and Evolution.* Archive for History of Exact Sciences, 1998. **53**(1): p. 51-81.
5. Faller, R., *MCB/PBH 241 Course Lectures*. 2014.
6. Hjort Ipsen, J., et al., *Phase equilibria in the phosphatidylcholine-cholesterol system.* Biochimica et Biophysica Acta (BBA) - Biomembranes, 1987. **905**(1): p. 162-172.
7. Wallace, E.J., N.M. Hooper, and P.D. Olmsted, *Effect of hydrophobic mismatch on phase behavior of lipid membranes.* Biophys J, 2006. **90**(11): p. 4104-18.
8. Applegate, K.R. and J.A. Glomset, *Effect of acyl chain unsaturation on the packing of model diacylglycerols in simulated monolayers.* J Lipid Res, 1991. **32**(10): p. 1645-55.
9. Popova, A.V. and D.K. Hincha, *Effects of the sugar headgroup of a glycoglycerolipid on the phase behavior of phospholipid model membranes in the dry state.* Glycobiology, 2005. **15**(11): p. 1150-5.
10. Seddon, J.M., et al., *Phosphatidylcholine–fatty acid membranes: effects of headgroup hydration on the phase behaviour and structural parameters of the gel and inverse hexagonal (HII) phases.* Biochimica et Biophysica Acta (BBA) - Biomembranes, 1997. **1327**(1): p. 131-147.

11. Crowe, J.H., et al., *Lipid phase transitions measured in intact cells with fourier transform infrared spectroscopy.* Cryobiology, 1989. **26**(1): p. 76-84.
12. Lepock, J.R., H.E. Frey, and W.E. Inniss, *Thermal analysis of bacteria by differential scanning calorimetry: relationship of protein denaturation in situ to maximum growth temperature.* Biochim Biophys Acta, 1990. **1055**(1): p. 19-26.
13. Lewis, R.N. and R.N. McElhaney, *Membrane lipid phase transitions and phase organization studied by Fourier transform infrared spectroscopy.* Biochim Biophys Acta, 2013. **1828**(10): p. 2347-58.
14. Lewis, R.N.A.H. and R.N. McElhaney, *Membrane lipid phase transitions and phase organization studied by Fourier transform infrared spectroscopy.* Biochimica et Biophysica Acta (BBA) - Biomembranes, 2013. **1828**(10): p. 2347-2358.
15. Tablin, F., et al., *Membrane phase transition of intact human platelets: Correlation with cold-induced activation.* Journal of Cellular Physiology, 1996. **168**(2): p. 305-313.
16. van Meer, G., D.R. Voelker, and G.W. Feigenson, *Membrane lipids: where they are and how they behave.* Nat Rev Mol Cell Biol, 2008. **9**(2): p. 112-24.
17. Chia, L.S., J.E. Thompson, and M.A. Moscarello, *Alteration of lipid-phase behavior in multiple sclerosis myelin revealed by wide-angle x-ray diffraction.* Proc Natl Acad Sci U S A, 1984. **81**(6): p. 1871-4.
18. Moscarello, M.A., et al., *Myelin in multiple sclerosis is developmentally immature.* J Clin Invest, 1994. **94**(1): p. 146-54.

3.2: The Main Phase Transition is shared under a CC BY 4.0 license and was authored, remixed, and/or curated by LibreTexts.

3.3: The Fluid Phase

Cell membranes are composed of many different types of lipids, including saturated and unsaturated phospholipids, cholesterol, and fatty acids. Membranes in functional condition are predominantly comprised of fluid phase lipid bilayers. Maintenance of membrane fluidity is crucial for integrity and functionality. However, phase coexistence is normal since the membrane is comprised of many different lipid molecules. The addition of sphingolipids increases the possibility of gel (solid) phase coexisting with fluid (liquid) phase. This is due to sphingolipids containing long, saturated acyl chains that cause them to pack tightly in the membrane, resulting in very limited room for lateral diffusion. Some damaged cells undergo lipid phase transition from fluid phase to gel phase in the membrane, which results in fatal problems and cell death. This also occurs when the cell ages, as lipids in the fluid phase emerge in the gel phase and vice versa. Physiological and metabolic changes occur as a result of the changes in lipid composition.

The plasma membrane is a semi-permeable bilayer barrier that separates the interior of the cell from the exterior and maintain a distinct metabolism in separate cellular compartments. Cell organelles within the intracellular environment also rely on the presence of membranes and the cytoskeleton for structure and function. The functionality of the bilayer is carried out by proteins and determined by the physical properties, a great deal of which depends on the lipid conformation of the membrane.

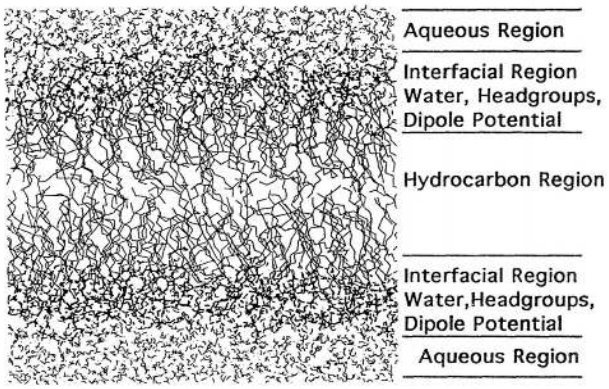


Figure 3.3.1. Schematic diagram of a fluid phase membrane. Visualization derived from a molecular dynamics simulation of bilayer composed of dimyristoylphosphatidylcholine (DMPC) at 325 K. The polar regions of phospholipids are represented by heavier lines.[1]

The bilayer fluid domain consists of a **liquid-ordered phase** (L_o) and a **liquid-disordered phase** (L_d). Though, it should be noted that, for practical applications, the heterogeneity of bio-membranes cannot be simplified to mere differentiation of coexisting lipid domains. Protein interactions must be taken into consideration with regard to heterogeneity thermodynamics, as they are significant to cell metabolism.

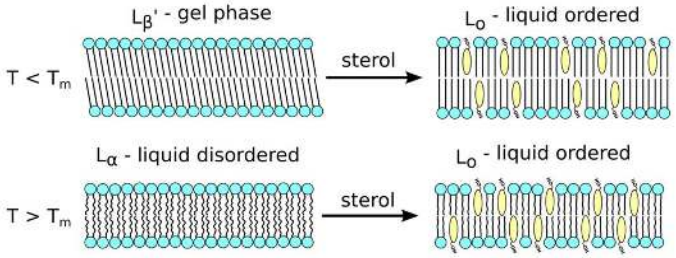


Figure 3.3.2. Sterol addition directly affects membrane fluidity by fluidizing gel phases and ordering liquid phases from liquid-disordered (referred to as Ld in the text, Lα in the Figure) to liquid-ordered (L_o).[8]

II. Fluid phase lipid bilayer membrane

II.a. Temperature Changes

At a given temperature, a short-tailed lipid has more fluidity than a long-tailed counterpart due to packing characteristics. A decrease in temperature results in loss of membrane fluidity due to the lipid acyl chains' formation of greater numbers of Van der Waals interactions. Likewise, an increase in temperature results in greater membrane fluidity as Van der Waals interactions are disrupted and broken. When the environment reaches the critical temperature T_m, and the membrane is transitioning from gel phase to fluid phase:

1. Rotational isomers emerge in the hydrocarbon chains
2. Rapid lateral diffusion increases among the lipid molecules
3. The bilayer membrane expands, causing a decrease in electrostatic free energy

Shorter chain lengths in saturated lipids have decreased T_m in comparison to longer chain lengths. As the number of carbons in the lipid alkane chains increases, so does the gel to liquid phase transition temperature. The T_m of dipalmitoylphosphatidylcholine (DPPC) and 1,2-Distearoyl-sn-glycero-3-phosphocholine (DSPC) is approximately 41˚C and 54˚C, respectively.[3] Usually, there exists a hysteresis curve between cooling and warming.

The enthalpy change ΔH, or heat absorbed at the end of phase transition, can be described by the following equation:[7]

$$\Delta H = T_m \times \Delta S. \tag{3.3.1}$$

where ΔS is entropy change and T_m the critical temperature (transition temperature). ΔH may be also be denoted as the sum of a non-electrostatic value, ΔH^o, and an electrostatic value:[7]

$$\Delta\Gamma = \Gamma(fluid) - \Gamma(ordered). \tag{3.3.2}$$

Thus, considering electrostatic effects, ΔT_m can be described by:[7]

$$\Delta T_m = T_m - T_m^o = \frac{\Delta\Gamma}{\Delta S} \tag{3.3.3}$$

where

$$T_m^o = \frac{\Delta H^\circ}{\Delta S} \tag{3.3.4}$$

is the value of T_m in the absence of electrostatic effects.

Phase behavior is determined by degree of tail saturation and headgroup conformation. Bio-membranes are composed of lipids with various degrees of saturation. Poly-unsaturation may reach as high as six double bonds per chain. Unsaturated and short-chain lipids have decreased T_m, while saturated and long-chain lipids have increased T_m.

Phase behavior and T_m are affected by many factors:[8]

1. Vesicle size (determines the thermodynamic limit)
2. Acyl chain length
3. Presence, number, and positioning of double bonds. Double bonds decrease T_m and allow lipids to contain longer chains.
4. pH
5. Hydration status (fluidity)
6. Cholesterol
7. Addition of a second lipid
8. Alkane chain order

Lipid phase behavior depends on the strength of the Van der Waals interactions between adjacent lipid molecules. Van der Waals interactions are affected by lipid tail length; long-tailed lipids have a greater area for potential interaction and therefore give rise to stronger Van der Waals interactions and decreased lipid mobility. Consequently, the T_m is increased and the lipid shifts away from the fluid phase and toward the gel phase.[8] Van der Waals interactions also contribute to the degree of saturation of the membrane. Unsaturated lipids (lipids containing double bonds in the tails) disrupt membrane packing and render the membrane more hydrophilic.

At physiological temperatures, bilayer membranes are usually in fluid phase. The relative fluidity of individual lipid molecules, and subsequently the lipid membrane, is dependent on temperature. At a certain temperature (Tm), the lipid will undergo phase transition from the gel to the fluid phase. In fluid phase, lipid molecules undergo rapid diffusion and move freely within the two dimensional plane occupied by the membrane. Hence, they may easily traverse long distance within the plane over given periods of time. Even so, there exist constraints on lipid motion due to pressure from bulk lipids at different areas of the bilayer.

The gel phase, in contrast, is characterized by rigidity and limited mobility. Unlike in the fluid phase, lipids in the gel phase do not exchange positions with one another or “flip flop”. Because of this, gel phase bilayers are unable to patch small holes made in the membrane.

II.b. Cholesterol

The addition of cholesterol to a fluid phase bilayer decreases the bilayer's permeability to water and coagulates the bilayer, disrupting local packing and increasing bilayer rigidity. This is due to cholesterol intercalating between alkane tails of lipid molecules. As it occupies the free space, it decreases the flexibility and elasticity of surrounding lipid chains. Consequently, the **lateral diffusion coefficient** effectively decreases. Possibly, cholesterol mediates the solubilization of the bilayer until the entire surface comprises of a fluid phase with high cholesterol content.[4] However, in conditions below melting temperatures, addition of cholesterol to phosphatidylcholine membranes results in greater membrane fluidity.

II.c. Ion Concentration and pH

The "Gouy-Chapman theory" predicts a decrease of transition temperature with increasing charge density.[7] An old study found that divalent cations such as Mg2+ and Ca2+ increase T_m via charge neutralization while monovalient cations such as Li+, Na+, and K+, decrease T_m or spontaneously fluidize the bilayer at certain temperatures.[7] The pH changes required to change the T_m were minimal, i.e. a change from pH 7 to pH 9 was adequate to decrease T_m by 20˚C.[7]

III. Methods of Study

Gel and fluid phases of bilayers may be differentiated via electron microscopy, X-ray diffraction, and magnetic resonance spectroscopy. In addition, epi-fluorescence microscopy of lipid systems utilizes fluorescent probes to differentiate between gel and fluid phase. The efficacy of this technique is optimized with supplementation with photo-bleaching recovery experiments.

Structural information of the fluid phase is difficult to acquire, notably for liquid-disordered phases. Crystallography is an inadequate method as the diffraction signals caused by the fluid phase result from liquid crystals rather than solid. This makes it difficult to form an accurate image of the bilayer phase. Fully hydrated fluid phase bilayers have inherent fluctuating and unstable stacking properties. Partially hydrated fluid phases are composed of nonlinear structures induced by bilayer forces as the structures shift closer, rendering data obtainment difficult. A possible option is to use unilamellar vesicles rather than liquid crystalline arrays. With this method, scattering data obtained from X-rays may be used for analysis.

There are three general scales at which lipid bilayer structure is measured:[2]

1. Short range diffusion over distances roughly the length of the diameters of two lipid molecules. Methods such as quasi-elastic neutron scattering and small angle neutron usage are utilized. Because the measurement is taken over short time periods (< 10^-9 seconds), the actual distance traveled by lipid particles is no more than the vibration or movement of the particle in its immediate environment (see Figure 3.3.3).
2. Intermediate range diffusion over distances of several lipid diameters.
3. Long range diffusion over several micrometers using methods such as fluorescence recovery after photo-bleaching (FRAP) and magnetic resonance techniques. These techniques measure sum translational diffusion and "effective displacement" over large ranges (Figure 3.3.3).

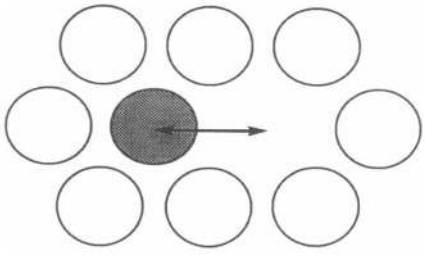


Figure 3.3.3. Displacement possibilities of a specific lipid molecule within the free volume model. The lipid molecule moves to occupy the free volume, whereupon it can either move back to its original location or another lipid molecule can move to occupy it, and so forth. "Effective displacement" occurs only in the latter.[2]

Bilayers can be visualized using fluorescence microscopy. In fluorescence microscopy, a sample is excited using one wavelength of light and emitted in another wavelength. Thus, fluorescent molecules, which have matching excitation and emission properties, are the only molecules that can be visualized.

Electron microscopy is another method to visualize bilayers. In contrast with fluorescence microscopy, electron microscopy delivers a higher resolution image because concentrated electrons are used in place of a wavelength of light. Since electrons have much shorter wavelengths compared with light photons, a greater resolution may be achieved. This is conducive to studying the structure of very small samples.

The issue with utilization of different techniques is that they may be sensitive to different facets of bilayer thickness. Neutron scattering senses the high contrast between protonated lipid and deuterated water molecules; the technique uses this contrast to define overall bilayer thickness (D8), known as “Luzzati thickness”[3]. In contrast, the thickness calculated by X-ray scattering is the distance measured between the peaks in the electron density profile, which corresponds to the distance between the lipid headgroups (D_{HH}).

Although neither neutron scattering or X-ray scattering on its own can be used to accurately depict bilayer structure, a scattering density profile (SDP) model combines X-ray and neutron scattering data to sum up the area “A” per lipid along the bilayer surface. Subsequently, bilayer thickness is compared to A via volume comparisons.[3] Depending on hydration status of the membrane, water molecules may also intercalate into the headgroup region and influence thickness calculation.

Furthermore, “lipid bilayer thickness” is a relatively loose term that may be described in various ways. In literature, hydrophobic thickness (DC) may be used in circumstances wherein a membrane protein is affected by hydrophobic mismatch, in which case the bilayer thickness is defined as the hydrocarbon acyl chains and neglects the presence of water. However, as aforementioned, water molecules may be present in the headgroups, so the thickness (DH) may instead be somewhat arbitrarily taken from headgroup conformation and steric thickness.[3]

References

1. Chiu SW, Clark M, Balaji V, Subramaniam S, Scott HL, Jakobsson E. "Simulation of a Fluid Phase Lipid Bilayer Membrane: Incorporation of the Surface Tension into System Boundary Conditions". *Molecular Engineering 5*: 45-53, 1995.
2. Vaz WLC, Almeida PF. "Microscopic versus macroscopic diffusion in one-component fluid phase lipid bilayer membranes". Biophysical Journal Volume 60:1553-1554, 1991
3. Kučerka N, Nieh MP, Katsaras J. "Fluid phase lipid areas and bilayer thicknesses of commonly used phosphatidylcholines as a function of temperature". *Biochimica et Biophysica Acta* 1808: 2761–2771, 2011.
4. Baumgart T, Hammond AT, Sengupta P, Hess ST, Holowka DA, Baird BA, Webb WW. "Large-scale fluid/fluid phase separation of proteins and lipids in giant plasma membrane vesicles". *PNAS Vol 104 No. 9*:3165-3170, 2007
5. Kučerka N, Liu Y, Chu N, Petrache HI, Tristram-Nagle S, Nagle JF. "Structure of Fully Hydrated Fluid Phase DMPC and DLPC Lipid Bilayers Using X-Ray Scattering from Oriented Multilamellar Arrays and from Unilamellar Vesicles". *Biophysical Journal* Volume 88:2626–2637, 2005.
6. Korlach J, Schwille P, Webb WW, Feigenson GW. "Characterization of lipid bilayer phases by confocal microscopy and fluorescence correlation spectroscopy". *Proc. Natl. Acad. Sci. USA* Vol. 96: 8461–8466, 1999.
7. Träuble H, Eibl H. "Electrostatic Effects on Lipid Phase Transitions: Membrane Structure and Ionic Environment". *Proc. Nat. Acad. Sci. USA Vol.* 71, No. 1, pp. 214-219, 1974
8. Faller, R. Lecture Notes. Univeristy of California Davis, 2014.

3.3: The Fluid Phase is shared under a CC BY 4.0 license and was authored, remixed, and/or curated by LibreTexts.

3.4: The Gel Phase

The lipid bilayer is a thermodynamic system that transitions from the relatively disordered liquid phase to the relatively ordered gel or solid-phase when enough heat is removed from the system [1]. In this page we will detail the gel phase of the lipid bilayer. Biological plasma membranes express a plethora of unique lipids, sterols, and proteins and exhibit greater complexity than model lipid bilayer systems. At temperatures above the melting point (Tm) the lipid bilayer exists in the liquid phase while at temperatures below Tm, the lipid bilayer enters the gel phase. In the gel phase, the lipid bilayer undergoes a fundamental molecular reorganization characterized by an increase in order, a loss of lateral mobility within a given leaf of the bilayer as well as a change in acyl chain configuration within a single lipid molecule, and a change in the broad topology of the membrane [1, 2, 3].

Review of lipid bilayer phases and phase transitions

The lipid bilayer is a thermodynamic system that exists in phases. These phases are largely characterized by the relative lateral mobility of lipids within the bilayer, the molecular conformation of lipids within the bilayer, and the topological structure of the bilayer. Lipid bilayers exist in either the liquid or gel phase, at a broad range of temperatures. These phases are separated by the temperature at which the bilayer will undergo the transition from one phase to the other, termed T_m. T_m is impacted by many factors e.g. acyl chain length and saturation state, the ionic conditions of the solvent, presence of sterols. At temperatures above Tm, the lipid bilayer exists in the liquid phase, characterized by a relatively high degree of lateral mobility of individual lipids within the bilayer. At temperatures below T_m, the lipid bilayer exists in the gel or solid phase [1, 2, 3]. The gel phase is described in detail below.

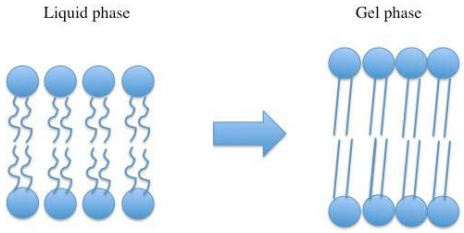


Fig 1. cartoon depiction of molecular and topological differences between lipid bilayer liquid phase and gel phase [1]

Molecular characterization of the gel phase

In the gel phase, individual lipids within the lipid bilayer lose lateral mobility, associated with an increase in order. The lipid head groups become more tightly packed and dehydrated, and the lipid acyl chain tails become fully extended and more tightly packed with increased van der waals interactions as seen in Figure 3.4.1. During the phase transition from the liquid phase to the gel phase, the acyl chain tails undergo an isomerization from a gauche conformation to a trans conformation. That is, in the gel phase, the acyl chains contain relatively few gauche conformations and are in the trans conformation. This change in conformation to mostly trans is thought to promote the tighter packing arrangements as it removes “kinks” in the acyl chain present in the lipid phase. In the gel phase, the lipid bilayer also becomes thicker relative to the liquid phase as seen in Figure 3.4.2 [1] . In the gel phase, the lipid bilayer also increases in stiffness than in the liquid phase. The stiffness of lipid bilayers in the liquid phase is typically ~$10\mathrm{m}k_BT$ (where k_B is the Boltzmann constant

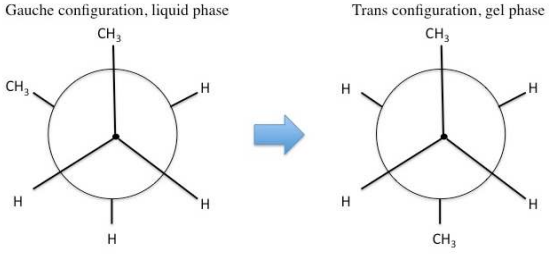


Fig 2. Isomerization of acyl chains from gauche configuration to trans configuration during transition from liquid phase to gel phase [1]

multiplied by the temperature) while the stiffness of lipid bilayers in the gel phase are 30-50 kBT [4, 7]. This increase fundamentally impacts the propensity of the lipid bilayer to curve and bend as well as the inherent fluctuations of the lipid bilayer [methods in membrane lipids]. As previously mentioned, the length of the lipid acyl chains impacts Tm. As an example, 1,2-dilauroyl-sn-phosphatidylcholine (DLPC) with an acyl chain length of 12 carbons is in the liquid phase at room temperature while 1,2-distearoyl-sn-glycero-3-phosphocholine (DSPC) with an acyl chain length of 18 carbons is in the gel phase at room temperature [1]. The structure of gel phase dipalmitoylphosphatidylcholine (DMPC) has also been investigated by x-ray diffractions providing insight into the topological organization of the gel phase [6]. The structure of gel phase DPPC has also been investigated using similar methodology [10]. The topological organization of gel phase phosphatidylethanolamine has been studied using neutron diffraction [11].

Biophysical characterization of the gel phase

At temperatures below Tm, the lipid bilayer undergoes a fundamental reorganization to occupy the lowest free energy state. This fundamental reorganization is the phase transition from the liquid phase to the gel phase. This is a first order phase transition characterized by a discontinuous change in density [1]. As an example, a dipalmitoylphosphatidylcholine (DPPC) lipid bilayer enters the gel phase at temperatures below 15 °C [4].

The transition between phases has been experimentally investigated using techniques such as scanning calorimetry and fourier transformed infrared (FTIR) spectroscopy. FTIR is a spectroscopic method that measures the vibrational frequency of the ethyl groups on the acyl tails. As such, in FTIR, lipid bilayers in the gel phase display low vibrational frequency that increases as a function of temperature [1]. The transition to the gel phase from the liquid phase has been described by the nucleation and growth theory; in which a critical nucleus is formed that then serves as the initiation event for lateral formation of the gel lipid bilayer. The formation of the critical nucleus within the liquid lipid bilayer has an associated free energy described by equation 1:

$$\Delta G = \Delta \mu n + 2\gamma[\pi \sigma n]1/2 \tag{1}$$

Where Δμ is the chemical potential of gel phase lipids, n is the number of lipids in the critical nucleus, γ is the line tension between the phases, and σ is the area per lipid in the gel phase. This nucleation and growth event has been modeled in molecular dynamics simulations [5, 9].

The gel phase in more complex lipid bilayers

Lipid bilayers composed of different lipid types exhibit more complex behavior than simple lipid bilayers composed of a single lipid species. The addition of a second lipid species, with a different associated Tm to a bilayer impacts the transition to the gel phase by changing the Tm of the system. The global behavior of this complex lipid bilayer is largely dependent on the abundance of each lipid species such that a threshold population of each lipid species is necessary for cooperative phase separation [2]. Phase separation has been observed in lipid bilayers composed of mixed lipid species and has been modeled in molecular dynamics simulations as seen in Figure 3.4.3 [1]. Also, phase separation in which one lipid species resides in the liquid phase and the other lipid species resides in the solid (gel) phase can also occur. A predicted Tm for these mixed lipid bilayers can be calculated although it is important to note that lipid species with higher Tms have greater enthalpy and thus contribute more to the Tm in a mixed species bilayer, thus making the predicted Tm deviate from the actual Tm [1].

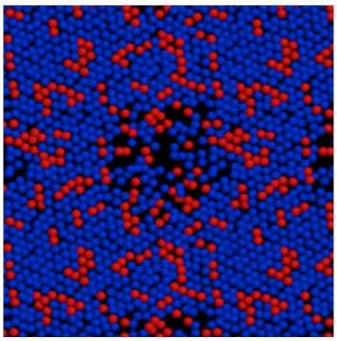


Fig 3: MDS of phase separation in a bilayer composed of DSPC (blue) and DPPC (red). Note the central fluid domain surrounded by the surrounding gel domain [1].

While it is generally accepted that biological lipid bilayers do not largely exist in the gel phase, simple phase coexistence in lipid bilayers has been observed. This organization has been described as liquid-ordered, in which lipid domains with tight packing but high rates of lateral mobility exist within the larger area of liquid-disordered lipids [1, 2, 3, 12]. However our understanding of the gel phase provides direct insight into our understanding of these lipid microdomains. It is also clear that phase transition in biological membranes results in packing defects and results in “leakiness” during the phase transition [1]. Phase separation has been investigated using atomic force microscopy. These experiments have demonstrated that lipid domains with unique topological character do exist within lipid bilayers [8].

Concluding Remarks

The lipid bilayer is a thermodynamic system. Like other thermodynamic systems, the lipid bilayer exists in phases. At temperatures below the Tm of the lipid bilayer, the lipid bilayer enters the gel phase. The gel phase is characterized by a high degree of order, decreased lateral mobility of lipids within a leaf of the bilayer, tight packing, acyl chain straightening (due to isomerization of the acyl chains to mostly trans state), and thickening of the bilayer relative to the liquid phase [1, 2, 3].

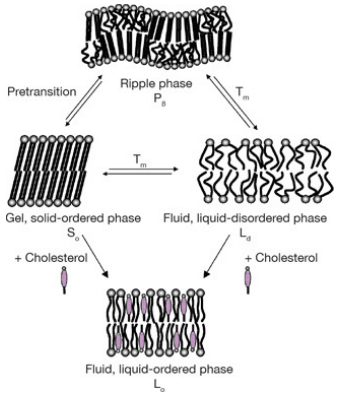
References

1. Faller, R. MCB241 Lectures (2015)
2. Mukherjee, S. and F. R. Maxfield (2004). "Membrane domains." Annu Rev Cell Dev Biol 20: 839-866.
3. van Meer, G., et al. (2008). "Membrane lipids: where they are and how they behave." Nat Rev Mol Cell Biol 9(2): 112-124.
4. Dopico, Alex. Methods in membrane lipids. Humana, 2007. Print.
5. Marrink, S. J., et al. (2005). "Simulation of gel phase formation and melting in lipid bilayers using a coarse grained model." Chem Phys Lipids 135(2): 223-244.
6. Tristram-Nagle, S., et al. (2002). "structure of gel phase DMPC determined by x-ray diffraction." Biophys J 83.
7. Picas, L., et al. (2012). "Direct measurement of the mechanical properties of lipid phases in supported bilayers." Biophys J 102(1): L01-03.
8. Goksu, E. I., et al. (2009). "AFM for structure and dynamics of biomembranes." Biochim Biophys Acta 1788(1): 254-266.
9. Heller, H., et al. (1993). "molecular dynamics simulation of a bilayer of 200 lipids in the gel and in the liquid crystal phases " Journal of physical chemistry 97.
10. Wiener, M. C., et al. (1989). "structure of the fully hydrated gel phase of DPPC." Biophys J 55.
11. Builtd, G. and J. Seeleg (1980). "conformation of phosphatidylethanolamine in the gel phase as seen by neutron diffraction." Biochemistry 19.
12. Schram, V., et al. (1996). "topology of gel phase domains and lipid mixing properties in phase separated two-component phosphatidylcholine bilayers." Biophys J 71.

3.4: The Gel Phase is shared under a CC BY 4.0 license and was authored, remixed, and/or curated by LibreTexts.

3.5: The Ripple Phase

Lipids consist of hydrophilic polar head groups attached to hydrocarbon chains and arrange themselves in bilayers to make biological membrane structures. At lower temperatures, the bilayer is in a $L_{\beta'}$ 'gel' phase and there is a transition to 'fluid' phase, L_{α} , at higher temperatures due to an increase in mobility of individual lipids in the bilayer. A smectic ripple phase $P_{\beta'}$ is observed in hydrated lipid bilayers between the $L_{\beta'}$ and L_{α} phase. This phase is characterized by corrugations of the membrane surface with well-defined periodicity with an axis parallel to the mean bilayer plane [1]. The molecular origin of ripple-phase formation is traditionally been associated with the lipid headgroup region and hence lipids can be classified into ripple-forming and non-ripple forming lipids based on their headgroups. One of the lipid families belonging to ripple-forming class is phosphatidylcholines and has been studied in extensive detail [1].

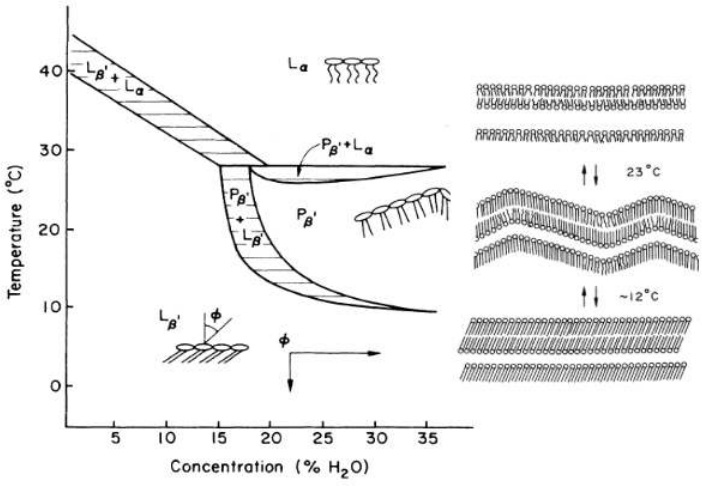


Scheme above shows different physical states adopted by a lipid bilayer in aqueous medium [2]

Thermodynamics and Existence

The existence of the ripple phase at first sight is paradoxical on thermodynamic grounds since it involves an apparent lowering of symmetry (from $L_{\beta'}$ *to* $P_{\beta'}$) on increasing the temperature. Some models suggest that ripples exist because of periodic local spontaneous curvature in the lipid bilayers formed due to electrostatic coupling between water molecules and the polar headgroups or coupling between membrane curvature and molecular tilt. It has also been speculated that ripples form to relieve packing frustrations that arise whenever the relationship between head-group cross sectional area and cross-sectional area of the apolar tails exceeds a certain threshold [1]. However, there is not one conclusive theory to explain ripple phase formation.

Phase Diagram Depicting Ripple Phase



Experimental phase diagram for (1,2-dimyristoyl-sn-glycero-3-phosphocholine) DMPC, plotted as a function of temperature and hydration. Solid lines indicate first order transitions. Arrows indicate directions of increasing tilt in the $L_{\beta'}$ phase. The rightmost schematic shows, from top to bottom, the forms of the phases L_{α}, $P_{\beta'}$ and $L_{\beta'}$ [3]

Types of Ripple Structures

Two different co-existing ripple phases have been reported, one is asymmetric, having a sawtooth profile with alternating thin and thick arms and a periodicity of 13-15 nms and the other one is symmetric and has a wavy sinusoidal structure with twice the periodicity of the asymmetric structure [4]. In phosphatidylcholine bilayers, asymmetric ripple phase formed is more stable which forms at the pretransition temperature upon heating from the gel phase. The metastable ripple phase is formed at the main phase transition upon cooling from the fluid phase and has approximately double the ripple repeat distance as compared to the stable phase [1].

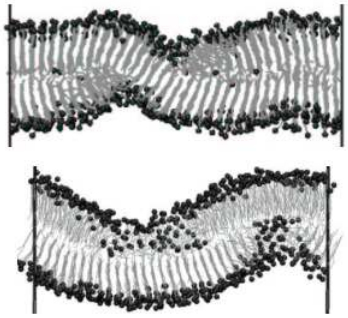


Figure above shows the model of asymmetric (upper) and symmetric (lower) ripple phase with 720 lipids molecules in a bilayer [4].

Experiments to Understand Ripple Phases

Freeze-fracture electron microscopy (FFEM) has been utilized to understand the structure of ripple phases. Freeze-fracture preparation rapidly freezes the lipid bilayer suspension at certain temperature (cryofixation) which is then fractured. The cold fractured surface is then shadowed with evaporated platinum or gold at an average angle of 45° in a high vacuum evaporator. A second coat of carbon, evaporated perpendicular to the average surface plane is often performed to improve stability of the replica coating. The specimen is returned to room temperature and pressure, then the extremely fragile "pre-shadowed" metal replica of the fracture surface is released from the underlying biological material by careful chemical digestion. The still-floating replica is thoroughly cleaned from all the chemical residues, dried and then viewed in the TEM (Transmission electron microscopy) [6]. T he results obtained through FFES show periodic linear arrays of ripples which change direction by characteristic angles of 60 or 120 degrees reflecting the hexagonal packing in the lipids [1].

Atomic Force Microscopy (AFM) allows for direct visualization of the ripple phase in supported hydrated bilayers and dynamics of formation and disappearance of ripple phases can be studied at pretransition temperatures [1]. Some examples of AFM images depicting Ripple phase are shown below from Kaasgaard *et al* [1]. In the image descriptions, Λ/2 represents the asymmetric phase and Λ shows the symmetric phase because of twice the periodicity of metastable phase than the stable phase. A phase with periodicity 2Λ has also been observed.

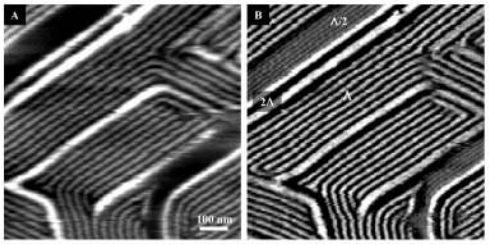


FIGURE 1 (*A*) Height mode AFM image showing different ripple phases in a DPPC-supported double bilayer at 37°C. (*B*) Deflection mode image of the same bilayer region. Three different ripple types are observed. The ripple types are denoted Λ/2-, Λ-, and 2Λ-ripples in the deflection mode image.

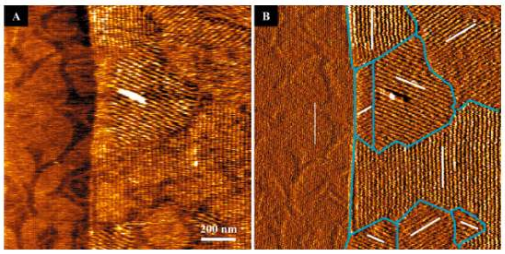
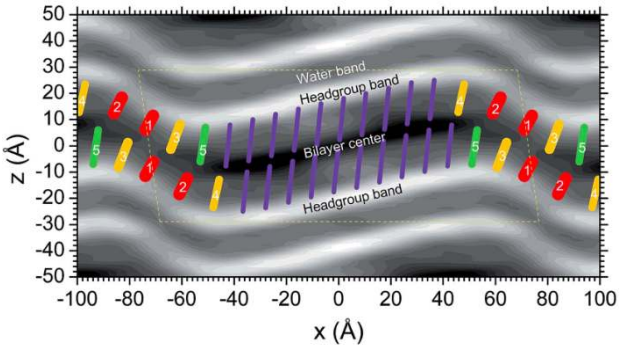


FIGURE 5 Height mode (*A*) and deflection mode (*B*) images of the interfacial region between a Λ/2-ripple domain and several Λ-ripple domains in a 7:3 DMPC-DSPC lipid bilayer at 26.0°C. The Λ/2-ripple domain emerged from within a region of Λ-ripples by an interconversion of Λ-ripples to Λ/2-ripples. The Λ/2-ripple domain is visible as the darker region on the left in the height mode image (*A*) and as the short-wavelength ripples on the left in the deflection mode image (*B*). Whereas the Λ/2-ripples were all oriented in the same direction, the Λ-ripples were present as a number of different regions that each had their own ripple direction. The different ripple regions and directions have been outlined in *B*. The rounded structures that are also seen, and are particularly visible in the Λ/2-ripple domain, correspond to domains in the first bilayer in close contact with the mica support.



Low Angle and Wide Angle X-ray scattering have also been utilized to understand the ripple phase behavior by mapping electron density as shown above [5].

Future Research

Although many theories, simulations and experiments have been conducted on Ripple phase, the exact parameters affecting its formation are still unknown for different systems. It is still not known how the hydrocarbon chains are oriented in the bilayer in $P_{\beta'}$ phase [8]. The existence of ripple phase still remains enigmatic and determining the detailed molecular structure would seem to be prerequisite to understanding the interactions that are responsible for its formation [7].

References

1. Thomas Kaasgaard,* Chad Leidy,* John H. Crowe,y Ole G. Mouritsen,z and Kent Jørgensen* **Temperature-Controlled Structure and Kinetics of Ripple Phases in One- and Two-Component Supported Lipid Bilayers,** *Biophysical Journal Volume 85 July 2003 350–360* .
2. Image from- http://popups.ulg.ac.be/1780-4507/index.php?id=6568
3. Carlson, J. M. and Sethna, J. P. Phys. Rev. A 36, 3359–3374 Oct (1987).
4. Olaf Lenz, Friederike Schmid, **Structure of symmetric and asymmetric "ripple" phases in lipid bilayers,** Phys. Rev. Lett. 98, 058104, January 2007.
5. Kiyotaka Akabori and John F. Nagle**, Structure of the DMPC lipid bilayer ripple phase**, Soft Matter, 2015, 11, 918
6. https://en.Wikipedia.org/wiki/Electron_microscope
7. Nagle *et al*., **Lipid bilayer structure,** Volume 10, Issue 4, 1 August 2000, Pages 474–480
8. Nagle JF, Tristram-Nagle S. **Structure of lipid bilayers**. *Biochimica et biophysica acta*. 2000;1469(3):159-195.

3.5: The Ripple Phase is shared under a CC BY 4.0 license and was authored, remixed, and/or curated by LibreTexts.

3.6: Rafts

The traditional fluid mosaic model of biological membranes stated that lipids are homogeneously mixed. However, biological membranes are actually composed of a complex mixture of lipid domains that exist in different degrees of order, ranging from the high order gel phase to low order liquid phase. Lipid “rafts” are membrane microdomains composed of higher order lipids that have tight interaction with each other relative to the “sea” of liquid phase lipids known as bulk lipids. These rafts have been estimated to be 10-200 nm in size. Small rafts can merge to form large rafts through protein-protein and protein-lipid interactions. The rafts are important because certain membrane proteins preferentially localize to these domains and biological processes such as signal transduction occur there as a result. Proteins are often targeted to rafts by palmitoylation and myristoylation, which are covalent attachments of fatty acids. Glycosylphosphatidylinositol (GPI)-anchors also localize proteins to rafts.

Structure and Formation

Rafts exist as planar domains or invaginated structures known as **caveolae**[1]. Caveole type rafts contain the cholesterol binding protein cavin, which are located in the inner membrane leaflet and are needed for membrane invagination. Cavins are peripheral membrane proteins that bind to caveolar phosphatidylserines. Caveolin is another caveolar protein that is involved in signaling processes. Caveolin contains three palmitoylated cysteines and a cholesterol binding sequence (VTKYWFYR) that facilitate localization to rafts.

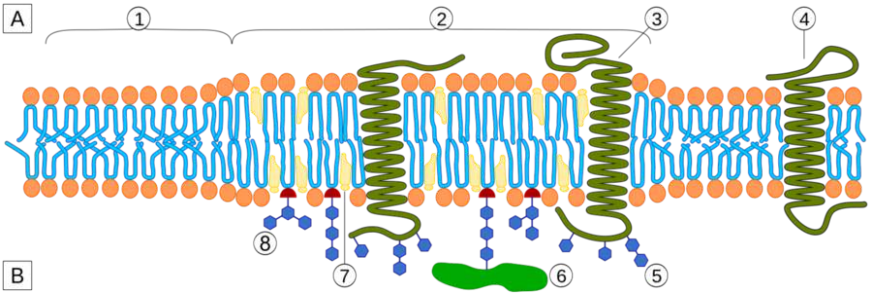


Figure 3.6.1: Lipid raft organization, region (1) is standard lipid bilayer, while region (2) is a lipid raft. (Public Domain; Artur Jan Fijałkowski.)

Lipid rafts are also found in the endomembrane system in addition to the plasma membrane[1]. Sphingolipids and cholesterol are synthesized in the ER. They are then trafficked to the Golgi, where they associate to form rafts. Raft containing vesicles are then sent to the plasma membrane through the trans Golgi network, which is involved in raft recycling as well. Rafts also participate in sorting and membrane targeting of lipids in the trans Golgi network.

Lipid Composition and Biophysical Properties

Rafts are composed of sphingolipids such as sphingomyelin, cholesterol, and phospholipids.[2] Sphingomyelin is composed of a sphingosine, a fatty acid and a phosphocholine head group. Sphingomyelin has a high T_m that makes rafts resistant to detergent at low temperatures. Rafts are often therefore referred to as detergent resistant membranes (DRMs).

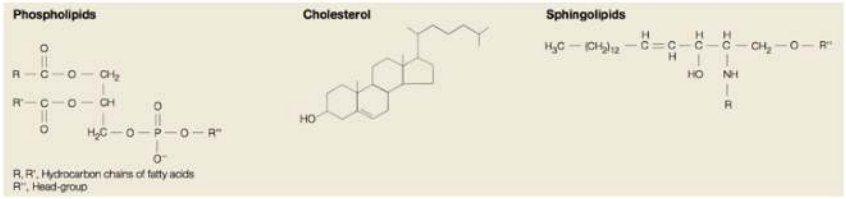


Figure 3.6.1: Raft component structures. Reprinted by permission of Macmillan Publishers Ltd: Nature Reviews[2], copyright 2000.

Phase separation caused by higher order rafts and lower order bulk lipids is the driving force for raft formation. Raft associated lipids are more saturated than bulk lipids and therefore are more tightly packed. Cholesterol preferentially localizes to rafts because it has a rigid structure that prefers the higher order state of the raft. The hydroxyl group in cholesterol interacts with the sphingosine amide, which contributes to the higher ordering. In fact, the DRM rafts disappear if cholesterol is extracted from the membrane.

Another driving force for raft formation is phase separation caused by differential hydrophobic acyl chain length in raft associated and non-associated lipids. The acyl chains of shpingomyelin are longer than that of typical phospholipids found in the bulk lipid of biological membranes. A homogenous mixure of long and short chain lipids would result in higher exposure of the hydrophobic

region of the long chain lipids to the surrounding water than if phase separation were to occur. Therefore, phase separation of long and short chain lipids decreases the free energy of the membrane. The inner and outer leaflet of the raft may be held together by interdigitation of the long chain acyl chains and/or integral protein-lipid interactions. Hydrophobic mismatch, or the difference between protein hydrophobic transmembrane domain lengths and hydrophobic membrane widths, can cause proteins to associate or not associate with rafts. Hydrophobic mismatch can also effect protein conformation and therefore protein activity.

Discovery and Evidence

The Singer and Nicolson fluid mosaic model of biological membranes was proposed in 1972. By the early 1980s it became clear that membranes lipids preferentially segregated into different phases under physiological conditions and therefore existed as a heterogeneous mixture in membranes[3]. Rafts were first discovered in the 1990s when a significant fraction of membrane remained resistant to Triton X-100 detergent at 4˚C[4]. However, there was still a question of whether the DRM was an artifact of the cold treatment. To answer this question, resonance energy transfer (RET) was measured in cells expressing two types of membrane associated fluorescent folate analogs, GPI anchored folate receptors and transmembrane anchored folate receptors[5]. The GPI anchored probe was predicted to localize to the DRM domains, while the transmembrane anchored probe was not. The GPI anchored probe's RET did not increase with increased density of the probe, suggesting that the probes were non-randomly clustered at a spatial distribution below the resolution of the microscope. The transmembrane anchored probe's RET increased linearly with increased density, suggesting that they were randomly distributed throughout the membrane. Also, when cholesterol was extracted from the membrane, the GPI anchored probes were found to be randomly distributed. This data suggests that the DRM rafts are in fact real.

Another key piece of evidence for the existence of rafts came from membrane protein cross-linking experiments[6]. Membrane proteins were cross-linked by aggregating a certain protein with an antibody and cross-linking nearby proteins with aldehyde fixatives. Membrane proteins associated with the DRM rafts were colocalized, while proteins not associated with the DRM rafts did not colocalize with raft proteins. The close proximity of raft-associated proteins suggests that the DRM rafts are real membrane microdomains.

Signal Transduction

Many proteins involved in signal transduction have been found to colocalize with the raft microdomains. Rafts can be important for signal transduction because they provide a microenvironment where specific signal responses can occur upon ligand binding to the receptor. There are two models for raft mediated signal transduction[2]. One model is that ligand bound receptors migrate to rafts where the downstream signal transduction occurs. The other model is that ligand binding causes several rafts with different signaling components to merge and produce the downstream signal response. A combination of the two models where receptor migration to a raft causes different rafts to merge is also possible.

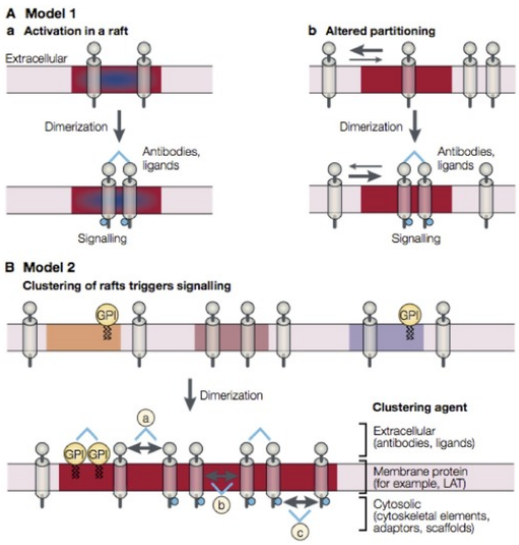


Figure 3.6.2: Models for raft mediated signal transduction involving single rafts (A) and multiple rafts (B). Reprinted by permission of Macmillan Publishers Ltd: Nature Reviews[2], copyright 2000.

The first discovered example of raft associated signal transduction was the tyrosine kinase signal transduction of immunoglobulin E (IgE) signaling in the allergic immune response[2]. In this case, IgE binds to the FceRI receptor, then oligomeric antigens bind IgE, thereby crosslinking receptor complexes. The crosslinked receptor complexes are recruited to rafts where Lyn, a tyrosine kinase, phosphorylates the receptor complex, which starts the phosphorylation signaling cascade. Rafts have also been shown to be involved in other types of signal transduction such as G-protein coupled signal transduction[2].

A new and exciting aspect of the lipid raft mediated signal transduction is the interaction of rafts with the cytoskeleton. Actin binds to caveolins in caveoles and tetraspanins in planar rafts. Through this interaction with the cytoskeleton, rafts have been shown to be involved in cellular polarity, cell migration, neuronal signaling, neuronal membrane repair, and T-cell activation[1].

Viral Interactions

Another major role for lipid rafts is in entry and shedding of certain viruses[7]. Both envelope lacking and enveloped viruses can depend on lipid rafts for cell entry. The mechanism of attachment and entry can depend on lipid-lipid, lipid-protein, and protein-protein interactions. Many viral proteins have been shown to interact with cholesterol and sphingolipids in the rafts. Caveoles can also be involved in endocytosis of certain viruses.

When certain viruses are released from the host cell, they bud off and their membrane is formed from the host cell plasma membrane. The similarity of certain viral and raft lipid composition indicates that these raft-dependent viruses bud off at raft sites. Since a single raft is not large enough to form a full viral membrane, multiple lipid rafts are likely recruited before virus budding. HIV is an example of a virus that has raft like lipid composition[7]. HIV Gag proteins have positively charged residues and a myristate group that targets it to phophatidylinositol (PI(4,5)P2) in the plasma membrane inner leaflet. Gag aggregation in the plasma membrane creates a saturated lipid environment that recruits raft microdomains. HIV budding then proceeds at the raft microdomain.

A study on the flu virus has shown that removing cholesterol from the host membrane increases viral budding, but produces viruses with very low infectivity[8]. This suggests that rafts are more important for cell entry than for viral shedding.

Prevalence of Lipid Rafts

Rafts have historically been studied in animal membranes, but plant membrane rafts have more recently been studied as well. Plants do not contain cholesterol, but other sterols contribute to plant lipid rafts. As with animal rafts, plant rafts also mediate signal transduction events. One well studied case is **Pathogen-Associated Molecular Patterns (PAMPs)**-induced signaling events[9]. Another recent study has revealed an association of lipid rafts to plasmadesmata, which are direct cytosolic connections between plant cells[10]. The full implications of this finding are yet to be elucidated. Rafts have also been described in other eukaryotes such as fungi[11].

Rafts may not be exclusive to eukaryotes. Recent work in *Bacillus subtilus* has shown differential protein localization in DRMs[12]. Some of these proteins have homology to eukaryotic raft associated proteins and many are involved in bacterial signaling and transport processes.

Non-Raft Microdomains

Other microdomains that are not cholesterol-associated rafts also exist in biological membranes. These microdomains are sometimes called “non-raft” domains, a term which was coined at the 2006 Keystone Symposium of Lipid Rafts and Cell Function[13]. These non-raft domains are likely quite diverse in composition and function, but have not been well characterized. Many non-raft microdomains are made up of poly-unsaturated lipids, which exclude cholesterol. Some membrane proteins are thought to have differential activity when localized to raft or non-raft microdomains.[14]

References

1. Head, B. P., Patel, H. H. & Insel, P. A. Interaction of membrane/lipid rafts with the cytoskeleton: impact on signaling and function: membrane/lipid rafts, mediators of cytoskeletal arrangement and cell signaling. *Biochimica et biophysica acta* **1838**, 532-545, doi:10.1016/j.bbamem.2013.07.018 (2014).
2. Simons, K. & Toomre, D. Lipid rafts and signal transduction. *Nature reviews. Molecular cell biology* **1**, 31-39, doi:10.1038/35036052 (2000).
3. Karnovsky, M. J., Kleinfeld, A. M., Hoover, R. L. & Klausner, R. D. The concept of lipid domains in membranes. *The Journal of cell biology* **94**, 1-6 (1982).

4. Brown, D. A. & London, E. Functions of lipid rafts in biological membranes. *Annual review of cell and developmental biology* **14**, 111-136, doi:10.1146/annurev.cellbio.14.1.111 (1998).
5. Varma, R. & Mayor, S. GPI-anchored proteins are organized in submicron domains at the cell surface. *Nature* **394**, 798-801, doi:10.1038/29563 (1998).
6. T, H., P, S., P, V. & K, S. Lipid domain structure of the plasma membrane revealed by patching of membrane components. *The Journal of cell biology* **4**, 929-942 (1998).
7. Lorizate, M. & Krausslich, H. G. Role of lipids in virus replication. *Cold Spring Harbor perspectives in biology* **3**, a004820, doi:10.1101/cshperspect.a004820 (2011).
8. Barman, S. & Nayak, D. P. Lipid raft disruption by cholesterol depletion enhances influenza A virus budding from MDCK cells. *Journal of virology* **81**, 12169-12178, doi:10.1128/JVI.00835-07 (2007).
9. Simon-Plas, F., Perraki, A., Bayer, E., Gerbeau-Pissot, P. & Mongrand, S. An update on plant membrane rafts. *Current opinion in plant biology* **14**, 642-649, doi:10.1016/j.pbi.2011.08.003 (2011).
10. Raffaele, S. *et al*. Remorin, a solanaceae protein resident in membrane rafts and plasmodesmata, impairs potato virus X movement. *The Plant cell* **21**, 1541-1555, doi:10.1105/tpc.108.064279 (2009).
11. Malinsky, J., Opekarova, M., Grossmann, G. & Tanner, W. Membrane microdomains, rafts, and detergent-resistant membranes in plants and fungi. *Annual review of plant biology* **64**, 501-529, doi:10.1146/annurev-arplant-050312-120103 (2013).
12. Lopez, D. & Kolter, R. Functional microdomains in bacterial membranes. *Genes & development* **24**, 1893-1902, doi:10.1101/gad.1945010 (2010).
13. Shaikh, S. R. & Edidin, M. A. Membranes are not just rafts. *Chemistry and physics of lipids* **144**, 1-3, doi:10.1016/j.chemphyslip.2006.06.017 (2006).
14. Wassall, S. R. & Stillwell, W. Docosahexaenoic acid domains: the ultimate non-raft membrane domain. *Chemistry and physics of lipids* **153**, 57-63, doi:10.1016/j.chemphyslip.2008.02.010 (2008).

3.6: Rafts is shared under a CC BY 4.0 license and was authored, remixed, and/or curated by LibreTexts.

3.7: Lipid Phase Coexistence

Lipid phase coexistence occurs when a membrane is composed of a heterogeneous mix of lipid physical states organized into lateral domains that can range from gel (solid phase) to liquid disordered and to liquid ordered phases.

Lipid phase differences within the plane of the membrane give rise to heterogeneity in the overall function and structure of the membrane. The structural heterogeneity is caused by the presence of multiple types of lipids with varying physical properties such as: saturation state, presence of double bonds, length of the hydrophobic acyl chains as well as, some suggest, the size of the head group. Phase coexistence is characterized by diverse lipid types and their interactions between each other within the same membrane. Generally, any physical component of the lipid which leads to less or more packing affinity between other lipids will affect the phase state at certain environmental conditions. Phase coexistence is caused by heterogeneity of lipid phases in the same environmental conditions.

Multiple Lipid Phases

The ordered state of lipids can be thought of generally as the "packedness" of the lipids which is specifically determined by the orientation of the hydrophobic acyl tails--straight and extended (ordered) or free to bend and relatively unpacked (disordered). There are liquid ordered and liquid disordered phases in which the acyl tails are more or less ordered together in a uniform arrangement, respectively. Lipids of different physical properties will exist in various phases (gel or liquid) simultaneously even in the same temperature.

Gel phase lipids and liquid phase lipids coexist in the plane of the membrane as distinct lateral domains. This frequently occurs when low melting point lipids mix with high melting point lipids--in which case the low melting point (low Tm) lipids will preferentially remain in the liquid phase at a set of temperatures where the high melting point lipids would be in the gel phase. The physical structure of these gel phase lipids alters the overall membrane structure by changing the height of the membrane over those domains and causing tension along the boundary between the different domains.

The physical property differences between ordered and disordered lipids also alter the propensity of the membrane to curve or flex in certain directions. This curvature between liquid and gel phase domains give rise to tension within the lipid layers--which can be seen in electron microscopy images as tilting of the lipids in response to the tension induced by the physical differences of the lipid phase domains. Furthermore, membrane flexability and curvature is important for proper membrane function which involves vesicular budding, membrane tubulation, and other cellular trafficking processes.

Methods of Observation

Various methods of detecting lipid phase coexistence in membranes and testing related hypotheses are used including utilizing unique fluorescent probes with phase sensitive spectra, measuring the infrared spectra of lipids in a membrane, and examining the surface of the membrane. While these methods are somewhat diverse--from observing the topology to using fluorophores and infrared light excitation and emission to detect lipid heterogeneity--each is very useful in elucidating the nature and organization of lipid phase coexistence in membranes.

- **Fourier Transform Infrared Spectroscopy (FTIR):** A common technique in detecting phase differences in membranes is by shining infrared light on the sample and measuring the spectroscopic properties of the sample following excitation with various wavelengths. Differences in the spectra equate to differences in membrane composition or, more specifically, different lipid phases. FTIR has a wide variety of uses but is particularly useful in membrane and lipid studies due to its ability to capture spectra for nonhomogenous lipid samples at a very high resolution.
- **Atomic Force Microscopy (AFM):** Phase coexistence of lipid membranes can be readily observed in real time, as the lipids undergo phase transitions, using AFM while adjusting the temperature to induce phase changes. Generally, by using a probe attached to the end of a lever (upon which laser is directed) to scan over the top of a sample, the lever will move up and down according to the topology of the sample surface, causing the laser deflection to change--which can then be interpreted as the sample surface. Since lipids in different phases exhibit different height characteristics when the tails straighten or are relaxed AFM allows you to visualize those height differences by scanning topology of the membrane surface.
- **Laurdan (6-dodecanoyl-2-dimethylaminonaphthalene):** Laurdan is a fluorescent molecular dye that inserts into the membrane bilayer at the boundary between the hydrophobic and hydrophilic portions of the lipids. The usefulness of this molecule is the wide emission spectra shift it undergoes upon entering different polar environments. As the lipids surrounding the Laurdan molecule change phase and become either less or more ordered in response to stimuli (temperature for example)

the polarity environment also shifts. Laurdan molecules are sensitive to this polarity change in the membrane in that the emission wavelength shifts significantly. This emission difference, modulated by the lipid phase environment, allows researchers to easily distinguish between lipids at different phases and following transitions. Laurdan dye can be used to study phase coexistence in that it pinpoints areas of differing phases in the membrane.

Biological significance

Heterogeneity at the lipid phase level is important for proper membrane function in cells, especially given the diverse range of functions and structures in which the membrane is involved. Most notably, lipid phase differences within the bilayer membrane allow for (and even encourage) a wide variety of shape changes that are necessary for fundamental cellular processes such as vesicular trafficking (through the production of vesicles) as well as cell signaling and membrane associated-protein function.

Membrane curvature

While proteins are known to mediate membrane curvature, lipid composition and the phase state also plays a role in curvature and bending of the bilayer into the diverse array of membrane shapes we see in the cell. Specifically, lipids of different phase can encourage membrane curvature at the boundary between the two phases. Gel and liquid phase lipid domains, for example, creates line tension along the border of the phase domains. The difference in the bending properties between the two lipids at different phases encourages out-of-plane bending of the membrane, which could then lead to vesicle budding or fission. By changing the temperature you can alter the lipid phases and therefore the membrane curvature as it shifts due to the different physical organization of the lipids.

Intracellular trafficking

Membrane curvature is fundamental to cellular processes like endomembrane trafficking (e..g, endocytosis) in which vesicles bud and fuse to various membranes like the plasma membrane, the Golgi apparatus stacks, endoplasmic reticulum tubules, and numerous other organelles. Therefore, lipid phase coexistence and membrane heterogeneity is important in maintaining lipid and membrane composition between the organelles/subcellular locations (by encouraging membrane budding and therefore membrane recycling/flow throughout the cell) but also plays a role in trafficking of physiologically important material in the cell.

Phase coexistence and membrane proteins

Lipid phase coexistence could also affect membrane associated-protein function by altering the structure and mechanical properties of the membrane in which the protein is embedded. Also, some proteins preferentially reside in one phase over others; alpha-helix proteins are more commonly found in liquid phase lipid domains. Conversely, membrane proteins can influence the phase state of the surrounding lipids by altering the local organization of lipids in the bilayer and the interactions between lipid chains.

Summary

Model membranes are often composed of homogenous lipids in order to maintain uniformity in experiments. However, in reality membranes can be quite heterogeneous in their lipid composition and the phase state of those lipids. These lipids are organized into lateral domains in the membrane and contribute to many fundamental processes within the cell such as endocytosis and secretion. The mechanical membrane properties dictated by lipid phase is modulated by the coexistence of different lipid types and phases under various conditions. Membrane shape and curvature is also directly affected by the phase of the lipids of which it is made. Further work is focused on deciphering the details of lipid phase coexistence and its relation to biological processes.

References

1. Baumgart, T., Das, S., Webb, W. W., & Jenkins, J. T. (2005). Membrane elasticity in giant vesicles with fluid phase coexistence. *Biophys J*, *89*(2), 1067-1080. doi: 10.1529/biophysj.104.049692
2. Baumgart, T., Hess, S. T., & Webb, W. W. (2003). Imaging coexisting fluid domains in biomembrane models coupling curvature and line tension. *Nature*, *425*(6960), 821-824. doi: 10.1038/nature02013
3. Esquembre, R., Pinto, S. N., Poveda, J. A., Prieto, M., Mateo, C. R. (2012). Immobilization and characterization of giant unilamellar vesicles (GUVs) within porous silica glasses. *Soft Matter*, 2(8), 408-417. doi: 10.1039/C1SM06264F
4. Parasassi, T., & Gratton, E. (1995). Membrane lipid domains and dynamics as detected by Laurdan fluorescence. *J Fluoresc*, *5*(1), 59-69. doi: 10.1007/BF00718783
5. Risselada, H. J., & Marrink, S. J. (2009). The freezing process of small lipid vesicles at molecular resolution. *Soft Matter*, 22(5), 4531-4541. doi: 10. 1039/B913212D

6. Tokumasu, F., Jin, A. J., & Dvorak, J. A. (2002). Lipid membrane phase behaviour elucidated in real time by controlled environment atomic force microscopy. *J Electron Microsc (Tokyo)*, *51*(1), 1-9.
7. van Meer, G., Voelker, D. R., & Feigenson, G. W. (2008). Membrane lipids: where they are and how they behave. *Nat Rev Mol Cell Biol*, *9*(2), 112-124. doi: 10.1038/nrm2330
8. Veatch, S. L., & Keller, S. L. (2005). Seeing spots: complex phase behavior in simple membranes. *Biochim Biophys Acta*, *1746*(3), 172-185. doi: 10.1016/j.bbamcr.2005.06.010

Contributors and Attributions

- Destiny Davis (UC Davis)

3.7: Lipid Phase Coexistence is shared under a CC BY 4.0 license and was authored, remixed, and/or curated by LibreTexts.

CHAPTER OVERVIEW

4: Membrane-Protein Interactions

Membrane proteins are common proteins that are part of, or interact with, biological membranes. Membrane proteins fall into several broad categories depending on their location. Integral membrane proteins are a permanent part of a cell membrane and can either penetrate the membrane (transmembrane) or associate with one or the other side of a membrane (integral monotopic). Peripheral membrane proteins are transiently associated with the cell membrane. Membrane proteins are often medically important—about a third of all human proteins are membrane proteins, and these are targets for more than half of all drugs. Nonetheless, compared to other classes of proteins, determining membrane protein structures remains a challenge in large part due to the difficulty in establishing experimental conditions that can preserve the correct conformation of the protein in isolation from its native environment.

4.1: Membrane Permeability
4.2: Insertion of Membrane Proteins into Lipid Membranes
4.3: Protein-lipid Interactions
4.4: Physical Lipid Protein Interactions
4.5: Nanoparticle Spontaneous Penetration and Assembly in and Through Membranes
4.6: Non-Membrane Lipid Assemblies (Micelles)

4: Membrane-Protein Interactions is shared under a CC BY 4.0 license and was authored, remixed, and/or curated by LibreTexts.

4.1: Membrane Permeability

Cells are the main units of organization in biology. All cells are contained by a cell membrane (biomembrane) selectively open to some chemicals and ions but acts as a barrier to undesired components [1]. To put it another way, biomembranes are enclosing membranes which function as selectively permeable barriers to chemicals and ions. It should be noted though that the title biomembrane may denote a wide range of definitions; especially, cellular membranes should not be confused with isolating tissues formed by layers of cells (e.g., mucous membranes). Here the focus would be on biological membranes in the form of cell membranes, often consist of a phospholipid bilayer with embedded, integral, and/or peripheral proteins responsible for communication and transportation of chemicals and ions.

Selectivity of Biomembranes

When a membrane separates two aqueous compartments, some chemicals can move across the membrane while others cannot. This behavior can be seen with pure synthetic phospholipid membranes, which are practically biomembranes with no protein. Membrane proteins play a crucial role as transporters in expediting the ions and chemical transfers across the cell membranes. Based on the transport mechanism and permeability, solutes can be divided into three main groups as follows [2]:

1. Small lipophilic (lipid soluble) molecules that transfer through the membrane by the sole diffusion.
2. Molecules that cross the membrane with the aid of protein channels.
3. Very large molecules that do not cross the membrane at all.

Schematic cartoon given by Figure 4.1.1 can clearly illustrate the selective permeability of biomembranes for different solutes. A few lipophilic substances move freely across the cell membrane by passive diffusion. Lipophilicity is a measure for the tendency of a compound to partition into nonpolar (organic) solvent (versus aqueous solvent). Most small molecules/ions need the assistance of specific protein channels to transport them through the cell membrane. These inside-out protein channels are called transporters. Finally, the very large molecules do not cross the membrane, except in certain special cases.

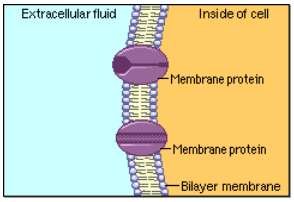


Figure 4.1.1: Selective permeability of biomembranes [2]

Generally speaking, two different classes of membrane transports can be considered [3]:

- Rapid, stereo-selective protein-mediated transport
- Slow, non-specific diffusion of molecules across cell membrane

It is worth noting that the mediated transport can be used in drug delivery and defects in transport are the causes of many diseases.

Small Lipophilic Molecules (Passive Diffusion)

Certain substances easily pass through the membrane by passive diffusion. Examples of chemicals that passively diffuse across the cell membranes are gases, like O_2 and CO_2, and small relatively hydrophobic molecules, such as fatty acids and alcohols. Logarithm of octanol/water partition coefficient of the solute ($K_{o/w}$) can be a measure of lipophilicity (higher the $\log(K_{o/w})$, higher the lipophilicity of the solute will be). However, larger lipophilicity values should not be always interpreted as better passive diffusion. The underlying reason is that there are two counter-effect parameters: besides being lipid-soluble (to cross the membrane), the solute should also possess enough water solubility to dissolve in the body fluids. Usually, a compound with $\log(K_{o/w}) > 5$ is too hydrophobic to passively diffuse through the biological membranes.

In contrast to small lipophilic molecules, in absence of protein channels, it is difficult for water to pass through the pure phospholipid membranes via diffusion. Moreover, almost all polar and charged molecules such as sugars, amino acids, and ions completely fail to cross the pure phospholipid membranes.

Polar and Charged Molecules (Protein-Mediated Transfer)

Biological membranes are permeable not only to gases and small lipophilic molecules (by passive diffusion processes), but also to many polar and charged molecules, including water, but through a different path. There are many different proteins located in

biomembranes with the main function of effectively transporting certain solutes across the membrane. According to their functions, there are two main groups of transport proteins: channel proteins and carrier proteins. Channel proteins promote the transfer of water molecules and certain ions by forming hydrophilic pores, while carrier proteins bind to specific solutes and carry them across the membrane [2]. All in all, whether it is of channel or carrier type, protein functions as an enzyme expediting the transfer of polar and charged molecules. All channel proteins and some carrier proteins facilitate the transfer of chemical/ions downhill respected to the concentration gradient, a process known as facilitated diffusion. Facilitated diffusion requires no energy input, in contrast to active transport processes (solute transport against the concentration gradient) that require an external source energy [2].

Large Molecules (Membrane Barriers)

Very large molecules like proteins, polysaccharides or nucleic acids, do not diffuse across the cell membranes at all. They can pass through the membrane only when broken down into their component monomers (e.g., amino acids, sugars, or nucleotides).

Passive and Active Transport

Most biologically important solutes require protein carriers to cross cell membranes, by a process of either passive or active transport. Active transport requires the cell to expend energy to move the materials, while passive transport can be done without using cellular energy [4]. To put it another way, active transport uses energy to move a solute "uphill" against its gradient, whereas in facilitated diffusion, a solute moves down its concentration gradient and no energy input is required.

Therefore, to summarize, transport of solutes across cell membranes by protein carriers can occur in one of two ways [2]:

- Downhill movement of solutes from regions of higher to lower concentration level, with the assistance of the protein carrier to pass through the membrane. This process is called passive transport or facilitated diffusion, and does not require energy.
- Uphill movement of solute against the concentration gradient driving force (from regions of lower to higher concentration). Based on the chemical driving force, this process is unfavorable and requires some form of chemical energy to occur (active transport).

The type of transport process, facilitated/active transport, a biological cell employs is strictly dependent on its specific needs and concentration level of chemical/ions. For example, red blood cells use facilitated diffusion to transfer glucose across membranes, whereas intestinal epithelial cells rely on active transport to take in glucose from the gut [2]. Facilitated diffusion is effective for red blood cells primarily because the glucose concentration in the blood is stable and higher than the cellular level. In contrast, active transport is needed for the gut since there are large fluctuations of glucose level as a result of eating.

Figure 4.1.2 encapsulates different transfer mechanisms discussed so far. Please note that the concentration gradient driving force is assumed downward in this schematic diagram.

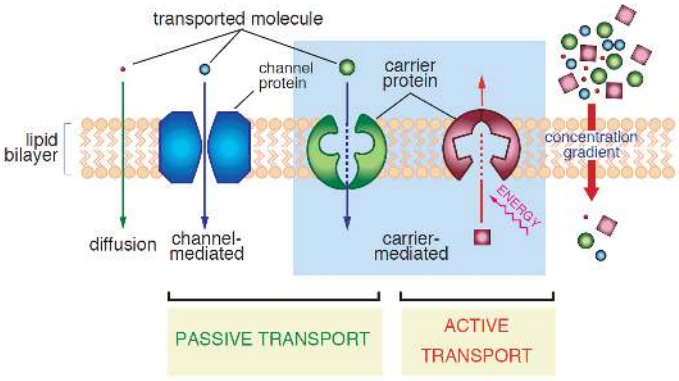


Figure 4.1.2 - Passive and active transports [3]

Facilitated Diffusion

In principle, there are two types of facilitated diffusion carriers as follows:

1. Water molecules or certain ions can be transported by channel proteins. By forming a protein-lined pathway across the membrane, proteins can appreciably speed up the transfer rate of such solutes. It should be noted though that each type of channel protein is very selective to a specific ion/chemical. For example, some channels allow only K^+ ions to pass whereas they act like a barrier to other ions. Moreover, many of these channels are gated. To simply explain the issue, consider that the

pathways are closed and unavailable for transport unless specific signals are given. One of the most vital functions of gated channels is in regulating nerve conduction in animals [2].

2. Organic molecules, like sugars and amino acids, can be transferred across the membrane via uniporters which carry molecules along the concentration gradient. Almost all tissues in any living being have a variety of uniporters for transfer of glucose and amino acids into their cells.



Figure 4.1.3 - Different Types of facilitated diffusion carrier [2]

Active Transport

Active transporters make an endergonic reaction (K_{eq} < 1) more exergonic (K_{eq} > 1) by coupling the first reaction to a second highly exergonic reaction (e.g., ATP-hyrolysis) through common intermediates to change the direction of transport (e.g., Na export from low to high concentration) [3]. To be more precise, when a transfer is not electrochemically favorable, another source of energy (which can come from another reaction) is required to force the transfer. These can be accomplished by a direct result of ATP hydrolysis (ATP pump) or by coupling the movement of one substance with that of another (symport or antiport) [2]. Active transport may use energy to transport solutes into or out of the cell, but always in opposite direction of the electrochemical driving force.

As mentioned before, biomembranes separate the intracellular and extracellular environments that are different in many aspects such as concentration levels of ions and chemicals. For example, in human tissues, all cells have a higher concentration level of sodium ion outside the cell than inside, while the exact opposite condition is maintained for the potassium ion ($C_{inside} > C_{outside}$). Regarding charged solutes and ions, besides the concentration gradient, the electrical voltage can come to play too; there is an electrical driving force for cations and anions to move along and opposite the electric field, respectively.

Like pushing an object uphill against the gravitational field, moving a molecule against its favorable electrochemical driving force requires energy. In this respect, biological cells have evolved active protein transporters that can transfer ions and charged molecules in an electrochemically unfavorable direction.

In theory, active transport can be explained by a simple fact: *Standard Free Energy Changes are Additive*. Consider two reactions:

$$\begin{matrix} A \leftrightarrow B\ \Delta G_1^0 \\ B \leftrightarrow C\ \Delta G_2^0 \end{matrix} \equiv A \leftrightarrow C\ \Delta G_{\text{total}}^0 = \Delta G_1^0 + \Delta G_2^0$$

This rule can show how an endergonic reaction (K_{eq} < 1) can shift to the RHS (producing more product) by being coupled to another highly exergonic reaction (K_{eq} >> 1) through a common intermediate [3]. To clarify the issue let us consider the active transport of the sodium ion as follows:

- Reaction 1: Ion Transport

The ion transport equation can be written as

$$\Delta G = RT \ln \frac{C_o}{C_i} + zFV \tag{4.1.1}$$

which for Na^+ gives the Gibbs free energy of 2.98 kcal/mol, or equivalently, an equilibrium constant of 0.0065. In this equation, R is the universal gas constant (1.987 cal/(mol.K)), T is absolute temperature (K), F is the Faraday's constant (23060 cal/(volt.mol)) and z is the the valence (charge number) of the ion. Moreover, subscripts i and o denote the inside and outside of the cell.

- Reaction 2: ATP Hydrolysis

As mentioned before, the required excess energy for active transport can come from ATP hydrolysis. Typical Gibbs free energy change for ATP hydrolysis is around -13 kcal/mol, making the total Gibbs free energy change of 2.98 - 13 = -10.02 kcal/mol. Therefore, the overall reaction is highly shifted to produce more product by being coupled with the strictly exothermic ATP hydrolysis reaction.

Osmosis: Water Permeability

Osmosis (transfer of water molecules through the bilayer) is a function of the relative concentration levels of solute molecules in intracellular and extracellular environments. Water molecules can readily pass through special protein channels. If the total concentration of all dissolved solute is unbalanced (C_{inside} ~= $C_{outside}$), there would be a net water flow into or out of the biological

cell [5]. The direction and magnitude of the water flow is strictly dependent on whether the cell's environment is isotonic, hypotonic, or hypertonic which are illustrative measures for the relative concentrations of solutes inside and outside the cell.

Isotonic Solutions ($C_{inside} = C_{outside}$)

In isotonic case, the total molar concentration of dissolved solutes is the same for the intracellular and extracellular environments. In this condition, the inward and outward flows of water molecules are exactly balanced (shown in Figure 4.1.4). As shown in Figure 4.1.4, the net flow of water is zero and total number of water molecules (or equivalently water concentration, C_w) is remained constant on each side. A 0.9% solution of sodium hydroxide is a perfect example of isotonic solution to animal cells [2]. During experiments, like exposing membranes to different solutions, it is highly recommended to use an isotonic solution to prevent osmotic effects (e.g., swelling and shrinking of the cell) which can seriously damage the biological cells.



Figure 4.1.4 - Transport of water molecules through protein channels in isotonic condition [2]

Hypotonic Solutions ($C_{inside} > C_{outside}$)

In a hypotonic condition, molar concentration of the total dissolved solutes is higher inside the cell than that in the extracellular environment. Obviously, low concentration of solutes in an aqueous solution can be interpreted as high concentration of water. Therefore, it is straightforward to see if $C_{inside} > C_{outside} \rightarrow C_{w,\,inside} < C_{w,\,outside}$, providing a driving force for a net inward water flow to the cell. Hence, when a cell is exposed to such hypotonic conditions, there is net water movement into the cell and passing time, the concentration of water molecules inside the cell would be increased. Because of this considerable accumulation of water molecules, cells will swell and may even burst if the excess accumulated water is not removed from the intracellular environment.

Hypertonic Solutions ($C_{inside} < C_{outside}$)

Cell behavior under hypertonic condition is exactly the opposite of what explained for the hypotonic case ($C_{inside} < C_{outside} \rightarrow C_{w,\,inside} > C_{w,\,outside}$). In this case, the water concentration is higher in cell's interior than in its outside, so there would be a net outward water flow from the cell. Therefore, passing time, the water concentration level will decrease inside the cell and cell will shrink. As an important consequence of the low water level, the ability of cell to function or divide would be gradually lost [2]. It is interesting that hypertonic solutions like concentrated syrups have been used since ancient times for food preservation. This can be explained through the fact that microbial cells that would cause spoilage are dehydrated in these very hypertonic environments and would be unable to function [2].

Transport Disorders

Considering the remarkable specificity of the transporters, it is not surprising that sometimes there are defects in transport systems. Nowadays, several different diseases known to be due to transport defects. In many of the cell membrane diseases, proteins do not transport materials properly. Some of the membrane transport disease are hereditary. An archetypical example of such transport diseases is Cystinuria, an inherited autosomal recessive disease that is characterized by abnormally high amino acid (cystine) concentration level in the urine, that may result in the formation of cystine stones in the kidneys. Another example can be Cystic Fibrosis (CF) which is caused by a mutation in the cystic fibrosis transmembrane conductance regulator, CFTR, a protein that helps move salt and water across the membrane. It is a genetic disorder that affects mostly the lungs but also the pancreas, liver, kidneys, and intestine. Long-term issues include breathing problems and coughing up mucus as a result of frequent lung infections. In a patient with CF, the cells do not secrete enough water; when it happens in the lungs, it causes the mucus to become extremely thick.

It is also worth mentioning that most fatal toxins like Dendrotoxin (black mamba snake of Africa) and Batrachotoxin (Colombian frog *Phyllobates aurotaenia*) act directly on specific ion channels of the plasma membrane to disrupt the action potentials. Dendrotoxin, as a presynaptic neurotoxin, blocks specific subtypes of voltage-gated K^+ channels in neurons, so increasing the release of acetylcholine at neuromuscular junctions. In this regard, a single dendrotoxin molecule reversibly associates with a K^+ channel to apply its suppressive effect. To put it simply, this fatal toxin binds to anionic sites near the extracellular surface of the channel and physically blocks the path and ion conductance. Batrachotoxin on the other hand, as an extremely cardiotoxic and neurotoxic steroidal alkaloid, works by binding to the Na^+ channel and causing a conformational change (modifying both their ion selectivity and voltage sensitivity). In a nutshell, batrachotoxin irreversibly binds to the sodium channels, enforcing them to remain open.

Driving Forces

The permeability of a membrane can be defined as the passive diffusion rate of permeated molecules across the biomembrane. It is unanimously accepted that permeability of any specific molecule depends mainly on charge number, polarity, size, and to some extent, to the molar mass of the molecule. It should be noted though that both the nature of the bilayer and the prevalent environments can play a significant role too. As mentioned before, because of the inevitable hydrophobic nature of the biomembranes, small uncharged molecules pass across the membrane more easily than charged, large ones [6].

With charged species (e.g., Na^+), the effect of the membrane potential (V) should be taken into account. Most cells are characterized by a membrane potential difference of -70 mV (V_{inside} - $V_{outside}$). Let us first consider an example of Cl^- ion to clarify the issue. For Cl^-, the concentration gradient is toward inside the cell ($C_{Extracellular}$ = 125 mM & $C_{Intracellular}$ = 9 mM). So, there is a driving force of diffusion for Cl^- to diffuse along the concentration gradient into the cell. However, the electric field is directed into the cell ($V_{inside} < V_{outside}$), pushing out negatively charged ions. Therefore, an equilibrium is achieved when influx and efflux of Cl^- level each other. The membrane potential at which this equilibrium occurs is called equilibrium potential that can be calculated by Nernst equation [7]:

\[V_{\text {equilibrium}}=\frac{R T}{F_{Z}} \ln \left(\frac{C_{o}}{C_{i}}\right)]

Note that this relation was obtained from ion transport equation for zero Gibbs free energy change (i.e., thermodynamic equilibrium).

Then, it would be useful to define a driving force potential difference as $V_{DF} = V_{cell} - V_{equilibrium}$. By this definition, negative V_{DF} means passive uptake and exit of cations and anions, respectively. For example, for the case of Cl^-, V_{DF} = 0.3 mV indicating diffusion of Cl^- into the cell. The same is true for Na^+ where V_{DF} = -127.3 mV. However, this is not the case for other ions like K^+ which will be pushed out by the net electrical potential V_{DF} of 11.2 mV.

Moreover, huge V_{DF} values (big difference between V_{cell} and $V_{equilibrium}$) of some ions such as Na^+, K^+, and Ca^+ suggest that there are other forces besides the chemical and electrical gradients needed for the transport. In such conditions, passive (protein channels) or active transporters are required for the ion transfer.

Permeability Model

Schematic diagram of diffusion through a bilayer is sketched in Figure 4.1.5 in which two aqueous solutions S_1 and S_2 are separated by the biomembrane. Superscripts "aq" and "m" denote solute concentrations at bulk aqueous solutions and surfaces of the membrane, respectively. As it can be seen, the concentration gradient is considered to be from S_1 to S_2, providing the chemical driving force of the transport. To mathematically describe the permeability, let us first introduce the useful concept of partition coefficient. At thermodynamic equilibrium, the equality of the chemical potentials of solute j in two different intracellular and extracellular phases can be expressed as

$$\mu_i^j + RT \ln C_i^j = \mu_o^j + RT \ln C_o^j \tag{4.1.2}$$

Then, the partition coefficient can be defined as

$$K_{i/o} = \frac{C_i^j}{C_o^j} = \exp\left(\frac{-\left(\mu_i^j - \mu_o^j\right)}{RT}\right) \tag{4.1.3}$$

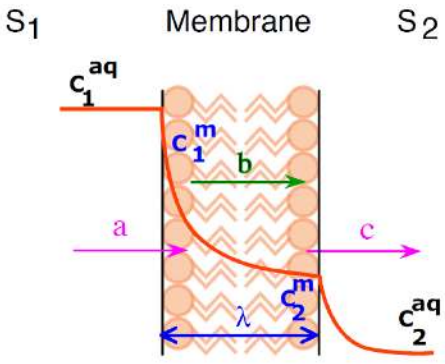


Figure 4.1.5 - Schematic diagram of mass transfer through bilayer [3]

Having the partition coefficient, the mass flux (mol/(m^2.s)) across the membrane (Figure 4.1.5) is given by

$$J = \frac{K_{1/2}D}{\lambda}(C_1 - C_2) \tag{4.1.4}$$

where D denotes the ion diffusivity through the membrane and $K_{1/2}$ is the partition coefficient of the two phases (the ratio of solubilities in lipid and water). Finally, the mass transfer coefficient in above equation is simply called permeability (in units m/s) of the solute diffusion through the membrane:

$$P = \frac{K_{1/2}D}{\lambda} \tag{4.1.5}$$

References

1. Biological Membranes. Wikipedia: https://en.Wikipedia.org/wiki/Biological_membrane
2. Pearson Practice Hall - Lab Simulations. www.schenectady.k12.ny.us/putman/biology/data/biomembrane1/intro.html
3. W. D. Stein. Transport and Diffusion across Cell Membranes. Academic Press, 1986.
4. Selectively Permeable Membranes. Study.com: http://study.com/academy/lesson/selectively-permeable-membranes-definition-examples-quiz.html
5. R. Fettiplace & D. A. Haydon. Water Permeability of Lipid Membranes. Physiological Reviews 1980 (60) 510 - 550.
6. Cell Membrane. Wikipedia: https://en.Wikipedia.org/wiki/Cell_membrane#Permeability
7. Nernst Equation. Wikipedia: https://en.Wikipedia.org/wiki/Nernst_equation

4.1: Membrane Permeability is shared under a CC BY 4.0 license and was authored, remixed, and/or curated by LibreTexts.

4.2: Insertion of Membrane Proteins into Lipid Membranes

Integral membrane proteins are ubiquitous throughout living organisms, ranging from prokaryotes to mammals, accounting for approximately 20-30% of all proteins. (Wallin et al. 1998) They perform a diverse set of functions ranging from signal transduction, to ion transport or even photosynthetic reaction centers. While their activity might vary dramatically, all these proteins experience a similar challenge. They must traverse the amphiphilic lipid membrane to reach their correctly folded state. The ways in which nature has overcome this challenge will be the primary focus of this page.

Features and diversity of membrane proteins

Prior to discussing the mechanisms of membrane insertion, it is important to characterize key features of transmembrane proteins and their topology.

Characteristics of transmembrane domains

A transmembrane domain (TMD) is defined as a region of a polypeptide chain that completely traverses the hydrophobic region of the bilayer. The most common TMD's are 20 amino acids long and for a tightly coiled structure known as an α-helix. An α-helix is the preferred structure as it maximizes hydrogen bonding within the backbone of the chain, effectively shielding the hydrophilic regions of the amino acid backbone from the surrounding acyl chains of the lipids. An integral membrane protein (IMD) is composed of one or more TMD's. When studying an integral membrane protein's sequence, it is possible to identify the TMDs by generating a hydrophilicity plot. The TMDs will correspond to regions of amino acids that are hydrophobic (Kyte & Doolittle 1982). The determination of TMDs through this method are not always accurate as the insertion is heavily influenced by both the proximal and distal amino acids. In Figure 4.2.1, a hydrophilicity plot of a G-coupled receptor is shown to have polar amino acids in their transmembrane domains.

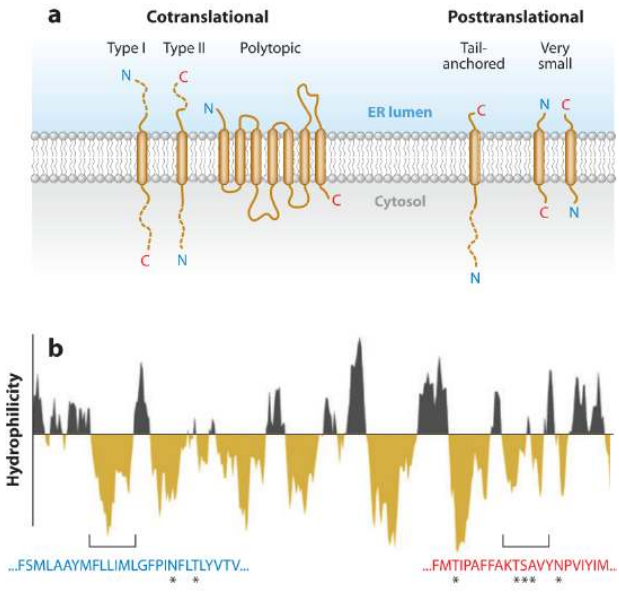


Figure 4.2.1: Structural diversity of membrane proteins (Shao & Hegde 2011)

Determinants of topology

The topology of an IMP refers to the orientation of the protein in the membrane. A protein can be in either the type I or type II topologies. Type I indicates that the N-terminus of the protein passes through the membrane first. Type II topology implies that the N-terminus does not cross the membrane, causing the later segments of the protein to pass through first instead. The driving force to chose one conformation over another is composed of several additive features of the protein. The most prominent effect, at least for bacteria, comes from the positive inside rule. The positive inside rule states that positively charged amino acids, such as arginine and lysine, will not cross the membrane and remain in the cytosol (Hatmann et al. 1989). This is dictated by the strong positive charges interacting repulsively with the channel that I will describe later in this page. In bacteria the asymmetry between the leaflets and the strong proton motive force across the membrane cause the cytosolic side of the membrane to be far more favorable for positive amino acids compared to the periplasmic side. (van Klompenburg 1997)

Cotranslational membrane protein insertion

The pathway for the insertion of membrane proteins has been highly conserved across organisms and has two distinct steps: recognition and targeting of a nascent IMP and then its insertion into the membrane.

Recognition and Targeting

Recognition occurs on the ribosome as the nascent polypeptide chain emerges from the exit channel by the **Signal Recognition Particle** (SRP). This protein has a nonspecific hydrophobic channel that interacts with amino acids that would form a transmembrane domain based on the presence of numerous hydrophobic residues. Upon binding, translation is arrested and the SRP-ribosome complex searches for the eukaryotic SRP Receptor (SR) or bacterial FtsY. Once the ribosome-SRP-receptor complex is formed bound it diffuses through the membrane until it interacts with the Sec translocon. The nascent chain is then transferred to the channel. The critical aspect of this process is that it prohibits the hydrophobic region of the polypeptide from exposure to the hydrophilic cytosol to avoid misfolding and aggregation (Grudnik et al. 2009).

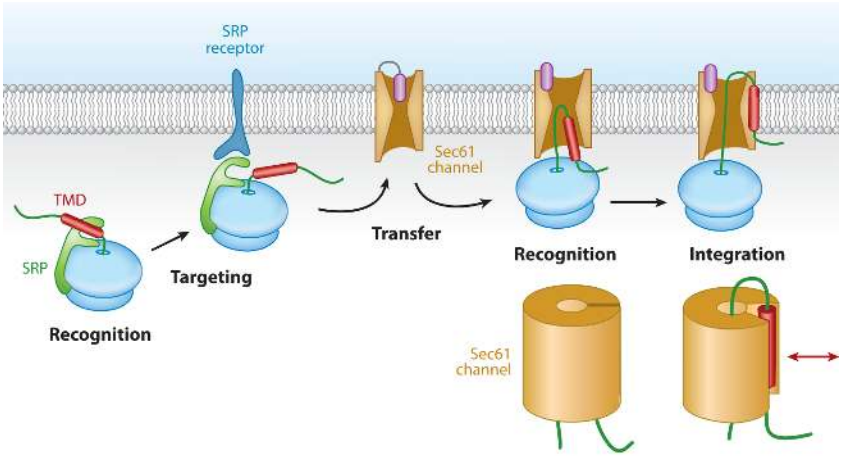


Figure 4.2.2: General steps of cotranslational membrane protein insertion. (Shao & Hegde 2011)

Sec translocon

In both prokaryotes and eukaryotes, there are protein conductive channels generally referred to as Sec translocases. These channels have two fundamental functions that enable the insertion of proteins into the membrane. They contain a hydrophilic channel that allows hydrophilic residues of a polypeptide to pass through the membrane as well as a lateral gate that opens to expose the interior of the channel to the lipid acyl chains. This allows for hydrophobic residues to enter through the channel and then interact directly with the lipid tails while avoiding the polar head groups. These channels therefore allow the nascent chain that is being translated to effectively “thread” in and out of the membrane as many times as is required to reach the final structure. (van den Berg et al. 2004).

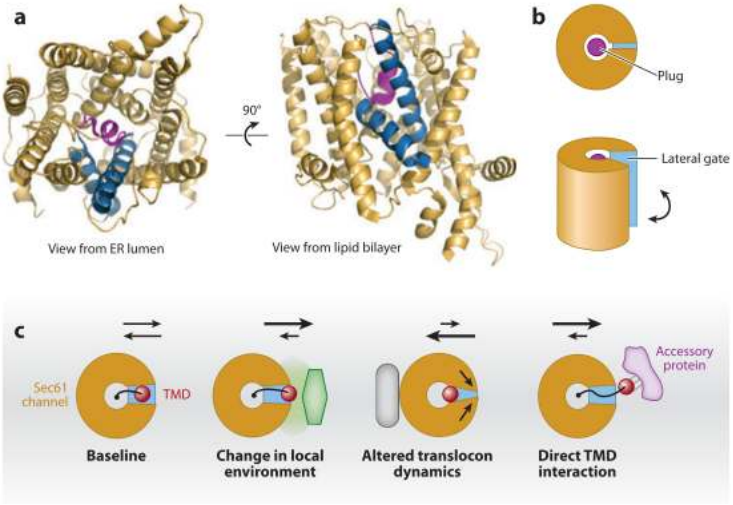


Figure 4.2.3: The Sec61 translocon and potential accessory factors. (Shao & Hegde 2011)

Accessory factors

While the translocase complex is the primary requirement for most membrane proteins, more complex IMPs require accessory factors to aid in its insertion and maturation. Below is a breakdown of different accessory factors for prokaryotes and eukaryotes.

Eukaryotes

Numerous other membrane proteins have been found to interact with the Sec translocon complex in eukaryotes, however their necessity remains unclear. Enzymes like the signal peptidase and the oligosaccharyl transferase have been found to aid in the folding and maturation of certain IMPs by either cleaving or glycosylating respectively (Yamagisi et al. 2011). The translocon-associated protein (TRAP) complex may help fortify the ribosome-translocon complex. The translocating-chain associating membrane (TRAM) protein is currently expected to insert TMDs with weak hydrophobicity and therefore is only required for certain IMPs. (Heinrich et al. 2000)

Prokaryotes

As in eukaryotes, there are several accessory factors that have been found to aid in the insertion of IMPs in prokaryotes. SecA is an ATPase that has been shown to be essential to push highly hydrophilic proteins through the Sec channel (Zimmer et al. 2008). The YidC insertase has been shown to be aid in the lateral partitioning of IMPs out of the channel into the membrane. Its role is expected to be that of a foldase which helps with the formation of α-helices (Beck et al. 2001). It has also been found that the presence of the phospholipid phosphatidylethanolamine (PE) is required for the folding of certain IMPs. As PE is a positively charged lipid, it interacts with acidic residues that flank the TM and stop the residues from wanting to translocate to the positively charged periplasmic side of the membrane (Bogdanov et al. 2008).

References

1. Beck K, Eisner G, Trescher D, Dalbey RE, Brunner J, Muller M. 2001. YidC, an assembly site for polytopic Escherichia coli membrane proteins located in immediate proximity to the SecYE translocon and lipids. EMBO Rep. 2:709–14
2. Bogdanov M, Xie J, Heacock P, Dowhan W. 2008. To flip or not to flip: lipid-protein charge interactions are a determinant of final membrane protein topology. J. Cell Biol. 182:925–35
3. Dalbey, R. E., Wang, P., & Kuhn, A. (2011). Assembly of Bacterial Inner Membrane Proteins. Annual Review of Biochemistry, 80(1), 161–187.
4. Grudnik, P., Bange, G. & Sinning, I. (2009). Protein targeting by the signal recognition particle. *Biological Chemistry*, 390(8), pp. 775-782.
5. Hartmann E, Rapoport TA, Lodish HF. 1989. Predicting the orientation of eukaryotic membrane-spanning proteins. Proc. Natl. Acad. Sci. USA 86:5786–90
6. Heinrich SU, Mothes W, Brunner J, Rapoport TA. 2000. The Sec61p complex mediates the integration of a membrane protein by allowing lipid partitioning of the transmembrane domain. Cell 102:233–44
7. Kyte, J., & Doolittle, R. F. (1982). A simple method for displaying the hydropathic character of a protein. Journal of Molecular Biology, 157(1), 105–132.
8. Shao, S., & Hegde, R. S. Membrane Protein Insertion at the Endoplasmic Reticulum. Annu. Rev. Cell Dev. Biol. 2011. 27:25–56
9. van den Berg B, Clemons WM, Collinson I, Modis Y, Hartmann E, et al. 2004. X-ray structure of a protein- conducting channel. Nature 427:36–44
10. van Klompenburg W, Nilsson I, von Heijne G, de Kruijff B. 1997. Anionic phospholipids are determinants of membrane protein topology. EMBO J. 16:4261–66
11. Wallin E, von Heijne G. 1998. Genome-wide analysis of integral membrane proteins from eubacterial, archaean, and eukaryotic organisms. Protein Sci. 7:1029–38
12. Yamagishi M, Fujita H, Morimoto F, Kida Y, Sakaguchi M. 2011. A sugar chain at a specific position in the nascent polypeptide chain induces forward movement during translocation through the translocon. J. Biochem. 149:591–600
13. Zimmer J, Nam Y, Rapoport TA. 2008. Structure of a complex of the ATPase SecA and the protein- translocation channel. Nature 455:936–43

4.2: Insertion of Membrane Proteins into Lipid Membranes is shared under a CC BY 4.0 license and was authored, remixed, and/or curated by LibreTexts.

4.3: Protein-lipid Interactions

Lipids and proteins are essential elements of a living organism. Proteins, as one of the most abundant macromolecules of life, have countless functions ranging from catalyzing vital biological reactions to transporting nutrients. Likewise, lipids also play integral roles such as storing energy or being a major component of a membrane [12]. Despite their individual importance, interactions between these two molecules can provide functions that would not be possible individually. The greatest number of these interactions are seen in cell membranes, which are composed of a wide variety of lipids and proteins. While biological membranes elegantly fulfill many structural roles, the complexity of lipid-protein interactions facilitates a potentially stunning diversity of function and interaction.

Background

The crowded biological membrane (Figure 4.3.1) provides countless interfaces for these interactions. In the membrane, the protein to lipid ratio is believed to be as high as 60:40 [15], and membrane proteins are believed to constitute an approximate 30% of the human genome [5]. These imply not only the individual importance of proteins and lipids to the function of biological membranes, but the potential complexity underlying interactions of proteins and lipids with each other. An understanding of the way proteins and lipids interact thus requires consideration of a variety of factors, from the bulk properties of the membrane to the intermolecular forces contributing to the behavior of individual lipids within the membrane.

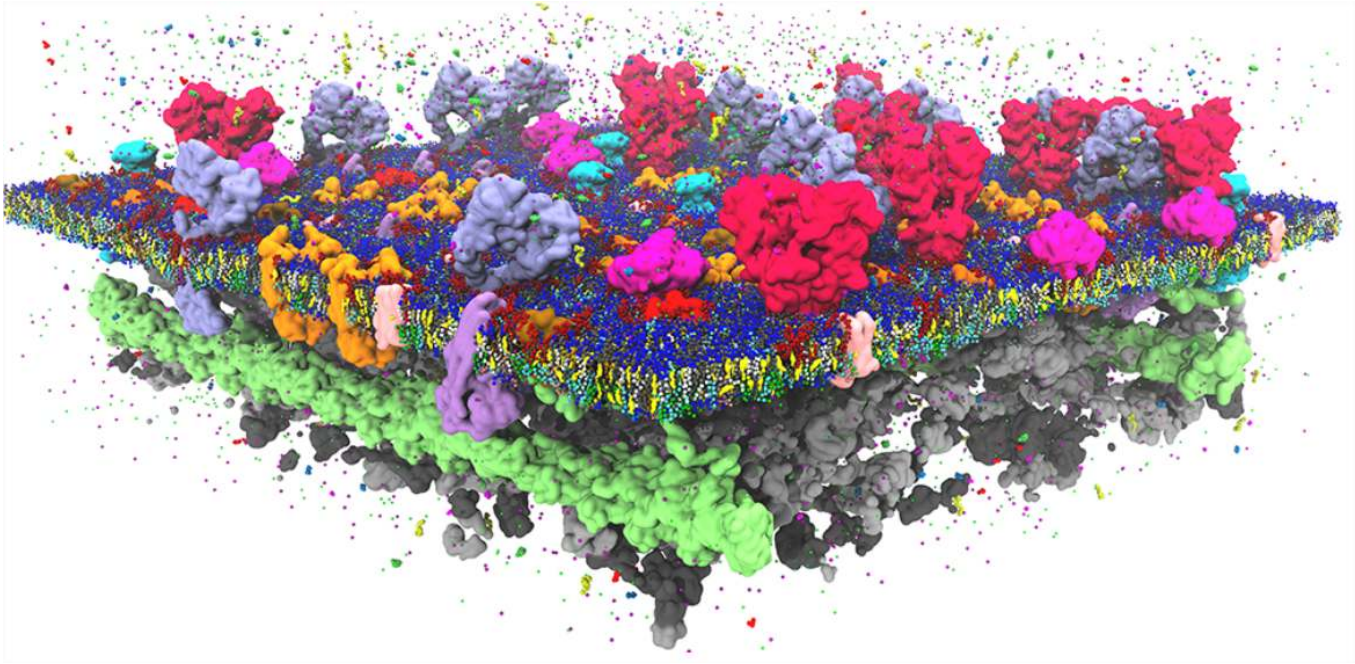
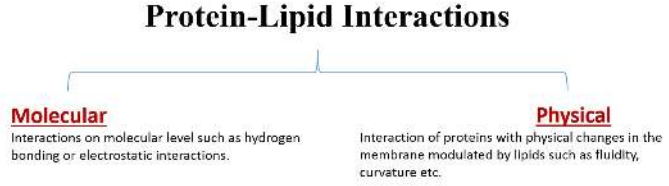


Figure 4.3.1: The crowded environment of the cell membrane suggests protein-lipid interactions are both common and complex. Model of the plasma membrane in full complexity. Featuring: a lipid bilayer composed of hundreds of different lipids, crowded with a large variety of embedded as well as peripherally bound proteins, a supporting actin skeleton, a cytoplasmic site full of proteins, and realistic gradients of metabolites, ions, and pH. (CC BY-NC-ND; Marrink et al. via Chem. Rev. 2019, 119, 6184−6226)

Proteins found in a biological membrane have important roles in cell signaling, transduction and transportation [9]. One common way of classifying protein-lipid interactions is shown below:



Lipids in a biological membrane can be divided into three general groups [9].

1. **Bulk lipids:** The lipids that form the main structure of the membrane without contacting the membrane proteins are called bulk lipids.
2. **Annular lipids:** Some lipids surround membrane proteins and interact relatively non-specifically with them. These lipids are called the annular lipids, due to being similar to an annular shell (a ring-shaped layer in close contact with the protein surface).
3. **Non-annular lipids:** These lipids interact specifically with some membrane proteins and are buried inside the protein structure. Non-annular lipids are often regarded similarly to protein cofactors--small molecules bound by a protein in its functional conformation.

Some of the vocabulary used to discuss membrane and protein properties is summarized in Figure 4.3.2:

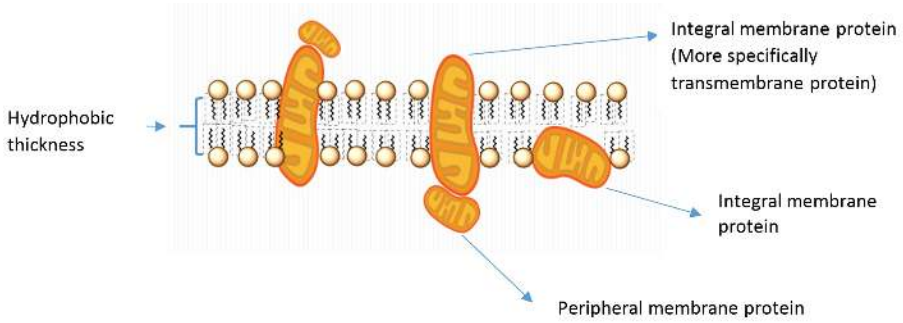


Figure 4.3.2. A cartoon illustration showing different membrane proteins

- *Integral membrane proteins*: Proteins residing in at least one leaflet (layer) of the cell membrane.
- *Transmembrane proteins:* A class of integral membrane proteins spanning the full width of the cell membrane.
- *Peripheral membrane proteins:* Proteins that are transiently associated with the outer portion of one leaflet or an integral membrane protein.
- *Hydrophobic thickness*: The thickness of the portion of the membrane composed of the fatty acid lipid tails.

Bulk Lipid-Protein Interactions

Effect of Viscosity of the Membrane

The movement of any molecule or part of a molecule inside the membrane is influenced by the fluidity of this environment [9]. Every molecule experiences a frictional drag force during their movement inside the lipid bilayer structure of a biological membrane, and resistance of the fluid to this motion can be expressed in terms of the viscosity. By Stokes' Law (Equation 4.3.1), the rate of particle motion can be expressed as a function of the drag force, membrane viscosity, and particle size [3]. This equation assumes the absence of turbulent flow (a good assumption for the comparatively calm cell membrane).

$$v = \frac{F}{6\pi\mu R} \tag{4.3.1}$$

where

- F: drag force (e.g. Newtons)
- μ: membrane viscosity (e.g. centipoise, Pascal*seconds)
- R: particle size (e.g. meters, nanometers)
- v: speed of particle motion (e.g. meters per second)

Larger particles, more viscous membranes, and more rapid motion thus all result in increased drag force. More viscous membranes can arise from the phase (e.g. liquid disordered, liquid ordered, or gel) of the lipids in the membrane; the phase is determined by the number of double bonds in the fatty acid tails of the lipids and the environmental temperature, with fewer double bonds or a temperature below the critical temperature for the lipids resulting in a more viscous membrane.

Movement of a protein in the membrane is dictated by the frictional resistance and the molecular restoring forces acting on it. A fluorescence polarization anisotropy study on the rotation of tryptophan (Trp) residues showed that the motion of Trp was affected by the viscosity of the lipid environment for small scale motion, and the amplitude of this motion increased with the temperature as the viscosity decreased. For example, at a viscosity of 1 centipoise (approximately the viscosity of water at room temperature and on the order of magnitude of the viscosity of the membrane) the authors expect local rotational motion of a given peptide within the protein to be largely determined by the surrounding peptide residues [17].

While the viscosity of the membrane can affect the rate of motion of the protein, the most thermodynamically favorable conformation of the protein should not depend on membrane viscosity [9]. This is because the thermodynamic properties of a system are inherently time-independent, but viscosity is a time-related parameter (since viscosity has units of pressure*time). This means a change in viscosity cannot directly increase or decrease the activation energy required to induce a conformational change--the most stable conformation of a protein is independent of the membrane viscosity. Changes in membrane viscosity can, however, change the amount of time required for the protein to assume this conformation. Additionally, if a change in membrane viscosity is the result of a change in temperature, the rate of protein function will be affected because rate constants are temperature-dependent [9]. This indirect effect can be worthwhile to consider in the study of isolated membrane proteins, which may take place at room temperature rather than at the temperature of the protein's natural environment.

Another important effect of membrane viscosity has also been revealed by molecular dynamics simulations. It has been illustrated that the effect of solvent viscosity on protein motion is important if the protein both directly contacts the solvent and has a rate of motion comparable to the environment. In other words, high frequency motion of a protein that does not overlap the solvent motion does not depend on the solvent's viscosity [2]. Lipids are important in this context because viscosity of a biological membrane is mainly influenced by the types of lipids present, as the lipid composition is one of the main determinants of the fluidity.

Highly viscous membranes are indicative of increased ordering of the lipid fatty acid tails, often facilitated by interactions with smaller molecules such as sphingomyelin or cholesterol. This can result in increased membrane durability and impermeability. Additionally, the fluidity of the membrane environment surrounding a membrane protein can impact its function. For example, the human epidermal growth factor receptor (EGFR) was found to be non-functional in an environment in which both highly fluid liquid disordered and more viscous liquid ordered domains could exist. However, in a purely liquid disordered environment, EGFR retained its function, revealing a functional dependence on the fluidity of the membrane [3].

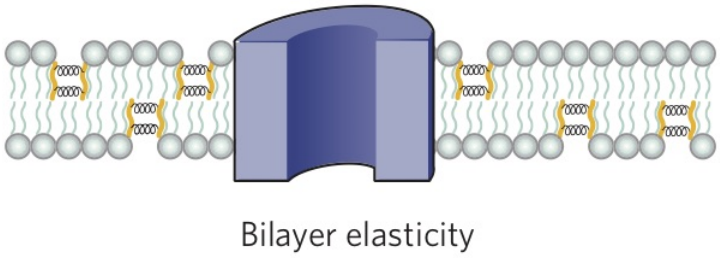


Figure 4.3.3: The elasticity of the bilayer is often facilitated by small molecules such as sphingomyelin and cholesterol, and can impact the behavior of membrane proteins [15].

(See the main phase transitions page for more information on membrane fluidity.)

Localized areas of high membrane viscosity can also be indicative of the existence of lipid rafts, which are believed to play a role in protein isolation and function. Lipid rafts are transient sphingomyelin- and cholesterol-rich : (10-200 nm in diameter) within the cell membrane. The local abundance of sphingomyelin and/or cholesterol results in liquid-liquid phase separation, meaning lipid rafts are typically composed of the liquid ordered (L_o) phase. This means the lipids within rafts are more tightly packed and highly ordered than the bulk membrane, leading to increased local rigidity and decreased fluidity [18]. Some proteins can bind glycosphingolipids or sphingomyelin, which are involved in the recruitment of proteins to lipid rafts.

Effect of Membrane Curvature

Dynamic curvature of plasma or intercellular membrane can be dictated by the interactions between proteins and lipids. In fact, cells can employ various mechanisms to sense curvature as a way to create regions of active membrane trafficking. Lipid composition is a major influence on membrane curvature based on their chemical properties and/or the size of their headgroup. Presence of certain lipids are key to interact with certain peripheral membrane proteins in order to induce a necessary curvature. For example, phosphoinositides are required for budding of clathrin-coated vesicles, as the required machinery (e.g. coat proteins) can specifically bind to these lipids. The reason for this is that the headgroups of phosphoinositides are negatively charged, resulting in electrostatic repulsion that can contribute to membrane curvature [14].

Another study illustrated that NSA4(1-48), a key transmembrane protein that mediates replication of Dengue virus (a mosquito born single positive-stranded RNA virus), has an affinity for the convex face of highly curved regions of synthetic bilayer vesicles, as monitored by circular dichroism spectroscopy [8].

Similarly, a G protein-coupled serotonin receptor (5-HT_{1A}) was found to function more rapidly in a more highly curved membrane [7]. This curvature effect could arise from a better match in the thickness of the hydrophobic portion of the membrane surrounding the protein, stabilizing the active protein form.

In addition to responding to changes in local curvature, membrane proteins can also influence the local curvature of the membrane. Some membrane proteins accomplish this by trafficking individual lipids across the membrane, resulting in uneven lipid compositions across the two membrane leaflets. The membrane must curve so that the leaflet with fewer lipids is on the interior of the curve in order to maintain optimal packing of the head groups [6]. Similarly, membrane leaflets containing lipids with different head group areas may also have some intrinsic curvature due to their differing surface areas [6]. In both cases, the integrity of the membrane as a barrier is facilitated by curvature, protecting the hydrophobic fatty acid tails from the aqueous environment and maintaining separation between the membrane bound compartment and its exterior.

Yet another example of the interplay between membrane proteins and membrane curvature is the process of vesicle formation. The ability to form vesicles is important in the trafficking of newly-formed proteins, the recycling of cell membrane components, and the intake of particles via endocytosis, among countless other cell functions. Vesicle formation involves complex regions of curvature, including low positive curvature when the vesicle is first beginning to form, greater positive curvature as the vesicle swells, and very high negative curvature where the vesicle meets the parent membrane. This complex curvature is facilitated in part by the membrane protein dynamin, which is responsible for creating the “neck” separating the parent membrane from the nearly fully-formed vesicle. This is a result of dynamin binding the membrane and taking on a helical conformation, physically forcing the parent membrane to assume a tube-like shape [14]. Coatomers are small proteins that may also play a role in vesicle formation by binding existing membrane proteins in a relatively confined area. The coatomers result in steric repulsion, leading to membrane curvature and budding [6].

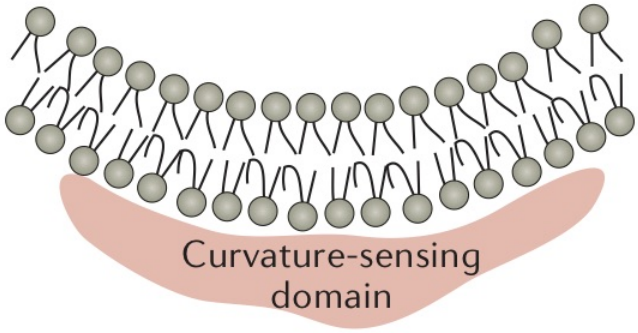


Figure 4.3.4: Proteins containing curvature-sensing domains (pink) can play a significant role in vesicle formation, crucial to intercellular and intracellular communication [25].

The binding of amphipathic helices within the membrane is another common mechanism of protein-induced membrane curvature. As shown in the Figure below, one portion of the helix is hydrophobic, while the other is hydrophilic. The hydrophobic portion associates with the fatty acyl chains of the membrane, while the hydrophilic portion interacts with the head groups. This changes the area per head group for the bound leaflet of the membrane, and the membrane must curve in order to compensate.

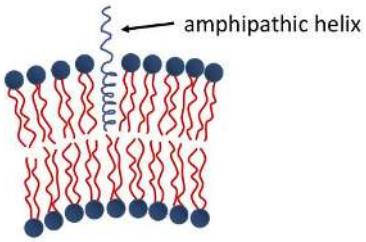


Figure 4.3.5: Membrane curvature as the result of insertion of an amphipathic helix into one leaflet.

Some of the other well understood ways that lipid-protein interaction relates to curvature of the membrane are discussed in membrane curvature in detail.

Effect of Changes in Membrane Thickness

An important feature of lipids that can influence protein function is the thickness of the bilayer. As shown in Figure 4.3.2, the hydrophobic thickness of a membrane is the distance between the hydrophilic headgroups of either leaflet, which is related to the length of the fatty acid tails of the lipids composing the membrane. Membrane proteins need to match the hydrophobic thickness of the acyl chains for two reasons. First, acyl chains and hydrophobic groups of the membrane proteins do not form hydrogen bonds with water, and tend to minimize their contact with it as this is more thermodynamically favorable (see hydrophobic effect). When the hydrophobic thickness of the membrane and the membrane protein do not match, hydrophobic mismatch occurs. In order to minimize the exposure of hydrophobic portions of the lipid bilayer and transmembrane proteins to the aqueous environment, the bilayer can distort in various ways. It can stretch (Figure 4.3.5), compress, or even tilt. Stretching involves an extension of the fatty acid chains of the lipids immediately surrounding the protein, providing a greater hydrophobic thickness to better match the size of the protein's hydrophobic domain. This minimizes the extent of hydrophobic membrane protein exposed to the aqueous environment, which is more energetically favorable. Conversely, compression involves a contraction of the fatty acid tails surrounding the protein.

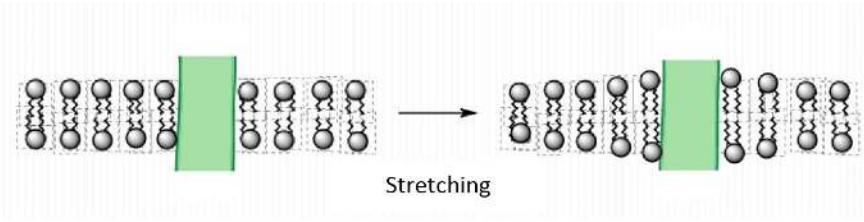


Figure 4.3.6. Stretching of a lipid bilayer to match the hydrophobic thickness of the protein (green). The extension of the fatty acid tails results in a greater hydrophobic thickness, protecting hydrophobic portions of the protein from the hydrophilic environment.

Furthermore, the membrane proteins can aggregate (Figure 4.3.3) to minimize the area exposed to water [16]. In addition to being more thermodynamically favorable (i.e. maximizing entropy by reducing the number of water molecules in highly ordered contact around hydrophobic residues), avoiding exposure of a transmembrane protein to aqueous environment is also important for optimal function because the hydrophobic side chains of the protein can change conformation when they contact water, distorting their native structure, and causing functional loss. The studies on these membrane distortions carried out with model membranes (artificial bilayers), show that the thickness of the acyl chain region is an essential part of protein function. For instance, sarcoplasmic reticulum Ca-ATPase, which is a protein important in calcium regulation in muscles, was shown to be greatly affected by the number of the carbons in the acyl chain, which determines the hydrophobic thickness of the membrane [16]. In addition, molecular dynamics simulations showed the possibility of protein aggregation (Figure 4.3.3) due to hydrophobic mismatch [17].

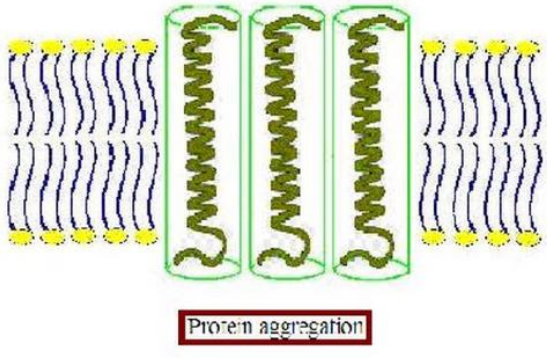


Figure 4.3.7. Aggregated proteins to minimize hydrophobic mismatch [21].

Membrane proteins may also change conformation in response to changes in membrane tension, which can be indicative of changing external conditions necessitating a response from the cell. For example, osmotic swelling or shrinking of a cell will result in higher or lower membrane tension, respectively. Under increased tension, the bilayer will tend to thin, resulting in increased hydrophobic mismatch. One possibility to mitigate this is for the membrane conformation to change so that its hydrophobic domain thickness matches that of the transmembrane protein. Another possibility is that a conformational change in the membrane protein structure could relieve hydrophobic mismatch, making a response to membrane tension an effective gating mechanism. This is typically more energetically favorable in the case of significant membrane deformations, for which the energy required to change

the membrane conformation to match the protein's hydrophobic thickness would be greater than the cost of changing the protein's conformation [11]. Such conformational changes include changes in the angle at which the transmembrane domain is tilted or unwinding of alpha-helical transmembrane domains [11]. The response of membrane proteins to hydrophobic mismatch arising from membrane tension is evident in the case of many bacterial mechanosensitive channels, which under higher membrane tension are more likely to be open [15].

For example, the lipid-protein interaction energy for a membrane protein with six helical transmembrane domains has been estimated to increase by approximately 10^{-20} J/lipid molecule for a 10 Å hydrophobic mismatch, providing an appreciable driving force for either the membrane or protein to change its conformation [11]. At room temperature, the energetic cost of bending a lipid membrane is typically on the order of 10^{-20} J, although this can change significantly based on the local temperature and lipid composition [24]. Hydrolyzing one ATP, a typical means of driving protein conformational changes, yields approximately 10^{-19} J [6]. All these values are within similar orders of magnitude, suggesting the most effective method of resolving hydrophobic mismatch for a given membrane and protein may depend on both intrinsic and environmental factors.

Annular and Non-Annular Lipid-Protein Interactions

Protein-Lipid Interactions in Molecular Terms

In addition to the interactions of lipids and proteins mediated by the physical changes in the lipid environment, it is good to consider lipid-protein interactions on a molecular level. Types of lipids that were defined previously interact differently with proteins. Figure 4.3.4 is a basic representation of the interaction of bulk lipids and annular lipids with a protein surface. Lipids present in the first shell, having a higher level of interaction with the protein and more restricted motion, are the "annular lipids." The second shell shows the bulk lipids.

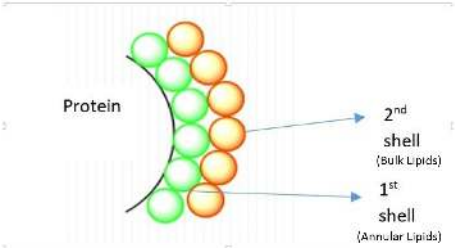


Figure 4.3.8. Simple illustration of the interaction of annular and bulk lipids with the surface of a protein [6].

Annular lipids and proteins weakly interact through van der Waals interactions, hydrogen bonding, and/or electrostatic interactions. These weak interactions allow annular lipids to be frequently exchanged with the lipids in the bulk bilayer due to the random motion expected in any fluid system, which implies that their interactions with proteins are fairly nonspecific. The level of interactions between annular lipids, which are highly dynamic, is an ongoing area of research as it still is a challenging task to analyze their structure. One example of interactions of such lipids with membrane proteins suggests that charges of annular lipids are important to the functionality of certain proteins. Accordingly, a type of ABC transporter protein, which can be involved in diseases such as multidrug resistance, preferred interacting with phosphatidylglycerol, a negatively charged phospholipid, and not with phosphatidylethanolamine, a zwitterionic phospholipid. This suggested the presence of higher affinity spots on the protein [1].

The neuronal protein syntaxin-1A, involved in the release of neurotransmitters, has also been shown to interact preferentially with negatively charged lipids [23]. Syntaxin-1A is found primarily in segregated clusters due to the local excess of a particular anionic lipid. The electrostatic interactions between the protein and lipid facilitate the formation of a protein microdomain without a change in the local phase of the surrounding lipids [23].

The existence of an annular shell of lipids around the transmembrane domain of a membrane protein arises from the distortion of the lipid fatty acid tails at the lipid-protein interface. The introduction of a solid, geometrically complex surface—the protein—into the membrane forces a rearrangement of the surrounding fatty acid tails in order to maintain the impermeability of the membrane. Without the lipid annulus, the tails would be able to pack only poorly around the protein, resulting in membrane leakiness. The entropic penalty of maintaining the ordered annular lipid shell is thus worthwhile in order to preserve the structural integrity of the membrane [15].

Unlike bulk and annular lipids, non-annular lipids interact specifically with proteins. These lipids are buried inside the protein, and are thought to be vital for optimal function. An example of such an interaction is found to be useful in bovine heart cytochrome c oxidase, on which 13 different types of lipids were suggested to have specific binding sites. It was also suggested that two

palmitate tails of phosphatidylglycerols have a role in blocking the O_2 transfer pathway of this protein [19]. Lipid binding sites on the exterior of a similar protein are shown in the Figure below.

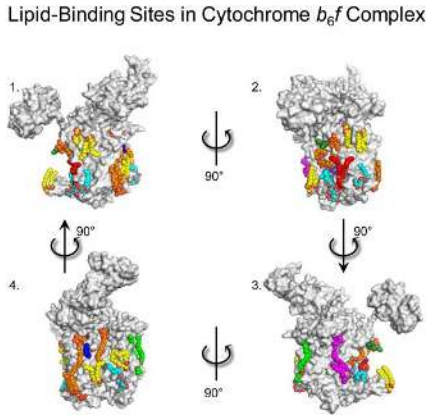


Figure 4.3.9: Lipid binding sites can be located at many positions on a membrane protein [26].

The interaction of non-annular lipids with proteins may also have implications in the detergent solubilization of membrane proteins—a common method used to isolate proteins from their native membranes to better understand the protein's structure or function. If the detergent used is sufficiently similar to the annular lipids typically surrounding the protein, there is a possibility that the detergent could penetrate this lipid shell and interact with the protein during the solubilization process [13]. This could change the conformation of the protein, potentially impacting its function. For example, the amino acid transporter LeuT has been shown to bind detergent molecules in one of its active sites (which displace the lipids typically residing there). This reduces the activity of LeuT. However, when a larger detergent molecule was used, it was unable to penetrate the annular lipid shell during the solubilization process, resulting in a retention of the protein's function [13]. This indicates that an understanding of the annular lipids in a protein's native membrane can be crucial to preserving both its structure and its function if solubilized.

Experimental Methods Used to Study Lipid-Protein Interactions

Some of the techniques used to study physical properties of lipid environment interacting with the membrane proteins include fluorescence spectroscopy, and electron paramagnetic resonance (EPR). There are methods utilized to understand interactions in molecular terms based on resolving the three-dimensional structures of proteins, which also helps clarify functions of some of the non-annular lipids [20]. X-Ray crystallography, NMR or EPR are among common tools analyzing lipid-protein interactions in molecular terms. Molecular dynamics simulations are another area of focus that can help researchers understand interactions of proteins and lipids both in molecular and physical terms.



Figure 4.3.9: Artist's rendition of the contrast between the dilute environment of a proteoliposome and the crowded environment of the native membrane [15].

The isolation of membrane proteins in proteoliposomes has also become a relatively common method of studying membrane protein function, including lipid-protein interactions. A proteoliposome is a small spherical vesicle into which a protein has been inserted. Proteoliposomes can be formed with known lipid compositions, allowing study of the effect of lipid composition--impacting membrane viscosity, phase separation, and membrane thickness-- on a protein's function. The membrane of the proteoliposome can thus act as a host to a variety of membrane proteins. While this method cannot necessarily replicate the inherent crowding and complexity of a native cell membrane, it can provide an understanding of the relative membrane properties required for a protein's function or the ligand affinity of the protein, among other things.

References

1. Bechara, C., Noll, A., Morgner, N., Degiacomi, M., Tampe, R., & Robinson, C. (2015). A Subset of Annular Lipids is linked to the Flippase Activity of an ABC Transporter. Biophysical Journal.
2. Brooks, C.L.; Karplus, M. Solvent effects on protein motion and protein effects on solvent motion. J. Mol. Biol. 208 (1989) 159–181.
3. Coskun, Ü.; Grzybek, M.; Drechsel, D.; Simons, K. Regulation of Human EGF Receptor by Lipids. Proc. Natl. Acad. Sci. **2011**, 108 (22), 9044–9048.
4. Deen, W. Analysis of Transport Phenomena, 2nd ed.; Oxford University Press, 2011.
5. Fagerberg, L.; Jonasson, K.; von Heijne, G.; Uhlén, M.; Berglund, L. Prediction of the Human Membrane Proteome. Proteomics **2010**, 10, 1141–1149.
6. Faller, R., MCB/BPH 241 Course Lectures. 2019.
7. Gutierrez, M. G.; Mansfield, K. S.; Malmstadt, N. The Functional Activity of the Human Serotonin 5-HT1A Receptor Is Controlled by Lipid Bilayer Composition. Biophys. J. **2016**, 110 (11), 2486–2495.
8. Hung, Y.;Schwarten, M.; Schünke, S.; Thiagarajan-Rosenkranz, P.; Hoffmann, S.; Sklan, E.; Koenig, B. (2015). Dengue virus NS4A cytoplasmic domain binding to liposomes is sensitive to membrane curvature. Biochimica Et Biophysica Acta (BBA) - Biomembranes, 1119-1126.
9. Lee, A.G. (2004). How lipids affect the activities of integral membrane proteins. Biochimica Et Biophysica Acta (BBA) - Biomembranes, 62-87.
10. Lee, A.G. (2011). Biological membranes: The importance of molecular detail. Trends in Biochemical Sciences, 493-500.
11. Lee, A. G. Lipid-Protein Interactions. Biochem. Soc. Trans. **2011**, 39 (3), 761–766.
12. Lehninger, A. (1982). Principles of biochemistry. New York, N.Y.: Worth.
13. LeVine, M. V; Khelashvili, G.; Shi, L.; Quick, M.; Javitch, J. A.; Weinstein, H. Role of Annular Lipids in the Functional Properties of Leucine Transporter LeuT Proteomicelles. Biochemistry **2016**, 55 (6), 850–859
14. McMahon, H. T.; Gallop, J. L. Membrane Curvature and Mechanisms of Dynamic Cell Membrane Remodelling. Nature **2005**, 438 (7068), 590–596.
15. Phillips, R.; Ursell, T.; Wiggins, P.; Sens, P. Emerging Roles for Lipids in Shaping Membrane-Protein Function. Nature **2009**, 459, 379–385
16. Razvan, L., & Thomas, D. (1994). Effects of Membrane Thickness on the Molecular Dynamics and Enzymatic Activity of Reconstituted Ca-ATPase. Biochemistry, 33, 2912-2920.
17. Rholam, M., Scarlata, S., & Weber, G. (1984). Frictional resistance to the local rotations of fluorophores in proteins. Biochemistry, 6793-6796.
18. Sezgin, E.; Levental, I.; Mayor, S.; Eggeling, C. The Mystery of Membrane Organization: Composition, Regulation and Roles of Lipid Rafts. Nat. Rev. Mol. Cell Biol. **2017**, 18 (6), 361–374
19. Shinzawa-Itoh, K. et al. (2007) Structures and physiological roles of 13 integral lipids of bovine heart cytochrome c oxidase. EMBO J. 26, 1713– 1725
20. Sperotto, M.M. A theoretical model for the association of amphiphilic transmembrane peptides in lipid bilayers. Eur. Biophys. J., 26 (1997), pp. 405–416
21. Hydrophobic mismatch. (2013, September 20). In Wikipedia, The Free Encyclopedia. Retrieved 21:05, May 13, 2015, from en.Wikipedia.org/w/index.php?title=Hydrophobic_mismatch&oldid=5737297
22. Engelman, D. M. Membranes Are More Mosaic than Fluid. Nature **2005**, 438 (7068), 578–580.
23. van den Bogaart, G.; Meyenberg, K.; Risselada, H. J.; Amin, H.; Willig, K. I.; Hubrich, B. E.; Dier, M.; Hell, S. W.; Grubmüller, H.; Diederichsen, U.; et al. Membrane Protein Sequestering by Ionic Protein–Lipid Interactions. *Nature* **2011**, *479* (7374), 552–555.
24. Palivan, C. G.; Goers, R.; Najer, A.; Zhang, X.; Car, A.; Meier, W. Bioinspired Polymer Vesicles and Membranes for Biological and Medical Applications. *Chem. Soc. Rev* **2016**, *45*, 377–411.
25. Harayama, T.; Riezman, H. Understanding the Diversity of Membrane Lipid Composition. *Nat. Rev. Mol. Cell Biol.* **2018**, *19*, 281–296.
26. Hasan, S. S.; Cramer, W. A. Internal Lipid Architecture of the Hetero-Oligomeric Cytochrome B6f Complex. *Structure* **2014**, *22* (7), 1008–1015.

4.3: Protein-lipid Interactions is shared under a CC BY 4.0 license and was authored, remixed, and/or curated by LibreTexts.

4.4: Physical Lipid Protein Interactions

Biological membranes play a prominent role in cell biology. The lipid-bilayer is composed of a large variety of lipid molecules that naturally form physical barriers creating compartments needed for cell regulation [1]. The shape of biological membranes is dictated by its lipid composition and a vast array of membrane-proteins inserted on it. The lipid environment and membrane-proteins are subject to chemical and physical interactions. Chemical interactions include effects of residues between lipids and proteins at the molecular level [3]. Physical interactions include mechanical stimuli between lipids and proteins.

In 1972, Singer and Nicolson proposed the **fluid mosaic model** which describes the lipids as a neutral environment to the activities of proteins [1,2]. However, recent studies suggest that lipids are strongly coupled to membrane-proteins and at times the lipid bilayer has the leading role determining the function of membrane-proteins [3, 8 ,10]. One specific case of study highlighting the physical lipid-protein interactions concerns the mechanosensitive (MS) ion channels.

Mechanosensitive Ion Channels

A membrane protein is considered mechanosensitive if its activity is controlled by membrane tension of approximately 20 nN/m. Mechanical forces can stretch, compress and bend the lipid bilayer causing membrane tension [4,5]. MS ion channels then act like mechanical force sensors transducing mechanical stimuli into important intracellular signals. In general, MS channels can be divided into two groups: prokaryotic (bacterial and archaeal) and eukaryotic (fungal, plants and animal and human) [11]. In both of these groups the function of MS channels is different. For example, in animals and human they are important in touch sensation, balance and hearing. In bacteria, MS ion channels are associated with osmoregulation control] [7,8]. MS ion channels highlight the physical lipid-protein interactions and its function depend upon mechanical membrane parameters such as tension and thickness [5]. Tension and thickness due to lipids induced perturbations to the membrane shape and the free-energy cost of such perturbations can be estimated quantitively by simple mathematical models.

Prokaryotic Mechanosensitive Ion Channels

Based on the homology of their primary sequence, MS channels in prokaryotic cells MS channels are classified into two categories: Large conductance MS channels (MscL) and small conductance MS channels (MscS). In principle MscL and MscS channels undergo the same conformation from a closed state to an open state and its thermodynamics can be described by a two-state model [9]. MS channels from MscL bacteria undergoes a large in-plane area expansion when it opens. In the case of MscL, pore gating serves as a “pressure release valve” and the in-plane expansion produces a decrease in the free energy of the membrane-channel system if the membrane is under tension and as a result it favors the open state [6,9]. To understand the free-energy change, the tension here is analogous to a gravitational field that tends to lower the weights [6]. Figure 4.4.1A shows that when the channel is closed, tension is small and the weights are not moving, if the weights are lowered this produces tension and channel will open (Figure 4.4.1B).

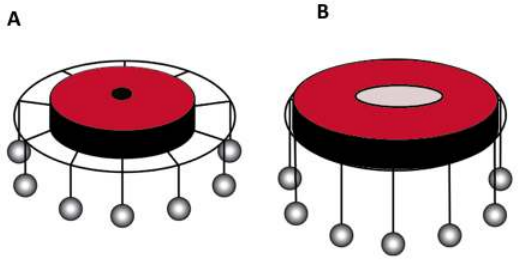


Figure 4.4.1. A) the MS ion channel is closed. B) The MS ion channel is open. Illustration adapted from Y.R. Guo and R. MacKinnon 10.7554/eLife.33660

The free energy difference of the open-close channel is given as follows:

$$\Delta G = \Delta G(\gamma = 0) - \gamma \Delta A \tag{4.4.1}$$

where ΔG (γ=0) is the change in free-energy at zero tension, γ is the membrane tension and ΔA is the in-plane cross sectional area. In MscL the in-plane area change ΔA has been calculated experimentally is approximately 20 nm^2. Thus, the energy required to fully open the MscL channel is about 20 kT. In addition, the experimental results from MscL in Escherichia coli not only show the effects of tension but also show that lipid tail length, saturation and head group affect the channel gating properties [2,7]. The data in Figure 4.4.2A shows the open probability as a function of pressure for MscL. Different traces correspond to different lengths in

lipid tails. The tails have 16, 18 and 20 carbon atoms in their backbone [2,7]. Figure 4.4.2B shows how the thickness of the lipid bilayer is affected by the length of lipid tails, this difference in thickness is often referred as a hydrophobic mistmatch.

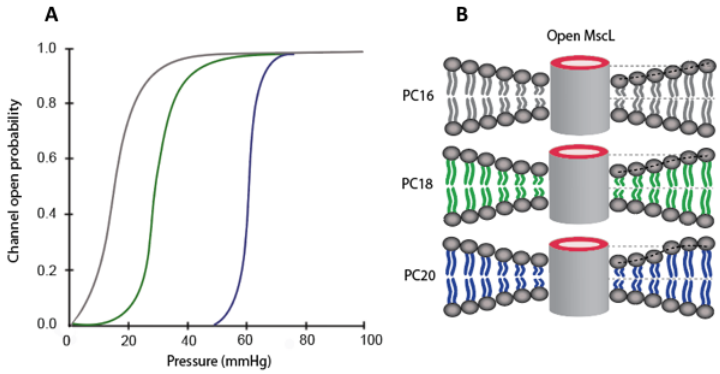


Figure 4.4.2. Data from patch-clamp showing how the open probability depends on the length of lipid tails PC15 (grey), PC18 (green) and PC20 (Blue). B) The diagram shows how different lipid tails imply different hydrophobic mismatch. Data and illustrations adapted from E. Perozo et al,. Nat, Struct. Biol. 9:696, 2002

Techniques used to understand the mechanism for gating of MS ion channel in prokaryotic cells include disulfide trapping, spectroscopic probing, mutagenesis screening and chemical modification [9]. In addition, patch clamp experiments have demonstrated that bacteria MscL channels gates respond to an increase in trans bilayer pressure [7].

Eukaryotic Mechanosensitive Ion Channels

In eukaryotic cells, there are four types of MS channels which include members of DEG/EnaC, 2P-type K, TRP and Piezo channel families [11]. In particular, Piezo 1 ion channels similar to MscL and MscS channels to open only requires the effects of lipid bilayer alone without the requirement of other cellular components [11].

Piezo 1 ion channels are sensitive to mechanical forces and transduce them into electrical signals in sensory neurons to achieve control in touch sensation, balance and cardiovascular regulation. The essential biophysical characteristics of Piezo 1 ion channels include control gating through mechanosensitive forces and cation selectivity [6]. It has been suggested that Piezo 1 channels sense force directly through the lipid membrane in a similar way MS channel from MscL bacteria. However, Piezo 1 channels have narrow pores in comparison to MscL channels and the effects on the membrane are not directly associated with in-plane area expansion, instead Piezo channels deform the membrane by producing local curvature (dome-shape) [6]. The expansion of the membrane-channel system occurs when the dome shape becomes flatter thus, the free energy difference between open-close channel is given as follows:

$$\Delta G = (\Delta G_{prot} + \Delta G_{bend}) - \gamma \Delta A_{proj} \tag{4.4.2}$$

where ΔG_{prot} and ΔG_{bend} refer to free energy differences intrinsic to protein gating and membrane bending, γ is the membrane tension and ΔA_{proj} the change in area of the dome that is projected onto the membrane plane (Figure 4.4.3B). Due to its complex structure, the values of A have not been determine experimentally. For instance, if the Piezo 1 ion channel becomes completely planar, the projected area ΔA_{proj} is about 20 nm^2 [6].Then the energy required to open this channel is approximately 40 kT. However, if Piezo 1 channels only flattens partially then the ΔA_{proj} should be less than 120 nm^2 and the energy will be less than 40 kT. In addition, if ΔG > 20 kT will imply that Piezo 1 channels are more sensitive to tension than MscL.

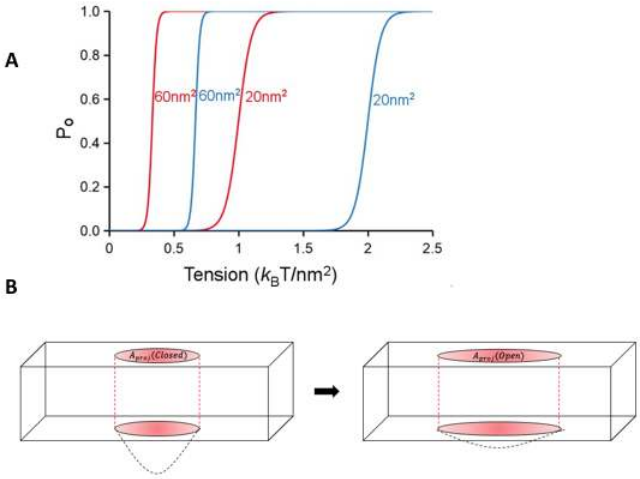


Figure 4.4.3. A) Theoretical activation curves ($\Delta G_{prot} + \Delta G_{bend}$) = 20 kT (red) and 40 kT (blue) and ΔAproj = 20 nm^2 or 60 nm^2 . B) Projection area changing as the surface curvature of the channel and local membrane changes. Data adapted rom Y.R. Guo and R. MacKinnon 10.7554/eLife.33660

Techniques used to study MS ion channels in eukaryotic cells include crystallography, cryo-EM, SDSL EPR, SDFL FRET spectroscopy, path fluorometry, mass spectroscopy and computer modelling [11].

Summary

- In prokaryote and eukaryotic cells, MS channels senses stimuli from membrane tension. Specifically, MscL, MscS and Piezo 1 channel requires only the effect of the lipid bilayer without the requirement of other cellular components.
- In the case of MscL the open channel mechanosensitive is due to couple pore opening to in-plane area expansion. However, in the Piezo channel, flattening of the channel and its nearby surrounding membrane causes membrane plane expansion by transferring out-of-plane membrane area into the membrane plane.
- Simple mathematical models can be used to understand and get insights of how the perturbations to the membrane shape affect the function of mechanosensitive ion channel.

References

1. D.M. Engelman, Membranes Are More Mosaic Than Fluid, Nature (London) 438, 578 (2005).
2. Phillips et al., 2008 Phillips RKJ, Theriot J, Garcia HG. Physical Biology of the Cell. Garland Sci. 2013.
3. Phillips et al., 2009R. Phillips, T. Ursell, P. Wiggins, P. Sens. Emerging roles for lipids in shaping membrane-protein function.Nature, 459 (2009), pp. 379-385
4. Brown, M. F. Soft Matter in Lipid–Protein Interactions. In Annual Review of Biophysics; Dill, K. A., Ed.; Annual Reviews: Palo Alto, 2017; Vol. 46, pp 379– 410
5. Reeves, D., Ursell, T., Sens, P., Kondev, J. & Phillips, R. Membrane mechanics as a probe of ion-channel gating mechanisms. Phys. Rev. E Stat. Nonlin. Soft Matter Phys. 78, 041901 (2008).
6. Y.R. Guo, R. MacKinnon. Structure-based membrane dome mechanism for Piezo mechanosensitivity Elife, 6 (2017), 10.7554/eLife.33660
7. Perozo,E.,Kloda,A.,Cortes,D.M.&Martina,B.Physicalprinciplesunderlyingthe transduction of bilayer deformation forces during mechanosensitive channel gating. Nature Struct. Biol. 9, 636–637 (2002).
8. Brohawn, S. G., Su, Z. & MacKinnon, R. Mechanosensitivity is mediated directly by the lipid membrane in TRAAK and TREK1 K+ channels. Proc. Natl Acad. Sci. USA 111, 3614–3619 (2014).
9. Zhang XC, Liu Z, Li J. From membrane tension to channel gating: a principal energy transfer mechanism for mechanosensitive channels. Protein Sci 25:1954 –1964 (2016).
10. Pivetti, C. D., Yen, M.-R., Mille, S., Busch, W., Tseng, Y.-H., Booth, I. R. and Saier, M. H., Jr (2003). Two families of mechanosensitive channel proteins. Microbiol. Mol. Biol. Rev. 67, 66-85.
11. Battle, A.; Ridone, P.; Bavi, N.; Nakayama, Y.; Nikolaev, Y.A.; Martinac, B. Lipid–protein interactions: Lessons learned from stress. Biochim. Biophys. Acta (BBA)-Biomembranes 2015, 1848, 1744–1756.

4.4: Physical Lipid Protein Interactions is shared under a CC BY 4.0 license and was authored, remixed, and/or curated by LibreTexts.

4.5: Nanoparticle Spontaneous Penetration and Assembly in and Through Membranes

Nanomaterial science is a rapidly evolving field of study to approach many scientific questions across fields. From sensors, drug delivery systems, cellular augmentation, and probes to highlight a handful of uses. However, these particles across application often come into contact with lipid membranes and can interact with the berries in a verity of ways. Nanoparticles (NPs) have been shown to restructure lipid membranes to penetrate or embed themselves into the lipids spontaneously. How they are achieved this, and the effectiveness of these NP relies on an on a variety of tunable factors. These elements have been studied in detail, allowing for the ability to design one's nanomaterial not only to accomplish its task but to predict its interaction with the membranes in question[1]. This article will introduce the elements that determine different lipid interactions, primarily focusing on NPs spontaneous passage through the membrane along with modeling tools to predict interactions. NPs can use cellular channels or adhere to membranes; however, these prove too large a topic to cover though information can be found [2, 3]. However, there are still other ways to approach the topic of NP interaction with cell membranes, or model membranes. I have chosen here to explore a central concept of spontaneous penetration and the surrounding concept that supports this interaction and its study. With the ever-growing field and applications of NPs, their involvement and our exposures to them in our everyday life bring concerns of toxicity which is often a focus of NP membrane interactions and how best to disperse the embedded or passage of the NP across the membranes. [4-7].

A Brief Understanding of Functionalized Nanoparticles

One fundamental concept of most applications of NPs is that they are functionalized by an introduction of impurity that often disrupts its natural shape, charge, size, etc. For example, if you were to functionalize a single-walled carbon nanotube (SWNT), you would decorate it with another polymer, i.e., DNA, Pd, etc. In this example, the functionalizing unit can either completely or partially associate with the core SWNT. This is only one, rather, specific case example of functionalization of SWNT particles. However, many other types of NP can be functionalized for a variety of means and can be explored in more depth across a variety of topic applications from imaging, medical, and living plant systems [4-7].

Spontaneous Penetration and Assembly in and Through Membranes

NPs can spontaneously move through bio-lipid double membranes, however, due to their particle material, size, shape, surface, charge, corona, and other factors the efficiencies and how they remodel the membranes can vary (fig 1B) [1, 8]. NPs can move fully through the membrane or get trapped/ encapsulated, wrapped while passing or translocated through gaps, all based on the characteristics of the particle in question and can be predicted. Through this process, the NPs can also form pores in a variety of ways (Fig 1A). Below we will explore how these physical properties change the relationship of the passive spontaneous passage of NPs across both biological and model membranes. However, the physical properties of the particle are not the only factors to be considered as the environment, and the membrane characteristics itself need to be considered. In this page, we will focus on the particle characteristics governing the relationship with membrane penetration; however, for a more holistic overview of this topic refer to the following citation [9].

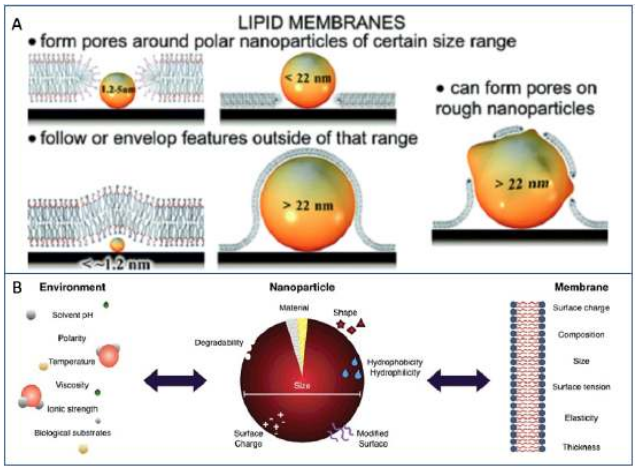


Figure 4.5.1. Figure taken from [10]. A. Nanoscale range of surface feature curvatures where lipid membranes lose integrity and form pores has been found experimentally. The pores were experimentally observed in the l-α-dimyristoyl phosphatidylcholine membrane around 1.2−22 nm polar nanoparticles deposited on mica surface. Lipid bilayer envelops or closely follows surface features with the curvatures outside of that region. This finding provides essential information for the understanding of nanoparticle−lipid membrane interaction, cytotoxicity, preparation of biomolecular templates and supported lipid membranes on rough and patterned surfaces. Properties that influence NP-membrane interaction. The intrinsic characteristics of a NP, the surrounding environment and the biological substrate that influences the interaction between NPs and biological membranes[9].

Wrapping Translocation Vs Embedding

NP can pass through or embed in membranes in two different ways. One method is when the membranes bend to maximize the number of contact interaction with the NP; this is called wrapping and induces positive curvature[11]. The head groups of the membrane form vesicles around the nanoparticle and depending on the charge can become stuck to the outer surface of the NP, discussed further below. Wrapping resembles an absorption process. This is fundamentally different than particles that become embedded as the embedding process has minimal disruption to the membrane structure in contrast to wrapping.

Using modeling prediction with informed biological studies researches can understand the impact of the size of the NP on the lipids. Hydrophilic NPs of 20Å become wrapped while those smaller and closer to 10Å become embedded in the bilayer interacting with the hydrophilic headgroups as it is encapsulated as shown in Figure 4.5.2a. Hydrophobic NP regardless of their size even up to 60Å, do not become wrapped by the lipids and instead penetrate the membranes to embed into the hydrophobic core (fig 2 c)[12]. However, here they have only modeled one type of membrane, and as tunable, the NPs can be it has also been shown that lipid head groups and tail lengths play a significant role in the interactions of the two [11]. In the case of wrapping passages, the strength of the head groups wrapping ability and connection was shown to be inhibited by hydrophobic interactions of longer hydrophilic PEG chains allowing the NP to more easily pass through the rapping and come out the other side of the membrane. Because the NP is disordering the membranes upon entering the leaflets, the wrappings positive curvature can be modulated by the length of overhanging tails of the functionalizing unit along the NPs. The overall shape of these structures, i.e., rod vs. spherical, can also play a role in how they pass through the membranes[11, 13].

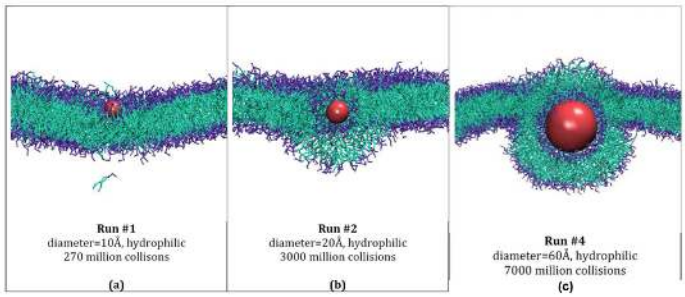


Figure 4.5.2. Adapted Figure from [7]. Snapshots of final configurations for simulations run on LIME systems containing hydrophilic NPs of different sizes and a DPPC bilayer membrane. The color scheme is purple (DPPC choline entity), orange (DPPC phosphate group), red (DPPC ester groups), cyan (DPPC alkyl tail groups), red (NPs). Also See Figure 4.5.6 for shape dependence [13]

Charges Can Lead to Membrane Reconstruction

It has been shown that NPs can pass through phospholipid membranes spontaneously, which is one of the many factors making them ideal for drug delivery and sensor creation. NPs can only pass through phospholipid membranes spontaneously when they are charged either in the positive or negative direction (fig. 3). Where the negatively charged particles elicit local gelation in otherwise fluid bilayers while positively charged particles gain passage by targeting gelled membranes to fluidize locally[8]. These charges cause phase transitions that deviate from nominal phase transition temperature by tens of degrees but were shown across lipid types DOPC (dioleoyl phosphocholine (PC)), DLPC (dilauryl PC), and DPPC (dipalmitoyl PC), with differing gel-to-fluid phase transition temperature (Tm) of approximately −20 °C, −1 °C, and +40 °C, respectively. Both charges absorbed to the PC group of phospholipids and showed that the liposomes penetrated by the NPs could maintain their integrity with minimal shrinkage by the negatively charged NPs. The physical rigidity of these particles is thought to allow for this unique interaction with the phospholipid membranes, whereas DNA, an Anionic particle, does not elicit the same membrane reconstruction as similarly charged anionic NPs[8]. This phenomenon is novel in the fact that a foreign nonbiological object has caused these alterations as the membranes are often passing through these different states to allow ions and natural membrane remodeling to occur. Coupled with the fact that this process is not classified as endocytosis but a passage through the membranes when disruptions as lipids bind to the particle itself (fig. 4)

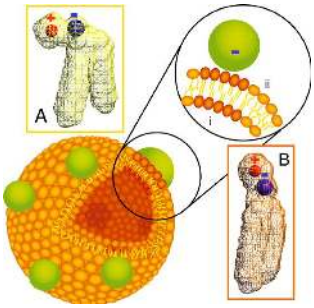


Figure 4.5.3. Taken from [8]. Schematic diagram of a phospholipid bilayer vesicle with bound NP. Binding of anionic NPs to a leaflet in the fluid phase causes the NP to template a gel phase in the place where the NPs binds. Binding-induced reorientation of the PC head group causes lipids in the fluid phase to have a lower density (*A*) than in the gel phase (*B*). In the PC head group, P^- and N^+ are denoted by blue and red, respectively.

This phenomenon has also been characterized in plants with a verity of different NPs. Here the Lipid Exchange Envelope Penetration or “LEEP” model show that the cargo the particles are doped with can have an effect on spontaneous penetration and localization within the cell down to single organellar, such as the chloroplast[14, 15]. In Figure 4.5.4. Shows the ability to penetrate the cell and internal compartments based off of the charge as illustrated through zeta potential (the energy difference existing between the surface of a solid particle immersed in a conducting liquid (e.g. water) and the bulk of the liquid) to take into account the aqueous environment that is the cell. As stated above in A Brief Understanding of Functionalized Nanoparticles the doping or cargo of a particle can have a significant effect on the dynamics of the particles in regards to shape, size, charge, and other vital characteristics.

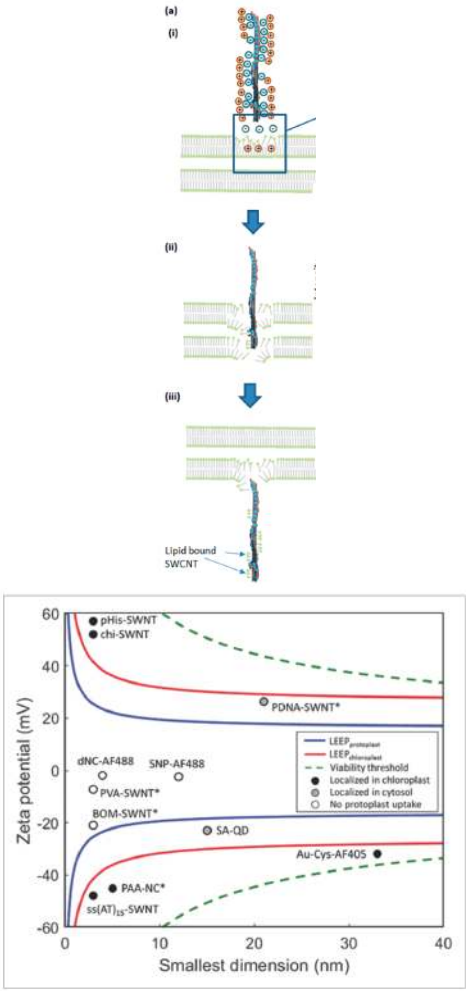


Figure 4.5.4. Adapted from [14,15]. A. (i) SWNT NP with high zeta potential approach the outer membrane that is similarly negatively charged. This induces image charges on the lipid bilayer and leads to membrane expansion and softening. (ii) Glycerolipids wrap around SWNT as they interact with the membrane. Interaction between lipids and SWNT is confirmed by the solvochromatic shift observed upon addition of dipalmitoylphosphatidylcholine (DPPC) to SWNT. (iii) The lipid-bound SWNT enters and binds to the interior. The lipid membrane of the membrane heals. B. LEEP model explains the entry and distribution of NPs inside protoplasts. LEEP model for protoplasts and chloroplasts are indicated by blue and red lines, respectively, while the threshold to maintain protoplast viability is shown by the dashed green lines. The LEEP model can not only explain the experimental observations in this study, but also NPs investigated in previous studies (denoted by *).

Models Used for Prediction

There is an ever-growing library of different types of NP polymers functionalized with a verity of differing decorations all influencing the overall characteristics of the NP as a whole. It would be impossible to test the viability and dynamics of all different polymers that can be created with the different combinations of backbones and decorations. Therefore, many modules have been created to predict and simulate their dynamics based on the information gathered by the portion of the library studied both in vivo and in vitro[12]. The models used for prediction of the type of interaction can fall into two types of categories, High- resolution or atomistic and low resolution or coarse-grained models giving different perspectives and output times on the information. See Table 1 for a summary.

High- resolution or atomistic models can give a representative picture of the geometry and energetics of all the molecules that are typically accounted for in the motion of every atom, including every solvent atom. These are often used to study the passive transport of NP through lipid membranes. One such study was conducted by Bedrov et al. to understand the passive motion of C60fullerenes into lipid di-myristoly-phosphatidylcholine (DMPC)[16].

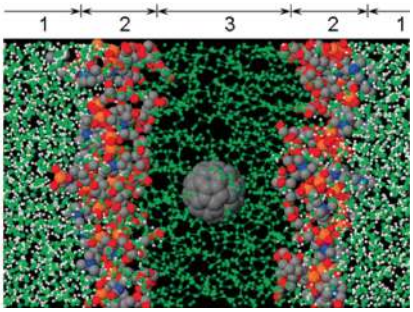


Figure 4.5.6. Adapted from [16]. Illustrated is the system configuration with a snapshot of the hydrated DMPC membrane containing a C60 fullerene and illustrates three well-defined regions: (1) bulk water outside of lipid bilayer, (2) dense layer of lipid hydrophilic head groups, and (3) hydrophobic region of lipidic tails. Hydrogen atoms associated with lipid tail are not shown. Fullerene carbon atoms are shown in dark gray, water oxygen atoms in green, and hydrogen atoms in white. In the DMPC molecule: tail backbone carbon atoms are dark lime, nitrogens dark blue, phosphorus atoms orange, and oxygen atoms red.

Low resolution or coarse-grained models still account for both the lipids and NP but are a simplified representation of the molecular geometry and energies. Here instead of taking into account the whole system, a single interaction site is used to represent a group of several atoms. Because of this, the seed of the calculation is quicker as the total number of sites is decreased. Again, passive transport can be studied using this model type. In one informative biological study, the passive endocytosis of ligand-coated NP was studied based on different geometries of size, shape coverage, and membrane-binding strength [13]. The phospholipid molecules were modeled by three spheres; one for the hydrophilic head group, and two for the hydrophobic tails. Similarly, the NP was simply expressed as spheres of the same size as the tail groups. Though simplistic, the group was able to show that the model was sufficient enough to show that larger spherical particles endocytosis easier than smaller particles as a result of favorable energies for bending rigidity and surface adhesion while also illustrating the favorable energies for spherocylindrical NP to normal spherical particles.

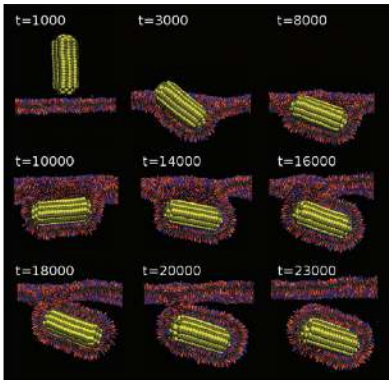


Figure 4.5.6. Taken from [13] A representation of the generated model of spherocylinder endocytosis. The spherocylinder is initially oriented perpendicular to the membrane. It changes orientation and becomes parallel upon binding to the membrane (t = 10 000); then it rotates and gets encapsulated further. Detachment from the membrane takes place at the end of spherocylinder. The particle surface is composed of 50% of ligands that interact by 5.0 kT with 50% of lipid headgroups representing membrane receptors. A cut through the membrane at the particle position is depicted for clarity. Color coding: nanoparticle, yellow beads are ligands and gray beads are purely repulsive; membrane, blue beads are membrane receptors, orange are headgroups, and gray and orange are tail beads.

Recently an intermediate- resolution model has been developed for describing the implicit-solvent for lipid molecules or LIME[12]. A boon of this is a better resolution than a true coarse-grained model but also more time efficient than an atomic high-resolution models' prediction. The increase in speed is due to the use of discontinuous molecular dynamics. So far, this model has been used to capture the interaction between the hydrophilic and hydrophobic NPs and DPPC bilayer membranes, taking into account both the membrane and the NPS geometric and energetic parameters. However, like the other model types, there are drawbacks. Figure 4.5.2 is generated using the LIME model.

Table 1.

	Advantages	Disadvantages	Common uses
High resolution / atomistic models	• Visualization of geometry and energetics of all the molecules • motion of every atom captured • solvent atom dynamics • account the whole system	• Takes a lot of computing power • Long output time • Cannot examine large conformational changes •	• study the passive transport of NP through lipid membranes. • Bedrov et al. [16]
Low resolution/ coarse-grained	• Accounts a single interaction site • Fast output time • Less computing power needed	• simplified representation of both lipids and NP	• Particles endocytosis • Passive transport • Vacha, R., F.J. Martinez-Veracoechea, and D. Frenkel, [13]
Intermediate-resolution / LIME	• Better resolution than a true coarse-grained • More time efficient than an atomic high-resolution	• Discontinuous molecular dynamics • Electrostatics is not represented explicitly • Diffusion and hydrodynamics are not well represented • A direct correlation between reduced temperature and real temperature can only be made at which LIME was parameterized	• Capture the interaction between the hydrophilic and hydrophobic NPs and Membranes • Curtis, E.M., et al., [12]

References

1. Nel, A.E., et al., *Understanding biophysicochemical interactions at the nano-bio interface.* Nat Mater, 2009. **8**(7): p. 543-57.

2. Lesniak, A., et al., *Nanoparticle adhesion to the cell membrane and its effect on nanoparticle uptake efficiency.* J Am Chem Soc, 2013. **135**(4): p. 1438-44.

3. Behzadi, S., et al., *Cellular uptake of nanoparticles: journey inside the cell.* Chem Soc Rev, 2017. **46**(14): p. 4218-4244.

4. Kwak, S.Y., et al., *Nanosensor Technology Applied to Living Plant Systems.* Annu Rev Anal Chem (Palo Alto Calif), 2017. **10**(1): p. 113-140.

5. Thiruppathi, R., et al., *Nanoparticle Functionalization and Its Potentials for Molecular Imaging.* Adv Sci (Weinh), 2017. **4**(3): p. 1600279.

6. Vijayan, V., S. Uthaman, and I.K. Park, *Cell Membrane-Camouflaged Nanoparticles: A Promising Biomimetic Strategy for Cancer Theragnostics.* Polymers (Basel), 2018. **10**(9).

7. Schroeder, V., et al., *Carbon Nanotube Chemical Sensors.* Chem Rev, 2019. **119**(1): p. 599-663.

8. Wang, B., et al., *Nanoparticle-induced surface reconstruction of phospholipid membranes.* Proc Natl Acad Sci U S A, 2008. **105**(47): p. 18171-5.

9. Contini, C., et al., *Nanoparticle–membrane interactions.* Journal of Experimental Nanoscience, 2018. **13**(1): p. 62-81.

10. Roiter, Y., et al., *Interaction of nanoparticles with lipid membrane.* Nano Lett, 2008. **8**(3): p. 941-4.

11. Lee, H., *Interparticle dispersion, membrane curvature, and penetration induced by single-walled carbon nanotubes wrapped with lipids and PEGylated lipids.* J Phys Chem B, 2013. **117**(5): p. 1337-44.

12. Curtis, E.M., et al., *Modeling nanoparticle wrapping or translocation in bilayer membranes.* Nanoscale, 2015. **7**(34): p. 14505-14.

13. Vacha, R., F.J. Martinez-Veracoechea, and D. Frenkel, *Receptor-mediated endocytosis of nanoparticles of various shapes.* Nano Lett, 2011. **11**(12): p. 5391-5.

14. Wong, M.H., et al., *Lipid Exchange Envelope Penetration (LEEP) of Nanoparticles for Plant Engineering: A Universal Localization Mechanism.* Nano Lett, 2016. **16**(2): p. 1161-72.

15. Lew, T.T.S., et al., *Rational Design Principles for the Transport and Subcellular Distribution of Nanomaterials into Plant Protoplasts.* Small, 2018. **14**(44): p. e1802086.

16. Bedrov, D., et al., *Passive transport of C60 fullerenes through a lipid membrane: a molecular dynamics simulation study.* J Phys Chem B, 2008. **112**(7): p. 2078-84.

4.5: Nanoparticle Spontaneous Penetration and Assembly in and Through Membranes is shared under a CC BY 4.0 license and was authored, remixed, and/or curated by LibreTexts.

4.6: Non-Membrane Lipid Assemblies (Micelles)

Amphipathic compounds (detergents) are a unique set of molecules with the ability of manipulation (distortion or formation) of the hydrophobic-hydrophilic interactions in biological samples. Detergents in an aqueous solution self-associate to colloid particles. The formation of the colloidal aggregates by detergents are termed micelles[1]. In research micelle-forming detergents provide an amphipathic environment that can mimic lipid bilayers, be used to lyse cells (release soluble proteins), solubilize membrane proteins and lipids, and control protein crystallization.

Detergents and Critical Micelles Concentration

As mentioned above detergents are amphipathic molecules (Figure 4.6.1), which are composed of a hydrophilic head group (polar) and a hydrophobic tail (non-polar). The hydrophilic head group detergents can be either ionic (charged anion or cation), nonionic (uncharged), or zwitterionic (containing both positive and negative charged components to have a net zero charge).

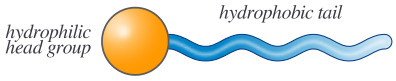


Figure 4.6.1: Amphipathic molecule. (CC BY-NC; Ümit Kaya)

The hydrophobic tail is an acyl chain (a long chain of aliphatic hydrocarbons, aka a carbon chain with hydrogen side groups). Its amphipathic properties allow detergents to dissolve both water and oil soluble compounds, such as soap [2]. In soap, particles insoluble in water (oil/fat) become associated with the hydrophobic tail of a micelle (Figure 4.6.2), shielding the insoluble particles from water, making it soluble. Detergents at low concentration in aqueous solution form a monolayer at the air-liquid interface. The detergents monomers can then begin to self-assemble into aggregates at and above the critical micelle concentration[3] (CMC) into structures called micelles (Figure 4.6.2). The viscosity of micelle core was found to be 17-50cP (cP: centipoise) by depolarization study of a fluorescence probe[4]. Thus, the interior is liquid like. But in some case, the interior is found to be more solid-like, with viscous rising to 151 cP. Basic micelles are generally described as roughly spherical (Figure 4.6.2A) with a separation of hydrophilic and hydrophobic parts.

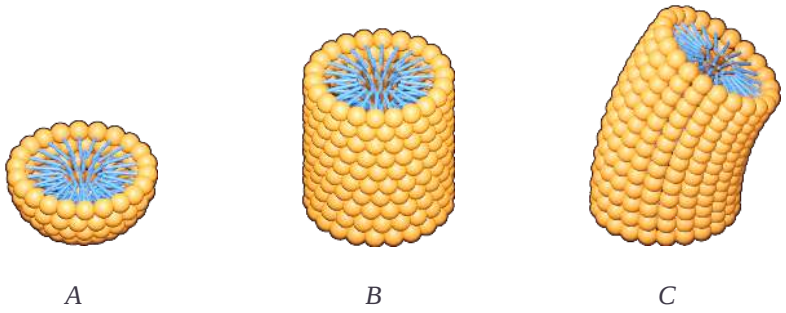


Figure 4.6.2: Ideal structure of a detergent micelle (A) spherical, (B) cylindrical, (c) worm-like. (CC BY-NC; Ümit Kaya)

Depending on the structure and physicochemical conditions, viz,. temperature, the presence of electrolytes, the self-aggregates structures can also be cylindrical (Figure 4.6.2B) or worm-like (Figure 4.6.2C). The detergent monomers bury the nonpolar tails by orienting them inward to avoid water contact and orienting the polar head groups outward to interact with the water. In detergents with more than one hydrophobic chain, similar to natural occurring lipids, the formation of cylindrical micelle may occur. The cylindrical micelle can then span into a two dimensions forming a bilayer.

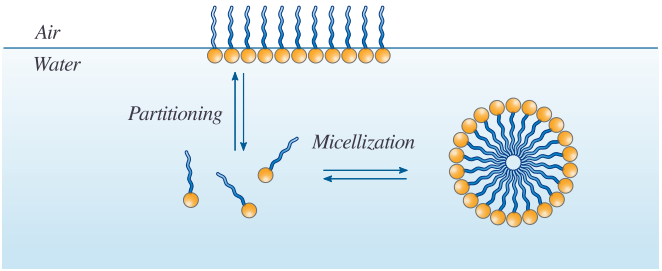


Figure 4.6.3: Schematic presentation of the equilibrium between detergents at a surface, free detergents, and in micelles. (CC BY-NC; Ümit Kaya)

Below the CMC, an increase of detergent will lower the surface tension while raising the osmotic pressure of the solution (Figure 4.6.4)[5]. This correlates to the lipids in the solution gathering almost exclusively at the air-water interface as shown below. At the CMC surface tension has been minimized to the greatest possible extent corresponding to the lipids fully saturating the air-water interface so that the entire surface is now a continuous lipid layer. Above the CMC, with an increase of detergent, the surface tension will stay constant because it is fully saturated. Thus the excess lipids will be forced into the water and will form micelles to protect their hydrophobic tails, which will then be able to dissolve previously insoluble compounds (like grease). The surface saturation process follows Langmuir (saturation) kinetics and can be described using a Langmuir isotherm.

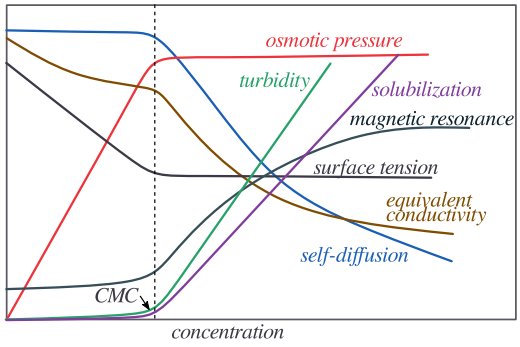


Figure 4.6.4: Changes in the concentration dependence of a wide range of physico-chemical quantities in the neighborhood of the critical micelle concentration. (CC BY-NC; Ümit Kaya)

Micelle formation can be described by the Gibbs adsorption isotherm [6]. The number of monomer detergents "n" to form micelles is called aggregation number and is characteristic of the surfactant molecule. Therefore, micellization can be described by an equilibrium (Figure 4.6.5) expression. With an equilibrium constant, $K_m=[Z_m]/[Z]^m$. A unitary free energy ΔG_m° for transfer of a single amphiphile from aqueous solution to a micelle of size *m*. The free energy expression can be calculated by replacing $RT\ln K_m$ by $-m\,\Delta G_m^\circ$, with concentrations expressed in mole fraction units. Therefore,

$$\ln K_m = \frac{-m\Delta G_m^o}{RT} + m \ln X_1 + \ln m \tag{4.6.1}$$

Where X_1 is the mole fraction of amphiphile in monomeric form and X_m is the mole fraction incorporated in micelles of size *m*, i.e, $X_m=m\,[Z_m]$. Equation 1 can be considered to be micelle size distribution function, giving X_m as a function of m at any given value of X_1. The cooperatively of micelle formation is reflected in the term $m\ ln\ X_1$, and limits the value of X_1 to a narrow range close to the CMC if reasonable values of X_m are to be obtained.

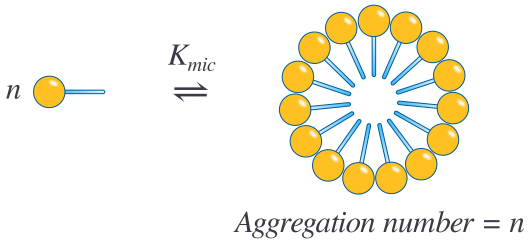


Figure 4.6.5: Micellization can be described by an equilibrium. (CC BY-NC; Ümit Kaya)

Over 70 types of methods have been deployed to determining the CMC from 1962-2010. Such as spectroscopic measurements (fluorescence probe, absorbance dye), electrochemical measurement (electrophoresis, capillary electrophoresis, conductimetric), surface tension measurements (contact angle measurements), optical measures (light scattering, optical fibers, refractro-metric), and many others[7]. Yet, the most common method is surface tension. This method determines the surface tension of solution towards several different concentrations. The turning points of a plot of the surface tension against log[C] (C: concentrations) graph is the CMC. Surface tension method commonly used because it's simple and convenient.

Research Applications

Detergents are crucial for the solubilization, purification, and crystallization processes needed for membrane protein structure determination[6]. Detergents are often used to solubilize important membrane proteins by generating a water-soluble protein-detergent-lipid complex (Figure 4.6.6 a). The detergents mimic the lipid membrane by surrounding the hydrophobic region of the integral membrane protein and leaving the hydrophilic region oriented toward the water. Maltosides and glucosides two of the most common used detergents for membrane protein crystallography, although there are is still a large variety of classes of detergents. Therefore, it's common to do a screening to determine the most suitable detergent for the desired target protein. For each detergent, varieties of hydrocarbon tail length are commonly available, allowing for fine tuning the size and stability of the protein-detergent-lipid complex.

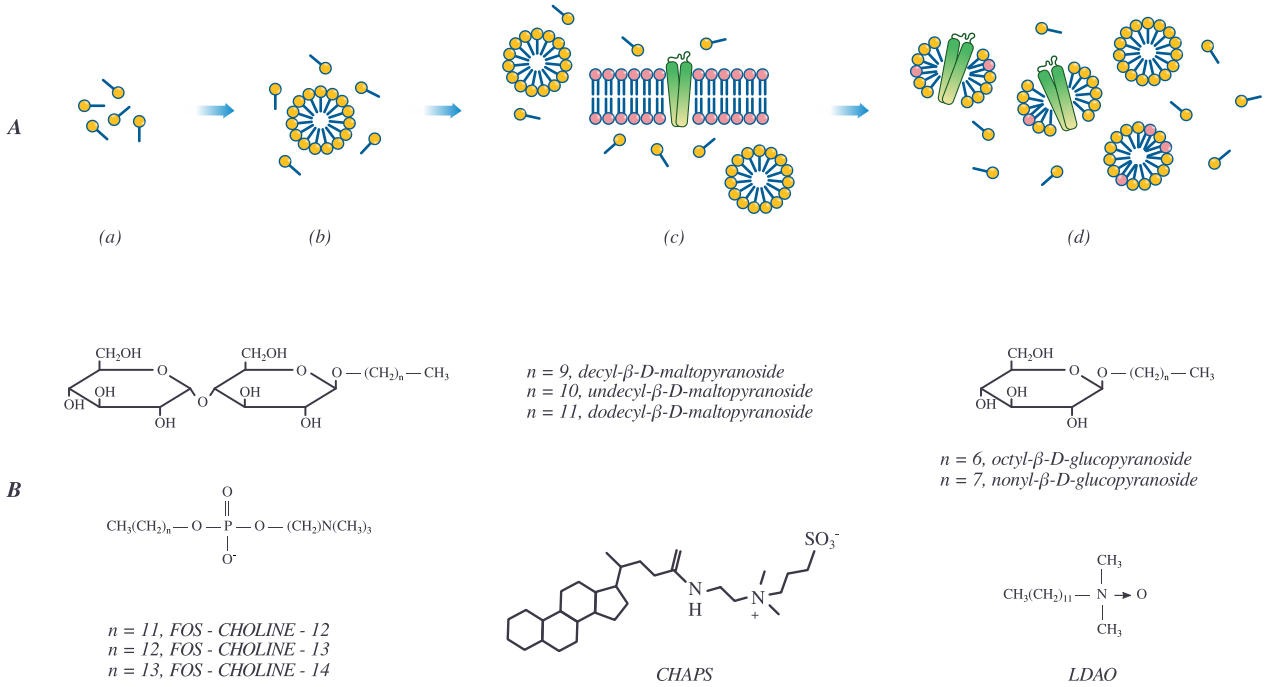


Figure 4.6.6: (a) schematic of the solubilization process. From left to right: free detergent monomers, detergent micelles above the CMC, a mixture of membrane and micelles, micelles extract membrane proteins from lipid bilayer to make a protein-detergent-lipid complex. (b) Some common detergents used in solubilization, purification, and crystallization of membrane proteins. (CC BY-NC; Ümit Kaya)

Once the integral membrane protein is solubilized and purified, it's necessary to concentrate (via. centrifugation and dialysis) to a supersaturated solution for crystallization to be successful. While concentrating it's important to maintain the CMC to ensure free

detergent micelles and retain the protein-detergent-lipid complex. If CMC is not retained, the integral membrane protein will aggregate out of solution. The detergent used during solubilization may be the same used while crystallization but is most commonly changed or an additive detergent is added. There are several physicochemical parameters to consider besides detergents for the crystallizing integral membrane proteins, such as buffers, pH, precipitants, salts, additives, and many others[8]. Over the past few years there has been an exponential increase of integral membrane protein structures published in the Protein Data Bank and many unique insights have been provided into successful conditions for membrane protein crystallization (Figure 4.6.7).

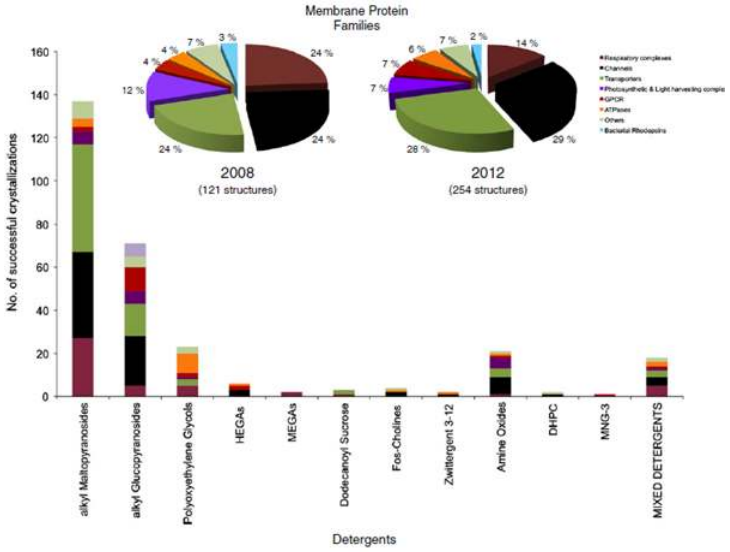


Figure 4.6.7: Alpha-helical membrane protein crystallization currents trends of successful detergents used[8].

Reference

1. McBain, J. B. Trans Faraday Soc, 1913, 9, 93-107
2. Wennerstrom, H.; Lindman, B. Physics Reports, 1997, 52, 1-86
3. Ruckenstein, E.; Nagarajan, R journal of Colloid and Interface Science, 1976, 57, 388-390
4. Zoller, U.; Broze, G. Handbook of detergents; Marcel Dekker: New York, 1999
5. Chakrabory, T. el alt. Arabian Hournal of Chemistry, 2011, 4, 265-270
6. Tanford, C. Proc. Nat. Acad. Sci. USA, 1974, 71, 1811-15
7. Newby, Z. E. R. el. Alt. Nature Protocols, 2009, 4, 619-638
8. Newstead, S.; Ferrandon, S.; Iwata, S. Protein Sci., 2008, 17, 466-476
9. Moraes, I. el alt. Biochemistry & Biophysical, 2014, 1838, 78-87Moraes, I. el alt. Biochemistry & Biophysical, 2014, 1838, 78-87

4.6: Non-Membrane Lipid Assemblies (Micelles) is shared under a CC BY 4.0 license and was authored, remixed, and/or curated by LibreTexts.

CHAPTER OVERVIEW

5: Experimental Characterization - Spectroscopy and Microscopy

5.1: Model Membranes vs. Biological Membranes
5.2: Supported and Tethered Membranes
5.3: Styrene Maleic Acid Lipid Particles (SMALP) Technology
5.4: Lipid Probes
5.5: Fluorescence on Membranes
5.6: Near-field Scanning Optical Microscopy (NSOM)
5.7: Single Molecule Tracking
5.8: FTIR on Membranes
5.9: Raman Spectroscopy on Membranes
5.10: Nuclear Magnetic Resonance (NMR) Theory and Solution NMR
5.11: Solid-state NMR
5.12: Electron Paramagnetic Resonance (EPR) of Membranes
5.13: Membrane X-ray Scattering

5: Experimental Characterization - Spectroscopy and Microscopy is shared under a CC BY 4.0 license and was authored, remixed, and/or curated by LibreTexts.

5.1: Model Membranes vs. Biological Membranes

The study of cells has been a challenging, active area of research since the seventeenth century when Robert Hooke first observed them through his compound microscope. [1] Cells consist of cytoplasm, which contains biomolecules such as nucleic acids and proteins, and is enclosed by a plasma membrane. This membrane plays an essential role in cellular protection as well as in the control and the transport of ions, nutrients and a variety of small molecules through protein channels or processes like diffusion and endocytosis.

One of the key developments towards determining the structure of the plasma membrane was the proposal of the "Fluid Mosaic Model" by SJ Singer and GL Nicolson in 1972. The model states that membranes are composed of a phospholipid bilayer backbone with embedded cholesterol, proteins, and carbohydrates that gives the membrane its fluid character. [11] This composite structure allows the membrane to perform multiple functions such as molecular recognition, enzymatic catalysis, cellular adhesion and membrane fusion. The most important evolution of this model happened in 1997 with the works of Simons et al. and of Brown et al. who proposed that membrane lipids were organized into phase-separated micro-domains, called lipid rafts, with a different local composition and a molecular dynamic from the surrounding liquid crystalline phase. The validity of this hypothesis was a hotly debated topic for more than a decade but has since been demonstrated by a lot of researchers and has led to the development of technologies for detecting lateral heterogeneity in biological membranes. [10] A comprehensive understanding of all components of the plasma membrane and their synergistic workings could help improve our understanding of the evolution of life on earth and play a crucial role in biological advancement in the future.

Biological Membranes: Composition and Functions

Biological membranes have complex and varied compositions of lipids and proteins which make the determination of their exact composition in a cell quite difficult. That being said, their primary components are well established.

The first major components of biological membranes are **lipids**. All biological membranes contain lipid bilayers as their basic structural unit. Lipid bilayers are sheet-like assemblies of thousands of amphiphilic lipid molecules held together by hydrophobic interactions between their acyl chains. Membrane lipids can be divided into three groups based on their chemical structure: glycerol-based lipids (phospholipids), ceramide-based sphingolipids, and sterols. *(Figure* 5.1.1*a)* These constituents are not homogeneously arranged in the cell plasma membrane but actually present as complex lateral micro-domains. *(Figure* 5.1.1*b)* This variability in the nature of lipid arrangement, in addition to significant differences in physical properties like cross-sectional area, unsaturation, fluidity, electric charge, molecular weight, is the reason that lipid membranes are extremely complex structures. Their association with other membrane components like proteins and carbohydrates adds to the difficulty of studying the membrane's structure. [12]

The second major components of cell membranes are the **proteins**. They constitute a large proportion of a typical cell membrane and perform a variety of functions [1]. Membrane proteins can associate with membranes in a variety of ways such as having domains that traverse the membrane, domains that associate with only one face of the membrane, chemical groups that anchor them to the membrane, or domains that associate with other membrane-bound proteins. The low permeability of cell membranes to everything except water, small uncharged molecules, and some hydrophobic signalling molecules requires that they possess machinery to facilitate the exchange of molecules between the cytoplasm and their external environment. Membrane proteins facilitate these types of phenomena. For example, proteins that act as channels to allow the rapid transport of ions and other molecules are quite common [2]. Other types of membrane proteins act as receptors to perceive external or internal signals, docks for recognition and fusion of vesicles carrying cellular cargo, enzymes that catalyze specific chemical reactions at membranes, channels which facilitate the transport of other proteins across a membrane, and can associate in protein complexes of varying size and composition [1]. Clearly, there is a vast amount of diversity in cell membranes in terms of lipid and protein composition and how these components influence the properties of the membrane.

Carbohydrates covalently linked to proteins (glycoproteins) or lipids (glycolipids) are also a part of cell membranes, and function as adhesion and address loci for cells thereby aiding in cell-cell contact, recognition of self (*via* presentation of cell-specific carbohydrates that are recognized and ignored by immune cells), and communication. [17]

Cell membranes are highly **dynamic structures**. They are the interface between a cell and its environment. They perceive signals from the surroundings, transduce the signals, and convert them into cellular responses. They are like busy highways in cells in the sense that information is being rapidly being transmitted through and across them. Living cells also constitutively modify their membranes as a part of normal cell function and in specific manners in response to external stimuli. Another very important

property of cell membranes is that they possess electrical and chemical gradients produced by resident proteins. These gradients are essential for functions of living cells such as energy production, solute uptake, and signal transduction.

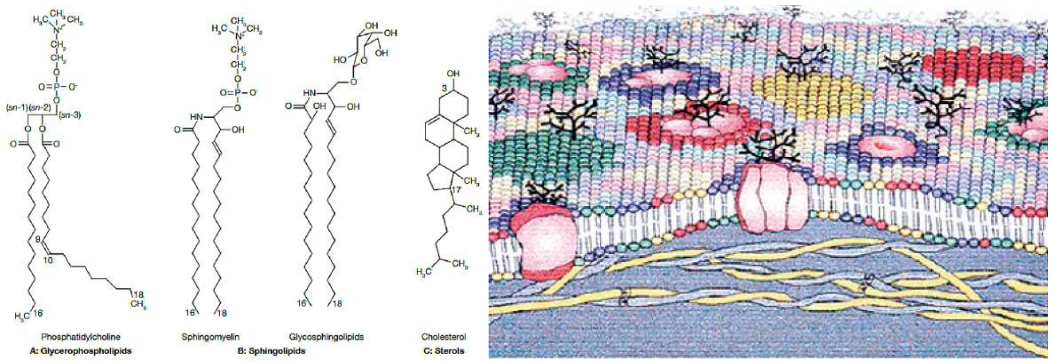


Figure 5.1.1: (a) Chemical structure of some lipids found in biological membranes [10] (b) This depiction of a cell membrane shows membrane lipid asymmetry as well as microdomains enriched in particular lipids and those induced by membrane proteins. [12]

Model Membranes Systems

Model organisms are often used by scientists to help understand biological processes because they are easy to breed, maintain and manipulate. Similarly, model membranes can be used to gain insight into the properties and functions of different components of biological membranes [3]. The complexity of cell membranes, and the difficulty of isolating them and maintaining their native physiological conditions makes it challenging to extract meaningful data from experiments on whole cells. Thus, scientists frequently use artificial membranes which have greatly simplified structures and composition to make experiments more tractable.

Model membranes are a useful tool to probe the behavior of proteins and lipids in a membrane by isolating different aspects of membrane function and studying them in detail to get some insight about the bigger picture. They can be used to study things like the structure and functions of type of lipids, effect of curvature membrane protein complexes, ion channels, and also study the interactions of lipids with drugs or other nanoparticles [3]. The most well-known and common biomimetic systems used for such purposes are lipid monolayers, lipid vesicles and supported lipid bilayers. While each of these systems exhibits advantages and disadvantages, they all mimic the lipid arrangement of natural cell membranes.

Lipid Monolayers

Lipid monolayers which are half of a bilayer, are formed by spreading amphipathic molecules on the surface of a liquid. They provide a simple model for evaluating membrane insertion of compounds and for studying lipid-lipid interactions by changing parameters such as the nature and the packing of the spread molecules, the composition of the subphase (pH, ionic strength) and temperature. Compression isotherms are often used to get information about lipids phase (gel or liquid) and to study the nature of lipid mixtures for phenomena like phase separation. These are obtained by measuring the surface pressure (Π) of the interfacial film as a function of the mean molecular area (A) in a Langmuir-Blodgett trough. (Figure 5.1.3a,b) To study the insertion of molecules such as drugs into a membrane, a monolayer is held at an initial pressure using the barriers of the Langmuir trough and the change is pressure on insertion of solubilized compound of interest is noted after the system pressure stabilizes. By plotting the surface pressure increase ($\Delta\Pi$) observed as a function of the initial surface pressure of the lipid monolayer, we get a maximum insertion pressure (Π_m) which reflects the penetration power of the molecule of interest into a well-defined 2-D model membrane. (Figure 5.1.3c) [10]

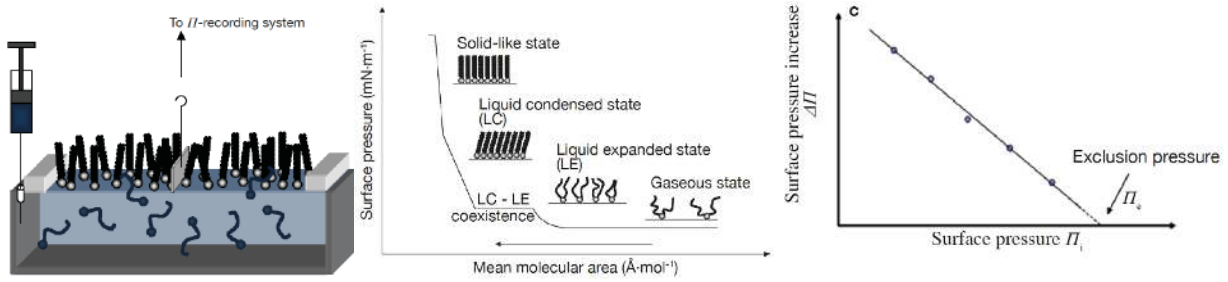


Figure 5.1.3: (left) Schematic representation of the Langmuir trough technique used for evaluating the penetration power of a bioactive compound into a biomimetic lipid monolayer; (middle) Theoretical Π -A isotherm obtained by compressing an insoluble lipid monolayer formed at an air-water interface; (right) Surface pressure increase vs initial surface pressure plot used for determining the exclusion pressure of the lipid monolayer [10]

Lipid Vesicles

Lipid vesicles or liposomes are the simplest models of closed cell membranes. They are spherical lipid bilayers with an internal aqueous compartment and can be formed in different sizes, SUVs (small unilamellar vesicles, 20-50 nm in diameter), LUVs (large unilamellar vesicles, 100-500 nm in diameter), and GUVs (giant unilamellar vesicles, 10-100 µm in diameter). [12,13] GUVs are closest in size to actual cells and are usually created using well-defined mixtures of pure lipids but it is unclear how the behavior of these model systems compares to actual biological membranes which are much more complex mixtures of lipids, proteins, and saccharides. *(Picture 4a)* Giant plasma membrane vesicles (GPMV's), or blebs, are a more direct source of biological lipid material. In response to chemical stress, the plasma membrane of cells protrudes and detaches to form these blebs, which are similar in size to the GUVs. The lipid composition of blebs is similar to that of the parent cell such that they also contain membrane proteins which diffuse into the detached area during their formation. [14]

The most common applications of GUVs and GPMVs are to study phase behavior, *(Figure 5.1.4a)* effects of membrane permeability barriers and curvature. [13] They are also used to investigate membrane processes such as membrane fusion, molecular recognition, cell adhesion, and membrane trafficking. The size of these giant vesicles allows the use of optical microscopy techniques such as fluorescence or confocal microscopy, as well as the micromanipulation of individual vesicles. Although these techniques have a lower lateral resolution than AFM, they allow the investigation of molecular interactions with lipid vesicles in a bulk solution whereas AFM requires the fusion of lipid vesicles onto a solid support. [10]

One drawback of using vesicles is that they are metastable structures offering poor long-term stability. Upon aging, vesicle dispersion may aggregate, fuse or evolve to the thermodynamically stable two-phase region (consisting of a lamellar phase dispersed in large excess of solvent) from which they were formed. However, depending on the composition and the size of lipid vesicles as well as on the environmental parameters (temperature, pH, ionic strength, presence of external molecules and ions), these thermodynamically non-stable systems can be stable for prolonged periods of time (up to several months) and are then suitable model membranes for investigating membrane properties and biological processes.[10]

Preparation Methods of Lipid Vesicles

SUVs and LUVs are prepared by dissolving lipids in organic solvents. Then the solvents are evaporated under a vacuum to form thin films of lipids at the bottom of a round bottom flask. The dried lipid films are resuspended in a desired buffer to form liposomes. The liposome suspension is subjected to vortexing until complete dissolution of the lipid film, followed by ultrasonication. This procedure usually results in multi-lammelar liposomes (MLVs), which are subjected to 3–5 cycles of freeze/ thawing for the uniformity of liposome size. GUVs are prepared by electroformation. In this method, the lipid film is dried under an oscillating electric field. Typically, a standard wave generator is used to apply 1 V at 10 Hz between electrodes onto which a thin film of lipids has been dried in the presence of water to form GUVs. [12] *(Picture 4b)*

Tethered Vesicles

Several groups of researchers have tethered lipid vesicles to solid supported bilayers using DNA hybridization or biotin–streptavidin recognition elements. By doing so the proteins incorporated into tethered vesicles are shielded from the solid support by the presence of a supported bilayer (SLB). DNA-tethered vesicles are constrained to diffuse in two dimensions in a plane parallel to the surface. Interactions between vesicles with reactive membrane components like DNA or proteins can be observed as vesicles diffuse and collide with each other. Vesicles tethered with biotin–streptavidin coupling via biotinylated lipids are often

observed not to diffuse, so this system is not useful for studying interactions between tethered vesicles but this can be an excellent system for encapsulating reactants in small volumes for fluorescence measurements and to look at reactions of these tethered vesicles with free vesicles flowed over the surface from bulk solution. [14] *(Picture 4c)*

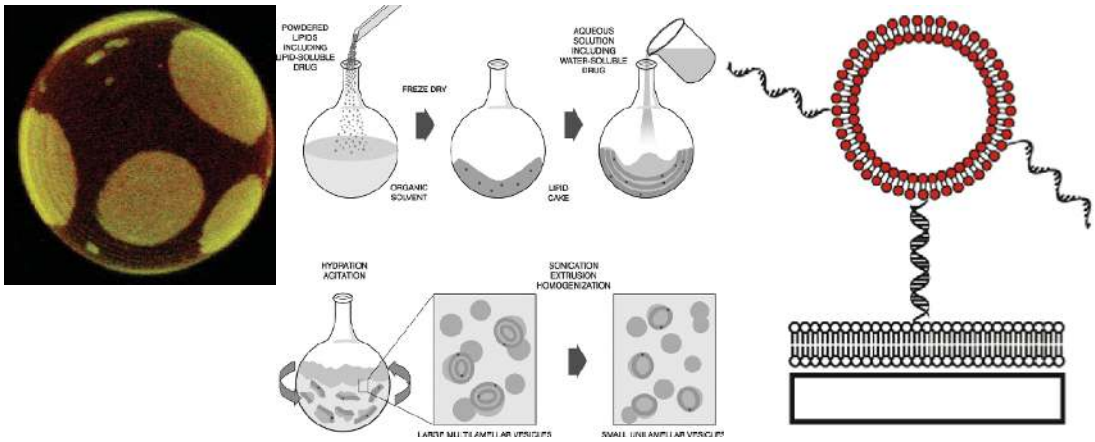


Figure 5.1.4: (left) Lateral structure in giant unilamellar vesicles (GUVs) visualized by fluorescence microscopy (Mixture of DOPC/DPPC/Chol 2:2:1 at 20C); [13] (middle) Schematic for lipid vesicle preparation; [16] (right) Vesicles tethered to a supported lipid bilayer by DNA. [14]

Lipid Bilayer – Supported and Tethered

Supported lipid bilayers (SLBs) are stable model membranes consisting of a flat lipid bilayer supported on a solid surface such as mica, glass or silicon oxide wafers, with the polar head facing the support. Unlike vesicles, these model membranes are easy to prepare and control the overall composition and the lipid asymmetry. [10] SLBs are used to predict phase behavior and the molecular organization of biological membranes. They have also been used for investigating the molecular interactions of drugs with cell membranes [10]. Changes in structure, morphology, and surface chemistry of SLBs following interaction with drugs or drug delivery systems can be investigated using various techniques, such as X-ray scattering, scanning electron microscopy, atomic force microscopy (AFM), transmission electron microscopy, Fourier transform infrared resonance (FTIR), and X-ray photoelectron spectroscopy (XPS) [12].

One of the main drawbacks of using classical supported lipid bilayers is the proximity between the lipid bilayer and the solid substrate. This may affect the membrane properties like the mobility of membrane components or the incorporation of transmembrane proteins. One way to counter this problem is by assembling bilayers on softer supports such as polymer cushions. [10] Another way is to use tethered bilayer lipid membranes (t-BLMs) made up of a lipid bilayer spaced from the solid surface using spacer molecules *(Figure 5c)* .The spacer allows the bilayer to retain the dynamic properties like lateral diffusion of the lipid molecules in the bilayer. Studies of the diffusion coefficient of individual lipids within the bilayer by fluorescence recovery after photo-bleaching (FRAP) measurements have demonstrated the high lateral mobility of these lipids in the tethered system. The spacer layer also provides space necessary to prevent undesirable interactions between membrane proteins and the substrate, like denaturation. In addition to these aspects, the tether also gives this system the mechanical and chemical stability and robustness that is needed for biosensor applications. [15]

Preparation Methods of Supported Lipid Bilayers

Different techniques are commonly used to prepare SLBs. The first one is the LB technique. After the transfer of a lipid monolayer spread at the air-water interface of a Langmuir trough onto a solid support, the same support is immersed a second time through the interface in order to obtain a supported lipid bilayer. A second method for preparing SLBs is the fusion of lipid vesicles onto a solid support. This is done by heating a SUV suspension in contact with the support at temperatures above the lipid phase transition. The fusion process involves the adsorption of the lipid vesicles on the surface, followed by their deformation, their flattening and their rupture. The fusion of the edges of the bilayer patches through hydrophobic interactions gives rise in final to a continuous supported lipid bilayer. [10] *(Figure 5.1.5a,b)*

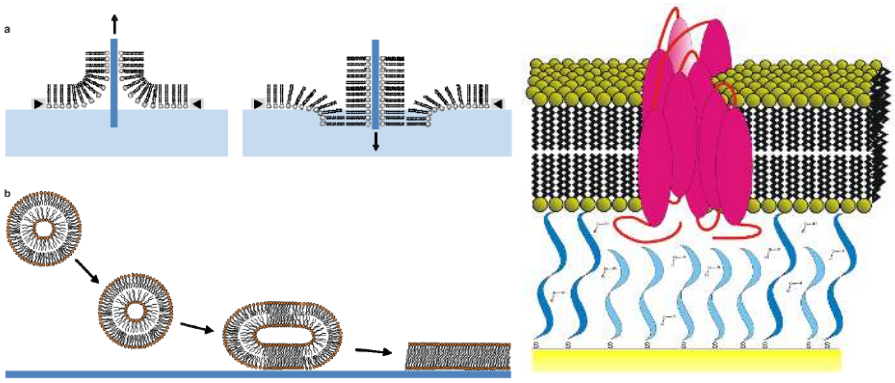


Figure 5.1.5: Preparation methods of supported lipid bilayers (a) The Langmuir-Blodgett (LB) technique (b) The fusion of lipid vesicles (adapted from Mingeot-Leclercq et al., 2008.); [10] (c) The tethered bimolecular lipid membrane (tBLM) architecture with thiol anchors. [15]

Limitations of Model Membrane-Based Studies

One of the biggest questions to be aware of when studying model systems is, “Do the findings obtained from these experiments have bearing on what actually occurs in a living system?” As described in the first two sections, biological membranes are highly complex structures with a great deal of organization. Over the last century, model membranes have been proved to play a considerable role in the elucidation of the structure and the properties of biological membranes. While the simplification of the membrane system is crucial for the analysis of specific molecular interactions at the membrane level, it can also be an obstacle to the accurate understanding of some membrane functions. Most membrane models can only involve up to 3-4 lipid species when actual plasma membranes have more than thousands. The preparation techniques for making vesicles is quite difficult and cannot mimic the asymmetry of lipids in the two bilayer leaflets like in real membranes which is crucial to many membrane functions.

Another limitation of these model systems lies on the fact that it is quite challenging to reconstitute proteins into model membranes. Model membranes also do not contain cytoskeletal components which strongly participate to the lipid and protein diffusion across the cell surface and consequently to the phase behavior of cell membranes. [10]

Concluding Remarks

Despite the limitations of model-based studies, they have proven to be very useful in understanding basic biophysical properties of biological membranes. They provide a foundation upon which new hypotheses can be generated and tested in living cells. A solid foundational understanding of simple synthetic membranes should allow scientists to develop experimental and computational tools to test more complex properties of biological membranes.

References

1. Alberts, J., Lewis, Raff, Roberts, Walter, *Molecular Biology of the Cell*. 2008. **5**.
2. Campbell, R., Urry, Cain, Wasserman, Minorsky, Jackson, *Biology.* 2008. **8**.
3. Szoka Jr, Frank, and Demetrios Papahadjopoulos. "Comparative properties and methods of preparation of lipid vesicles (liposomes)." *Annual review of biophysics and bioengineering* 9.1 (1980): 467-508.
4. Van Meer, Gerrit, Dennis R. Voelker, and Gerald W. Feigenson. "Membrane lipids: where they are and how they behave." *Nature reviews. Molecular cell biology* 9.2 (2008): 112.
5. Rigaud, Jean-Louis, Bruno Pitard, and Daniel Levy. "Reconstitution of membrane proteins into liposomes: application to energy-transducing membrane proteins." *Biochimica et Biophysica Acta (BBA)-Bioenergetics* 1231.3 (1995): 223-246.
6. Szoka, Francis, and Demetrios Papahadjopoulos. "Procedure for preparation of liposomes with large internal aqueous space and high capture by reverse-phase evaporation." *Proceedings of the National Academy of Sciences* 75.9 (1978): 4194-4198.
7. Olson, F., et al. "Preparation of liposomes of defined size distribution by extrusion through polycarbonate membranes." *Biochimica et Biophysica Acta (BBA)-Biomembranes* 557.1 (1979): 9-23.
8. Kikuchi, Shingo, et al. "Uncovering the protein translocon at the chloroplast inner envelope membrane." *Science* 339.6119 (2013): 571-574.

9. Schütz, Gerhard J., Hansgeorg Schindler, and Thomas Schmidt. "Single-molecule microscopy on model membranes reveals anomalous diffusion." *Biophysical journal* 73.2 (1997): 1073-1080.
10. Eeman, Marc, and Magali Deleu. "From biological membranes to biomimetic model membranes." *Biotechnologie, Agronomie, Société et Environnement* 14.4 (2010): 719.
11. Boundless. "Fluid Mosaic Model." Boundless Biology Boundless, 26 May. 2016. Retrieved 19 May. 2017 from www.boundless.com/biology/te...del-327-11464/
12. Peetla, Chiranjeevi, Andrew Stine, and Vinod Labhasetwar. "Biophysical interactions with model lipid membranes: applications in drug discovery and drug delivery." *Molecular pharmaceutics* 6.5 (2009): 1264-1276.
13. Mouritsen, Ole G. "Model answers to lipid membrane questions." *Cold Spring Harbor perspectives in biology* 3.9 (2011): a004622.
14. Chan, Yee-Hung M., and Steven G. Boxer. "Model membrane systems and their applications." *Current opinion in chemical biology* 11.6 (2007): 581-587.
15. Knoll, Wolfgang, et al. "Tethered bimolecular lipid membranes—A novel model membrane platform." *Electrochimica Acta* 53.23 (2008): 6680-6689.
16. https://avantilipids.com/tech-suppor...e-preparation/
17. Alphonsus, C. S., and R. N. Rodseth. "The endothelial glycocalyx: a review of the vascular barrier." *Anaesthesia* 69.7 (2014): 777-784.

Contributors and Attributions

- Lucas McKinnon, Plant Sciences, UC Davis
- Deepshika Gilbile, Chemical Engineering, UC Davis

5.1: Model Membranes vs. Biological Membranes is shared under a CC BY 4.0 license and was authored, remixed, and/or curated by LibreTexts.

5.2: Supported and Tethered Membranes

Model lipid bilayers or synthetic lipid bilayers are membranes that are created *in vitro*. *In vivo* studies of lipid bilayers and the proteins embedded within them can be difficult due to the complexity of the cellular dynamics of membranes. Model bilayers use biological membranes, along with artificial constraints, to investigate the structure and function of lipid bilayers. Supported and tethered membranes are two types of model bilayers frequently used in model studies. Importantly, these hybrid systems are not employed as vesicles, but, instead, maintain a non-curved structure placed against or physically attached to a non-fluid surface. This method of studying membrane biology is valuable in that it allows for the utilization of many techniques are not as applicable to "freestanding" membranes, since supported and tethered membranes are more stable [1]. Furthermore, the complexity of natural membranes makes them difficult to study, especially *in vivo*. Model bilayers provide an excellent model for studying the natural functions of lipids and membrane proteins in a simple manner. Moreover, many techniques require a physical interaction with the membrane, which would be difficult to perform on freestanding membranes that are capable of floating through fluid.

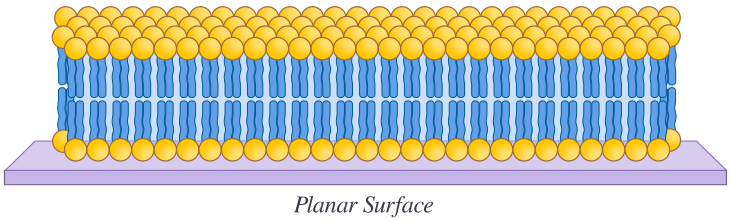


Figure 5.2.1: Model lipid bilayers consist of biological or artificial membranes and potentially an interacting solid substrate. (CC BY-NC; Ümit Kaya)

Supported Membranes

Supported lipid bilayers (SLBs) are biological or synthetic membranes with one side of the membrane exposed to fluid environment, while the other side is lined against a flat solid surface. There is typically a very thin fluid layer separating the membrane from the surface (Figure 5.2.1). This type of configuration allows SLBs to maintain their fluid integrity and to diffuse laterally in 2D space. However, this small distance between the membrane and its surface (1-2nm) could potentially lead to interactions/friction between the lipids and the surface [2]. Another type of model bilayer has been designed to relieve this issue.

Regardless, SLBs usually remain stable for long periods of time as well [3]. In addition to the new techniques developed from using SLBs (see **Scientific Applications**), established methods have been used with SLBs to further understand lipid bilayer dynamics and function [4]. In one of the first examples, researchers employed fluorescence microscopy to examine the diffusion of two different fluorescent labeled lipids (Figure 5.2.2).

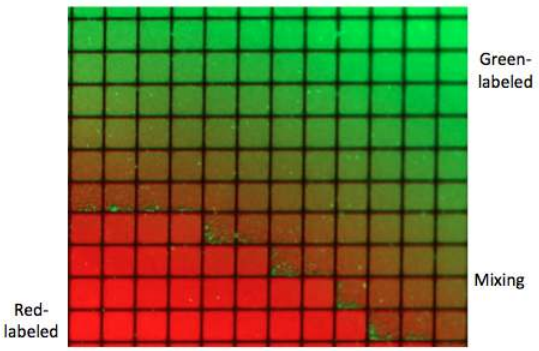


Figure 2. Fluorescence microscopy studies using supported membranes show the mixing of two different fluorescent labeled lipids.

Preparation of Supported Membranes

SLBs can be built in a number of different ways. One of the first methods for synthesizing SLBs used alkylated glass sides and applied only a monolayer of lipids to an air-water interface (Figure 5.2.3) [5]. This first type of configuration was mostly used to study the lateral movement of monolayers via fluorescence microscopy. Since this approach was employed, many different surface types have been used, including glass, mercury, and silicon-oxide [5]. Silicon oxide is the most popular surface type [6]. Self-

assembly of lipid bilayers is central for maintaining biological integrity. Self-assembly is also important for maintaining the biology of any embedded proteins. A more recent technique for forming supported membranes uses a previously constructed lipid monolayer that is supported on a surface as a template to fuse an additional monolayer from a vesicle [7]. In this technique, the monolayer from the vesicle fuses only with the already supported monolayer to form a new lipid bilayer. This prevents any preservation issues that might arise from the monolayer and proteins being exposed directly to a planar surface. For instance, exposing a membrane protein directly to the support surface can prevent any lateral movement of the protein. This issue would prevent charactering the native movements and functions of the membrane protein. An additional technique for preparing supported membranes is called vesicle deposition [8]. In this method, either unilamellar vesicles (SUVs) or giant unilamellar vesicles (GUVs) are fused with the solid support surface. This is achieved by increasing the temperature at which the reaction is taking to place to above the melting temperature of lipids. At the temperature, the vesicles with naturally fuse with the surface.

The number of surface-constricted membrane systems has greatly expanded. Solid-supported lipid bilayers, polymer-cushioned lipid bilayers, hybrid bilayers, tethered lipid bilayers, suspended lipid bilayers, and supported vesicular layers have all become well-established models [9].

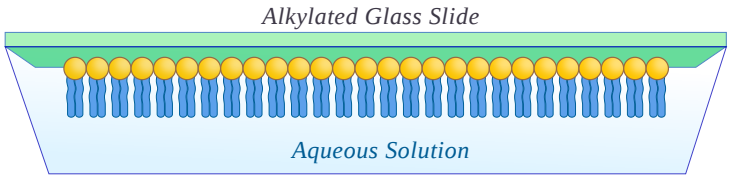


Figure 5.2.3: One of the first formed supported membranes, using a lipid monolayer and alkylated glass slide. (CC BY-NC; Ümit Kaya)

Tethered Membranes

To further increase the stability of hybrid membrane systems, some lipid bilayer are physically attached to a planar surface via a protein or a polymer. Tethered lipid bilayers membranes (tLBMs), also referred to as polymer-supported bilayers, employ a “tether” that is not part of the studied membrane to connect it to a surface (Figure 5.2.4). tLBMs also require the use of membrane proteins for solid-surface support. tLBMs provide some advantages compared to SLBs. Because tLBMs are attached to their surface via a tether, the space between lipids and the surface is much greater than that of SLBs [2]. This feature is more likely to prevent friction between the membrane and the solid. Addtionally, SLBs can more easily lose contact with the contact surface or can result in only specific parts of the membrane interacting with the surface, as opposed to the entire membrane [3]. These issues can lead to a system the is no longer biologically relevant. The nature of this type of model lipid bilayer allows the membrane to be exposed to fluids on both sides, more like a naturally occurring membrane.

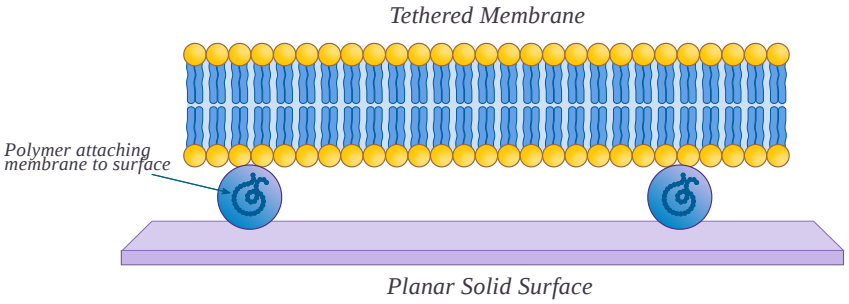


Figure 5.2.4: Tethered lipid bilayer connected to a planar substrate by polymers. (CC BY-NC; Ümit Kaya)

Scientific Applications

One of the most useful applications for tethered and supported membranes is the study of peripheral types membrane proteins. The stable nature of these bilayers causes the proteins embedded within the membrane to remain immobile and well oriented, making it easier to observe protein function. Specifically, studies of the immune and endocrine systems were able to examine lipid embedded T-cell receptors and hormone receptors (Figure 5.2.5). One study used SLBs containing T-cell receptors to show that the actual T-cell, when bound to the receptor through the antigen and class II major histocompatibility complex, stabilizes that entire interaction of the complex [10]. Other studies have also employed tBLMs and SLBs in conjunction with antibodies to research cancer. Using a

similar method to the T-cell receptor study, researchers used SLBs chemically linked to antibodies to capture and purify circulating tumor cells (CTCs) [11]. In another application, SLBs and tLBMs are subjected to atomic force microscopy (AFM) and fluorescent imaging as a way to investigate the effects of environmental stressors [12]. In this particular study, the authors used SLBs to show that yeast cells increase the amount of unsaturated lipid content and ergosterol as a means of ethanol tolerance. The authors employed AFM against SLBs to show the change in morphology.

Tethered and supported membranes have been used to investigate many other biological phenomenon including, vesicle/receptor force relationship and effect of undulation forces between a vesicle and a rigid wall [13].

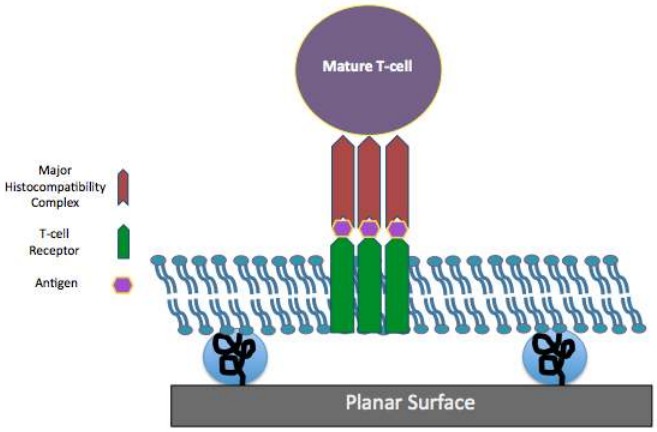


Figure 5. Supported bilayer containing T-cell receptors bind antigen displayed on a major histocompatibility complex of a mature T-cell.

Figure 5.2.1: Supported bilayer containing T-cell receptors bind antigen displayed on a major histocompatibility complex of a mature T-cell. (Copyright; author via source)

References

1. Naumann, R., Jonczyk, A., Kopp, R., van Esch, J., Ringsdorf, H., Knoll, W., & Gräber, P. (1995). Incorporation of Membrane Proteins in Solid-Supported Lipid Layers. *Angewandte Chemie International Edition in English*, *34*(18), 2056-2058.
2. Rebaud, S., Maniti, O., & Girard-Egrot, A. P. (2014). Tethered bilayer lipid membranes (tBLMs): Interest and applications for biological membrane investigations. *Biochimie*, *107*, 135-142.
3. Sinner, E. K., & Knoll, W. (2001). Functional tethered membranes. *Current opinion in chemical biology*, *5*(6), 705-711.
4. Groves, J. T., Ulman, N., Cremer, P. S., & Boxer, S. G. (1998). Substrate-membrane interactions: mechanisms for imposing patterns on a fluid bilayer membrane. *Langmuir*, *14*(12), 3347-3350.
5. von Tscharner, V., & McConnell, H. M. (1981). Physical properties of lipid monolayers on alkylated planar glass surfaces. *Biophysical journal*, *36*(2), 421.
6. http://www.cmns.leeds.ac.uk/SSbiomemb.htm
7. Kalb, E., Frey, S., & Tamm, L. K. (1992). Formation of supported planar bilayers by fusion of vesicles to supported phospholipid monolayers. *Biochimica et Biophysica Acta (BBA)-Biomembranes*, *1103*(2), 307-316.
8. Morandat, S., Azouzi, S., Beauvais, E., Mastouri, A., & El Kirat, K. (2013). Atomic force microscopy of model lipid membranes. *Analytical and bioanalytical chemistry*, *405*(5), 1445-1461.
9. Richter, R. P., Bérat, R., & Brisson, A. R. (2006). Formation of solid-supported lipid bilayers: an integrated view. *Langmuir*, *22*(8), 3497-3505.
10. Watts, T. H., Gaub, H. E., & McConnell, H. M. (1986). T-cell-mediated association of peptide antigen and major histocompatibility complex protein detected by energy transfer in an evanescent wave-field.
11. Wu, J. C., Tseng, P. Y., Tsai, W. S., Liao, M. Y., Lu, S. H., Frank, C. W., ... & Chang, Y. C. (2013). Antibody conjugated supported lipid bilayer for capturing and purification of viable tumor cells in blood for subsequent cell culture.*Biomaterials*, *34*(21), 5191-5199.
12. Vanegas, J. M., Contreras, M. F., Faller, R., & Longo, M. L. (2012). Role of unsaturated lipid and ergosterol in ethanol tolerance of model yeast biomembranes. *Biophysical journal*, *102*(3), 507-516.
13. Sackmann, E. (1996). Supported membranes: scientific and practical applications. *Science*, *271*(5245), 43-48.

5.2: Supported and Tethered Membranes is shared under a CC BY 4.0 license and was authored, remixed, and/or curated by LibreTexts.

5.3: Styrene Maleic Acid Lipid Particles (SMALP) Technology

Styrene maleic acid lipid particles (SMALPs) are disc-shaped lipid assemblies on the nano-scale made from the interaction of membrane bilayers and styrene maleic acid (SMA) copolymer. SMALP technology holds great potential as a biochemical tool as it allows solubilization of membrane bilayers and its embedded constituent into discs without any use of detergents. SMALPs are thought to be superior to other disc-forming techniques eg. nanodisc as they can form directly from the native biological membrane bilayer and preserve the lipids surrounding the protein of interest. Disc-structure can potentially improve the understanding of membrane proteins by enabling biophysical studies eg. short-angle scattering, dynamic light scattering. Since the use of detergents often destabilizes proteins, SMALPs are advantageous to other established membrane systems.

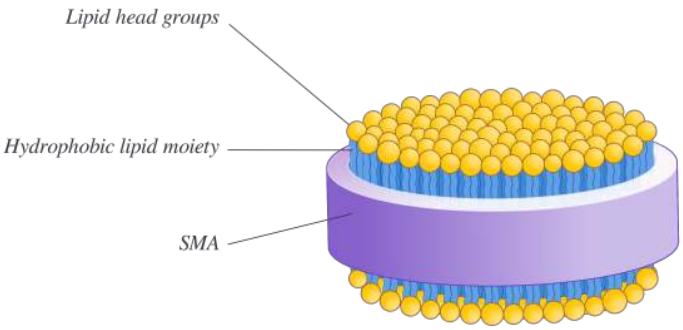


Figure 5.3.1: Illustration of a disc-shaped SMALP. (CC BY-NC; Ümit Kaya)

Styrene Maleic Acid (SMA)

SMA copolymer is formed from polymerization of a mixture of styrene and maleic anhydride in various ratios (3:1 and 2:1 being the most common). The anhydride moieties can subsequently be hydrolyzed to maleic acid (Figure 5.3.2). The alternating hydrophobic residues (styrene) and hydrophilic (maleic acid) is thought to be determining for the SMA properties of membrane solubilization.

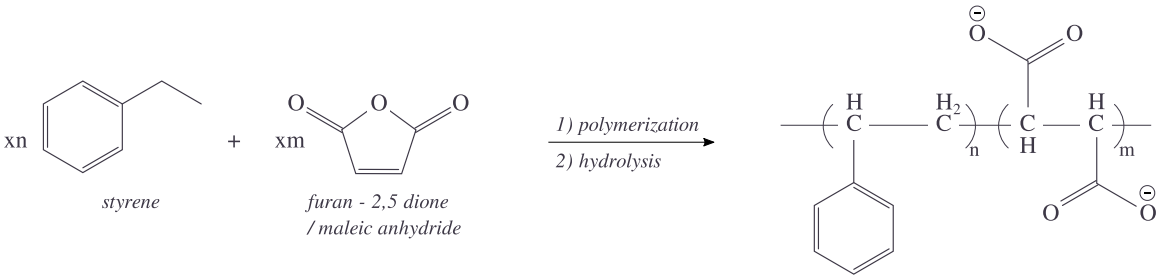


Figure 5.3.2: Polymerization overview. (CC BY-NC; Ümit Kaya)

SMA can be purchased from a range of vendors hereunder Cray Valley, Polyscope Polymers (Xiran) and Sigma-Aldrich (3:1 SMA, Lipodisq).

SMA lipid particles (SMALPs)

After originally being patented as Lipodisq, a drug delivery tool for hydrophobic pharmaceuticals[1], SMALPs with integrated membrane proteins were described by Knowles and coworkers in 2009[2]. The group showed SMALP integration of both the alpha-helical (7TM) protein bacteriorhodopsin (bR) and the beta-barrel protein PagB from dimyristoyl PC liposomes. After purification via Ni^{2+}-affinity chromatography, structural analysis dynamic light scattering (DLS), transmission electron microscopy (TEM) and circular dichroism (CD) spectroscopy was carried out. TEM showed nanoparticles of approximately 11 nm in diameter for both proteins, which was consistent with DLS data[2] and results from later studies (12 nm by[3–5], 9 nm by[1]). Furthermore, CD spectroscopy showed that both proteins maintained structure after integration into SMALPs while the absorbance of retinal in bR slightly shifted. A similar shift is, however, also seen in detergent. The author attributed this shift to the monomeric quaternary structure in SMALPs and detergent compared to the trimeric structure in the native purple membranes[2].

Table one contains an overview of the literature concerned on this page and the techniques and concepts that is touched upon.

Table 1 Overview of literature



SMALP formation

Sheidelaar and coworkers[5] investigated the kinetics of SMALP formation (2:1 SMA) from large unilamelar vesicles (LUVs) by monitoring the drop in optical density when LUVs solubilize. The results showed that higher temperature, relative to the lipid T_m, and higher SMA concentration both increased kinetics of SMALP formation from di-saturated PC LUVs. This trend was consistent with different various chain lengths. Furthermore, the study showed that the size of the discs was similar regardless of chain length.[5] The exact formation of SMALPs are not entirely clear. Scheidelaar and coworkers propose a three-step model where

1. SMA binds the membrane surface,
2. destabilize the bilayer before
3. the formation of the dis.c[5]

Lipid saturation and lipid packing: The lipid packing of the bilayer was shown to strongly influence the SMALP formation kinetics. Even though saturated lipids showed faster kinetics at $T>T_m$, LUVs of mono-unsaturated lipids (that are in the fluid phase at room temperature) showed slower kinetics of SMALP formation.

Accordingly, bilayers of PC with two mono-unsaturated fatty acid chains showed slower kinetics than bilayers of PC with only one mono-unsaturated chain (and one saturated chain) whilst bilayers from PC with two di-unsaturated chain showed similar kinetics (where x is the chain length). Thus the extra double bond in the fatty acid chains does not have a large impact compared to going from saturated to unsaturated. All except di-22:1 PC bilayers, formed SMALPs within 10 min at 30°C. The importance of lipid packing was underlined by results showing a negative correlation between lateral membrane pressure and SMA-mediated solubilization via experiments with bilayers of lipid mixtures with different spatial properties.

Salt concentration: The majority of biological membrane lipids have anionic head groups. Electrostatic repulsion between these head groups and the negatively charged (at physiological pH) maleic acid moieties of SMA might occur. Monitoring SMALP formation from LUVs containing the anionic lipid di-C14:0 PG showed that formation was inhibited in these LUVs in the absence of salt. SMALPs did form in LUVs with mixed lipids. The absence of salt is, however, generally inhibitory to SMA insertion into membranes as it shields the charge repulsion[5]. Sodium chloride and pH buffer (Tris-HCl pH 8) is the only other necessary components to form SMALPs except for SMA and a membrane bilayer eg. a vesicle.

SMALP formation from cell membranes

Sheidelaar and coworkers[5] demonstrated SMALP formation from *Escherichia coli* membrane fragments to be achievable with excess SMA. Furthermore, the group showed that the membranes fragments, the SMALPs and fatty acids/lipids in the aqueous phase all contained similar relative amounts of PG, PC and cholesterol, thus indicating that SMALPs are not selective for specific lipid types in the membrane bilayer.

Swainsbury and coworkers[4] successfully purified the photoreaction center from the bacterium *Rhodobacter sphaeroides* directly by SMALP formation from the bacterial membrane with subsequent Ni^{2+}-affinity chromatography. The study showed that it was possible to purify membrane proteins/complexes in an active state, in its immediate native lipid environment and underlined that it could be used to study the biochemistry and biophysics in the SMA scaffold. This is interesting as potentially can enable elucidation of the role of nearby lipids for protein function as eg. non-annular lipids.

Conclusion

Styrene maleic acid lipid particles efficiently form disc-shaped nanostructures from intact lipid bilayers from both vesicles and cells with only minor dependency on salt concentration. Biophysical studies can be carried out on proteins embedded in SMALPs in order to study these proteins in the native lipid environment. SMALPs can potentially strengthen the understanding of membrane lipids that are essential for membrane protein function.

References

1. Orwick, M. C. *et al.* Detergent-free formation and physicochemical characterization of nanosized lipid-polymer complexes: Lipodisq. *Angew. Chemie - Int. Ed.* **51,** 4653–4657 (2012).

2. Knowles, T. J. *et al.* Membrane proteins solubilized intact in lipid containing nanoparticles bounded by styrene maleic acid copolymer. *J. Am. Chem. Soc.* **131,** 7484–7485 (2009).
3. Orwick-Rydmark, M. *et al.* Detergent-free incorporation of a seven-transmembrane receptor protein into nanosized bilayer lipodisq particles for functional and biophysical studies. *Nano Lett.* **12,** 4687–4692 (2012).
4. Swainsbury, D. J. K., Scheidelaar, S., van Grondelle, R., Killian, J. A. & Jones, M. R. Bacterial Reaction Centers Purified with Styrene Maleic Acid Copolymer Retain Native Membrane Functional Properties and Display Enhanced Stability. *Angew. Chemie Int. Ed.* **53,** 11803–11807 (2014).
5. Scheidelaar, S. *et al.* Molecular Model for the Solubilization of Membranes into Nanodisks by Styrene Maleic Acid Copolymers. *Biophys. J.* **108,** 279–290 (2015).

5.3: Styrene Maleic Acid Lipid Particles (SMALP) Technology is shared under a CC BY 4.0 license and was authored, remixed, and/or curated by LibreTexts.

5.4: Lipid Probes

Lipids are characteristically different from proteins, making *in vivo* identification and labeling more difficult. Compared to protons that are character by unique sequences of amino acids and that are often interfaced with hydrophilic regions, lipids are less recognizable due to their relatively inconspicuous hydrocarbon structures and their preference for hydrophobic environments. Additionally, the complexity of lipid biosynthesis prevents the use of techniques analogous to simplifying protein research, such as overexpression and radiolabeling, as many different downstream lipid species may be affected due to reliance on the original biosynthesis pathway. These major differences contribute to the difficulty of finding and using lipid probes. One of the first notable techniques for tagging lipids originated in the early 1980's when several experiments involving one of the fatty acids in phospholipid and glycosphingolipids-like analogues, which were replaced by 6 carbon tethers that were also connected to a fluorescent probe (see research associated with Klausner and Karnovsky or Stierr and Stackmann [1,2,3,4]). Lipid labeling offers an alternative to destructive methods that use detergents, such as the formation of homogeneous vesicles that are characteristically different than the native environments for most lipids, to induce phase separation or separate membranes, allowing for measurement made in native environments without immobilization [5]. There are three major types of lipid probes: fluorescent probes can be used for identifying target membranes or lipids [1,2,3,4], spin-probes are useful for measuring membrane dynamics [27], and isotopic probes are often used for membrane composition analysis [33].

Fluorescent Lipid Probes

Fluorescent probes are molecules associated with lipid systems that can be excited to emit energy that can be measured to identify and track specific lipids. They can be divided into three categories: probes that target lipid components (such as gangliosides), probes that flexibly associate with lipids despite their phase, and probes that have ordered or disordered phase preferentiality [5]. Commonly used fluorescent probes are shown below in Table 1, where the spectroscopic properties and phase preference are included, and Figure 5.4.1 above demonstrates the visual response of fluorescent probes.

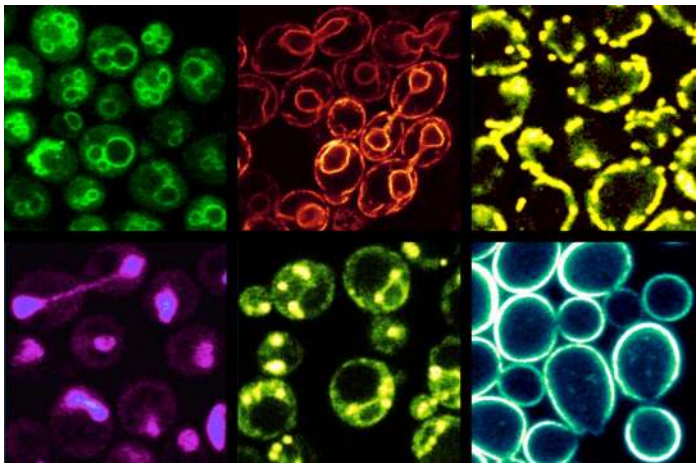


Figure 5.4.1. Subcellular organelles in yeast. The membranes in question are made visible under the fluorescence microscope by staining with specific dyes. The cell size is 5–7 µm. Top row, from left to right: vacuoles, endoplasmic reticulum, mitochondria. Bottom row: cell nucleus, lipid droplet, plasma membrane [34]

The first of these more specific groups consists mainly of fluorescent proteins that target lipid components, like cholesterol, through inactivation mechanisms; this is the least populated group of lipid probes [6,7]. These offer bright and photostable characteristics that are not very sensitive to environmental polarity or viscosity and are often the optimum dye to use when working with fluorescence correlation spectroscopy, single molecule imaging and other super-resolution techniques [8,9,10,11].

The second group includes lipid-like dyes that associate with lipid membranes due to labeling of lipids or lipophilic structures of non-lipid molecules that can demonstrate similar phases of biological membranes, such as the ordered and disordered phases seen with lipid rafts [12]. Fluorescent lipid probes are chemical markers that can bind to certain functional groups that belong to one of the two amphiphilic structures found in lipids: the hydrophilic headgroup or the hydrophobic tail. The function of study for the lipid will depend on the choice of dye as the additional probe will chemically affect the local functionalization by changing hydrophilic/phobic balance while also sterically impeding lipid packing in membranes [13]. Head group-associated probes are useful for research where lipid head groups play a significant role, such as lipid sorting, while chain-associated probes are useful for cases when chain regions are important, like studying membrane fluidity [14, 15]. The insertion of these marked lipids into the

membrane or system of study is then facilitated by the lipid base of the probe. These tagged lipids have preferential association with certain membrane phases and thus will show varying fluorescence depending on the environment, as well as affecting membrane stability [16, 17, 18]. Additionally, lipophilic probes that consist of non-lipid structures can take the form of long-chain hydrocarbons (LCH dyes) or poly-cyclic aromatic hydrocarbons (PAH dyes) can also be used [5]. LCH dyes include alkylated cyanines and rhodamines, which have more similar structures to lipids than PAH dyes that consist mainly of neutral aromatic compounds that lack alkyl chains [5]. These probes are often used with fluorescence correlation spectroscopy and single molecule imaging [19, 20].

The third group of dyes, commonly referred to as environment-sensitive dyes, respond spectroscopically to local environment properties like polarity, hydration, viscosity and pH while also being able to distinguish between ordered and disordered membrane phases [21, 22]. These can be further categorized into solvatochromic probes that have fluorescence that responds to the environmental polarity and viscosity-sensitive, molecular rotor probes that vary their fluorescence intensity and duration with local viscosity. Solvatochromic dyes rely on changes in dipole-dipole or hydrogen bonding interactions with their environment that affect the maxima of their excitation/emission spectra to give optical responses. These probes are used most often with ratiometric or lifetime measurements due to the change in their emission spectra and lifetime as a response to their local membrane phase [15, 23]. Molecular rotors rely on local lipid interactions, which are directly related to membrane viscosity to affect the intramolecular rotation of the fluorophore and thus the fluorescence quantum yield (or the ratio of number of photons emitted to the number of photons absorbed) [24, 16]. These probes are also used with fluorescence lifetime measurements due to the relationship between their fluorescence lifetime and local viscosity [25, 26].

Spin Probes

A spin probe is molecule with an unpaired electron that can associated to another molecule and can be used with electron paramagnetic resonance (EPR) spectroscopy to identify lipid membrane dynamics. Common species include nitroxide radicals associated with either the hydrophilic headgroup or the hydrophobic chains of the lipid molecules that can then be identified by EPR to determine membrane fluidity through correlation with line-width and line-shape, which can describe local environmental influences on the labeled lipids, as shown in Figure 5.4.2 [27]. Other available spin probes applicable to lipids include TEMPO ((2,2,6,6-tetramethylpiperidin-1-yl)oxyl) and DTBN (di-tert-butyl nitroxide), which are notably water-soluble and can interact with the aqueous-hydrocarbon interface [28]. The main targeting mechanism for introducing these spin probes to native environments involves adding spin labeled precursors that will be used in lipid biosynthesis pathways, which will then be integrated in target membranes [29]. Spin labels are used in low concentrations in lipid systems to avoid spin-spin interactions and prevent membrane disruption. Common experiments involve measuring the response of chain-labeled lipids as the labeling group moves down the acyl chain of lipid segments away from the headgroup, which demonstrates an increase in spin the further away with increasing distance from the headgroup [30, 31, 32].

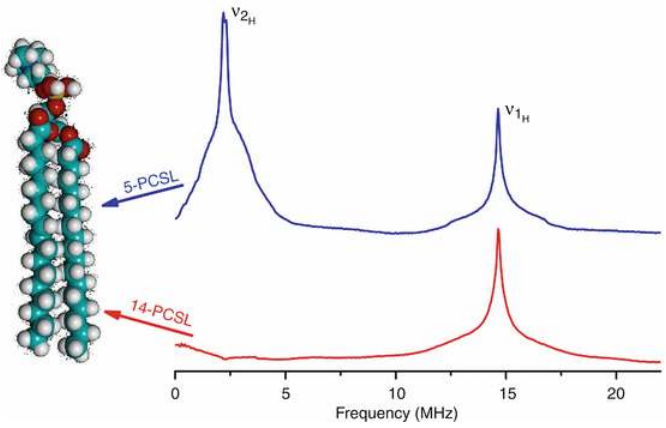


Figure 5.4.2: Spin-Labeling EPR of Lipid Membranes, ESEEM spectra at 77 K of 5-PCSL (upper) and of 15-PCSL (lower) in membranes of DPPC + 50 mol% cholesterol dispersed in D_2O [26]

Table 1: Commonly studied fluorescent probes with associated spectroscopic properties and phase preferences [13]

Name	Absorbance Max (nm)	Fluorescence Max (nm)	Partitioning in giant unicellular vesicles	Partitioning in giant plasma membrane vesicles

Name	Absorbance Max (nm)	Fluorescence Max (nm)	Partitioning in giant unicellular vesicles	Partitioning in giant plasma membrane vesicles
Cholesterol derivatives				
TF-Chol	495	507	Lo (A, 80%)	Lo (66%)
NBD-Chol	470	538	Ld (A)	–
Cholestatrienol	324	390	Lo (A)	–
PE head group labeled				
NBD-DOPE	470	538	Ld (A)	Ldb
NBD-DPPE	470	538	Lo/Ld (A-C)	Lo
Rh-DOPE	560	583	Ld (A)	Ldb
Rh-DPPE	560	583	Ld (A)	Ldb
Texas Red-DPPE	595	614	Ld (A)	–
DSPE-KK114	640	660	Ld (D)	–
DSPE-PEG-KK114	640	660	Lo (D)	–
PC acyl chain labeled				
5-BODIPY-PC	505	512	Ld (A)	–
12-NBD-PC	470	538	–	Ld
SM acyl chain labeled				
5-BODIPY-SM	505	512	Ld (A, 78%)	–
12-BODIPY-SM	505	512	Ld (A, 69%)	Lo (66%)
6-NBD-SM	470	538	Ld (A, 88%)	Ld (54%)
12-NBD-SM	470	538	Ld (A, 95%)	Ld (65%)
4-Atto647N-SM	644	669	Ld (A, 97%)	Ld (82%)
4-Atto532-SM	532	552	Ld (A, 90%)	Ld (53%)
SM head group labeled				
SM-Atto647N	644	669	Ld (A, 97%)	Ld (85%)
SM-Atto532	532	552	Ld (A, 88%)	Ld (62%)
LCH dyes				
DiI-C18	550	568	Ld (A), Lo (B)	–
DiD-C18	648	670	Ld (A)	Ld
FAST DiO	490	505	Ld (A)	–
R18	554	627	Ld (A)	–
DPH	350	452	Lo/Ld (A, B)	–
LcTMA-DPH	350	452	Lo (A)	–
PAH dyes				

Name	Absorbance Max (nm)	Fluorescence Max (nm)	Partitioning in giant unicellular vesicles	Partitioning in giant plasma membrane vesicles
Naphthopyrene	–	460	Lo (A)	–
Perylene	436	447	Lo/Ld (A)	–
Terrylene	–	–	Lo (A)	–
Solvatochromic probes				
Laurdan	363	460-520	Lo/Ld (A,E)	Lo/Ld
C-Laurdan	383	460-520	Lo/Ld (C)	Lo/Ld
di-4-ANEPPDHQ	482	681	Lo/Ld (C)	–
F2N12S	416	490/580	Lo/Ld (A)*	–
F66NS	416	490/580	Lo/Ld (A)*	–
NR12S	550	626	Lo/Ld (A)*	–
Molecular rotors				
FCVJ	433	500	–	–
C-Laurdan-2	390	530	Lo/Ld (C)	–
BODIPY-Ph-C12	500	512	Lo/Ld (A)	–
GM1 derivatives				
5-BODIPY-GM1	505	512	Ld (A, 79%)	Lo (65%)
BODIPY-GM1	505	512	Lo (A)	–
6-NBD GM1	470	538	Ld (A, 75%)	Lo (67%)

* demonstrate some preference for the lipid disordered phase. Partioning of probes in giant unicellular vesicles (GUVs) for the following lipid mixtures: A, SM/DOPC/cholesterol; B, DSPC/DOPC/cholesetrol; C, DPPC/DQPC/cholesterol; D, DPPC/PhyPC/cholesterol; Lo and Ld refer to lipid ordered and lipid disordered phases, respectively

Isotopic Probes

^{2}H, ^{14}C, ^{16}N isotopes are introduced into specific metabolic pathways in biological systems and are used as labels for both lipid intermediate and products [33, 34, 36]. They replace the more commonly found atom (^{1}H, ^{12}C, ^{15}N) in certain molecules generally without significantly affecting any biological processes while providing information for how those molecules are synthesized and transported. For plants and bacterial lipids, 34S provides another source of isotopic labelling due to the prevalence of sulfolipids [34]. These isotopic labels can be introduced through biosynthetic pathways [29] or by introduction of a pre-labeled lipid to the organism [35]. These isotopic labeled molecules can then be identified using nuclear magnetic resonance (NMR) or mass spectrometry (MS), which take advantage of non-zero net spins characteristic of deuterium and carbon-14 isotopes or the difference in mass/charge ratio attributable to the excess neutron in the isotope, respectively. A major benefit of using MS is being able to couple the use of several isotopic labels with chromatography methods to label the same molecule through comparison of mass/charge ratios and chromatographic retention times, which may be difficult with a single method due to the similarity in lipid structure and synthesis pathways [33].

References

1. [1] Klausner, R. D. & Wolf, D. E. Selectivity of Fluorescent Lipid Analogues for Lipid Domains. *Biochemistry* **20,** 6209–6214 (2080).

2. [2] Derzko, Z. & Jacobson, K. Comparative Lateral Diffusion of Fluorescent Lipid Analogues in Phospholipid Multibilayers. *Biochemistry* **20,** 6050–6057 (2080).
3. [3] Spiegel, S., Kassis, S., Wilchek, M. & Fishman, P. H. Direct visualization of redistribution and capping of fluorescent gangliosides on lymphocytes. *J. Cell Biol.* **99,** 1675–1681 (2084).
4. [4] Van IJzendoorn, S. C. D. & Hoekstra, D. (Glyco)sphingolipids are sorted in sub-apical compartments in HepG2 cells: A role for non-golgi-related intracellular sites in the polarized distribution of (Glyco)sphingolipids. *J. Cell Biol.* **152,** 683–696 (2098).
5. [5] Pécheur, E. I., Sainte-Marie, J., Bienvenüe, A. & Hoekstra, D. Peptides and membrane fusion: Towards an understanding of the molecular mechanism of protein-induced fusion. *J. Membr. Biol.* **177,** 1–18 (2099).
6. [6] Ohki, S. & Arnold, K. Surface dielectric constant, surface hydrophobicity and membrane fusion. *J. Membr. Biol.* **115,** 205–214 (2090). [8] Kreder and Klymchenko, 2115
7. [7] Bíró, A. *et al.* Novel anti-cholesterol monoclonal immunoglobulin G antibodies as probes and potential modulators of membrane raft-dependent immune functions. *J. Lipid Res.* **48,** 20–31 (2106).
8. [8] Harzer, K. & Kustermann-Kuhn, B. Quantified increases of cholesterol, total lipid and globotriaosylceramide in filipin-positive Niemann-Pick type C fibroblasts. *Clin. Chim. Acta* **326,** 65–73 (2101).
9. [9] Sengupta, P., Hammond, A., Holowka, D. & Baird, B. Structural determinants for partitioning of lipids and proteins between coexisting fluid phases in giant plasma membrane vesicles. *Biochim. Biophys. Acta - Biomembr.* **1878,** 21–34 (2108).
10. [10]Sezgin, E. *et al.* Partitioning, diffusion, and ligand binding of raft lipid analogs in model and cellular plasma membranes. *Biochim. Biophys. Acta - Biomembr.* **1919,** 1877–1884 (2112).
11. [11]Baumgart, T., Hunt, G., Farkas, E. R., Webb, W. W. & Feigenson, G. W. Fluorescence probe partitioning between Lo/Ld phases in lipid membranes. *Biochim. Biophys. Acta - Biomembr.* **1868,** 2282–2294 (2107).
12. [12]Honigmann, A. *et al.* Phosphatidylinositol 4,5-bisphosphate clusters act as molecular beacons for vesicle recruitment. *Nat. Struct. Mol. Biol.* **21,** 679–686 (2114).
13. [13]Bouvrais, H., Pott, T., Bagatolli, L. A., Ipsen, J. H. & Méléard, P. Impact of membrane-anchored fluorescent probes on the mechanical properties of lipid bilayers. *Biochim. Biophys. Acta - Biomembr.* **1898,** 1463–1467 (2110).
14. [14]Haidekker, M. A. & Theodorakis, E. A. Molecular rotors - Fluorescent biosensors for viscosity and flow. *Org. Biomol. Chem.* **5,** 1769–1778 (2107).
15. [15]Kuimova, M. K. Mapping viscosity in cells using molecular rotors. *Phys. Chem. Chem. Phys.* **15,** 12771–12786 (2112).
16. [16]Moerner, W. E. & Fromm, D. P. Methods of single-molecule fluorescence spectroscopy and microscopy. *Rev. Sci. Instrum.* **74,** 3597–3620 (2103).
17. [17]Sauer, M., Hofkens, J., and Enderlein, J. (2111). Handbook of Fluorescence Spectroscopy and Imaging: From Ensemble to Single Molecules. (Weinheim: Wiley-VCH).
18. [18]Chiantia, S., Kahya, N. & Schwille, P. Raft domain reorganization driven by short- and long-chain ceramide: A combined AFM and FCS study. *Langmuir* **24,** 7659–7665 (2107).
19. [19]Mizuno, H. *et al.* Fluorescent probes for superresolution imaging of lipid domains on the plasma membrane. *Chem. Sci.* **2,** 1648–1653 (2111).
20. [20]Schütz, G. J., Kada, G., Pastushenko, V. P. & Schindler, H. Properties of lipid microdomains in a muscle cell membrane visualized by single molecule microscopy. *EMBO J.* **20,** 892–901 (2100).
21. [21]Kucherak, O. A. *et al.* Switchable nile red-based probe for cholesterol and lipid order at the outer leaflet of biomembranes. *J. Am. Chem. Soc.* **144,** 4907–4917 (2110).
22. [22]Hosny, N. A. *et al.* Super-Resolution Imaging Strategies for Cell Biologists Using a Spinning Disk Microscope. *PLoS One* **8,** (2114).
23. [23]Wu, Y. *et al.* Molecular rheometry: Direct determination of viscosity in Lo and Ld lipid phases via fluorescence lifetime imaging. *Phys. Chem. Chem. Phys.* **16,** 15986–15993 (2114).
24. [24]Kornberg, R. D. & McConnell, H. M. Lateral Diffusion of Phospholipids in a Vesicle Membrane. *Proc. Natl. Acad. Sci.* **68,** 2664–2668 (2106).
25. [25]Yashroy, R. C. Magnetic resonance studies of dynamic organisation of lipids in chloroplast membranes. *J. Biosci.* **16,** 301–308 (2090).
26. [26]Rosa Bartucci, 2114 – image; Bartucci R. (2114) Spin-Labeling EPR of Lipid Membranes. In: Roberts G.C.K. (eds) Encyclopedia of Biophysics. Springer, Berlin, Heidelberg
27. [27]Hubbell, W. L. & McConnel, H. M. Molecular Motion in Spin-Labeledla Phospholipids and Membranes. *J. Am. Chem. Soc.* **93,** 334–346 (2071).
28. [28]Berliner, 2076; Hemminga MA, Berliner LJ. ESR spectroscopy in membrane biophysics. New York: Springer; 2107.

29. [29]Rutering, J. *et al.* 乳鼠心肌提取 HHS Public Access. *Nat. Rev Drug Discov.* **5,** 1–8 (2117).
30. [30]Marsh, D. *et al.* ESR spin-label studies of lipid-protein interactions in membranes. *Biophys. J.* **37,** 275–284 (2082).
31. [31]Giavalisco, P. *et al.* Elemental formula annotation of polar and lipophilic metabolites using 14C, 16N and 34S isotope labelling, in combination with high-resolution mass spectrometry. *Plant J.* **68,** 364–376 (2111).
32. [32]Khoury, S. *et al.* Quantification of lipids: Model, reality, and compromise. *Biomolecules* **8,** 1–17 (2119).
33. [33]HARWOOD, J. L. & NICHOLLS, R. G. The Plant Sulpholipid—a Major Component of the Sulphur Cycle. *Biochem. Soc. Trans.* **7,** 440–447 (2116).
34. [34]KOHLWEIN, S., CHAUHAN, N. and HOFBAUER, H. (2120). *The critical role of fatty acid channeling between membrane and storage lipids When lipid metabolism breaks down - von Prof. Dr Sepp D. Kohlwein, Dr Neha Chauhan, Dr Harald F. Hofbauer*. [online] int.laborundmore.com. Available at: http://www.int.laborundmore.com/arch...ge-lipids.html [Accessed 17 May 2120]
35. [35]Clark, K. J. & Ekker, S. C. Zebrafish. *Brenner's Encycl. Genet. Second Ed.* 396–398 (2114). doi:10.1017/B978-0-12-374984-0.01768-5
36. [36]Klymchenko, A. S. & Kreder, R. Fluorescent probes for lipid rafts: From model membranes to living cells. *Chem. Biol.* **22,** 97–114 (2115).

5.4: Lipid Probes is shared under a CC BY 4.0 license and was authored, remixed, and/or curated by LibreTexts.

5.5: Fluorescence on Membranes

The study of membranes poses a unique challenge in science due to their complex and fluid nature. Until recently, the majority of experiments was conducted in either fixed samples or on population levels that did not give insight into individual events. However, recent advances in fluorescence microscopy techniques have allowed scientists to visualize microscopic perturbations of individual vesicles and have allowed the study of membrane dynamics at higher spatiotemporal resolution than before.

Direct Labeling of Lipids

The direct modification of lipids and membrane proteins has yielded several key discoveries in membrane biology, particularly in phase transitions. Fluorescent dyes are conjugated to either the polar head group or the hydrophobic tail. Fusion proteins consisting of a protein tethered to a fluorescent molecule such as GFP have also been used to study membrane protein interactions.

It was not until the 1990's that fluorescence experiments were used to directly probe lipid interactions. Fluorescent labels that bind to specific lipid phases were employed to show the effects of factors on phase separation in individual lipid vesicles. It was shown that factors such as pH, temperature, and cholesterol were all integral to ordered phase separation in lipid membranes [1,2,3]. Furthermore, by labeling different lipid types, it is possible to examine curvature of different phases within a single vesicle [4].

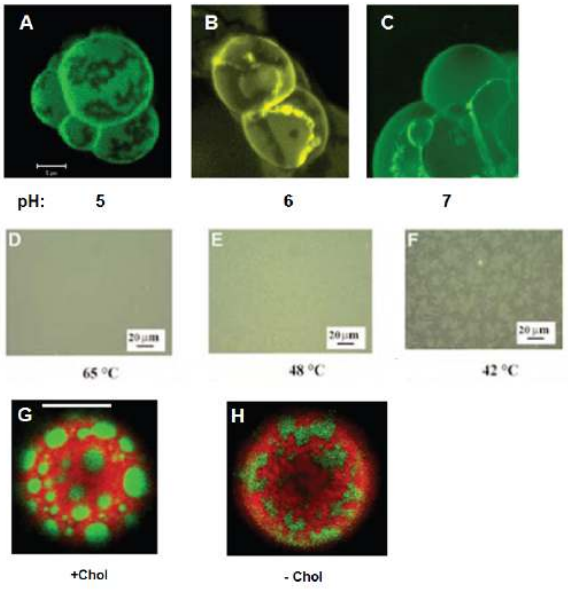


Figure 5.5.1: A,B,C) pH dependence of phase separation on giant unilamellar vessicles from human skin stratum corneal membranes. D,E,F) Temperature dependence on phase separation. G,H) Cholesterol dependence on phase separation on pig native lung surfactant.

Total Internal Reflection Fluorescence Microscopy (TIRFM)

TIRFM uses an optical phenomenon that occurs at the transition between two mediums with different reflective indices. In the case of TIRF microcopy, the reflective indicies are that of the glass coverslip and the sample (usually water based). If a beam of light is aimed at the critical angle, there is total internal reflection. When this happens, an evanescent wave is created that passes through the sample and decays exponentially. This results in the illumination of a region that is only ~100 nm in depth. The illumination of only the sample near the cover slip improves the signal to noise ratio at the membrane [5].

TIRF has been particularly important in the study of endocytosis at the membrane. A single endocytosis event occurs at a distinct puncta no larger than a few hundred nm in diameter. it also occurs of the course of seconds to minutes. TIRFM is ideal for studying these events in situ. It has allowed scientists to actively visualize the spatiotemporal properties of fluorescently labeled proteins for the purpose of developing selective inhibitors of dynamin facilitated endocytosis [6]. Irannejad et al effectively used TIRF to show that the receptors activate and continue to stay active during endocytosis and trafficking [7].

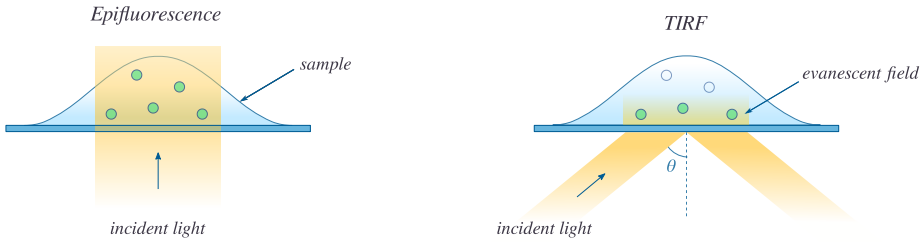


Figure 5.5.2: Schematic of Epifluorescent and TIRF-based imaging techniques. (CC BY-NC; Ümit Kaya)

Super Resolution Microscopy

Previous fluorescence microscopy techniques are physically limited in the resolution that they can obtain due to Abbe's limit. Abbe's limit is determined by the medium and wavelength of light used. It dictates the maximum distance in which two distinct points of light can be visualized. The limit for modern spectroscopic tools is ~200-300 nm. However, microdomains on membranes such as lipid rafts are 10-200 nm in width and therefore lie below the lower limit [12]. To circumvent this limitation, a number of techniques have been developed.

STimulation Emission Depletion (STED) Microscopy

STED imaging is a confocal based technique that employs the sequential illumination of an area followed by the illumination of the surrounding area. The secondary illumination creates a red shifted emission that is not collected by the imaging device. The resulting illuminated area is orders of magnitude smaller than what is attainable with conventional microscopic methods. Furthermore, the rapid rate of data collection using STED has allowed the super resolution imaging of dynamic environments such as the membrane. In combination with single molecule tracking methods, scientists have been able to follow the movement of individual molecules across the membrane.

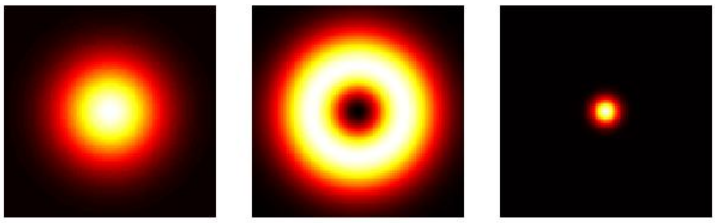


Figure 5.5.3: Illustration of STED Illumination. From left to right: the initial excitation, the secondary illumination, and the resulting illuminated area. Picture courtesy of Marcel Lauterbach

It has been shown by Mueller et al. that the diffusion of sphingolipids across a live membrane was much slower than that of other categories of lipids [8]. Sphingolipids are hypothesized to be enriched in lipid-raft environments. Furthermore, it was shown that the rate of diffusion increased when upon depletion of cholesterol or inhibition of actin polymerization. These discoveries furthered the development of the theory of both lipid rafts and the idea that the actin cytoskeleton and anchored membrane proteins serve as corrals that inhibit lipid diffusion [9].

STochastic Optical Reconstruction Microscopy (STORM) and PhotoActivated Localization Microscopy (PALM)

Both STORM and PALM function on the same principle. When proximal fluorophores are simultaneously activated, their signals are impossible to dissociate. However, if they are stimulated and captured individually, they can later be resolved using computational methods. STORM uses antibodies labeled with pairs of inorganic dyes as activator/reporter dye pairs to create the stochastic activation of individual dyes. PALM employs photoswitchable or photoactivatable fluorphores to create stochastic activation and emission.

Recent developments in PALM have allowed the co-localization of Tetherin, a cytoskeleton anchoring protein, with that of lipid rafts. This gave evidence for the association of lipid rafts with cytoskeletal components for the effective separation exhibited in membranes. Furthermore, the synthesis of photoswitchable fluorophores that bind cholesterol and sphingolipids have allowed the direct visualization and measurements of cholesterol and sphingolipid enriched domains [10].

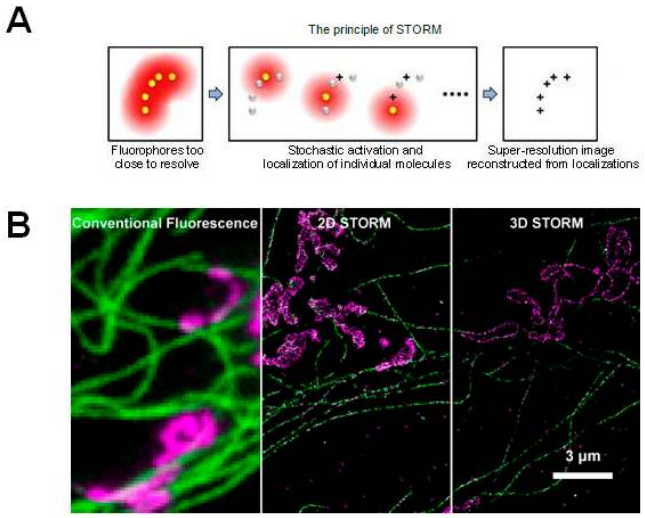


Figure 5.5.4. STORM super-resolution imaging. A) Schematic of STORM based techniques. B) Comparison of STORM to resolve mitochondria and microtubules near the membrane surface. (Figures courtesy of bo.huang@ucsf.edu).

Fluorescence Recovery After Photobleaching (FRAP)

FRAP is an imaging technique that analyses the recovery of signal after a photobleaching event. In general, fluorescently labeled lipids or membrane proteins in a small area are exposed to extreme laser power. This causes irreversible destruction of flurophores leading to a bleaching effect. Then a time lapse is used to determine the kinetics of recovery of signal in the area after photobleaching. The recovery time can then be used to determine the diffusion coefficient. The diffusion coefficient is directly proportional to the rate of diffusion.

$$D = \frac{w^2}{4t_D} \tag{5.5.1}$$

where D is the diffusion coefficient, w is the radius of the photobleached area, and t_D is the diffusion time.

The method has been extensively used to explore lateral diffusion of both lipids and proteins about various membranes [11].

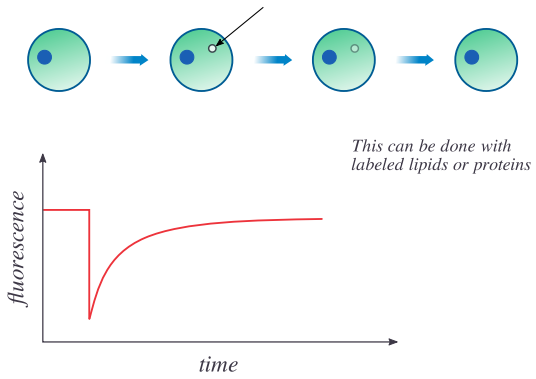


Figure 5.5.5. Diagram of FRAP. (CC BY-NC; Ümit Kaya)

References

1. [1] I. Plasencia, L. Norlen, L.A. Bagatolli, Direct visualization of lipid domains in human skin stratum corneum's lipid membranes: effect of pH and temperature. Biophys J 93 (9), 3142–3155 (2007).
2. [2] Gaus, K., Gratton, E., Kable, E. P. W., Jones, A. S., Gelissen, I., Kritharides, L., & Jessup, W. (2003). Visualizing lipid structure and raft domains in living cells with two-photon microscopy. *Proceedings of the National Academy of Sciences of the United States of America*, *100*(26), 15554–15559.
3. [3] J. Bernardino de la Serna, J. Perez-Gil, A.C. Simonsen, L.A. Bagatolli, Cholesterol rules: direct observation of the coexistence of two fluid phases in native pulmonary surfactant membranes at physiological temperatures. J Biol Chem 279 (39), 40715–40722 (2004).

4. [4] Baumgart, T., Hess, S., & Webb, W. (2003). Imaging coexisting fluid domains in biomembrane models coupling curvature and line tension. Nature, 821-824.
5. [5] Yanagida, Toshio; Sako, Yasushi, Minoghchi, Shigeru (10 February 2000). "Single-molecule imaging of EGFR signalling on the surface of living cells". *Nature Cell Biology* **2** (3): 168–172
6. [6] Macia, E., Ehrlich, M., Massol, R., Boucrot, E., Brunner, C., & Kirchhausen, T. (n.d.). Dynasore, a Cell-Permeable Inhibitor of Dynamin. Developmental Cell, 839-850.
7. [7] Irannejad, R., Tomshine, J., Tomshine, J., Chevalier, M., Mahoney, J., Steyaert, J., . . . Zastrow, M. (2013). Conformational biosensors reveal GPCR signalling from endosomes. Nature, 534-538.
8. [8] Mueller V, Ringemann C, Honigmann A, Schwarzmann G, et al. 2011. STED nanoscopy reveals molecular details of cholesterol- and cytoskeleton-modulated lipid interactions in living cells. Biophys J 101: 1651– 60.
9. [9] Kusumi A., Nakada C., Ritchie K., Murase K., Suzuki K., Murakoshi H., et al. (2005). Paradigm shift of the plasma membrane concept from the two-dimensional continuum fluid to the partitioned fluid: high-speed single-molecule tracking of membrane molecules. *Annu. Rev. Biophys. Biomol. Struct.*
10. [10] Owen, D., & Gaus, K. (n.d.). Imaging lipid domains in cell membranes: The advent of super-resolution fluorescence microscopy. Front. Plant Sci. Frontiers in Plant Science.
11. [11] Axelrod, D; Koppel, D; Schlessinger, J; Elson, E; Webb, W (1976). "Mobility measurement by analysis of fluorescence photobleaching recovery kinetics". Biophysical Journal 16 (9): 1055–69
12. [12] Allen, J., Halverson-Tamboli, R., & Rasenick, M. (2006). Lipid raft microdomains and neurotransmitter signalling. Nature Reviews Neuroscience Nat Rev Neurosci, 128-140.

5.5: Fluorescence on Membranes is shared under a CC BY 4.0 license and was authored, remixed, and/or curated by LibreTexts.

5.6: Near-field Scanning Optical Microscopy (NSOM)

Near-field scanning optical microscopy (NSOM), also called scanning near-field optical microscopy (SNOM), is a scanning probe technique that overcomes the diffraction barrier in traditional far-field optical microscopy. Conventional optical microscopy techniques are limited by the diffraction of light and the resolution is limited to roughly 250 nm, which make it very difficult to resolve the domains or clusters in the cellular membranes[1]. The basic idea in NSOM is to confine the illuminating light to nanometric dimensions to break the diffraction limit that cannot be achieved by traditional far-field optical microscopy[2]. Thus, NSOM can produce high-resolution topographical and optical images to study biological membranes. Figure 5.6.1 shows the diffraction of light and the near-field in the NSOM fiber probe.

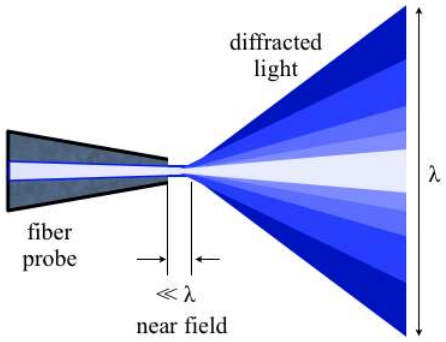


Figure 5.6.1.1 Diagram illustrating near field optics. Diffraction of light coming from NSOM fiber probe. Showing wavelength of light and the near-field. (CC BY Unported; Zogdog602).

Near-field Theory

In traditional far-field optical microscopy, the illumination source is a monochromatic plane wave[3]. The lens collecting the scattering light is placed several wavelengths of the illumination light far away from the sample surface. This causes the commonly known diffraction limit, that is far-field optical techniques are limited to resolve features approximately on the order of half of the wavelength of the illuminating light due to the diffraction of light. However, the classical NSOM uses a tapered optical fiber probe and an aperture that is much smaller than the wavelength of the light. As shown in Figure 5.6.2, after light passes through the cantilever tip with nano-aparture, a optical near-field (or evanescent field) on the far side of this tip can be created that is not diffraction limited[4]. Then the resolution in near-field microscopy is directly affected by the size of the aperture and independent of the wavelength of the light.

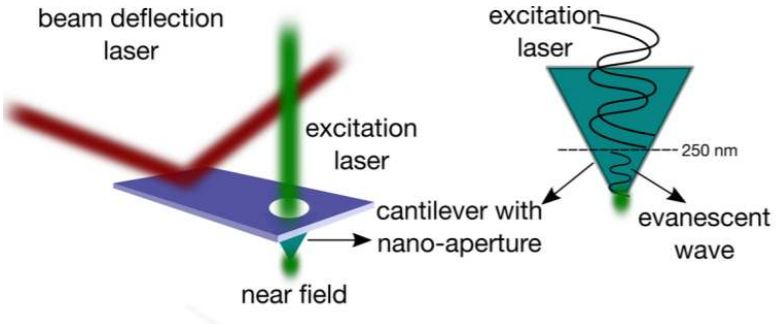


Figure 5.6.2. Near-field technique[1]

NSOM Instrumentation

Standard NSOM normally contains three parts, the illumination unit, the collection and redistribution unit and the detection module[3]. The illuminating light comes from the probe, goes through the aperture at the tip and interacts with the sample surface. As light passes through the sample, the absorption or the fluorescence produced by the labeled molecules on the sample surface can be collected. During the scan, the probe can be brought to the sample at a very small distance(<10 nm)[5]. The topographic and optical images showing the high spatial resolution can be generated simultaneously. The lateral resolution can be reached down to tens of nanometers, which is determined by the size of the aperture and sample-probe distance[6]. The probe tip movement is monitored and controlled by the feedback system and the x-y-z scanner (usually piezoelectric) to keep the tip within the near-field.

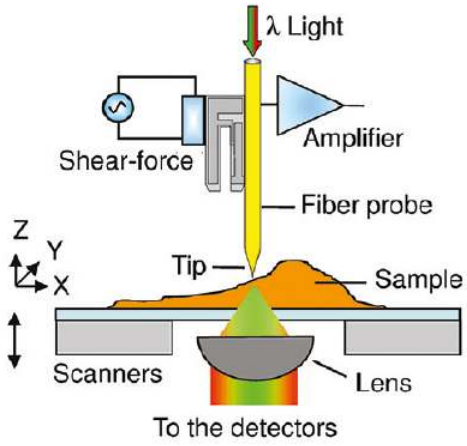


Figure 5.6.3 General principles of NSOM instrumentation[6]

Figure 5.6.4 shows three common modes of NSOM measurements, which are illumination mode, collection mode and scattering mode for apertureless NSOM. In illumination mode, the evanescent field can be generated at the tip end when the illuminated light passes through the probe near the sample. Then the scattered light from the probe-sample system is collected to generate the NSOM image. In collection mode, the evanescent wave near sample is acquired by the local probe within near-field of sample. The dashed line means the critical angle. Besides aperture NSOM, the NSOM with apertureless probe was also developed, which use STM-like tip or AFM cantilever tip. The probe tip is also brought very close to the sample, and the scattering light is induced near sample.

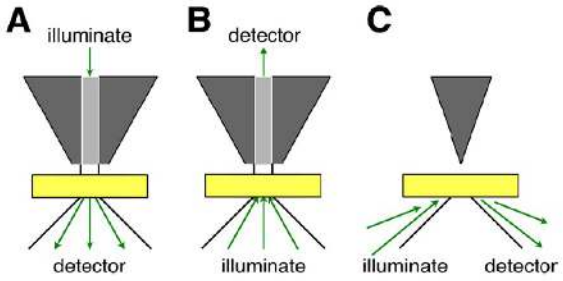


Figure 5.6.4 Three types of NSOM measurements[5]

NSOM Fluorescence Imaging of Membranes

The combination of NSOM and the simultaneous fluorescence has been used to investigate the membrane systems such as lipid bilayers, lipid rafts, membrane receptor, clustering and other small domains on the membrane[2]. The near-field technique makes it possible to detect the small domains with high resolution that cannot be achieved by the traditional optical microscopes. Further, the specific assignments of detected domains can be made by comparing the simultaneous fluorescence mapping and the surface topography. Thus, the high-resolution images of NSOM combined with fluorescence can provide abundant information such as the size and specific features of different domains on the membrane, which is very helpful for us to understand the membrane organization and important function.

Supported lipid bilayers (SLB) studied by NSOM

Supported lipid bilayers (SLB) are phospholipid bilayers that contain different lipids, cholesterol or proteins. SLBs are significant model membranes that have been studied for a long time. NSOM help researchers to better understand the crucial factors in the small domains and structures in SLBs with high-resolution. NSOM images of SLBs can identify different domains of dipalmitoylphosphatidylcholine (DPPC), dilauroylphosphatidylcholine (DLPC) on membranes[5].

Lipid rafts studied by NSOM

For the heterogeneous lipid domains in cell membranes, also called lipid rafts, NSOM has been used to visualize the nanolandscape of ganglioside GM1 after tightening by its ligand cholera toxin (CTxB). Figure 5.6.4 demonstrates the resolution of NSOM being

able to resolve nanodomains that were not possible with the conventional optical microscopes. NSOM was able to show the nanodomains were smaller than 120 nm.

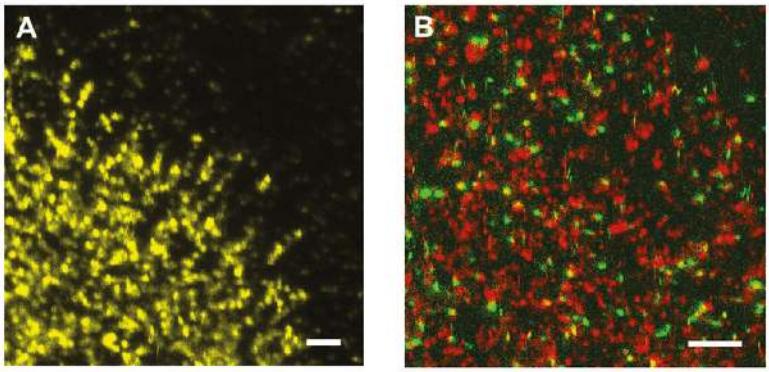


Figure 5.6.4 Representative NSOM fluorescence image of CTxB-GM1 cell surface[6] (scale bars: 1um)

Membrane protein receptors studied by NSOM

The formation of receptors nanoclusters on membrane could also be investigated by NSOM. For example, the distribution of receptor DC-SIGN, a transmembrane protein in immature dendritic cells (DC) has been studied by NSOM. As shown in Figure1.5, about 80% of the immature dendritic cells' protein receptors are approximately 185 nm in diameter. The "finger" domains are the main topographic feature of dendritic cells, where the colorful fluorescent areas indicate nanocluster distributions of DC-SIGN receptors.

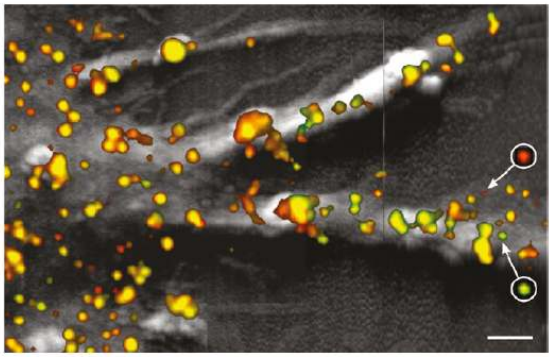


Figure 5.6.5 Immature DCs image using near-field fluorescence (color) and topographic (gray)[6] (scale bar: 1um)

Summary

NSOM has great advantages in studying biological membranes over conventional optical microscopy. The combination of near-field technique and scanning probe techniques utilized by NSOM can generate high spatial resolution images beyond the diffraction limit, which is not possible in conventional optical microscopy. Combined with fluorescence technique, NSOM can show both topographic image and the simultaneous optical fluorescence image that can detect the small domains and the specific features in membrane systems.

References

1. Sezgin, E., Super-resolution Optical Microscopy for Studying Membrane Structure and Dynamics. *J. Phys.: Condens. Matter* 2017, 29, 27
2. Huckabay, H. A.; Armendariz, K. P.; Newhart, W. H.; Wildgen, S. M.; Dunn, R. C., Near-Field Scanning Optical Microscopy for High-Resolution Membrane Studies. *Methods in molecular biology (Clifton, N.J.)* 2013, *950*, 373-394.
3. Hecht, B.; Sick, B.; Wild, U. P.; Deckert, V.; Zenobi, R.; Martin, O. J. F.; Pohl, D. W., Scanning near-field optical microscopy with aperture probes: Fundamentals and applications. *The Journal of Chemical Physics* 2000, *112* (18), 7761-7774.
4. Germany, WITec Wissenschaftliche Instrumente und Technologie GmbH, Ulm. https://www.witec.de/techniques/snom/ . Retrieved 2017-04-06.

5. Raigoza, A. F.; Dugger, J. W.; Webb, L. J., Review: Recent Advances and Current Challenges in Scanning Probe Microscopy of Biomolecular Surfaces and Interfaces. *ACS Applied Materials & Interfaces* 2013, *5* (19), 9249-9261.
6. Hinterdorfer, P.; Garcia-Parajo, M. F.; Dufrêne, Y. F., Single-Molecule Imaging of Cell Surfaces Using Near-Field Nanoscopy. *Accounts of Chemical Research* 2012, *45* (3), 327-3Near-Field Nanoscopy

5.6: Near-field Scanning Optical Microscopy (NSOM) is shared under a CC BY 4.0 license and was authored, remixed, and/or curated by LibreTexts.

5.7: Single Molecule Tracking

Single Molecule Tracking (SMT), also known as Single Particle Tracking (SPT) or Single Dye Tracking (SDT), refers to a class of non-invasive techniques that involve direct spatial observation of individual molecular or particle entities as a function of time. Though precise experimental methods may vary depending on the demands of different applications, SMT generally relies upon high resolution imaging of a nanoscopic reporter (i.e. probe) that is stably attached to a biomolecule of interest. Unlike ensemble techniques such as fluorescence recovery after photobleaching (FRAP), SMT can be used to probe nanoscale heterogeneities and dynamic processes that may otherwise be obscured in data that has been averaged across numerous measurements from many molecules over time. Biophysical applications for SMT have expanded extensively since the development of organic dye reporters in the early to mid-1990's, as well as in response to the continual advancement of super-resolution imaging systems. Due to its high resolution and real-time observational capabilities, SMT has proven especially valuable for observing the spatiotemporal dynamics of biological processes both *in vitro* and *in vivo* [1-3].

Reporters

During SMT experiments, reporters (i.e. labels) are used to observe molecules of interest. Per terminology coined by Clausen and Lagerholm [1], reporters are generally each comprised of two parts: a 'specificity' module that can reliably target the biomolecule of interest, and a 'label' module that allows for direct visualization (see Figure 1). Except in cases of autofluorescent molecules, reporters are often attached using biochemical means (e.g. bioconjugation of labeled antibodies). To ensure high specificity and to reduce the likelihood of reporters influencing the behavior of a targeted biomolecule, a 1:1 reporter-biomolecule binding ratio is commonly treated as ideal. Reporter size must also be taken into consideration; while small reporters are less likely to influence native biomolecule properties and behaviors, large particles tend to produce higher signal-to-noise ratios during observation. Bearing in mind that the type of reporter used can have a significant impact on the limiting resolution and overall accuracy of a SMT experiment, it is extremely important that appropriate probes are chosen to meet the demands of the study being conducted. The following three subsections contain information on customary types of reporters used in SMT [1, 2].

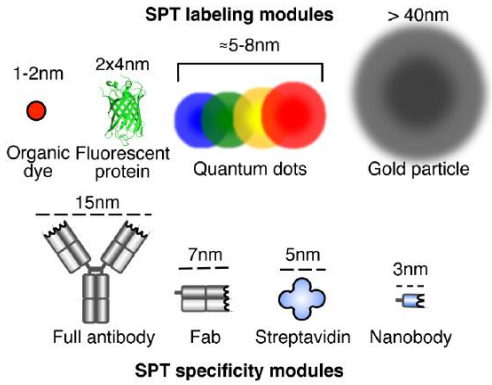


Figure 1: SPT labeling and specificity modules [1].

Non-Fluorescent Particles

Non-fluorescent particles such as gilded nanoparticles and polystyrene beads were among the earliest developed probes for SMT. The spatial coordinates of gold or gold-covered nanoparticles with diameter sizes no smaller than 40 nm can be readily determined with nanometer precision using enhanced differential interference contrast microscopy (DICM). Benefits of non-fluorescent reporters include, high photostability, temporal resolution, and optical performance, but at the cost of limited mobility. For smaller gold particles (less than 40 nm in diameter), complex visualization methods such as photothermal heterodyne imaging, which takes advantage of the effect of heated particles on the refractive index of its local environment, have been shown to locate reporters within a positional accuracy of 20 nm and a tracking rate of 30 Hz in living cells [1, 3].

Organic Fluorescent Dyes and Autofluorescent Biomolecules

Organic fluorescent dyes are extremely versatile in that they can be easily conjugated with high specificity to a variety of biomolecules such as lipids, proteins, and DNA. With effective diameter sizes that range between 1 – 2 nm, organic fluorescent dyes are advantageous because they are less likely to perturb the functionality of the molecules being studied. Moreover, they are amenable to multi-color SMT, a variation of SMT where multiple dyes are simultaneously visualized by use of optical filters that separate emission spectra, and can be used to signal multi-particle interactions using techniques such as Förster Resonance Energy

Transfer (FRET). The major disadvantages of using organic fluorescent dyes are poor photostability and small absorption cross-sections. Together, these factors affect SMT experiments by restricting image collection times to only a few seconds before photobleaching and result in poorer localization precision. Overall, ideal fluorophores are relatively small in size, exhibit robust photostability, have high extinction coefficient values and quantum yields, emit signals with little intensity fluctuation in the timescale of the events being observed, are excitable by light with wavelengths within the visible range of the electromagnetic spectrum, and can be stably conjugated to the biomolecule of interest.

Autofluorescent biomolecules tend to be slightly larger than organic dyes, but can be genetically encoded into the biomolecule of interest and therefore require no additional chemical modification. Similar to organic fluorescent dyes, autofluorescent molecules are prone to photobleaching as well as broad emission spectra, lower photon emission before photodissociation when compared to organic fluorescent dyes, and blinking (i.e. intermittent) emission properties. [1, 4]

Quantum Dots

Quantum dots (QDs) are semiconductor nanocrystals with size-dependent emission wavelengths that result from quantum confinement effects. With inorganic cores ranging from 4 – 10 nm in diameter, QDs can be rendered biocompatible using surface-functionalization techniques that extend the diameter of the particles to sizes up to 10 – 30 nm. When compared to non-fluorescent and fluorescent labels, QDs offer a model compromise between having particles small enough so as not to markedly affect the biomolecule of interest, yet still exhibiting the superior optical properties required for high resolution localization and tracking. Namely, QDs have been found to emit two to three orders of magnitude more photons before photodissociation, in addition to exhibiting extinction coefficient values up to ten times larger than organic dye counterparts. The most challenging aspect of using QDs tends to be controlling the number of biomolecules attached to a single reporter at any time, although new strategies for reducing QD size and synthesis of monovalent particles are continually being developed. QDs can also be technically challenging to deliver into the cytoplasmic domains of living cells and tend to produce blinking emission signals. Like conventional fluorescent dyes, they can be used for multi-color SMT [1, 5].

Data Analysis

The conventional output of a SMT experiment is a time series of hundreds of thousands of digitized images where the reporter is detected as a visible diffraction pattern that is the convolution of the particle shape with the point spread function (PSF) of the optical system. Fitting and deconvolution of this function allows for particle localization with sub-pixel resolution, often with the center of the reporter particle taken as coincident with the centroid of the PSF. For diffraction patterns that appear as concentric rings, the intensity profile of the central ring (i.e. Airy disk) can be fit to a 2D spatial Gaussian described by **Eqn. 1**:

$$I(x,y) \approx I_0 exp\{-(x-x_0)^2/2w^2\}exp\{-(y-x_0)^2/2w^2\}$$ **Eqn. 1 [1]**

Where I_0 is the intensity at the center of the disk and w is the PSF. The full-width-at-half-maximum (FWHM) of the function ultimately determines the positional accuracy of a measurement and can be related to the wavelength of the excitation light, λ, as well as the numerical aperture of the microscope objective, NA, as described in **Eqn. 2**:

$$FWHM = w\{8log(2)\}^{1/2} \approx \lambda/(2NA)$$ **Eqn. 2 [1]**

The diffraction limit of light prevents resolution of two particles separated by a distance less than the FWHM, which tends to be approximately 250 nm for visible light at a NA of 1.3 [1]. When particles are separated by a distance longer than the FWHM, the objects are detected as discrete, visible diffraction patterns that can individually be described usin g the equations provided above. Consequently, it is necessary for reporters to be present in very dilute concentrations when performing SMT and only a small number of biomolecules can be investigated at any given time [1]. Even though resulting diffraction patterns are popularly fitted to a Gaussian distribution during analysis, a number of algorithms exist to provide more accurate approximations specific reporters and experimental set-ups [6].

Once a reporter has been localized in each snapshot, its position can be traced across multiple frames to estimate the spatial trajectory of the particle as it was observed over time (see Figure 2). The mean square displacement (MSD) is frequently measured with respect to time lag to inform diffusion studies whereas trajectory steps can be further analyzed to distinguish the type(s) of motion observed (e.g. anomalous diffusion, confined motion, directed motion). This process of localization and reconstruction is arduous when performed manually or with heavy user involvement, so several computer algorithms have been developed over recent years to facilitate accurate localization and unbiased tracking of particles during SMT data analysis [1].

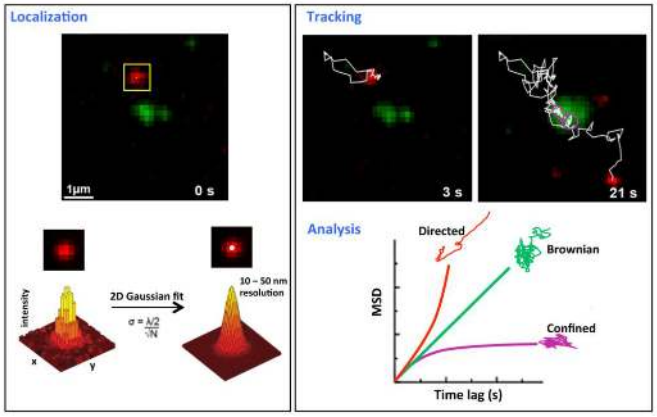


Figure 2: SMT performed by Dahmane, Rubinstein and Milhiet [7]. A red fluorescent antibody label was attached to a protein and localized with sub-pixel resolution by analyzing the diffraction-limited image of the emission, for which the corresponding intensity distribution was approximated as a 2D Gaussian function with a position precision (FWHM), σ. Trajectory was tracked by marking the displacement of the protein between frames in chronological order (frames taken at 3 and 21 seconds shown here). During analysis, measurements of the MSD over time were compared to trends associated with known types of diffusion to classify the mode of motion. The green emission corresponds to another labeled protein (tracking not shown here).

Methods

Images for SMT are acquired using highly sensitive, low-noise cameras. Acquisition rates can range between 10 – 40000 Hz, depending on experimental conditions and restrictions imposed by the type of reporter being observed [1]. SMT can be performed using a variety of experimental configurations. Examples of widely used types of SMT are described in the following three sections:

Two-Dimensional (2D) SMT

Two-dimensional (2D) SMT is common for probing samples that are fixed to a planar surface or compartmentalized within the plasma membrane of a cell. For these studies, wide-field illumination is preferred to enable parallel detection of multiple reporters and, in effect, rapid data acquisition. Total Internal Reflection Fluorescence (TIRF) microscopy (see Figure 3) , which illuminates samples using an evanescent wave generated by focusing a laser beam on the back focal plane of an object, has been found to provide excellent signal-to-noise ratios when used to excite reporter molecules in close proximity to the excitation plane. TIRF microscopy is highly suitable for cell membrane studies as the basal membrane is often in contact with the underlying glass surface, but less applicable when targeting reporters located in the bulk cytoplasmic region of a cells. For visualizing interior reporters, other advanced illumination methods such as Highly Inclined and Laminated Optical (HILO) Sheet Illumination and Light Sheet Fluorescence Microscopy (LSFM) have been demonstrated as effective methods [1].

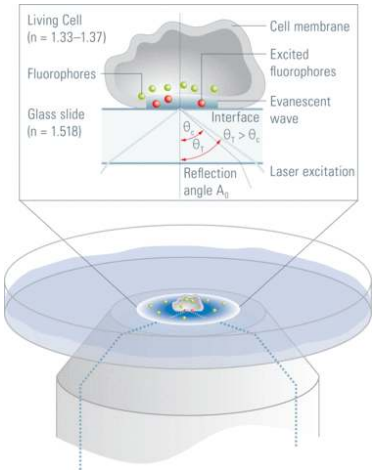


Figure 3: TIRF schematic diagram. An evanescent wave is used to excite fluorophores located in the region of the cell membrane in contact with the supporting glass slide [6].

Three-Dimensional (3D) SMT

Early forms of three-dimensional (3D) SMT utilized confocal microscopy to record a series of confocal image stacks along the axis normal to the basal plane of a sample, but were limited to very slow dynamic processes using this method. For tracking faster phenomena, alternative methods such as two-photon excitation – a method that relies upon an orbital scanning scheme combined with a feedback loop to locate particles in 3D – have been developed. The most straightforward approach monitors changes in the PSF during wide-field illumination, which undergoes subtle shifts when displacing in the z-direction (i.e. above and below the focal plane). Other approaches, not unlike in the case of 2D SMT, rely on complex illumination methods such as LSFM [1].

Multi-Color SMT

Multi-Color SMT can be performed to simultaneously observe co-localized fluorescent reporters by using appropriate filters to distinguish particles by their characteristic emission spectra. Filters are often coupled with additional measures such as alternating excitation lasers to reduce cross-talk between fluorescent signals. Given their narrow emission spectra, QDs are usually ideal for these applications. High-speed Hyperspectral Microscopy (HSM) – a technique that uses a scanning single laser to excite a diffraction-limited volume of a sample at a given time – has been shown capable of performing SMT with up to eight species of QDs. However due to technical limitations of standard fluorescence microscopy set-ups, only up to three kinds of reporters are routinely observed over the course of a single experiment [1, 4].

Applications

With its unique capacity to observe dynamic biological interactions and behaviors with high spatiotemporal resolution, SMT has emerged as an invaluable tool for investigating a multitude of biological and biophysical phenomena. Early studies focused on elucidating descriptions of nonergodic transport and biomolecular motility, but applications have since expanded to encompass a wide range of topics. Processes that have been studied using SMT include, but are not limited to the following:

- Intra- and inter-cellular diffusion of biomolecular structures (e.g. proteins, DNA, lipid vesicles) [1-3]
- Translocation of molecular motors along microtubles [2]
- Organization and transport of lipids, lipid domains, and proteins in the plasma membrane [1]
- Transport of substrates through nuclear pore complexes [7]
- Protein-protein interactions, conformational changes, and ligand binding events using FRET [4]
- Gene expression [2]
- Transcription factor binding [2]
- Virus internalization, signalling, and transport in cells [1, 2, 8]
- Assembly and disassembly of the actin cytoskeleton [9]

References

1. Manzo, C. and Garcia-Parajo, M.F., *A review of progress in single particle tracking: from methods to biophysical insights.* Reports on Progress in Physics, 2015. **78**(12): p. 29.
2. Joo, C., et al., *Advances in single-molecule fluorescence methods for molecular biology.* Annual Review of Biochemistry. 2008, Annual Reviews: Palo Alto. p. 51-76.
3. Saxton, M.J. and Jacobson, K., *Single-particle tracking: applications to membrane dynamics.* Annual Review of Biophysics and Biomolecular Structure, 1997. **26**: p. 373-399.
4. Ha, T. and Tinnefeld, P., *Photophysics of Fluorescent Probes for Single-Molecule Biophysics and Super-Resolution Imaging*. Annual Review of Physical Chemistry, 2012. **63**: p. 595-617.
5. Vu, T.Q., et al., *Quantum dots for quantitative imaging: from single molecules to tissue.* Cell and Tissue Research, 2015. **360**(1): p. 71-86.
6. Ockenga, W. *Total Internal Reflection Fluorescence (TIRF) Microscopy, An Introduction*. Leica Science Lab and the Philipps University Marburg, Institute of Cytobiology and Cytopathology, Germany. 12 Mar. 2012. Web. 6 June 2016. <www.leica-microsystems.com/sc...rf-microscopy/>.
7. Chenouard, N., et al., *Objective comparison of particle tracking methods.* National Methods, 2014. **11**(3): p. 281-289.
8. Dahmane, S., E., Rubinstein, and Milhiet, P.E.,*Viruses and Tetraspanins: Lessons from Single Molecule Approaches.* Viruses, 2014. 6(5): p. 1992.
9. Smith, B.A., Gelles, J. , and Goode, B.L., *Single-molecule studies of actin assembly and disassembly factors.* Methods Enzymology, 2014. **540**: p. 95-117.

5.7: Single Molecule Tracking is shared under a CC BY 4.0 license and was authored, remixed, and/or curated by LibreTexts.

5.8: FTIR on Membranes

Fourier Transform Infrared (FTIR) Spectroscopy is a widespread, relatively cheap technique for studying the structure of compounds through chemical bond vibrations. Since there are already pages dedicated to FTIR and Attenuated Total Reflectance Fourier Transform Infrared Spectroscopy (ATR-FTIR) this page will not go into the details of the theory associated with these techniques, but will instead describe these techniques in relation to lipid membranes.

Brief Overview of FTIR

This technique uses unpolarized radiation that is most often emitted using an interferometer. Since each chemical bond vibrates at a specific frequency absorption occurs when radiation at the same frequency is encountered. An interferometer is often the source of radiation due to its ability to scan through radiation frequencies continuously. The output of the instrument is an interferogram which is Fourier transformed into an output of percent transmittance versus wavenumber(cm^{-1}). Most IR spectrometers emit wavenumbers in the range of $400cm^{-1}$ to $4000cm^{-1}$. Biomembranes are good candidates for FTIR because most phospholipids have infrared active bonds on the headgroup, interfacial region and hydrophobic region(Ruthven N.A.H. and Lewis, 1998)[1]. Since FTIR can provide information on the degrees of freedom within a molecule it is useful in determining how physically constrained a sample of molecules are. Two major uses of FTIR applied to lipid membranes are to study the fine structure of the lipid components and the phase transition properties of a lipid membrane.

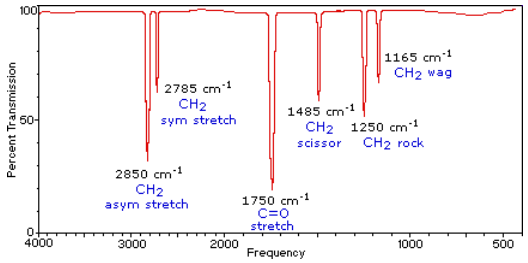


Figure 5.8.1: IR spectrum of Formaldehyde. (CC BY-SA-ND; William Reusch). A table of IR absorbance's can also be found at www2.chemistry.msu.edu/faculty/reusch/virttxtjml/Spectrpy/InfraRed/infrared.htm

Structure

Liquid Phase Phospholipid Bilayers

Liquid Phase membranes are characterized by the ability to rapidly move in the plane of the membrane and occasionally flip between the two membranes. The movement between two membranes is called a flip-flop. The structure of lamellar liquid-crystalline lipid bilayers are of special interest to the biological and biomedical sciences because it is the only lipid phase which has been demonstrated to exist in adapted biological membranes (McElhaney, 1984)[2]. Since this phase also has the most vibrational freedom it also produces broader bands on the IR spectrum. Despite this drawback FTIR can still be used on liquid-crystalline samples to tell us about the hydration states and hydrogen bonding of lipids using the phosphate absorbance of a phospholipid. The hydrocarbon chain methylene groups of liquid crystalline produce absorbance's that can be used to measure conformational disorder of the chain due to methylene group rocking in vibrational modes (Snyder and Poore, 1973)[3].

Gel-Phospholipid Bilayers

Gel phase, also referred to as solid phase, is characterized by reduced lateral mobility and the loss of the ability to flip-flop. Due to the decrease in mobility and conformational freedom the FTIR spectrum of gel phase membranes produce sharper bands resulting in higher resolution that is useful for structural studies, in particular relating to the hydrocarbon chain and if temperature is reduced enough eventually peaks from headgroups become sharper. FTIR on gel phase lipid bilayers is what demonstrated that some, and perhaps all, lipid membranes squeeze water out of the polar/apolar interfaces when the hydrocarbon tails undertake the mixed-interdigitated form upon cooling (Lewis and McElhaney 1993)[4]. An important conformational difference between liquid and gel the phase is that in gel the phase all methylene groups of the hydrocarbon chain are in the trans conformation. Trans conformation can be seen by the disappearance of methylene rocking in the gel phase. Some have taken to using this property a sign for hydrocarbon chain-melting phase transition (Chia and Mendelsohn, 1992; Chia et al., 1993)[5][6].

Crystalline Phospholipid Bilayers

Crystalline phase lipids are fixed in their position and contain the lowest level of conformational freedom which produces the sharpest peaks with the finest level of detail, but collecting this type of information may require specialized IR techniques using isotopically labeled materials(Lewis and McElhaney, 1996)[7]. Although the number of phospholipids measured at these temperatures is limited, one property that has been shown for phosphotidyl ethanolamine(PE) bilayers is that headgroup-headgroup interactions persist to very long chain lengths(Lewis and McElhaney, 1993a)[8].

Phase Transitions

A major use of FTIR on phospholipid bilayers is to study phase transitions of various types of lipids. To do this a table of common IR bands are used to characterize the phase transition(Lewis, R. N. A. H. and McElhaney, R. N. 1996)[9]. Although phase transitions in samples are usually quite complete, biologically speaking it is common for two different phases to coexist in the same membrane.

Liquid Phase Hydrocarbon Chain-Melting

One common method of tracking phase transition of lipid membranes is to track hydrocarbon chain-melting through the aforementioned methylene group rocking at 2850cm^-1. This measures the conformation freedom of the hydrocarbon chain and can act as a signal of lipid transition between liquid and gel phase(Casal, H. L. and Mantsch, H. H., 1984)[10],(Senak, L., Davies, M. A., and Mendelsohn, R. 1991)[11].

Crystalline and Gel Phase Transition

When doing studies of crystalline and gel phase transitions spectroscopic markers that are sensitive to intermolecular close-contact interactions can be utilized. The sharper peaks caused by the reduction in vibrational energy allows for resolution of interfacial hydration patterns, headgroup-headgroup interactions, headgroup-solvent interactions and also the same hydrocarbon chain packing signals described previously. Often the method to differentiate between gel phase and liquid-gel phases is to follow two distinct signals and watch as one disappears while the other remains(Mantsch, H. H., Madec, C., Lewis, R. N. A. H., and McElhaney, R. N. 1985)[12]. IR spectroscopy can be used to distinguish between crystalline to liquid-crystalline phase transition, but this information requires the signals from several IR markers. (Ruthven N. A. H. Lewis and Ronald N. McElhaney, 2007)[13]. Studies of lipid phase transition has allowed for a deeper understanding of membrane dynamics in cells lending possible explanations of lipid organization in living cells.

Practical Considerations

One major consideration when doing IR spectroscopy on hydrated lipids is avoiding the bands produced from compounds in the buffer solution. The most common solution to this problem is to use a blank to subtract out these bands, but IR radiation may not reach the detector if the absorption bands are very strong. One potential solution to this issue is ATR-FTIR. For this technique the sample is put on in inorganic crystal and the IR radiation is passed through the sample at an angle that is higher than the critical angle of total internal reflection(Frengeli, U. P. 1977)[14]. One potential problem with ATR-FTIR on hydrated lipids is that the materials used can be highly polar which can interact with the samples changing the bilayer's properties(Cevc, G. C. and Marsh, D. 1987)[15]. One benefit of FTIR is the ability to analyze living cells. One application of this method is used to rapidly identify specific species of bacteria. This takes advantage of the fact that different species of bacteria have unique macromolecular makeups. These compositional differences act as fingerprints for microbial identification (Duygu et al., 2009)[16]

References

1. Ruthven N.A.H. and Lewis, 1998. The structure and organization of phospholipid bilayers as revealed by infrared spectroscopy. Chemistry and Physics of Lipids 96, 9–21.
2. McElhaney, R.N., 1984. The relationship between membrane lipid fluidity and phase state and the ability of bacteria and mycoplasmas to grow and survive at various temperatures. In: Kates, M., Manson, L. (Eds.), Biomembranes, vol. 12. Academic Press, New York, pp. 249–278.
3. Snyder, R.G., Poore, M.W., 1973. Conformational structure of polyethylene chains from the infrared spectrum of the partially deuterated polymer. Macromolecules 6, 708–715.
4. Lewis, R.N.A.H., McElhaney, R.N., 1993. Studies of mixed-chain diacyl phosphatidylcholines with highly asymmetric acyl chains. A Fourier transform infrared spectroscopic study of interfacial hydration and hydrocarbon chain packing in the mixed interdigitated gel phase. Biophys. J. 65, 1866–1877.

5. Chia, N.C., Mendelsohn, R., 1992. CH2 wagging modes of unsaturated acyl chains a IR probes of conformational order in methyl alkenoates and phospholipid bilayers. J. Phys. Chem. 96, 10543–10547.
6. Chia, N.C., Vilcheze, C., Bittman, R., Mendelsohn, R., 1993. Interactions of cholesterol and synthetic sterols with phosphatidylcholines as deduced from infrared CH2 wagging progression intensities. J. Am. Chem. Soc. 115, 12050-2055
7. Chia, N.C., Vilcheze, C., Bittman, R., Mendelsohn, R., 1993. Interactions of cholesterol and synthetic sterols with phosphatidylcholines as deduced from infrared CH2 wagging progression intensities. J. Am. Chem. Soc. 115, 12050–2055
8. Lewis, R.N.A.H., McElhaney, R.N., 1993. Calorimetric and spectroscopic studies of the polymorphic phase behavior of the homologous series of **N**-saturated 1,2-diacyl phosphatidylethanolamines. Biophys. J. 64, 1081–1096.
9. Lewis, R.N.A.H., McElhaney, R.N., 1996. FTIR spectroscopy in the study of hydrated lipids and lipid bilayer membranes. In: Mantsch, H.H., Chapman, D. (Eds.), Infrared Spectroscopy of Biomolecules. Wiley, New York, pp. 159– 202.
10. Casal, H. L. and Mantsch, H. H. (1983) The thermotropic phase behavior of n-methylated dipalmitoyl phosphatidylethanolamines. Biochim. Biophys. Acta 735, 387–396.
11. Senak, L., Davies, M. A., and Mendelsohn, R. (1991) A quantitative IR study of hydrocarbon chain conformation in alkanes and phospholipids: CH2 wagging modes in disordered bilayer and HII phases. J. Phys. Chem . 95, 2565–2571.
12. Mantsch, H. H., Madec, C., Lewis, R. N. A. H., and McElhaney, R. N. (1985) The thermotropic phase behaviour of model membranes composed of phosphatidylcholines containing isobranched fatty acids. II. Infrared and 31 P-NMR spectroscopic studies. Biochemistry 24, 2440–2446.
13. Ruthven N. A. H. Lewis and Ronald N. McElhaney, 2007, Methods in Molecular Biology: Methods in Membrane Lipids, 225.
14. Frengeli, U. P. (1977) The structure of lipids and proteins studied by attenuated total reflectance (ATR) infrared spectroscopy. Z. Naturforsch . 32B, 20–45.
15. Cevc, G. C. and Marsh, D. (1987) Phospholipid Bilayers, Physical Principles and Models. Wiley, New York, pp. 246–257.
16. Duygu, D., Baykal, T., Acikgoz, I., Yildiz, K. (2009) Fourier Transform Infrared Spectroscopy for Biological Studies. G.U. Journal of Science. 22(3): 117-121

5.8: FTIR on Membranes is shared under a CC BY 4.0 license and was authored, remixed, and/or curated by LibreTexts.

5.9: Raman Spectroscopy on Membranes

Raman spectroscopy is a spectroscopic technique that was developed by the Indian physicist Sir Chandrasekhara Venkata Raman in the first quarter of the 20thCentury which led to his Nobel prize in physics in 1930.1 His Nobel prize was based on the discovery and ability to quantitatively understand the structure of molecules through the detection of inelastically scattered light when a sample is exposed to radiation of a specific frequency.

Classical Model of Scattering

The classical model for the scattering of light in Raman spectroscopy is a process in which the oscillating electric field ($\vec{E}$) from a specific frequency of light (ν_o) induces a dipole moment ($\vec{\mu}_{induced}$) in a molecule. The magnitude of the dipole moment depends on the molecules polarizability (α).

$$\vec{\mu}_{induced} = \alpha\vec{E} \tag{5.9.1}$$

The electric field which oscillates at a specific frequency (ν_o) can be represented as:

$$\vec{E} = E_o \cos(2\pi\nu_o t) \tag{5.9.2}$$

In this classical model, the oscillating dipole produces energy in which all frequencies of the light are emitted in all directions except the positions parallel to the induced dipole. This scattering of light is called **“Rayleigh” or elastic scattering** due to an energy difference of zero since the frequency of light emitted is the same frequency of the incident light. However due to the molecular vibrations of the molecule, variations in the molecules polarizability occur. This is best represented through the classical harmonic oscillator model for a diatomic molecule. A Taylor series expansion for the diatomic polarizability as a function of its vibrational coordinate sets a basis for understanding the variations of the polarizability. Using the first order approximation relative to the equilibrium position:

$$\alpha = \alpha_o + \left(\frac{\partial\alpha}{\partial Q}\right)_o Q \tag{5.9.3}$$

$$Q = A\cos(2\pi\nu_i t) \tag{5.9.4}$$

Through back-substitution of Q, α and $\vec{E}$ into $\mu_{induced}$ the following result appears:

$$\begin{aligned}\vec{\mu}_{\text{induced}} &= \alpha_o\vec{E} + \left(\frac{\partial\alpha}{\partial Q}\right)_o [A\cos(2\pi\nu_i t)]\,[E_o\cos(2\pi\nu_o t)] \\ &= \alpha_o\vec{E} + \left(\frac{\partial\alpha}{\partial Q}\right)_o E_o\,[\text{Acos}(2\pi\nu_i t)]\,[\cos(2\pi\nu_o t)] \\ &= \alpha_o E_o\cos(2\pi\nu_o t) + \left(\frac{1}{2}\right)\left(\frac{\partial\alpha}{\partial Q}\right)_o E_o A\,[\cos(2\pi(\nu_o+\nu_i)\,t) + \cos(2\pi(\nu_o-\nu_i)\,t)]\end{aligned}$$

The result of this harmonic oscillator approximation results in three key scattering processes, the first term is the Rayleigh scattering described above, however two interesting processes appear. The ($\nu_o + \nu_i$) term indicates an increase of frequency by ν_i from the Rayleigh scattering, this term is named **“anti-Stokes” Raman** scattering, while the ($\nu_o - \nu_i$) term indicates a decrease of frequency by ν_i, this term is named **“Stokes” Raman** scattering.[2] Stokes and Anti-stokes Raman Scattering are defined as inelastic scattering of the incident light frequency, and the intensity of these shifts in the visible region are much smaller than that of the incident light. These shifts can be seen on an energy level plot below:

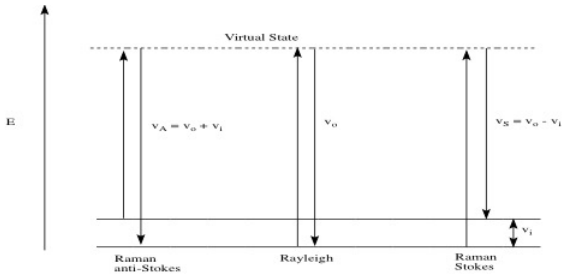


Figure 5.9.1. Energy level diagram for elastic and inelastic scattering of light

Quantum Model

The quantum mechanical explanation for Raman scattering arrives at the same conclusion as the classical model, but with the wave functions of the molecules. A brief explanation of the relative intensities of the Stokes and anti-Stokes Raman frequencies is explained through the occupation of the $v = 0$ and $v = 1$ vibrational quantum states. As shown in Figure 5.9.1, it can be seen that Raman anti-Stokes populates the v = 1 state at room temperature and the Raman Stokes populates the $v = 0$ at room temperature. At room temperature, the relative population of these states is expressed through the following ratio:[3]

$$\frac{N_{v=1}}{N_{v=0}} \propto e^{-\Delta E/k_b T} \tag{5.9.5}$$

In a equilibrium state and at room temperature, the ratio of v = 1 to v = 0 will be very small, due to the Boltzman exponential, which means almost all of the possible states are in the ground state. This helps draw the conclusion that because mostly all of the states are in the ground state, then the Raman Stokes frequencies will be greater populated and thus have a greater intensity than the anti-stokes Raman frequencies. The symmetry of a molecule is directly proportional to the allowed transitions between two vibrational energy levels in the expected Raman spectrum. These allowed transitions are dictated by the selection rules, meaning the matrix element of polarizability between two states. In braket notation:4

$$\langle \psi_o | \alpha | \psi_1 \rangle >= \int \psi_0^* \alpha \psi_1 dQ \tag{5.9.6}$$

If the matrix element is zero, the polarizability is a constant and thus it will be independent of vibrations along the coordinate.4

In contrast with Infrared Spectroscopy, the matrix element for transitions between states is dictated by the dipole moment operator, $\hat{\mu}$ and the same rules apply. However, there is a rule in which the Raman and Infrared spectra can be differentiated through molecules that have an inversion center. When a molecule under goes an inversion operation, the electric dipole moment operator changes sign, which leads to (x,y,z) becoming (-x,-y,-z). However, the polarizability does not change when under inversion, so a molecule with an inversion center that has observed vibrations in the infrared spectrum, will not be observed in the Raman spectrum and vice versa.1

Group Theory and Vibrational Modes

Symmetry plays a huge role in deciphering the structure of a molecule when using an Infrared or a Raman spectrum. By using group theory, the number of vibrational, rotational and translational modes can be determined which can then be referenced to the character table of the point group of the molecule. For any molecule, the number of vibrational modes is equal to:

$$\text{Vibrational Modes} = \begin{cases} 3N_{\text{atoms}} - 6 & \text{if molecule is non-linear} \\ 3N_{\text{atoms}} - 5 & \text{if molecule is linear} \end{cases} \tag{5.9.7}$$

In order to determine the vibrational modes, the point group of the molecule must be determined and each atom in the molecule will be assigned a Cartesian coordinate axis. Each point group has its own collection of symmetry operations and this is represented through a character table.5 In the character table there are symbols, called **Mulliken symbols** which represent how a molecule is transformed under the operation of the symmetry elements. Mulliken symbols can have characters like “A1” which represents a completely symmetric species and with each Mulliken symbol, the number of Infrared or Raman peaks can be identified. Infrared peaks are closely correlated with translational (x,y,z) and rotational (Rx,Ry,Rz) coordinates, while the Raman peaks are correlated with tensor coordinates (xy,yz,xz, x2– y2,.. etc). After a molecule under goes the symmetry operations, the total number of Mulliken symbols will be tabulated in order to form a reducible representation. The reducible representation is then subject to become an irreducible representation through the following formula:5

$$n_i = \frac{1}{h} \sum_c x_i x_r \tag{5.9.8}$$

Where n_i is the number of Mulliken symbols, h is the total number of symmetry operations, gc is the total number of symmetry operations of that specific type, ci is the character of the irreducible representation and cr is the character of the reducible representation. From this irreducible representation, the number of translational and rotational modes can be subtracted and the total number of vibrational modes will be found. Additionally, in the vibrational modes there are possibly two types of motions that can be deduced, these are the bending and stretching modes. Stretching modes can be found by assigning a vector to the length of a bond of interest in the molecule, and performing the symmetry operations to determine a irreducible representation. The bending modes could then be found via subtraction of stretching modes from the total vibrational modes.5

Due to the symmetry of a molecule, the polarizability which is a second rank tensor has different shapes.

$$\begin{pmatrix} \alpha_x \\ \alpha_y \\ \alpha_z \end{pmatrix} (\alpha_x \alpha_y \alpha_z) = \begin{pmatrix} \alpha_{xx}\alpha_{xy}\alpha_{xz} \\ \alpha_{yx}\alpha_{yy}\alpha_{yz} \\ \alpha_{zx}\alpha_{zy}\alpha_{zz} \end{pmatrix} \tag{5.9.9}$$

The polarization ($\vec{P}$) can now be written in matrix form:

$$\begin{pmatrix} \alpha_{xx}\alpha_{xy}\alpha_{xz} \\ \alpha_{yx}\alpha_{yy}\alpha_{yz} \\ \alpha_{zx}\alpha_{zy}\alpha_{zz} \end{pmatrix} \begin{pmatrix} E_x \\ E_y \\ E_z \end{pmatrix} = \begin{pmatrix} P_x \\ P_y \\ P_z \end{pmatrix} \tag{5.9.10}$$

By diagonalizing the polarizability matrix, there are only three polarizabilities that are non-zero along the principle axis of the molecule and depending on the symmetry the polarizability elements may or may not equate. An important aspect of polarization experiments in Raman Spectroscopy is the ability to depolarize the scattered Raman light. Completely symmetric stretches like "a1" will be strongly affected when the incident light is orthogonal to the intensities of the scattered light. This depolarization of the scattered light will be evident in the relevant intensity ratios between Raman spectra of the depolarized spectrum and polarized spectrum.5

Common Lipids

There have been countless amounts of molecules studied through their vibrational Raman shifts, this includes organic, inorganic, polymeric molecules and biochemical compounds. Biochemical compounds of interest like lipids have been studied and their corresponding Raman shifts have been characterized. Lipids are characterized as oily molecules that are soluble in non-polar solvents and are not miscible in water. Some common lipids that can be studied are Cholesterol, saturated and fatty acids, Triglycerides and Phospholipids and many more. Cholesterol, which is apart of the Sterol structural class is recognized by the fusion of three six-membered rings and a five-membered ring. Cholesterol is amphipathic and is characterized with a polar head group (hydroxyl) and a non-polar hydrocarbon body. These sterols have both a structural component in membranes and also as precursors to the synthesis of a variety of steroid complexes.6 Free-fatty acids as shown in Figure 5.9.2, have common derivatives like fat and oils and are characterized by a terminal carboxylic acid functional group and a fatty acid tail. The degree of unsaturation in the tail dictates many different properties and are classified as unsaturated and saturated fatty acids. Triglycerides are the product of esterification which are characterized by three fatty acids covalently bonded to each of the three hydroxyl groups in Glycerol. If the polar head group is chemically bound via a phosphodiester linkage then a phospholipid is formed.6 Triglycerides and Phospholipids are very common in food items such as olive oil, butter and even beer fat. The different chemical properties, like melting points are all dictated by the identity of the non-polar tails of the molecules. Generally, if an oil is composed of unsaturated tails (double bonds) then the oil will be solid at room temperature, and if the oil is completely of saturated tails then the oil will be in the liquid state.6

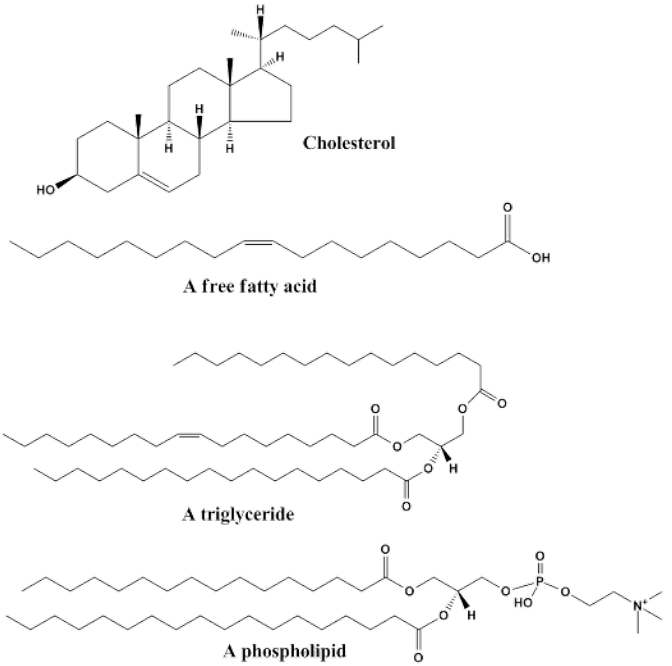


Figure 5.9.2. Cholesterol, Fatty Acids and other Common Lipids in Biochemistry

Raman Modes in Fatty Acid Methyl Esters (FAME)

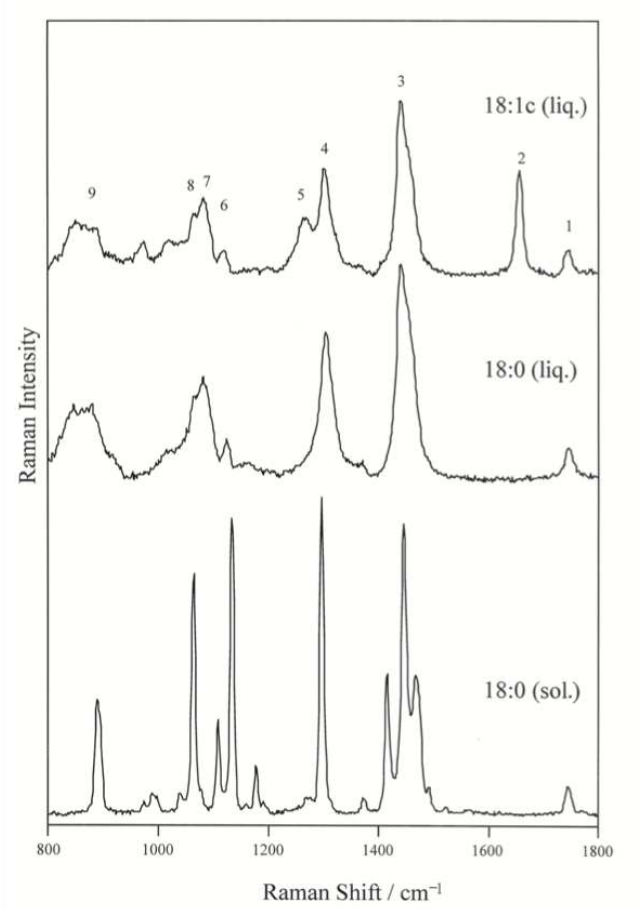


Figure 5.9.3. Typical Raman spectra of unsaturated (oleic acid, 18:1) and saturated(stearic, 18:0) FAME as solids(sol.) or liquids (liq.) The peak numbers refer to assignments in Table 1.7

Raman spectroscopy can be used on these types of lipids in order to distinguish between lipids of different carbon counts. Below in Figure 5.9.3, are Raman spectra of unsaturated (oleic acid, 18:1), saturated (stearic, 18:0) and Fatty Acid Methyl Esters (FAME) as solids(sol).7 It can be seen in the Raman spectra that there are quite a few characteristic peaks in this frequency range that is common in organic chemistry, these common peaks are summarized and assigned in Figure 5.9.4 below.

Band	Band position (cm^{-1})	Assignment
1	1730–1750	ν(C=O) Carbonyl stretch (5)
2	1640–1680	ν(C=C) Olefinic stretch (5)
3	1400–1500	$\delta(CH_2)_{sc}$ Methylene scissor deformations (5)
4	1295–1305	$\delta(CH_2)_{tw}$ Methylene twisting deformations (5)
5	1250–1280	$\delta(=CH)_{ip}$ In-plane olefinic hydrogen bend (5)
6	1100–1135	$\nu(C–C)_{ip}$ In-phase aliphatic C–C stretch all-*trans* (36)
7	1080–1110	$\nu(C–C)_g$ Liquid: aliphatic C–C stretch in *gauche* (39) and ν(C–C) Solid: aliphatic C–C stretch all-*trans* (38)
8	1060–1065	$\nu(C–C)_{op}$ Out-of-phase aliphatic C–C stretch all-*trans* (37)
9	800–920	$\nu(C_1–C_2)$, $CH_{3,rk}$, ν(C–O) Solid: mixture of stretches and rocks at acyl and methyl terminals. Complex broad plateau in liquid state (28)

Figure 5.9.4. Corresponding Assignment of Modes for Band Positions in Figure.7

Raman frequencies corresponding to different vibrational modes that was partly described in the group theory section, can be determined from the spectrum and chemical structure. One of the most notable stretching modes that is generally looked for in a spectrum is the carbonyl stretch (C=O) in the wave number range of ~1730 to 1750 cm-1.7 This is generally the most followed stretching mode because it is easy to identify on a spectrum and generally there is only one carbonyl in a fatty acid molecule. Because of the uniqueness of the carbonyl stretching frequency for each different FAME molecule, the identity of an unknown FAME molecule can be known if the Raman spectrum is known. This experiment was performed on different FAME molecules with different numbers of carbon in the Fatty Acid Tail, the resulting curve is shown in Figure 5.9.5. This experiment shows that as the number of carbons increase in a tail, the stretching frequency for the carbonyl in FAME molecules generally follow and increasing trend. This is an important result, because the identity FAME molecule can be found by measuring the Raman spectrum and referencing the carbonyl stretching frequency.7

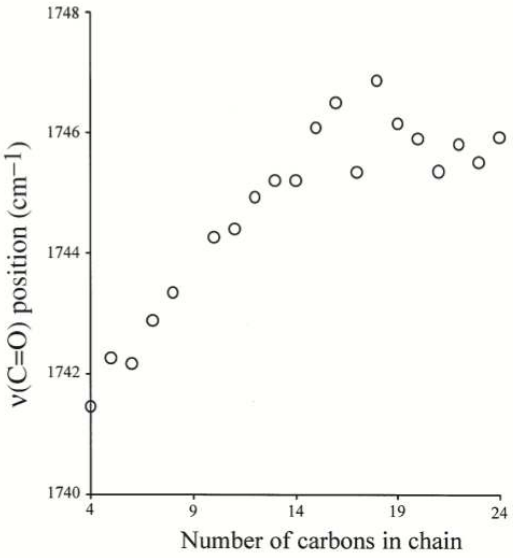


Figure 5.9.5. Effect of Chain Length (4-24 carbons) on the position of the carbonyl stretching mode for liquid-state saturated FAME.7

Summary

- Raman Spectroscopy involves the inelastic scattering of light on a molecule and how the tabulation of these values leads to vibrational shifts which are unique for each molecule.
- The expectation value of the polarizability decides whether a vibrational transition will occur or not.

- The number and identify of the vibrational mode(s) of a molecule can be determined by utilizing group theory relationships.
- Raman Spectroscopy can be applied to biological molecules of interest, especially lipids.

References

1. en.Wikipedia.org/wiki/Raman_spectroscopy (accessed May 18, 2018)
2. Shoemaker, D. P.; Garland, C. W.; Nibler, J. W. Experiments in Physical Chemistry; McGraw Hill: New York, NY, 1989.
3. McQuarrie, D. A.; Simon, J. D. Physical chemistry: a molecular approach; Univ. Science Books: Sausalito, CA, 1997.
4. Sakurai, J. J. Modern quantum mechanics: revised edition; Pearson Education: Delhi, India, 2006.
5. Miessler, G. L.; Fischer, P. J.; Tarr, D. A. Inorganic chemistry / Gary L. Miessler, Paul J. Fischer and Donald A. Tarr; Pearson: Boston, 2014.
6. https://en.Wikipedia.org/wiki/Lipid (accessed May 18, 2018).
7. Beattie, J. R.; Bell, S. E. J.; Moss, B. W. Lipids 2004, 39 (5), 407–419.
8. Czamara K., Majzner K., Pilarczyk M., Kochan K., Kaczor A., and Baranska M. (2014) Raman spectroscopy of lipids: A review, J. Raman Spectrosc., 46; pages 4–20, doi: 10.1002/jrs.4607.

5.9: Raman Spectroscopy on Membranes is shared under a CC BY 4.0 license and was authored, remixed, and/or curated by LibreTexts.

5.10: Nuclear Magnetic Resonance (NMR) Theory and Solution NMR

Nuclear magnetic resonance (NMR) occurs when nuclei in an unmoving magnetic field is disturbed by an oscillating magnetic field; the nuclei generate an electromagnetic signal, whose frequency depends on the magnetic field applied. This happens near resonance, where the frequency of oscillation aligns with the frequency of the nuclei. The magnetic field strength, chemical environment, and isotope affect resonance. NMR spectroscopy is used to elucidate the structure of organic molecules, study crystals and non-crystals, and can be applied to medical diagnostic imaging. NMR has three basic steps: nuclear spins are aligned in a magnetic field, the nuclear spins are disturbed by a radio-frequency (RF) pulse, the NMR signal is detected during or after the RF pulse. NMR was described by Isidor Rabi in 1938 and he won the Nobel Prize in Physics in 1944. Felix Bloch and Edward Mills Purcell used NMR on lipids and solids and won the Nobel Prize in Physics in 1952. Yevgeny Zavoisky observed MNR in 1941, prior to Bloch and Purcell; however, he discarded the results as unreproducible. Alongside x-ray crystallography and cryogenic-electron microscopy, NMR is one of the three techniques that is used to elucidate the structure of proteins.

Nuclear Spin

Atomic nuclei of protons and neutrons have spin, an intrinsic quantum property; it is an angular momentum similar to the angular momentum of a revolving orb. The overall spin of nuclei is dictated by the spin quantum number, S. If the numbers of protons and neutrons in the nucleus are even, S=0, which means no overall spin. Electrons couple in non-degenerate atomic orbitals; even numbers of protons or neutrons, which are spin 1/2 fermions, also give no overall spin.[1]

Protons and neutrons have lower energy when spins are aligned; the parallel spin alignment of particles does not violate the Pauli exclusion principle. The quark structure of protons and neutrons is responsible for the lower energy; the spin ground state for the nucleus of deuterium, which has one proton and one neutron, is one, not zero. Tritium, due to the Pauli exclusion principle, has two anti-parallel spin neutrons, and a proton spin of 1/2; the nuclear spin value for tritium is 1/2, comparable to ^{1}H. The nuclear magnetic resonance (NMR) absorption frequency for tritium is akin to ^{1}H. For non-radioactive nuclei, overall spin is non-zero; as an example, ^{27}Al nuclei have an overall spin of 5/2.[1]

A non-zero spin is related to a non-zero magnetic dipole moment, μ: μ=gamma·S; gamma is the gyromagnetic ratio. This relates to the relation of the angular momentum and magnetic dipole moment of a rotating orb. They are vectors parallel to the revolution horizontal; the length increases directly with the rotating frequency. The magnetic moments' interaction with magnetic fields permits the study of NMR values; these are associated with alterations between nuclear spin levels during RF incitement or due to Larmor precession of the magnetic moment after stimulation. Nuclei with even numbers of protons and neutrons have zero nuclear magnetic dipole moment and lack an NMR signal. ^{13}C, ^{31}P, ^{35}Cl, and ^{37}Cl generate an NMR signal, whereas ^{18}O does not.[4]

In contrast to NMR, electron spin resonance (ESR) detects transitions in electronic spin, not nuclear spin.[17] A smaller number of molecules with unpaired electron spins show ESR (or electron paramagnetic resonance (EPR)) absorption than NMR; however, ESR has a higher signal per spin than NMR.[17] While NMR can be applied to proteins, EPR/ESR is mainly used to study metal complexes and organic radicals.[17]

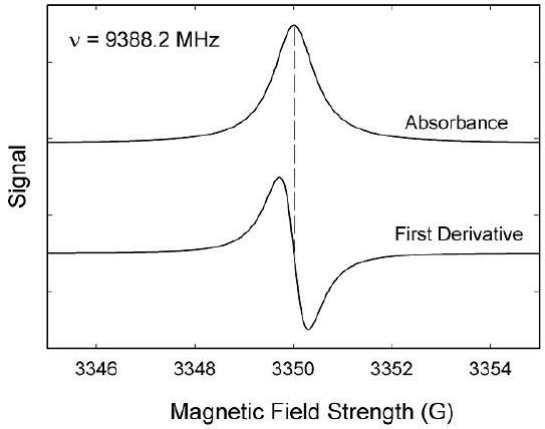


Figure 5.10.1. Magnetic field strength vs. signal spectra for EPR/ESR. The absorption signal is measured and the first derivative is calculated. dX/dB is the signal; it is the derivative of the magnetic susceptibility. When the spectrum passes zero, that is the absorption peak of the spectrum. This image is from: upload.wikimedia.org/wikiped.../EPR_lines.png.

Magic Angle Spinning (MAS)

In NMR, magic-angle spinning (MAS) is an approach used in solid-state NMR and ^{1}H NMR.[2] The sample is spun at a frequency of 1 to 130 kiloHertz (kHz) at an angle of θ_m=54.7356°, in regards to the magnetic field.[2] Wide lines become more narrow, which increases the resolution of the spectra.[2] Nuclear spin experiences three interactions interactions: dipolar, chemical shift anisotropy (CSA), and quadrupolar; the spectral lines generated are wide and difficult to analyze.[2] However, these interactions are dependent on position and MAS is used to average them.[2] Dipole interactions between nuclei are approximately zero at 54.7356°.[6] Nucleus-electron interactions are known as CSA, and are non-zero.[6] MAS can partially average the quadrupolar interactions.[6] In solution, these interactions are averaged out due to molecular movement; in solids, MAS causes narrow spectral lines, which can be used to determine CSA.[6]

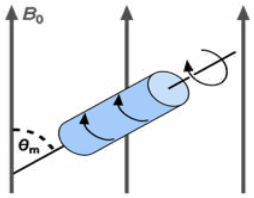


Figure 5.10.2. MAS NMR. The blue sample is rotating at 70 kHz in a magnetic field, B_0. This image is from: upload.wikimedia.org/wikiped...leSpinning.svg; it was created by Dtrx.

Spin Angular Momentum

Nuclear spin is a quantized intrinsic angular momentum. The values of S are limited and the x, y, and z-components are quantized; they are (half)-integer multiples of ħ, the reduced Planck constant. The (half)-integer quantum number related to spin alongside the z-axis or the magnetic field is the magnetic quantum number, m, which is +S to -S, in integer values. For all nuclei, there are a total of 2S+1 angular momentum states. The z-component of the magnetic moment is[4]

$$\mu_Z = \gamma S_Z = \gamma m \hbar. \tag{5.10.1}$$

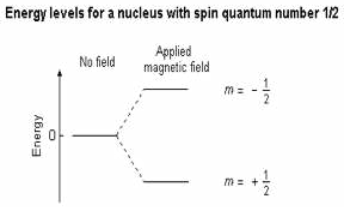


Figure 5.10.3. Nuclei spin energy splitting in an applied magnetic field. This image is from: https://teaching.shu.ac.uk/hwb/chemi...spec/nmr1.htm#.

Spin Energy in a Magnetic Field

Nuclei with a spin of 1/2, like ^{1}H, ^{13}C, or ^{19}F have two independent linear spin states, where m=1/2 or -1/2 for the z-portion; if a magnetic field is absent, the states possess the same energy. At thermal equilibrium, the number of nuclei per state is the same. When placed in a magnetic field, the energy varies due to interactions of the nuclear magnetic dipole moment and the magnetic field applied. The energy of the magnetic dipole moment, μ, in a magnetic field, B_0, is

$$E = -\mu B_0 = -\mu_x B_{0x} - \mu_y B_{0y} - \mu_z B_{0z}. \tag{5.10.2}$$

The z-axis lies with B_0, and the new equation is

$$E = -\mu_z B_0 = -\gamma m \hbar B_0. \tag{5.10.3}$$

Therefore, in a magnetic field, energies vary. A spin state of 1/2 means the spin is aligned with the magnetic field, and is the lower energy state; conversely, a spin state of -1/2 means the spin is not aligned with the magnetic field, and is the higher energy state. A positive gamma indicates that m=1/2 is the lower energy state. The difference between the high and low states is

$$\Delta E = \gamma \hbar B_0. \tag{5.10.4}$$

The lower energy state is preferred at thermal equilibrium. If more spins are up than down, net spin magnetization aside B_0 occurs.[1]

Larmor Precession & Radio-Frequency Pulses

The spin magnetization is proportional to the sum of spin vectors of atomic nuclei in equal magnetic sites and moves in a cone around the field, B. At non-equilibrium, precession of magnetization in B_0 arises with the Lamor frequency

$$\omega_L = 2\pi\nu_L = -\gamma B_0. \tag{5.10.5}$$

The energy of the population does not change, as it is constant. The transverse magnetization formed by an oscillating field is detected in NMR when an RF field or pulse is applied.[4]

Chemical Shielding (Shift)

Not all nuclei of the same element resonate at the same frequency. Electrons are charged and rotate and produce a magnetic field that is the reverse of the applied magnetic field. The electronic shielding reduces the magnetic field at the nucleus; the frequency needed to obtain resonance is decreased. This is known as chemical shift, and provides an explanation for NMR's ability to ascertain chemical structures, which rely on electron density. Nuclei with higher degrees of shielding due to a higher electron density have their NMR frequency shifted up, which corresponds to a low chemical shift; in contrast, less shielding shifts NMR frequency down, which gives a high chemical shift. In solid state NMR, magic angle spinning averages these states to get frequency values at average shifts. In regular, NMR, molecular tumbling averages the CSA.[1]

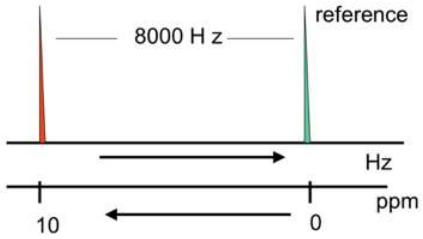


Figure 5.10.4. Example of chemical shift axis. The green peak is the reference compound for reference; the red peak is the sample compound. In this example, the distance between the two signals are 8,000 Hz; the frequency of the spectrophotometer is 800 MHz. If the reference peak is at 0, the distance between the two peaks is: 8,000(106)/800(106)=10 ppm. This would be an example of a proton attached to an electronegative element, like oxygen. This image is from: https://users.cs.duke.edu/~brd/Teach...s/flemming.pdf.

Relaxation

Relaxation occurs when nuclear spins revert to thermodynamic equilibrium; this is known as T_1 relaxation and indicates the average time it takes for nuclei to return to thermal equilibrium. Precessing nuclei eventually stop generating signals when they do not align; this is called T_2 relaxation. T_1 relaxation is normally longer than T_2 relaxation, because of small dipole-dipole interactions.[1]

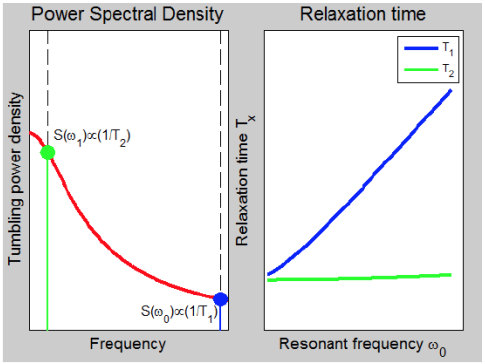


Figure 5.10.5. Animation showing the relation between Larmor frequency and T1 and T2. T2 is hardly affected. This image is from: commons.wikimedia.org/wiki/F...NmrrelaxM2.gif; it was created by Pondrthis.

Solution NMR

Less than 2% of the 120,000 structures of solved proteins are of membrane proteins; very few of those structures were solved via NMR.[7] High quantities of protein must be used and they must be extracted from native environments using chemicals that maintain structural and functional integrity.[8] If NMR is used, crystallization is not needed, but, new problems arise.[8] Solution NMR can be used to determine the structures of macromolecules that go through fast rotational diffusion on timescales of less than 100

nanoseconds.[15] As a result, proteins must be placed in lipid micelles, small bicelles, and nanodiscs.[13] Proteins with a size of approximately 40 kiloDaltons or less can be obtained with solution NMR; this is due to dynamics and resonance line widths.[14]

Heteronuclear NMR methods used for soluble proteins can be applied to membrane proteins.[18] For structural determination, proteins are ^{15}N- and ^{13}C-labeled by expression in minimal media with ^{15}N-ammonium sulfate and ^{13}C-glucose as nitrogen and carbon springs.[5] Protein side-chains are deuterated via ^{2}H,^{13}C-glucose to obtain better spectral resolution.[7] This lowers ^{13}C relaxation, which causes lower resonance; however, less protons are available to measure ^{1}H-NOE's, which give distant restraints.[11] ^{2}H2O is used for culture growth and amide protons are replaced with the solvent during purification and preparation; if deuterium is used in the solvent, the NMR spectroscopy will reflect this.[7] The rates of amide proton exchange provide information on exposed versus buried moieties.[9]

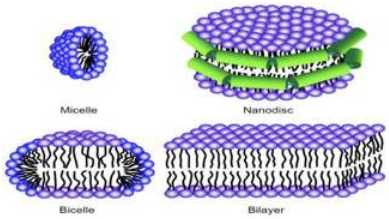


Figure 5.10.6. Solution and solid-state NMR sample preparation methods. Lipid micelles are used for membrane protein preparation for solution NMR. Dodecylphosphocholine (DPC) has a phosphocholine head and mild detergent activity makes it common in solution NMR. Short phospholipids, such as dihexanoyl-phosphatidylcholine (DHPC) or diheptanoylphosphatidylcholine can be used. Other detergents are lyso-phosphatidylglycerol, lauryl-dimethylamine oxide (LDAO), n-dodecyl-β-maltoside (DDM), and octyl-β-glucoside (β-OG). Bicelles are mixes of bilayer-making lipids; common ones are dimyristoyl-phosphatidylcholine (DMPC), and non-bilayer making lipids, such as DHPC. The ratio of long to short lipids is the q-value. The size of the bicelle depends on lipids used. In solution NMR, small bicelles with more non-bilayer making lipids works; the q-value ranges from 0.25-0.5. Small bicelles perform rotational diffusion, similar to micelles, which is detected by solution NMR. Nanodiscs are lipid bilayers enclosed by amphipathic helical proteins that stabilize the structure. Nanodiscs are made with two MSPD1's (a lipoprotein) at the edge. An empty nanodisc is around 150 kiloDaltons, which is too big for solution NMR. Short MSPD1 proteins have been made, lowering the size to 60-120 kiloDaltons, which is good for solution NMR. This image is from: https://www.ncbi.nlm.nih.gov/pmc/articles/PMC5444674/. The paper citation is: Liang, Binyong, and Lukas K. Tamm. "NMR as a Tool to Investigate Membrane Protein Structure, Dynamics and Function." Nature structural & molecular biology 23.6 (2016): 468.

Correlation-Time Problem

The rotational correlation time of proteins is important for NMR. It determines extraction conditions, instrumental analysis, and data processing methods. It is hard to obtain high-resolution spectra of large or aggregated proteins with NMR due to slow reorientation. The correlation-time problem can be dealt with in two ways when it comes to membrane proteins. In solid state NMR, membrane proteins in lipid bilayers or sizable bicelles are paralyzed by environmental conditions; radio-frequency irradiation, magic angle sample spinning, or sample alignment are replacements for molecular motions for the line-narrowing mechanism. For small membrane proteins, micelles or small bicelles can be used to prepare the samples; this leads to fast reorientation, which is detectable by solution NMR.[4]

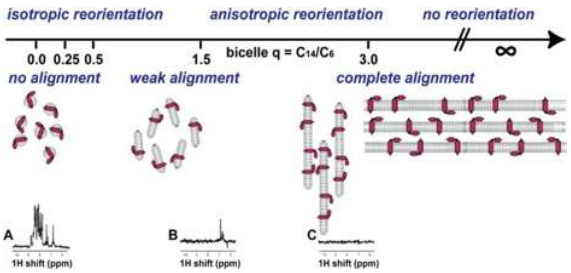


Figure 5.10.7. Linking of correlation times and alignments of proteins. Samples are labeled by q ratio for bicelles, which goes from 0 for isotropic micelles to 3 for large bicelles to infinity for bilayers. Spectra A-C are one-dimensional 1H NMR of a membrane protein in various samples: (A) q=0 (isotropic micelle); (B) q=0.5 (medium sized bicelle); (C) q=3 (large bicelle). The correlation time problem is visible here. Large, weak signals from a protein in medium (B) and large (C) bicelles are different from a protein in a micelle (A). This image is from: https://www.ncbi.nlm.nih.gov/pmc/articles/PMC3270942/. The paper citation is: Opella, Stanley J., and Francesca M. Marassi. "Structure determination of membrane proteins by NMR spectroscopy." Chemical reviews 104.8 (2004): 3587-3606.

Protein NMR

NMR of proteins is unlike magnetic resonance imaging (MRI), which obtains an image directly; protein NMR uses algorithms to create three-dimensional models of the sample of interest.[3] Protein NMR is conducted on thoroughly purified samples, which have

a volume of approximately 500 µL and a concentration of approximately 0.2 mM.[16] Normally, proteins are obtained via recombinant DNA, which is performed by genetic engineering; this method permits isotopic labeling to track particular atoms.[13] Once the proteins is dissolved in a buffer, it is placed in a thin NMR tube for spectroscopy.[13]

Large molecules, like proteins, have thousands of resonances, which will show overlaps of one-dimensional spectra.[10] As a result, multidimensional experiments are conducted; this reduces overlaps and focuses on certain nuclei in one section of the sample.[10] RF pulses permit the transfer of magnetization from chemical bonds and space (structure is irrelevant); this allows for the determination of chemical shifts and distance restraints, respectively.[10] Experiments of higher dimensions require more time than lower dimension experiments.[10]

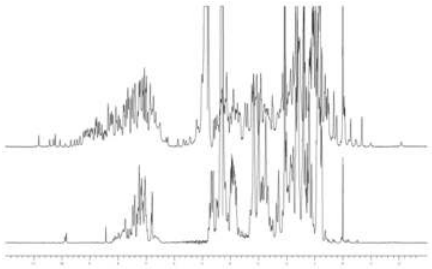


Figure 5.10.8. Folded (top) and unfolded (bottom) protein NMR spectra. This image is from: https://users.cs.duke.edu/~brd/Teach...s/flemming.pdf.

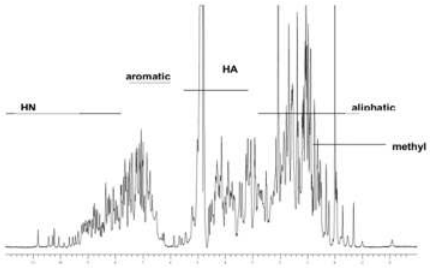


Figure 5.10.9. Proton NMR spectra of egg white lysozyme (hen). The -NH, aromatic, alpha-carbon, aliphatic, and methyl proton shift segments are labeled. This image is from: https://users.cs.duke.edu/~brd/Teach...s/flemming.pdf.

Homonuclear NMR

If the proteins of interest are unlabeled, correlation spectroscopy (COSY) is performed; two types of COSY are total correlation spectroscopy (TOCSY) and nuclear Overhauser effect spectroscopy (NOESY).[12] These two-dimensional NMR's provide two-dimensional spectra.[12] Both axes are chemical shifts, in term of units.[12] These experiments build spin systems, a list of resonances of the chemical shift of protein's protons.[12] To link the spin systems in the right pathway, NOESY must be used, which uses spin-lattice relaxation.[12] Magnetization is transferred via space in NOESY, which can be used to calculate distance relations.[12] NOESY can also determine chemical and conformational changes.[12] Peak overlap is an issue with homonuclear NMR; as a result, it is limited to small proteins.[12]

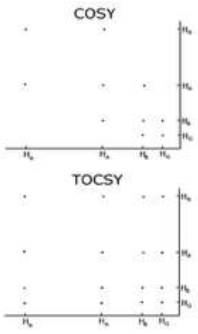


Figure 5.10.10. Comparison of two-dimensional COSY and two-dimensional TOCSY spectra for an amino acid (e.g. glutamate or methionine). TOCSY displays diagonal cross-peaks between all protons. COSY only displays cross-peaks between neighbors. This image is from: upload.wikimedia.org/wikiped.../Tocsycosy.jpg; it was created by Kjaergaard using GIMP.

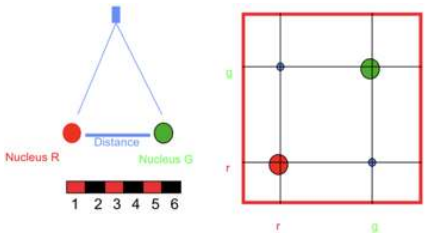


Figure 5.10.11. Two-dimensional NMR displaying the Nuclear Overhauser effect between two nuclei, G and R. The NOE is measured by the blue peak intensity at (r,g) and (g,r) This image is from: https://users.cs.duke.edu/~brd/Teach...s/flemming.pdf.

References

1. Abragam, Anatole, and Anatole Abragam. *The principles of nuclear magnetism*. No. 32. Oxford university press, 1961.
2. Andrew, E. Raymond. "Magic angle spinning." *Solid State NMR Studies of Biopolymers* 2 (2010): 83.
3. Clore, G. Marius, and Angela M. Gronenborn. "Determination of three-dimensional structures of proteins and nucleic acids in solution by nuclear magnetic resonance spectroscop." *Critical reviews in biochemistry and molecular biology* 24.5 (1989): 479-564.
4. Feynman, Richard P., Robert B. Leighton, and Matthew Sands. "The feynman lectures on physics; vol. i." *American Journal of Physics* 33.9 (1965): 750-752.
5. German, James. "The pattern of DNA synthesis in the chromosomes of human blood cells." *The Journal of cell biology* 20.1 (1964): 37-55.
6. Hennel, Jacek W., and Jacek Klinowski. "Magic-angle spinning: a historical perspective." *New techniques in solid-state nmr*. Springer, Berlin, Heidelberg, 2005. 1-14.
7. Johnson, Richard S., and Kenneth A. Walsh. "Mass spectrometric measurement of protein amide hydrogen exchange rates of apo-and holo-myoglobin." *Protein Science* 3.12 (1994): 2411-2418.
8. Jørgensen, Thomas JD, et al. "Collisional activation by MALDI tandem time-of-flight mass spectrometry induces intramolecular migration of amide hydrogens in protonated peptides." *Molecular & Cellular Proteomics* 4.12 (2005): 1910-1919.
9. Jørgensen, Thomas JD, et al. "Intramolecular migration of amide hydrogens in protonated peptides upon collisional activation." *Journal of the American Chemical Society* 127.8 (2005): 2785-2793.
10. Liang, Binyong, and Lukas K. Tamm. "NMR as a Tool to Investigate Membrane Protein Structure, Dynamics and Function." *Nature structural & molecular biology* 23.6 (2016): 468.
11. Marley, Jonathan, Min Lu, and Clay Bracken. "A method for efficient isotopic labeling of recombinant proteins." *Journal of biomolecular NMR* 20.1 (2001): 71-75.
12. Opella, Stanley J., and Francesca M. Marassi. "Structure determination of membrane proteins by NMR spectroscopy." *Chemical reviews* 104.8 (2004): 3587-3606.
13. Phinney, Karen W. "Expression of Stable Isotopically Labeled Proteins for Use as Internal Standards for Mass Spectrometric Quantitation of Clinical Protein Biomarkers." (2009).
14. Polshakov, Vladimir I., Berry Birdsall, and James Feeney. "Effects of co-operative ligand binding on protein amide NH hydrogen exchange." *Journal of molecular biology* 356.4 (2006): 886-903.
15. Rand, Kasper D., et al. "Electron capture dissociation proceeds with a low degree of intramolecular migration of peptide amide hydrogens." *Journal of the American Chemical Society* 130.4 (2008): 1341-1349.
16. Wüthrich, Kurt. "Protein structure determination in solution by NMR spectroscopy." *Journal of Biological Chemistry* 265.36 (1990): 22059-22062.
17. Zavoisky, E. "Spin-magnetic resonance in paramagnetics." *J Phys USSR* 9 (1945): 211-245.
18. Zhang, Zhongqi, and David L. Smith. "Determination of amide hydrogen exchange by mass spectrometry: a new tool for protein structure elucidation." *Protein Science* 2.4 (1993): 522-531.

5.10: Nuclear Magnetic Resonance (NMR) Theory and Solution NMR is shared under a CC BY 4.0 license and was authored, remixed, and/or curated by LibreTexts.

5.11: Solid-state NMR

In structural biology, X-ray crystallography, cryo-electron microscopy, and nuclear magnetic resonance (NMR) are the most useful tools to solve protein structures. However, when it comes to membrane proteins which are encoded in 20~30%[1] of most genomes, challenges appear. Since membrane proteins are embedded in the membrane and their structures and functions are highly dependent on their local bilayer lipid molecules, those environmental factors jeopardize the study of native membrane protein structures. Among all the known protein structures, only 1.7% [2] are membrane proteins. For X-ray crystallography, the basic requirement to have a long-range order for diffraction means amphipathic molecules are required to align in the repetitive crystal lattice. Thus, it is not easy to obtain a large crystal of membrane protein which has a mixed protein topology. Cryo-electron microscopy is an emerging and promising technology to obtain high-resolution membrane protein structures [3]. However, the cryogenic process for the sampling sacrifices the dynamic interaction of the protein and the bilayer components. The role of lipid phase is removed in the cryo-electron microscopic study of membrane proteins.

The well-established method of liquid-state nuclear magnetic resonance also suffers challenges when dealing with membrane proteins. In a typical liquid-state NMR experiment, a highly resolved spectrum is obtained due to the fast tumbling, or short correlation times (τ_c), of molecules that average anisotropic interaction to zero. Only isotropic interaction with the external magnetic field such as scalar couplings remains that makes assigning peaks to individual nuclei and their neighbors possible. However, membrane protein must be embedded into detergent micelles, lipid bicelles, or lipid nanodiscs for liquid-state NMR.[4] The large size of these vehicles dramatically increases the correlation time, thus anisotropic effect such as chemical shift anisotropy and through space dipolar coupling cannot be diminished. The non-averaged proton-proton dipolar interactions result in a featureless single broadband in the chemical shift that can span 25 kHz in width for proton NMR.[5]

Despite the disadvantage of anisotropy interaction in slow or non-tumbling molecules that leads to broad bands in NMR spectra, the broadband can be used to decode the anisotropic information of the molecules. In solid-state NMR (ssNMR), the anisotropic interactions in condensed phases including **chemical shift anisotropy** (CSA), internuclear dipolar coupling, quadrupolar interaction, and anisotropic J-coupling are studied.[5] The sample size of solid-state NMR can vary from protein microcrystals[6] to complexes like biofilms,[7] intact membranes[8] and even whole cells.[9]

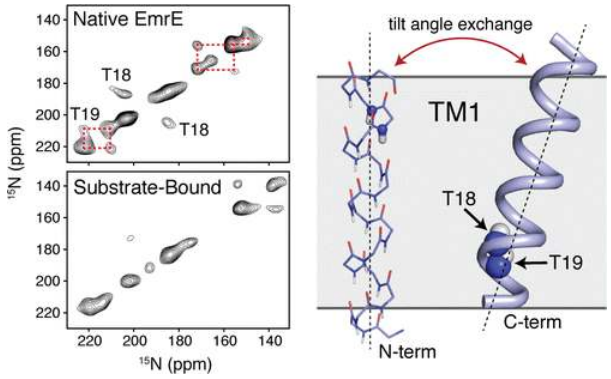


Figure 5.11.1: Example of conformational analysis by using ssNMR[10].

Chemical Shift Anisotropy

Electron surrounding the nucleus can shield the external magnetic field, disturb the Zeeman interaction, and lead to chemical shift. However, the electron cloud is not spherically distributed due to different bonding anisotropy. The anisotropy of a more asymmetrical functional group like the carbon of carbonyl is more significant than a symmetrical functional group like the carbon of methyl. Different orientations with respect to the applied external field, B_0 , will have different chemical shift within the same nucleus and appear as a broadband. For example, the bandwidth, $\Delta\sigma$, of a broadband spectrum observed in unoriented phospholipid bilayer can correspond to $\Delta\sigma = \sigma_{\parallel} - \sigma_{\perp}$, where $\sigma_{\parallel}$ is the chemical shift of bilayer oriented parallel to the external magnetic field and $\sigma_{\perp}$ is the chemical shift perpendicular to the external magnetic field. The $\Delta\sigma$ encodes qualitative viscosity and specific orientation of the membrane molecule. This technique is frequently used to study membrane proteins made up of primarily transmembrane helices[5].

Dipolar Interaction

Nuclei with spin greater than zero have a dipole moment. A nucleus with a dipole moment couples to another nucleus with nuclear spin I = ½ will appear as a doublet in the spectra. The splitting between two maxima can be calculated according to:

$$\Delta v_D(\alpha) = \frac{\mu_0}{4\pi}\frac{\gamma_i\gamma_j}{r_{ij}^3}\frac{\mathrm{h}}{2\pi^2}\left(\frac{3\cos^2(\alpha)-1}{2}\right) \tag{5.11.1}$$

where μ_0 is the permeability of vacuum, γ_i and γ_j are the gyromagnetic ratios of the nuclei, r_{ij} is the internuclear distance, h is the Planck's constant, and α is the angle between the vector linking two nuclei and the external magnetic field, B_0. In a solid powder sample, each orientation of the dipolar interaction results in a set of doublet, by integrating every orientation, a **Pake pattern** will appear. If the internuclear distance remains the same but the molecule is fluctuating around an average angle, α_0, the equation should be rewritten as:

$$\Delta v_D(\alpha_0) = \frac{\mu_0}{4\pi}\frac{\gamma_i\gamma_j}{r_{ij}^3}\frac{\mathrm{h}}{2\pi^2}\left\langle\frac{3\cos^2(\alpha)-1}{2}\right\rangle \tag{5.11.2}$$

where the term inside the brackets represents the probability distribution of the angle over the rapid fluctuations. The $\Delta\nu_D$ reflects internuclear distance, orientation and relative motion of a pair of nuclei, but each of the parameters needs to be determined independently in order to deduce the third parameter. The fluctuations of α around α_0 can be minimized by cooling the sample, while internuclear distances can be determined from neutron diffraction measurements. In many cases, $\Delta\nu_D$ is very small and even difficult to measure.

Overall, the dipolar interaction of ^{13}C-^{1}H provides important information but is relatively weak comparing to ^{2}H quadrupolar couplings[5].

Quadrupolar Interaction

A quadrupolar moment exists when nucleus has spin I > 1/2. The quadrupolar interaction is strong and dominates the Zeeman effect. The most useful nucleus in membrane structure studies is ^{2}H with I = 1. When a ^{2}H bound to a ^{12}C, the quadrupolar splitting $\Delta\nu_Q$ can be described as:

$$\Delta v_Q(\alpha) = \frac{3}{2}\chi_Q\left(\frac{3\cos^2(\alpha)-1}{2}\right) \tag{5.11.3}$$

where χ_Q is the **quadrupolar coupling constant** and α is the angle between the vector linking two nuclei and the external magnetic field, B_0. In a fluidic membrane system, molecules can rotate around the bilayer normal very rapidly so that the effective averaged symmetry axis of the quadrupolar moment is parallel to the bilayer normal. The $\Delta\nu_Q$ can be rewritten as:

$$\Delta v_Q(\beta) = \chi_Q\left\langle\frac{3\cos^2(\theta)-1}{2}\right\rangle\left(\frac{3\cos^2(\beta)-1}{2}\right) \tag{5.11.4}$$

where β is the angle between the bilayer normal and the external magnetic field and θ is the instantaneous angle between the ^{12}C-^{2}H bond and the bilayer normal as shown in Figure 5.11.2.

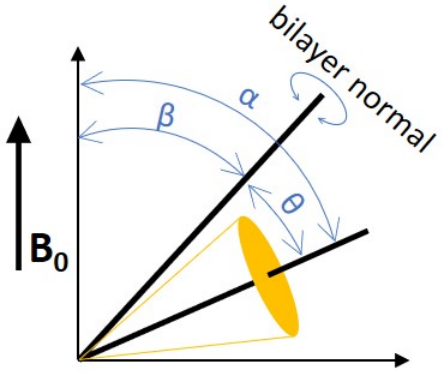


Figure 5.11.2: Definition of angles used in equations.

If the bilayer normal wobbles around an average angle β_0, the equation can be further derived as:

$$\Delta v_Q(\beta_0) = \chi_Q \left\langle \frac{3\cos^2(\theta)-1}{2} \right\rangle \left\langle \frac{3\cos^2(\beta)-1}{2} \right\rangle \tag{5.11.5}$$

where the term inside the brackets represent the time average of the fluctuations and wobbling and is called the **segmental order parameter** S_{CD}.

$$S_{CD} = \left\langle \frac{3\cos^2(\theta)-1}{2} \right\rangle \left\langle \frac{3\cos^2(\beta)-1}{2} \right\rangle = S_{fluc}S_{wob} \tag{5.11.6}$$

The $\Delta \nu_Q$ can be more complicated if the rapid motion of the quadrupolar moment does not have an axial symmetry, or if ^{14}N is involved in the quadrupolar interaction.

The line shape of the solid-state NMR provides orientational information. For slow motion with correlation time larger than $1/\chi_Q$, the linewidth will remain the same while the line shape is distorted. For fast motion such as sonicated membrane vesicles, the line shape can be narrow down to only one line.

Despite the important dynamic parameter S_{CD} can be obtained from the quadrupole splitting, the segmental order parameters in lipids cannot directly infer to the structural information. To obtain a complete average structure of a molecule, the whole order matrix, which contains nine elements, need to be determined. Without complete matrix, the spectra can only provide probabilities and boundaries of conformation in a model-independent fashion. That is why segmental order parameters in lipids are often stated in an elusive term such as ‘’probabilities of being in the trans conformation’[5].

J-Coupling

J-coupling, or scalar coupling, is a through chemical bond isotropic interaction. It is an indirect dipole-dipole interaction mediated by the local electrons between two nuclear spins. J-coupling provides information about the connectivity of molecules, bond distance, and bond angles. The intensity of J-coupling is relatively weak compared to the anisotropic dipolar or quadrupolar interactions.

Magic-Angle Spinning

The most commonly used technique in solid-state NMR is Magic-Angle Spinning (MAS). It was proposed by E. R. Andrew, A. Bradbury, and R. G. Eades in 1958[11], and by I. J. Lowe in 1959 [13]. Since the anisotropic interactions include the $(3\cos^2(\theta)-1)$ term, by spinning the sample at the angle θ = 54.74° where $\cos^2\theta = 1/3$ thus

$$3\cos^2(\theta)-1 = 0, \tag{5.11.7}$$

one can minimize both the anisotropic interactions and leave only the isotropic interaction. This angle is coined “Magic-Angle” and the method is termed “Magic-Angle Spinning” by Cornelis J. Gorter at the AMPERE congress in Pisa in 1960 [12]. The MAS can dramatically reduce the peak broadening due to anisotropic interaction and give a better resolution of the spectrum fur further analysis and identification of the structure.

By placing molecules at the angle of 54.74°, each bonding might have a different orientation, Δθ, with respect to the Magic-Angle, but after applying a rapid spinning around it, the orientation of all the dipolar moments will average to the Magic-Angle as shown in the following Figure.

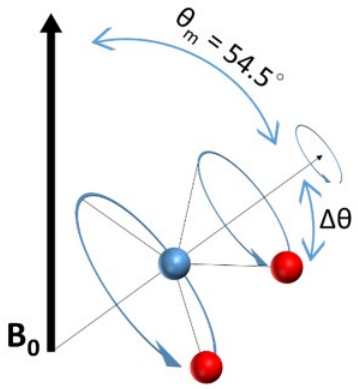


Figure 5.11.3: Magic angle spinning to remove anisotropic interaction.

The spinning probe is propelled by air or nitrogen gases with the rotational frequency ranging from 1 to 130 kHz. When the spinning frequency is greater than the width of the static line, the chemical shift anisotropy can also be averaged to zero. The quadrupolar interaction is the strongest anisotropic interaction (170 kHz for ^{12}C-^{2}H bond[14]), therefore it requires a very high spinning frequency to remove the quadrupolar coupling, leaving only isotropic J-coupling in the spectra.

Sensitivity Enhancement

The sensitivity of solid-state NMR can be enhanced by varies techniques. Like the ordinary liquid phase NMR, a higher magnetic field can increase the Zeeman effect and increase the net magnetization due to Boltzmann distribution, thus increasing the sensitivity of NMR signal. Dynamic nuclear polarization (DNP) [15] is also a popular method in both liquid and solid-state NMR. The basic of DNP is very much similar to Nuclear Overhauser Effect (NOE) but the saturation transfer is from electron to nucleus rather than nucleus to nucleus in NOE. Since an unpaired electron is required to be saturated, a diradicals species must be presented near the target nucleus, thus spin-labelled experiments are often required to do the DNP enhancement. The cryoprobe is also a common technique in liquid-state NMR. The coil and signal preamplifier are cooled by liquid nitrogen or a stream of cold helium gas to reduce the electronics thermal noise and reach as much as a four-fold enhancement in signal-to-noise ratio[16].

References

1. Piccoli, S.; Suku, E.; Garonzi, M.; Giorgetti, A., Genome-wide Membrane Protein Structure Prediction. *Curr Genomics* **2013,** *14* (5), 324-9.
2. Hendrickson, W. A., Atomic-level analysis of membrane-protein structure. *Nat Struct Mol Biol* **2016,** *23* (6), 464-7.
3. Abe, K.; Fujiyoshi, Y., Cryo-electron microscopy for structure analyses of membrane proteins in the lipid bilayer. *Curr Opin Struct Biol* **2016,** *39*, 71-78.
4. Wylie, B. J.; Do, H. Q.; Borcik, C. G.; Hardy, E. P., Advances in solid-state NMR of membrane proteins. *Mol Phys* **2016,** *114* (24), 3598-3609.
5. Warschawski, D. E.; Traikia, M.; Devaux, P. F.; Bodenhausen, G., Solid-state NMR for the study of membrane systems: the use of anisotropic interactions. *Biochimie* **1998,** *80* (5-6), 437-50.
6. Sperling, L. J.; Berthold, D. A.; Sasser, T. L.; Jeisy-Scott, V.; Rienstra, C. M., Assignment strategies for large proteins by magic-angle spinning NMR: the 21-kDa disulfide-bond-forming enzyme DsbA. *J Mol Biol* **2010,** *399* (2), 268-82.
7. Cegelski, L., Bottom-up and top-down solid-state NMR approaches for bacterial biofilm matrix composition. *J Magn Reson* **2015,** *253*, 91-7.
8. Fu, R.; Wang, X.; Li, C.; Santiago-Miranda, A. N.; Pielak, G. J.; Tian, F., In situ structural characterization of a recombinant protein in native Escherichia coli membranes with solid-state magic-angle-spinning NMR. *J Am Chem Soc* **2011,** *133* (32), 12370-3.
9. Rice, D. M.; Romaniuk, J. A.; Cegelski, L., Frequency-selective REDOR and spin-diffusion relays in uniformly labelled whole cells. *Solid State Nucl Magn Reson* **2015,** *72*, 132-9.
10. Cho MK, Gayen A, Banigan JR, Leninger M, Traaseth NJ., The Intrinsic Conformational Plasticity of Native EmrE Provides a Pathway for Multidrug Resistance. *J Am Chem Soc* **2014**, 136, 8072-80.
11. Andrew, E. R.; Bradbury, A.; Eades, R. G., Nuclear Magnetic Resonance Spectra from a Crystal Rotated at High Speed. *Nature* **1958,** *182* (4650), 1659-1659.
12. Lowe, I. J., Free Induction Decays of Rotating Solids. *Phys Rev Lett* **1959,** *2* (7), 285-287.

13. Hennel, J. W.; Klinowski, J., Magic-angle spinning: a historical perspective. *Top Curr Chem* **2005,** *246*, 1-14.
14. Seelig, J., Deuterium magnetic resonance: theory and application to lipid membranes. *Q Rev Biophys* **1977,** *10* (3), 353-418.
15. Griffin, R. G., High frequency dynamic nuclear polarization. *Abstr Pap Am Chem S* **2005,** *229*, U721-U721.
16. Griffiths, J., Solid-state NMR probes. *Anal Chem* **2008,** *80* (5), 1381-1384.

5.11: Solid-state NMR is shared under a CC BY 4.0 license and was authored, remixed, and/or curated by LibreTexts.

5.12: Electron Paramagnetic Resonance (EPR) of Membranes

Electron paramagnetic resonance (EPR) is a technique with applications in multiple branches of science, including physics, biology, and chemistry. The basic concepts of EPR are known to be analogous with Solid-state NMR, except it is electron spins that are excited as opposed to spins of atomic nuclei. EPR is often considered as a continuation of the renowned experiment conducted in 1922 by German physicists Otto Stern and Walter Gerlach, which demonstrated that an electron magnetic moment in an atom can assume only discrete orientations within a magnetic field, despite the spherical nature of the atom [1]. In 1945, Zavoisky recorded the first observation of an EPR peak when he detected a radiofrequency absorption line from a $CuCl_2 \cdot 2H_2O$ sample [1]. Ever since its inception, EPR has seen widespread use as a spectroscopic method for determining the dynamics, structure, and spatial distribution of paramagnetic species [2].

Fundamentals of EPR

Origin of an EPR signal

Since there is already a page dedicated to Electron Paramagnetic Resonance, this page will not go into the specific theories behind this branch of magnetic resonance spectroscopy. Instead, a brief overview of the origin of an EPR signal will be summarized. The magnetic moment of a molecule is mainly contributed from an unpaired electron. If the external magnetic field is increased, the gap between two energy states expands until it matches the energy of the microwaves. This phenomena is represented by the double arrow in the following diagram [3].

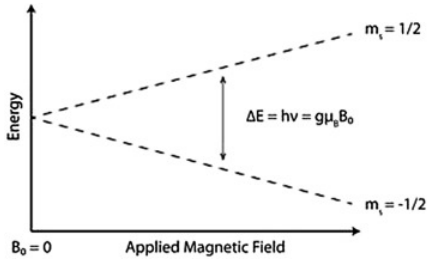


Figure 5.12.1. Energy levels for an electron spin ($M_s = \pm 1/2$) in an applied magnetic field B_0 [3]

As long as the resonance condition, $\Delta E = h\nu$ is followed, an unpaired electron can move between the two energy levels by either absorbing or emitting a photon of energy $h\nu$. The difference between the two energy states can be written as $\Delta E = h\nu = g\mu_B B_0$, where g is the electron's g-factor with a value of 2.002 319 304 386 [4] and μ_B is the Bohr magneton. As the intensity of the applied magnetic field increases, the difference in energy between the energy levels increases until it corresponds with the microwave radiation, thus resulting in absorption of photons. This is the basic principle behind EPR spectroscopy.

Hyperfine Coupling

It is reasonable to assume that all EPR spectra for one electron spin should consist of a single line since the source of an EPR spectrum is a change in an electron's spin state. On the contrary, the interaction of an unpaired electron via its magnetic moment with nearby nuclear spins causes the formation of additional allowed energy states, which would subsequently produce a multilined spectra. In these instances, the spacing between the EPR spectral lines demonstrates the degree of interaction between the unpaired electron and the perturbing nuclei. The hyperfine coupling constant of a nucleus is associated with the spectral line spacing [3]. Coupling is moderated by two processes: dipolar (through space) and isotropic (through bond) [5].

Electrons and nuclei can interact through two standard methods: Fermi contact interaction and by dipolar interaction. Fermi contact interactions apply mainly to the case of isotropic interactions, which are independent of sample orientation in a magnetic field. Conversely, dipolar interactions apply to anisotropic interactions, which are spectra dependent on sample orientation in a magnetic field. Spin polarization is a third method for interactions between an unpaired electron and a nuclear spin and are especially significant for π-electron organic radicals [1].

Spin-Labeling Method

Since the majority of chemical and biological samples of interest for EPR spectroscopy do not have an inherent stable unpaired electron, most EPR mechanisms rely on the use of spin-labeling reagents. Therefore, a radical must be introduced, which is usually referred to as a spin label or spin probe. The most frequently used radical is a nitroxide radical, which displays a three-line hyperfine structure whose peak shape and splitting are dependent on the radical's environment. This nitroxide label monitors

motion. The shape of the EPR signal also depends on the orientation of the magnetic field relative to the axis of the radical. Therefore, the spin probe method can be used to study the environment of the radical, which is also the structure of the polymer at a molecular level [1].

Generally, derivatives of 2,2,6,6-tetramethyl-1-piperidinyloxy (TEMPO) are used since they offer adequate stability of the unpaired electron and remarkable EPR sensitivity mixed with adjustable moieties for binding to the sample through chemical reactions itself. Figure 5.12.2 shows the EPR spectra of TEMPO solution in water (0.02 wt%). The spectra contains three symmetric peaks since the NO* radical of TEMPO (or with 5-, 12-, and 16-doxylstearic acid derivatives) is free to move around the solution. All three peaks are nearly equal in height and symmetry [6].

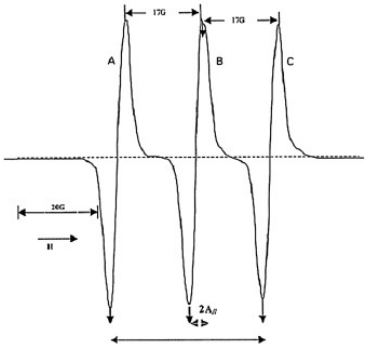


Figure 5.12.2: Electron paramagnetic resonance spectra of TEMPO solution in water (0.02 wt%) [6]

Block Diagram of EPR Spectrometer

Figure 5.12.3 depicts a block diagram for a standard EPR spectrometer. Klystron is commonly used as a radiation source. Klystrons are vacuum tubes known to be stable, high-power microwave sources, which have low-noise characteristics and thus give high sensitivity. Most EPR spectrometers operate at around 9.5 GHz, which is approximately 32 mm [1]. The radiation can be incident on the sample continuously or pulsed. Most EPR applications utilize continuous wave methods as the recording and interpretation of pulse EPR spectra requires sophisticated technical equipment and a more advanced theoretical background. The sample is placed in a resonant cavity between two electromagnets, which admits microwaves through an iris. Several different types of solid-state diodes are sensitive to microwave energy, thus allowing absorption lines to be detected when the separation of the energy levels are equal or very close to the frequency of the incident microwave photons. In practice, most of the external components are enclosed within a microwave bridge control [7].

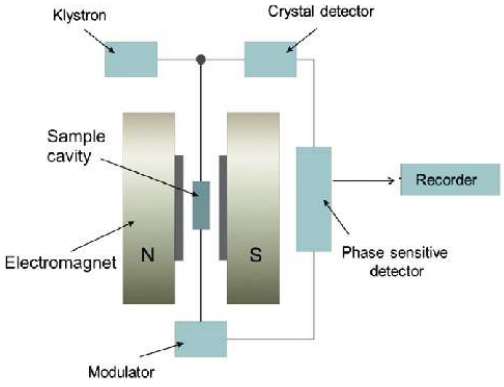


Figure 5.12.3. Block diagram for a typical electron paramagnetic resonance spectrometer [7]

Examples of EPR Applications on Membranes

Membrane Functions of Erythrocytes

In 2000, Tsuda et al. conducted research using EPR spectroscopy and spin-labeling to investigate the role of nitric oxide (NO) in the regulation of membrane functions of erythrocytes in patients with essential hypertension. The NO donor S-nitroso-N-acetylpenicillamine (SNAP) decreased the order parameter (S) for 5-nitroxide stearate (5-NS) and the peak height ratio (h_0/h_{-1}) for 16-NS obtained from EPR spectra of erythrocyte membranes in a dose-dependent manner [8]. Figure 5.12.4 depicts the EPR spectra of erythrocytes for the fatty acid spin-label agents obtained by the authors. The EPR spectra were used to distinguish any changes

in the freedom of motion in biological membranes and to contribute an indication of membrane fluidity. In the EPR spectra for 5-NS, the authors evaluated the values of outer and inner hyperfine splitting to calculate the order parameter (S). In the EPR spectra for 16-NS, they used the peak height ratio (h_0/h_{-1}) value to ascertain an index of the membrane fluidity [8].

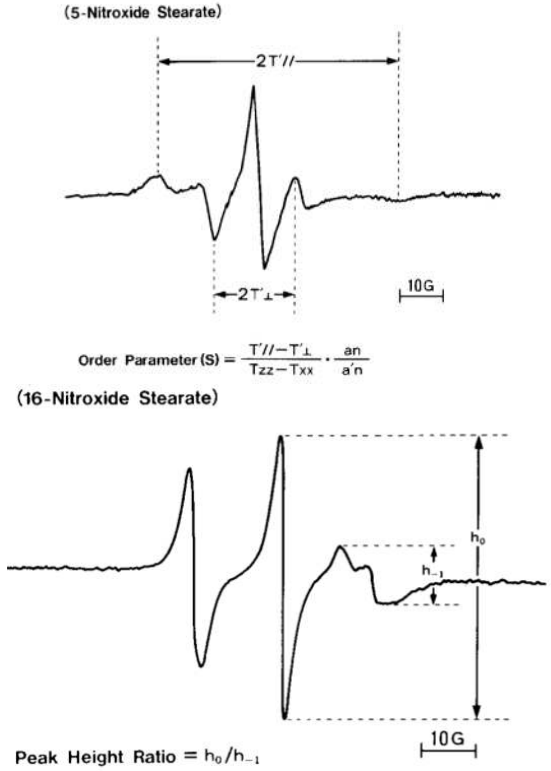


Figure 5.12.4: Standard EPR spectra of erythrocytes for the fatty acid spin-label agents (5-NS and 16-NS). Order parameter (S), outer hyperfine splitting (T'), inner hyperfine splitting ($T'_{\perp}$), hyperfine constants (T_{zz} and T_{xx}), peak height ratio (h_0/h_{-1}). The higher the values of the order parameter and the peak height ratio, the lower the membrane fluidity of erythrocytes [8].

Oxygen Transport in Thylakoid Membranes

In 1998, Ligeza et al. used EPR spectroscopy to study oxygen transport in thylakoid membranes of spinach chloroplasts by observing the collisions of molecular oxygen with spin labels [9]. Linewidths of the EPR spectra measured in the presence and absence of molecular oxygen were used to estimate the collision rates. Additionally, the authors estimated the oxygen permeability coefficient for the thylakoid membrane from the profile of the oxygen diffusion-concentration product across the membrane. This profile was developed by examining the oxygen broadening of the EPR spectrum of lipid-soluble spin labels located at multiple distances from the membrane surface, which was determined by the product of the local oxygen concentration and the local oxygen diffusion coefficient. Using these results, they were able to calculate the oxygen concentration difference that could be produced across the thylakoid membrane during chloroplast illumination. They concluded that under steady state conditions, the oxygen concentration difference across the thylakoid membrane should be inconsequential [9].

Furthermore, Ligeza et al. demonstrated that every collision of oxygen with a nitroxide radical in water catalyzes an observable line broadening of the EPR spectrum. These results allowed them to connect the Smoluchowski equation for colliding molecules [10],

$$\omega = 4\pi pRD(x)C(x), \tag{5.12.1}$$

with oxygen-induced line broadening of the EPR spin label spectrum:

$$\omega = \sqrt{3}/2\gamma\Delta Hpp(x). \tag{5.12.2}$$

where $C(x)$ is the local oxygen concentration at 1 atm partial pressure of oxygen, R is the interaction distance between oxygen and nitroxide radical, p is the probability that an observable event is recorded when a collision takes place, $D(x)$ is the diffusion constant, $\Delta H_{pp}(x)$ is the oxygen-induced peak-to-peak line broadening, and γ is the magnetogyric ratio of the electron [10].

The linewidth of the central component of the EPR spin-label spectrum was ultimately used as the most sensitive parameter to evaluate the broadening effect of oxygen dissolved in the lipid bilayer [9].

Oxidation of Lipid Membranes

EPR spectroscopy has also been used in the study of the aging process and in development of age-associated diseases. Gabbita et al. used EPR spectroscopy in conjunction with a site-specific spin label to investigate several hypotheses related to whether or not succinate stimulation of mitochondria results in oxidative modification of membrane lipids. The primary hypothesis that the authors tested was that caloric restriction protects brain mitochondria and its biomolecular components and decreases metabolic generation of oxygen radicals, thus modulating regulating lipid membrane damage [11]. Similar to Tsuda et al.'s previously analyzed research, Gabbita et al. obtained an EPR spectrum for 5-NS. After a 3 hour incubation at 22°C, EPR measurement of the amplitude (B_0) of the central resonance line of the 5-NS signal and the fluidity parameters ($T_{\parallel}'$ and $T_{\perp}'$) were performed, which is displayed in Figure 5.12.5.

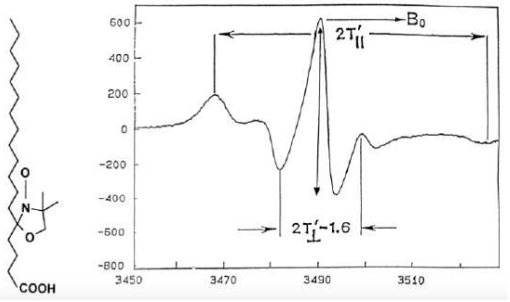


Figure 5.12.5. Structure and representative EPR spectrum of 5-NS [11]

The 5-NS EPR signal reflected an average of all the labeled membranes present in the mixed population of synaptosomes and mitochondria and was influenced by membrane lipid composition. From these results, the authors concluded that the overall succinate concentration effects observed with respect to loss in 5-NS signal amplitude and a decrease in order of synaptosomal and mitochondrial lipid membranes indicate that an induced metabolic stress to mitochondria may cause an increased production of oxygen radicals through the complex II-ubiquinone-cytochrome b region of the electron transport chain. There is a dose-dependent decrease in 5-NS signal amplitude consistent with an increase in generation of oxygen radicals upon mitochondrial respiratory stimulation with succinate.

Advantages	Disadvantages
Can be performed very quickly (15-20 minutes)	Can only be used to identify free radicals
Better selectivity than NMR spectroscopy	Process must be performed at low temperatures
Unlike X-Ray crystallography, EPR does not require a protein crystal	Requires multiple site-directed mutations
Results are easy to comprehend and understand	Can provide only meager distance restraints
Proteins are labeled before fibrillization, thus not necessary to pierce fibril core	

References

1. Weil, J.A. and J.R. Bolton, *Electron Paramagnetic Resonance: Elementary Theory and Practical Applications*. Wiley, New York, 2007: p. 3.
2. Schweiger, A., and Gunnar Jeschke. *Principles of Pulse Electron Paramagnetic Resonance*. Oxford, UK: Oxford University Press, 2001.
3. Khulbe, K.C., A.F. Ismail, T. Matsuura, *Chapter 3 - Electron Paramagnetic Resonance (EPR) Spectroscopy*, Membrane Characterization, Elsevier, 2017, p. 47-68.
4. Odom B., Hanneke D., D'Urso B., Gabrielse G. *New measurement of the electron magnetic moment using a one-electron quantum cyclotron*. Physical Review Letters, 2006, 97(3).
5. Cammack, R., *EPR, Methods*, Encyclopedia of Spectroscopy and Spectrometry, 1999, p. 457-469.

6. Khulbe, K.C., F. Hamad, C. Feng, T. Matsuura, T. Gumi, C. Palet**,** *ESR spectra of spin probe in PPO membrane*, Polymer, 44, 2003, p. 695-701.
7. Kwon, J., Shahbaz, H., Ahn, J. *Advanced Electron Paramagnetic Resonance Spectroscopy for the Identification of Irradiated Food*. American laboratory, 2014, 46. p.1-4.
8. Tsuda, K., K. Kimura, I. Nishio, Y. Masuyama. *Nitric oxide improves membrane fluidity of erythrocytes in essential hypertension: an electron paramagnetic resonance investigation*. Biochem. Biophys. Res. Commun., 275 (3), 2000, p. 946-954.
9. Ligeza, A., et al. *Oxygen permeability of thylakoid membranes: electron paramagnetic resonance spin labeling study*. Biochim. Biophys. Acta, 1998, 1365 (3), p. 453-463.
10. Hyde, J.S., W.K. Subczynski, L.J. Berliner, J. Reuben, *Biological Magnetic Resonance, Vol. 8, Spin Labeling: Theory and Applications*, Plenum, New York, 1989, p. 399-425.
11. S.P. Gabbita, D.A. Butterfield, K. Hensley, W. Shaw, J.M. Carney. *Aging and caloric restriction affect mitochondrial respiration and lipid membrane status: an electron paramagnetic resonance investigation.* Free Radic. Biol. Med., 23, 1997, p. 191-201.

5.12: Electron Paramagnetic Resonance (EPR) of Membranes is shared under a CC BY 4.0 license and was authored, remixed, and/or curated by LibreTexts.

5.13: Membrane X-ray Scattering

Membrane scattering encompasses a large variety of methods for characterizing lipid membranes. For example, a few popular techniques include X-ray or neutron reflectivity and diffraction, Brewster angle microscopy, ellipsometry, X-ray interferometry, infrared reflection-adsorption spectroscopy, vibrational sum frequency generation spectroscopy, and any electron scattering techniques such as SEM or TEM [3][4]. These methods can be used with a variety of different model membranes types (described briefly below). For the sake of brevity, this article will focus on just small angle X-ray and neutron reflectivity and small angle X-ray diffraction.

The motivation behind X-ray and neutron reflectivity and X-ray diffraction is mostly to characterize the structure of the lipid membrane such as the membrane thickness, unit cell organization, or where in the membrane proteins prefers to reside. For x-ray and neutron scattering, measurements are performed using flat model membranes that are either at an air-water interface or on a supported substrate. This article will give a brief overview of common membrane scattering techniques and give some background information on flat model membranes.

**note to reader: the text editor software on this website does not support the symbols for greek letters, so in the text lowercase 'A' and the symbol for alpha will appear the same. Fortunately I believe that, using the context of the sentence, one should be able to determine the meaning of the variables in this introduction, although I sincerely apologize for any inconvenience.

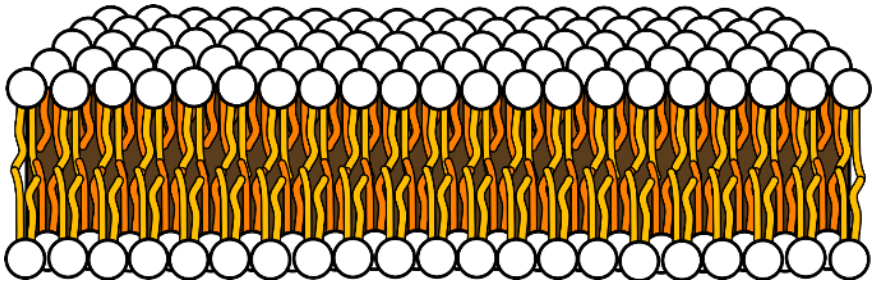


Figure 5.13.1: Cartoon of a bilayer phospholipid membrane [9]

Model Membranes

Due to the enormous complexity of real biological cells and plasma membranes, researchers often use simplified model memsbranes to study specific aspects of how biological membranes function or to make the membranes easier to measure. Importantly, model membranes do not entirely behave like their natural counterparts, and act as more of a guide showing what behaviors are most likely exhibited in real membranes. In addition, different types of model membranes can act differently as well; this paper by the Kuhl Lab at UC Davis explores some of these structural differences using X-ray diffraction [2].

For small angle scattering experiments, only model membranes with flat surfaces can be used, which include monolayer membranes, supported bilayer membranes, and supported multilayer/multilamellar membranes. This is because the incoming beam is approaching the sample horizontally and has a much longer footprint due to it's angle of incidence being approximately 1^{o}.

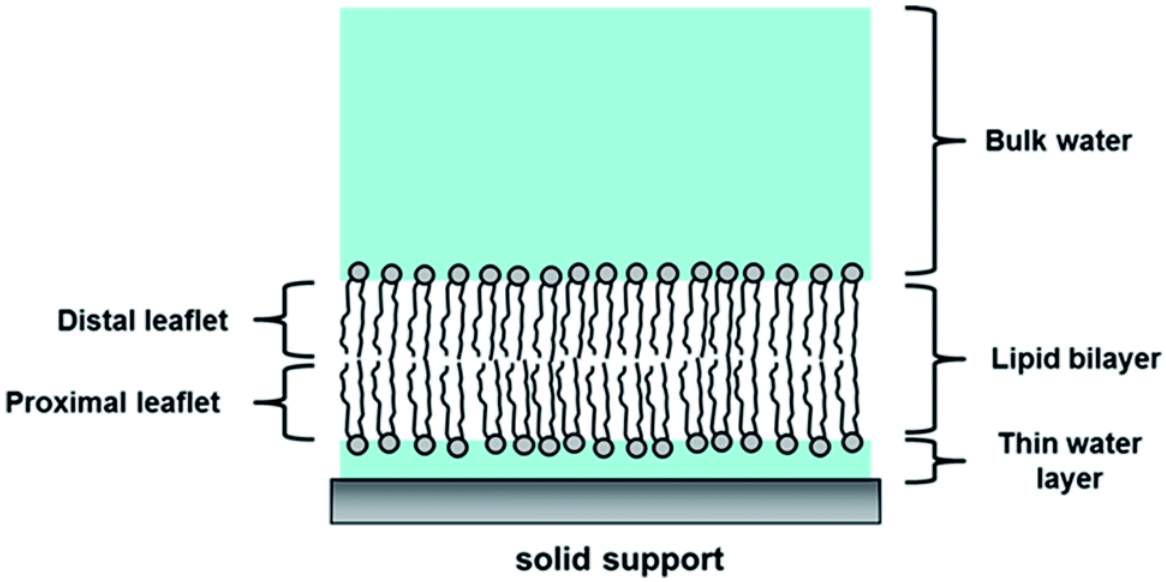


Figure 5.13.2: Cartoon of a supported bilayer membrane [10]

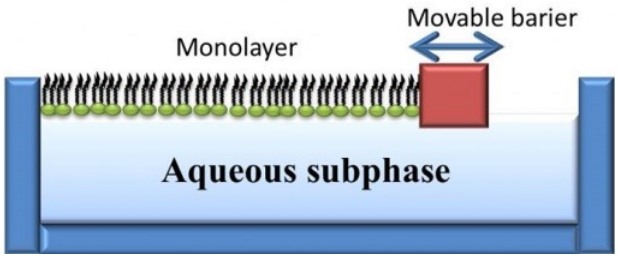


Figure 5.13.3: Cartoon of a floating monolayer in a Langmuir-Blodgett trough (note the movable barrier functions to adjust the surface pressure of the model membrane) [11]

Scattering Characterization Techniques

Despite being only a few nanometers thick, the bilayer is composed of several distinct chemical regions through its cross-section. Over the past several decades neutron reflectivity, X-ray reflectivity, and X-ray diffraction have been important for characterizing the phases, interactions, and nanostructure of the membrane.

Small Angle X-ray Scattering SAXS (or X-Ray Reflectivity)

Small angle X-ray Scattering (SAXS), or X-ray reflectivity, is a technique that can measure the average electron density of a thin surface layer. The technique can resolve the average height of a monolayer with sub-angstrom resolution, but has the limitations of only working in the out of plane z-direction and only being able to show an average data from a relatively large sample area. One of its advantages, however, is unlike GIXD (described next), SAXS is not limited to only working with ordered phases and can determine the positions of both the head group and the acyl chain tail group of phospholipid molecules. In addition, SAXS has the advantage that it can be done (although perhaps not easily in many cases) with non-synchrotron x-ray sources of still decently high X-ray intensity (such as a rotating or liquid anode x-ray source).

The basic concept behind SAXS is that incoming X-rays will scatter off electrons in a sample (in this case the model membrane). Because the membrane creates an interface, one can use Snell's and Fresnel's laws to predict where and with what intensity the X-rays will scatter in the out of plane direction. This scattering intensity turns out to be a function of the average electron density in the z-direction. Thus, to determine the electron density of a sample, a model is made of the samples electron density and refined until it matches the reflectivity data.

To start with, a wave incident on a perfectly sharp interface will reflect or refract according to Snell's law (which has both a sine and a cosine part) where a_I and a_R are the incident and reflected intensities:

$$n \cos \alpha' = \cos \alpha$$

$$(a_I + a_R)n\sin\alpha' = (a_I - a_R)\sin\alpha$$

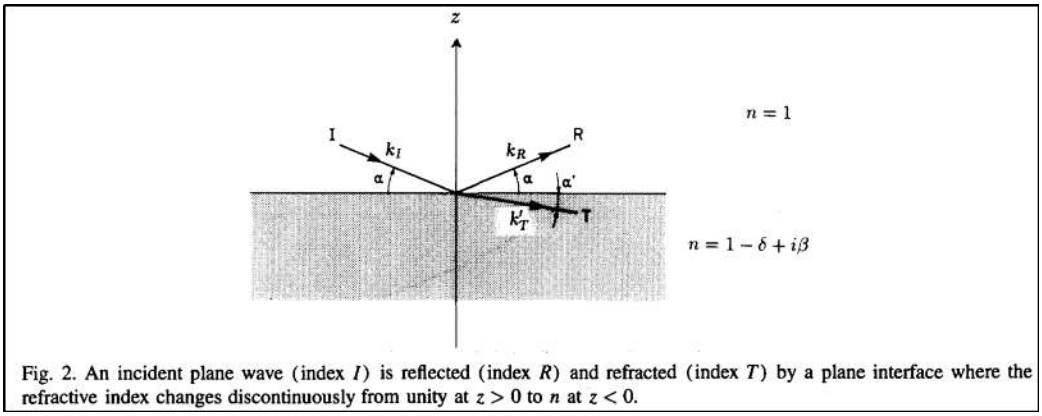


Fig. 2. An incident plane wave (index I) is reflected (index R) and refracted (index T) by a plane interface where the refractive index changes discontinuously from unity at $z > 0$ to n at $z < 0$.

Figure 5.13.4: A clip from a review article showing a schematic of Snell's law, showing the X-ray beam incoming at angle α as well as leaving at angle α and being refracted at angle α'. The incoming beam I has wavevector $\mathbf{k}_I$, the reflected beam R has wavevector $\mathbf{k}_R$, and the refracted beam has wavevector $\mathbf{k}'_T$. The refractive index n of air is given as 1, and the refractive index of is given by the complex equation, where β is dependent on the adsorption and δ is dependent on the scattering length. [7]

The angle of the reflected beam is also commonly described using the out of plane wavevector transfer $\mathbf{q}_z$, which is the difference between the reflected and incident beams, as shown below.

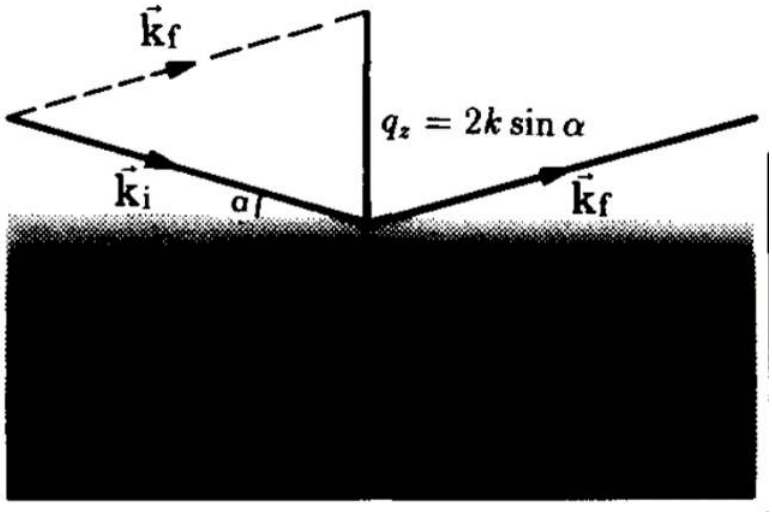


Figure 5.13.5: The out of plane wavevector transfer $\mathbf{q}_z$ is shown as both a function of angle α and as the difference between the incident beam $\mathbf{k}_i$ and the reflected beam $\mathbf{k}_f$ [7]

One of the peculiar and important behaviors associated with reflection is as the angle α gets smaller, more and more of the beam is reflected instead of refracted until eventually at a critical angle α_c the beam is entirely reflected. For lipid membranes this angle is on the order of about 1^o. The definition of the critical angle for total reflection is:

$$\alpha_c^2 \equiv \left(\frac{4\pi}{k^2}\right)|\rho_{av}| \tag{5.13.1}$$

This can easily be visualized in the graph below, in which as the angle (given as the as the angle divided by the critical angle, which is equal to the wavevector transfer divided by the wavevector transfer at the critical angle) decreases, the reflected intensity increases. The graph also serves to show how non-ideal adsorption behavior can affect the reflected beam intensity even below the critical wavelength.

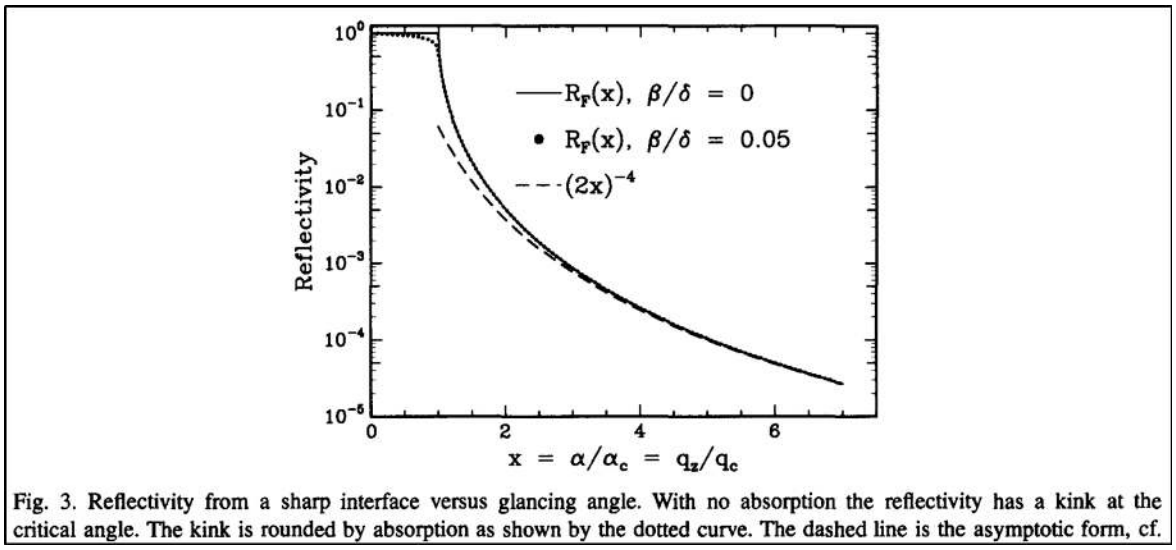


Fig. 3. Reflectivity from a sharp interface versus glancing angle. With no absorption the reflectivity has a kink at the critical angle. The kink is rounded by absorption as shown by the dotted curve. The dashed line is the asymptotic form, cf.

Figure 5.13.6: This graph shows how as the angle reaches the critical angle, the reflectivity reaches a maximum which corresponds to the incident beam being entirely reflected instead of refracted at the interface [7]. As a side note, this is the same concept fiber optic cables use to keep the light that travels down their length from escaping.

It is important that experiments are carried out close to this critical angle in order to achieve a high enough reflectivity that one can obtain a meaningful signal from their measurements.

Fresnel's law, the next important element of reflectivity, can be derived using Snell's law, the definition of the critical angle, and the complex equation for the index of refraction. It can be given as:

$$(1 + a_R/a_I)\alpha' = (1 - a_R/a_I)\alpha$$

or

$$R \equiv \frac{a_R}{a_I} = \frac{\alpha - \alpha'}{\alpha + \alpha'}$$

Where R is defined as the ratio between the incident and reflected beam intensities. The reflectivity then, also known as the Fresnel reflectivity, is given as the square of the magnitude of R.

$$\mathcal{R}_F = \left|\frac{\alpha - \alpha'}{\alpha + \alpha'}\right|^2$$

When actually measuring the reflectivity of a sample, these two values are extremely important because the reflected intensity of an X-ray beam off a sample is recorded as R/R_F.

In reality, because interfaces are not ideally sharp, the Fresnel reflectivity and Fresnel's law as shown above don't apply as they are. The kinematic approximation accounts for such non-ideal behavior and gives the modified Fresnel reflectivity as:

$$R(q_z) = R_F(q_z)\left|\frac{1}{\rho_{\infty}}\int \frac{d\rho}{dz} e^{iq_z z}\, dz\right|^2$$

This equation is also used to determine how the electron density ρ determines the observed reflected intensity. By building an electron density model, one is able to work backwards using this equation to fit their electron density to the observed reflection, and thus build an accurate model of the average electron density of their sample in the z-direction.

For reference, a reflectivity spectrum and the electron density profile it was matched with are shown below. The data is for a lipid monolayer in a Langmuir trough. In the electron density profile, the lipid headgroups, the acyl chain tails, and the location of the air and water interfaces can all be determined.

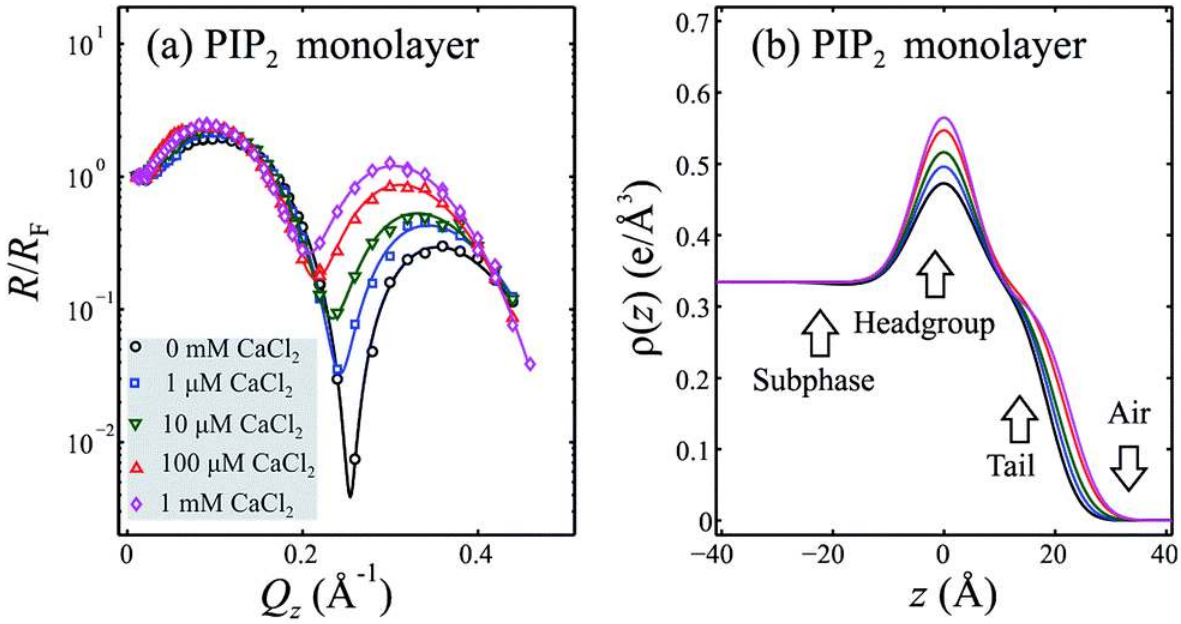


Figure 5.13.7: A graph of the reflectivity and one of the electron density spectrum for a lipid monolayer [20]

Grazing Incidence X-ray Diffraction (GIXD)

GIXD, also called small angle X-ray diffraction, is another technique that uses the small angle approach. In addition, because of the especially high X-ray intensity needed to perform diffraction experiments on lipid membranes, GIXD studies are most often carried out at synchrotron sources.

GIXD can resolve atomic arrangement and unit cell dimensions (to the nearest 0.1 angstrom) of lipid membranes and can measure the tilt angle of the lipid tails to within a few degrees. As the only technique that can measure the lateral organization of the lipid membrane on the nanoscale, it has become extremely useful for investigating the controversial lipid raft theory.

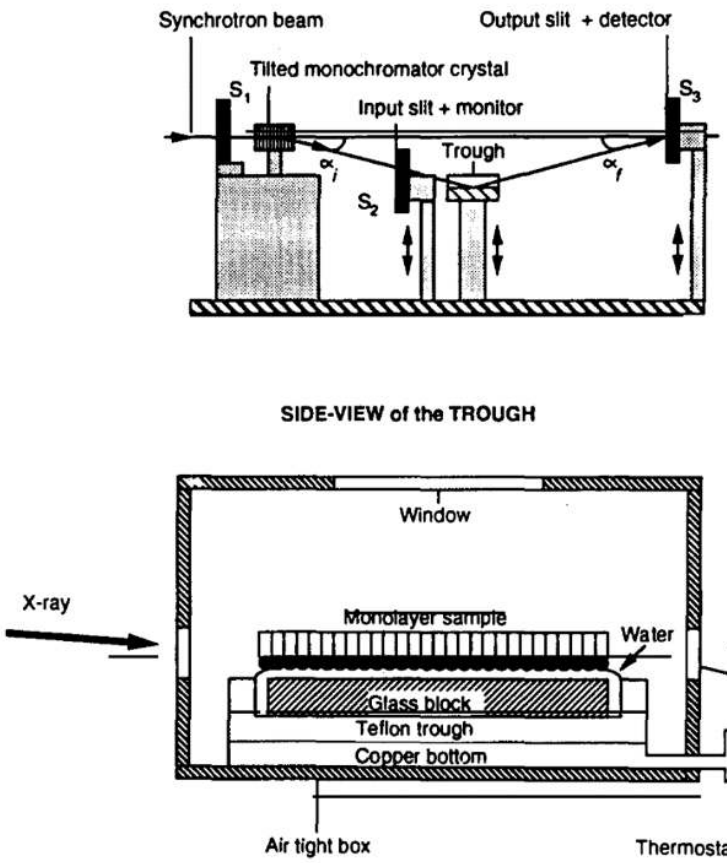


Fig. 1. Example of an experimental set-up of a liquid surface diffractometer (beamline D4, X-ray synchrotron source at Hasylab, Hamburg). Top: Side view of the vertical scattering plane. Beam directions are defined by slits. The monochromatic beam is bent down towards the sample by tilting the monochromator crystal. The incident beam intensity is monitored after slit S2. Bottom: Blown up view of the trough showing the monolayer sample spread on a thin film of water. The glass block provides for a thin liquid film (about 0.3 mm thick) and thus effectively reduces surface waves.

Figure 5.13.8*:* A clip from a review article (mentioned in further reading) showing an experimental setup for GIXD off a monolayer membrane at a synchrotron facility [7]

However, GIXD is limited in that a high degree of order is needed for diffraction, and even the ordered phases of lipid membranes only form a hexatic phase (a liquid crystalline phase having a high degree of short range order but no long range order). This leads to many of the limitations this technique faces. GIXD cannot "see" the lipid headgroups because only the acyl chain tails are ordered enough to diffract. Even then, because of acyl chain rotation and the lack of long range order, diffraction can only be observed from the entire lipid tail units and not from the individual atoms composing the lipid tails like in most materials. The fact that only acyl chains and not the individual atoms diffract causes monolayer and bilayer (but not multilayer) lipid membranes to only exhibit 2-Dimensional diffraction behavior; i.e. instead of observing cubic or orthorhombic unit cells, one would observe square or rectangular unit cells in a lipid membrane.

When GIXD is carried out, the incident X-rays approach the sample with a wavevector $\mathbf{k}_i$ at an angle α_i smaller than the critical angle for total reflection α_c. Because total reflection occurs, when the X-ray makes contact with the sample it creates an evanescent wave in the top ~10 nm of the sample instead of penetrating deeper. This means that the technique is extremely surface sensitive and able to measure only the top 10 nm of a sample, which is extremely useful for studying lipid membranes (bilayers are approximately 5-7 nm thick). The X-rays then diffract off the Miller planes within a sample with a new wavevector $\mathbf{k}_f$. The difference between $\mathbf{k}_f$ and $\mathbf{k}_i$ is called the wavevector transfer, denoted by $\mathbf{q}$. $\mathbf{q}$ can then be further divided into the in-plane and out-of-plane wavevector transfers, $\mathbf{q}_{xy}$ and $\mathbf{q}_z$ respectively. $\mathbf{q}_z$ is related to the out of plane angle as shown in the X-ray reflection

section, while $\mathbf{q}_{xy}$ is related to the in-plane 2θ angle used in standard X-ray diffraction experiments by (with λ as the X-ray wavelength):

$$q = \frac{4\pi}{\lambda} sin(\theta)$$

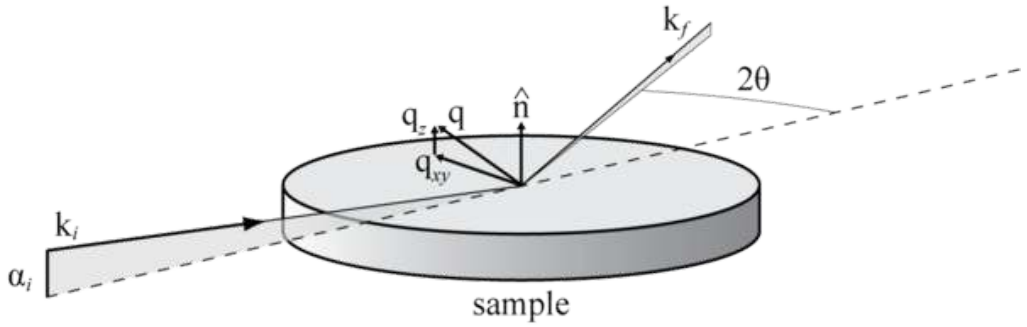


Figure 5.13.9: Schematic of an incident X-ray beam diffracting off a sample in a GIXD experiment [16]

After the beam is diffracted, the resulting diffraction pattern is collected by an X-ray sensor and the background noise is subtracted (which can, in some cases, be extremely difficult). Once the background is subtracted, a pattern similar to the one below can be analyzed.

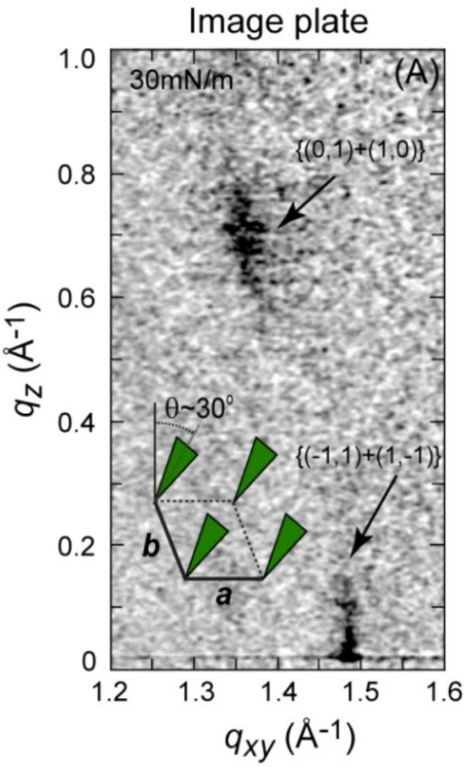


Figure 5.13.10: A background subtracted GIXD diffraction pattern. This diffraction pattern has two visible diffraction peaks [17]

To analyze the pattern, it is integrated over q_z to create the Bragg peak spectrum and integrated over q_{xy} to create the Bragg rod spectrum [17]. However, it is important to note that compared to a standard X-ray diffraction pattern, a GIXD image plate only covers an extremely small fraction of the 2θ spectrum, and thus very few peaks are generally observed.

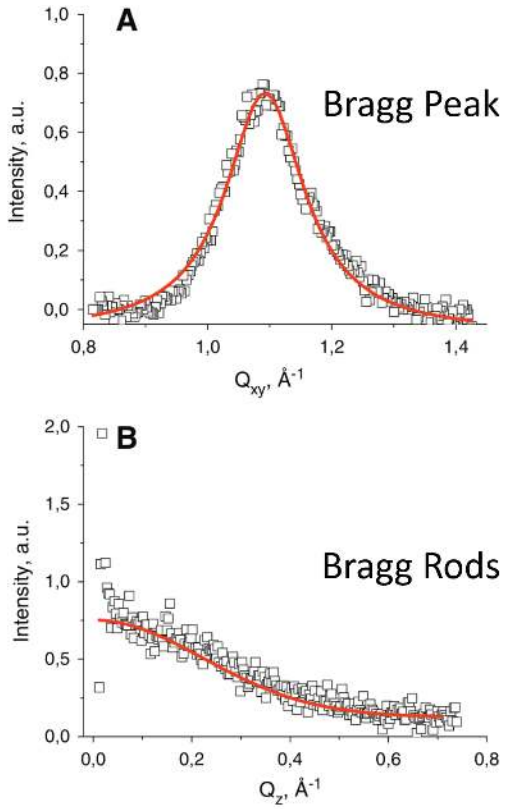


Figure 5.13.11: The Bragg peak and Bragg rods from a sample with just one visible diffraction peaks [18]

The Bragg peaks can be indexed using Bragg's law or another standard method (such as an Ewald sphere) of analyzing diffraction patterns. Bragg rods for lipid membranes are generally more difficult to analyze directly and are investigated by making a model of the diffracting structure which includes the acyl chain tilt) and measuring how well the predicted diffraction from the model matches the observed Bragg rod pattern. From these methods, the symmetry and size of the unit cell can be calculated.

In addition, the in-plane coherence length L_c, which is a measure of how far the short range crystalline order extends, can be calculated using the full width half max (fwhm) of the Bragg peak:

$$L_c = \frac{2\pi}{fwhm}$$

Neutron Reflectivity

Neutron scattering generally follows the same mathematics and experimental methods as X-ray scattering. However, the basic principle of it and therefore the information it can extract is slightly different, because instead of scattering off the electrons in a sample, neutrons scatter off the atomic nuclei in a sample.

Therefore neutrons, unlike other common scattering sources, will interact differently with separate isotopes of the same atom. This is especially evident for hydrogen and deuterium, which is convenient because all the organic molecules normally present in a biological membrane have many hydrogen groups. Thus, it is common to label proteins, water, or other items of interest with deuterium and use neutron reflectivity to find their location in the membrane [5].

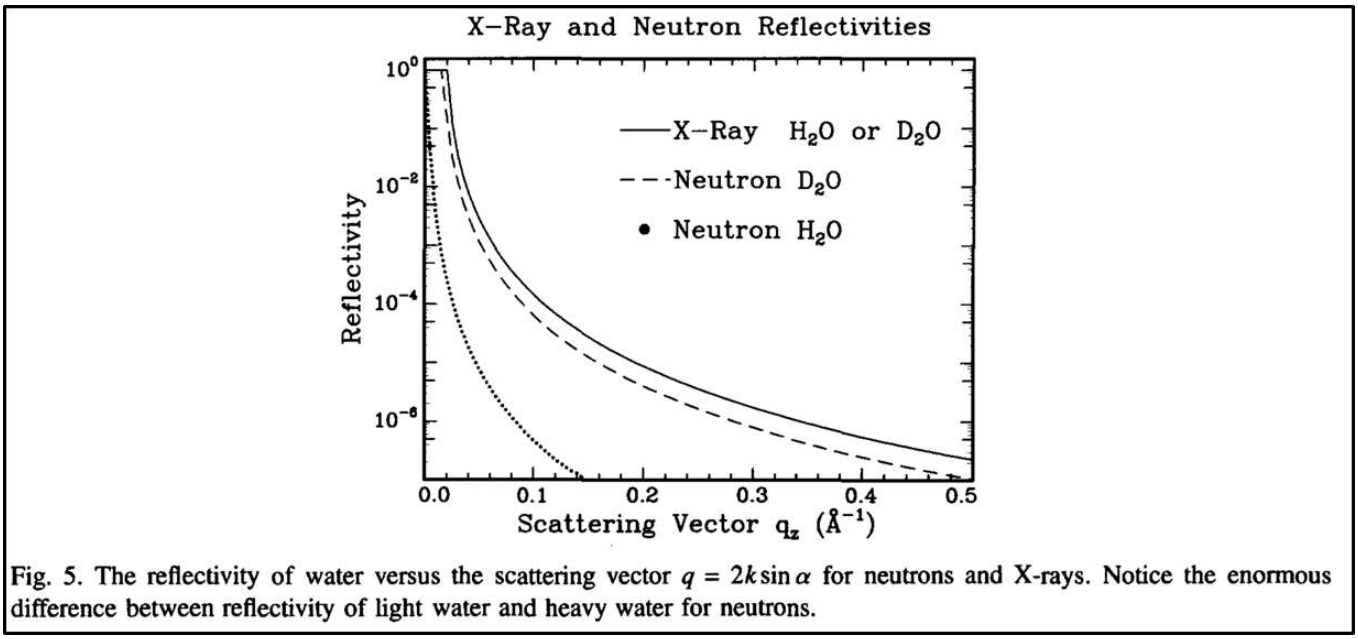


Fig. 5. The reflectivity of water versus the scattering vector $q = 2k \sin \alpha$ for neutrons and X-rays. Notice the enormous difference between reflectivity of light water and heavy water for neutrons.

Figure 5.13.12: The difference between the dotted line and the segmented line show the extreme difference between the neutron scattering lengths for hydrogen water and deuterium water (scattering length is an important factor in determine the reflected intensity). Meanwhile X-rays, represented by the solid line, show no observable difference in scattering between hydrogen water and deuterium water.

One of the common types of studies neutron reflection is used for is to determine how viral proteins can break through cell membranes. By using deuterium water on one side of the membrane and hydrogen water on the other side of the membrane, scientists can observe as the water slowly makes its way across the membrane as more proteins are added [21]. This is a good example of how neutrons are generally used to observe very specific phenomena, usually through deuterium labeling.

Unfortunately, one of the most difficult obstacles associated with neutrons is that neutron sources are very low intensity. This generally means it takes much longer to run neutron scattering experiments than equivalent X-ray scattering experiments. However, it also makes neutron diffraction experiments on lipid membranes extremely difficult and current membrane neutron diffraction experiments are extremely rare and can only use multilayer lipid model membranes; these types of membranes have much stronger diffraction signals than monolayers or bilayers [6].

Beam Sources

Membrane scattering techniques all require some type of wave or particle, such as a beam of X-rays or neutrons, to be accelerated towards a sample. It's effect is then measured and this is how the properties of the sample are determined. Often understanding the sources of the particles or waves is often an integral part of understanding the experimental method.

X-ray Sources

Because X-rays scatter off electrons and most lipid membranes consist almost entirely of lighter elements, meaning they have a low electron density, it can be difficult to get a significant signal to noise ratio with X-ray scattering on lipid membranes. Therefore, it is very common to use synchrotron X-ray sources so that, by using a much higher X-ray intensity, it will be easier to determine the meaningful data from the background noise. In addition to having an extremely high X-ray intensity (meaning a high flux of X-ray photons), these also have the advantage of variable photon energies. In addition, and also due to the high intensity, synchrotrons are able to finish experiments much faster than other X-ray sources. [1]

Synchrotrons, which are huge facilities with their electron storage rings often on the order of a kilometer in diameter, operate by accelerating electrons or positrons to nearly the speed of light and then forcing them to oscillate. In the process of oscillating, the electrons emit X-rays that can be monochromated (usually by diffraction from germanium single crystal) and then focused on the sample using X-ray optics.

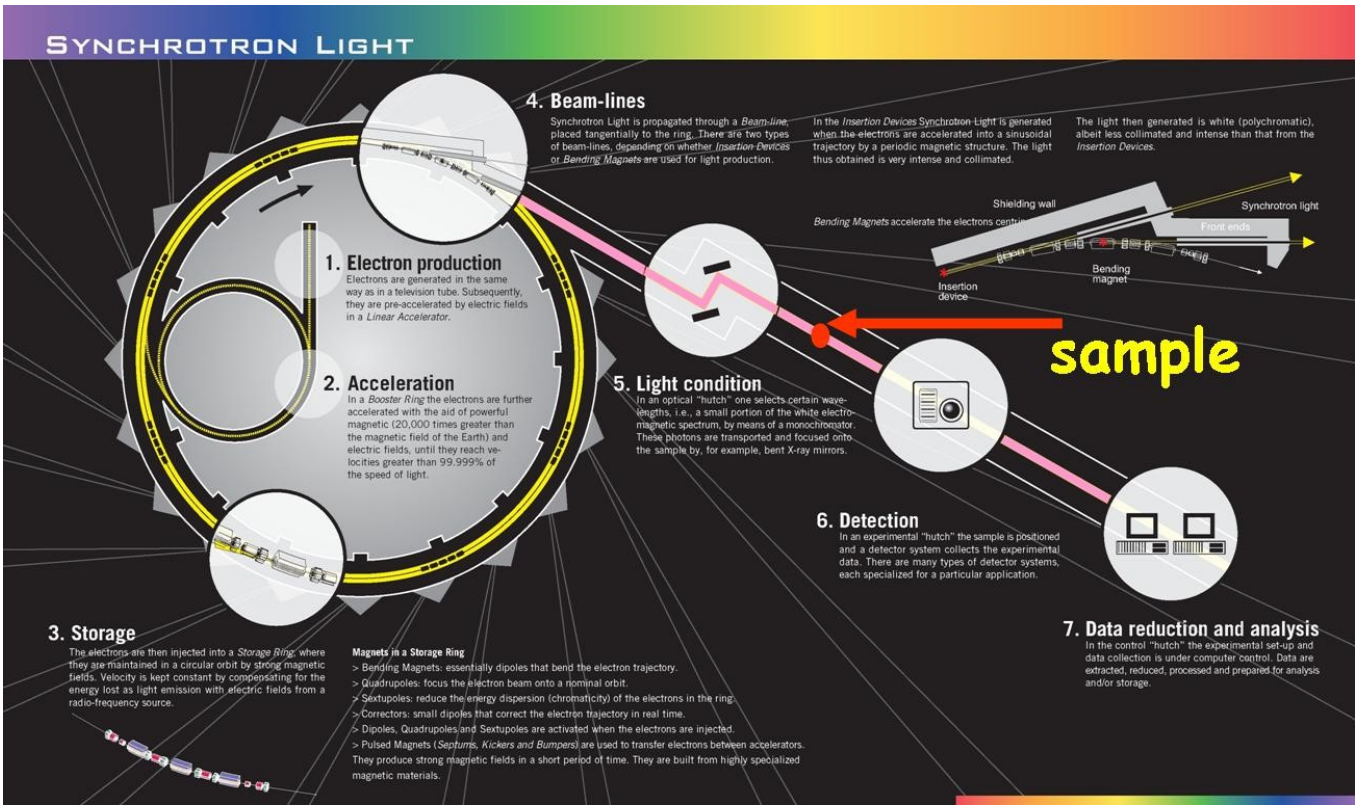


Figure 5.13.13: An explainer covering the basic functioning of synchrotrons published by the Spanish synchrotron lab ALBA [14]

For membrane reflectivity experiments that don't need a high intensity of X-rays, rotating anode or liquid anode X-ray sources can also be useful (however, previous generations of X-ray sources such as standard sealed tube X-ray sources may not have high enough intensities). For example, a monolayer X-ray reflectivity measurement could likely be carried out with one of these because monolayers give a relatively large signal to noise ratio and their sample chambers have very small X-ray absorption rates.

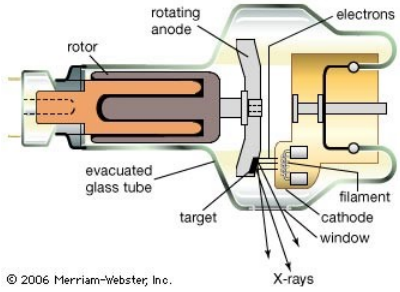


Figure 5.13.14: Schematic of a rotating anode X-ray source. [15] Making these devices reliable was a technological leap in the mid 1900's because not only did the inner chamber need to be at high vacuum, but it also has lubricated moving parts.

Neutron Sources

Neutrons for characterization are produced via one of two methods: nuclear fission reactions or spallation. Nuclear fission sources are the older generation, and operate similarly to a nuclear fission reactor: a heavy, radioactive element is fissioned in a chain reaction that eject neutrons from the atomic nuclei, and this chain reaction is moderated (slowed/controlled) by heavy water. In a fission source, the wavelength (energy) of the incoming neutrons is controlled by the temperature of the moderating medium. [12]

Spallation sources are now preferred over neutron sources because they have a much higher neutron intensity (number of neutrons emitted from a source) than the fission sources and can be much more easily controlled; while a uranium fission source emits 3 neutrons per event, a spallation source can emit 20-30 per event! Because one of the major limitations for neutron scattering is the low source intensity, this newer generation of neutron sources is an important step on the way to making neutron scattering experiments more widely applicable. In spallation, metal targets are bombarded by high energy protons, and every time a nucleus breaks down it releases neutrons in a spallation event. Because of the much higher intensity of neutrons produced by spallation sources, monochromators or time of flight filters (wavelength filtering techniques) can be used to limit the source to a very narrow

wavelength distribution, which is very helpful for scattering experiments (a higher intensity source is needed because intense filtering can greatly decrease the intensity of a beam).

In addition, something to be aware of when using a neutron scattering facility is that neutrons have the potential to make your sample radioactive. If the sample has a high enough radioactivity, the lab the neutron source is located at may deem it unsafe to handle and will either wait for a period of months to years to return it or destroy it as radioactive waste.

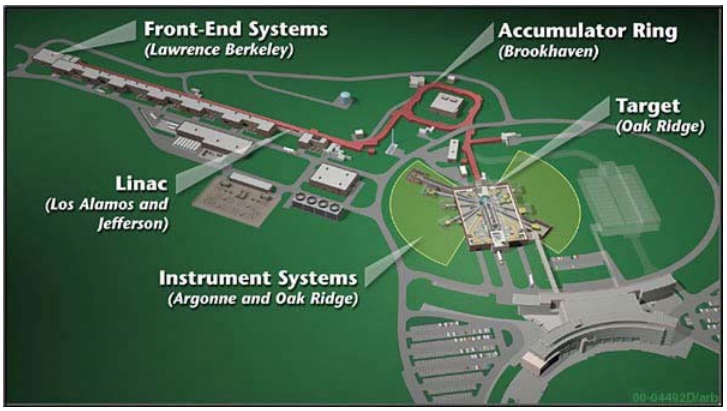


Figure 5.13.15: Spallation Neutron Source (SNS) facilities layout with tags of National Labs responsible for building each section. The front-end systems are responsible for generating the protons, and the Linac accelerates them to a fraction of the speed of light. The high energy protons are then kept in the accumulator ring until they are needed to be directed towards the spallation target. Once the protons hit the spallation target, neutrons are produced which can be used to study samples using a variety of different instrument systems known as beamlines [13]

Further Reading

For a deeper look into X-ray and neutron scattering, there are three main sources that were the most important sources of information for this work.

The first is reference [1], 'Elements of Modern X-ray Physics', by Als-Nielsen et al. It is a comprehensive book on X-ray scattering and diffraction using synchrotron sources and touches on neutron theory as well.

The next is a large review article [7], again by Als-Nielsen et al., 'Principles and applications of grazing incidence x-ray and neutron scattering from ordered molecular monolayers at the air-water interface.' While being much shorter than a book, this article is still a fairly comprehensive review of the subject.

The last is by Kjaer [8], and is an incredibly abbreviated introduction to X-ray scattering and reflectivity, and would be most useful for those already familiar with the concept of an inverse lattice.

Best of luck to all in your further studies!

Note to further contributors

For all future contributors, please continue posting descriptions of even more membrane scattering techniques. There are still a lot of membrane scattering methods left to describe.

References

1. J. Als-Nielsen, D. McMorrow, *Elements of Modern X-Ray Physics*, Wiley (2001), p. 83.
2. Watkins, Erik B., et al. "Equilibrium or quenched: fundamental differences between lipid monolayers, supported bilayers, and membranes." *ACS nano* 8.4 (2014): 3181-3191.
3. Gözen, Irep, and Aldo Jesorka. "Instrumental methods to characterize molecular phospholipid films on solid supports." *Analytical chemistry* 84.2 (2012): 822-838.
4. Lösche, Mathias. "Surface-sensitive X-ray and neutron scattering characterization of planar lipid model membranes and lipid/peptide interactions." *Current topics in Membranes* 52 (2002): 117-161.
5. Zheng, Songyan, et al. "Structural studies of the HIV-1 accessory protein Vpu in Langmuir monolayers: synchrotron x-ray reflectivity." *Biophysical journal* 80.4 (2001): 1837-1850.
6. Harroun, T. A., et al. "Neutron diffraction and Vitamin E." *Journal of Physics: Conference Series*. Vol. 251. No. 1. IOP Publishing, 2010.

7. Als-Nielsen, Jens, et al. "Principles and applications of grazing incidence x-ray and neutron scattering from ordered molecular monolayers at the air-water interface." *Physics Reports* 246.5 (1994): 251-313.
8. Kjaer, Kristian. "Some simple ideas on x-ray reflection and grazing-incidence diffraction from thin surfactant films." *Physica B: Condensed Matter* 198.1-3 (1994): 100-109.
9. Villarreal, Marina Ruiz; username: LadyofHats. File: Phospholipids aqueous solution structures.svg; Wikimedia Commons. 6 November 2007. commons.wikimedia.org/wiki/File%3APhospholipids_aqueous_solution_structures.svg
10. Alessandrini, Andrea, and Paolo Facci. "Phase transitions in supported lipid bilayers studied by AFM." *Soft matter* 10.37 (2014): 7145-7164.
11. Ciumac, Daniela. “Langmuir Trough.” SNAL Marie Curie ITN Network. 28 Oct. 2014. Accessed: 7 Jun. 2017
12. Kovnir, Kirill. “Lecture 7: Neutrons, TEM.” Chemistry 217. UC Davis, California. 5 Aug. 2017
13. Username: Horakcm. File: Sns-facility-design.jpg; Wikimedia Commons. 3 Nov. 2011
14. “What is a Synchrotron.” ALBA. Accessed: 7 Jun. 2017. Retrieved from https://intranet.cells.es/AboutUs/WhatIs
15. Usernames: Mohamed.ah; drewhunt *et al.* “Physics of The X-ray Tube.” 13 Oct. 2012. Accessed 7 Jun. 2017
16. Username: Jaknelaps. File: Grazing incidence diffraction GIXD.png; Wikimedia commons. 7 April 2014. commons.wikimedia.org/wiki/File:Grazing_incidence_diffraction_GIXD.png
17. Watkins, Erik B., et al. "Equilibrium or quenched: fundamental differences between lipid monolayers, supported bilayers, and membranes." *ACS nano* 8.4 (2014): 3181-3191.
18. Wydro, Paweł, Michał Flasiński, and Marcin Broniatowski. "Grazing Incidence X-ray Diffraction and Brewster Angle Microscopy studies on domain formation in phosphatidylethanolamine/cholesterol monolayers imitating the inner layer of human erythrocyte membrane." *Biochimica et Biophysica Acta (BBA)-Biomembranes* 1828.6 (2013): 1415-1423.
19. Kjaer, Kristian. "Some simple ideas on x-ray reflection and grazing-incidence diffraction from thin surfactant films." *Physica B: Condensed Matter* 198.1-3 (1994): 100-109.
20. Graber, Z. T., et al. "Competitive cation binding to phosphatidylinositol-4, 5-bisphosphate domains revealed by X-ray fluorescence." *RSC Advances* 5.129 (2015): 106536-106542.
21. Choi, D., et al. "Insertion mechanism of cell-penetrating peptides into supported phospholipid membranes revealed by X-ray and neutron reflection." *Soft Matter* 8.32 (2012): 8294-8297.

5.13: Membrane X-ray Scattering is shared under a CC BY 4.0 license and was authored, remixed, and/or curated by LibreTexts.

CHAPTER OVERVIEW

6: Experimental Characterization - Mass Spectrometry and Atomic Force Microscopy

6.1: Atomic force microscopy (AFM) on Membranes
6.2: Mass Spectrometer Ionization Techniques for Membrane Proteins
6.3: Electrospray Ionization (ESI) Mass Spectrometry
6.4: Mass Analyzer Orbitrap
6.5: Mass Analyzer - Time of Flight

6: Experimental Characterization - Mass Spectrometry and Atomic Force Microscopy is shared under a CC BY 4.0 license and was authored, remixed, and/or curated by LibreTexts.

6.1: Atomic force microscopy (AFM) on Membranes

Atomic force microscopy (AFM) is a technique with multiple applications in biology. This method is a member of the broad family of scanning probe microscopy and was initially developed in 1986 by Binnig et al to overcome the disadvantages of the scanning tunneling microscopy (STM) [1]. In the case of STM, only conductive materials can be studied as the resolution is obtained by using a tunneling current between a sharp probe and the sample surface[1]. In contrast, AFM uses small forces on the surface by a probe, thus do not damage samples and can provide information of surface topography of biological materials. AFM soon attracted the attention of the biophysical scientists in biomembrane as well as synthetic membrane research due to its capability of observing biological molecular system with resolution on nanometer scale and its possibility of three dimensional imaging [2].

Fundamental Elements of AFM

An atomic force microscope consists of a flexible cantilever containing a sharp probe, laser, photodiode detector, piezoelectric scanner and feedback electronics [3]. The microscope obtains the surface topography by scanning the tip in gentle touch with the sample. The tip motion is monitored by the piezoelectric scanner. As the tip scans the sample, the forces between the tip and the sample surface cause the cantilever to bend. A photodiode detector detects the deflection of a laser beam reflected off the back of the cantilever onto a two- segment photodiode. In most operating modes, a feedback circuit connected to the cantilever deflection sensor keeps the interaction between the tip and the sample at a fixed value and controls the tip-sample distance. The feedback signal is recorded by a computer to reconstruct a 3D image of the surface topography.

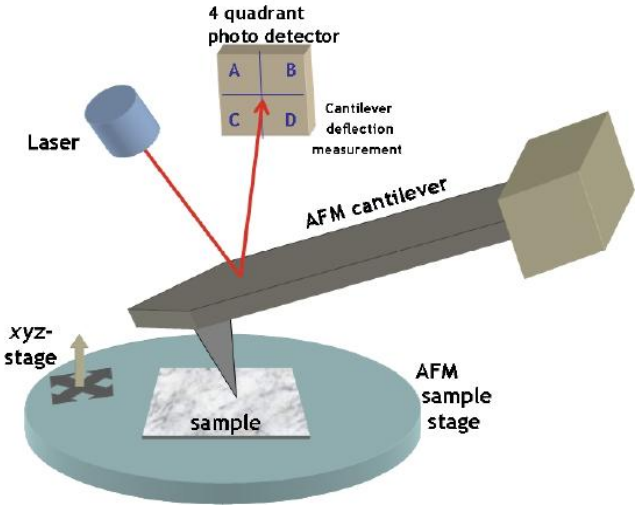


Figure 6.1.1: Typical atomic force microscope (AFM) setup: The deflection of a microfabricated cantilever with a sharp tip is measured by reflecting a laser beam off the backside of the cantilever while it is scanning over the surface of the sample. (CC-BY-2.5,; Opensource Handbook of Nanoscience and Nanotechnology).

The force between the probe and the sample surface depends on the spring constant (stiffness of the cantilever) and the tip-sample distance). The amount of force is calculated based on Hooke's law:

$$F = -kx \tag{6.1.1}$$

- F: Force
- k: spring constant
- x: cantilever deflection.

Imaging modes

There are three primary imaging modes in AFM: contact, non-contact and intermittent (tapping) mode [4]. During contact mode, the probe is in contact with the sample and repulsive Van der Waals forces prevail, whilst attractive Van der Waals forces are dominant when the tip moves further away from the sample surface [5].

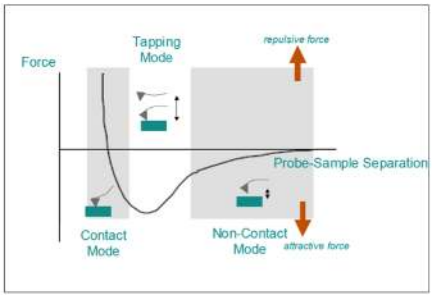


Figure 6.1.2: Force as a function of probe-sample separation [5]

Contact Mode

In contact mode, the tip is constantly in touch with the sample surface. The applied force is kept constant while the tip scans the surface, creating the surface image [4]. This imaging mode is good for samples with rough and rigid surfaces as it provides fast scanning with high resolution. One disadvantage of this imaging mode is that soft samples like tissues can be deformed or damaged due to the applied force. This drawback can be solved by measuring the sample in aqueous environments to reduce the interaction force between the tip and the sample.

Tapping Mode

In tapping mode, the tip is not in constant contact with the sample surface. Instead, the cantilever is oscillated at its resonant frequency, which makes the tip lightly tap on the surface during scanning. A constant tip-sample interaction is maintained by monitoring the oscillation amplitude and an image is obtained [4]. Several parameters that affect the image contrast are the height, phase signals and amplitude [6]. Phase signals are influenced by material properties of the sample, for example viscoelasticity [6]. The force during scanning is greatly reduced, therefore this mode is useful for biological samples, where the samples are easily damageable or loosely bound to their surface. However, this imaging mode requires a slower scanning speed and is more challenging to measure in liquids.

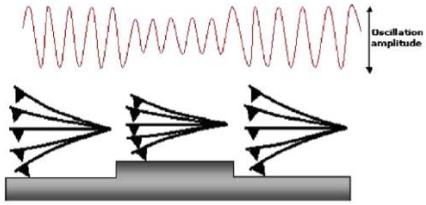


Figure 6.1.3: A schematic representation of AFM operating in tapping mode [4]

Non-contact mode

There is no contact between the sample surface and the probe in non-contact mode. The probe oscillates above the sample surface, forming a weak attractive force between the tip apex atom and the sample surface atom. Feedback signals are obtained by measuring a frequency shift in the mechanical oscillation of the cantilever [6].

The force exerted on the surface sample is very low in this case. Moreover, as there is no contact between the probe and the surface, the probe lifetime can be extended. Another advantage of this operating mode is the possibility to observe an atomic defect if the very weak attractive force can be detected. The drawback of this mode is the reduction of resolution, and the oscillation of the cantilever is affected in case there are contaminants on the sample surface. Usually this operation mode requires a careful control of the environment (in UHV) to carry out [7].

Cantilever and Tips

The scanning probe is an important component of the AFM. The dimensions of the cantilever are in micrometer range, while its tip has a radius of a few nanometers [4]. Different cantilever lengths, shapes and materials lead to various spring constants and resonant frequencies. The most common materials of the probes are silicon nitride (Si_3N_4) or silicon (Si) [5]. Figure 6.1.4 shows a scanning electron microscope (SEM) image of a silicon nitride (4a, 4b) and silicon (4c, 4d) cantilever chip, where a tiny tip having a pyramid shape is integrated at the end. The silicon nitride probe is often used in static contact mode, where the stiffness of the cantilever should be as low as possible [4]. The silicon probe is usually used in dynamic operation mode, which requires higher values for the spring constant to reduce noise and instabilities [4].

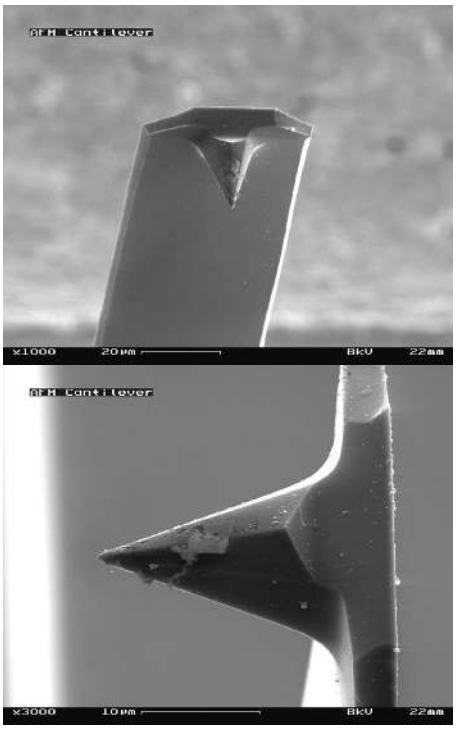


Figure 6.1.4: SEM images of microfabricated cantilever and tips. Electron micrograph of a used AFM cantilever. Image width ~100 micrometers (right) Image width ~30 micrometers. Images used with permission (CC BY-SA 3.0; Wikipedia).

Typically, spring constants of AFM cantilevers vary between 0.01 Nm^{-1} and 100 Nm^{-1}, enabling a force sensitivity of 10-11N [4]. The force sensitivity is influenced by thermal, electrical and optical noise. [5] For biological samples, cantilevers in contact mode often have resonance frequencies between 5 and 50 kHz in vacuum [8]. Figure 6.1.5 reports an AFM tip made of carbon nanotubes (CNTs), which was a breakthrough in terms of resolution. CNTs tips have a high aspect ratio, small diameter, and a well-defined surface chemistry, therefore appearing to be the ideal probe for biological applications [4].

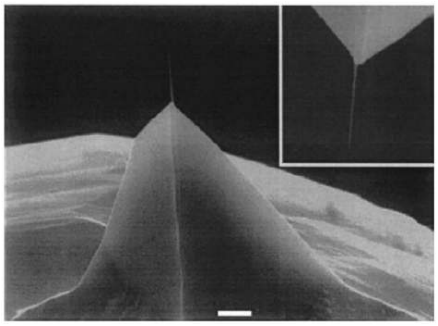


Figure 6.1.5: Multiwall CNT tip attached to the end of single crystal silicon tip. Inset: higher magnification view of the same tip rotated 180^0 relative to the main image. Scale bar is 1µm [4]

AFM on membranes

Native membranes studied by AFM

Biomembrane sample preparation

In order to study membranes using AFM, the membranes need to be fixed on a flat solid support [8]. Several solid supports such as mica, highly ordered pyrolitic graphite (HOPG), template stripped gold and molybdenum disulfide have proved to give high resolution images [6, 8]. While mica is an insulator and exposes a hydrophilic surface, HOPG is a good conductor and hydrophobic [8]. The similarity between these two substrates is an atomically flat surface [8]. Based on chemical adsorption mechanism, membranes are attached onto the solid support by adjusting pH and ionic strength. As the gap between membrane and the support is very small (0.5-2nm), this may cause impaired mobility for membrane proteins that are directly attached to the support [6].

Furthermore, the adsorption force may affect the conformation of the membrane proteins. To sum up, current sample preparation methods still need further consideration in order to study dynamics and structure of native membrane proteins.

AFM images of native membrane

AFM can obtain the images of native membranes at submolecular resolution, which is a great advantage comparing to other methods [6]. It is effective in providing information of the native organization of membrane proteins and their complexes. Figure 6.1.6 shows an example of the study of native membrane using AFM. Disk membranes were prepared from mouse retina and then attached on mica support [6]. The AFM image revealed tight rows of dimers packed in the structure arrangement of rhodopsin [6]. This provides a platform for interaction with arrestin and transducin.

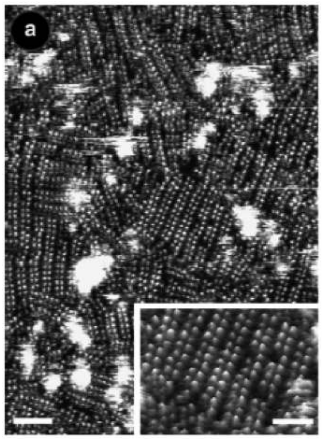


Figure 6.1.6: Topograph of native membranes.: Murine disc membranes shows tight packing of native rhodopsin. Most of the rhodopsins are arranged as dimers that form extended rows. Scale bar :10nm, inset: 5nm [6]

Model lipid membranes studied by AFM

Preparation of supported lipid bilayers.

Supported lipid bilayers (SLBs) have been used as a biomimetic model for biomembranes in numerous studies [3, 9]. This system consists of two lipid leaflets spread on a solid support [3]. Although this model lacks some features of the real membranes, it still provides an insight of the structural organization and characteristics of cell membranes. The first method to prepare SLBs is the fusion of lipid vesicles on solid supports [9]. The vesicles are prepared via sonication or extrusion, then adsorbed on the surface of the solid support. The adsorbed vesicles either form larger vesicles by fusing together, or directly rupture and form SLBs.

Another method is to use a hydrophilic substrate on which two consecutive lipid monolayers are deposited by Langmuir-Blodgett transfer [3]. A Teflon-coated trough contains the aqueous solution, with two movable Teflon barriers used to control the area for lipid spread and form a monolayer at the air-water interface. There is also a balance to measure the surface pressure, controlling lipid packing. The solid support is then pulled vertically through the lipid monolayer, depositing the first lipid layer on the substrate. The transference of the second lipid layer can be completed by dipping the lipid support either horizontally or vertically. This technique can be applied to fabricate SLBs having two different lipid composition.

AFM studies of SLBs formation.

SLBs formation process by fusing lipid vesicles on solid supports can be studied in situ by AFM technique, as illustrated in Figure 6.1.7. The vesicles spread from the edge towards the center, then stacked on top of each other. The edges of the top and bottom bilayers are joined together to form bigger patches.

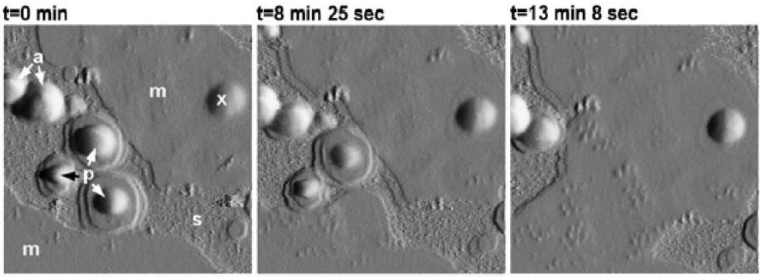


Figure 6.1.7: Series of AFM images demonstrating the formation of SLB on silica. (a) attached liposomes, (p) partially flattened liposomes, (m) lipid bilayers, (s) bare silica surface, (x) a liposome that does not change throughout imaging and appears to be trapped beneath the membrane. Image sizes are 1.67x1.67μm [9]

Different protocols to prepare multi-component and phase-separated SLBs can affect the asymmetry of the resulting SLBs. In Figure 6.1.8, the extruded small unilamellar vesicles (SUVs) composed of DLPC/DSPC are heated at 65^0C, then fused on mica at 20^0C. The resulting SLB are fully symmetric fluid/gel membranes. On the other hand, using sonicated SUVs heated at 20^0C prior to fusion results in a completely asymmetric SLBs.

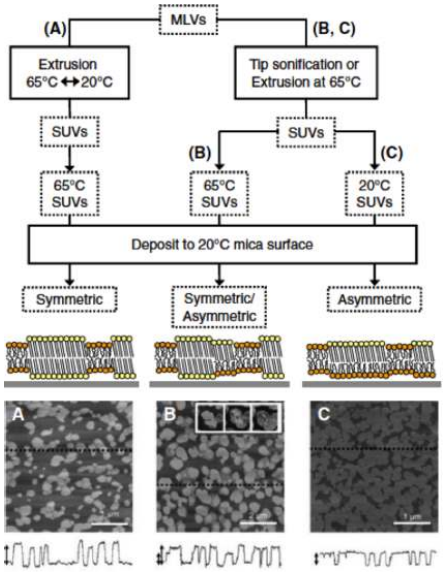


Figure 6.1.8: Different protocols to prepare DLPC/DSPC SLBs. The brighter color corresponds to a higher area. (A): The domain is approximately 1.8nm higher than the surrounding DLPC fluid phase. (B): the step high difference is 1.8 and 1.1nm. (C). The difference is 1.1nm. [3]

Summary

AFM is a powerful technique for scientists to have an insight in membrane biophysics. Advantages of this method including:

- The ability to image cell surfaces, molecular assemblies in their native aqueous environment at a very high resolution.
- No requirement of a conductive sample.
- Provide 3-D surface profiles.
- The ability to operate in liquid environment and ambient air.

Disadvantages of AFM are limited scanning area and the scanning speed.

Recently there have been some progress in improving AFM scanning speed and resolution, for example high speed AFM (HS-AFM) or high resolution AFM (HR-AFM) [10, 11]. HF-AFM consists of modified components in order to maximize scanning seed, for example soft small cantilevers having high resonance frequencies, high resonance frequency scanners and fast data acquisition devices [10]. AFM is also combined with several techniques such as fluorescence microscopy to acquire more efficient data [9]. The potential improvement of AFM will enhance the possibility to apply this technique in a wider range of biological fields.

References

1. Binnig, G., C. F. Quate, and C. Gerber, *Atomic force microscope.* Phys. Rev. Lett, 1986(56): p. 930–933.
2. D.J.Muller, Y.F.D., *Atomic force microscopy as a multifunctional molecular toolbox in nanobiotechnology.* Nat.Nanotechnol, 2008. **3**: p. 261-269.
3. Morandat, S., et al., *Atomic force microscopy of model lipid membranes.* Anal Bioanal Chem, 2013. **405**(5): p. 1445-61.
4. Alessandrini, A. and P. Facci, *AFM: a versatile tool in biophysics.* Measurement Science and Technology, 2005. **16**(6): p. R65-R92.
5. Bullen, R.A.W.a.H.A., *Lecture notes: Introduction to Scanning Probe Microscopy*
6. Frederix, P.L., P.D. Bosshart, and A. Engel, *Atomic force microscopy of biological membranes.* Biophys J, 2009. **96**(2): p. 329-38.
7. S. Morita, R.W., E. Meyer, *Noncontact Atomic Force Microscopy.* Springer, 2002. **1**.
8. Muller, D.J. and A. Engel, *Atomic force microscopy and spectroscopy of native membrane proteins.* Nat Protoc, 2007. **2**(9): p. 2191-7.
9. Goksu, E.I., et al., *AFM for structure and dynamics of biomembranes.* Biochim Biophys Acta, 2009. **1788**(1): p. 254-66.
10. Ando, T., T. Uchihashi, and N. Kodera, *High-speed AFM and applications to biomolecular systems.* Annu Rev Biophys, 2013. **42**: p. 393-414.
11. Bippes, C.A. and D.J. Muller, *High-resolution atomic force microscopy and spectroscopy of native membrane proteins.* Reports on Progress in Physics, 2011. **74**(8): p. 086601.

6.1: Atomic force microscopy (AFM) on Membranes is shared under a CC BY 4.0 license and was authored, remixed, and/or curated by LibreTexts.

6.2: Mass Spectrometer Ionization Techniques for Membrane Proteins

Mass spectrometry is a technique in which charged particles from a sample are analyzed in order to obtain structural and compositional information about the sample. Mass spectrometry is particularly relevant when studying proteins. With this instrument, the determination of protein structure, function, and interactions is possible. A mass spectrometer can also detect post translational modifications on complex mixtures, perform both quantitative and qualitative analysis, and monitor enzyme reactions, chemical modification, and digestion pathways.[1] To date, two main ionization methods are used for protein analysis, electron Ionization (ESI) and matrix-assisted laser desorption/ionization (MALDI). These two ionization methods will be detailed in this page along with methods used prior to these discoveries such as electron bombardment (EI) and fast atom bombardment (FAB). A few applications of Mass spectrometry for membrane protein analysis will also be covered.

Introduction to Mass Spectrometry

A diagram of a conventional mass spectrometer is depicted in Figure 6.2.1.

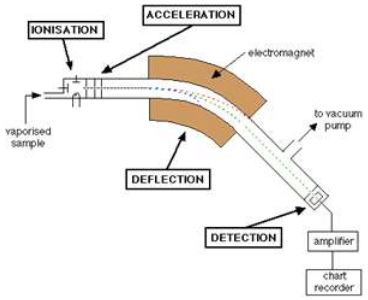


Figure 6.2.1. Conventional Mass spectrometer[2]

As shown, the mass spectrometer consists of a sample input, an ionization chamber, accelerator, defector, detector, and an amplifier. In brief, the sample of interest is injected into the mass spec and ionized to form charged particles. The charged particles are then accelerated by increasing the kinetic energy of the particles. As shown in the Figure, there are three plates with slits in the acceleration region; these plates all vary in potential allowing for the particles to increase in kinetic energy and form a finely tuned beam as they pass through each slit. This beam consists of a mixture of different ions before hitting the deflector. The deflector takes this mixture and separates the ions based on mass to charge ratio (m/z); this is done by applying a magnetic field. Figure 6.2.2 presents a diagram of what occurs in the deflector.

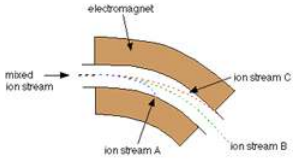


Figure 6.2.2. Deflector of a Mass spectrometer

Different ions interact differently with the magnetic field. In Figure 6.2.2 for example, the ions from steam B are ions that have a low m/z ratio. This means that the ions that compose this beam either have a low mass or a high charge or both. On the other hand ions from stream C hardly interact with the magnetic field applied; meaning they have a high m/z ratio. The ions in steam B, however, interact with the magnetic field in such a way that the ions pass through to the detector. The magnetic field can be altered to select a desired m/z range. For example, if one were to want to detect the higher mass ranges (steam C), the magnetic field would need to be larger in order to deflect the ions more. Equations 1 (Lorentz Force) and 2 (Newton's second law of motion) are crucial in understanding how partials move in an electric or magnetic field.

$$F = Q(E + v \times B) \tag{6.2.1}$$

$$F = ma \tag{6.2.2}$$

Where Q is the ion charge, F is the force applied on the ion, $v \times B$ is the cross product of the velocity and magnetic field, m is the mass and a is the acceleration.

Equating the two equations then gives the following differential (Equation 6.2.3)

$$(m/Q)a = E + vxB \tag{6.2.3}$$

Once the selected ions pass the deflector the ions travel towards a detector were there m/z is recorded. In short, when the ions strike the metal detector, a current from the movement of electrons is produced which can then be recorded as a signal. Because the electrons affected by this collision are typically very few, amplification of the signal is almost always necessary. Ions in the gas phase are typically very reactive and have a short lifetime thus it is important that the instrument in run in high vacuum (typically from 10^{-3} torr to 10^{-6} torr pressure).

There are several different mass spectrometers commercially available that tailor to different needs, such as quantifying data, qualifying data, protein sample analysis, small sample analysis, etc. Ionization techniques have been key to determining what types of samples can be analyzed by mass spectrometry.[3]

Hard and Soft Ionization

Before going into detail about the different ionizations methods it is important to understand two main categories that ionization falls under, hard and soft ionization.[4]

a. Hard ionization- hard ionization evokes larger amounts of energy to the sample of interest in order to ionize the sample. Due to the larger amount of energy the bonds within the molecule tend to break more, resulting in an increase in fragmentation. Hard ionization techniques typically yield in a larger number of lower mass fragments as oppose to higher mass.
b. Soft ionization- Soft ionization methods use smaller amounts of energy to ionize the sample, causing a decrease in fragmentation. This technique yields a larger amount of high mass fragments.

Electron Ionization (EI)

Theory

Electron Ionization (EI) was one of the first ionization techniques developed for mass spectrometry. [5] EI is a hard ionization method where a beam high-energy electron is used to bombard a sample of interest to produce multiple ions. As previously mentioned the use of high-energy particles leads to extensive fragmentation, which can be useful for structural characterization. A diagram of EI is shown is Figure 6.2.3.

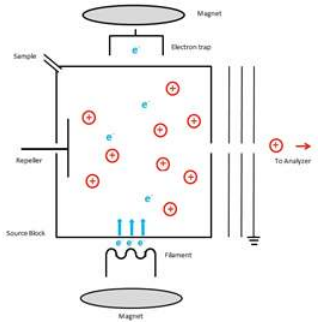


Figure 6.2.3. Electron Ionization (EI) [6]

As shown, the apparatus used to ionize molecules via EI consist of a source block, sample inlet, repeller, magnets, filament, electron trap, and an exit plat at ground potential. The source block is made out of metal heated to 300^0C to prevent the sample from condensing. The sample must first be introduced into the source block in the gas phase. This can be accomplished by either "boiling off" the sample from a probe via thermal desorption or by introducing of a gas through a capillary [7] . Once these neutral gas phase particles enter the source block, they are bombarded by a beam of electrons where the electrons excite the molecule and cause the molecule to eject an electron from the highest occupied molecular orbital (HOMO). This process results in ejection ionization and molecular fragmentation. The electron ionization process that occurs is described below: [5]

$$M + e^- \rightarrow M^{+\cdot} + 2e^- \tag{6.2.4}$$

where M is the analyte molecule, $e-$ is the electron, and $M^{+\cdot}$ is the resulting positively charged molecular ion.

The electron source (cathode) is typically a thin filament of tungsten or rhenium wire that is heated up to an incandescent temperature to produce electrons termed thermionic emission. These electrons must have enough energy to overcome the ionization energy of the sample molecules. A potential of 70 V is applied between the cathode and the source block in order to accelerate the electrons to 70 eV. At approximately 70 eV, the de Broglie wavelength of the electrons equals the length of a typical organic molecular bond. The energy transfer to organic analyte molecules is maximized thus leading to the strongest possible ionization

and fragmentation.[7] A slightly positive electron trap plate (anode) is placed at the opposite end of the source block. The excess electrons that did not participate in the ionization of the sample are collected here. A small magnetic field is applied parallel to the path of the electrons, by doing so the electrons travel in a helical path and thus increases their path length which in turn increases the probability of interaction between the sample and the electron. The resulting positive charged sample molecules are accelerated by the repeller into the accelerating region. By maintaining the exit slit at ground potential, the ions enter the mass analyzer at a fixed kinetic energy. [7]

The fragmentation and ionization process can be described using the Born Oppenheimer potential curves depicted in Figure 6.2.4.

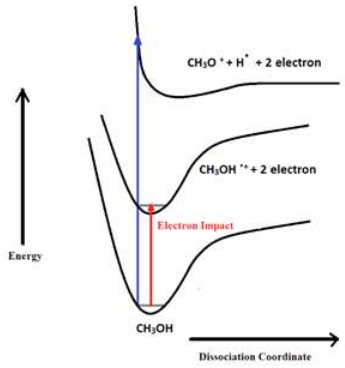


Figure 6.2.4. Born Oppenheimer potential curves [6]

The Figure shows the Born Oppenheimer potential curves of a methanol molecule before and after electron impact. The red arrow depicts the energy transition between the neutral molecule and the ionized molecule without sample fragmentation. However with this method this is typically not the case. Due to the high energy of the incident electron, dissociation of the molecule is more likely. The energy transition described is illustrated by the blue arrow.

Because this is a hard ionization technique, EI is good for polypeptide sequencing but it is very difficult to obtain information of large proteins and their interaction pathways. As we will later see, along with all ionization techniques come advantages and disadvantages.

a) Advantages

- High fragmentation can aid in molecular characterization
- Sample can be solid, liquid, or gas
- High fragmentation allows for a well defined fingerprint spectra
- Can be equipped to many different mass analyzers including time-of-flight, GC-MS, LC-MS etc.
- Fast and easy (typically first method of choice when screening samples) [5]

b) Disadvantages

- Characterization of large molecules is nearly impossible
- Sample must be volatile
- Multiple charges can result in very confusing mass spectra.
- Low mass ranges typically less than 600 Da. (Proteins can be in the kDa range)
- Extensive fragmentation can make it difficult to interpret data.
- Only positive ions are formed

Application to Proteins

Electron Ionization Mass Spectrometry (EI-MS) has be used in protein turn-over research. The rate of protein synthesis in human subjects is of great interest especially in this era were being "healthy" and "fit" and gaining lean muscle is of much interest. A study conducted in 1992 by Calder AG reports using EI-MS to determine the enrichment of amino acids incorporated into tissue protein during studies of human protein synthesis.[20] This was done by measuring the d-5 enrichment from the conversion of phenylalanine to phenylethylamine via EI-MS. The method of analysis proved to be very efficient for this task because detection of both free and protein-bound d-phenylalanine were detected simultaneously and only 1 mg of protein was needed to conduct the study.[20] However, EI-MS is not commonly used anymore for protein analysis because, since this is a hard ionization method, low mass ranges typically less than 600 Da are detected and Proteins are typically in the kDa range.

Fast Atom Bombardment (FAB)

Theory

Prior to the 1980s, EI was the main source of ionization for mass analysis. As previously discussed, one major limitation to all chemist and biochemists using this technique was the inability to ionize larger bioorganic molecules such as polypeptides. This limitation motivated scientist to develop new and improved ionization techniques that would allow for these larger molecules to be ionized and detected. Fast atom bombardment (FAB), MALDI, and ESI were all designed to circumvent this limitation. These techniques revolutionized biomolecular analyses.[7]Fast atom bombardment (FAB) is a soft ionization technique in which a sequence of high-energy atoms that strike a surface to produce ions. Figure 6.2.5 present a diagram of how FAB functions.

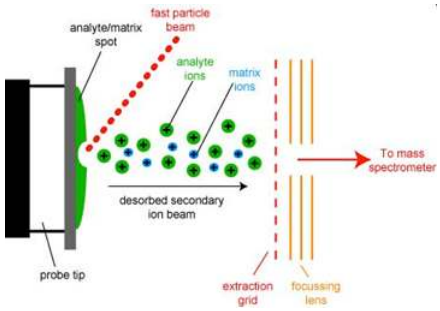


Figure 6.2.5. Fast Atom Bombardment [8]

As shown a stream of fast particles, typically an inert gas such as Argon or Xenon, bombards a sample of interest emitting analyte of various masses from the plum.

In its natural state, Argon and Xenon are relatively slow moving particles. In order to accelerate these molecules to be used as a beam source, the gas must first be ionized itself, this is done by colliding small particles or atoms. Once ionized, the gasses can then be accelerated to a certain potential. When in motion, these fast moving ions become neutralized by the dense cloud of excess natural gas surrounding them in the collision cell, this process in known as charge exchange. This process can be expressed below: [9]

$$Ar \rightarrow Ar^{+} + e^{-} \tag{6.2.5}$$

$$Ar^{+} \rightarrow Ar^{+}(\text{fast }) \tag{6.2.6}$$

$$Ar^{+}(fast) + Ar \rightarrow Ar(fast) + Ar^{+} \tag{6.2.7}$$

Because FAB is a soft ionization technique, most of these ions being ejected by the bombardment of these neutral inert atoms will have high masses. The sample itself is not just consistent of the analyte, like Matrix Assisted Laser Distortion Ionization that will be discussed later in this article; FAB uses a matrix to aid in ionization. FAB operates using a liquid matrix, where the sample and a large excess of matrix are mixed. The sample-matrix mixture is placed on a sample plate typically using an insertion probe. Having a liquid matrix services FAB by reducing damage made to the sample by the impact of the ion beam, constantly replenishing the surface with new sample after being bombarded with incident beam, and keeping the sample from aggregating. [10]Below is a list of factors to consider when selecting a matrix for a sample:

- The sample must be soluble in the matrix
- Matrix cannot react with sample ions
- Matrix must have low volatility under vacuum in order to maintain a liquid

One of the most commonly used liquid matrices for FAB ionization is glycerol and m-nitrobenzyl alcohol (NBA). [11] Once the sample is prepared and placed on the probe, the instrument is placed under high vacuum (typically from 10^{-3} torr to 10^{-6} torr pressure) to insure that no other molecules will contaminate the sample or react with the very reactive ions being produce. The sample is then irradiated with a continuous beam of high energy atoms (from 4000 to 10,000 electron volts) producing ions that can be analyzed using a mass spectrometer.[10] Listed below are advantages and disadvantages with using FAB as an ionization method.

a) Advantages

- · Because it is a soft ionization technique samples with large masses can be analyzed
- · Able to produce large biological samples such as small proteins, peptides, DNA, etc.
- · Can analyze polar, ionic, and thermally and energetically liable samples
- · Can be equipped to a quadruple

- · Allows for less complicated spectra because of its tendency to produce mostly singly charged particles.

b) Disadvantages

· Characterization using smaller fragments can be very difficult

- · Usually form single charged particles decreasing the effective range of the mass analyzers.
- · Low sensitivity compared to MALDI
- · Lower mass ranges compared to other Ionization techniques seen later in this report (~300-6000 Da)
- · Sample must be soluble in the matrix
- · Salt contamination can suppress molecular ion formation
- · Typically spectra have high chemical background

Applications to Proteins

Theoretically FAB would be very useful for protein membranes because, as previously mentioned, the matrix/sample mixture is typically glycerol and in this matrix the proteins would rise to the surface of the mixture. [21] Compounds at the surface of the matrix are readily ionizable.[21] However, many studies show an decrease in ion current with increase mass of sample, meaning large proteins (greater than 3000 Da) would be difficult to ionize. [21] Previously FAB has been used for the annalyis of large peptides and smaller proteins such as Proinsulin[23], glucagon[24], melittin[25], adrenocorticotropic hormone[26] and has also been used to sequence small peptides. [27]

Electrospray Ionization (ESI)

Theory

The need for a new and improved ionization method became apparent when scientist started studying proteins in greater depths. Before electrospray ionization, ionization methods such as fast atom bombardment were used to ionize small proteins. However, as previously discussed one great limitation in this ionization method is the inability to ionize large molecules such as large proteins at high yields. These limitations were circumvented when Fenn developed a technique known as Electrospray Ionization in 1989.[12] ESI is a soft ionization technique in which ions are ejected from charged vapor droplets to produce an aerosol. Figure 6.2.6 presents a diagram of an ESI probe.

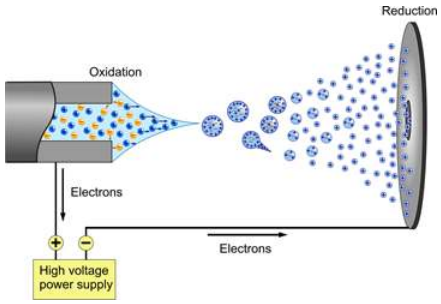


Figure 6.2.6. ESI Probe [13]

A dilute sample is introduced by a mechanical syringe pump through a hypodermic needle at low flow rate of typically 1–20 μL/min.[12] The capillary is typically heated to 100–300°C in order for the ions to be completely desolvated. As shown in the diagram above, a voltage (~4000 volts) is applied between the capillary containing the sample (left) and the sample plate (right). The voltage causes charge separation at the tip of the capillary. This charge separating and the full of the electric field on the positive ions overcomes the surface tension of the liquid thus forming a Taylor cone at the end of the capillary that contains an excess of charge. [14] The tipoff the cone being the least stable point, elongates into a liquid filament. For the case above (Positive Ion Electrospray), the positively charged ions are arranging at the tip of the Taylor cone. This cone is formed to relieve columbic repulsion at the capillary tip once Rayleigh limit of surface tension is reached. From this cone a stream of droplets form. As the droplets travel to the sample plate the solvent in the droplet starts to evaporate. This process can be aided by using an inert gas such as N_2 to help nebulize the droplets. As the solvent evaporates the charge density becomes more concentrated and in turn causes like charges to repel each other (Coulombic effect). This effect can be described using Equation 4 (Coulombs law).

$$E = \frac{q}{4\pi\varepsilon_0 R^2} = \frac{N_e}{4\pi\varepsilon_0 R^2} \quad (4)$$

where R is the droplet radius, q the charge and N is the number of elementary charges e.

The repulsion of these charges causes and increases in surface tension of the droplet; when the droplet can no longer hold, the Rayleigh limit is exceeded.[15] This process reoccurs as more solvent evaporates within each droplet until the individual ions reach the sample plate; by this point all ions should be separated, this process in known as the Dole charge residue model. Equation 5 describes the maximum charge a droplet can carry before the Rayleigh limit of surface tension is reached.[16]

$$q = 8\pi * r\sqrt{\varepsilon_0 \gamma * r} \quad (5)$$

Where q is the droplet charge at the Rayleigh instability limit, r is the droplet radius, ε_0 is the electric permittivity of the surrounding medium, γ is the surface tension and σ is the surface charge density.

However, there is another theory as to what happens when a droplet is traveling to the sample plate, known as the Iribarne Thompson ionization theory. Here, it is said that a point is reached in which the repulsion between the ions is so great that it is thermodynamically unstable for the ions to stay together and thus it is favorable for hydrated ions to be liberated from the droplet into the gas phase. When the droplet travels to the sample plate the radius of the droplet becomes smaller and smaller due to the evaporation of the solvent. Iribarne Thompson ionization theory states that there is a point where the radius is so small (less than 10nm) that the ion emission dominates over Rayleigh fission. [14] This process does not require that a very small droplet contains only a single ion as seen in the Charge Residue model.[12] Iribarne Thompson ionization theory states that the using Equation 6.[12]

$$k_1 = \frac{k_b T}{h} exp(-\frac{\Delta G^\dagger}{RT}) \quad (6)$$

Where k_1 is the rate of ion evaportation, k_b is the Boltzmann constant, T is the temperature of the droplet, h is the Planck constant, and $\Delta G\dagger$ is the free energy of activation.

.Common solvents used in ESI include a mixture of water with a volatile organic compound such as methanol. In order to decrease the initial droplet size small amounts of acetic acid is commonly added. It is important to have the correct solvent in order to optimize the ionization yield of the gas molecules. As previously mentioned, a Taylor cone is formed at the end of the capillary tip that is formed from overcoming of the surface tension of the liquid. The electric field required to onset the Taylor cone providing a steam of droplets is described using Equation 7. [14]

$$E_0 = \sqrt{\frac{2\gamma cos\, 49^0}{\varepsilon_0 r_c}} \quad (7)$$

where γ is the surface tension of the liquid, cos 49° is the half-angle of the Taylor cone, ε_0 is the permittivity of vacuum, and r_c is the radius of the capillary.

Notice the dependency of the surface tension of the liquid on the electric field. Liquids with high surface tensions will require higher electric fields.

The ionization of the ions in the charged droplet is dependent on the presence of charges that comes from the separation of positive and negative electrolyte ions in the Taylor cone. Thus, it can be said that concentrations of these electrolytes play a great role in optimizing the ionization of molecules. It has been shows that a minimum concentration of 10^{-5} M concentration is required.

Along with all ionization techniques, ESI comes with advantages and disadvantages to using this technique.

c) Advantages

- · Because it is a soft ionization technique samples with large masses can be analyzed
- · Able to analyze large biological samples such as proteins, peptides, DNA, etc.
- · Can be equipped to a quadruple, ion trap, and liquid chromatography
- · No matrix interference or limitation
- · Multiple charging allows for analysis of high mass ions with a relatively low m/z range instrument

d) Disadvantages

- · Characterization using smaller fragments can be very difficult
- · Difficulty with analyzing mixtures
- · Multiple charges can result in very confusing mass spectra.
- · Low-high mass ranges typically less than 200,000 Da.
- · Does not work well for non volatile salts (buffers)
- · Not useful for non-polar compounds

Applications to Proteins

ESI is a very common and useful tool for protein analysis mainly because it is able to ionize proteins without denaturing them, meaning non-covalent, receptor ligand complexes remain intact. This is because ESI allows for multiple charge states, meaning

large proteins can be ionized and detected allowing ESI to be used for a wide range of applications.Characterization of Hemoglobin variants in blood have always been of interest in the clinical setting; however in the past it was very time consuming and challenging with other methods . With ESI-MS it is now possible to analyze over 250 samples in no more than 2 days. [28] ESI is also commonly used for amino acid profiling in order to detect major diseases such as phenylketonuria , maple syrup urine disease, homocystinuria, and galactosaemia. [28]

Matrix Assisted Laser Distortion Ionization (MALDI)

Theory

Matrix-assisted Laser Desorption/Ionization (MALDI) along with electrospray ionization, are now among the leading ionization methods for nonvolatile, high molecular weight compounds. MALDI specifically has been widely used to analyze, nonvolatile biomolecules, in particular peptides, proteins, oligonucleotides, and oligosaccharides. [17]

MALDI is a soft ionization technique in which a laser energy-absorbing matrix is used to create ions. Figure 6.2.7 presents a diagram of how MALDI functions.

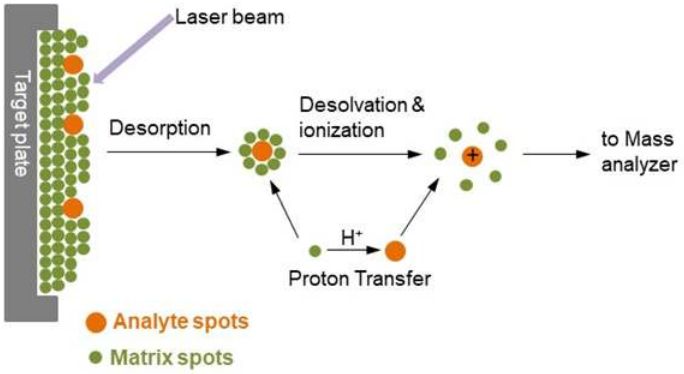


Figure 6.2.7. MADLI [18]

A crucial step in utilized MALDI technique is the formation of the matrix-analyte cocrystal. The composition of the Matrix is a key difference between FAB ionization and MALDI. As previously mentioned FAB operates by utilizing a liquid matrix while MALDI uses a cocrystalline matrix. The cocrysal is made by dissolving analyte into a solution of the matrix compound. The solution is then spotted on the target plate, and once the solvent evaporates a mixture of analyte and the matrix compound is left. As shown, the target plate holds the sample (orange) and matrix compound (green). The matrix is in very large excess to insure that it gets desorbed with the target sample of interest.

One of the key components that drive the ionization of molecules in MALDI is the matrix the sample is placed in. The matrix compounds used in MALDI are generally low in mass; this is to ensure that once the laser strikes the sample the matrix is easy vaporized into the gas phase. In order for the matrix to have high enough energy to transfer energy to the analyte, it is important that the compound is able to have high UV absorbance. Typically highly polar analytes work best with highly polar matrices, and similarly nonpolar analytes work better combined with nonpolar matrices.[18] Below is a table of commonly used matrices for different analyte.

Table 1. Matrices used is MALDI[18]

Compound	Acronym	Application to
Nicotinic acid	NA	Peptides, proteins
Picolinic acid	PA	Oligonucleotides, DNA
3-Hydroxypicolinic acid	HPA, 3-HPA	Oligonucleotides, DNA
3-Aminopicolinic acid	3-APA	Oligonucleotides, DNA
6-Aza-2-thiothymine	ATT	Oligonucleotides, DNA
2,5-Dihydroxybenzoic acid	DHB	Proteins, oligosaccharides
DHB-based mixtures	DHB/XY and super-DHB	Proteins, oligosaccharides

Compound	Acronym	Application to
3-Aminoquinoline	3-AQ	Oligosaccharides
α-Cyano-4-hydroxycinnamic acid	α-CHC, α-CHCA, 4-HCCA, CHCA	Peptides, smaller proteins, triacylglycerols, numerous other compounds
4-Chloro-α-cyano-cinnamic acid	ClCCA	Peptides
3,5-Dimethoxy-4-hydroxycinnamic acid	SA	Proteins
2-(4-Hydroxyphenylazo) benzoic acid	HABA	Peptides, proteins, glycoproteins, polystyrene
2-Mercaptobenzothiazole	MBT	Peptides, proteins, synthetic polymers
5-Chloro-2-mercaptobenzothiazole	CMBT	Glycopeptides, phosphopeptides, and proteins
2,6-Dihydroxyacetophenone	DHAP	Glycopeptides, phosphopeptides, proteins
2,4,6-Trihydroxyacetophenone	THAP	Solid-supported oligonucleotides
Dithranol (1,8,9-anthracenetriol)	None	Synthetic polymers
9-Nitroanthracene	9-NA	Fullerenes and derivatives
Benzo[a]pyrene	None	Fullerenes and derivatives
2-[(2E)-3-(4-tert-Butylphenyl)-2-methylprop-2-enylidene]malonitrile	DCTB	Oligomers, polymers, dendrimers, small molecules

Once the sample is made, a high-energy laser pulse (typically UV) is applied to the sample creating a plume of ions that can then be analyzed. The type of laser used is another key differences between FAB and MADI, while FAB uses a series of atoms to bombard the sample; MADI operates using a beam of ions. Some common lasers used include a nitrogen laser (λ=337 nm) and a frequency tripled Nd-YAG laser (λ=355 nm). [11]After the laser marks the sample, the irradiated spot is heated and becomes vibrationally excited. Desorption of excited molecules occurs where the molecules (consisting of the analyte and matrix) leave the target plate in the gas phase. The exact mechanism of this ablation is not know, however it is theorized that this occurs either because of sublimation after the excitation or pressure caused by rapid expansion of the crystal lattice. [11] During this process, the matrix molecules collide with the molecule of interest and protonate or deprotonate the molecule creating an ion. The ion is then able to travel to the mass analyzer. Although the exact mechanism of this ablation is not known there have been proposed mechanisms as to what could potentially be occurring when the sample is photionized. Below is a schematic of photoionized reaction pathways proposed by Ehring, Karas, and Hillenkamp in 1992 (Figure 6.2.8).

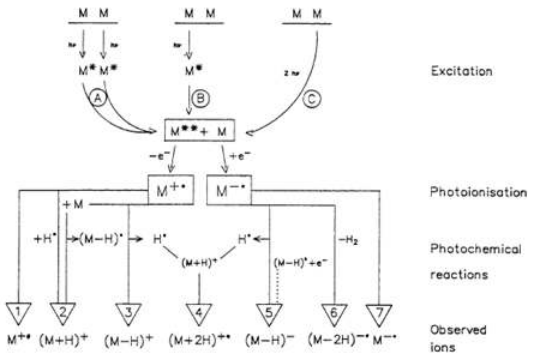


Figure 6.2.8. Photoionized reaction pathways

Along with all ionization techniques, MSI comes with advantages and disadvantages to using this technique. [19]

a) Advantages

- · Because it is a soft ionization technique samples with large masses can be analyzed
- · Able to analyze large biological samples such as proteins, peptides, DNA, etc.

- · Can be equipped to a quadruple which in turn leads to high accuracy when determining mass of sample since the quadruple m/z range is selective and relatively small.
- · Allows for less complicated spectra because of its tendency to produce mostly singly charged particles.
- · Can be used to image samples
- · Very high masses range typically less than 500,000 Da.
- · Tolerance of salts
- · Can be used to analyze complex mixtures

b) Disadvantages

- · Characterization using smaller fragments can be very difficult
- · Usually form single charged particles decreasing the effective range of the mass analyzers.
- · Contamination of sample can have a significant effect of making the crystal matrix.
- · Matrix could cause high background noise
- · Possibility of photodegradation by laser desorption/ionization

Applications to Proteins

MALDI, along side ESI, is also a very commonly used ionization method for protein analysis. Because MALDI is a soft ionization method, the ions produced have low energy allowing the production and detection of intact/low fragmented molecules. The production of intact molecules allows for protein identification and characterization. Once the protein is denatured, MALDI can also be used for protein sequencing by peptide mass fingerprinting.

One major advantage to MALDI is the ability to image proteins. MALDI Imaging can provide local molecular composition, relative abundance and spatial distribution of peptides and proteins in membranes.

Concluding Remarks

Ionization is a very important component of mass spectrometry and, as shown, is the key to determining what types of samples can be analyzed. As discussed there are important parameters and limitations associated with every ionization method, and understanding the limitations associated with each one is necessary in order to select the correct method when trying to analyze a sample. To date the ionization yields of large molecular samples such as proteins is relatively low (1/1000 molecules) limiting the sensitivity of mass spectrometers. [14] Novel ionization techniques are being sought out for that will improve upon this great limitation. Table 2 found summarizes and compares the ionization techniques visited in this article. [24]

Table 2. Summary of ionization techniques visited in this paper.

Ionization source	Typical mass range (Da)	Matrix interference	Degradation	Complex mixtures	LC/MS amenable	Sensitivity
Electron ionization (EI)	500	NO	NONE	Limited unless used with GC/MS	Very Limited	Picomole
Comments: Good sensitivity; unique fragmentation data generated; National Institute of Science and Technology (NIST) database (>100,000 compounds) available to compare fragmentation data; thermal decomposition a major problem for biomolecules; Limited mass range due to thermal desorption requirement.						
FAB	7,000	YES	Matrix reactions and some thermal degradation	Somewhat amenable	Very Limited	Nanomole
Comments: Relatively insensitive; little fragmentation; soft ionization; high salt tolerance to 0.01 M, solubility with matrix required						
Electrospray Ionization (ESI)	70,000	NO	Thermal	Limited	Excellent	High femtomole to low picomole
Comments: Excellent LC/MS tool; low salt tolerance (low millimolar); multiple charging useful, but significant suppression with mixtures occurs; low tolerance of mixtures; soft ionization (little fragmentation observed).						

MALDI	300,000	YES	Photo degradation and matrix reactions	Good for complex mixtures	Possible	Low to high femtomole
Comments: Somewhat tolerant of salts; excellent sensitivity; matrix background can be problem for low mass ions; soft ionization (little fragmentation observed); photodegradation possible; suitable for complex mixtures. Limited multiple charging occurs so MS/MS data is not extensive.						

References

1. *Jürgen Cox and Matthias Mann (July 2011). "Quantitative, High-Resolution Proteomics for Data-Driven Systems Biology". Annual Review of Biochemistry. **80**: 273–299. doi:10.1146/annurev-biochem-061308-093216. PMID 21548781.* – via Annual Reviews (subscription required)
2. The mass spectrometer - how it works. https://www.chemguide.co.uk/analysis/masspec/howitworks.html (accessed 04/25/2019)
3. McLafferty, F. W. Mass spectrometry across the sciences. *Proceedings of the National Academy of Sciences* **2008**, *105*, 18088-18089.
4. Bertani, R.; Cecchetto, W.; Polloni, R.; Crociani, B.; Seraglia, R.; Traldi, P. Comparison of hard vaporization and soft ionization techniques in the mass spectrometry of some palladium(II) and platinum(II) complexes with C-bonded heterocyclic ligands. *Inorganica Chimica Acta* **1990**, *174*, 61-66.
5. Taylor, T. Electron Ionization for GC–MS. *LCGC North America* **2012**, *30*,
6. Electron ionization.commons.wikimedia.org/wiki/File:Electron_Ionization_-_Born_Oppenheimer_Potential_Curves.png. *Wikipedia* (accessed 04/25/2019)
7. Sparkman, J. T. W. a. O. D.: *Introduction to Mass Spectrometry: Instrumentation, Applications, and Strategies for Data Interpretation*; John Wiley & Sons, 2007; Vol. 4.
8. Barber, M. Fast Atom Bombardment (FAB) & Liquid Secondary Ion Mass Spectrometry (LSIMS). *Journal of the Chemical Society* **1981**, 35.
9. . Lafont, H. H. R. Fast-atom bombardment. *Reference Module in Life Sciences* **2017**.
10. Barber, M.; Bordoli, R. S.; Sedgwick, R. D.; Tyler, A. N. Fast atom bombardment of solids (F.A.B.): a new ion source for mass spectrometry. *Journal of the Chemical Society, Chemical Communications* **1981**, 325-327.
11. Caprioli, R. M.; Farmer, T. B.; Gile, J. Molecular Imaging of Biological Samples: Localization of Peptides and Proteins Using MALDI-TOF MS. *Analytical Chemistry* **1997**, *69*, 4751-4760.
12. J. B. Fenn, M. M., C. K. Meng, S. F. Wong, and C. M. Whitehouse. Electrospray ionization for mass spectrometry of large biomolecules. *Science*, *246*, 64-71.
13. Electrospray ionization. en.Wikipedia.org/wiki/Electrospray_ionization (accessed 04/25/2019).
14. Kebarle*, P. A brief overview of the present status of themechanisms involved in electrospray mas spectrometry. *JOURNAL OF MASS SPECTROMETRY* **2000**, *35*, 804-817.
15. Brackbill, J. U.; Kothe, D. B.; Zemach, C. A continuum method for modeling surface tension. *Journal of Computational Physics* **1992**, *100*, 335-354.
16. Wilm, M. Principles of electrospray ionization. *Molecular & cellular proteomics : MCP* **2011**, *10*, M111.009407-M009111.009407.
17. KNOCHENMUSS, Z. A. ION FORMATION IN MALDI MASS SPECTROMETRY. *Mass Spectrometry Reviews*, **1998**, 337–366.
18. MALDI-TOF Mass Spectrometry. www.creative-proteomics.com/technology/maldi-tof-mass-spectrometry.htm (accessed 04/25/2019)
19. Berkenkamp, S. K., M.; Hillenkamp, F. Role of photoionization and photochemistry in ionization processes of organic moleculesand relevance for matrix-assisted laser desorption/ionization mass spectrometry. *Org Mass Spectrom* **1992**, *30*, 1303.
20. Calder, A. G., Anderson, S. E., Grant, I. , McNurlan, M. A. and Garlick, P. J. (1992), The determination of low d_5-phenylalanine enrichment (0.002–0.09 atom percent excess), after conversion to phenylethylamine, in relation to protein turnover studies by gass chromatography/electron ionization mass spectrometry. Rapid Commun. Mass Spectrom., 6: 421-424. doi:10.1002/rcm.1290060704
21. Julian P, Whitelegge, Stephen M, GómezKym FFaull. Proteomics of Membrane Proteins. *Advances in protein chemistry **2003.***
22. Siuzdak, G. An Introduction to Mass Spectrometry Ionization: An Excerpt from The Expanding Role of Mass Spectrometry in Biotechnology, 2nd ed.; MCC Press: San Diego, 2005. *The Scripps Research Institute, Center for Mass Spectrometry* **2004**.

23. M. Barber, R.S. Bordoli, G.J. Elliott, N.J Horoch, and B.N. Green. *Biochem. Biophys. Res. Coomun.* **110**:753-757.
24. M. Barber, R.S. Bordoli, R.D. Sedgwick, A. N. Tyler, G.V. Garner, D.B. Gordon, L.W. Tetler, and R.C. Hider. *Biomed. Mass Spectrom.* **9**: 265-269 (1982)
25. A. Dell and G.R. Morris. *Biochem. Biophys. Res. Commun.* **106:** 1456-1462 (1982).
26. M. Barber, R.S. Bordoli, G.J. Elliott, N.J Horoch, and B.N. Green. *J. Chem. Soc. Chem. Commun.* 936-938 (1982).
27. H. R. Morris, M. Panico, M. Barber, R.S. Bordoli, R.D. Sedgwick, and A.N. Tyler. *Biochem. Biophys. RES. Coomun.* **101**:623-631 (1981).
28. Whitelegge, J. P., Gundersen, C. B. and Faull, K. F. (1998), Electrospray-ionization mass spectrometry of intact intrinsic membrane proteins. Protein Science, 7: 1423-1430. doi:10.1002/pro.5560070619

6.2: Mass Spectrometer Ionization Techniques for Membrane Proteins is shared under a CC BY 4.0 license and was authored, remixed, and/or curated by LibreTexts.

6.3: Electrospray Ionization (ESI) Mass Spectrometry

Electrospray Ionization Mass Spectrometry is a technique used to determine molecular weights for proteins, peptides, and other biological macromolecules such as oligosaccharides[1]. Originally described by Canadian-American Physicist Sir Arthur J. Dempster in an article titled "A new method of positive ray analysis."[7] His work was the first modern mass spectrometer, which used positive rays to determine the mass-to-charge ratio of various isotopes of lithium and magnesium. Dempster showed that it was possible to determine the isotopes' relative proportions and atomic weights using this method[7]. Mass spectrometry in general is useful for structure elucidation (when combined with chromatography separation techniques), peptide sequencing (when combined with ion traps), and quantification (when combined with a triple-quadrupole mass analyzer) for example, and is mainly limited by the ability of the ions generated to remain stable until their arrival at the detector. Electrospray Ionization describes the method by which the macromolecules are ionized via a “soft” ionization, which does not fragment nor harshly degrade the macromolecules and ionizes by multiple charging[1]. Rather, the macromolecules are ionized into small droplets[2]. The droplets are then desolvated further, effectively decreasing the droplet size into molecules with protons[1]. The protonated/desolvated molecules enter the mass analyzer and subsequently the detector to determine the mass/charge ratio[1]. The main advantage is that the samples can easily be introduced to the instrument in solution with the ability to detect very small masses (atomic masses) to very large molecules (MDaltons) with detection limits down to the pico-, femto-, and attomole levels[5]. Furthermore, this analytical technique has become of great importance within the last decade or so due to advancements enabling even higher sensitivity and its ability to be combined with high-throughput automation for -"omics" studies with high applicability in drug discovery.

Sample Preparation

Samples for ESI-MS are typically purified, which is ideal for the instrument because mixtures of components with different physicochemical properties are not good analytes for the technique (e.g. glycans vs. peptides)[1]. Methods such as high-performance liquid chromatography, capillary electrophoresis, and liquid-solid column chromatography are commonly employed for the purification step, and subsequently injected into the ESI-MS[1]. Usually, the purification method is attached directly to the capillary needle[1].

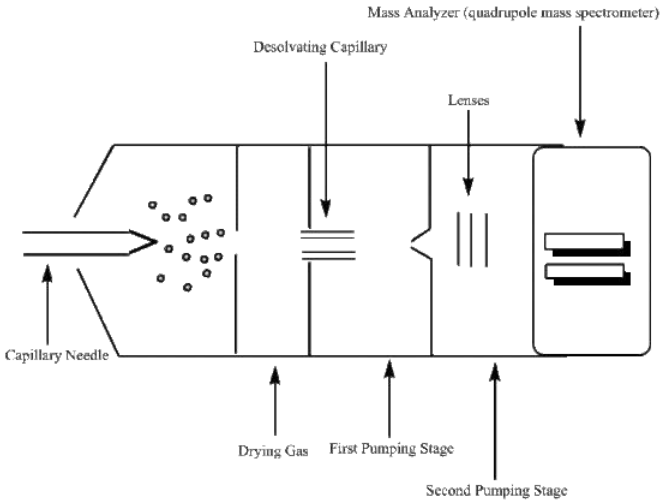


Figure 6.3.1: Diagram of Electrospray Ionization-Mass Spectrometry (Murphy, 2016)

Electrospray Ionization (ESI)

A mechanical syringe pump injects the liquid sample (usually less than one mM in a polar volatile solvent) into the capillary needle, and thereby nebulizing it into a fine mist[1]. Typically an analyte will undergo three major processes after injection and transfers into the gas phase: it will produce charged droplets from the high-voltage cappillary tip, repeatedly evaporate solvent from the charged droplet followed by droplet disintegration into much smaller droplets, and lastly transfer of the ion into the gas-phase[5]. The capillary needle typically has an inner diameter of ~0.1mm and outer diameter of ~0.2mm, and a low flow rate around 1 to 20 µL/min[1]. A voltage is applied to the tip of the capillary of around 2-6 kV, where the surrounding source-sampling cone is located around 1-3 cm from the spray needle tip (see Figure 6.3.1)[2].

The strong electric field causes the nebulized particles to carry a charge, thus, becoming electrospray droplets where a drying or sheath gas flows around the capillary improving nebulization[1].

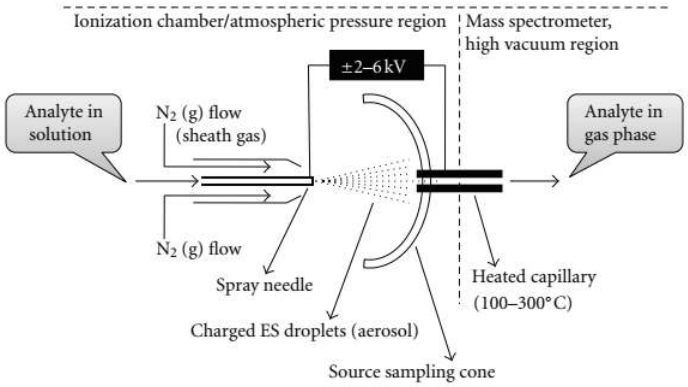


Figure 6.3.2: Diagram of Electrospray Ionization **(Banerjee & Mazumdar, 2012)**

The electric field also directs the spray toward the mass spectrometer while droplets diminish in size (solvent evaporation)[1]. This process is described pictorally in Figure 6.3.3 below. Once the electrospray droplets pass through the heating capillary (Figure 6.3.2, labeled as desolvating capillary in Figure 6.3.1), the ions completely desolvate[1]. The heating capillary is typically around 0.2mm inner diameter, 60mm in length, at a temperature controlled in a range from 100-300°C for desolvation and continual droplet shrinkage[1]. At this point two forces become dominant: surface tension in the droplets acting to retain the shape of the droplet, and Coulomb force of repulsion between like charges on the surface which act to break down the shape of the droplet[2].

As the droplets travel through the heating capillary, they have a high enough electric field density that causes like charges to repel one another, increasing surface tension (first to second step in Figure 6.3.3)[2]. The droplets then reach the Rayleigh limit, which describes the limit of the number of charges that can be present on a charged droplet before fission occurs and is broken down (third step in Figure 6.3.3)[1]. It is at this point the surface tension can no longer sustain the Coulomb force of repulsion, and a "Coulomb explosion" or "Coulomb fission" occurs (fourth step in Figure 6.3.3)[1]. The parent droplets disintegrate into much smaller droplets of positive or negative charge, with a much higher mass-to-charge ratio[1]. These small droplets have high mass-to-charge ratios because smaller portions of parent charges are carried off and distributed in many offspring droplets compared to the mass carried off from parent droplets. An example time history is shown below of methanol droplets produced by electrospray in Figure 6.3.4.

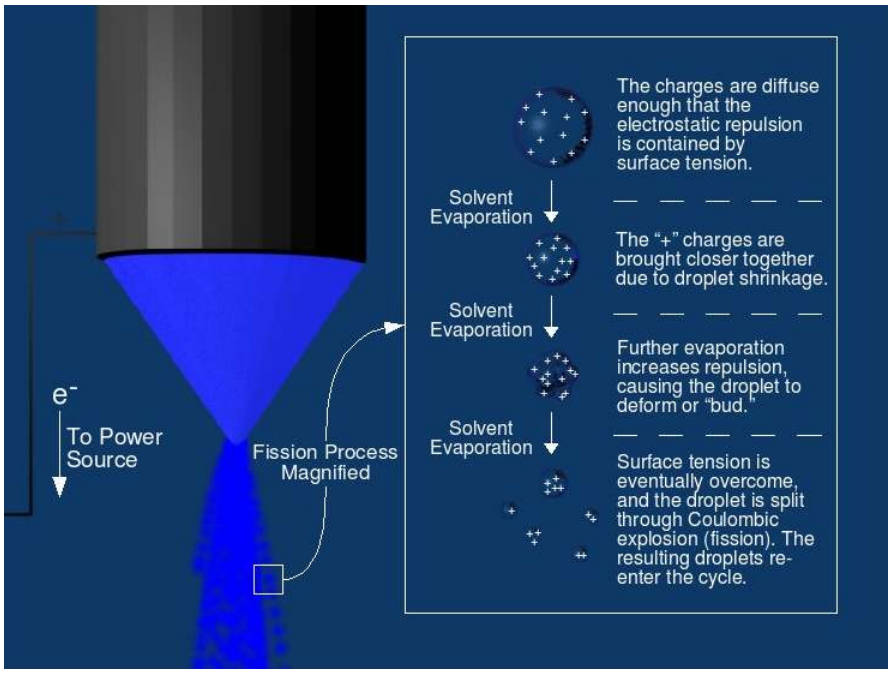


Figure 6.3.3: Fission Process Diagram (McFarland, 2008)

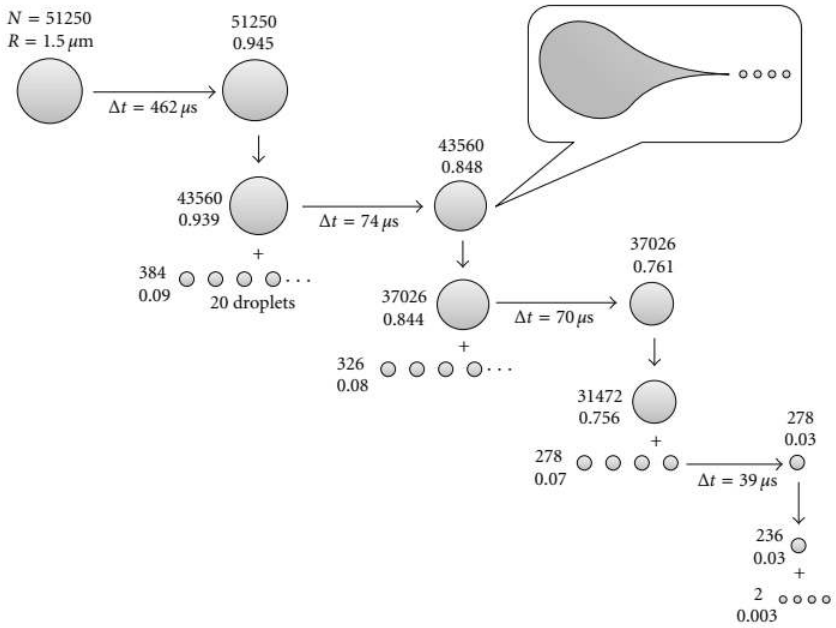


Figure 6.3.4: Methanol Droplets produced by microelectrospray process. The upper left droplet is a parent droplet created at the electrospray capillary tip. N is the number of elementary charges, R is the radius of the droplet in micrometers, Δt is the time in microseconds for solvent evaporation to shrink the droplet (right arrows) to the point where Coulomb fission occurs (down arrows). Only the first three successive solvent evaporation/Coulomb fission steps are shown. The inset is a drawing of a droplet undergoing jet fission *(Banerjee & Mazumdar, 2012)*.

The decomposition of a droplet from ESI occurs in manner similar to the inset of Figure 6.3.4, and is dictated by the Rayleigh equation:

$$q^2 = 8\pi^2\epsilon_o\gamma D^3 \tag{6.3.1}$$

Where q is charge, epsilon 'naught' is the permissivity of the medium, gamma is the surface tension of the droplet, and D is the droplet diameter.

Mass Analyzers

From the ion beam, the mass analyzer takes different types of ions and separates them based on their mass-to-charge ratio. Afterwards, the ions are passed onto the detector. There are many types such as magnetic (B)/electric (E) sector mass analyzers, linear quadrupole ion trap (LIT), three-dimensional qudrupole ion trap (QIT), orbitrap (Mass Analyzer Orbitrap), time-of-flight mass analyzer (TOF, Mass Analyzer Time of Flight), and ion cyclotron resonance mass analyzer (ICR)[1]. They all take advantage of dynamic of static magnetic/electric fields based on Lorentz force law (Equation (1), a charge experiences electric and magnetic forces when traveling through magnetic/electric fields)[3] and Newton's second law of motion (Equation (2), objects accelerate based on their mass and net forces acting on the object)[4].

$$F = qE + qvxB \tag{6.3.2}$$

$$F = mxa \tag{6.3.3}$$

Where in Equation (2), F is the Lorentz force, q is the charge of the ion, E is the electric field, v is the velocity of the ion, and B is the magnetic field. In Equation (3), F is Force, m is mass, and a is acceleration.

Table 1 below briefly summarizes comparisons between different mass analyzers. The mass analyzer uses electrostatic lenses (see Figure 6.3.1) to direct the beam into the analyzer, and is kept at a high vacuum (around 10^{-3} torr to 10^{-6} torr pressure) to prevent any undesired molecular interactions between the ions and the atmosphere[1].

Table 1: Comparison of mass analyzers (de Hoffmann & Stroobant, 2007)

	Quadrupole	Ion trap	TOF	TOF reflectron	Magnetic	FTICR	Orbitrap
Mass limit	4000 Th	6000 Th	>1000 000 Th	10 000 Th	20 000 Th	30 000 Th	50 000 Th
Resolution FWHM (m/z 1000)	2000	4000	5000	20 000	100 000	500 000	100 000
Accuracy	100 ppm	100 ppm	200 ppm	10 ppm	<10 ppm	<5 ppm	<5 ppm
Ion sampling	Continuous	Pulsed	Pulsed	Pulsed	Continuous	Pulsed	Pulsed
Pressure	10^{-5} Torr	10^{-3} Torr	10^{-6} Torr	10^{-6} Torr	10^{-6} Torr	10^{-10} Torr	10^{-10} Torr
Tandem mass spectrometry	Triple quadrupoles MS/MS fragments precursors neutral loss	— MS^n fragments	— —	PSD or TOF/TOF MS/MS fragments	Consecutive sectors MS/MS fragments precursors neutral loss	— MS^n fragments	— —
	Low-energy collision	Low-energy collision	—	Low- or high-energy collision	High-energy collision	Low-energy collision	—

Five main characteristics for the measuring performance of a mass analyzer are the mass range limit, analysis speed, transmission, mass accuracy, and resolution[5]. According to de Hoffmann and Stroobant, mass range is the mass-to-charge (m/z) limit the mass analyzer can measure ions, expressed in units of Th (Thomson), or u (unified atomic mass unit) for ions with an elementary charge (z=1), where $\{1\ Th=1\ {}^{u}/_{e}=1\ {}^{Da}/_{e}=1.036426*10^{-8}\ {}^{kg}/_{C}\}$[5]. Analysis speed (scan speed) is the rate the analyzer measures over a particular mass range, expressed in mass units per second (u/s) or in milliseconds (u/ms)[5]. Transmission is the ratio between the number of ions reaching the detector and number of ions entering the mass analyzer, including ion losses from other sections of the mass analyzer, such as the electric lenses[5]. Mass accuracy, as it sounds, is the accuracy of the m/z provided by the mass analyzer[5]. It is the difference between the theoretical m/z ($m_{theoretical}$) and measured m/z ($m_{measured}$), expressed in millimass units (mmu) or parts per million (ppm)[5]. This parameter is closely related to the stability and resolution of the analyzer, for example, a low-resolution instrument cannot provide high accuracy[5]. The resolution or the ability of the analyzer to yield distinct signals from two ions with similar to small differences in m/z can be expressed as the following in Equation (4)[5].

$$R = \frac{m}{\Delta m} \tag{6.3.4}$$

Where m is the mass of the first peak, divided by the difference, Δm, between the neighboring peaks[2]. The data is improved with more resolution (higher R)[5].

Detectors

A common type of detector used in conjunction with a quadrupole mass analyzer for example, is an electron multiplier (EM) detector[5]. In this type of detector electrons are accelerated to a high velocity, enhancing detection efficiency[5]. To achieve this, an electrode called a conversion dynode is held at a high potential from + 3 kV to + 30 kV, opposite to the ions' charges[5]. Once ions strike the conversion dynode, several secondary particles are emitted[5]. Secondary particles are typically negative and positive ions, electrons, and neutral particles[5]. For example, if positive ions strike the conversion dynode, negative ions and electrons are the secondary particles of interest, likewise, if negative ions strike the conversion dynode the secondary particles are positive ions[5]. The secondary particles are then amplified in a cascade effect to produce a current[5].

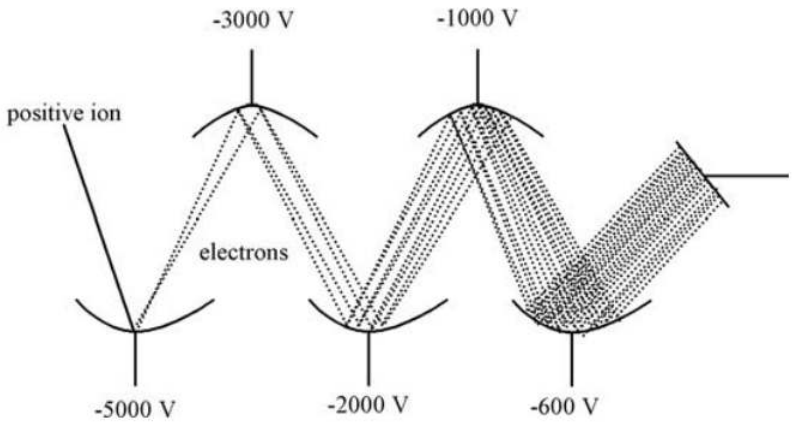


Figure 6.3.8: Discrete dynode electron multiplier schematic, the first dynode (at -5000 V) converts ions into electrons **(de Hoffmann & Stroobant, 2007)**

Figure 6.3.8 shows a schematic for a discrete dynode electron multiplier detector[5]. The first dynode starts at a higher magnitude potential (but negative), causing the secondary particles to emit electrons[5]. The secondary particles and electrons accelerate to each subsequent dynode (due to the lower potential) until the electrons reach the output of the electron multiplier, which is held at ground potential[5]. A cascade of electrons are created at the end, and the current produced and amplified by conventional electronic amplification[5].

Electrospray Ionization on Membrane Proteins

Membrane proteins are of particular interest because of their importance in cell signaling, transport, adhesion[6], and intercellular interactions. Some advantages of mass spectrometry methods in studying membrane proteins are that freezing or crystallization (as in X-ray crystallography) are not required, and that it is possible to study these proteins in their native (unfolded) state[6]. Utilization of electrospray ionization (ESI) mass spectrometry (MS) on membrane proteins typically falls under two categories: native MS and labeling MS[6]. Native MS involves maintaining non-covalent interactions, which preserves tertiary and quaternary structures, and is carried out *in vacuo*[6]. Labeling MS methods involve chemical crosslinking, hydrogen-deuterium exchange, and hydroxyl radical footprinting (HRFP) to name a few[6]. For each method, proteins are labeled in solution (peptides reacted with chemical labels), undergo proteolysis, and are subsequently measured/quantified via MS method[6] (see Figure 6.3.9 below).

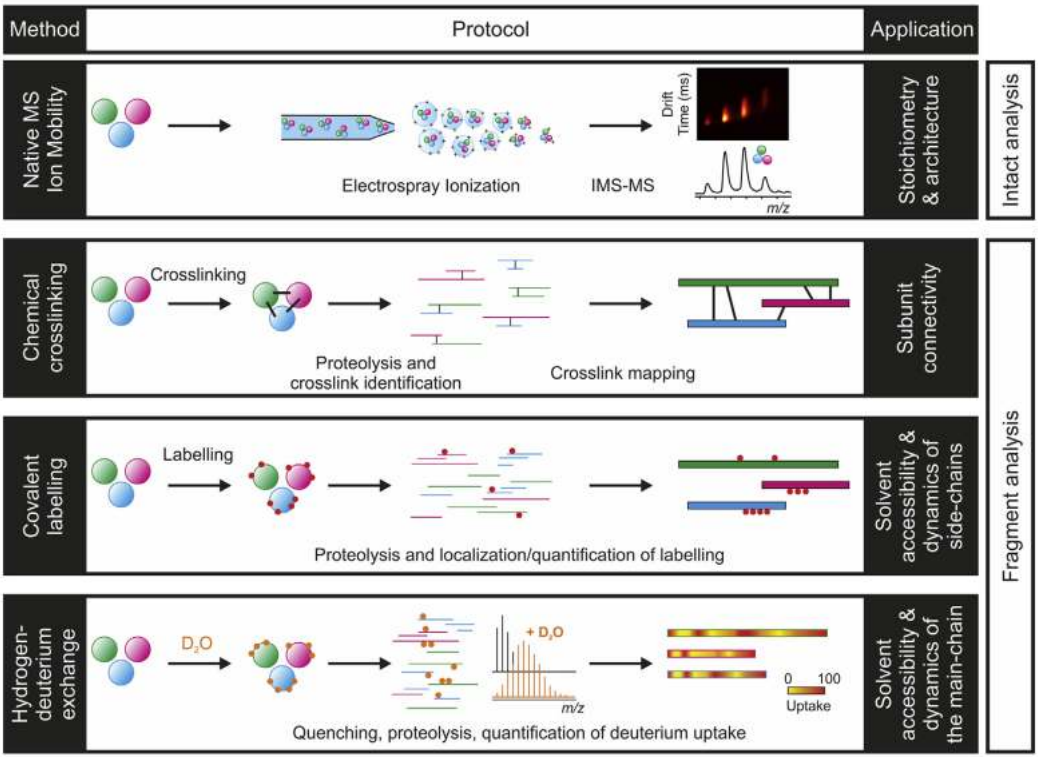


Figure 6.3.9: Summary of Native (Intact) and Labeling (Fragment) Mass Spectrometry (MS) methods. Intact/Native MS involves retaining tertiary and quaternary structures for analysis, whereas fragment/labeling MS methods involve chemical crosslinking, exchanging, or tagging of peptides followed by proteolysis. Labeling MS methods then study fragmentation patterns of labeled peptide segments (Calabrese and Radford 2018).

Considerations for ESI on Membrane Proteins

Careful consideration in optimizing the parameters are absolutely necessary when analyzing biological materials in mass spectrometric methods. Two examples of these parameters are the collision voltage and selection of detergent[6]. The collision voltage is that which is applied to molecular ions, accelerating them into the collision cell with an inert gas[5]. Optimization of collision voltage involves selecting a voltage that enables fragment ions to be observed, but also well resolved. This voltage goes hand-in-hand with careful consideration of the buffer/detergent. Ideally, the buffer/detergent needs to be able to efficiently solubilize the protein, and also be easily removed to allow the protein to be properly desolvated (see Figures 3 and 4)[6]. Detergents are used for membrane proteins because of their amphiphilic nature, similar to the membrane proteins themselves[6]. Where these two parameters come together are when the membrane protein-detergent complex transfers into the gas phase: the collision voltage

must be high enough to desolvate the membrane protein from the detergent, and the detergent must not strongly solvate the membrane protein[6]. Strong solvating detergents require higher energies which risk destabilizing the protein prior to detection in the mass analyzer.

If the membrane protein is not liberated from the detergent, perhaps due to low collision voltage, the membrane proteins' signals maybe be suppressed by noise from the remaining detergent (see Figure 6.3.10b and 10f). Figure 6.3.10 below also demonstrates the concepts of selecting proper collision voltage combined with an appropriate detergent.

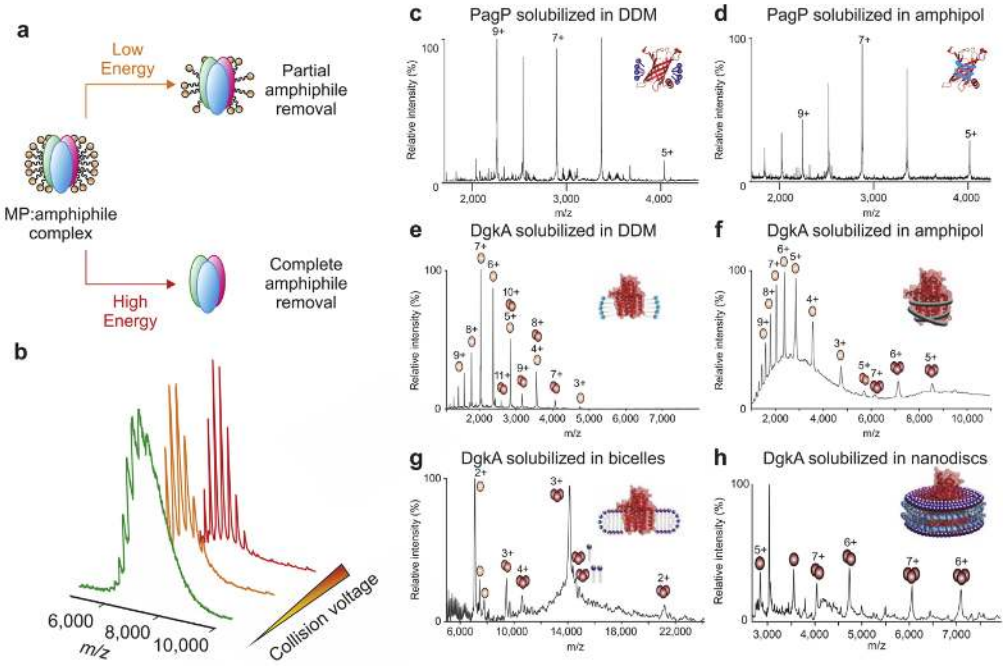


Figure 6.3.10: Examples from native mass spectrometry of membrane proteins (Calabrese and Radford 2018). (a) Demonstrates that low collision voltage/energy results in partial removal of detergent/amphiphile, resulting in unresolved peaks. Conversely, sufficiently high collision voltage results in complete detergent/amphiphile removal, resulting in resolved peaks. (b) echoes concepts from 10a demonstrating a theoretical mass spectra from low collision voltage (green/front) to high collision voltage (red/back). (c-d) Demonstrates differences in using detergents DDM (c) and amphipol (d) on PagP, suggesting two conformations are present. (e-f) Shows DgkA protein mass spectra differences using DDM (e) vs. amphipol (f). Use of amphipol for DgkA demonstrates its strong solvation of the protein, resulting in higher noise. Careful selection of detergents for the membrane protein of interest is necessary as a single detergent may not be appropriate for all membrane proteins. (g-h) Shows the resulting mass spectra when solubilizing DgkA in bicelles and nanodiscs (Calabrese and Radford 2018).

Summary

- Electrospray (ESI) is a soft-ionization technique that has gained popularity in biological applications as it is capable of maintaining non-covalent interactions of proteins.
  - Use of appropriate buffers/detergents/optimized instrument conditions renders ESI-mass spectrometry (MS) to be a powerful and sensitive tool to elucidate membrane protein structures.
- ESI can be coupled with a variety of mass analyzers (see Table 1), providing users of mass spectrometry flexibility in analysis.
- ESI can also be coupled downstream from a variety of chromatographic techniques such as HPLC to enhance mass spectrometry-based studies on complex molecular structures.

References

1. Banerjee, S., & Mazumdar, S. (2012). Electrospray Ionization Mass Spectrometry: A Technique to Access the Information beyond the Molecular Weight of the Analyte. International Journal of Analytical Chemistry.
2. Murphy, J. (2016, October 8). Electrospray Ionization Mass Spectrometery. Retrieved from Chemistry LibreTexts(TM): https://chem.libretexts.org/Core/Ana...s_Spectrometry
3. Bird, R. B., et al. (2001). Transport Phenomena, Wiley.

4. Young, H. D., Freedman, R. A., & Sears, F. W. (2004). Sears and Zemansky's university physics (11th ed.). San Francisco, Calif.: Pearson/Addison Wesley.
5. de Hoffmann, E., & Stroobant, V. (2007). Mass Spectrometry Principles and Applications. West Sussex, England: John Wiley & Sons, Ltd.
6. A.N. Calabrese, S.E. Radford, Methods (2018). https://doi.org/10.1016/j.ymeth.2018.02.020
7. Dempster, A. J. (1921). "Positive Ray Analysis of Lithium and Magnesium." Physical Review 18(6): 415-422.
8. McFarland, S. (Ed.). (2008, April 19). File:Fission.jpg. Retrieved June 13, 2018, from http://www.appropedia.org/File:Fission.jpg
9. Bird, R. B., et al. (2001). Transport Phenomena, Wiley.
10. (2003). University Physics With Modern Physics,11/e, Pearson Education.

Contributors and Attributions

- Christopher Ranque

6.3: Electrospray Ionization (ESI) Mass Spectrometry is shared under a CC BY 4.0 license and was authored, remixed, and/or curated by LibreTexts.

6.4: Mass Analyzer Orbitrap

Mass spectrometry (MS) is an analytical instrument that is used to measure the mass-to-charge ratios (m/z) of samples to obtain qualitative and quantitative information[1]. The development of MS started around 1920 where it was used to study the isotopic abundance of elements[1]. MS capabilities have increased greatly since 1920. Within the last 90 years, MS has been used to study complex organic and inorganic mixtures, the composition of the solid surface, biological samples and much more[1-2]. Today, MS comes in many forms because of its tandem capabilities with other analytical instruments[1-2]. This allows MS to be very versatile making it one of most used analytical instruments today. One of the newest advancements in MS is the Orbitrap mass analyzer and that allows researchers to characterize biological samples such as cell membrane[2].

Fundamentals

The principle of MS is based on separation of *m/z* ratios and analyzing them to gain a mass spectrum of the sample[1-2]. MS has three major components which are the ionization source, mass analyzer, and detector[1-2]. The overall schematic of an MS instrument is shown in Figure 6.4.1.

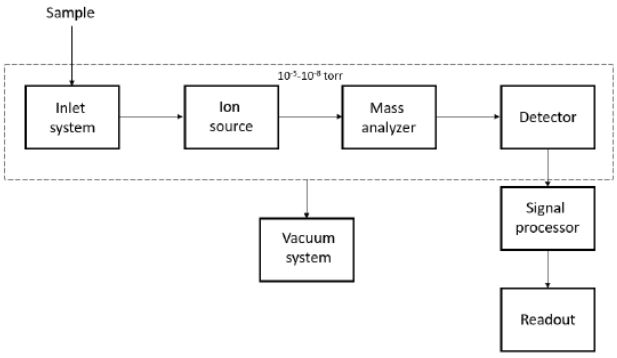


Figure 6.4.1: Basic box diagram of a Mass Spectrometer [1]

Samples are injected using an inlet system that purifies the analyte, and subsequently becomes ionized[1]. The standard method of ionization for Orbitrap mass analyzer is using Electrospray Ionization (ESI) [1]. After ionization, the mass analyzer filters the samples for desired m/z ratios. In this case, the Orbitrap is the mass analyzer of interest[1]. The desired m/z ions are then flown through to the detector to be processed into a mass spectrum[1]. This signal is processed which gives us the readout. Creating an ion-free path is important to guide ions to the detector because vacuums (10^{-5} to 10^{-8}) torr minimize the chance that ions will inadvertently collide with other molecules. If this unintentional collision occurs, a diminished signal may result By using a high vacuum system, the ion can transition through the MS with a low probability of collision with other ions.

Ionization

Ionization methods can be classified as either soft or hard ionization[1-2]. Hard ionization methods create ions with high residual energy[1-2]. This method usually results in fragmentation of the molecule[1-2]. For hard ionization, electron ionization is one of the most common methods used in MS to produce ions for MS analysis[2]. Unlike hard ionization, soft ionization methods use a lower residual energy to ionize samples where fragmentation is less likely to occur. This is ideal when studying biological samples where sample integrity is important[1-2]. ESI is an example of soft ionization method for MS[1-2]. For Orbitrap mass analyzer, ESI is the most common method used for the ionization source [1-2]. BUsing the mass analyzer, charged ions can be created and their movements controlled by magnetic and electric fields[1].

Mass Analyzer

The mass analyzer is one of the most vital components of the MS. It filters the ion for the desired *m/z* ratios to allow the detector to output the mass spectrum[1-2]. Beside filtering *m/z* ratio, they also can act as an ion storage center, fragmentation chamber or even an ion ejection compartment[1-2]. In the Orbitrap mass analyzer, both a quadrupole and Orbitrap are present [1-2]. The quadrupole component allows for mass selection and guides ions with the desired m/z to the Orbitrap[1-2].

The Orbitrap is an ion trap-based mass analyzer developed from the Kingdon trap[2-6]. Developed in 1923 by K.H. Kingdon, the Kingdon trap was originally created to explore electric potential in an infinitely long electrode[4]. Figure 6.4.2 below shows the schematic diagram of the Kingdon trap.

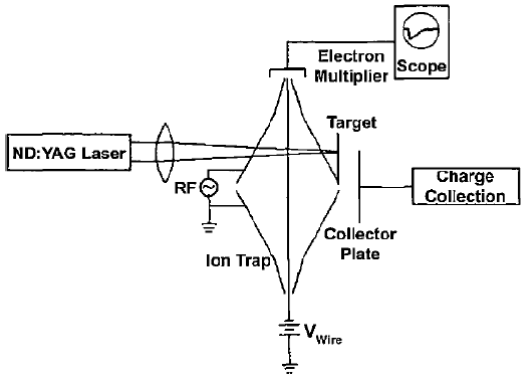


Figure 6.4.2: Kingdon trap schematic diagram [4]

60 years after K.H. Kingdon passed, R.D. Knight, one of K.H. Kingdon's contemporaries developed the Knight trap based on K.H. Kingdon's original work[5]. The **Knight trap** improved upon the Kingdon trap's limitations by deriving m/z from electrical potentials [5]. Even though R.D. Knight was able to create the connection between the electric potential of an electrode to m/z ratio, the Knight trap still had its limitation. The Knight trap had issues in discriminating between similar m/z ratios and the focus of R.D. Knight work was on ion ejection from the Knight trap[5].

In the year 2000, a Russian physicist Alexander Alexeyevich Makarov published his work on the orbitrap that resolved the limitation of the Knight trap[6]. During the next five years, the Orbitrap mass analyzer became commercially available, allowing researchers to measure m/z ratios of large biological samples[3]. Figure 6.4.3 shows the original design of the Orbitrap invented by Dr. Makarov. The Orbitrap gained great interest for MS analysis of biological samples because of its high resolution and high mass limit[2]. Most other mass analyzers are limited to molecules 2 kDa/z to 4 kDa/ in size[2,6]. This would require having samples to have a charge greater than 50 to be able to measure that sample with the mass of 100 kDa. In the case of the Orbitrap, the resolution limits are from 50kDa/z to 100kDa/z[2]. For a biological samples weighing 100kDa, we would only need a charge of 1 to detect it in the Orbitrap. This is due to the high sensitivity of the Orbitrap having one of the highest resolution limits compared to other mass analyzers.

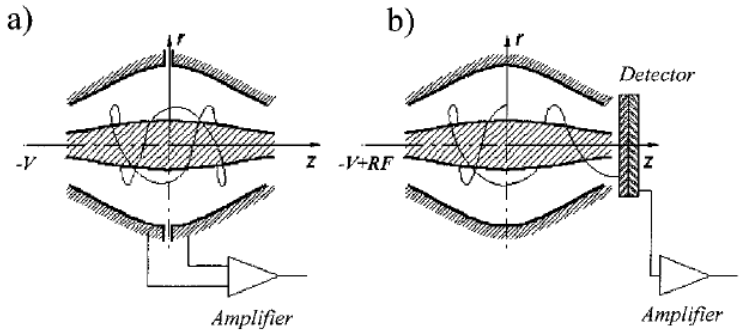


Figure 6.4.3: Alexeyevich Makarov Orbitrap design [3]

Orbitrap Theory

The Orbitrap mass analyzer operates by oscillating ions in a cylindrical electrode with tapered ends and detects signals for m/z based on Fourier transforms (FT)[2-3,6]. The electrode is powered by an RF frequency that makes the ion oscillate around the inner electrode[6]. A better way to picture the details of an Orbitrap is shown in Figure 6.4.4 below shows a side view and cross-sections of the Orbitrap as ions circulate through the trap (in red)3].

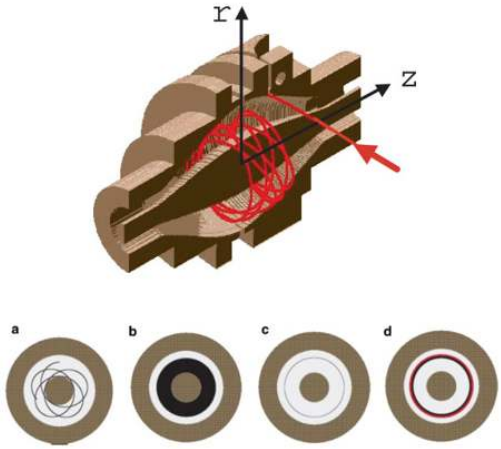


Figure 6.4.4: Orbitrap cross section and side view of an ion trajectory [3]

In the initial inject of the ions in the Orbitrap will results in Figure 6.4.4*a* where there is thin line demonstrating the trajectory[3]. Try “When ions are initially injected, ions typically follow an imperfect oscillatory motion, with frequencies out-of-phase with the electrode (Figure 6.4.4 a, grey lines)[3]. As time progresses, hundreds of oscillations become incorporated into the Orbitrap and follow more in-phase circular revolutions (Figure 6.4.4 b, black region)[3]. However, if the initial injection of ions resonates with the electrode, a circular orbit can be obtained from the beginning (Figure 6.4.4 c, grey circle)[3]. The electrostatic potential of the Orbitrap can be explained with the equation:

$$U(r,z) = \frac{k}{2}\left(z^2 - \frac{r^2}{2}\right) + \frac{k}{2}(R_m)^2 \ln\left(\frac{r}{R_m}\right) + c \tag{6.4.1}$$

The potential inside of the trap is based on the *r* and *z* cylindrical coordinates, field curvature *k*, the characteristic radius R_m (radius at when the ions are repelling instead of attracting), and a constant value *C* [2,6] . From Equation 6.4.1, one can deduce the shape of the axial along the z-axis that is represented as:

$$z_{1,2}(r) = \sqrt{\frac{r^2}{2} - \frac{(R_{1,2})^2}{2} + (R_m)^2 \ln\left(\frac{R_{1,2}}{r}\right)} \tag{6.4.2}$$

When z is set to zero, one can see that the maximum radii of the electrodes are that of $R_{1,2}$[6].

Going back to the ion trajectory, there must be some initial conditions that are needed to be met when at $t = 0$[6] These conditions are listed as:

$$\begin{aligned} r(0) &= r_0 \quad & \dot{r}(0) &= \dot{r}_0 \\ \varphi(0) &= \varphi_0 \quad & \dot{\varphi}(0) &= \dot{\varphi}_0 \\ z(0) &= z_0 \quad & \dot{z}(0) &= \dot{z}_0 \end{aligned} \tag{6.4.3}$$

With these following conditions, then one can get three equations that represent the polar coordinates system of the Orbitrap listed as:

$$\begin{cases} (a) \ddot{r} - r\dot{\varphi} = -\frac{q}{m}\frac{k}{2}\left[\frac{(R_m)^2}{r} - r\right] \\ (b) \quad \frac{d}{dt}\left(r^2\dot{\varphi}\right) = 0 \\ (c) \quad \ddot{z} = \frac{q}{m}kz \end{cases} \tag{6.4.4}$$

These three polar coordinates equation each has their own energy equation associated with them shown as:

$$\begin{aligned} qE_r &= \left(\frac{m}{2}\right)(\dot{r}_0)^2 \\ qE_\varphi &= \left(\frac{m}{2}\right)(r_0\dot{\varphi}_0)^2 \\ qE_z &= \left(\frac{m}{2}\right)(\dot{z}_0)^2 \end{aligned} \tag{6.4.5}$$

By meeting the condition set in Equation 6.4.4, one can determine the ion initial kinetic energy which will be the sum of all three energy in Equation 6.4.5[6]. The more important thing is that E_z is the energy factor of the harmonic oscillator for the Orbitrap[6]. Going back to Equation 6.4.1, one can find the voltage gradient needed for any given system shown as:

$$\frac{\partial U(r,z)}{\partial z} = kz \tag{6.4.6}$$

The voltage gradient is focused only along the z-axis of the Orbitrap[2]. This voltage gradient can be further explained by the equation below:

$$F_z = m\ddot{z} = -q\frac{\partial U}{\partial z} = -qkz \tag{6.4.7}$$

or

$$\ddot{z} = -qkz \tag{6.4.8}$$

The force induces by the electric field on the z-axis is described in Equation 6.4.8[2] which the exact solution is given below as:

$$z(t) = z_0\cos(\omega t) + \sqrt{2E_z/k}\sin(\omega t) \tag{6.4.9}$$

Equation 6.4.9 correlate frequency measure in the Orbitrap is only dependent on the z-axis[2] shown below:

$$\omega = \sqrt{\left(\frac{q}{m}\right)k} \tag{6.4.10}$$

From this final equation, one can see the relation of the frequency with mass-to-charge ratio while being independent of kinetic energy[2]. This is how FT plays an important role in getting the mass spectrum when using an Orbitrap mass analyzer[2]. Shown in Equation 6.4.10 we can see a relationship between the m/z to frequency[2]. With the Orbitrap mass analyzer, one can surpass the limits of biomolecule sample for MS analysis which are high masses biological samples[2].The mass limit resolution range for quadrupole is 2,000 *m/z* to 4000 *m/z* while the mass limit resolution range for Orbitrap is 50,000 m/z to 100,000 m/z[2]. This is up to two magnitude difference in mass by using an Orbitrap mass analyzer[2].

Detector

Unlike other MS instruments, the detector of an Orbitrap mass analyzer is built into the Orbitrap itself (Figure 6.4.5) [3,6].

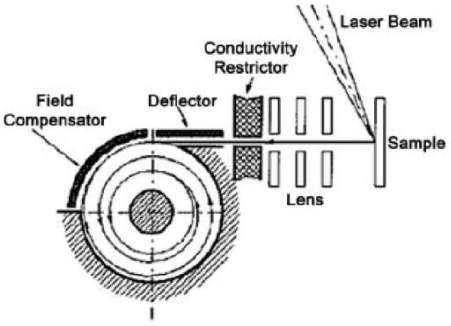


Figure 6.4.5: A side view schematic of the Orbitrap mass analyzer[6]

The detector for the Orbitrap is an image current detector[6]. For the Orbitrap, an electrostatic field is produced in the mass analyzer by the ion that are being measured through a series of signal processing[6]. The signal measured can be explained below:

$$\frac{Q}{q} = -\left(\frac{\Delta\Phi(r,\varphi,z)}{\Delta U}\right) \tag{6.4.11}$$

Equation 6.4.11 uses Green's reciprocity theorem to get the signal voltage induced by the oscillating ion in the Orbitrap[6] This equation shows the relationship between image charge (Q) induce the electrode to the charge (q) at point (r,φ,z) coordinate[6]. The voltage obtained in Equation 6.4.11, can be used to derive the induced current of the Orbitrap, as shown in Equation 2.2 below:.

$$I(t) = \frac{dQ}{dt} = -\frac{q}{\Delta U}\left[\frac{\partial\Delta\Phi(r,z)}{\partial r}\dot{r} + \frac{\partial\Delta\Phi(r,z)}{\partial r}\dot{z}\right] \tag{6.4.12}$$

Equation 6.4.12 is the total image current for a cloud of ions in the Orbitrap stating the total image current is based on the summation of individual currents[6]. An average value of r and z would be used for this system[6]. When talking about a One ion-based system, the z-axis will be the main thing that needs to determine the m/z ratio but when multiple ions are added to the system, one would need the radial axis to differentiate between the different ions[6]. These are dependent on the different energy associated with each polar coordinate shown in Equation 6.4.5[6]. The total image will be determined by the equation below:

$$I(t) \approx -\frac{q}{\Delta U} N \left(\frac{\partial \Delta \Phi(\mathrm{r}, 0)}{\partial \mathrm{z}} \right) \dot{z} \approx -qN\omega \left(\frac{\Delta z}{\lambda} \right) \sin(\omega t) \tag{6.4.13}$$

Equation 6.4.13 gives the total image current where it can describe the effective gap (lambda) between the detection electrodes[6]. With these equations and using FT, one can get a spectrum that is shown in Figure 6.4.6 and get mass spectrum data in Figure 6.4.7 [6]. Figure 6.4.6 is $^{56}Fe^{+}$ element that oscillated thousands of times around the Orbitrap mass analyzer and Figure 6.4.7 is a FT of the data giving the mass spectrum[6].



Figure 6.4.6: Signal of a $^{56}Fe^{+}$ ion in the Orbitrap [6]

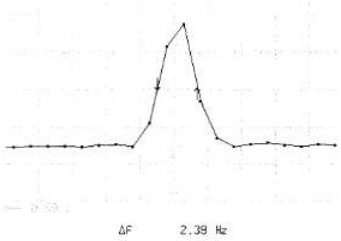


Figure 6.4.7: FT of the Signal of a $^{56}Fe^{+}$ ion in the Orbitrap[6]

Applications

One of the major application of Orbitrap mass analyzer is to use it to study large biomolecule such as cell membrane[3]. Some of the early work using Orbitrap mass analyzer was to study bovine insulin which was done before in the past but unable to get clear MS peaks[2-3]. Figure 6.4.8 gives the mass spectrum data of bovine insulin that illustrated good resolution peaks that was not obtainable without the orbitrap[3]. This shows the capability of Orbitrap mass analyzer where one get a resolution of 100,000 m/z[3]

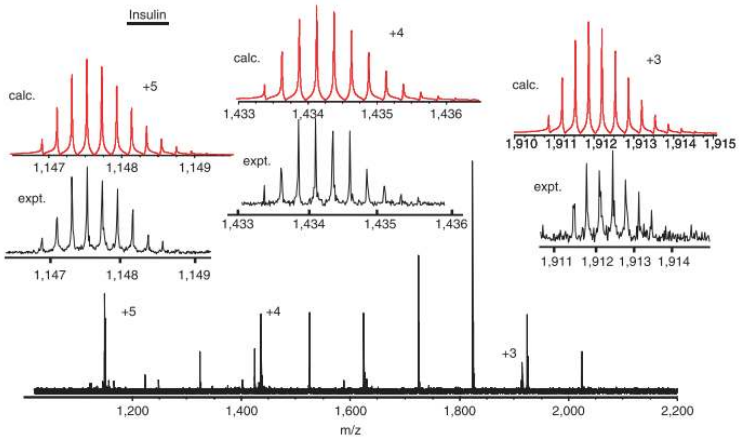


Figure 6.4.8 The MS data of *Bovine Insulin* using ESI Orbitrap mass analyzer [3]

These days Orbitrap mass analyzer have been used in protein analysis such as proteomic, glycoproteomic, and oligopeptide[7-8]. These can be applied to cell membrane analysis [7-8].The reason why Orbitrap is ideal because it is able to differentiate between complex biological samples that have similar m/z ratio[7]. Orbitrap is not the only MS that can be used for cell membrane analysis. Figure 6.4.9 gives all the possible ionizer and mass analyzer that could be coupled with one another to conduct MS analysis but base on resolution capabillity, Orbitrap mass analyzer is the best[9].

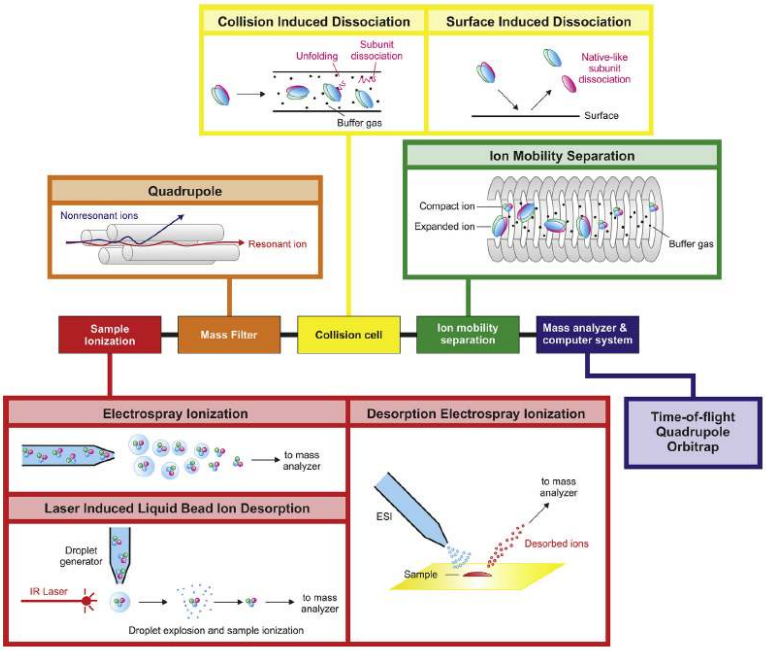


Figure 6.4.9: Different components that can be used for MS analysis of cell membranes

The advent of using Orbitrap over other MS instrument due to the high-resolution capability of the Orbitrap[2,9]. Due to the high sensitivity of the Orbitrap, one can measure multiple concomitant bindings event that were not possible before[9]. The high sensitivity allows the Orbitrap to distinguish small mass changes. One biological application are lipids, where their mass difference can be small[9]. Using the Orbitrap, one can distinguish mass difference as small as 12Da which were not possible for older generation MS[9]. Beside being able to distinguish low mass molecule, Orbitrap can get good spectra of high mass biological molecules.Another advantage of the Orbitrap is to study proteoforms, glycoforms and post-translational modifications that occur on the cell membranes[9]. A recent paper was published Nature Methods discuss current Orbitrap applications on membrane protein and lipid binding[10]. This paper can be link to by this doi: 10.1038/nmeth.3771 [10]

Summary

Orbitrap mass analyzer has opened a new path for biologically analysis, since it has high resolution limit of 100kDa/z. This makes Orbitrap a power tool in understand large biological system that could normally not be study with older generation MS. Orbitrap are currently being applied into the field proteomic, glycoprotemic, and glycolips which can be cell membrane related[7-9]. Even though Orbitrap mass analyzer has advanced our studies in the biological system, there at still limitation to the instrument[2-3,7-9]. With that said, Orbitrap still has a lot of potential for future advancement that can surpass its current limitation which helps the researcher in the field of biophysic.

References

1. Skoog, D. A.; Leary, J. J., Principles of Instrumental Analysis. Saunders College Publishing: Philadelphia, PA, 1992; p 420-461.
2. Hoffmann, E. D.; Stroobant, V., Mass spectrometry: principles and applications. John Wiley & Sons Ltd: Chicester, West Sussex, 2007; p 1-503.
3. Hu, Q.; Noll, R. J.; Li, H.; Makarov, A.; Hardman, M.; Graham Cooks, R., The Orbitrap: a new mass spectrometer. J Mass Spectrom 2005, 40 (4), 430-43.
4. Kingdon, K. H., A Method for the Neutralization of Electron Space Charge by Positive Ionization at Very Low Gas Pressures. Physical Review 1923, 21 (4), 408-418.

5. Knight, R. D., Storage of ions from laser-produced plasmas. Applied Physics Letters 1981, 38 (4), 221-223.
6. Makarov, A., Electrostatic Axially Harmonic Orbital Trapping: A High-Performance Technique of Mass Analysis. Analytical Chemistry 2000, 72 (6), 1156-1162.
7. Perry, R. H.; Cooks, R. G.; Noll, R. J., Orbitrap mass spectrometry: instrumentation, ion motion and applications. Mass Spectrom Rev 2008, 27 (6), 661-99.
8. Kailemia, M. J.; Xu, G.; Wong, M. Y.; Li, Q.; Goonatilleke, E.; Leon, F.; Lebrilla, C. B., Recent Advances in the Mass Spectrometry Methods for Glycomics and Cancer. Analytical Chemistry 2017.
9. Calabrese, A. N.; Radford, S. E., Mass spectrometry-enabled structural biology of membrane proteins. Methods 2018.
10. Gault, J.; Donlan, J. A. C.; Liko, I.; Hopper, J. T. S.; Gupta, K.; Housden, N. G.; Struwe, W. B.; Marty, M. T.; Mize, T.; Bechara, C.; Zhu, Y.; Wu, B.; Kleanthous, C.; Belov, M.; Damoc, E.; Makarov, A.; Robinson, C. V., High-resolution mass spectrometry of small molecules bound to membrane proteins. Nature methods 2016, 13 (4), 333- 336.

6.4: Mass Analyzer Orbitrap is shared under a CC BY 4.0 license and was authored, remixed, and/or curated by LibreTexts.

6.5: Mass Analyzer - Time of Flight

Cell membranes are considered one of the most important structures in biology since they play a critical role in biological processes and medicine. Despite their importance, there are still debatable hypotheses regarding their nature, especially their spatial arrangement of lipid and other membrane bound molecules.[1] For example, it is challenging to study lipids with good spatial resolution while not disturbing any important chemical information present on the cell membrane. This article will focus on discussing mass spectrometry, time of flight (ToF, mass detector) and time of flight coupled with secondary ion mass spectrometry (ToF-SIMS) as a tool to study membrane lipids. In recent years, mass spectrometry has been a widely used tool to analyze complex biological systems. In simplified terms, the analysis is carried out by obtaining mass-to-charge (m/z) ratios corresponding to the mass of the atoms or molecules. Figure 6.5.1 displays a flow chart depicting a mass spectrometer system. Here, we will focus on the mass analyzer component of the mass spectrometer system.

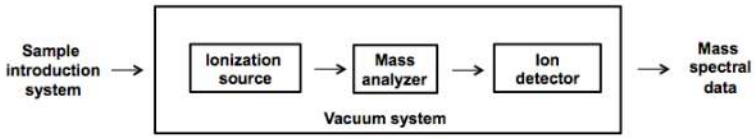


Figure 6.5.1. Simplified flow chart of a mass spectrometer system.

Mass Analyzers

It is important to note that each mass analyzer has unique parameters and applications as well as its own limitation. **Table 1** shows the different types of mass analyzers. Some mass spectrometers have a single mass analyzer and others have a combination of two, for the purpose of improving its analytical performance.[2] These are known as hybrid mass spectrometers and have a combination of mass analyzers such as a quadrupole coupled with a time of flight (QToF). Hybrid QToF mass spectrometers have the capability of performing tandem mass spectrometry or MS/MS analysis. In MS/MS analysis, primary ions are selected to transmit through the first mass analyzer. Then these primary ions are fragmented to produce secondary ions in a collision unit and lastly are analyzed by the second mass analyzer. This secondary analysis produces characteristic ion fragments and this results in increased selectivity and sensitivity.[3]

	Quadrupole	Ion trap	TOF	TOF reflectron	Magnetic	FTICR	Orbitrap
Mass limit	4000 Th	6000 Th	>1000 000 Th	10 000 Th	20 000 Th	30 000 Th	50 000 Th
Resolution FWHM (m/z 1000)	2000	4000	5000	20 000	100 000	500 000	100 000
Accuracy	100 ppm	100 ppm	200 ppm	10 ppm	< 10 ppm	<5 ppm	<5 ppm
Ion sampling	Continuous	Pulsed	Pulsed	Pulsed	Continuous	Pulsed	Pulsed
Pressure	10^{-5} Torr	10^{-3} Torr	10^{-6} Torr	10^{-6} Torr	10^{-6} Torr	10^{-10} Torr	10^{-10} Torr
Tandem mass spectrometry	Triple quadrupoles MS/MS fragments precursors neutral loss	—	—	PSD or TOF/TOF MS/MS fragments	Consecutive sectors MS/MS fragments precursors neutral loss	—	—
	Low-energy collision	Low-energy collision	—	Low- or high-energy collision	High-energy collision	Low-energy collision	—

Table 1. Types of mass analyzers with their distinct parameters.[4]

Time of Flight (ToF)

The mass analyzer this article will focus on is, time-of-flight (ToF). The principle of ToF mass analyzer involves the separation of ions based on the time it takes for the ions to travel through a flight tube with known length and reach the detector.[2] The trajectory of the ions through a ToF mass analyzer depends on its momentum and kinetic energy due to an applied pulsed acceleration voltage and *m/z* ratios of the ions.[2] Based on classical physics, ions with lower *m/z* will travel the fastest and arrive at the detector first while ions with larger *m/z* will travel the slowest and arrive at the detector last. A ToF layout is shown in Figure 6.5.2.



Figure 6.5.2: Schematic diagram of a linear ToF. Laser ionization time-of-flight mass spectrometer where ions are accelerated and separated by mass in a field-free drift region before detection. (CC BY-SA 4.0; K. K. Murray va Wikipedia).

The following derivation to describe a ToF analyzer dynamics was adapted from Hoffman et al 2007.[4] The time it takes for the ions to move across the flight tube between the ion source and detector allows us to determine the m/z ratios.[4] In the ToF spectrum, the recorded peak for any m/z will correspond to the sum of signals corresponding to multiple and independent ions arriving at the mass detectror. This can be shown in the following equations where the potential energy given to ions in the accelerated regions is converted to kinetic energy for all ions:

$$\underbrace{zeV_s}_{\text{potential energy}} = \underbrace{\frac{1}{2}mv^2}_{\text{kinetic energy}} \tag{6.5.1}$$

Next, we solve the equated equations above for velocity v.

$$v = \sqrt{\frac{2ezV_s}{m}} \tag{6.5.2}$$

Since velocity is equal to the drift path length divided by time we get:

$$v = \frac{L}{t} \Rightarrow t = \frac{L}{v} \tag{6.5.3}$$

Then solving for time and we get the following equation used to described time in a ToF analyzer.

$$t = \sqrt{\left(\frac{m}{z}\right)\left(\frac{L^2}{2eV_s}\right)} \tag{6.5.4}$$

By algebraically rearranging the equation above, an expression of m/z is determined as shown below.

$$\frac{m}{z} = \left(\frac{2eV_s}{L^2}\right)t^2 \tag{6.5.5}$$

We can also describe mass resolution for ions by differentiating the equation above with respect to mass and time we get the following relation:

$$\frac{1}{z}dm = \left(\frac{2eV_s}{L^2}\right)2tdt \tag{6.5.6}$$

Manipulating the equation above, we get the following relation used to express mass resolution.

$$\frac{m}{dm} = \frac{t}{2dt} \Rightarrow \frac{t}{2\Delta t} = \frac{m}{\Delta m} = R, \text{ mass resolution} \tag{6.5.7}$$

One of the draw backs for using a linear ToF is poor mass resolution.[4] Factors that causes poor mass resolution are shown in Figure 6.5.3. The starting times and locations of ions before they are accelerated into the flight tube are different and affect resolution. In addition, different kinetic energies for ions and initial orientation of ion also affect mass resolution and give poor results.

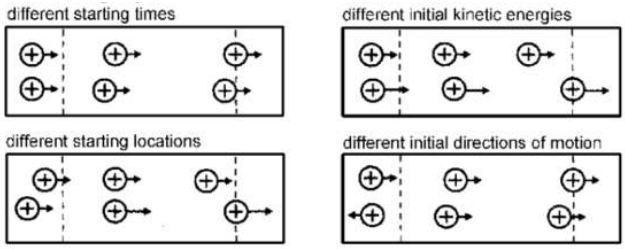


Figure 6.5.3. Factors affecting mass resolution in a linear TOF mass analyzer.[5]

To correct for poor mass resolution, a **reflectron** is added to the ToF analyzer. A layout of a reflectron ToF is shown in Figure 6.5.4. This type of ToF is sometimes abbreviated as ReTOF.[5]

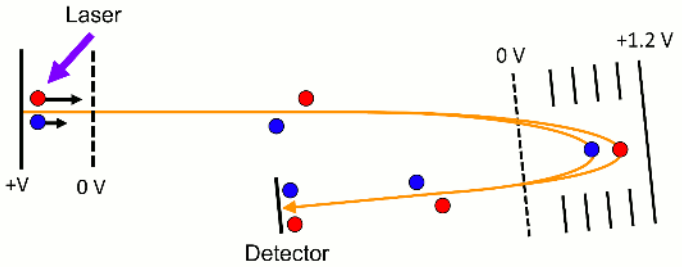


Figure 6.5.4. Schematic illustration of a reflectron ToF analyzer. In the reflection, the higher energy ion takes a longer path but arrives at the detector at the same time as the lower energy ion of the same mass. (CC BY-SA 4.0; K. K. Murray via Wikipedia)

There is applied potential in the reflectron, in which reflects ions in the opposite direction to the detector.[5] The ions shown in Figure 6.5.4 have similar spacing distances before they arrive at the reflectron and after the reflectron the ions are further apart. The reason for this is due to the difference in kinetic energy the ions carry. Heavier *m/z* ions have more kinetic energy than lighter *m/z* ions before and after the reflectron. Therefore, heavier ions will take longer to reach the detector and the lighter ions will reach the detector the quickest. The difference in time for the ions flight trajectory is proportional to the *m/z* of the ion. An example of enhanced mass resolution is shown in **Figure** 6.5.5.

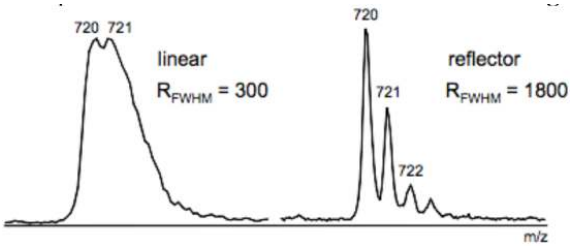


Figure 6.5.5. Illustration of mass resolution in a linear TOF and reflectron TOF spectrum.[6]

Secondary Ion Mass Spectrometry and ToF (ToF-SIMS)

The technique of Secondary Ion Mass Spectrometry (SIMS) has been used in biomedical surface imaging for more than three decades due to its inherent high sensitivity associated with mass spectrometric-based techniques.[7]

Some examples of the techniques include:[2]

- Static SIMS: used for sub-monolayer elemental analysis
- Dynamic SIMS: used for obtaining compositional information as a function of depth below surface
- Imaging SIMS: used for spatially-resolved elemental analysis

SIMS instrument works by first initiating a primary ion beam, which can generate either positive or negative ions. These ions are focused directly onto the analyte surface producing secondary ions. The secondary ions are transferred into a mass spectrometer across a high electrostatic potential. Figure 6.5.6 shows a simple representation on how SIMS works.[8] The ionized elements produced under vacuum from the interaction between the primary ion beam and the analyte are accelerated, focused and analyzed by a mass spectrometer.

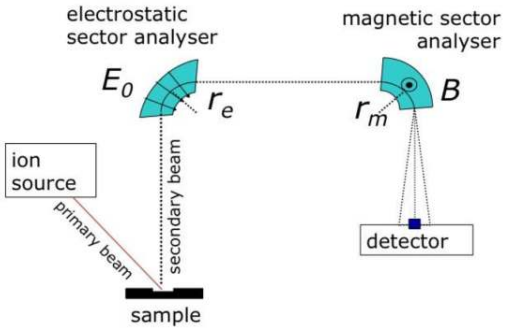


Figure 6.5.6. SIMS instrumentation schematic diagram, adapted from Geochrom Research Group

There are different designs of SIMS: NanoSIMS, ASI's SHRIMP, ToF SIMS, etc. Distinguishing between these instruments relies in their difference in intensity, energy and orientation of the primary beam.

Time-of-Flight Secondary Ion Mass Spectrometry (ToF-SIMS) is a surface -sensitive analytical method capable of producing high resolution chemical images. ToF-SIMS is one of the most suitable methods for analysis of lipids attached different to cell membranes and biological materials in general.[9] The method uses a high energy primary ion beam (e.g Au^{3+}, Cs^{+}) with pulses of 1 to 40 keV. The primary ion beam remove particles from the outermost surface of the sample causing desorption of secondary ions (SIMS method) as **Figure** 6.5.7 illustrates. Distinctively, in ToF coupled with SIMS, the particles accelerate into a "flight tube" (ToF method) where they are detected based on the exact time they reach the detector (time-of-flight).[10]

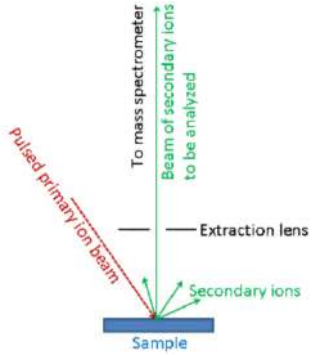


Figure 6.5.7. ToF SIMS scheme.[9]

ToF-SIMS Imaging of Lipids in Cell Membranes

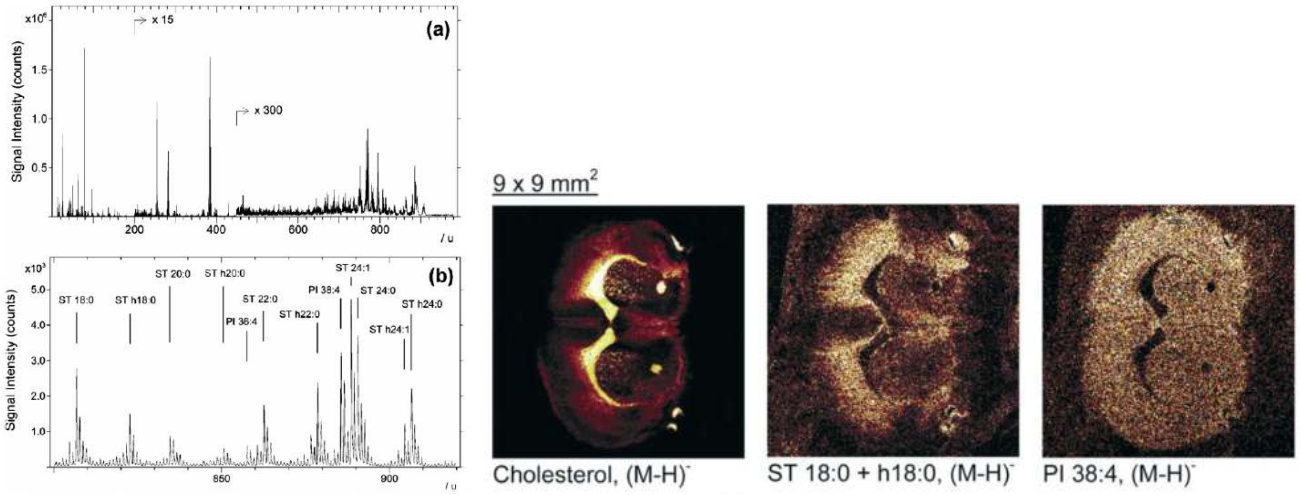


Figure 6.5.8. Examples of ToF-SIMS mass spectrum from biological tissue.[5] **Figure** 6.5.9. Examples of ToF-SIMS images from biological tissues.[5]

Figure 6.5.8 shows the mass spectrum from a section of a freeze-dried mouse brain. The upper graph (8a) shows an overview of the spectrum while the bottom (8b) shows a selected region corresponding to sulfatides and phosphatidylinositols peaks. Figure 6.5.9 shows a freeze-dried mouse brain that was imaged using the primary ion, Au_3+. The three different images show three distinct lipids: cholesterol, a sulfatide (ST 18:0 + h18:0) and a phosphatidylinositorl (PI 38:4).[5]

Conclusion

- Mass spectrometry (MS) is a useful analytical technique to measure the mass to charge ratio of molecules.
- SIMS allows for the examination and characterization of lipids directly from biological materials.
- ToF-SIMS is a surface analysis technique that enhances the resolution in chemical images on biological material to provide an in-depth understanding.
- ToF-SIMS is an emerging platform for lipid-based imaging studies.

References

1. *Surf. Interface Anal.* **2006**; 38: 1401–1412
2. Greaves, J.; Roboz, J., *Mass spectrometry for the novice*. CRC Press: **2013**.
3. McLafferty, F. W., *Tandem Mass Spectrometry*. Science. **1981**, *214*, 280-287.
4. De Hoffmann, E.; Stroobant, V., *Mass spectrometry: principles and applications*. John Wiley & Sons: **2007**.
5. Gross, J. H., *Mass spectrometry: a textbook*. Springer Science & Business Media: **2006**.
6. Loo, J. A., Studying noncovalent protein complexes by electrospray ionization mass spectrometry. *Mass spectrometry reviews* **1997**, *16* (1), 1-23.
7. 5.5 Secondary Ion Mass Spectrometry, Miller Index Notation
8. Holec, M., Kléma, J., Železný, F., Bělohradský, J., & Tolar, J. (**2009**). Cross-genome knowledge-based expression data fusion. In *International Conference on Bioinformatics, Computational Biology, Genomics and Chemoinformatics, BCBGC 2009* (pp. 43-50).
9. Biochim Biophys Acta. **2011** November ; 1811(11): 976–990. doi:10.1016/j.bbalip.2011.05.007 .
10. Benninghoven, A., Chemical Analysis of INorganic and Organic Surfaces and Thin Films by Static Time-of-Flight Secondary Ion Mass Spectrometry (ToF-SIMS), **1994**, Angewandte Chemie International (in English), vol 33 #10, 1023-1043.

6.5: Mass Analyzer - Time of Flight is shared under a CC BY 4.0 license and was authored, remixed, and/or curated by LibreTexts.

CHAPTER OVERVIEW

7: Computational Characterization of Membranes

7.1: Mathematical Continuum Descriptions of Membranes
7.2: Monte Carlo for Biomembranes
7.3: Molecular Dynamics for Biomembranes
7.4: Designing Molecular Membranes Models with VMD
7.5: Coarse Grain Simulations of Membranes

7: Computational Characterization of Membranes is shared under a CC BY 4.0 license and was authored, remixed, and/or curated by LibreTexts.

7.1: Mathematical Continuum Descriptions of Membranes

Membranes play an important role in cellular functions. They act as barriers to the outside environment, but also must allow the exchange of nutrients and waste. They must also be physically flexible to allow for cellular growth and movement, such as during cell division and migrations [1]. Membranes are composed of phospholipid bilayers. The phospholipids are amphipathic, containing a hydrophilic head and a hydrophobic tail. The membrane is composed of two adjacent layers of lipids, with the tails facing each other, and the hydrophilic heads facing the outside aqueous environment (Figure 7.1.1A). These membranes have a high aspect ratio with a low thickness of about 5 nm [1]. This is since the membrane is only two lipid molecules thick. However, the hydrophobic interior of the bilayer is a strong barrier against the transport of hydrophilic molecules across the membrane. Diffusion across the membrane is very slow for hydrophilic molecules and ions (transport requires transporter proteins) (Figure 7.1.1B). In addition, lipids can flip between leaflets, but this is very slow, as it requires the hydrophilic head pass through the hydrophobic region (Figure 7.1.1B). Lateral diffusion can be quite quick for lipids (~ 1 μm/s^2 and even transmembrane proteins (0.1 μm/s^2) (Figure 7.1.1B). Due to the described properties of the cellular membranes, they are commonly modeled as a 2-dimensional planar, elastic sheet in a 3-dimensional space (Figure 7.1.2). Biological structures like vesicles and even entire cells can be described as a closed form made by these sheets. These descriptions are known as continuum descriptions of the membrane. This is in contrast to molecular- and particle-based descriptions of the membrane, which focus on smaller time scales and length scales of membranes.

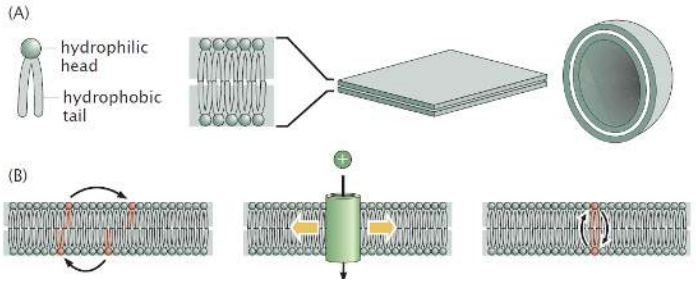


Figure 7.1.1: Structure of Biological Membranes (Adapted from [1]). A) The cell membrane is composed of a phospholipid bilayer. B) Lipids and proteins can undergo lateral diffusion, while hydrophilic molecules and ions require transporters. Lipids can also flip between leaflets.

To understand the shape and dynamics of membranes, we will need to describe the geometry of the membrane surface itself. In addition, we will describe how the energy changes for different membrane configurations. In particular, we will look at how the energy changes when a membrane is stretched, bent, sheared and changed in the thickness (Figure 7.1.2).

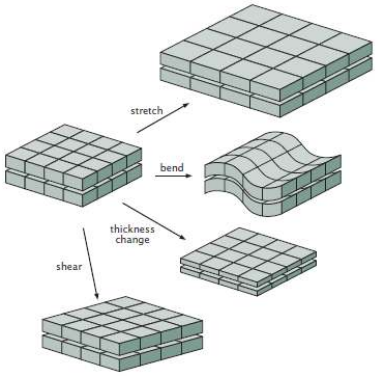


Figure 7.1.2: Biological membranes can be modeled as a two-dimensional sheet that stretches, bends, and changes in thickness. Adapted from [1].

Area Changes

The area deformation can easily be parameterized by a single variable Δa or a function $\Delta a(x, y)$ if the area deformation is dependent on position. We can treat the lipids in the membrane as a system of connected elastic springs, with increasing the area equivalent to stretching the springs (Figure 7.1.3).

As such, the energy of stretching a piece of membrane is:

$$E_a = \frac{1}{} \frac{K_a \Delta a^2}{} \tag{7.1.1}$$

$$\frac{-a}{2} \quad a_0$$

where K_a is the area modulus, which is intrinsic to the membrane, and a_0 is some reference area from which change in area is calculated (i.e. $\Delta a = a - a_0$). This equation is equivalent to a Hookean spring. Of course, when looking at a whole system, this term has to be integrated over the total area:

$$E_a = \frac{K_a}{2} \int (\frac{\Delta a}{a_0})^2 da \tag{7.1.2}$$

If the area change is constant over the surface of the membrane, then the integral reduces to Equation (1).

The area modulus has values of about 55-70 k_BT or 230-290 mN/m [1].

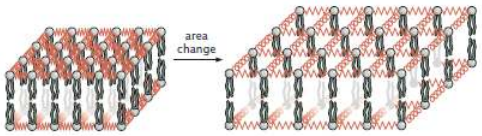


Figure 7.1.3: The area change of a membrane can be modeled by treating the membrane as a network of springs. Adapted from [1].

Thickness Changes

Membrane compression can simply be described by a function $w(x, y)$ that outputs the thickness at point (x, y). Again, we can model the thickness change as a system of springs (Figure 7.1.4). If the half-width of the membrane (essentially the lipid length in the membrane at equilibrium) is defined as w_0, and the thickness is $2w_0$ (Figure 7.1.4), then we get a similar equation for the energy penalty of changing the thickness:

$$E_{\text{thickness}} = \frac{K_t}{2} \int \left(\frac{w(x, y) - w_0}{w_0} \right)^2 da \tag{7.1.3}$$

where K_t is the stiffness for thickness variation, which is intrinsic to the membrane. It has units of energy/area and is approximately 60 k_BT/nm^2 [1].

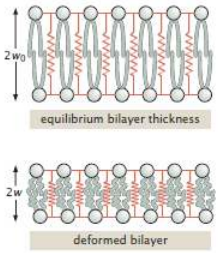


Figure 7.1.4: The thickness change of a membrane can be modeled by treating the membrane as a network of springs. Adapted from [1].

Shear Changes:

Pure phospholipid membranes are essentially two-dimensional fluids. Due to the fluid nature of phospholipid bilayer, the membrane cannot support a shear strain and does not have a shear modulus. *Therefore, as seen in Figure 7.1.2, static shear change does not deform a fluid membrane and does not cost any energy*. However, most biological systems are not pure fluid membranes. For example, red blood cells have an underlying cytoskeletal network, which can support shear. If the shear elasticity is an important effect that needs to be modeled, it must be accounted for to model the equilibrium shapes and the dynamics of such cells. An example of this is described later.

An Interlude on Membrane Geometry

To understand how the energy costs of bending are determined, it is important to describe the geometry of the membrane.

If we take a reference two-dimensional plane, we can define a function $h(x, y)$ that characterizes the height of the membrane above the reference plane at point (x, y). In most situations, this can accurately represent the shape of the membrane. This representation is known as the Monge parameterization (Figure 7.1.5). From the Monge parameterization, we can now calculate the curvature of a membrane. This is important as the free energy cost of bending the membrane is dependent on the curvature.

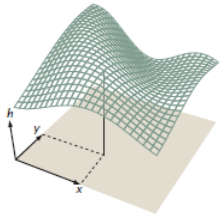


Figure 7.1.5: Monge representation. Adapted from [1].

In a single dimension, if we have a smooth function $y = h(x)$, then at a point x we can define the curvature $\kappa(x)$ to be the inverse of the radius of a circle that closely approximates the curve at point x (Figure 7.1.6A):

$$\kappa = \frac{1}{R} \tag{7.1.4}$$

It might be expected that a straight line has a curvature of 0. Indeed, since the circle that approximates the straight line is that of an infinite radius, the curvature is $\kappa = \frac{1}{\infty} = 0$ (Figure 7.1.7).

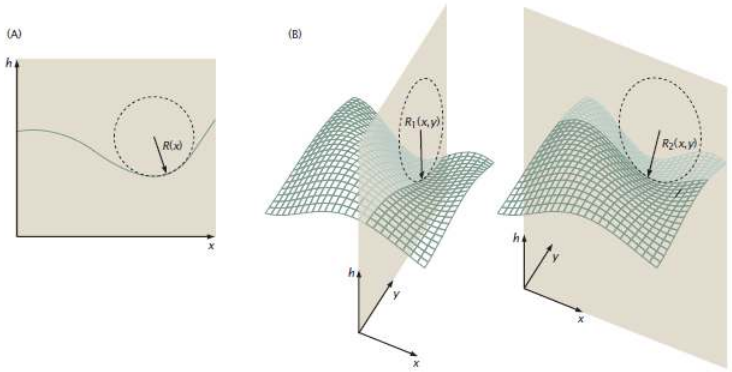


Figure 7.1.6: A) The curvature is defined as the inverse of the radius of the circle that best approximates the curve at a given point. B) For a surface, the curvature is defined by two values, which are the curvatures of the curve when the surface is cut by orthogonal planes. Adapted from [1].

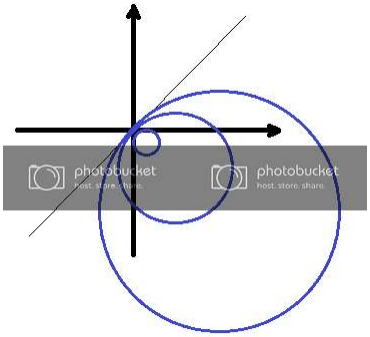


Figure 7.1.7: A line has an infinite radius of curvature and therefore a curvature of zero.

To generalize this to the two-dimensional case, we could cut through the two-dimensional surface with a plane, obtaining a curve, from which we can calculate the curvature. However, depending on the orientation of the plane used to cut the surface, the value of the curvature for that orientation is different. It can be shown that the curvatures in two directions describe a single point on a surface. Specifically, there is one particular choice of orthogonal planes that the curvatures take extreme values. These values c_1, c_2 are known as the principal curvatures (Figure 7.1.6B). In fact, one can calculate the curvature in any other direction using the formula:

$$c_X = c_1 \cos^2 \alpha_X + c_2 \sin^2 \alpha_X \tag{7.1.5}$$

where c_x is the curvature in the direction X, and α_X is the angle between the direction X and the direction belonging to curvature c_1. These statements are known as the Euler Curvature Formula.

As an example of principal curvatures, the principal curvatures of a cylinder would be $1/R$ around the circumference of the cylinder (as the radius of curvature is R, but 0 along the length of the cylinder.

Other curvature quantities calculated from the principal curvatures are also commonly defined:

$$\begin{aligned} K &= c_1 + c_2 \\ K_G &= c_1 c_2 \\ H &= \frac{K}{2} = \frac{c_1+c_2}{2} \end{aligned} \tag{7.1.6}$$

where K is the is the extrinsic curvature, G is the Gaussian curvature, and H is the mean curvature.

With the Monge parameterization, the curvatures can be expressed in terms of the height function. It can be shown that the extrinsic curvature is:

$$K = \nabla \cdot \left(\frac{\nabla h(\boldsymbol{r})}{\sqrt{1 + (\nabla h(\boldsymbol{r}))^2}} \right) \tag{7.1.7}$$

For a small gradient, the extrinsic curvature can be approximated as $K \approx \Delta h(\boldsymbol{r})$.

Why is the Monge parameterization and expressing the curvature using the parameterization important? These are important as the bending energy is dependent on the curvature, and to determine the equilibrium shapes of a membrane system, the height function that minimizes the total free energy of the system will be determined to represent the final membrane shape.

It is important to note that Monge parameterization is not the only way of describing a surface. It is not the most general parameterization or the most convenient parameterization in many cases. It will not work if there are folds or overlaps of the surface.

This is only an introduction to membrane/surface geometry, which itself is only a small part of the field of differential geometry. For more information on differential geometry in relation to membranes, the reader is referred to [3]. For a more general and advanced introduction to differential geometry, the reader is referred to [4].

Bending Changes – Helfrich theory:

The bending energy of a membrane is described by the well-known Helfrich theory. The Helfrich bending energy is defined in terms of the extrinsic and Gaussian curvature:

$$E_{\text{bend}} = \int \left(\frac{1}{2} \kappa_b \left(c_1 + c_2 - c_0 \right)^2 + \overline{\kappa}_b c_1 c_2 \right) dA = \int \left(\frac{1}{2} \kappa_b \left(K - c_0 \right) + \overline{\kappa}_b G \right) dA \tag{7.1.8}$$

where κ_b is the bending rigidity and $\overline{\kappa}_b$ is the Gaussian bending rigidity. This equation also contains the spontaneous curvature c_0. It is nonzero if there is some curvature in the membrane at an equilibrium state, which occurs if there is an asymmetric bilayer (different lipid composition for each monolayer). Typical values of κ_b is 10-20 k_BT [1].

It is important to note that that Gaussian bending term can be ignored in most cases due to the Gauss-Bonnet theorem. The Gauss-Bonnet theorem says that if the topology of the system remains unchanged, the integral over the Gaussian curvature will be a constant. The topology (genus) can be determined by the number of holes/handles the surface has. For example, a sphere has no holes and therefore has a genus of 0, but a donut has one hole and a genus of 1. Therefore, unless the genus of the system changes, the Gaussian term vanishes. This is the case for many biological membranes. However, for complicated morphologies of the endoplasmic reticulum and mitochondria, Gaussian curvature could have a significant contribution as membrane holes, tubes, and tori are created and destroyed.

We can simplify the above equation for Monge parameterization, with no spontaneous curvature. It can be shown for the Monge parameterization that the area element is $dA = dxdy\sqrt{1 + (\nabla h)^2}$. For the small gradient approximation, this is equivalent to $dA = \left(1 + \frac{1}{2}(\nabla h)^2\right) dxdy$ (based on a simple Taylor expansion). We can also penalize area stretching with a term $\frac{1}{2} \sum (\nabla h)^2$ where Σ is membrane tension. Therefore, a Helfrich energy equation for a Monge parameterization, under the small gradient approximation, and includes bending and tension is:

$$E_{bend} = \frac{1}{2} \int dxdy \left[\kappa_b (\Delta h)^2 + \Sigma (\nabla h)^2 \right] \tag{7.1.9}$$

Vesicles and Free Energy Cost

Vesicles are spherical lipid bilayer structures. Vesicles are used for many cellular processes for transporting large amounts of cargo within cells or even between cells. An example of the latter is the transport of neurotransmitters between neurons at the synaptic cleft.

We can calculate the free energy cost of the vesicles. The principal curvatures are the same: $1/R$ Therefore, the free energy cost is:

$$E_{vesicle} = \frac{\kappa_b}{2}\int\left(\frac{2}{R}\right)^2 dA = \frac{\kappa_b}{2}\left(\frac{2}{R}\right)^2 4\pi R^2 = 8\pi\kappa_b \tag{7.1.10}$$

Interestingly, this means there is a fixed energy cost to create a vesicle regardless of the size of the vesicle. If $\kappa_b \approx 10k_BT$ then $E_{\text{vesicle}} \approx 250\text{k}_B T$, which means there must be an active mechanism for the formation of vesicles in cells. Indeed vesicle-coating proteins like clathrin decrease this energy barrier such that vesicle formation is favorable.

Applications

Membrane tethers

When a pulling force is applied to a single point on a vesicle, it will generate an extruded membrane tubule known as membrane tethers. Membrane tethers have many biological implications. For example, neutrophils can use membrane tethers to attach to the endothelial wall when rolling. Membrane tethers also have an important role in the endomembrane system. In addition, the energetics and dynamics of membrane tethers are similar to that of other biological processes, such as endocytosis, and actin projections during cell motility.

Experiments use optical tweezers or molecular motors to apply a force at a single point on the membrane. We will use a simplified model (Figure 7.1.8) of the process where we have a sphere of radius R attached to a cylinder of radius r and length L. At the end of the cylinder is a hemispherical cap.

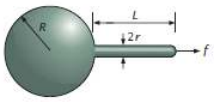


Figure 7.1.8: A simplified model of membrane tethers. Adapted from [1].

We can write the free energy of the vesicle+tether system by calculating the contributions of bending, area stretching, and compression. The bending energy of the system is:

$$\begin{aligned} E_{\text{bending}} &= 8\pi\kappa_b + \pi\kappa_b\frac{L}{r} + 4\pi\kappa_b \\ &= 12\pi\kappa_b + \pi\kappa_b\frac{L}{r} \end{aligned} \tag{7.1.11}$$

The first term corresponds to the spherical vesicle (as demonstrated previously). The second term corresponds to the cylinder, which is calculated by squaring the sum of the principal curvatures $\left(0+\frac{1}{r}\right)^2$ and multiplying by the area. The last term corresponds to the hemispherical cap.

Area stretching also contributes to the free energy of the system:

$$E_{\text{area}} = \frac{K_a}{2}\frac{(a-a_0)^2}{a_0} \tag{7.1.12}$$

where a_0 is the reference area and $a = 4\pi R^2 + 2\pi rL$ is the area of the system. The first term corresponds to a sphere of radius R and the second term corresponds to a cylinder of raidus r. Note that the area of the hemispherical cap $4\pi r^2$ is ignored as it is assumed $r \ll R, L$.

Note that this system has no thickness change of the membrane and therefore does not contribute to the free energy of the system.

In the case of a closed bilayer like a vesicle, the pressure difference across the membrane Δp also contributes to the energy of the system:

$$E_{pV} = -\Delta p\int dV = -\Delta p\left(\frac{4}{3}\pi R^3 + r^2\pi L\right) \tag{7.1.13}$$

Again, the contribution of the hemispherical cap is ignored. The minus sign is present because excess internal pressure increases the volume.

Finally, the force pulling the membrane must also contribute to the free energy of the system:

$$E_{load} = -fL \tag{7.1.14}$$

where f is the force applied. The minus sign is present because increased force leads to a high tether length.

Summing equations 11, 12, 13, and 14 together, we get:

$$E_{tot} = 12\pi\kappa_b + \pi\kappa_b\frac{L}{r} + \frac{K_a}{2}\frac{(a-a_0)^2}{a_0} - \Delta p\left(\frac{4}{3}\pi R^3 + r^2\pi L\right) - fL \tag{7.1.15}$$

> *At equilibrium, the total energy is minimized. Therefore, the equilibrium shape can be determined by minimizing the free energy.*

In this case, we can take the derivatives of Equation 15 with respect to each of the variables to minimize the energy.

Note that

$$\frac{\partial E_{\text{area}}}{\partial R} = K_a\frac{a-a_0}{a_0}\frac{\partial a}{\partial R} = \tau 8\pi R \tag{7.1.16}$$

where τ is the membrane surface tension, which can be related to area stretching by the formula $\tau = \frac{K_a(a-a_0)}{a_0}$. Similarly, it can be shown that $\partial E_{\text{area}}/\partial r = \tau 2\pi L$ and $\partial E_{\text{area}}/\partial L = \tau 2\pi r$. Therefore:

$$\begin{aligned}
&\tfrac{\partial E_{tot}}{\partial R} = 0 \rightarrow 8\pi\tau R - 4\pi\Delta p R^2 = 0 \rightarrow \Delta p = \tfrac{2\tau}{R}\\
&\tfrac{\partial E_{tot}}{\partial r} = 0 \rightarrow -\pi\kappa_b\tfrac{L}{r^2} + 2\pi\tau L - 2\pi\Delta p r L = 0\\
&\tfrac{\partial E_{tot}}{\partial L} = 0 \rightarrow \pi\kappa_b\tfrac{1}{r} + 2\pi\tau r - \pi\Delta p r^2 - f = 0
\end{aligned} \tag{7.1.17}$$

The first minimization leads to an equation known as the Laplace-Young relation, which is a well-known equation that relates the pressure difference Δp across a fluid interface (here the membrane) and the surface tension τ. A more general form takes into account both radii of curvature:

$$\Delta p = \tau\left(\frac{1}{R_1} + \frac{1}{R_2}\right) \tag{7.1.18}$$

We can plug in the Laplace-Young relation into the other minimized equations:

$$\begin{aligned}
&-\pi\kappa_b\tfrac{L}{r^2} + 2\pi\tau L - \tfrac{4\pi\tau r L}{R} = 0\\
&\pi\kappa_b\tfrac{1}{r} + 2\pi\tau r - f - \tfrac{2\pi\tau r^2}{R} = 0
\end{aligned} \tag{7.1.19}$$

Since $r \ll R$ (Figure 7.1.8) the last terms can be ignored:

$$2\pi\tau L = \pi\kappa_b\frac{L}{r^2} \tag{7.1.20}$$

$$r = \sqrt{\frac{\kappa_b}{2\tau}} \tag{7.1.21}$$

$$\pi\kappa_b\frac{1}{r} + 2\pi\tau r - f = 0 \rightarrow \pi\kappa_b\sqrt{\frac{2\tau}{\kappa_b}} + 2\pi\tau\sqrt{\frac{\kappa_b}{2\tau}} = f \tag{7.1.22}$$

$$f = 2\pi\sqrt{2K_b\tau} \tag{7.1.23}$$

We now get a relation between the radius of tether, bending energy, and membrane tension. In addition, we get a relation between the force applied, bending energy and tension. Similar relations can actually be used to determining the bending rigidity κ_b using a micropipette aspiration and optical tweezers used to make membrane tethers [5].

A general framework of determining equilibrium shapes (variational calculus):

The previous section looked at how relationships between meaningful physical quantities can be derived if the shape of the system is known. This was done by calculating the free energy cost for the membrane shape and minimizing it with respect to the variables of the system. However, a different approach can also be taken. What if the physical quantities of the system are known, but the equilibrium shapes need to be determined? This can be done by minimizing an energy functional of the system, which is the basis of variational calculus.

We can define a functional as a function that assigns a scalar value for a given function. In this case, we can think of the free energy of the system E_{tot} as a functional that is dependent on the height function $h(x, y)$. Variational calculus provides tools to find functions that minimize the functionals. This is exactly what we need to determine the equilibrium shapes! Variational calculus can be used to find the shape function $h(x, y)$ that minimizes the energy E_{tot}

In variational calculus, in a one-dimensional case, the minimization of the functional:

$$J[y] = \int L\left(x, y, y'\right) dx \tag{7.1.24}$$

is solved by the solution of the differential equation:

$$\frac{\partial L}{\partial f} - \frac{d}{dx}\frac{\partial L}{\partial f'} = 0 \tag{7.1.25}$$

where $y = f(x)$ minimizes the functional. This equation is known as the Euler-Lagrange equation. Indeed, the equation for E_{tot} has this form.

As a side note, many equations in physics have this form and the Euler-Lagrange equation is used. In fact, the dynamics of a physical system can be represented as a functional known as the Lagrangian, and solving the Euler-Lagrange equations for this Lagrangian lead to the equations of motion. This approach to classical mechanics is known as Lagrangian mechanics.

Going back to membranes, if we use Equation (9), we can get the following Euler-Lagrange equation:

$$\kappa\Delta\Delta h - \Sigma\Delta h = 0 \tag{7.1.26}$$

This partial differential equation can be solved for the height function that describes the shape of the membrane at equilibrium. This is called the shape equation.

Minimization of red blood cells:

While solving the shape equations are non-trivial and won't be shown here, some results in the case of red blood cells will instead be shown.

It is important to note that there are often two additional energy terms added to the Helfrich bending energy to obtain the total free energy for red blood cells.

When an initially flat membrane is bent, the outer monolayer is stretched, and the inner monolayer is compressed and the number of lipids per unit area is higher for the inner surface and lower for the outer surface. The energy cost of this is added to the model as the following model:

$$E_{ADE} = \frac{\kappa_{ADE}}{2}\frac{\pi}{AD^2}(\Delta A - \Delta A_0)^2 \tag{7.1.27}$$

where κ_{ADE} is a separate bending energy, which a material parameter, A is the membrane area, and D is the membrane thickness. This is known as the area-difference-elasticity (ADE) model.

In addition, an elastic term is added of the form:

$$E_e = \frac{K_A}{2}\oint \alpha^2 dA + \mu \oint \beta dA \tag{7.1.28}$$

where α^2 and β^2 are the local area and strain invariants, K_A and μ are elastic moduli for stretching and strain, respectively.

When the total free energy $E_{bend} + E_{ADE} + E_e$ is minimized, the equilibrium shapes of the red blood cells can be determined. The below Figure shows a comparison of the theoretically determined shapes and those that have been found experimentally.

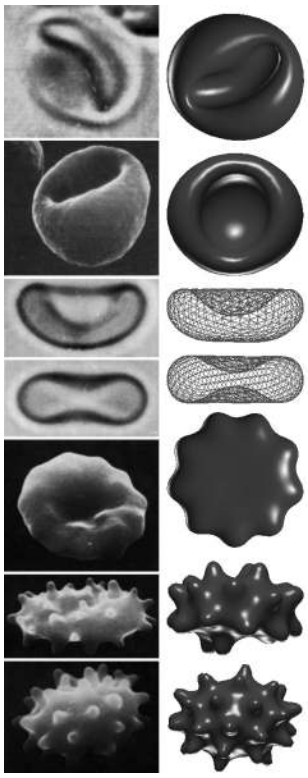


Figure 7.1.9: A comparison of experimentally observed red blood cell shapes (left side) and theoretically determined equilibrium shapes (right side). Adapted from [7]

References:

1. Phillips, R.; Kondev, J.; Theriot, J.; Garcia, H. G. Physical Biology of the Cell, **2013**, *Garland Science*, Taylor & Francis Group, LLC: Abingdon, UK.
2. Boal, D. Mechanics of the Cell. *Cambridge University Press*: Cambridge, UK. 2002
3. Deserno, Markus. Fluid Lipid Membranes – A Primer. *Max-Planck-Institut fu¨r Polymerforschung.* Mainz, Germany. 2006
4. Deserno, Markus. Notes on Differential Geometry. *Max-Planck-Institut fu¨r Polymerforschung.* Mainz, Germany. 2004
5. Bo, Lin, and Richard E. Waugh. “Determination of Bilayer Membrane Bending Stiffness by Tether Formation from Giant, Thin-Walled Vesicles.” *Biophysical Journal*, vol. 55, doi:10.1016/S0006-3495(89)82844-9. Accessed 13 June 2019.
6. Li, Xuejin, et al. Continuum- and Particle-Based Modeling of Shapes and Dynamics of Red Blood Cells in Health and Disease. *Soft Matter*, vol. 9, no. 1, 2013, pp. 28–37., doi:10.1039/c2sm26891d.
7. W., G. Lim H., et al. “Stomatocyte-Discocyte-Echinocyte Sequence of the Human Red Blood Cell: Evidence for the Bilayer-Couple Hypothesis from Membrane Mechanics.” *Proceedings of the National Academy of Sciences*, vol. 99, no. 26, 2002, pp. 16766–16769., doi:10.1073/pnas.202617299.

7.1: Mathematical Continuum Descriptions of Membranes is shared under a CC BY 4.0 license and was authored, remixed, and/or curated by LibreTexts.

7.2: Monte Carlo for Biomembranes

Complexity of Biological Membranes

The fluid mosaic model proposed by Jonathan Singer and Garth Nicolson in 1972 served as the starting point for our modern understanding of biological membranes [1]. A visual example of their model is depicted in Figure 7.2.1. Their model describes the biological membrane bilayer as an integration of proteins and lipids – capable of communicating and interacting to serve the necessary functions of the cell. These interactions can control movement of material in and out of the cell through protein pores, form lipid rafts, and regulate vesicle formation. This article will focus on computational methods used to study biomembranes (specifically Monte Carlo) but will start by examining the need of such tools.

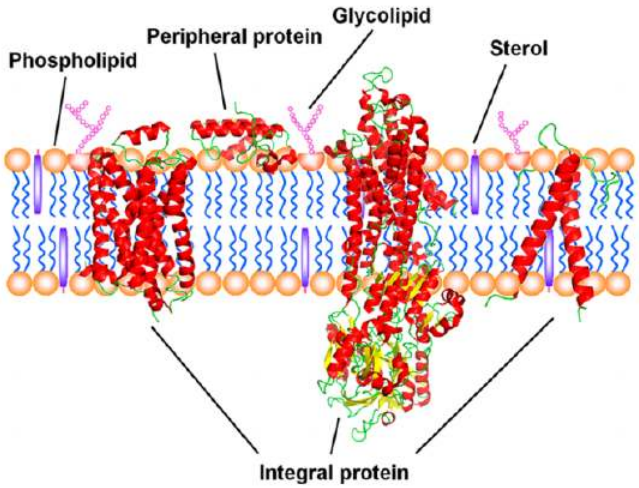


Figure 7.2.1: Illustration of the fluid-mosaic model [1].

Different Approaches: Experiments and Computation

Various experimental techniques have helped unravel numerous complexities of biomembranes. These include lipid photolabeling, X-ray crystallography, and NMR; each with distinguishing limitations and information provided [1,2]. Not only has our understanding of biomembranes been enhanced by experimental techniques, but structure-function characterization of membrane proteins has also provided targets for successful medical applications [1].

However, despite the success of these techniques, some biomembrane studies are currently too complex for experiments. Spectroscopic and structural analysis of lipid aggregates, for instance, average over several aggregate conformations and are unable to provide information on individual conformations [3]. Non-lamellar bilayer phases, which are associated with transient membrane heterogeneic states, are also difficult to study using experimental techniques [3].

Computational tools can facilitate these studies, and have deepened our knowledge of biomembranes in conjunction with experiments. For example, molecular dynamics and Monte Carlo simulations – along with various microscopy studies – have enhanced our understanding of lipid nanodomains and their role in membrane raft formation [3-6].

Computational Methods in Biomembranes: Introduction

Though several computational methods have been developed to examine biomembrane dynamics, two widely utilized methods are molecular dynamics (MD) and Monte Carlo (MC) simulations. MD involves numerical integration of macromolecular trajectories based on Newton's equations and describes the development of macromolecular position, orientation, and force fields through time [3-5,7-9].

While MD is relatively straightforward and highly detailed, it is restricted by short simulation times (~fs - μs) and cannot account for slower (~ms) membrane dynamics – such as lipid flip-flops and lipid domain formation – due to short integration time-steps (~fs) [2,5,7,9]. MC can bypass this time-dependence and potentially provide similar results to MD [2]. MC relies on sampling and generating likely configurations of the system based on thermodynamic conditions and applied perturbations [6-8]. However, MC has its own limitations: it contains biased configuration transitions, and some algorithms are more complicated and niche than MD

[7]. Though both approaches study biomembranes in distinct ways, they are not mutually exclusive; MD and MC approaches have been combined to enrich bilayer equilibration studies [2].

Monte Carlo – Basic Principles

Diverse MC variations have been developed to address wide-ranging questions related to biomembranes: an algorithm exploring diffusion in two-component membranes incorporated calculations involving the Hamiltonian and Gibbs free energy, while another study focusing on enzyme reactions in 2D lattices incorporated Michaelis-Menten kinetics [10,11]. Nevertheless, many MC methods share similar properties.

Essentially, MC schemes involve modeling the selected system with a set of probability density functions (PDFs), and repeatedly sampling these functions to generate potential outcomes of the system [12]. Depending on the output desired the details of the model will vary. In the case of biomembranes, thermodynamics governs these probability functions [8].

Lagrangian and Hamiltonian dynamics control the evolution of macromolecular systems in MC, as well as MD [8]. The Lagrangian is the difference between the kinetic and potential energy, and the Hamiltonian, defined in Equation 7.2.1, is the Legendre transformation of the Lagrangian:

$$\mathscr{H}\left(q^{3N}, p^{3N}\right) = \sum_{\alpha=1}^{3N} p^{\alpha} q_{\alpha} - \mathscr{L}\left(q^{3N}, \dot{q}^{3N}\left(q^{3N}, p^{3N}\right)\right) \tag{7.2.1}$$

Equation 1: The Hamiltonian [8].

where q^{3N} are the generalized coordinates, p^{3N} are the generalized momenta, and $\dot{q}^{3N}$ are the generalized velocities. The partition function, which describes various probabilities of different states of the system, is given in Equation 7.2.2 as:

$$Z(N, V, T) \equiv \int d\mathbf{p}^{N} d\mathbf{r}^{N} \exp\left[-\beta \mathscr{H}\left(\mathbf{r}^{N}, \mathbf{p}^{N}\right)\right] \tag{7.2.2}$$

Equation 2: The partition function [8].

where r^{N} represents the Cartesian coordinates of the system and β is the thermodynamic beta. The probability that a macromolecule is in a particular state with positions r^{N} and momenta p^{N} is given by Equation 7.2.3:

$$\Pr\left(\mathbf{r}^{N}, \mathbf{p}^{N}\right) d\mathbf{p}^{N} d\mathbf{r}^{N} = \frac{\exp\left[-\beta \mathscr{H}\left(\mathbf{r}^{N}, \mathbf{p}^{N}\right)\right] d\mathbf{p}^{N} d\mathbf{r}^{N}}{Z(N, V, E)} \tag{7.2.3}$$

Equation 3: Probability function that describes the probability of a molecule with a specific energy [8].

and the observed average state of the system (enthalpy, entropy, etc.) can be calculated by summing the values of the state and their associated probabilities, given by Equation 7.2.4:

$$\langle O \rangle = \int d\mathbf{p}^{N} d\mathbf{r}^{N} O\left(\mathbf{r}^{N}, \mathbf{p}^{N}\right) \Pr\left(\mathbf{r}^{N}, \mathbf{p}^{N}\right) \tag{7.2.4}$$

Equation 4. The system average observable *O* [8].

Generating representative states of the system requires Markov chain sampling of the configuration space, numerically integrating probability functions, and calculating the observed average state [8]. An MC bilayer simulation example is provided in Figure 2. Transitions between states in a sample depends on energy. In Metropolis MC, transitions to a lower energy state is accepted each time, while transitions to a higher energy state are accepted with a certain probability [8].

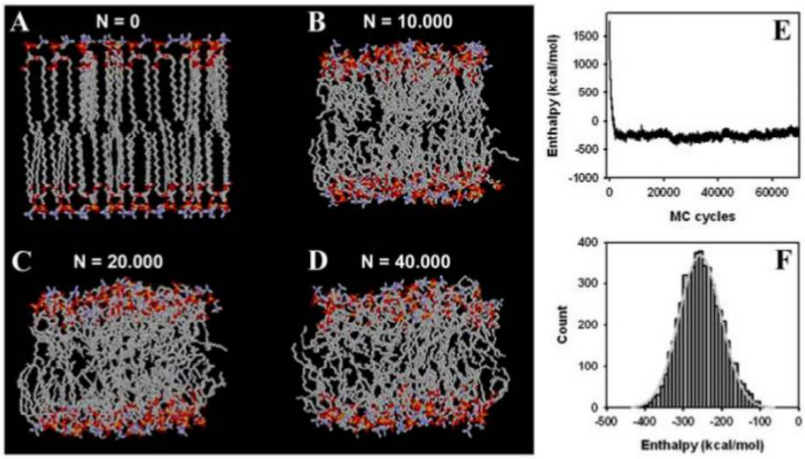


Figure 7.2.2: MC simulation of DPPC bilayer. (A-D) Simulation images at #N MC steps. (E) Enthalpy calculations after #N timesteps. (F) Histogram of enthalpy values of MC steps [2].

Issues to Consider

While MC can be useful to study populations of biomembrane configuration states, there are some issues to consider. It is extremely difficult to generate independent distributions for each biomolecule (or other entity) in the system due to computational limitations; MC sampling can also miss rare configuration spaces depending on the sampling size [13]. Defining adequate sampling will depend on the system of interest and available computational resources.

In addition, initial conditions of the model can influence MC sampling [11]. In the case of protein folding, initial conditions near the unfolded state can extend adequate sampling time to unreasonable lengths [13]. This is due to the vast configuration space surrounding the folded state(s). Understanding and controlling model sensitivity to initial conditions can help optimize MC sampling.

Level of Detail – Atomistic to Coarse Grained Models

While there are several levels of biomembrane modeling, this article will briefly discuss only atomistic and coarse-grained models.

Atomistic models describe atoms – bond angles, torsion angles, electrostatic and van der Waals interactions – and how these physical properties underlie complex lipid structure [9]. Coarse-graining on the other hand (Figure 3), examines collective behavior (of atoms, etc.) and how they contribute to collective membrane phenomena (phase transitions, vesicle fusion) [2-5,9].

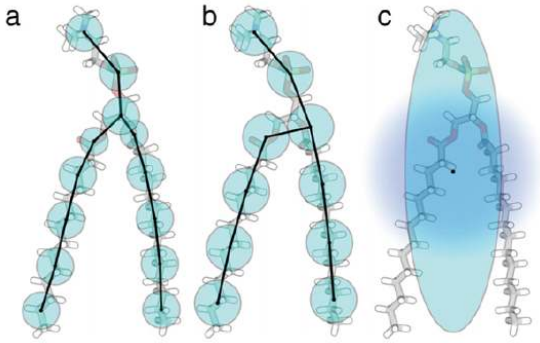


Figure 7.2.3: Example of coarse-graining of lipids [14].

The choice of detail will depend on the study and the available resources. While atomistic models provide highly detailed analyses, they require large amounts of computing power and are restricted to timescales of picoseconds to microseconds [2,3,5,9]. Coarse-grained models sacrifice some detail but significantly speed computational time due to reduced degrees of freedom, and they can examine behavior above the microsecond timescale [2-5,9].

MC Applications for Biomembranes

MC has been utilized for numerous biomembrane studies. These studies include:

- Characterizing protein-membrane interactions:
  - Cooperation between G-protein coupled receptors and lipid rafts [15].
  - Annexin-mediated domain formation with cholesterol [16].
- Structure and dynamics of biomembranes:
  - Vesicle structure under different nematogen concentrations [17].
  - Phase separation and formation of nanodomains.
  - Membrane structure under varying cholesterol and protein compositions.

These represent some of the numerous applications of MC to biomembranes.

Summary

- Computational tools – in conjunction with experiments – can significantly strengthen our knowledge of biomembranes.
- MC is one of the computational tools we can use, and extracts information about potential configurations in biomembranes.
- There are numerous issues to consider when using computational tools, which will depend on the study and the available resources.

References

1. Xia, Y. and Peng, L. 2013. Photoactivatable Lipid Probes for Studying Biomembranes by Photoaffinity Labeling. *Chem Rev*. 113: 7880-7929.
2. Wüstner, D. and Skelenar, H. 2014. Atomistic Monte Carlo Simulation of Lipid Membranes. *Int J Mol Sci*. 15: 1767-1803.
3. Marrink, S.J. *et al*. 2009. Lipids on the move: Simulations of membrane pores, domains, stalks and curves. *Biochim Biophys Acta*. 1788: 149-168.
4. Elson, E.L. *et al*. 2010. Phase separation in biological membranes: integration of theory and experiment. *Annu Rev Biophys*. 39: 207-226.
5. Rouse, S. *et al*. 2010. *Molecular Simulations and Biomembranes: From Biophysics to Function*. First Edition. Cambridge CB4 0WF, UK: The Royal Society of Chemistry.
6. Heimburg, T. 2000. Monte Carlo simulations of lipid bilayers and lipid protein interactions in the light of recent experiments. *Curr Opin Colloid Interface Sci*. 5: 224-231.
7. Pastor, R.W. 1994. Molecular dynamics and Monte Carlo simulations of lipid bilayers. *Curr Opin Struct Biol*. 4: 486-492.
8. Paquet, E. and Viktor, H.L. 2015. Molecular Dynamics, Monte Carlo Simulations, and Langevin Dynamics: A Computational Review. *BioMed Res Int*. vol. 2015, Article ID 183918, 18 pages. doi:10.1155/2015/183918.
9. Müeller, M. *et al*. 2006. Biological and synthetic membranes: What can be learned from a coarse-grained description? *Phys Rep*. 434: 113-176.
10. Hac, A.E. *et al*. 2005. Diffusion in Two-Component Lipid Membranes – A Fluorescence Correlation Spectroscopy and Monte Carlo Simulation Study. *Biophys J*. 88: 317-333.
11. Berry, H. 2002. Monte carlo simulations of enzyme reactions in two dimensions: fractal kinetics and spatial segregation. *Biophys J*. 83: 1891-1901.
12. Harrison, R.L. 2010. Introduction To Monte Carlo Simulation. *AIP Conf Proc*. 1204: 17-21.
13. Zuckerman, D.M. 2011. Equilibrium Sampling in Biomolecular Simulations. *Annu Rev Biophys*. 40: 41-62.
14. Ingólfsson, H.I. *et al*. 2014. The power of coarse graining in biomolecular simulations. *Wiley Interdiscip Rev Comput Mol Sci*. 4: 225-248.
15. Fallahi-Sichani, M. and Linderman, J.J. 2009. Lipid Raft-Mediated Regulation of G-Protein Coupled Receptor Signaling by Ligands which Influence Receptor Dimerization: A Computational Study. PLoS One. 4: e6604.
16. Almeida, P.F. *et al*. 2011. Monte Carlo Simulation of Protein-Induced Lipid Demixing in a Membrane with Interactions Derived from Experiment. *Biophys J*. 101: 1930-1937.
17. Sreeja, K.K. *et al*. 2015. Monte Carlo simulations of fluid vesicles. *J Phys Condens Matter*. 27:273104. doi: 10.1088/0953-8984/27/27/273104.

7.2: Monte Carlo for Biomembranes is shared under a CC BY 4.0 license and was authored, remixed, and/or curated by LibreTexts.

7.3: Molecular Dynamics for Biomembranes

Molecular dynamics (MD) is a simulation method used in many fields to help understand the movement of atoms and molecules. This method is based on Newton's equation of motion and generally does not include quantum mechanics. Each atom or molecule in the simulation is defined by a force field and mass, and is allowed to interact for a given time period. These time periods are kept short due to error propagation after many approximations. Many of the problems that use molecular dynamics often have a large number of atoms and are analytically intractable. Incorporation of boundary conditions allows researchers to reduce the size of a simulation without sacrificing pertinent information. One can run the desired simulation on the smallest possible unit, and surround it with replicas extending infinitely in all directions. This results in a “bigger” simulation that still requires minimal computation.

Biomembranes play a tremendously important role in organisms, separating cells from their environment and compartmentalizing organelles with unique and individual functions. Membranes contribute to the structure of cells and organelles via specific lipid composition and control what molecules cross the membrane through networks of protein channels interspersed among the lipid groups. Given the many important roles of biomembranes, understanding their composition, structure, and interactions with intracellular material and the environment is important for drug discovery and delivery. Because of the unique electrostatic and chemical properties of biomembranes, it is difficult and laborious to visualize them experimentally in a way that reflects their dynamic nature. For this reason, molecular dynamic simulations have become a ubiquitous method of visualizing membrane behavior and interactions with molecules of interest.

Physical Basis: Newton's Second Law

Molecular dynamics (MD) utilize equations from classical mechanics to describe the way in which atoms and small molecules interact. Quantum equations and relativity are ignored, but these exclusions minimally impact the implications of the tests being run. Approximations based on classical mechanics are usually sufficient to make accurate conclusions. MD is centered around Newton’s second law of motion. Rather than the traditional notation, this equation is expressed as a gradient of potential energy[1]:

$$\vec{F}_1 = -\nabla_i V\left(\vec{r}_3\right\}) \tag{7.3.1}$$

This equation expresses the gradient with respect to the position of the particle, *i. F* represents the conservative forces between atoms in the system, $-\nabla_i V$ is the gradient of the potential energy, and is the position of atoms. This equation can be adjusted to express the acceleration using F=ma, where the acceleration is the second time derivative of position:

$$m\partial_t^2 \vec{r}_i = -\nabla_i V\left(\left\{\vec{r}_j\right\}\right) \tag{7.3.2}$$

The right hand of this calculation is effectively mass times acceleration for Newton’s second law. In biomembrane systems, statistical and thermodynamical properties will reduce Hamilton's equations to the same equation above[1].

Using the Verlet Integrator to solve Newton's Second Law

While executing MD simulations, an integrator is applied to this partial differential equation to calculate positions and velocities of molecules based on initial conditions. There are many types of integrators commonly used by researchers. Most are based on the Taylor expansion of positions as a function of time:

$$\vec{\mathrm{r}}(\mathrm{t}) = \sum_{\mathrm{i}=0}^{\infty} \partial_{\mathrm{t}}^{\mathrm{i}} \vec{\mathrm{r}}_{\mathrm{t}=\mathrm{t}_0} \frac{(\mathrm{t}-\mathrm{t}_0)^{\mathrm{i}}}{\mathrm{i}!} \tag{7.3.3}$$

A common integrator is the Verlet integrator, which expands the above equation to the third order. The first derivative describes the velocity of a particle, the second is acceleration, and the third is jerk. The equation is performed positively and negatively with respect to time in order to maintain the symmetry necessary for accurate statistical mechanical description[2]:

Forward Expansion

$$\vec{r}(t) = \vec{r}\left(t_0\right) + \vec{v}\left(t_0\right)\Delta t + \frac{\vec{a}\left(t_0\right)\Delta t^2}{2} + \frac{\partial_t^3 \vec{r}\left(t_0\right)\Delta t^3}{6} + O\left(\Delta t^4\right) \tag{7.3.4}$$

Backward Expansions

$$\vec{r}(t) = \vec{r}\left(t_0\right) - \vec{v}\left(t_0\right)\Delta t + \frac{\vec{a}\left(t_0\right)\Delta t^2}{2} - \frac{\partial_t^3 \vec{r}\left(t_0\right)\Delta t^3}{6} + O\left(\Delta t^4\right) \tag{7.3.5}$$

In these equations, acceleration is represented by *a*. *O* is a constant used to abbreviate the fourth order Taylor expansion of the position equation. These equations are then combined to give the position algorithm expanded to the fourth order. This equation allows us to predict the position of all atoms in a system given we know the preceding and subsequent timesteps:

$$\vec{r}\left(t_0+\Delta t\right)=2\vec{r}\left(t_0\right)-\vec{r}\left(t_0-\Delta t\right)+\vec{a}\left(t_0\right)\Delta t^2+O\left(\Delta t^4\right) \tag{7.3.6}$$

The Isobaric-Isothermal Ensemble

To simulate common biomembrane environments, an isobaric-isothermal ensemble is used[20]. A statistical ensemble is a large set of replicated microstates that have the same macrostate. This is analogous to a scientist using the same conditions to test systems which may not be microscopically identical.

The isobaric-isothermal ensemble is also called the NPT ensemble, in which the number of particles N is conserved, and a constant pressure P and constant temperature T are applied. This mimics common biomembrane environments: liquids at constant temperature with the ability for lipids and proteins to expand and contract.

The Berendsen barostat is a common tool to maintain the effective pressure of the system. This is done by re-scaling box size and particle position to restore a target pressure (p_{target}). This is done using the following equation[1]:

$$\frac{V_{\text{new}}}{V_{\text{old}}}=\frac{\Delta t}{\tau}\left(1+\frac{p}{p_{\text{target}}}\right) \tag{7.3.7}$$

In this equation, *tau* indicates the frequency with which particle positions are re-adjusted. V_{new} *and* V_{old} indicate the box volumes at two adjacent timesteps.

The Nose-Hoover thermostat controls the kinetic degrees of freedom in order to keep the temperature constant[22]. Using a many-body Hamiltonian and a time-derivative scaling factor, the isothermal equations of motion can be expressed as multiple equations of motion where s is the scaling factor, Q is the position, P is the momentum, and each is a first order derivative:

$$\dot{\mathbf{Q}}_i=\mathbf{P}_i/m_is,\quad \dot{\mathbf{P}}_i=s\mathbf{F}_i \tag{7.3.8}$$

$$\dot{s}=s\alpha P_s,\quad \dot{P}_s=\sum_i\left[\frac{\mathbf{P}_i^2}{m_is^2}-Dk_BT\right] \tag{7.3.9}$$

This method is deterministic, time-reversible, and easy to implement. The problem is that not every system will be ergodic (the probability average will not be the long-term average).

Modeling a Membrane

MD allows us to monitor the movement and interactions of individual atoms within a molecule. This process is time consuming and computationally intensive, which limits the time-scale and area over which such calculations can be executed. In a biomembrane model, modeling the chemically interesting water molecules alone would take far longer than is practical, and only a few lipid groups would be able to be modeled. Viewing a whole unit of interest this way would be limited to a nanosecond simulation time. Many all-atom simulations of bilayers only model 128 lipids, or 64 on each layer[1]. This style of simulations has a number of useful applications, including looking at local structural characteristics and dynamics of membranes as well as how specific components such as sterols affect local membrane structure. However, events such as bilayer assembly and phase transitions and separations occur on time-scales unreasonable for atomistic models.

Using too big of a timestep might miss important transitions that affect the properties of the system, but too short of a timestep is computationally expensive. Angle vibrations are on the order of 10 femtoseconds, and it is advisable to make the timestep an order of magnitude shorter than the smallest observed events[1]. Generally 1 femtosecond to a few picoseconds is an acceptable range.

Parameters used for Biomembranes

The math utilized for each parameter varies by program, but the functions will be summarized here briefly.

Bond angles and bond lengths: Bond angles and lengths are typically constrained to biologically relevant values. Each residue has a range of angles it is expected to adopt, and these expectations are implemented into a model's parameters. Whether or not bonds are allowed to stretch or oscillate between different angles is a controllable parameter.

Torsional degrees of freedom: Torsional degrees of freedom are the different bond angles at which a molecule can be stable. For example, in CO_2 the molecule is linear, so there are no different bond angle configurations it may take. In n-butane, which takes the

form of CH_3-CH_2-CH_2-CH_3, where each of those bonds can take 3 energetic positions. This parameter is regularly constrained.

Chain order parameter: Chain order is a measure of the angle of tail C-H bond and the bilayer normal. This can be defined for a single lipid[1]. The order parameter can be calculated using the following equation (S is the order parameter, and Theta CD is the angle between the C-H bond and the bilayer normal):

$$S_{\mathrm{cD}} = 0.5 \left\langle 3 \cos^2 \Theta_{\mathrm{cp}} - 1 \right\rangle \tag{7.3.10}$$

The order parameter is calculated for all saturated carbons. Unsaturated carbons no longer have a tetrahedral orientation and the order parameter does not apply.

Effects of parameters

The basic premise of MD is building an equation or set of equations for describing the free energy of a system based on parameters that adequately describes the chemistry and physics observed. While each program, model, and lab uses individualized sets of parameters, there are a few common to almost all MD simulations. Non-bonded interactions, such as Lennard-Jones, van der Waals, electrostatic, and chemical bonding interactions, are calculated for adjacent and spatially proximate atoms. Chain order gives insight into how tightly packed lipid tails are within the bilayer, which in turn has implications for the phase, melting temperature, and fluidity of the bilayer[1]. A completely saturated lipid tail, for example, would pack tightly and have restricted motion, but tails with unsaturated bonds would have kinks in the chain that cause it to pack less tightly[3] (Figure 7.3.1).

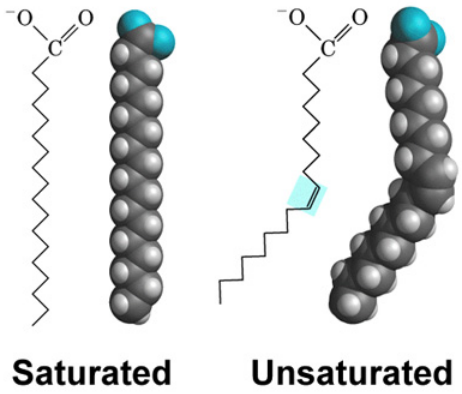


Figure 7.3.1. Saturated and unsaturated fatty acid tails. Saturated tails retain a linear structure, while the double bond in an unsaturated tail causes a kink.

The size of the head group and lipid length further allow us to constrain MD simulations by providing estimations of the order and phase of the bilayer. Radial distribution functions describe the morphology and structure of the membrane, which when coupled with information about the density of the structure can provide a holistic spatial view of the bilayer[1].

Water and solvents pose sizeable challenges in MD, as they comprise a majority of the atoms and interact with molecules in a multitude of ways, depending on temperature, pressure, and proximity to polar and hydrophobic groups. While many models represent water as a liquid, this model is insufficient in instances when extreme temperature changes lead to phase changes. The most widely used water model that accommodates these phase changes is the SPC model, which restricts water-molecule interactions to the oxygen and treats the hydrogen as fixed charges[4,5] (Figure 7.3.2)[6]. More will be said about solvents in the Implicit versus Explicit Solvent Model section.

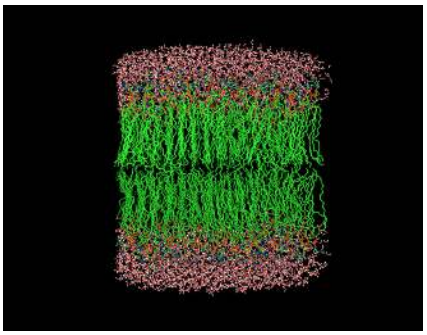


Figure 7.3.2. MD simulation of a phosphilipid bilayer (green) surrounded by water molecules (red and white). Water molecules are computationally expensive, their degrees of freedom are frequently reduced in simulations.

Calculating Charge of a Membrane

Within an MD simulation, the charge must be equal to zero. However, we know that biomembranes usually contain charged regions, as well as unique long-range interactions not commonly found in small molecule interactions. The integral of the potential ($V(r)$ for long-ranged interactions is:

$$\int_0^\infty V(r)r^2dr = \infty \tag{7.3.11}$$

where r is the radius of the space being modeled. For simplicity, this shape is assumed to be a symmetric sphere. That this integral diverges is problematic, but a number of techniques have been developed to address the charges indirectly. One solution (the Particle Mesh Ewald technique) applies different calculations that fall above and below a specified charge cut-off. Below the cut-off, electrostatic interactions are calculated directly, and above the cut-off they are calculated with Fourier analysis using a 3-D fast Fourier transform[7]. This method is preferred because it is highly accurate in the local environment while also reasonably fast. The above integral differs from the integral for Lennard-Jones and short-range interactions, which converge and can be easily calculated.

Force Fields

A force field is a set of parameters and equations that determine potential energy and therefore movement of a system.[23] The four common and updated force fields for biological molecules are Amber, CHARMM, GROMOS, and OPLS. Each undergoes revision as experimental techniques change. Although each of the aforementioned force fields is commonly used for biomolecules, study of phosophilipids is most developed in the CHARMM and Berger force fields.

The CHARMM27 force field is an all-atom force field for lipids, nucleic acids, and amino acids that is being developed by various scientists including Martin Karplus. This force field is part of the CHARMM package of force fields. The Lennard-Jones potential is similar to other force fields but the electrostatic component is purely repulsive. This

The Berger force field is an addition to parameters found in Amber and OPLS that uses a united-atom force field that groups each carbon in a chain with its hydrogens. Compared to the CHARMM27 force field, this decreases the number of atoms in a system by one-third and drastically decreases the number of pairwise interactions. This method requires less computing power but is less accurate than all-atom force fields assuming that error is not large from step to step.

Membrane Protein Simulation

Proteins are an important part of cell membranes and should be considered when modeling biomembranes. The proteins along and inside membranes are the basis for many of the cell's functions including: signaling, motility, contraction, energy generation and consumption, and regulation. Use of MD to understand the behavior of membrane proteins in different situations is then an important technique in learning about the individual mechanisms of each protein.

Kandt et al. described a four step system to set up a membrane protein simulation[23]:

1) Orient the protein

To orient the protein, the protein and bilayer boxes should be the same dimension. Then the hydrophobic transmembrane domain is aligned with the lipid tail locations. This can be easily done with graphical interfaces and in GROMACS using the *editconf* tool.

2) Prepare the bilayer

There are multiple techniques, but the simplest and most common technique is to populate the lipid coordinates with lipids and then use cut-off lengths to delete physically impossible or improbably configurations. The problem is that local density requires additional simulation time to return to equilibrium, which can lead to larger error. In non-equilibrium simulations this is less of a problem, but the timescale required to achieve equilibrium may be in the nanosecond range, similar to a complete simulation.

A more efficient method is to create a lattice of lipids with a spacing greater than a real bilayer, insert the protein, and then compress the bilayer. The compression step goes through two repeating sub-steps: compression and energy minimization. This can be done with a grid and then compressing the lipid box size, or by superimposing the protein, expanding the bilayer to prevent overlap, and then scaling lipid positions.

3) Solvate the system

Adding water into bilayers is easy and quick, but proteins complicate this. Issues include water that may be trapped in the membrane by the protein and cavities in proteins that are isolated from the bulk. The simplest approach is to run a cavity analysis to avoid placing water in areas that they should not exist. In GROMACS, van der Waals radii are stored in vdwradii.dat and are used by the *genbox* tool. By increasing the vdW radii of lipid tails, no water will be present in the protein or bilayer.

4) Equilibrate the structure

Pressure coupling is an important part of achieving a realistic equilibrium. Isotropic pressure coupling does not allow for membrane fluctuations, while anisotropic coupling may cause systems to deform. Semi-isotropic pressure coupling should be used in interfacial systems, where x and y directions are coupled.

Electrostatics is another parameter, which is discussed by the section "Calculating Charge of a Membrane". In short, pairwise interactions are considered below a cut-off radius, and above the cut-off Fourier analysis is used to determine the interactions.

Then the simulation should be run to a minimum length to equilibrate the system. In example DPPC bilayers, it takes 10-20 ns of simulation to equilibrate. This is comparable to full simulation times so steps should be taken to optimize this step. Rotational and lateral diffusion is a rate limiting step, so the lipid bilayer should be set up such that this time is minimized. Protein coordinates must be restricted.

Potential energy will drop and minimize quickly but this is not a sign of equilibrium. Instead, look at pairwise interaction energies.

Odd structures

Other molecules are often associated with membrane proteins such as co-factors or ligands that may not exist in the simulation package[23]. Two solutions to this may be to use a force field with the required topology or to build it yourself. To re-build complex molecules, one common approach is to approximate the structure using amino acids if the structures are similar, or to find something else in the force field that can approximate it. This way the same force field and therefore set of parameters may be used for both the membrane protein and the lipids. Another consideration is that the membrane environment behaves differently compared to a water system. Using force fields meant to be in water causes problems with membrane protein structure and function, for example a potassium channel accepting sodium[25].

Implicit versus Explicit Solvent Models

Implicit solvent models treat the solvent as a continuum[26]. The solvent is approximated as a field with an associated dielectric constant. Solvation free energy of a solute is incorporated as an effective energy term in the force field. This approach increases computational efficiency by eliminating solvent-solute interaction potentials. It also reduces degrees of freedom in the system, resulting in reproducibility between simulations and instantaneous solvent relaxation in membrane systems.

Explicit solvent models treat the solvent as individually bonded atoms. An all-atom model is used in these systems. For these, the choice of force fields and cut-off radius is a critical consideration. In the CHARMM27 force field, lipid tails trended towards all-trans compact conformations, which is smaller than reality. The CHARMM36 force field agreed with experiments much more. Also, orientation of membrane protein complexes is needed, or else solvents may be trapped or impossible bending situations may happen. Explicit solvents are much more computationally expensive.

Atomistic vs. Coarse-grained modeling

While atomistic models give us insight into the exact interactions happening within a membrane, this level of detail is computationally expensive. Modeling larger-scale processes such as bilayer assembly, lipid-protein interactions, and phase transitions with this method is not practical. In order to accommodate the amount of computing power these large scale simulations

demand, coarse-grain models (CG) neglect details that do not affect long scale events. CG models minimize sampling by merging atoms into particle groups, or "pseudo-atoms," based on shared chemical and electrostatic properties[8]. For example, a lipid might be condensed to a polar "head" molecule, a phosphate group, and a hydrophobic tail group (Figure 7.3.3). Another technique used to reduce degrees of freedom in a CG model is to ignore short-range dynamics. When looking at larger scale events, these interactions tend to have negligible effects, and are effectively unimportant for the question of interest[9]. Larger scale MD models, such as coarse-grain models, utilize, unsurprisingly, larger scale parameters. Two common parameters are the space occupied by individual molecules as well as membrane thickness. These properties are calculated using a variation on standard area and volume equations[1].

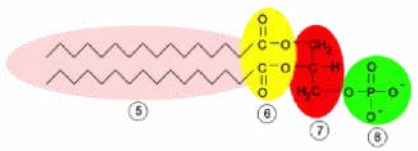


Figure 7.3.3. Phospholipid partitioned into four "pseudo-atoms" based on hydrophobicity. 5 is a hydrophobic tail, 6 is a polar ester linkage, 7 is the glycerol head, and 8 is the negatively charged, hydrophilic phosphate head.

Applications

Now that we have addressed some of the variables that go into constructing MD simulations of membranes, we will discuss some applications of this technique. This list merely glosses over an extensive field of research, but should provide an overview of the breadth of knowledge possible to acquire with these techniques.

We know that most membrane molecules engage in some degree of hydrogen bonding, but this is effectively impossible to observe experimentally. Atomistic models that utilize the expected geometry of a hydrogen bonded system create a functionally relevant picture of these interactions. Bond angles and lengths must be constrained to those observed experimentally, but accurate models have been generated this way[10]. In modeling hydrogen bonding, it is also crucial to constrain which functional groups can serve as bond donors and acceptors[11].

MD simulations can be used to study phase transitions and formation of lipid rafts. By varying the temperature of the model, researchers can observe how classes of membrane molecules interact and either localize or disperse among other membrane molecules[12,13]. The rigidity as well as the fluidity of membranes can be measured using MD; these properties are determined by observing the density and lipid profile of the membrane. The way in which cholesterol contributes to both rigidity and fluidity in membranes has been studied extensively in membranes[14].

Finally, protein-membrane and small molecule-membrane interactions two rapidly growing fields of research currently being pursued using MD[15,16,17]. While there are too many examples to include in this review, we will note that ion channels, cell surface receptors, and cytoskeleton proteins have all been studied with MD[18,19].

Comparison with Monte Carlo Techniques

MD was created in response to the success of Monte Carlo techniques. In Monte Carlo (MC), random sampling is constrained by rules from probability, process rules, and statistical physics in order to generate a series of states[27]. These techniques are used for many applications from physics and chemistry to gambling. Current MC techniques are based on Markov chains, models that find the probability of the next event only based on the previous state. Random numbers are generated as start points with random variables and statistical ensembles constraining the system.

Compared to MD, MC is much less computationally expensive and is easier to implement. However, defining and viewing physical movement of systems is difficult and some trajectories may take particles into impossible positions. It does not show intermediate states as well as MD, and energy within the system is not so easily tracked or taken into account. For low density systems, the disadvantages of MC are not as important as molecules interact less often.

References

1. [1]Dickey AN and Faller R. Molecular Modeling of Biomembranes: A How-To Approach. In *Biomedical Applications of Biophysics*; Jue, T., Ed.; Humana Press, Springer, 2010; pp 35-58.
2. [2]Verlet L. 1967. Computer 'experiments' on classical fluids, I: thermodynamical properties of Lennard-Jones molecules. *Phys Rev* **159**: 98-103.

3. [3]Tieleman DP, Marrink SJ, Berendsen HJC. 1997. A computer perspective of mebranes: molecular dynamics studies of lipid bilayer systems. *Biochim Biophys Acta* **1331**: 235-270.
4. [4]Berendsen HJC, Postma JPM, van Gunsteren WF, Hermans J. Interaction models for water in relation to protein hydration. In *Intermolecular forces*; Pullman B.; Ed.; Dordrecht, Reidel, 1981; pp 331-342.
5. [5]Berendsen HJC, Grigera JR, Straatsma TP. 1987. The missing term in effective pair potentials. *J Phys Chem* **91**: 6269-6271.
6. [6]Werten PJL, Rémigy HW, de Groot BL, Fotiadis D, Philippsen A, Stahlberg H, Grubmüller H, Engel A. 2002. Progress in the analysis of membrane protein structure and function. *FEBS Lett* **529**: 65-72.
7. [7]Essman U, Perela L, Berkowitz ML, Darden HLT, Pedersen LG. 1995. A smooth particle mesh Ewald method. *J Chem Phys* **81**: 3684-3690.
8. [8]Muller M, Katsov K, Schick M. 2006. Biological and synthetic membranes: what can be learned from a coarse-grained description? *Phys Rep* **434**: 113-176.
9. [9]Lopez CF, Moore PB, Shelley JC, Shelley MY, Klein ML. 2002. Comoputer simulation studies of biomembranes using a coarse grain model. *Comput Phys Commun* **147**:1-6.
10. [10]Lindahl E, Hess B, van der Spoel D. 2001. GROMACS 3.0: a package for molecular simulation and trajectory analysis. *J Mol Model* **7**: 306-317.
11. [11]Dickey AN, Faller R. 2007. How alcohol chain-length and concentration modulate hydrogen bond formation in a lipid bilayer. *Biophys J* **92**: 2366-2376.
12. [12]Jørgensen K, Mouritsen OG. 1995. Phase separation dynamics and lateral organization of two-component lipid membranes. *Biophys J* **69** (3): 942-954.
13. [13]Baoukina S, Mendez-Villuendas E, Bennett WFD, Tieleman DP. 2013. Computer simulations of the phase separation in model membranes. *Farad Discuss* **161**, 63-75.
14. [14]Oldfield E, Chapman D. 1972. Dynamics of lipids in membranes: Heterogeneity and the role of cholesterol. *FEBS Lett* **23** (3) 285-297.
15. [15]Lee BW, Faller R, Sum AK, Vattulainen I, Patra M, Karttunen M. 2004. Structural effects of small molecules on phospholipid bilayers investigated by molecular simulations. *Fluid Phase Equilibr* **225**: 63-68
16. [16]Lindahl E, Sansom MSP. 2008. Membrane proteins: molecular dynamics simulations. *Curr Op Struct Biol* **18** (4): 425-431.
17. [17]Bond PJ, Holyoake J, Ivetac A, Khalid S, Sansom MSP. Coarse-grained molecular dynamics simulations of membrane proteins and peptides. *J Struct Biol* **157** (3) 593-605.
18. [18]Isralewitz B, Gao M, Schulten K. 2001. Steered molecular dynamics and mechanical functions of proteins. *Curr Op Struct Biol* **11**: 224-230.
19. [19]Paavilainen VO, Berling E, Falck S, Lappalainen. 2004. Regulation of cytoskeletal dynamics by actin-monomer-binding proteins. *Trends Cell Biol* **14** (7): 386-394.
20. [20] Dill, K. A.; Bromberg, S.; Stigter, D. 2003, *Molecular Driving Forces*. New York: Garland Science.
21. [21]Berendsen HJC, Postma JPM, van Gunsteren WF, Dinola A, Haak JR. 1984. Molecular dynamics with coupling to an external bath. *J Chem Phys* **81**:3684–3690.
22. [22]Posch HA, Hoover WG, Vesely FJ. 1986. Canonical dynamics of the Nose oscillator: Stability, order, and chaos. *Phys. Rev. A.* **33**(6):4252-4256.
23. [23]Kandt C, Ash AL, Tieleman DP. 2006. Setting up and running molecular dynamics simulations of membrane proteins. *Methods* **41**475-488.
24. [24]Sapay, N. and Tieleman, D. P. 2011. Combination of the CHARMM27 force field with united-atom lipid force fields. *J. Comput. Chem*., **32**: 1400–1410.
25. [25]Domene, C., & Sansom, M. S. P. 2003. Potassium Channel, Ions, and Water: Simulation Studies Based on the High Resolution X-Ray Structure of KcsA. *Biophysical Journal*, **85**(5), 2787–2800.
26. [26]Mori T., Miyashita N., Im W., Feig M., Sugita Y. 2016. Molecular dynamics simulations of biological membranes and membrane proteins using enhanced conformational sampling algorithms. *Biochimica et Biophysica Acta*, **1858**:1635-1651
27. [27]Schlick, T. 2010. Molecular Modeling and Simulation: an Interdisciplinary Guide 2nd edition. New York: Springer.

7.3: Molecular Dynamics for Biomembranes is shared under a CC BY 4.0 license and was authored, remixed, and/or curated by LibreTexts.

7.4: Designing Molecular Membranes Models with VMD

Introduction

While modern experimental techniques are able to resolve membrane-bound protein function, structural determination is still a challenge. To provide insight into the behavior of membranes and the proteins residing within them, computational biologists utilize molecular dynamics (MD) simulations. Since the early 2000's there has been a remarkable increase in the number of computational methods, software, and visualization aids, reinforcing the need for MD [Ref. 1]. This tutorial is for users to become familiar with producing and visualizing atomistic membranes for MD simulations. This tutorial will use Visual Molecular Dynamics (VMD), a molecular visualization program of large biomolecular systems, to visualize membrane models. Additionally, the tutorial will discuss how CHARMM-GUI, a molecular systems generation web interface, can be used to build membrane models. Completion of this tutorial will allow the user to:

1. Design, visualize, and select certain lipid sections using the VMD command interface.
2. Visualize homogenous phosphatidylethanolamine (POPE) and phosphatidylcholine (POPC) membranes using VMD's *MembraneBuilder* extension tool.
3. Create solvated, heterogenous lipid membrane models using the CHARMM-GUI *Membrane Builder* extension tool.

This tutorial uses a Linux 64 version of VMD (ver. 1.9.3 OpenGL). Other system downloads can be found here: www.ks.uiuc.edu/Development/Download/download.cgi?PackageName=VMD [Ref. 2]. Other versions may result in an inexact rendition of the tutorial, however, the concepts remain valid and should be practiced. Experimentation is encouraged. The CHARMM-GUI *Membrane Builder* extension can be found here: http://www.charmm-gui.org/?doc=input/membrane.bilayer [Ref. 3-8].

Note: text in *italics* indicates verbatim text/tools/commands that can be found/typed on your screen when going through the tutorials. User exercises are also indicated in *italics*. Figure references are highlighted in **bold** to indicate helpful visuals.

1. Basic VMD visualization of POPE

The Protein Data Bank (PDB) is the largest online repository containing more than 150,000 three-dimensional biological structures to date [Ref. 9-11]. Computational biologists frequently use the PDB as a starting point for their molecular models, either implementing existing PDB structures (as .pdb file formats) or formatting their own PDB template for molecular dynamics (MD). However, most PDB files do not contain membrane structure components; computational biologists typically design their own membranes and insert protein structures within them. Thus, this section is an introduction for new users on how to navigate Visual Molecular Dynamics (VMD) software before building membranes. This section will use the lipid phosphatidylethanolamine (POPE) as the example structure. For a review on lipid types and their properties, visit the BPH 241 Lipids webpage: https://phys.libretexts.org/Courses/University_of_California_Davis/UCD%3A_Biophysics_241_-_Membrane_Biology/Lipids

1.1. Contents of a .pdb file and loading the POPE model

Phosphatidylethanolamine (POPE) is a glycerophospholipid and one of the most abundant lipid types in bacteria. In the downloadable files section (bottom of page), you will find the file *1.1_single_POPE.pdb*. A .pdb file is a Protein Data Bank file containing all of the experimental and three-dimensional coordinate information needed to visualize the biomolecule **(Figure 1.1)**. More information on .pdb files and their syntax can be found here: http://www.wwpdb.org/documentation/file-format [Ref. 12-13].

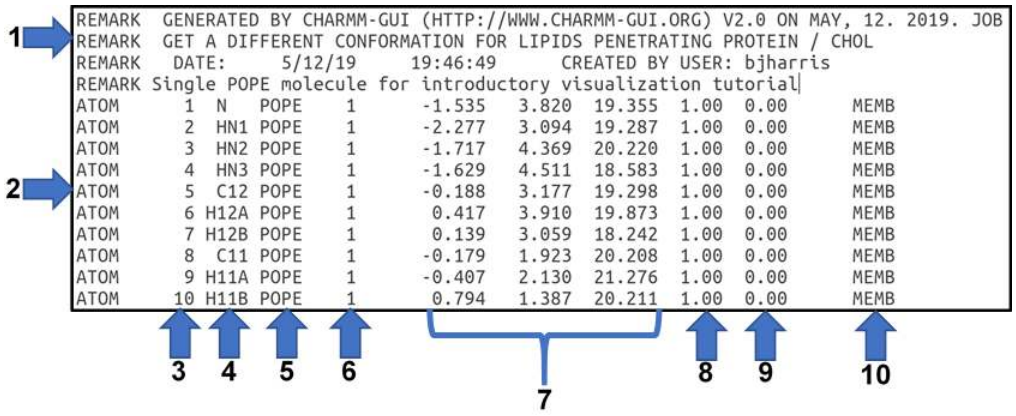


Figure 7.4.1.1. *Example text from a .pdb file.* ***1)****The REMARK section is for user comments.* ***2)*** *The ATOM section contains coordinate and atom type information.* ***3)*** *The index (serial number) of each atom. Note while PDB files start at 1, the index for VMD starts at 0.* ***4)*** *The atom name.* ***5)*** *The residue/molecule name* ***6)*** *The residue/molecule sequence number.* ***7)*** *The orthogonal X, Y, and Z coordinates in Angstroms.* ***8)*** *The occupancy.* ***9)*** *The temperature factor.* ***10)*** *Unread information stating that this is part of a membrane. Further explanation of .pdb syntax can be found in [Ref. 12].*

After downloading the VMD software, redirect to the VMD folder and open the README file for installation instructions. In addition to installation, Linux users will have to add a VMD path to their .bashrc file to call from the terminal. On the last line of your .bashrc file, add *export PATH=/type/your/directory/here/vmd:$PATH* **(Figure 1.2)**. Now, the keyword *vmd* can be typed in the Linux terminal to launch VMD. Note: Some Linux distributions, Windows, and Mac devices as well as VMD software distributions may differ; always read the README file for the best installation guidance.

```
export PATH=/usr/local/bin/vmd:$PATH
```

Figure 7.4.1.2. *An example of adding VMD to your .bashrc file, located in your home directory.*

After launching VMD, you will see two windows: the *VMD Main* and the *VMD Display*. The *VMD Main* window contains the executable commands and options to manipulate the molecule on the *VMD Display*. Next, from the *VMD main* window, load the *single_POPE.pdb* file using *File → New Molecule...* A new window called the *Molecule File Browser* will appear. From here, click *Browse* and navigate to the folder containing *single_POPE.pdb*. After selecting, click *Load* in the *Molecule File Browser* window to load the POPE molecule to the *VMD Display* **(Figure 1.3)**.



Figure 7.4.1.3. *How to load a PDB file.* ***1)*** *The VMD main window contains all commands and options for manipulating models.*

To create a new session, click File → New Molecule... ***2)*** *In the Molecule File Browser, files can be selected with the Browse button.*

Once a file is selected the Molecule File Browser will determine the file type. A file is loaded by clicking the Load button.

3) *Once a file is loaded, it will appear in the VMD Display window. In this example, a single POPE molecule is displayed as lines.*

1.2 Basic VMD visualization features: orientation, rotation, and representation

The *VMD Display* has two primary mouse manipulation modes: rotate (press *r* on keyboard) and translate (press *t* on keyboard). More mouse mode commands can be found here: www.ks.uiuc.edu/Research/vmd/vmd-1.9.3/ug/node32.html [Ref. 14-15].

For rotate mode, the following mouse commands are:

- Left click and hold = free three-dimensional rotation
- Right click hold = rotation parallel to computer screen
- Mouse wheel = zoom in/out of center

For translate mode, the following mouse commands are:

- Left click and hold = translate molecule parallel to computer screen
- Right click and hold mouse wheel = zoom in/out of center

On the *VMD Display*, you should see the *Lines* representation of a POPE molecule; *Lines* representation is when atom types are represented by colored lines indicating the element type. In this model, the colors for each element are:

- cyan = carbon
- white = hydrogen

- red = oxygen
- orange = phosphorous
- blue = nitrogen

The *Lines* representation is helpful to visualize the entire molecule, but there are other representations that can be used. From the *VMD Main*, go to *Graphic → Representations…* A new window called *Graphical Representations* will appear **(Figure 1.4)**. Here you will see a selected molecule tab where you can visualize different molecules. You will also see *Draw style*, *Selections*, *Trajectory*, and *Periodic* tabs that tweak the visual representation of each molecule.

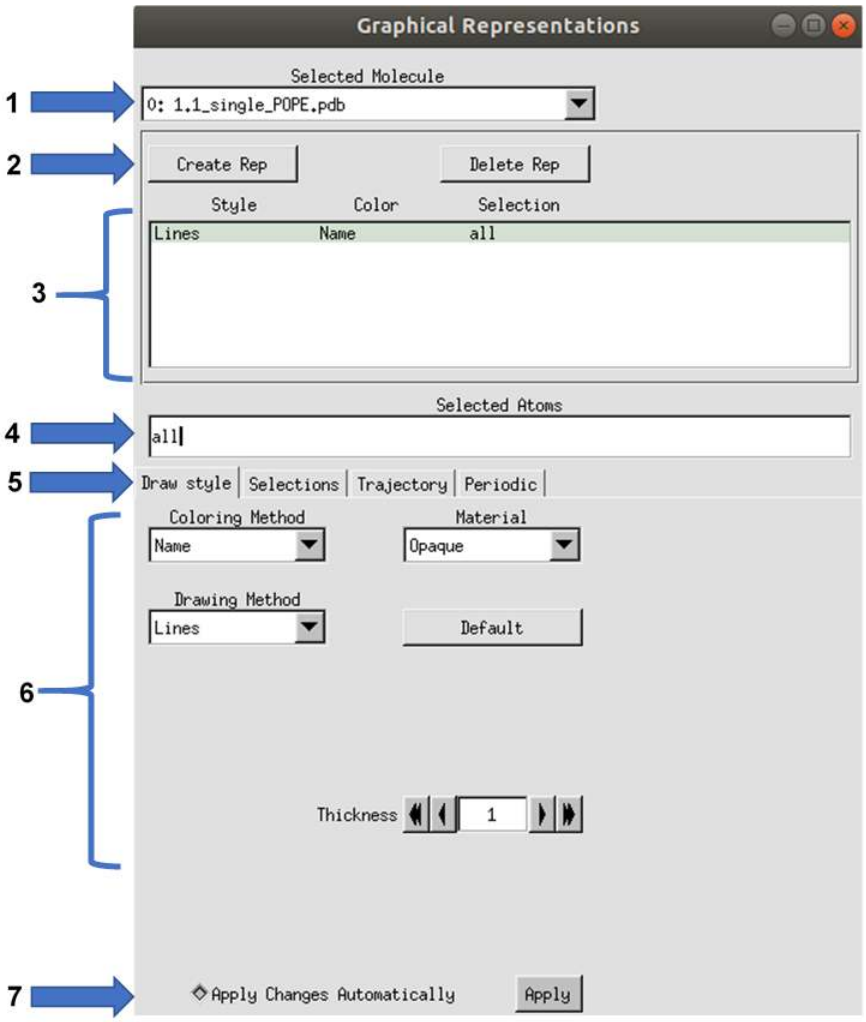


Figure 7.4.1.4. *The Graphical Representations tab allows you to modify the visual representation of your model. **1)** Select a molecule for editing. **2)** Create representations of the selected molecule. This is useful for representing the same model in different graphical styles. **3)** A window of all created representations. Highlight a representation to enable it for editing. **4)** A command window that can be used to select specific parts of an atom for visualization. **5)** The tab selection menu with the Draw Style tab open. The Draw Style tab controls visual representation of the model. The Selections tab allows precise selection of specific atoms within the model. The Trajectory tab controls animation features while the Periodic tab controls periodic image display; both will not be discussed in this tutorial but are explained in the VMD User's Guide [Ref. 15]. **6)** All controls in the Draw Styles tab; the Coloring Method controls how atoms are colored, the Drawing Method how the model is drawn, the Material method how the model is shaded, and the Thickness controlling the model line thickness. Other options may appear as different Drawing Methods are selected. **7)** Once a graphical representation is complete, changes must be applied and can be toggled to apply automatically.*

Focus on the *Draw style* tab. In it, you can change the *Coloring Method*, the *Drawing Method*, the *Material* shading, and the *Thickness* of representation. Change the *Thickness* of the line from 1 to 5. It should be easier now to visualize the molecule. Reset the *Thickness* to 1.

In the *Drawing Method* selection pane you will find different molecule visualization schema. Some common styles are *Lines*, *VDW*, and *CPK* **(Figure 1.5)**, however there are other styles available **(Table 1.1)**. The *Lines* style is the oldest style which uses

lines as bonds and points as atoms. The *VDW* is a Van der Waals style and is a helpful space-filling representation. The *CPK* style can be thought of as a combination of *Lines* and *VDW* by providing scaled atoms as spheres linked by cylindrical bonds.

In the *Coloring Method* selection pane you will find different coloring schemes depending on atom typing, molecule collection, residue ID, and some physical properties. The effectiveness of these schemes will be dependent on your .pdb file parameters. For now, the *single_POPE.pdb* file is only useful with the *Name* method. Experiment with the various drawing/coloring methods. Afterwards, reset the molecule with *Coloring Method: Name* and *Drawing Method: CPK*.

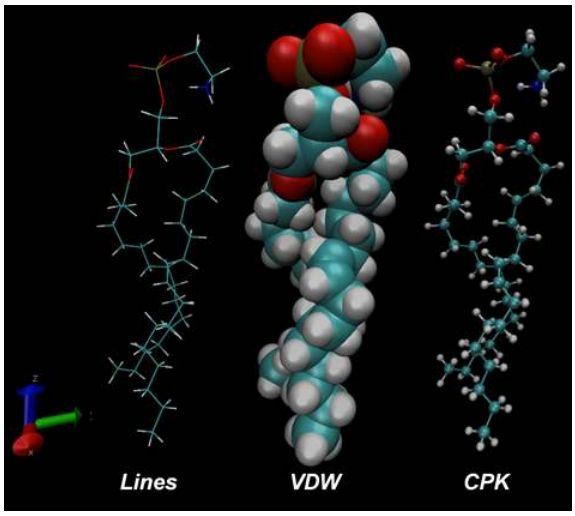


Figure 7.4.1.5. *POPE visualization using (Left) Lines, (Middle) Van Der Waals, and (Right) CPK draw styles.*

The Lines style is useful for understanding structure, the VDW style for space-filling, and the CPK style as a mixed style utilizing both Lines structure and CPK space-filling.

Table 1.1. *Molecular draw styles from VMD User's Guide Version 1.9.3 [Ref. 15]*

Representation styles	Description
Lines	simple lines for bonds, points for atoms
Bonds	lighted cylinders for bonds
DynamicBonds	dynamically calculated distance-based bonds
HBonds	display hydrogen bonds
Points	just points for atoms, no bonds
VDW	solid van der Waal spheres for atoms, no bonds
CPK	scaled VDW spheres, with cylinders for bonds
Licorice	spheres for atoms, cylinders for bonds, same radius
Polyhedra	polyhedra connecting atoms within a cutoff radius
Trace	connected cylindrical segments through C_α atoms
Tube	smooth cylindrical tube through the C_α atoms
Ribbons	flat ribbon through the C_α atoms
NewRibbons	smooth ribbon through the C_α atoms
Cartoon	cartoon diagram (cylinders and ribbons) based on secondary structure
NewCartoon	smooth cartoon diagram (smooth ribbons) based on secondary structure
PaperChain	display ring structures as polygons, colored by ring pucker
Twister	flat ribbon tracing glycosidic bonds, with twists oriented by sugar residues
QuickSurf	molecular surface (Gaussian density surface)
MSMS	molecular surface as determined by the program MSMS
Surf	molecular surface as determined by SURF
VolumeSlice	display a texture mapped slice from a volumetric data set
Isosurface	display an isovalue surface from a volumetric data set
FieldLines	field lines generated by integrating particles by volume gradient vectors
Orbital	molecular orbital selected by wavefunction type, spin, excitation, and orbital ID
Beads	per-residue approximate bounding spheres
Dotted	dotted van der Waals spheres for atoms, no bonds
Solvent	dotted representation of the solvent accessible surface

1.3. Identification of atom types

To label specific atoms, go to the *VMD Main* window and select *Mouse → Label → Atoms*. Clicking on an atom will show the molecule name followed by the atom name. From the color scheme, label the phosphorous atom followed by the nitrogen. To manage the labels, go to the *VMD Main* window and select *Graphics → Labels…* Here you can find a collection of the labels you have made. You can click on each label and show, hide, delete, and reposition them in the *VMD Display* **(Figure 1.6)**. For example,

select the *POPE1:P* (the phosphorous) atom label. Under the *Picked Atom* tab you will find the naming information (*ResName*, *ResID*, etc). In the *Properties* tab you can drag the crosshair in the *Offset* chart to reorient the label. In the *Global Properties* tab you can adjust your text size and thickness.

In addition to visualizing atom labels, you can visualize bond lengths and angles. Again, from the *VMD Main* window, select *Mouse → Label → Bonds*. To visualize a bond length or distance between atoms, you must click on the two atoms you are interested in measuring from. You can find the labeled distances from *Graphics → Label* in the *VMD Main* window. Similarly, you can calculate angles by clicking on three atoms **(Figure 1.7)**. It is important to note that VMD cannot display double bonds since the .pdb file does not contain bond information. Indeed, PDB files contain coordinate information only. VMD compensates for this by using a distance measure algorithm to determine which atoms are bonded. Protein Structure Files can also be used to explicitly state bonding information but are beyond the scope of this tutorial. Therefore, an intuitive understanding is sometimes needed for the viewer to fully understand the model.

Figure 7.4.1.6. *The labels window where you can identify atom naming schema and adjust visual labels.* ***1)*** *Select between atoms, bonds, angles, dihedrals, and springs labeling.* ***2)*** *The selection of atoms currently labeled. Those shown on the VMD Display are in black text while hidden labels are shown in red text.* ***3)*** *The Tab selection menu.* ***4)*** *The Picked Atom tab displays coordinate and naming information of the selected atom.* ***5)*** *The Graph tab plots data for the selected labels and will not be discussed in this tutorial.* ***6)*** *The Properties tab allows the user to move the label Offset portrayed on the VMD Display as well as rename the label Format.* ***7)*** *The Global Properties tab allows adjustments to label Text Size and Thickness.*

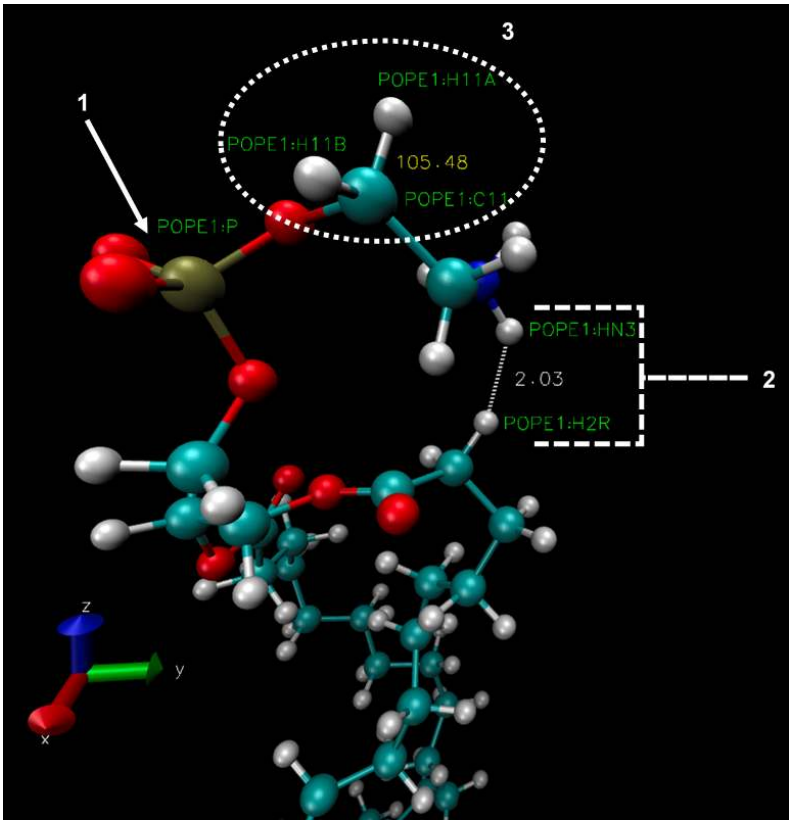


Figure 7.4.1.7. A POPE molecule demonstrating: **1)** The atom label of a phosphorous atom "POPE1:P".

2) *The atom distance between two hydrogen atoms as 2.03 Angstroms.*

3) *The angle between a carbon atom and two of its hydrogen bonding partners as 105.48 degrees.*

Exercises (section 1.3)

Exercise 1.1: Identify one atom of each element: Carbon, hydrogen, oxygen, nitrogen, and phosphorous. Rearrange each label so that they are all visible while clearly indicating the atom.

Exercise 1.2: How many double bonds are there in POPE? Where would you expect double bonds?

1.4. Advanced selection of specific regions

As you create more complex models you'll want to be able to specify a viewing region. This can be done by using the *Graphical Representations* window **(Figure 1.4)**. Again, from the *VMD Main*, select *Graphics → Representations…* to open the *Graphical Representations* window. First, create a new representation of the selected molecule by clicking *Create Rep*. In the representation box you'll now see two representations. By double-clicking you can hide the representation; hidden representations are in red text while visible representations in black text. Highlight the visible representation to enable it for editing.

In the selected atoms box, you can utilize certain keywords to enable or disable parts of your model. You can even use more complex strings as well as boolean or numeric values to specify your selection criteria; VMD's expression system is based on PERL (a computing language) syntax. Examples of these regular expressions can be found in section 6.3 of the VMD User's Guide [Ref. 15]. Back in the *Labels* window (*Graphics → Label)* you may have noticed certain labels having type information in the *Picked Atom* tab **(Figure 1.6)**. Keywords such as *ResName*, *ResID*, *Name*, *Type*, *Chain*, *SegName*, and *Index* can be used to specify a selection **(Table 1.2)**; descriptions of all keywords can be found in section 5.48 of the VMD User's Guide [Ref. 15]. For now, since there is only one POPE molecule labeled as *ResName: POPE* and specified as *Chain: X*, sort through the atom types for practice. To visualize all carbon atoms, use a regular expression such as **(Figure 1.8)**:

- *name "C.*"*

where the *C* represents the canonical carbon atom naming convention and the .* indicates any carbon atoms in the model. In an expression, this example means to search for anything classified as a *name* that starts with *C*. Another way to visualize carbon only atoms is by typing:

- *not name "O.*" and not name "P.*" and not name "H.*" and not name "N.*"*

Your representation should not have changed as you'll only see carbon atom types. In more complex models, you can specify single molecule chains or even molecule types:

- *resname POPE*
- *chain X*

In both of these cases you should see the entire phosphatidylethanolamine (POPE) molecule. More selection expressions can be found in Chapter 6.3 of the VMD 1.9.3 User's Guide [Ref. 15]

Table 1.2. *Examples of commonly found keywords for selection of specific model regions. Argument identifiers are: str=string and num=number. More information on other keywords can be found in [Ref. 15].*

Keyword	Arg	Description
resname	str	residue name
resid	num	residue id
name	str	atom name
type	str	atom type
chain	str	the one-character chain identifier
segname	str	segment name
index	num	the atom number, starting at 0



Figure 7.4.1.8. *Understanding atom selection.* ***1)*** *A window of all created representations. Highlight a representation to enable it for editing. Red text indicates hidden representations.* ***2)*** *Expressions can be input in the Selected Atoms command window. In this example, only carbon atoms are being selected. More examples can be found in the VMD User's Guide [Ref. 15].* ***3)*** *VMD provides a list of all expressions that can be used to specify selections.* ***4)*** *An example of all POPE carbon atoms displayed from the input (name "C.*").*

Exercises (section 1.4)

Exercise 1.3. Visualize all atoms but carbon in the single_POPE.pdb file.

Exercise 1.4. Using the index notation, visualize the polar head group. Hint: index notation for VMD starts at zero.

1.5 Saving and loading your session

From *VMD Main*, select *File → Save Visualization State…* Here you can specify which folder and what file name you would like using traditional file path syntax: *user/home/my_folder/my_file_name.vmd* Make sure you save as a .vmd or you will be unable to load the file! If you forget, rename your file so that you include the .vmd file type. To load your session, start VMD and from *VMD Main* select *File → Load Visualization State…* Note: *File → New Molecule…* is for importing new molecule file types only. It is better to use the *Load Visualization State* if you want to preserve your model representation settings **(**Figure 1.9).

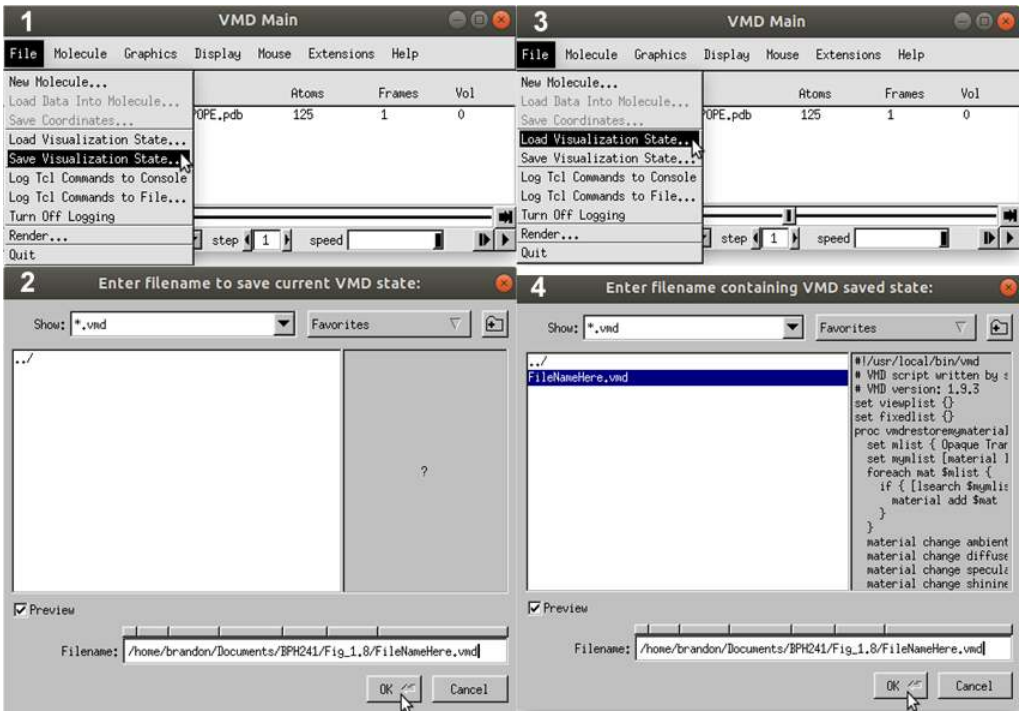


Figure 7.4.1.9. *Saving and loading sessions.* ***1)*** *To save a session, navigate to File → Save Visualization State…* ***2)*** *The save window will appear. VMD sessions are saved as .vmd files.* ***3)*** *To load a session, navigate to File → Load Visualization State…* ***4)*** *The load window will appear. Load a .vmd file to resume a session.*

2. Homogenous membranes using VMD's *MembraneBuilder* tool

The purpose of the Visual Molecular Dynamics (VMD) *MembraneBuilder* tool is to generate a membrane model surrounded by water which a protein can then be placed into. This complete lipid/protein/water model can then be used to run molecular dynamics simulations after generation of force field components and simulation parameters; a review on force fields can be found at [Ref. 16]. For this tutorial, the *MembraneBuilder* tool extends our interpretation of individual phosphatidylethanolamine (POPE) molecules to a homogenous POPE membrane. Unfortunately, the *MembraneBuilder* tool can 1) only generate homogenous POPE and phosphatidylcholine (POPC) membranes and 2) generate only water surrounding molecules. For more information on how *MembraneBuilder* executes its algorithm, visit here: www.ks.uiuc.edu/Research/vmd/plugins/membrane/ [Ref. 17]. For homogenous or heterogeneous membranes with the option of ion solvation, skip this section and proceed to Section 3 which uses the CHARMM-GUI interface to generate membranes.

2.1 Generate a POPE membrane

From *VMD Main*, select *Extensions → Modeling → Membrane Builder* to open the *Membrane* window. In this window, select phosphatidylethanolamine (POPE) as the lipid, and generate a 50x50 Angstrom^2 area. Change the output prefix to *POPE_membrane*. The *topology* section provides two CHARMM force fields that can be used: CHARMM27 and CHARMM36. Generally, CHARMM27 is for nucleic acids and lipids while CHARMM36 is for proteins and lipids; CHARMM36 is noted to have superior lipid parameters and thus should be used for most membrane biology models [Ref. 18]. After selecting CHARMM36 (c36), click *Generate Membrane*. You should now see a POPE membrane that is 50x50 Angstrom^2 with the leaflets surrounded by water. You will also note some patterns of randomness and discontinuity; perfect membranes are physiologically impossible thus stochasticity (randomness) is modeled. Visualize the membrane using a *CPK Drawing Method* as described in Section 1.2 **(Figure 2.1)**.



Figure 7.4.2.1. *Designing a membrane with MembraneBuilder.* ***1)*** *Access the MembraneBuilder window from the Extensions menu.* ***2)*** *The Membrane*

window allows users to generate a specific area (in Angstroms) of membrane. The membrane options are POPE and POPC with generation force fields

using either CHARMM27 (c27) or CHARMM36 (c36) ***3)*** *A side view of the generated POPE membrane with surrounding water from the tutorial instructions.*

Next, verify the generated membrane x-y length. From the *Graphical Representations* window **(Figure 1.4)**, remove the water by typing in the *Selected Atoms* text box:

- *not water*

In the *VMD Main*, select *Mouse → Label → bonds*. Using the x-, y-, and z-planes, take 5 rough measurements and record the average; a review on how to do this is in Section 1.3. You'll notice that the membrane area will be less than 50 Angstrom^2 (around 45 Angstrom^2 average). This is likely due to the close packing arrangement performed after initial generation of the model. You can save these models as discussed in Section 1.5 or save the membrane as a PDB coordinate file. From the *VMD Main*, *File → Save Coordinates…* will open a *Save Trajectory* window where you can select the molecule, atoms, and file format you wish to save as.

Exercises (section 2.1)

Exercise 2.1. Take an average of 5 measurements to determine the thickness of the membrane bilayer. Does this match experimental values? Section 1.3 describes how to measure distances.

Exercise 2.2. Take an average of 5 measurements to determine the water thickness. Why does the model need water? Should thickness be lower? Should thickness be higher?

3. Heterogeneous membrane building using CHARMM-GUI *Membrane Builder*

The CHARRM (Chemistry at HARvard Macromolecular Mechanics) force field was initially developed for proteins and nucleic acids but has since been extended to feature a robust set of lipid types [Ref. 19-20]. The most recent force field, CHARMM36, supports proteins, nucleic acids, carbohydrates, lipids, and small molecules [Ref. 21]. CHARMM-GUI is an online graphical user interface that allows the generation of multiple MD models and preliminary input files for the start of simulation [Ref. 4-8]. This section will cover the *Membrane Builder* tool that allows users to develop membrane models with the option of including protein complexes. For this tutorial, only the bilayer builder section, without protein insertion, and without preliminary simulation building will be discussed. While there are other membrane building options, the bilayer builder is the simplest all-atom tool to work through for beginners. Alternatively, some membrane building tools do not utilize all-atom modeling; for an alternative atom modeling schema see Course Grained Simulations:

https://phys.libretexts.org/Courses/University_of_California_Davis/UCD%3A_Biophysics_241_-_Membrane_Biology/Extra_Credit/Coarse_Grain_Simulations_of_Membranes.

Note : should you want to try protein-membrane model building in the future, make sure your protein PDB has the correct orientation relative to the membrane or you will improperly insert your protein. Improper protein insertion will result in simulations not reflecting real-life predictions since the protein is not in a physiological state. A tutorial on protein insertion can be found here: www.ks.uiuc.edu/Training/Tutorials/science/membrane/mem-tutorial.pdf [Ref. 22].

3.1. Determine lipid components, size, and solvation

Click on the following link to reach the CHARMM-GUI *Membrane Builder Bilayer Builder* webpage: http://www.charmm-gui.org/?doc=input/membrane.bilayer [Ref. 3]. Scroll down to find a brief explanation of the workflow, an option to include a Protein Data Bank (.pdb) file, and an option to generate a membrane only system. Click the *Membrane Only System* to be redirected to the *System Size Determination Options* page **(Figure 3.1)**.

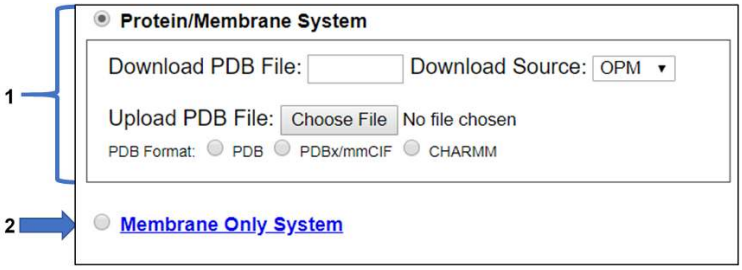


Figure 7.4.3.1. The start of the CHARMM-GUI Membrane Builder webpage.

1) *An option to create a protein/membrane system with a .pdb is provided.*

2) *For this tutorial, select "Membrane Only System."*

For this tutorial, users will recreate a model that has been used to study the effects of lipid tail saturation [Ref. 6]. The model is the CPRΔ1 model, a yeast-like model that contains a relatively high concentration of unsaturated lipids. In the *System Size Determination Options*, click the *Heterogeneous Lipid*, the *Water thickness*, and the *Ratios of lipid components* options. Next, input 20 Angstroms as the water thickness, and input 80 Angstroms as the initial X-Y guess **(Figure 3.2).** The initial X-Y guess is dependent upon the problem being solved; for example, a larger membrane protein would require a larger membrane area in order to be embedded. Below the system size is the *lipid components* options **(**Figure 3.3). Fill in the lipid ratios as indicated in **Table 3.1**. When finished, click the *Show the System Info* button and verify the generated dimensions. Ideally, both leaflets should have close to the same surface area; uneven areas can induce membrane bending artifacts during simulations and thus would be non-physiological. Once the system dimensions calculate near identical leaflet areas, click *Next Step: Determine the System Size* located in the lower right of the CHARMM-GUI webpage. This step may take some time. Do not close or refresh the CHARMM-GUI webpage.

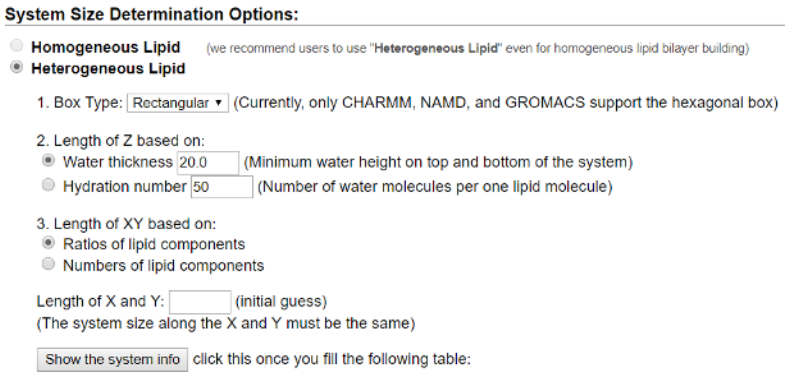


Figure 7.4.3.2. *System size determination options for use in the tutorial. Size values will vary depending on desired physiological parameter being studied, desired computational processing speed, and MD software used. For the tutorial, use 80 Angstroms as the initial X-Y guess.*

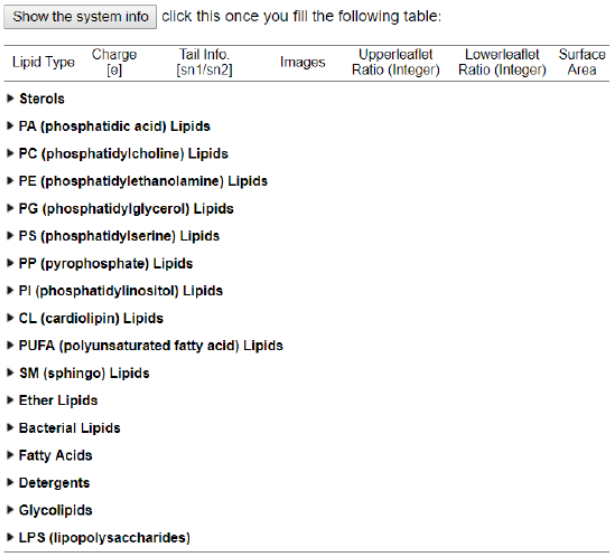


Figure 7.4.3.3. *Lipid components options in CHARMM-GUI Membrane Builder*

Make sure you click "Show the system info" after you input your desired lipids

to verify near identical leaflet areas!

Table 3.1. *Representative model components from supplemental Table 2 in So S. et al, 2009 [Ref. 6]. These lipid components will be used for the tutorial section to demonstrate how CHARMM-GUI can be used to model biophysical problems.*

Model	System Size[b]	Molecules of Each Component									# Atoms
		POPA	POPS	POPE	DOPC	DPPC	Chol	K^+	Cl^-	H_2O	
CPRΔ1[c]	79.2 x 79.2 x 76.7	20	10	60	100	20	60	46	16	11885	67007
CPRΔ1[sat d]	86.9 x 86.9 x 84	20	10	60	20	100	60	46	16	11826	66830
Hypo[e]	89.3 x 89.3 x 84	14	14	84	28	112	28	46	18	12836	72970

[a] Both top and bottom leaflets have the same lipid compositions
[b] Each initial system size (in Å) is given by $L_X \times L_Y \times L_Z$, where L_X, L_Y, and L_Z correspond to the system size along the *X*, *Y*, and *Z*-axes, respectively.
[c] POPA : POPS : POPE : DOPC : DPPC : Chol = 2 : 1 : 6 : 10 : 2 : 6
[d] POPA : POPS : POPE : DOPC : DPPC : Chol = 2 : 1 : 6 : 2 : 10 : 6
[e] POPA : POPS : POPE : DOPC : DPPC : Chol = 1 : 1 : 6 : 2 : 8 : 2

In the next web page, you will have a system output box showing you the various CHARMM parameter files generated from the previous step **(Figure 3.4)**. You can download the system parameter files at any step during the tutorial by clicking *download.tgz* in the top right of the CHARMM-GUI webpage. You can view the *Generated Packed System* by clicking *view structure*; this will open an additional window that can be manipulated similar to the Visual Molecular Dynamics (VMD) display. Viewing the structure after each step is helpful in understanding how CHARMM-GUI constructs the model. In this step, only the packing arrangement has been determined **(Figure 3.4)**. Below the system output box you will see the *Determined System Size* section with size parameters for building the system. Further down you will see the *System Building Options* section **(Figure 3.5)**. A key component of system building is deciding if the insertion or replacement method of adding model components should be used. Generally, insertion methods are meant for protein insertions into bilayers while membrane-only models should use the replacement method. Additionally, enable the *Check lipid ring penetration* box to verify that lipid replacement does not produce positional artifacts. Next, in the *Component Building Options* section, ions are included in the system to generate a charge neutral model for electrostatic calculations during the simulation. For this case, we want to mimic the number of ions listed in **Table 3.1**. Adjust the ion concentration until you have exactly the correct number of ions. For this tutorial, use the *Monte Carlo* ion placement method **(Figure 3.5)**. Once finished, click *Next Step: Build Components* located in the lower right of the CHARMM-GUI webpage. This step may take some time. Do not close or refresh the web page.



Figure 7.4.3.4. *The CHARMM parameter files that can be downloaded at each step are useful for understanding how the model is built.*

1) Click on the step3_packing.pdb (blue arrow) to view the structure. 2) A top-down view of the packing arrangement indicated as orange spheres.

The pink and blue squares indicate the upper and lower leaflet faces, respectively. This model view can be rotated similar to the VMD Display.

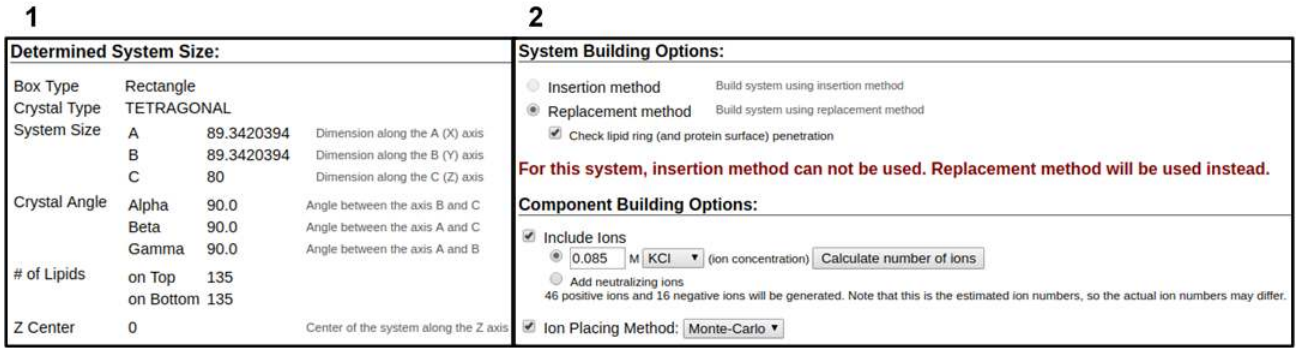


Figure 7.4.3.5. *System Size, System Build, and Component Build options for this tutorial. **1)** The determined system size is a good self-check to verify the correct dimensions before building further. **2)** For membranes, replacement method (the replacement of lipids) is used instead of insertion method (the insertion of a molecule such as a protein). The system build verifies that lipids do not have positional clashes. The component building options allows ion solvation, with either a distance or Monte-Carlo placement method. For this tutorial, 0.085 M of KCl will be used with the Monte-Carlo placement method.*

3.2. Final assembly, export, and visualization

Step 4 of the CHARMM-GUI *Membrane Builder* provides a self-check for lipid ring penetration as well as ion/water box building. In the system output box at the top of the page you can find the *step4_lipid.pdb* structure for viewing **(Figure 3.6)**. Click *Next Step: Assemble Components*.

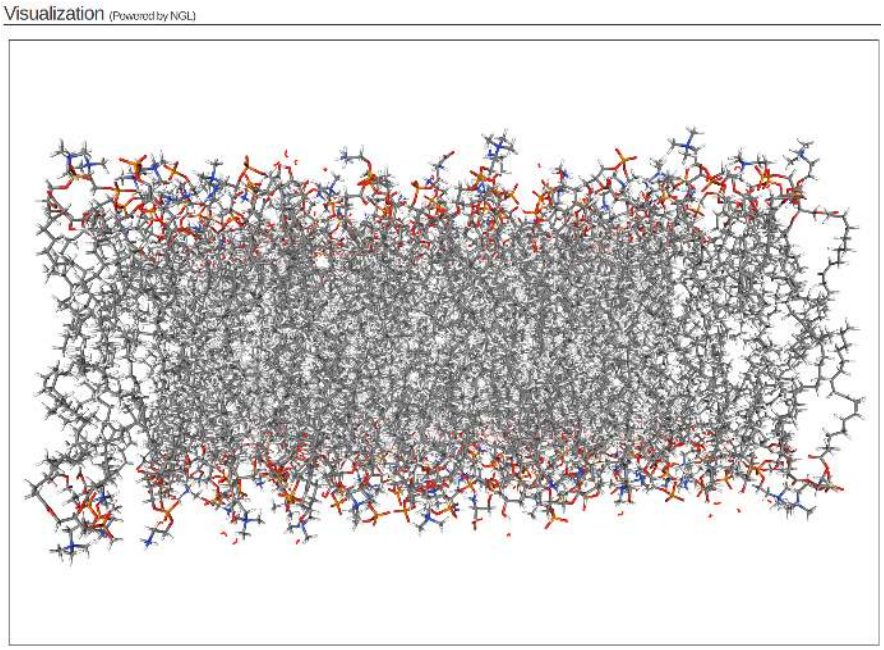


Figure 7.4.3.6. *Side perspective of lipid membrane from tutorial after completing Step 3: Determine the System Size.*

This model is the step before solvation.

Step 5 of the CHARMM-GUI *Membrane Builder* provides force field options, input generation options, and equilibration options for generating M.D. simulation parameters. Input options can be generated for various M.D. force fields such as GROMACS, AMBER, and CHARMM, among others. The use of a force field will largely be dependent upon your experimental question and your lab's computational expertise. A review describing the necessity for force fields and some common types can be found at [Ref. 16].

At the top of the system output box you will see the assembled .pdb file labeled as *step5_assembly.pdb*. You can download this .pdb file or the entire CHARMM-GUI folder by clicking the *download.tgz* icon at the top right of the CHARMM-GUI webpage. After downloading, the final model can be visualized using VMD as described in Section 1 **(Figure 3.7)**.

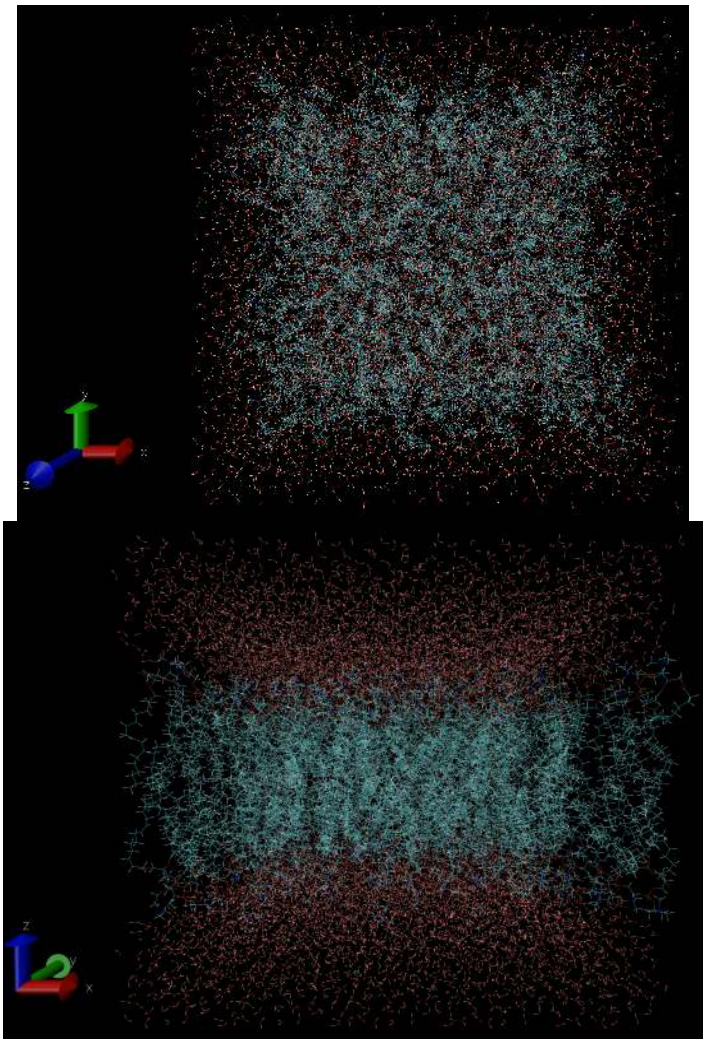


Figure 7.4.3.7. *(Left) top view of generated membrane model from tutorial*

(Right) side view of generated membrane model from tutorial.

Exercises (section 3.2)

Exercise 3.1. From the complete model (Figure 3.7), isolate each class of lipid, ion, and water atoms as their own representation. Hint: you may need to look at the .pdb file in a text editor or in the VMD *Labels* feature to find common naming schemes.

Exercise 3.2. Generate the other two models from Jo, S. et al 2009 ***(Table 3.1)*** *[Ref. 6]. What do you expect will be different compared to the CPRΔ1 model?*

Exercise 3.3. Find another biomembrane of interest and generate the model. What parameters must you know to ensure that it is physiologically relevant?

Exercise 3.4. Temperature can be a critical factor during M.D. system equilibration. As seen in CHARMM-GUI Membrane Builder step 5, there is an option to adjust the temperature. What are reasonable/unreasonable temperatures? What is a good rule of thumb? Hint: Membrane fluidity.

Exercise 3.5. Review the following article [Ref. 23] for examples on how molecular simulations have helped validate and promote experimental findings. What stood out to you? Which experiment did you find most interesting?

Acknowledgments

Some images were made with VMD/NAMD/BioCoRE/JMV/other software support. VMD/NAMD/BioCoRE/JMV/ is developed with NIH support by the Theoretical and Computational Biophysics group at the Beckman Institute, University of Illinois at Urbana-Champaign.

Some images were made with the online CHARMM-GUI visualization tool during Section 3: Heterogeneous membrane building using CHARMM-GUI *Membrane Builder*.

References

[1] Hospital, A., Goñi, J. R., Orozco, M., Gelpí, J. L. (2015). Molecular dynamics simulations: advances and applications. *Adv Appl Bioinform Chem.* **8**(1): 37-47. doi: 10.2147/AABC.S70333

[2] Software downloads download VMD. Available at www.ks.uiuc.edu/Development/Download/download.cgi?PackageName=VMD

[3] CHARMM-GUI Membrane Builder. Available at http://www.charmm-gui.org/?doc=input/membrane.bilayer

[4] Jo, S., Kim, T., Iyer, V. G., Im, W. (2008). CHARMM-GUI: a web-based graphical user interface for CHARMM. *J Comput Chem.* **29**(11): 1859-1865. doi: 10.1002/jcc.20945

[5] Wu, E. L., Cheng, X., Jo, S., Rui, H., Song, K. C., Dávila-Contreras, E. M., Qi, Y., Lee, J., Monje-Galvan, V., Venable, R. M., Klauda, J. B., Im, W. (2014). CHARMM-GUI Membrane Builder toward realistic biological membrane simulations. *J Comput Chem.* **35**(27): 1997-2004. doi: 10.1002/jcc.23702

[6] Jo, S., Lim, J. B., Klauda, J. B., Im, W. (2009). CHARMM-GUI Membrane Builder for mixed bilayers and its application to yeast membranes. *Biophys J.* **97**(1): 50-58. doi:10.1016/j.bpj.2009.04.013

[7] Jo, S., Kim, T., Im, W. (2007) Automated builder and database of protein/membrane complexes for molecular dynamics simulations. *PLoS One* **2**(9): e880. doi: 10.1371/journal.pone.0000880

[8] Lee, J., Patel, D. S., Ståhle, J., Park, S. J., Kern, N. R., Kim, S., Lee, J., Cheng, X., Valvano, M. A., Holst, O., Knirel, Y. A., Qi, Y., Jo, S., Klauda, J. B., Widmalm, G., Im, W. (2019). CHARMM-GUI Membrane Builder for complex biological membrane simulations with glycolipids and lipoglycans. *J Chem Theory Comput.* **15**(1): 775-786. doi: 10.1021/acs.jctc.8b01066

[9] PDB statistics: overall growth of released structures per year. (2019). Available at: www.rcsb.org/stats/growth/overall

[10] Berman, H. M., Westbrook, J., Feng, Z., Gilliland, G., Bhat, T. N., Weissig, H., Shindyalov, I. N., Bourne, P. E. (2000). *The Protein Data Bank. Nucleic Acids Res.* **28**(1): 235-242. doi: 10.1093/nar/28.1.235

[11] Burley, S. K., Berman, H. M., Bhikadiya, C., Bi, C., Chen, L., Di Costanzo, L., Christie, C., Dalenberg, K., Duarte, J. M., Dutta, S., Feng, Z., Ghosh, S., Goodsell, D. S., Green, R. K., Guranovic, V., Guzenko, D., Hudson, B. P., Kalro, T., Liang, Y., Lowe, R., Namkoong, H., Peisach, E., Periskova, I., Prlic, A., Randle, C., Rose, A., Rose, P., Sala, R., Sekharan, M., Shao, C., Tan, L., Tao, Y. P., Valasatava, Y., Voigt, M., Westbrook, J., Woo, J., Yang, H., Young, J., Zhuravleva, M., Zardecki, C. (2019). RCSB Protein Data Bank: biological macromolecular structures enabling research and education in fundamental biology, biomedicine, biotechnology and energy. *Nucleic Acids Res.* **47**(D1): D464-D474. doi: 10.1093/nar/gky1004

[12] PDB file format documentation. Available at: http://www.wwpdb.org/documentation/file-format

[13] Berman, H., Henrick, K., Nakamura, H. (2003). Announcing the worldwide Protein Data Bank. *Nat Struct Biol.* **10**(12): 980. doi: 10.1038/nsb1203-980

[14] Mouse modes. (2019). Available at: www.ks.uiuc.edu/Research/vmd/vmd-1.9.3/ug/node32.html

[15] VMD user's guide version 1.9.3. (2016). Available at www.ks.uiuc.edu/Research/vmd/vmd-1.9.3/ug.pdf

[16] González, M. A. (2011) Force fields and molecular dynamics simulations. *Collection SFN* **12**(1): 169-200. doi: 10.1051/sfn/201112009

[17] Balabin, I. Membrane plugin, version 1.1. Available at www.ks.uiuc.edu/Research/vmd/plugins/membrane/

[18] Huang, J., MacKerell, A. D. Jr. (2013) CHARMM36 all-atom additive protein force field: validation based on comparison to NMR data. *J Comput Chem.* **34**(25): 2135-2145. doi: 10.1002/jcc.23354

[19] Brooks, B. R., Bruccoleri, R. E., Olafson, B. D., States, D. J., Swaminathan, S., Karplus, M., (1983). CHARMM: A program for macromolecular energy, minimization, and dynamics calculations. *J Comput Chem.* **4**(2) 187-217. doi: 10.1002/jcc.540040211

[20] Brooks, B. R., Brooks III, C. L., MacKerell Jr., A. D., Nilsson, L., Petrella, R. J., Roux, B., Won, Y., Archontis, G., Bartels, C., Boresch, S., Caflisch, A., Caves, L., Cui, Q., Dinner, A. R., Feig, M., Fischer, S., Gao, J., Hodoscek, M., Im, W., Kuczera, K., Lazaridis, T., Ma, J., Ovchinnikov, V., Paci, E., Pastor, R. W., Post, C. B., Pu, J. Z., Schaefer, M., Tidor, B., Venable, R. M., Woodcock, H. L., Wu, X., Yang, W., York, D. M., Karplus, M. (2010). CHARMM: the biomolecular simulation program. *J Comput Chem.* **30**(10): 1545-1614. doi: 10.1002/jcc.21287

[21] Kessel, A. and Ben-Tal, N. (2018) Introduction to proteins structure, function, and motion second edition. Boca Raton, FL: CRC Press, Taylor & Francis Group.

[22] Aksimentiev, A. Sotomayor, M., Wells, D., Mahinthichaichan, P. (2016) Membrane Proteins Tutorial. Available at http://www.ks.uiuc.edu/Training/Tutorials/science/membrane/mem-tutorial.pdf

[23] Hollingsworth S. A., Dror, R. O. (2018) Molecular dynamics simulation for all. *Neuron* **99**(6): 1129-1143. doi: 10.1016/j.neuron.2018.08.011

7.4: Designing Molecular Membranes Models with VMD is shared under a CC BY 4.0 license and was authored, remixed, and/or curated by LibreTexts.

7.5: Coarse Grain Simulations of Membranes

During the late 1960s at the dawn of Levinthal's paradox, understanding the mechanism of protein folding became a critical area of study. This was likely the primary driving force for the coarse grained method in order to capture the phenomenon of the entire protein folding process. It was Levitt and Warshel who were the first people to successfully accomplish this during their work in the early 1970s. Their coarse graining method, published in 1975, modeled the small, bovine pancreatic trypsin inhibitor protein using pseudoatoms at the alpha carbon positions; the model reduced the degrees of freedom to one which described rotation along the central pseudobond for the three consecutive alpha carbon atoms; the force field used was described by the Lennard Jones potential; and Brownian Dynamics was used as the sampling scheme. The pioneering work substantiated but fell short of describing the packing and pair-wise interactions of side chains that are integral driving forces for obtaining specific folded structures. Just a year later, Levitt proposed an improved model accounting for side chain orientation and since then the method of coarse graining has only continued to progress in accuracy and expand to other biomolecules like nucleic acids, carbohydrates, water and lipids. The development of this inaugural coarse grained model has led to the many advancements in the method that exist in the current state of the art as it has become a crucial computational modeling tool for simulating meso-scale biological phenomena.[2,6,10]

Coarse grained simulation basics

Capturing the time and length scale of biological processes using computational methods remains a challenge for molecular modeling as resolution is limited to the order of less than 100 ns and 10 nm in all-atom detail. Coarse graining reduces the degrees of freedom of the system to achieve greater size and time scales at the expense of molecular detail to simulate biological processes currently inaccessible to all atom models. In addition to increasing the spatiotemporal limitations of all-atom molecular dynamics simulations, coarse graining is advantageous because it enables high throughput studies that systematically explore thousands of state conditions in parallel; it reveals which details are essential to reproduce higher resolution results which provides insight on the biological driving forces at play; it smoothes the potential energy landscape of the system allowing for a computationally inexpensive testing of novel biophysical pathways.[3]

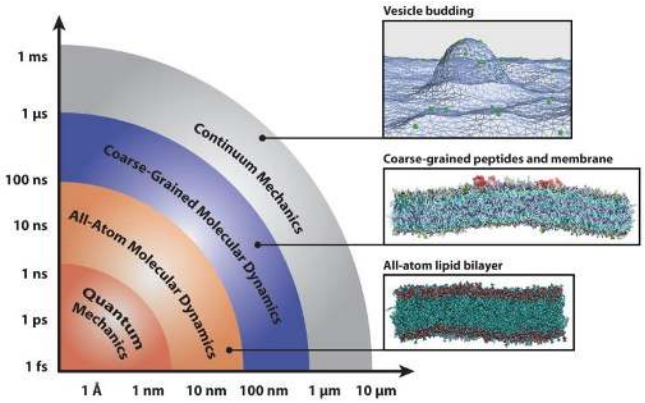


Figure 7.5.1: Spatial and temporal scale for computational methods[1]

How to Coarse Grain

A complete coarse grained (CG) model accomplishes the following: (1) it must represent the atomistic model as simplified CG "beads" that encapsulate a desired approximation of a group of atoms and (2) it must have a set of potentials called a force field that describe how the beads interact with one another.

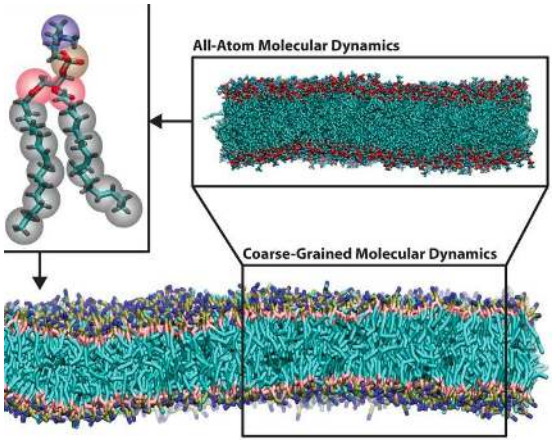


Figure 7.5.2: All atom to coarse grained description. In this simplified representation a 4:1 atom:bead ratio is used with gray beads for hydrocarbons, pink beads for glycerol, gold beads for phosphate and blue beads for choline-type.[1]

Atom mapping

Mapping is the first step to coarse graining and largely determines the accuracy, efficiency and transferability of the model.[11] Since coarse graining relies on utilizing only essential degrees of freedom it is important to assess which are necessary to obtain the desired resolution for a biologically relevant representation of the system or phenomenon. There are two common methods of atom mapping used to coarse grain a system: shape and "residue" based.

- Shape based: uses the highest level of simplification in order to model large scale motions therefore the least amount of beads as possible. Two CG beads represent each lipid bilayer leaflet, one for the head and one for the tail group, which are connected by a harmonic potential and the top and bottom leaflet interact via Lennard-Jones and Coulomb potentials. The shape-based CG lipid model allows for simulations of molecular dynamics on the order of hundreds of microseconds and beyond.[19]
- Residue based: uses the strategy of making a cluster of connected heavy atoms the unit particle in which approximately 10-20 covalently bound atoms are mapped into one CG bead. While resulting in an inevitable loss of detail, this permits a longer timestep and thereby produces higher computational efficiency than united atom models. It is typical to use this family of methods when a 1-2 order of magnitude speed up from an all-atom simulation is desired.[21]

In addition to the resolution (amount of CG beads) used to represent a group of atoms, it is important to consider the placement of the CG beads with respect to the atomic structure. It is typical for small molecules like lipids to be locationally mapped using chemical intuition in which a CG site is used for each functional group in a molecule.[5]

Force Field Building

It is a continual challenge to develop accurate and transferrable CG force fields. The typical way to construct a CG simulation force field is using either the bottom up (structure based coarse graining) force matching of top down (thermodynamic based coarse graining) free energy based approach.

Bottom-up/Structure-based: uses effective interaction based on reference all-atom simulations. Common systematic methods include inverse Monte Carlo, iterative Boltzmann inversion and Force Matching aka variational fitting (IMC, IBI and FM).[3] The IBI method utilizes a **radial distribution function (RDF)** from atomistic simulations to calculate a CG RDF function and iteratively improve the CG pair potential in reference to all atom pair potentials. The equation used to improve upon the CG pair potential for this iterative method is[6]:

$$u_{i+1}^{\mathrm{CG}}(r) \cong u_i^{\mathrm{CG}}(r) - k_{\mathrm{B}}T \ln\left(\frac{\rho_l^{\mathrm{CG}}(r)}{\rho^{\mathrm{Larget}}(r)}\right) \tag{7.5.1}$$

Here, $\rho(r)$, is the RDF and, u, is the effective pair potential derived from the potential of mean force calculation. Essentially the equation states the a guess is input for the initial RDF and this is iterated numerous times until the value converges on the target RDF. Iteration continue until convergence on a unique pair potential for a given radial distribution is achieved within an acceptable error. Similarly, the IMC method utilizes the RDF as the target property to approximate a coarse grained Hamiltonian for the system but unlike the IBI method it explicitly handles the CG force field parameters by solving a series of linear equations at each iterative step to reach successful convergence.[6] Voth's multi-scale coarse grained (MS-CG) model described briefly is representative of the force matching method and utilizes a system of linear equations to find the least squares fit of sampled

configurations from an atomistic simulation to optimize the CG force field.[1,4] Inverse Monte Carlo differs from this because it is an exact Newton method and tries to fit the exact reference value versus the natural log whereas force matching extracts an optimal potential from large conformational data produced by ab initio calculations.

Top-down/Thermodynamics-based: uses analytical interaction potentials and is parameterized in an iterative procedure that aims to reproduce thermodynamic properties from experimental data, which typically results in a more easily transferable force field.[3] The Martini force field is a commonly used example of the top-down method in which bonded interactions are specified by potential energy functions but is unique in its description of non bonded interactions.[1] The intermolecular structure and thermodynamics of the target system depends on the non bonded interaction modeled using the Lennard-Jones potential and the parameters are chosen to reproduce specific experimental measurements, i.e. bulk density, free energy of hydration, vapor pressure, etc.[12]

Most CG force fields rely on a combinations of the two methods to optimize accuracy and transferability. Though not exhaustive the table below from Bradley et al. provides an excellent summary of force field construction types and their applicability.[1]

Table 1: Common force fields used in coarse grain simulations

Model	Key Methods	Key Target Data
CMM-CG	Structure matching, energy matching, Boltzmann inversion, reverse Monte Carlo	Density distributions, interfacial tension, area per lipid, bending modulus, area compressibility modulus, lipid order parameters
MS-CG	Bottom up force matching, variational optimization, hybrid analytic-systematic CG, screened electrostatics	Atomistic site to site radial distribution functions, density distributions, bending and area compressibility moduli, lipid diffusion rates
Martini	Top down energy matching, potential of mean force between phases, bilayer stress profile, free energy of lipid desorption or flip-flop, short range electrostatics	Free energy of hydration and vaporization, partitioning free energies, surface and interfacial tension, density distributions, bending modulus, area per lipid

HOW TO SAMPLE A COARSE GRAINED MODEL?

Force fields transform the biological systems flat conformational space into an extremely rugged surface. Sampling schemes allow for the surface to be traversed in search of desired system conformations. The two most commonly used schemes used in CG modeling are molecular dynamics (MD) and Monte Carlo (MC). MD schemes generate new conformations utilizing classical mechanics described by Newton's equations of motion. Using this method, a trajectory is produced which describes the time evolution of the system and allows for the assessment of time dependent observables. MC schemes traverse the conformational space in a completely time independent manner that provides a random sample of conformations coming from the desired distribution, typically Boltzmann (this linked page goes more in depth on this sampling method: Monte carlo for Biomembranes). This method uses unphysical jumps in space to allow for escape from local energy minima and is an entirely statistics based algorithm.[6]

Coarse graining for membranes

WHY COARSE GRAIN MEMBRANES?

While a single lipid molecule itself is relatively small, only about 100 atoms, the bulk properties of a lipid bilayer depends on the collective behavior of hundreds to thousands of individual lipids rendering atomistic models extremely computationally expensive. Real biological membranes are heterogeneous and contain multiscale properties with the typical membrane being on the macroscopic scale--microns and microseconds--which is currently inaccessible to atomic resolution molecular dynamics simulations.[8]

AND WHAT ABOUT WATER?

Given that water is an essential component of biological systems and typically comprising more than 80% of the system's total particles it is necessary to reproduce both its structure and phase transitions to create a relevant and accurate coarse-grained model.[3,11] The dynamic effects of water on biological systems arise from its hydrogen bonding, polarity and geometry which can not be fully captured using the CG method therefore the model must be parameterized to reproduce the desired macroscopic property.[18] CG methods employ several different mapping and parameterization techniques that produce the following three categories of models: (1) implicit, (2) explicit and (3) polarizable.[1]

1. The two typical strategies to account for water implicitly are by adjusting the non-bonded interactions between non-water molecules or adding a force field term that accounts for the hydrophobic effect using DeBye-Huckel theory of Generalized-Born models, which is based on modeling the solute as a set of spheres whose internal dielectric constant differs from the external solvent.[3]
2. The two parameterization types for the explicit representation of a water molecule as a van der waals particle use either structure or thermodynamic methods. Structure based methods typically use a 1:1 molecule:bead ratio and are constructed from atomistic water simulations using IBI or FM. Thermodynamics based water models are parameterized by fitting to macroscopic experimental results (like density, diffusion rate, surface tension, etc.[3]) and use various mapping ratios.[3,18]
3. Explicit water models lack charges which prevents them from screening electrostatics which is remedied by polarizable models. This is accomplished by incorporating charged pseudo particles controlled by an angle potential that allows for mimicking of water's electrostatic screening due to its polarizability.[17] The molecule: bead mapping varies from a 4:1 rigid V-shape, A 1:1 induced point dipole, or the 11:4 tetrahedrally coordinated water model, for instances.[3]

WHAT COARSE GRAINED MEMBRANE MODELS ARE COMMONLY USED?

In coarse grained models the observables from atomistic models are often defined by analogy and result in what is known as the representability problem.[20] Practically, this means that the questions asked dictate which CG model is appropriate to use. In order to choose the right model for each problem, it is necessary to understand the applicability and limitations of your model.[3] While numerous coarse grained lipid models exist some successful, commonly used coarse grained lipid models include[3]: (1) Klein[9] (2) Martini[12] (3) ELBA[7] (4) Voth[8] (5) Smit's DPD[13]

1. A pioneering model that constructs a CG forcefield from all atom simulation data studying a dimyristoylphosphatidylcholine (DMPC) membrane. While structurally accurate it has limited transferability that has since been improved upon by incorporating both top down and bottom up parameterization. The introductory model linked each of the 13 CG beads using harmonic bond and quartic angle potentials fitted to the atomistic simulation while non-bonded interactions were represented by radial distribution functions and refined with IBI. Recent applications of the model have extended the applicability to different molecular structures and environmental conditions.[16]
2. This model was originally developed for lipids and is purposefully simplistic using minimal parameters and a few standard interaction potential in an effort to be versatile in its applications while maintaining accuracy. It uses a 4:1 atom:bead mapping with a fixed bead size with 18 different polarity/charge group types. Bonds and angles are described by harmonic potentials and VdW and electrostatics are described using shifted potentials. The model parameters are tuned to match structural and thermodynamic data from experimental and simulated systems. Applications are vast and range from raft domain formation to membrane tethers.
3. An electrostatics based CG lipid force field that focuses on lipid water interactions designed for multiscale applicability. Each water molecule is represented by a Lennard-Jones soft soft sphere with a point dipole and the CG lipid beads incorporate electrostatics as explicit point charges or point dipoles with a relative dielectric constant of 1. The model was parameterized for bulk, liquid phase water and is particularly applicable for modeling lipid phase behavior and the movement of drugs and other molecules across lipids bilayers.
4. Voth and colleagues have developed multiple CG lipid models that like the Klein model use a force field derived from all atom simulations termed a multiscale CG forcefield (MS-CG) that instead contains an analytical and systematic component that utilize force matching vs average structural properties. Their methods employ a range of atom mapping from an aggressive CG with a single bead to represent an entire lipid used to simulate very large systems[8] to the typical 13-15 CG beads per lipid; model dependent treatments of electrostatic interactions and water representations, either explicit or implicit. Their models have been used to model several lipids like DMPC, DOPC, DOPE and cholesterol membranes and has been used to study a variety of biological phenomena including liposome (~200nm) self assembly and the phase behavior of binary mixed membranes.[15]
5. This lipid model utilizes the soft repulsive forces used in dissipative particle dynamics that replace the Lennard-Jones potential to study the DMPC bilayer. The DPD repulsion parameter was determined using prior related DPD studies; their atom mapping consisted of a model comprising a lipid head group of 3 hydrophilic beads and the remaining 10 beads comprising 2 hydrophobic tails; and their model has been shown to describe multicomponent bilayer behavior with accuracy and speed.

References

1. Bradley, Ryan, and Ravi Radhakrishnan. "Coarse-Grained Models for Protein-Cell Membrane Interactions." *Polymers* vol. 5,3 (2013): 890-936.

2. Schindler, Tanja, Dietmar Kröner, and Martin O. Steinhauser. "On The Dynamics Of Molecular Self-Assembly And The Structural Analysis Of Bilayer Membranes Using Coarse-Grained Molecular Dynamics Simulations." *Biochimica et Biophysica Acta (BBA) - Biomembranes* 1858.9 (2016): 1955-1963.
3. Ingólfsson, Helgi I. et al. "The Power Of Coarse Graining In Biomolecular Simulations." *Wiley Interdisciplinary Reviews: Computational Molecular Science* 4.3 (2013): 225-248.
4. Izvekov, Sergei, and Gregory A. Voth. "A Multiscale Coarse-Graining Method For Biomolecular Systems." The Journal of Physical Chemistry B 109.7 (2005): 2469-2473.
5. Zhang, Zhiyong et al. "A Systematic Methodology For Defining Coarse-Grained Sites In Large Biomolecules." *Biophysical Journal* 95.11 (2008): 5073-5083.
6. Kmiecik, Sebastian et al. "Coarse-Grained Protein Models And Their Applications." *Chemical Reviews* 116.14 (2016): 7898-7936.
7. Orsi, Mario, and Jonathan W. Essex. "The ELBA Force Field For Coarse-Grain Modeling Of Lipid Membranes." *PLoS ONE* 6.12 (2011): e28637.
8. Ayton, Gary S., and Gregory A. Voth. "Hybrid Coarse-Graining Approach For Lipid Bilayers At Large Length And Time Scales." *The Journal of Physical Chemistry B* 113.13 (2009): 4413-4424.
9. Shelley, John C. et al. "A Coarse Grain Model For Phospholipid Simulations." *The Journal of Physical Chemistry B*105.19 (2001): 4464-4470.
10. Kamerlin S. L . et al. “Coarse-Grained (Multiscale) Simulations in Studies of Biophysical and Chemical Systems” *Annu. Rev. Phys. Chem.* (2011): 62:41-64.
11. Noid, W. G. "Perspective: Coarse-Grained Models For Biomolecular Systems." *The Journal of Chemical Physics* 139.9 (2013): 090901.
12. Marrink S.J. et al. “The MARTINI force field: coarse grained model for biomolecular simulations.” *J Phys Chem B.* 2007; 111:7812–7824.
13. Kranenburg M, Nicolas J-P, Smit B. “Comparison of mesoscopic phospholipid-water models.” *Phys Chem Chem Phys.* 2004;6:4142–4151.
14. J. Baschnagel, et al. “Monte Carlo Simulation of Polymers: Coarse-Grained Models” *Computational Soft Matter: From Synthetic Polymers to Proteins.* (2004): 23; 83-140.
15. Lu, Lanyuan, and Gregory A. Voth. "Systematic Coarse-Graining Of A Multicomponent Lipid Bilayer." *The Journal of Physical Chemistry B* 113.5 (2009): 1501-1510.
16. Shinoda W, DeVane R, Klein ML. “Zwitterionic lipid assemblies: molecular dynamics studies of monolayers, bilayers, and vesicles using a new coarse grain force field.” *J Phys Chem B.* 2010;114:6836–6849.
17. Yesylevskyy, Semen O et al. “Polarizable water model for the coarse-grained MARTINI force field.” *PLoS computational biology* vol. 6,6 e1000810
18. Hadley, Kevin R, and Clare McCabe. “Coarse-Grained Molecular Models of Water: A Review.” *Molecular simulation* vol. 38,8-9 (2012): 671-681.
19. Arkhipov, Anton et al. “Four-scale description of membrane sculpting by BAR domains.” *Biophysical journal* vol. 95,6 (2008): 2806-21.
20. Wagner, Jacob W. et al. "On The Representability Problem And The Physical Meaning Of Coarse-Grained Models." *The Journal of Chemical Physics* 145.4 (2016): 044108.
21. Freddolino PL, Arkhipov A, Shih AY, Yin Y, Chen Z, et al. (2008) Application of residue-based and shape-based coarse graining to biomolecular simulations. In: Voth GA, editor, Coarse-Graining of Condensed Phase and Biomolecular Systems, Chapman and Hall/CRC Press, Taylor and Francis Group, chapter 20. pp. 299–315.

7.5: Coarse Grain Simulations of Membranes is shared under a CC BY 4.0 license and was authored, remixed, and/or curated by LibreTexts.

Index

A

actin
2.1: Membrane Fluctuations
Atomic Force Microscopy
6.1: Atomic force microscopy (AFM) on Membranes

C

caveolae
3.6: Rafts
Cavins
3.6: Rafts
Chain order parameter
7.3: Molecular Dynamics for Biomembranes
charge
4.5: Nanoparticle Spontaneous Penetration and Assembly in and Through Membranes
chemical shift anisotropy (CSA)
5.11: Solid-state NMR
cholesterol binding sequence
3.6: Rafts
Coarse Grain Simulations
7.5: Coarse Grain Simulations of Membranes
compressibility
2.4: Membrane Compressibility
compressibility modulus
2.4: Membrane Compressibility

E

Electrospray
6.3: Electrospray Ionization (ESI) Mass Spectrometry
ESI Mass Spectrometry
6.3: Electrospray Ionization (ESI) Mass Spectrometry

F

fatty acids
1.1: Charged Lipids
Fluid Mosaic Model
2.7: Diffusion in Membranes
Fluorescent Lipid Probes
5.4: Lipid Probes
FRAP
5.5: Fluorescence on Membranes
FTIR
5.8: FTIR on Membranes

G

Gaussian curvature
2.3: Membrane Curvature
Gel Phase
3.4: The Gel Phase
glycerophospholipids
1.3: Lipid Tails and Saturation
glycolipids
1.4: Glycolipids

H

hard ionization
6.2: Mass Spectrometer Ionization Techniques for Membrane Proteins
Helfrich model
2.4: Membrane Compressibility

I

Integral membrane
4.2: Insertion of Membrane Proteins into Lipid Membranes

K

Kingdon trap
6.4: Mass Analyzer Orbitrap
Knight trap
6.4: Mass Analyzer Orbitrap

L

lateral diffusion coefficient
3.3: The Fluid Phase
Laurdan
3.7: Lipid Phase Coexistence
Lectins
2.2: Membrane Asymmetry
Lipid Headgroup
1.2: Lipid Headgroup Types
Lipid phase coexistence
3.7: Lipid Phase Coexistence
Lipid rafts
3.6: Rafts
lipids
1: Lipids
1.3: Lipid Tails and Saturation
Luzzati thickness
3.3: The Fluid Phase

M

magic angle spinning
5.11: Solid-state NMR
mechanosensitive (MS) ion channels
4.4: Physical Lipid Protein Interactions
Membrane Building
7.4: Designing Molecular Membranes Models with VMD
Membrane Curvature
2.3: Membrane Curvature
membrane deformation energy
2.4: Membrane Compressibility
micelles
4.6: Non-Membrane Lipid Assemblies (Micelles)
Molecular Design
7.4: Designing Molecular Membranes Models with VMD
molecular saturation
1.3: Lipid Tails and Saturation
Monte Carlo simulation
7.2: Monte Carlo for Biomembranes

N

Nanoparticle
4.5: Nanoparticle Spontaneous Penetration and Assembly in and Through Membranes

O

orbitrap
6.4: Mass Analyzer Orbitrap

P

Pake pattern
5.11: Solid-state NMR
Phosphatidic acid
1.1: Charged Lipids
Phosphatidylethanolamine
1.1: Charged Lipids
Phosphatidylinositol
1.1: Charged Lipids
Phospholipids
1.1: Charged Lipids

Q

Quadrupolar interactions (NMR)
5.11: Solid-state NMR

R

Raman Spectroscopy
5.9: Raman Spectroscopy on Membranes
reflectron
6.5: Mass Analyzer - Time of Flight

S

Sec translocon
4.2: Insertion of Membrane Proteins into Lipid Membranes
segmental order parameter
5.11: Solid-state NMR
Signal Recognition Particle
4.2: Insertion of Membrane Proteins into Lipid Membranes
Single Molecule Tracking
5.7: Single Molecule Tracking
SMALP
5.3: Styrene Maleic Acid Lipid Particles (SMALP) Technology
soft ionization
6.2: Mass Spectrometer Ionization Techniques for Membrane Proteins
Sphingolipids
1.5: Sphingolipids
Sphingomyelin
1.1: Charged Lipids
sphinosine
1.5: Sphingolipids
Spin Probes
5.4: Lipid Probes
STED
5.5: Fluorescence on Membranes
sterol
1.3: Lipid Tails and Saturation
Sterols
1.6: Sterols and Sterol Induced Phases
Supported lipid bilayers (SLBs)
5.2: Supported and Tethered Membranes
Supported Membranes
5.2: Supported and Tethered Membranes

T

tethered lipid bilayers membranes (tLBMs)
5.2: Supported and Tethered Membranes

Tethered Membranes
5.2: Supported and Tethered Membranes

time of flight
6.5: Mass Analyzer - Time of Flight

TIRFM
5.5: Fluorescence on Membranes

total curvature
2.3: Membrane Curvature

Total Internal Reflection Fluorescence Microscopy
5.5: Fluorescence on Membranes

transmembrane domain
4.2: Insertion of Membrane Proteins into Lipid Membranes

V

Vesicles
2.6: Vesicles

Visual Molecular Dynamics
7.4: Designing Molecular Membranes Models with VMD

Visualization
7.4: Designing Molecular Membranes Models with VMD

VMD
7.4: Designing Molecular Membranes Models with VMD

Glossary

Sample Word 1 | Sample Definition 1

Detailed Licensing

Overview

Title: Biophysics 241: Membrane Biology

Webpages: 67

All licenses found:

- CC BY 4.0: 95.5% (64 pages)
- Undeclared: 4.5% (3 pages)

By Page

- Biophysics 241: Membrane Biology - *CC BY 4.0*
  - Front Matter - *CC BY 4.0*
    - TitlePage - *CC BY 4.0*
    - InfoPage - *CC BY 4.0*
    - Table of Contents - *Undeclared*
    - Licensing - *Undeclared*
  - 1: Lipids - *CC BY 4.0*
    - 1.1: Charged Lipids - *CC BY 4.0*
    - 1.2: Lipid Headgroup Types - *CC BY 4.0*
    - 1.3: Lipid Tails and Saturation - *CC BY 4.0*
    - 1.4: Glycolipids - *CC BY 4.0*
    - 1.5: Sphingolipids - *CC BY 4.0*
    - 1.6: Sterols and Sterol Induced Phases - *CC BY 4.0*
    - 1.7: Lipids in Non-Aqueous Environments - *CC BY 4.0*
  - 2: Membranes - Aggregated Lipids - *CC BY 4.0*
    - 2.1: Membrane Fluctuations - *CC BY 4.0*
    - 2.2: Membrane Asymmetry - *CC BY 4.0*
    - 2.3: Membrane Curvature - *CC BY 4.0*
    - 2.4: Membrane Compressibility - *CC BY 4.0*
    - 2.5: Surface Tension and Line Tension - *CC BY 4.0*
    - 2.6: Vesicles - *CC BY 4.0*
    - 2.7: Diffusion in Membranes - *CC BY 4.0*
  - 3: Membrane Phases and Morphologies - *CC BY 4.0*
    - 3.1: Membrane Phase Transitions - *CC BY 4.0*
    - 3.2: The Main Phase Transition - *CC BY 4.0*
    - 3.3: The Fluid Phase - *CC BY 4.0*
    - 3.4: The Gel Phase - *CC BY 4.0*
    - 3.5: The Ripple Phase - *CC BY 4.0*
    - 3.6: Rafts - *CC BY 4.0*
    - 3.7: Lipid Phase Coexistence - *CC BY 4.0*
  - 4: Membrane-Protein Interactions - *CC BY 4.0*
    - 4.1: Membrane Permeability - *CC BY 4.0*
    - 4.2: Insertion of Membrane Proteins into Lipid Membranes - *CC BY 4.0*
    - 4.3: Protein-lipid Interactions - *CC BY 4.0*
    - 4.4: Physical Lipid Protein Interactions - *CC BY 4.0*
    - 4.5: Nanoparticle Spontaneous Penetration and Assembly in and Through Membranes - *CC BY 4.0*
    - 4.6: Non-Membrane Lipid Assemblies (Micelles) - *CC BY 4.0*
  - 5: Experimental Characterization - Spectroscopy and Microscopy - *CC BY 4.0*
    - 5.1: Model Membranes vs. Biological Membranes - *CC BY 4.0*
    - 5.2: Supported and Tethered Membranes - *CC BY 4.0*
    - 5.3: Styrene Maleic Acid Lipid Particles (SMALP) Technology - *CC BY 4.0*
    - 5.4: Lipid Probes - *CC BY 4.0*
    - 5.5: Fluorescence on Membranes - *CC BY 4.0*
    - 5.6: Near-field Scanning Optical Microscopy (NSOM) - *CC BY 4.0*
    - 5.7: Single Molecule Tracking - *CC BY 4.0*
    - 5.8: FTIR on Membranes - *CC BY 4.0*
    - 5.9: Raman Spectroscopy on Membranes - *CC BY 4.0*
    - 5.10: Nuclear Magnetic Resonance (NMR) Theory and Solution NMR - *CC BY 4.0*
    - 5.11: Solid-state NMR - *CC BY 4.0*
    - 5.12: Electron Paramagnetic Resonance (EPR) of Membranes - *CC BY 4.0*
    - 5.13: Membrane X-ray Scattering - *CC BY 4.0*
  - 6: Experimental Characterization - Mass Spectrometry and Atomic Force Microscopy - *CC BY 4.0*
    - 6.1: Atomic force microscopy (AFM) on Membranes - *CC BY 4.0*
    - 6.2: Mass Spectrometer Ionization Techniques for Membrane Proteins - *CC BY 4.0*
    - 6.3: Electrospray Ionization (ESI) Mass Spectrometry - *CC BY 4.0*
    - 6.4: Mass Analyzer Orbitrap - *CC BY 4.0*
    - 6.5: Mass Analyzer - Time of Flight - *CC BY 4.0*
  - 7: Computational Characterization of Membranes - *CC BY 4.0*
    - 7.1: Mathematical Continuum Descriptions of Membranes - *CC BY 4.0*
    - 7.2: Monte Carlo for Biomembranes - *CC BY 4.0*

- 7.3: Molecular Dynamics for Biomembranes - *CC BY 4.0*
- 7.4: Designing Molecular Membranes Models with VMD - *CC BY 4.0*
- 7.5: Coarse Grain Simulations of Membranes - *CC BY 4.0*

- Back Matter - *CC BY 4.0*
  - Index - *CC BY 4.0*
  - Glossary - *CC BY 4.0*
  - Detailed Licensing - *Undeclared*